

DISSERTATION

BIOMARKERS OF DISEASE PROGRESSION AND CHEMOTHERAPEUTIC
RESISTANCE IN CANINE OSTEOSARCOMA

Submitted by

Liza E. O'Donoghue

Department of Clinical Sciences

In partial fulfillment of the requirements

For the Degree of Doctor of Philosophy

Colorado State University

Fort Collins, Colorado

Fall 2011

Doctoral Committee:

Advisor: Dawn L. Duval

Douglas H. Thamm

Gerrit J. Bouma

Michael Weil

ABSTRACT

BIOMARKERS OF DISEASE PROGRESSION AND CHEMOTHERAPEUTIC RESISTANCE IN CANINE OSTEOSARCOMA

Osteosarcoma is the most common primary bone malignancy in both humans and dogs. Over 10,000 canine patients develop this highly aggressive cancer annually and many succumb to metastatic disease in less than a year. In recent years, canine osteosarcoma has been increasingly recognized as an excellent model for the disease in humans, especially with regard to the molecular biology of the disease. Thus, research targeted at canine osteosarcoma benefits not only dogs but the field of human oncology as well. Research into the genetic and molecular derangements of osteosarcoma in both species has identified a number of oncogenes and tumor suppressor genes that may contribute to tumorigenesis. Additionally, some mediators of invasion and metastasis have been recognized (e.g. Ezrin, matrix metalloproteinases). Despite this, only a limited number of studies have been performed that examine the molecular genetics of osteosarcoma in the context of patient outcome.

Thus, with the aim of identifying new target genes and pathways that contribute to disease progression and chemoresistance in osteosarcoma, we first performed transcriptomic and genomic analyses of primary tumors from dogs that had experienced

good or poor outcomes following definitive treatment for osteosarcoma. These broad survey experiments yielded a selection of targets for future investigation. To further focus in on the genes that were most deranged from "normal" expression patterns, we compared gene expression patterns from tumors to those of normal bone. This study provided valuable perspective on genes that were identified in the outcome-based experiments, allowing selection of four promising gene targets to pursue. We next set out to validate *in vitro* models of canine osteosarcoma so that mechanistic studies could be pursued. Assays to test species and short tandem repeat identity were adapted to cell lines in use in our facility and presumed osteosarcoma cell lines were verified to be bone-derived via PCR testing of a bone-specific marker. Additionally, four anti-human antibodies were validated for use in canine samples.

Two genes whose expression progressively altered with increased tumor aggressiveness were chosen for further study: insulin-like growth factor 2 mRNA binding protein 1 (IGF2BP1) and n-Myc downstream regulated gene 2 (*NDRG2*). IGF2BP1 has been identified as an oncofetal protein and its mRNA was strongly overexpressed in patients with the worst outcome while it was virtually undetectable in normal bone. We identified one possible mechanism for dysregulation of this gene in OSA and we also discovered that knock down of this gene in a canine osteosarcoma cell line inhibited cell invasion. *NDRG2* has been dubbed a tumor suppressor in a number of different tumor types yet had not been previously investigated in osteosarcoma. We found *NDRG2* mRNA to be underexpressed in all tumors relative to normal bone; patients with poor outcomes had the lowest expression levels. Multiple isoforms of the gene were found to be expressed in canine samples: these were cloned and transfected

into a low-NDRG2-expressing cell line. Exogenous expression of NDRG2 in this *in vitro* system enhanced sensitivity to doxorubicin, one of the drugs most commonly used to treat osteosarcoma. Additionally, three possible mechanisms of dysregulation of this gene were identified.

The studies presented herein progress from fact-finding surveys to in-depth functional examination of two genes that likely contribute to osteosarcoma invasion and chemoresistance. Furthermore, additional genes identified in our survey experiments offer promise for future studies into molecular mechanisms of osteosarcoma metastases and chemotherapeutic resistance. Finally, these studies have laid the groundwork for the development of gene-expression-based prognostic screens for dogs with osteosarcoma.

ACKNOWLEDGEMENTS

There are many people I must acknowledge, as, without their support, this body of work would not have been possible. First and foremost, I want to thank my advisor, Dr. Dawn Duval, for her years of support and her willingness to take a chance on the desperate dual degree student who showed up in her office one spring day in 2007. Her enthusiasm for science and endless data manipulation have always inspired me to keep going. I would also like to thank the current and former members of my graduate committee, Drs. Thamm, Weil, Bouma and Ptitsyn, for their guidance and occasional skepticism throughout this process. I could have not have accomplished this without their help.

Special thanks are due to Dr. Terry Nett. As a founding influence of the dual degree program, he has always been there to support me when I needed it. He sent me to meet my advisor and he "went to bat" for all the students in the program on critical educational issues. Similarly, I would like to thank all the faculty and student members of the dual DVM-PhD program for making this opportunity possible.

I would like to thank all the members of the Duval lab for putting up with my antics: Sara Anglin, Anne Handschy, Brian Kalet, Deanna Dailey, Dorna Khamsi. I would also like to thank all of the researchers in the ACC for their companionship and for sharing their expertise over the years. Barb Rose, Laura Chubb, Luke Wittenburg, Joe Sottnik, Jenette Shoeneman, Ryan Hansen, Brad Charles, Susan Hudacheck, Jared Fowles, Kelvin Kow, Debra Kamstock, Chuck Halsey have all been a huge help.

Much of this work was funded by a grant from the Morris Animal Foundation: they have my heartfelt thanks. Additional funding was provided by the CSU College

Research Council, Infinity Pharmaceuticals, CSU Center for Companion Animal Studies PVM Student Grant Program and the CSU CVMBS Dual Degree Program. Thank you all so much for giving me this opportunity.

Last but not least, I would like to thank my family: Bruce, Deborah and Sam Pfaff and Richard O'Donoghue. Although we are separated by many miles, I've always felt your support. I love you all very much.

TABLE OF CONTENTS

Abstract.....	ii
Acknowledgements.....	v
List of Tables and Figures.....	ix
 Chapter One: Introduction	
Literature Review	
Osteosarcoma in the Dog.....	1
Comparative Oncology: Canine Osteosarcoma as a Model for Human Osteosarcoma.....	4
Molecular Pathogenesis of Osteosarcoma.....	7
Metastasis.....	14
Tools for Identification of Molecular Contributors to Carcinogenesis and Metastasis.....	19
Molecular Mechanisms of Gene Regulation.....	21
Chemoresistance: Mechanisms and Associated Genes.....	25
Project Rationale.....	28
References.....	33
 Chapter Two: Expression profiling in canine osteosarcoma: identification of biomarkers and pathways associated with outcome.	
Synopsis.....	57
Introduction.....	58
Methods.....	61
Results.....	67
Discussion.....	77
Conclusions.....	87
Acknowledgements.....	88
References.....	89
 Chapter Three: Gaining perspective: Gene expression analysis of canine osteosarcoma in relation to normal bone.	
Synopsis.....	95
Introduction.....	96
Methods.....	97
Results & Discussion.....	101
Conclusions.....	108
References.....	110
 Chapter Four: Validation of <i>in vitro</i> models for canine osteosarcoma.	
Synopsis.....	113
Introduction.....	114
Methods.....	116
Results.....	122

Discussion.....	133
Acknowledgements.....	138
References.....	139
Chapter 5: Overexpression of the oncofetal protein IGF2BP1 contributes to an invasive phenotype in canine osteosarcoma.	
Synopsis.....	142
Introduction.....	143
Methods.....	147
Results.....	155
Discussion.....	164
Acknowledgements.....	169
References.....	171
Chapter 6: The putative tumor suppressor gene, NDRG2, contributes to doxorubicin resistance in canine osteosarcoma.	
Synopsis.....	176
Introduction.....	177
Methods.....	179
Results.....	187
Discussion.....	199
Acknowledgements.....	204
References.....	205
Chapter 7: Conclusions	
General Conclusions.....	210
Future Directions.....	215
Appendix A - Pathway maps: GeneGo MetaCore analysis.....	217
Appendix B - Lists of genes obtained from pairwise t-test intersections of three study cohorts.....	220
Appendix C - Chromosomal expression maps: array comparative genomic hybridization versus microarrays for tumor and normal bone.....	239
Appendix D - Chromosomal expression maps: array comparative genomic hybridization versus microarrays for good- and poor-responder tumors.....	279
Appendix E - NDRG2 Sequences: Expression Constructs.....	319

LIST OF TABLES AND FIGURES

Chapter 2

Table 2.1 – Study Population.....	62
Table 2.2 – Primer sequences and amplicon size for selected genes.....	65
Figure 2.1 - Fold change analysis of microarray data.....	69
Figure 2.2 - qRT-PCR validation of genes selected from fold change analysis of microarray data.....	71
Figure 2.3 - Pathway analysis, most significant pathways.....	73
Figure 2.4 - Hedgehog and parathyroid hormone signaling pathways in bone and cartilage development.....	74
Figure 2.5 - qRT-PCR analysis of the Hedgehog pathway.....	75
Table 2.3 – Results of classification modeling.....	76

Chapter 3

Table 3.1 – Signalment, tumor location and treatment information for patients included in the normal bone versus matched tumor studies.....	99
Figure 3.1 – Heat map and principal components analysis of gene expression in canine OSA compared to normal bone.....	102
Figure 3.2 – Venn diagram displaying overlapping features from pairwise comparisons of microarray expression data.....	103
Figure 3.3 – Extracted microarray expression data for previously identified genes of interest.....	104

Chapter 4

Figure 4.1 – Multiplex PCR agarose gel electrophoresis.....	123
Table 4.1 – Observed allele sizes in 29 canine cell lines.....	124
Figure 4.2 – Abbreviated STR profile of two cell lines originally presumed to both be D17.....	126
Table 4.2 – Allele distribution in 29 cell lines as determined by STR analysis.....	127

Figure 4.3 – PEZ 6 locus.....	128
Figure 4.4 - Validation of ADHFE1 expression in canine cell lines.....	130
Figure 4.5 - Validation of SCN1B expression in canine cell lines.....	131
Figure 4.6 - Immunohistochemical staining of canine kidney sections with anti-ADHFE1 antibody.....	132
Figure 4.7 - Immunohistochemical staining of canine kidney, skin and tumor sections with anti-SCN1B antibody.....	134

Chapter 5

Figure 5.1 - Schematic of IGF2BP1 genomic DNA.....	145
Figure 5.2 – Alignment of IGF2BP1 antibody epitope and canine IGF2BP1.....	151
Figure 5.3 - IGF2BP1 expression from microarray and qRT-PCR studies.....	156
Figure 5.4 – Immunohistochemical staining of primary OSA sections for IGF2BP1 and survival curves based on IHC scores.....	158
Figure 5.5 – Expression of IGF2BP1 in canine OSA cell lines.....	159
Figure 5.6 – IGF2BP1 knockdown and subsequent invasion and migration assays in the Abrams cell line.....	161
Figure 5.7 – Array CGH analysis of the chromosomal region surrounding IGF2BP1.....	163
Figure 5.8 – Analysis of IGF2BP1 3' UTR via qRT-PCR.....	165

Chapter 6

Figure 6.1 – Messenger RNA Expression of NDRG2 in primary OSA tumors, cell lines and normal bone.....	188
Figure 6.2 – Protein and isoform analysis of NDRG2 in canine OSA cell lines.....	190
Figure 6.3 – Isoform analysis of NDRG2 mRNA comparing primary canine OSA tumors from good and poor-responder cohorts.....	192
Figure 6.4 – Mechanisms of NDRG2 dysregulation in canine OSA.....	193

Figure 6.5 – NDRG2 mRNA and protein expression in Abrams transfectants.....	195
Figure 6.6 – Resazurin-based viability assays of Abrams-NDRG2 and Abrams-CAT cells following DOX treatment.....	198
Table 6.1 – Doxorubicin sensitivity in transfected Abrams cells.....	199

Chapter 1

Literature Review and Project Rationale

Osteosarcoma in the Dog

Osteosarcoma (OSA) is a primary bone tumor of mesenchymal origin that occurs in canine patients at a rate of roughly eight per 100,000 pet dogs per year in the United States, totaling over 8,000 new cases annually (1). It is the most common primary bone tumor and the most frequent sites affected are the metaphyseal regions of long bones, particularly the front limbs (2-4). Large and giant breed dogs are most often affected by appendicular OSA: mixed breed as well as purebreds are at risk but, some breeds, including Greyhounds and Rottweilers, appear to have an elevated susceptibility (5-8). Age distribution of OSA patients is bimodal with a small peak in young animals (18-24 months) and a larger peak in older dogs (median = 7 years), the youngest patients tend to have the most aggressive disease and concordantly poor survival (3, 7, 9). Axial OSA also occurs in dogs but is less common (~25% of cases) and tends to involve a more varied population: it will not be addressed further (9). Although large body size is the primary OSA risk factor in dogs, other factors, including prior bone fracture, surgical implants, radiation treatment and infarction have been identified as possible contributors to tumorigenesis at the site of such trauma (7, 10-18).

Osteosarcoma patients typically present with lameness and localized swelling of the affected limb; pathologic fractures are relatively common in cases where the tumor has significantly weakened the existing bone matrix (9, 19, 20). Radiographically, OSA appears as a simultaneously osteolytic and osteoblastic lesion, with destruction of normal bone and aberrant growth of tumor "bone," this has been described as having a "sunburst" appearance (20, 21). The radiographic appearance of new periosteal bone formation has been dubbed Codman's triangle and, while not always present in OSA, does occur in some patients (9). Osteosarcoma tumors are histologically characterized by eosinophilic matrix (osteoid) and cells with large nuclei, multiple nucleoli and various stromal components. A wide range of differentiation states are observed. There are many different histotypes of OSA including osteoblastic, chondroblastic, fibroblastic, telangectatic, giant cell, and poorly differentiated: these classifications identify the primary cell type within the tumor but do not appear to affect clinical outcome except in the case of the highly vascular telangectatic OSA, a tumor histotype typically associated with a poor outcome (20-22).

The primary cause of morbidity and mortality in OSA patients is aggressive metastatic disease of the lungs. Less than 10% of dogs present with clinically detectable metastasis ($\geq 1\text{ cm}^3$) at the time of OSA diagnosis (9). It is estimated that upwards of 90% of OSA patients without detectable metastatic disease have micrometastases at presentation and many of these dogs will subsequently develop lung metastases (19, 23). Prior to the addition of systemic chemotherapy to treatment protocols, post amputation survival was generally 3-4 months; this was extended by the addition of adjuvant chemotherapy protocols (9, 24). Thus, treatment failures are primarily failures to treat

distant disease and improved management of distant disease can extend disease-free survival.

Standard of care treatment for OSA involves amputation of the affected limb followed by adjuvant chemotherapy with doxorubicin, a platinum-based drug or a combination of the two aimed at inhibiting distant disease (9, 25-29). More recently, a limb-sparing surgical technique has been developed and is implemented in cases where amputation is not desired or is unfeasible (30, 31). In some cases, radiation therapy is used as a palliative treatment but shows limited benefit as a curative agent (32-36).

Several prognostic factors have been identified in canine OSA. One of the strongest predictors of outcome is the presence of clinically detectable metastases at diagnosis: although pulmonary metastasectomy has been described in a number of canine patients, it is not frequently pursued and does not always confer prolonged survival (9, 37). Time to development of lung metastases and the number of pulmonary metastases developed have also been identified as prognostic factors as have serum alkaline phosphatase levels (ALP) and histological grade (22, 38, 39). Humeral location and large tumor size have been related to a negative outcome (3, 9, 27, 40, 41). Lymph node metastases are notably rare in OSA but their presence has been identified as a negative prognostic indicator (22, 42). Furthermore, microvascular density of the tumor may serve some prognostic function, as tumors with very high microvascular density have demonstrated a shorter time to metastases (43). Finally, recent work indicates that elevated pre-treatment monocyte and lymphocyte counts, albeit still within normal ranges, are associated with shorter disease-free intervals (DFI) (44).

Long term disease-free survival is influenced by treatment protocols as well as other prognostic factors noted above. Amputation alone has demonstrated a median survival time of less than 20 weeks although it can be considered a palliative treatment when owners do not wish to pursue chemotherapy. The vast majority of patients treated with amputation alone are euthanized within a year due to metastatic disease (19). The addition of systemic adjuvant chemotherapy to treatment protocols increases median survival to 10-11 months with some patients surviving disease-free for well over a year (27, 29, 45-50). In dogs that present with clinically detectable metastases, survival time is dramatically shortened (days to weeks) but the addition of chemotherapy and palliative radiation to treatment protocols nonetheless improves survival (51). Limb sparing techniques have introduced an interesting twist to patient survival as it appears that localized infection around the surgical site may actually prolong time to metastasis (52-54). Unfortunately, despite these advances, one-year survival is only 30% (55, 56).

Comparative Oncology: Canine Osteosarcoma as a Model for Human Osteosarcoma

Canine OSA is an exemplary model for the same disease in humans (1, 4, 57, 58). Not only do dogs share an environment with their human companions, the tumor lesions are also virtually identical: they occur in the same locations, present the same histologies, and primarily metastasize to the same organ (59). Many of the above-noted prognostic factors in dogs are also shared by human patients (60). Furthermore, greater than 10 times more canine patients present for OSA annually than human patients (61), dramatically increasing the potential study pool. Unfortunately, survival following

treatment is equivalently poor in human patients with a 5-year survival rate of 60% and only 15% for patients who present with metastatic disease (57).

Perhaps the greatest value of the canine model is that these tumors are spontaneous and not the result of laboratory-induced chromosomal aberrations or gene mutations (57-59, 62). A number of mouse models of OSA exist but these have been induced in controlled experiments and do not represent the genetic diversity in humans or even the relatively inbred canine population (63-66). The somewhat inbred nature of the pet dog population, however, is beneficial in that this limited genetic variance can aid in identifying genetic markers of disease or progression that may otherwise be masked in the more-diverse human population (67, 68). Indeed, canine OSA studies have identified breed-specific genetic factors that may predispose to OSA and/or influence prognosis. For instance, a recent comparison of OSA cytogenetic aberrations between Golden Retrievers and Rottweilers revealed that there was a strong influence of genetic background on resulting tumor karyotypes (68). Additionally, heritability of an OSA-predisposing phenotype in Scottish Deerhounds was determined to have a Mendelian dominant effect (69). Thus, identification of causative factors in this inbred population may help identify previously unknown or cloaked factors in the human disease.

Additional benefits of dogs as a model system include a relatively large body size and similar metabolic rate to humans that allow more-direct translation of treatment protocols between species; also, dogs' faster disease progression allows for shorter study periods to assess clinical outcomes (21). In fact, clinical trials in dogs with OSA have successfully translated into the human population: muramyl tripeptide (MTP) increased

survival time in canine OSA patients and, similarly, increased time to relapse in humans with OSA (70-72)

Treatments between canine and human patients are quite similar with tumor removal and adjuvant chemotherapy as the primary treatment protocols (9, 21, 58). However, human patients tend to receive a wider selection of chemotherapy protocols and also often receive neoadjuvant chemotherapy to de-bulk the tumor prior to surgery (57, 73-75). While this latter strategy is successful as a treatment option, it reduces scientific value of tumor tissue removed at the time of surgery as gene expression signatures are dramatically altered by exposure to these drugs. In this sense, canine tumors that were naïve to chemotherapy at the time of amputation provide an excellent resource for discovery of OSA biomarkers and novel treatment targets that may well translate across species.

The greatest difference between OSA in dogs and humans is that appendicular OSA primarily affects human adolescents whereas the majority of canine patients are middle-aged or older (21, 57, 76). Despite this, faster growing children are most prone to developing the disease and this seems a relevant link to the large-breed tendency toward developing OSA in canines: genetic makeup contributing to large size and fast growth likely predispose to oncogenic transformation in bone in both systems.

Finally, a number of molecular characteristics are shared between canine and human OSA (57). Recent work by Paoloni and colleagues compared gene expression signatures of canine and human OSA and normal tissue samples (77). Hierarchical clustering of these gene expression signatures was unable to differentiate between the two species on the basis of gene expression. Furthermore, they identified several progression-

related genes in canine samples that were verified as prognostic factors in an independent human OSA sample set.

Molecular Pathogenesis of Osteosarcoma

There is no known etiology for OSA in either dogs or humans but a number of molecular contributing factors have been identified in recent years. The most common chromosomal aberration observed in OSA is aneuploidy, however, hallmark translocations like those observed in a number of sarcomas have not been identified in OSA (78). With regard to gene expression signatures, the most common unifying factor in both human and canine OSA is that there is no unifying factor: dysregulation of many genes has been observed but they are not consistent among individuals (21).

Several human disease syndromes predispose patients to developing OSA and mutations in the contributing genes have been studied extensively in canine and non-syndrome-related human OSA. In humans with hereditary retinoblastoma, mutations of the tumor suppressor gene *RB1* lead to childhood retinoblastoma as well as secondary tumors including OSA (79-83). This pathway is also often dysregulated in canine OSA cell lines and human patients without germ-line mutations, indicating that spontaneous mutation of the gene may promote osteosarcomagenesis (84-86). Interestingly, however, in a study of 21 canine primary tumors, altered expression of the *RB1* gene was not observed (87). Whether or not functional RB1 protein confers any survival advantage to OSA patients is unclear as studies have found dissimilar results in different patient populations (84, 86, 88).

Similarly, in Li-Fraumeni syndrome, *TP53* mutations are inherited and predispose patients to a number of tumors, often OSA (89-92). *TP53* is a pro-apoptotic tumor suppressor gene that demonstrates dominant negative behavior when mutated in the DNA-binding domain, effectively inhibiting wild-type TP53 from activating target genes (93). As TP53 is involved in a negative feedback loop governing its own expression, these dominant negative mutations lead to excessive buildup of TP53 protein in the cell; this mechanism is commonly observed in tumors via immunohistochemistry (IHC) (94). Additionally, *TP53* expression can be ablated by a number of large-scale mutations, including rearrangement of intron 1 which has been observed in several human OSA cell lines (95, 96). Beyond Li-Fraumeni syndrome, aberrant *TP53* expression is observed in many canine and human OSA tumors from patients without germ-line mutations, suggesting a possible role for this gene in tumorigenesis and/or progression (85, 87, 97-102). In one study of 24 primary canine OSAs with *TP53* mutations, these mutations correlated significantly with decreased survival time following surgery (103). Furthermore, a study of 167 canine osseous tumors found that, of all subtypes, OSAs expressed more TP53 protein than any others and that TP53 overexpression in OSA correlated with breed predisposition for development of the disease (104). In a number of human OSA studies, however, TP53 expression has not been correlated with clinical outcome (100-102). It is also important to note that *TP53* mutations, like *RBI* mutations, while found in a number of OSA samples, are by no means necessary to induce disease or metastasis (105).

Rothmund-Thomson syndrome (RTS) has also been identified as predisposing to OSA in human patients but only in the subset of patients with mutations in the DNA

helicase RecQ protein-like 4 (*RECQL4*) (106). In a population of 33 RTS patients, 29 *RECQL4* sequence-affecting mutations were observed and eleven of these patients developed OSA (107). In a study addressing the frequency of *RECQL4* mutations in spontaneous non-RTS-related OSAs, however, no mutations in this gene were observed other than a small number of SNPs that were also present in normal tissue (108). Werner syndrome is another cancer predisposition syndrome caused by helicase dysfunction: Werner Syndrome, RecQ helicase-like (*WRN/RECQL2*) is the culprit in this case. A smaller percentage of these patients develop OSA than RTS patients, but OSA is, nonetheless, more prevalent in this group than in the population at large (109, 110). The *WRN* gene shares functionality with the Bloom syndrome, RecQ helicase-like (*BLM/RECQL3*) gene, another gene mutated in the cancer-predisposing Bloom syndrome (BS) (111, 112). As the primary role of these three helicase genes is maintenance of genomic stability, it logically follows that loss of function mutations would lead to genomic instability, increased genomic mutation rates and a higher likelihood of cancer. Additionally, both the *BLM* and *WRN* helicases have been shown to physically interact with *TP53* and support its role in apoptosis (113-115). Thus, disruption in these genes not only encourages genetic mutation but inhibits appropriate cellular response to mutation and DNA breaks. While patients harboring loss-of-function mutations in the *RECQ* genes are prone to developing OSA, spontaneous mutations do not appear to be major contributing factors to osteosarcomagenesis in the general population (61, 78).

In addition to these human mutation syndromes, a number of individual gene mutations have been identified as contributing to osteosarcomagenesis. Many of these genes are involved with the *TP53* or *RB1* pathways in one way or another, suggesting

that dysregulation of these tumor suppressor pathways is an important step in tumorigenesis (78). For example, the *INK4A* locus on human chromosome 9p21 encodes two gene products crucial to regulation of both the TP53 and RB1 pathways. The larger gene product, Cyclin-Dependent Kinase Inhibitor 2A (CDKN2A/p16INK4A), affects RB1 expression via modulation of Cyclin D and is often suppressed in OSA either by locus deletion or other mechanisms (116-118). CDKN2A also suppresses expression of Cyclin-Dependent Kinase 4 (CDK4) in a healthy cell. In cases of OSA where neither the *RB1* gene nor the *CDKN2A* gene are mutated, amplification or over-expression of the *CDK4* gene has been observed, identifying an additional point for dysregulation in this pathway (84, 119). Similarly, in canine OSA cell lines, dysregulation in *CDKN2A* has been observed in cells with low levels of the RB1 protein (85).

An alternate gene product from the *INK4A* locus, p14ARF, stabilizes TP53 by direct binding as well as down-regulation of Mouse Double Minute 2 (MDM2), a protein that promotes degradation of TP53 (120, 121). An inverse correlation between wild type TP53 expression and p14ARF expression has been observed in OSA indicating that downstream targets of the TP53 pathway can be effectively dysregulated by p14ARF loss even when normal TP53 functionality is present (122). Similarly, *MDM2* amplification has been demonstrated in OSA resulting in rapid and inappropriate degradation of the TP53 gene product and dysregulation of downstream targets (123, 124). Interestingly, *MDM2* and *CDK4* localize to Hsa 12q15 and 12q13, respectively; amplification of this entire region is not uncommon in OSA and leads to dysregulation of both TP53 and RB1 pathways via degradation of TP53 and overexpression of a downstream RB1 target (125,

126). Similarly, the *COPS3* gene, overexpression of which results in TP53 degradation, has been identified as being overexpressed in OSA (127).

The v-Myc Myelocytomatosis Viral Oncogene Homolog (*MYC*) and the related neuroblastoma-derived v-Myc Myelocytomatosis Viral Related Oncogene (*MYCN*) have both been identified as oncogenes that can be overexpressed in OSA (100, 128-130). Additionally *MYC* expression has been associated with methotrexate and cisplatin resistance in OSA (131, 132) and mouse models of *MYC* alteration have demonstrated that reduction of *MYC* expression can cause tumor regression (133). A number of other genes that interact with the *MYC* genes have been identified as being dysregulated in OSA. Platelet-Derived Growth Factor (*PDGF-β*), Insulin-Like Growth Factor II mRNA Binding Protein I (*IGF2BP1*) and N-MYC Downstream Regulated Gene 2 (*NDRG2*) are three notable cases. *PDGF* has been shown to activate *MYC* transcription and in at least one OSA cell line, overexpression of this mRNA is coincident with *MYC* overexpression (134). *IGF2BP1* is also known as *CRD-BP* for its role in binding to the coding region determinant portion of *MYC* mRNA and stabilizing the transcript, effectively increasing its translatability (129, 135). *MYC* directly binds to the *NDRG2* promoter and suppresses the transcription of this putative tumor suppressor gene (136). Additionally, genes discussed above in the context of their involvement with TP53 and RB1 such as *p16INK4A*, *p14ARF* and *MDM2* have also been found to modulate *MYC* activity, emphasizing the entwined nature of many of these pathways (137-141).

Several other oncogenes have been identified as being overexpressed in OSA, including FBJ Murine Osteosarcoma Viral Oncogene Homolog (*FOS*) (100, 130), v-erb-b2 Erythroblastic Leukemia Viral Oncogene Homolog 2 (*ERBB2/HER-2*) (142, 143), and

Glioma-Associated Oncogene Family Zinc Finger 1 (*GLI1*) (144, 145). Interestingly, *GLI1* localizes to Hsa 12q13-14, the same region occupied by *CDK4*, *MDM2* and Tetraspanin 31 (*TSPAN31*). *TSPAN31*, also called "sarcoma associated sequence" has been found to be amplified in OSA, often concurrently with other genes in this region (126). Thus, this region may be a hotspot for osteosarcomagenesis with a single chromosomal amplification being able to simultaneously induce *GLI1* expression, suppress *RB1* expression and degrade *TP53* protein. *GLI1* is part of the hedgehog (HH) signaling pathway, a pathway that plays a major role in bone development and dysregulation of which has been implicated in the proliferation of OSA cells (146-148). Ligands for the pathway, Sonic Hedgehog (SHH), Desert Hedgehog (DHH) and Indian Hedgehog (IHH) bind to the Patched receptor (PTCH). Upon binding, Smoothed (SMO) is de-repressed and activates downstream transcription factors *GLI1* and *GLI2*. This cascade carries on to regulate cell-cycle control mechanisms including Cyclins and *MYC* (149). Inhibition of the HH pathway has reduced proliferation in OSA models (150).

As OSA is a tumor of bone, it naturally follows that expression of bone development factors is often abnormal. The role of genes such as Runt Related Transcription Factor 2 (*RUNX2*) and Osterix (*OSX/SP7*) in osteosarcomagenesis has been investigated but is still unclear. *RUNX2* is modulated by *RB1* interaction and exerts transcriptional control over bone-specific genes including Osteocalcin and Alkaline Phosphatase (151, 152). The end results of *RUNX2* overexpression, however, are contradictory: in some cases it mediates apoptosis and prevents transformation (153, 154) whereas, in others, it appears to be pro-proliferative and pro-transformation (155-

158). *OSX* is a downstream target of *RUNX2* and so it is not surprising that the role of this gene has been equally confounding. *OSX* expression inhibited tumor growth and metastasis in one murine OSA model (159) yet enhanced proliferation in a different model (160). Thus, it has been suggested that cellular context may dictate whether *RUNX2* and *OSX* are pro- or anti-tumorigenic (61).

Tumors essentially begin as excessive tissue growth diseases; thus, the expression of growth factors and their receptors has been an attractive line of investigation in OSA. Insulin-Like Growth Factor I (IGF1) was found to be a potent mitogen in the human OSA cell line MG-63 indicating that some tumors may be inhibited by blockade of this pathway (161). This responsiveness is likely due to the frequent overexpression of the IGF1 Receptor (IGF1R) in OSA; numerous antibodies and small-molecule inhibitors have been generated to inactivate this receptor and are in clinical trials (162-166). Similarly, dysregulation in Vascular Endothelial Growth Factor Receptor (VEGFR), Platelet Derived Growth Factor Receptor (PDGFR), Epidermal Growth Factor Receptor (EGFR), Fibroblast Growth Factor Receptor (FGFR2), Met Proto-Oncogene (MET) and their ligands have all been observed in OSA (162, 167-175). Due to the redundancy of many of these growth factors, it has been suggested that the expression of these pathways in OSA represent bystander effects as opposed to bona fide requirements for tumor establishment and progression (78).

In conclusion, TP53 and RB1 pathways as well as growth factor signaling disruptions are, undoubtedly, large contributors to tumor growth and evasion of apoptosis in this system. Genome-wide studies have identified countless additional molecules that may be involved in osteosarcomagenesis that, as yet, have received only limited study.

With regard to patient treatment and survival, however, discovering mechanisms of tumorigenesis in this disease is of less immediate importance than determining how and why these tumors metastasize and developing effective treatments to counter this next stage of OSA progression.

Metastasis

The term *metastasis* describes both the process by which tumor cells become established in a distant organ as well as the resulting lesion. The development of metastasis is, essentially, a bipartite process in which cells from the primary tumor must first escape the tissue of origin then become established in a new and, presumably, hostile tissue. This process is of such great import to cancer that it is considered one of the "hallmarks of cancer" (176, 177). Indeed, as noted previously, failure to control metastatic disease is the primary cause of morbidity and mortality in OSA patients.

As malignant tumors grow, they also invade surrounding tissue, the first step in the metastatic cascade (176, 178). Tumor cells and associated stromal components break down extracellular matrix in neighboring tissue by expressing matrix metalloproteinases (MMPs) and by altering intercellular interactions (179-181). In a number of different tumor types, expression of MMPs has demonstrated prognostic significance: tumors with the highest MMP levels show the most evidence of metastasis (182-184). MMPs have also been identified as contributing to OSA invasion and metastasis: MMP-1, 2 and 9 have all been known to be expressed in these tumors (185, 186). Until recently, it was presumed that a small population of metastatic subclones arose within a tumor then escaped to form metastases. While this is still accepted to a degree, the permissive nature

of the tumor microenvironment has received increasing interest in recent years. Were metastasis due to only a small population of metastatic subclones, the gene expression differences of this group should not be apparent on large scale genomic studies. However, the seminal work of van de Vijver and colleagues, in which they analyzed almost 300 primary breast carcinomas, demonstrated that gene expression signatures differ between patients depending on prognosis and time to metastasis (187). Similarly, in a murine OSA model, gene expression signatures differed between highly metastatic and less aggressive tumor types (188). These studies and others provided strong evidence that more-aggressive tumors have different phenotypes in both tumor cells and stroma compared to their less-aggressive counterparts.

Tumor cells that escape the primary tumor utilize blood or lymphatic vessels to travel to distant sites. Tumors have been described as highly vascular entities, indeed, were they to rely on existing vascular supply, their size would be dramatically limited (189). Thus, tumors utilize a variety of mechanisms to attract or grow new vessels termed *neovasculature*. Some neovasculature is formed by "sprouting" angiogenesis, a process in which an existing blood vessel receives extracellular signals that induce the sprouting off of new vessels. The subsequent coalescing endothelial cells polarize toward the initiating signal, often FGF and/or VEGF, form a lumen, and provide new blood supply to the target region (190). Intussusceptive angiogenesis is a process by which existing vessels are rapidly multiplied: endothelial cells expand to form a pillar inside the lumen which then divides the resulting two vessels from each other (191). This form of angiogenesis has concerned cancer researchers as it is unlikely that anti-angiogenic agents will be effective against this process simply because the endothelial

cells are not dividing (190). Thus, it may serve as a means for tumors to develop resistance to anti-angiogenic drugs.

Endothelial progenitor cells (EPC) are a relatively new topic of study but it has been determined that this population can be recruited from the bone marrow to form vessels *de novo* (190, 192). Angiogenic signaling molecules such as VEGF mobilize these EPCs and direct them to sites of tissue damage, ischemia or growing tumor lesions (193). Furthermore, EPCs may secrete additional angiogenic factors themselves, exponentially amplifying recruitment signals (192). Due to this positive feedback loop, inhibition of EPC recruitment by tumors may be highly beneficial to tumor and metastasis control. *Vessel co-option* is the term used to describe tumor expansion specifically around existing blood vessels (190). In several tumor types, especially those in highly vascular tissue, the initial avascular tumor mass contacts and travels along vessels in lieu of secreting angiogenic factors to develop neovasculature (194, 195). As tumor size increases, it may outstrip the original blood supply and begin to secrete pro-angiogenic factors (196). It has been determined that VEGF is also a player in this process as are angiopoietins, thus, VEGF inhibition could successfully target many types of neovasculogenesis (196, 197).

The process of vasculogenic mimicry was first identified in highly aggressive melanoma cells but has been since noted in many tumor types (190, 198). This phenomenon occurs when tumor cells begin expressing endothelial cell markers and organize into luminal structures that can convey fluids. There is evidence that this occurs in OSA and is mediated by VE-cadherin and VEGF among other factors (199, 200). VE-cadherin is an endothelial-specific cell adhesion molecule whose activation in tumor cells

appears to be necessary for vascular mimicry (201). Additionally, siRNA mediated knockdown of VEGF inhibited vascular mimicry in OSA cells: whether this was due to downstream VE-cadherin signaling or different pathway effects is unclear (199). Tumor cells that take part in this mimicry have undergone a dramatic phenotypic switch from the source tissue and, thus, pose a challenge to researchers seeking to undermine angiogenesis in tumors. The lymphatic route of metastasis and lymphangiogenesis is important in a number of cancers (e.g. breast cancer) but seems to be of less relevance in OSA considering the remarkable rarity of associated lymph node metastases.

Once tumor cells manage to escape the primary tumor and enter the vascular system, they must exit the circulation and take up residence in a new tissue to form a metastasis. Not all tumors form macroscopic metastases and some metastases do not become macroscopic until after the primary tumor is excised (202). In OSA, however, up to 15% of patients present with macrometastases at the time of diagnosis indicating that primary tumors don't necessarily suppress metastasis growth while *in situ* as has been observed in other cancer types (202). Tumor metastases generally demonstrate a preference for which distant tissue they will arise in (203). It has been postulated that some tissues or niches in a given tissue provide an accommodating environment and metastases will undergo fewer selection pressures should the initiating cells terminate their migration there (204). This "seed and soil" hypothesis has been argued extensively and is often invoked to explain why metastases occur in regions that are not the first major capillary bed encountered by circulating tumor cells (176, 205). However, what is currently unclear is whether cells in the primary tumor evolve mechanisms that will support colonization of distant sites or if selection pressures in those distance sites induce

changes in metastatic cells when they arrive. It is likely a combination of both scenarios that leads to only a small proportion of circulating tumor cells surviving the initial encounter with foreign tissue then, over time, adapting to that tissue (176).

A number of large-scale genomic studies comparing gene expression in metastases to primary tumors have been performed and some have identified genes that play a role in establishing metastases at distant sites. For instance, the cytoskeletal linker protein Ezrin promotes establishment of metastasis in OSA by conferring a survival advantage on tumor cells that express it when they reach distant sites. Suppression of Ezrin expression dramatically reduced survival of tumor cells in non-osteoid tissues (206). Similarly, β 4-Integrin is upregulated in highly metastatic OSA cells and interacts with Ezrin, filling a pro-metastatic role (207). Additionally, the NOTCH signaling pathway and associated microRNAs have been linked with OSA metastasis success in distant tissues (208). Conversely, Fas expression has been inversely correlated to metastatic potential of OSA cells (209). Surface expression of Fas on OSA cells that have entered lung tissue leads to apoptosis induction; thus, Fas-negative cells receive positive selective pressures in the lungs and the resulting lesions express significantly less Fas than primary tumors. This phenomenon has been observed in human OSA, canine OSA and mouse models of the disease (210-213). For many targets identified by new large genomic studies, the stage of metastasis that is promoted by a given target is not immediately apparent. Thus, at this time, elucidating the precise roles of differentially regulated metastatic genes is crucial to further understand the process and devise treatments.

Tools for Identification of Molecular Contributors to Carcinogenesis and Metastasis

Computer processing power and associated genome/transcriptome analysis technologies have grown by leaps and bounds since the Human Genome Project was first initiated in 1989 and since the human genome was published in 2001 (214). Consequently, researchers are now able to generate and analyze vast data sets in order to identify dysregulated genes and pathways in cancer.

Microarray technology was adapted from Southern blotting as a means to probe many oligonucleotide sequences on a solid scaffold (215). It has been applied to a number of different uses, one of which probes mRNA sequences. Since the early years of development, millions of expressed sequence tags (ESTs) for a variety of species have been published; thus, current expression arrays probe in excess of 40,000 gene tags in a given species (216). These expression arrays allow broad assessment of global expression patterns in tumors and serve as excellent survey tools for discovering new markers of disease. Similarly, this technology has also been applied to expression analysis of microRNAs (217). Microarrays have also been used for comparative genomic hybridization (CGH), a technique that probes copy number of loci in genomic DNA (218). This technology is especially useful in cancer profiling to assess amplification and deletion status of chromosomal regions. Fluorescence *in situ* hybridization (FISH) can serve the same purpose but requires the user to focus on specific target regions of chromosomes as opposed to surveying the entire genome (218). The latest development in genome and transcriptome analysis is deep sequencing. This technology provides not only sequence data but also copy number analysis for gDNA, mRNA, microRNA and/or

any other oligonucleotide of interest (219). This data-intensive methodology is already challenging microarray dominance of the field and will likely replace microarray technology when costs become similar (220).

With these data-intensive technologies, data management and interpretation becomes challenging. Expression microarrays are pre-processed with a variety of algorithms prior to analysis to normalize the data. These algorithms differ from each other in the linearity of variance relative to expression as well as absolute expression values (221). Resulting pre-processed data can differ greatly across algorithms (222). Furthermore, microarray chips can possess physical flaws that are not immediately apparent yet compromise portions of data (223). Thus, it is standard practice to validate microarray expression of individual biomarkers with reverse transcription quantitative polymerase chain reaction (qRT-PCR) (224). Deep sequencing removes some of these unknown variables by generating such a huge volume of data that small errors are outweighed. Beyond identification of individual factors related to disease and progression, microarray or deep sequencing data can be processed with gene association algorithms (e.g. Ingenuity, GeneGo) to identify dysregulated pathways (223). This pathway analysis supersedes error caused by chip flaws or algorithm differences as pathways must possess multiple dysregulated genes to cross significance thresholds.

High throughput proteome analyses have also been devised, for instance matrix-assisted laser desorption ionization-time-of-flight-mass spectrometry (MALDI-TOF-MS) following 2-dimensional gel electrophoresis has been used to identify differentially regulated proteins in canine mammary carcinoma (225). This technology can also be used to analyze post translational modifications of proteins including phosphorylation,

ubiquitination and acetylation among others (226). Beyond the new high-throughput methodologies, older standard molecular biology techniques are still very much in use, especially for researchers seeking to go beyond identification of gene dysregulation and investigate the functional roles of gene products.

Molecular Mechanisms of Gene Regulation

Following identification of dysregulated genes or pathways in cancer, researchers must determine the mechanism underlying this dysregulation for effective therapeutic targeting of the gene products. Genes and their mRNA and protein products are regulated at many levels; this complexity adds to the difficulty of devising treatments but also provides the opportunity to design more-targeted therapies with potentially fewer side effects.

Chromosomal aberrations are a frequent cause of gene dysregulation in many different types of cancer. This category includes locus amplification and deletion as well as translocations. In locus amplification, a region of a chromosome is preferentially copied excessively; this mechanism has been observed to cause amplification of the *ERBB2* and *MYCN* genes in breast cancer and neuroblastoma, respectively (227, 228). Locus deletion occurs when regions of chromosomes are lost due to breakage or failed crossover events. If these regions contain tumor suppressor genes, the result can be malignant transformation. One such example is the *CDKN2A* region: it is frequently homozygously deleted in both OSA and the related Ewing sarcoma (117, 229, 230). Translocations occur when a piece of chromosome is traded between two non-homologous chromosomes resulting in fusion genes. This often puts an oncogene under

the translational control of a highly active, unrelated promoter (e.g *MYC-Ig* translocation in Burkitt's lymphoma and *bcr-abl* in leukemias) (94). This has been observed in a number of tumor types but is not a typical cause of OSA.

In order for transcription of DNA to proceed at an optimal rate, transcription factors must assemble on the promoter regions of genes. Transcription factor binding site mutations as well as mutations in the transcription factors themselves can cause a gene to be silenced or constitutively activated. Silencing of a tumor suppressor gene via promoter mutations can have devastating effects. For example, at least two germ line mutations in the *RBI* promoter have been identified that inhibit binding of transcription factors and effectively silence the gene; these mutations were identified in retinoblastoma familial clusters (231). Similarly, RB1 binds to the *MYC* oncogene promoter and suppresses transcription. Mutation in the RB1 binding domain, the *MYC* promoter binding site, or overall suppression of RB1 protein can lead to overexpression of the oncogene product (232). The tumor suppressor TP53 forms homodimers and homotetramers and acts as a transcriptional transactivator (94, 233). Mutation in the DNA binding domain of even one allele of this gene has a dominant negative effect because much of the wild type protein will be dimerized with mutant protein. This results in the failure of TP53 to transactivate targets involved in apoptosis and subsequent apoptotic escape by mutant cells (233).

Aberrant control of the epigenetic complement of genes is observed in many different tumor types and leads to dysregulation of involved genes without the need for mutations (234). Methylation of CpG islands, especially in the promoter region of genes, is a normal mechanism of cellular control of transcription: high levels of methylation

effectively silence nearby genes. Hyper- and hypo-methylation of genes has been observed in a number of different tumor types and is directly related to repression of tumor suppressor genes and release of oncogene or mitogen expression. For instance, the Insulin-Like Growth Factor II (*IGF2*) locus is imprinted in normal cells - one copy of the gene is naturally silenced by methylation. In OSA, however, it has been observed that the *IGF2* locus can undergo loss of imprinting, releasing the second allele from suppression and initiating expression of this mitogen from both alleles (235). On the opposite end of the spectrum, the gene Wnt Inhibitory Factor 1 (*WIF1*) is often downregulated in OSA by hypermethylation; this blockade releases downstream targets promoting tumorigenesis and metastasis (236). Similar gene effects can be caused by histone acetylation or lack thereof. Acetylation of histones by histone acetyltransferases (HATs) opens up chromatin structure to make DNA more accessible to transcription machinery and transcription factors. Histone Deacetylases (HDACs) perform the opposite function, removing acetyl groups and rendering DNA less accessible and thereby less transcribed (237). Several drugs targeting HDACs have been applied to anti-cancer treatments with the intent of inhibiting deacetylation of tumor suppressor type genes. One such drug, valproic acid, has been found to sensitize both human and canine OSA cells to doxorubicin chemotherapy indicating that a gene or genes that promote cell death in response to doxorubicin are suppressed by deacetylation of regional histones (238).

This discussion, thus far, has focused on DNA, however, a number of post-transcriptional and post-translational disruptions also contribute to tumorigenesis and progression. The relatively new field of microRNA study has yielded much insight into

the post-transcriptional control of mRNA transcripts (239, 240). MicroRNAs are small, non-coding RNA sequences that can act as tumor suppressors or oncogenes depending on which transcripts they target. In these targets, they can effect translational repression and mRNA degradation, effectively limiting the amount of protein generated from a given transcript (241). Expression of microRNAs is partially controlled by epigenetic factors which adds an additional layer of complexity to any strategy aimed at targeting them (242). In OSA, a number of microRNA-transcript interactions have been identified that either promote or inhibit tumor growth. For instance, in U2OS cells, microRNA-31 was able to inhibit proliferation and promote apoptosis in the face of a defective TP53 pathway (243). Conversely the "oncomiR" microRNA-21 is overexpressed in OSA tissues and cell lines; knockdown of this microRNA decreases cell invasion and migration (244). These microRNAs may be under- or overexpressed by any of the mechanisms previously discussed for protein-coding genes. Additionally, cancer cells can evade microRNA regulation of transcripts by removing microRNA response elements frequently found in the 3' untranslated region (UTR) . Many genes possess a constitutive UTR that is present on all transcripts and a longer UTR that is only present if the first poly-adenylation signal in the gene is not used. Recent studies have found that cancer cells tend to have more constitutive UTRs relative to long UTRs; this effectively removes microRNA response elements from the RNAs and limits control over translation (245).

Post-translational protein modification as well as altered control of protein half-life can also contribute to disruptions in cellular behavior. One such disruption was alluded to previously with regard to MDM2 downregulation of TP53 protein. MDM2 is

a ubiquitin E3 ligase which ubiquitylates TP53 protein, targeting it for degradation, and, thus, greatly decreasing its half-life (246). MMPs are also targeted by post-translational mechanisms and their overexpression that contributes to invasion is partially due to failures in post-translational balance (247). Additionally, survey experiments of OSA have determined that many proteins are excessively phosphorylated in tumor cells suggesting hyperactivity of kinases (248). One such highly phosphorylated protein is RB1: in a resting cell, it exists in its least phosphorylated form but when cells transition to rapid division, it is highly phosphorylated, thus, inappropriate phosphorylation of RB1 may drive proliferation (249). In conclusion, genes can be dysregulated at the DNA, RNA and protein levels; determining the means of dysregulation is an important step in designing targeted therapies that can allow proper cell-control functions to reassert themselves in tumor cells.

Chemoresistance: Mechanisms and Associated Genes

Gene dysfunction not only drives tumorigenesis and progression but also provides the means for cancer cells to resist chemotherapy. Treating a patient with chemotherapeutic regimens exerts strong selective pressure on tumor cells: those that have activated genes that reduce their susceptibility to drugs will survive treatment and continue proliferating while those that have not will die. Chemoresistance comes in many forms, from molecular pumps that remove drugs from cells to impaired DNA damage response mechanisms that allow damaged cells to continue dividing. As metastatic disease following systemic chemotherapy is the primary cause of negative

outcomes in OSA, it is important to identify chemoresistance mechanisms so that drugs can be designed to subvert these mechanisms.

Some mechanisms of chemoresistance are likely in place in tumor cells long before they ever encounter therapeutic agents. For instance, evasion of apoptosis is a "hallmark of cancer" and derangement in pathways that allow this also contributes to chemoresistance (250). The TP53 pathway is one such apoptotic mechanism and LOH of TP53 and related genes has been associated with chemoresistance in OSA (251, 252). Similarly, Parathyroid Hormone Related Protein (PTHrP) has been shown to inhibit apoptosis in OSA cells by blocking the TP53 pathway as well as mitochondrial apoptosis pathways (253). Finally, dysregulation of microRNAs that target apoptotic pathway members has been identified as a mechanism of OSA chemoresistance in several studies (254, 255).

Decreased membrane permeability to drugs has also been implicated in OSA chemoresistance as one study found significantly less drug accumulation in resistant murine cell lines (256). This phenomenon may also be attributable to cellular mechanisms that remove drugs from cells such as ABC transporters that confer multi-drug resistance (257). Chemoresistance in OSA has been strongly correlated with expression of these transporters and inhibition of these genes has been shown to increase drug sensitivity (257, 258). In addition to removing drugs, tumor cells can limit the effects of drugs by altering regulation of genes that detoxify them and/or suppress the accumulation of reactive oxygen species (ROS). One such gene, Glutathione S-Transferase P1 (*GSTP1*), not only detoxifies drugs but also modulates the expression of protein kinases that have been implicated in cell survival following stress (259, 260).

Overexpression of this gene in OSA has been correlated with chemoresistance and knockdown in experimental models has increased sensitivity to both cisplatin and doxorubicin (259).

Several microarray studies comparing gene expression signatures from chemoresistant OSA to chemosensitive OSA have been undertaken in human, canine and mouse models (261-266). Most of these studies, however, are comparing good-responder patients to poor-responder patients and, while this inevitably includes chemoresistance as a factor, these expression profiles may also include initial tumor aggressiveness that is unrelated to chemoresistance. Thus, it is important to follow up survey studies with work examining the genes identified and defining their roles in OSA. Bruheim and colleagues compared gene expression signatures of OSA xenografts based upon their resistance to different chemotherapeutic regimens and found a number of genes to be differentially regulated between ifosfamide, doxorubicin and cisplatin treatments (261). Of all the survey experiments mentioned here, this study goes furthest toward identifying chemoresistance genes that are not necessarily related to tumor aggressiveness. HDAC activity likely leads to suppression of genes that confer chemosensitivity to doxorubicin as both human and canine OSA cell lines have been shown to have increased sensitivity when pre-treated with the HDACi valproic acid (238). Follow-up studies by the same group have used microarrays to identify which pathways are altered by VPA, increasing the body of knowledge regarding gene contributions to chemoresistance (267).

Significant progress has been made in identifying genes and pathways that contribute to chemoresistance in OSA but more contributors are identified with each new related publication. Mastering the mechanisms that promote chemoresistance and

metastasis in this disease and, hence, devising new therapies, can lead to great improvements in patient survival.

Project Rationale

Osteosarcoma continues to defy medical treatments and, even with state-of-the-art therapies, causes a high mortality rate in both dogs and humans that develop this cancer. At the initiation of this research, there had been several reports of microarray studies of gene expression in human OSA but none in dogs despite the much higher incidence rate in this species (262-264). Considering the many similarities between dogs and their human companions, we set out to explore gene expression in this model with the aims of identifying genes that may provide prognostic information for patients of both species and defining new gene targets for drug development. Thus, we first hypothesized that primary tumor gene expression signatures would vary based upon patient outcome. This hypothesis is explored in **Chapter 2 (Expression profiling in canine osteosarcoma: identification of biomarkers and pathways associated with outcome)** where we performed microarray analysis of gene expression in two cohorts of dogs: those that responded well to definitive treatment and those that responded poorly. These two cohorts were defined on the basis of disease free interval (DFI) and were straddled around the median DFI of 200 days. Fold change and pathway analyses were used to identify genes and pathways that were different between the two cohorts. Additionally, quantitative RT-PCR was performed on select microarray-identified genes to validate the microarray data and to generate expression-based classification models. These models

identified several genes that were predictive of outcome in this population and may be useful for developing prognostic profiles.

Having identified some promising targets in Chapter 2, we next wanted to examine gene expression and copy number aberrations in the context of normal tissues. As OSA is typically classified as karyotypically chaotic, we hypothesized that copy number alterations (CNAs) would be associated with dysregulation of some genes important in tumorigenesis and progression. Additionally, we hypothesized that tumor gene expression profiles would differ from normal bone gene expression profiles and these differences would provide context for the biomarker identification begun in Chapter 2.

Chapter 3 (Gaining perspective: Gene expression analysis of canine osteosarcoma in relation to normal bone) explores these hypotheses with expression microarrays and array comparative genomic hybridization (aCGH). We first developed a methodology for obtaining high-quality RNA from normal bone samples that were obtained from amputees. Next, expression microarrays were performed on these samples and resulting expression profiles were compared to tumor expression profiles from Chapter 2. Over two thousand genes were dysregulated between normal bone and all primary tumors, identifying a vast number of tumor-specific genes for future study. Additionally, only a subset of biomarkers identified in Chapter 2 were significantly dysregulated from normal bone; this allowed us to narrow our pool of genes for prognostic use. Array CGH analysis emphasized the previously-reported chaotic nature of OSA karyotypes and identified CNAs that correlated to mRNA expression for several genes including *MYC* and *PTEN*.

Prior to moving forward with functional investigations of specific genes in *in vitro* models, we first wanted to validate these models for species identity, uniqueness and tissue of origin. Cell line contamination has been acknowledged for decades but only recently have funding agencies and publication groups begun requiring cell line validation (268, 269). Additionally, many tools for molecular biology studies are not yet available for canine samples so we found it necessary to validate several anti-human antibodies for use in dog tissues and cell lines. As it has been estimated that 18% to 36% of all cell lines are contaminated (270), we hypothesized that some proportion of cell lines in our facility would be contaminated. Thus, in **Chapter 4 (Validation of *in vitro* models for canine osteosarcoma)**, we adapted a species-specific PCR to test cell lines for species identity and applied a commercially available short tandem repeat (STR) genotyping kit to canine cell lines to determine if they were derived from different individuals. Both contamination and genetic drift were detected in these studies, emphasizing the need for good cell culture practices. Additionally, we performed quantitative RT-PCR on presumed OSA derived cell lines to evaluate expression of the OSA marker *RUNX2*. Furthermore, we successfully validated anti-human antibodies for use in future canine studies.

Having verified that the seven available canine OSA cell lines were, indeed, canine, OSA and derived from different individuals, we next pursued functional studies of two genes identified in Chapters 2 and 3: *IGF2BP1* and *NDRG2*. The first, *IGF2BP1*, has been identified as an oncofetal gene in several tumor systems and was overexpressed in poor responder tumors relative to good responder tumors. It was also overexpressed in all tumors relative to normal bone, suggesting a stepwise upregulation of this gene

with increasing tumor aggressiveness. Thus, we hypothesized that IGF2BP1 expression would be increased in tumors relative to paired normal bone samples and that inhibition of this transcript in *in vitro* systems would alter indices of tumor aggressiveness.

Chapter 5 (Overexpression of the oncofetal protein IGF2BP1 contributes to an invasive phenotype in canine osteosarcoma) explores mRNA and protein expression of IGF2BP1 via qRT-PCR, western blot and immunohistochemistry (IHC) in primary tumors, normal bone and canine OSA cell lines as well as the outcome of expression modification *in vitro*. Findings indicate that only a subset of primary tumors overexpress IGF2BP1 and that IHC staining of primary tumor tissue does not correlate with outcome. However, *in vitro*, siRNA mediated knockdown of IGF2BP1 transcript reduced invasion in OSA cells. Additionally, no CNAs were found to be associated with altered gene expression for *IGF2BP1* but 3' untranslated region shortening correlated with outcome in good and poor responder cohort samples, identifying one method by which this gene may escape regulation in OSA.

NDRG2 was identified in Chapters 2 and 3 as a gene whose expression was suppressed in a progressive fashion with highest expression in normal bone and least expression in poor-responder primary tumors. Very little is known about the structure and function of the protein product(s) of this gene but it has been identified as a putative tumor suppressor in several cancer types. Thus, we set out to explore the expression profile of this gene in cell lines as well as tumor and tissue samples and hypothesized that suppression of this gene in OSA contributes to tumor aggressiveness. **Chapter 6 (The putative tumor suppressor gene, *NDRG2*, contributes to doxorubicin resistance in canine osteosarcoma)** explores this hypothesis via analyzing mRNA and protein

expression of NDRG2 in tissues and cell lines as well as determining the functional outcome of restoring expression of this gene in an *in vitro* model. We identified two expressed isoforms of NDRG2 in canine samples and, although isoform expression did not correlate with outcome, exogenous expression of these isoforms in the *in vitro* model altered cellular chemoresistance. Additionally we determined that, in this system, NDRG2 expression positively correlates with bone morphogenetic protein 4 (BMP4) expression in cells expressing exogenous transcript. Seeking to determine the means of NDRG2 (dys)regulation in OSA, we analyzed MYC transcript expression, CNAs and cell response to the demethylating agent 5-azacytidine. Thus, we determined that NDRG2 regulation is multifactorial and may be determined by a combination of MYC-based suppression, copy number loss and hypermethylation.

The primary overarching goal of this dissertation was to identify new gene targets in OSA that contribute to disease progression and/or chemoresistance. To reach this goal, we utilized an inverse pyramid methodology, starting with broad whole-genome and transcriptome studies. Results from these studies were exhaustively analyzed to identify a smaller pool of genes for further study. Characterization and functional analyses of two of these genes were then pursued to better define their roles in OSA, potentially laying the groundwork for development of targeted therapies in the future.

References

1. Vail DM, MacEwen EG. Spontaneously occurring tumors of companion animals as models for human cancer. *Cancer Investigation* 2000;18(8):781-92.
2. Nielsen SW. Comparative pathology of bone tumors in animals, with particular emphasis on the dog. *Recent Results in Cancer Research* 1976;54:3-16.
3. Misdorp W, Hart AA. Some prognostic and epidemiological factors in canine osteosarcoma. *Journal of the National Cancer Institute* 1979;62:537-45.
4. MacEwen EG. Spontaneous tumors in dogs and cats: models for the study of cancer biology and treatment. *Cancer and Metastasis Reviews* 1990;9(2):125-36.
5. Ru G, Terracini B, Glickman LT. Host related risk factors for canine osteosarcoma. *The Veterinary Journal* 1998;156(1):31-9.
6. Rosenberger JA, Pablo NV, Crawford PC. Prevalence of and intrinsic risk factors for appendicular osteosarcoma in dogs: 179 cases (1996-2005). *Journal of the American Veterinary Medical Association* 2007;231(7):1076-80.
7. Chun R, de Lorimier L-P. Update on the biology and management of canine osteosarcoma. *Veterinary Clinics of North America: Small Animal Practice* 2003;33(3):491-516.
8. Urfer SR, Gaillard C, Steiger A. Lifespan and disease predispositions in the Irish Wolfhound: A review. *Veterinary Quarterly* 2007;29(3):102-11.
9. Dernell WS, Ehrhart NP, Straw RC, Vail DM. Tumors of the skeletal system. In: Withrow SJ, Vail DM, editors. *Withrow and MacEwen's Small Animal Clinical Oncology*. 4th ed. St. Louis: Saunders Elsevier; 2007. p. 540-67.
10. Arthur JJ, Kleiter MM, Thrall DE, Pruitt AF. Characterization of normal tissue complications in 51 dogs undergoing definitive pelvic region irradiation. *Veterinary Radiology & Ultrasound* 2008;49(1):85-9.
11. Schneider U, Lomax A, Hauser B, Kaser-Hotz B. Is the risk for secondary cancers after proton therapy enhanced distal to the Planning Target Volume? A two-case report with possible explanations. *Radiation and Environmental Biophysics* 2006;45(1):39-43.
12. McEntee MC, Page RL, Théon A, Erb HN, Thrall DE. Malignant tumor formation in dogs previously irradiated for acanthomatous epulis. *Veterinary Radiology & Ultrasound* 2004;45(4):357-61.

13. Barnes M, Duray P, Deluca A, Anderson W, Sindelar W, Kinsella T. Tumor induction following intraoperative radiotherapy: Late results of the national cancer institute canine trials. *International Journal of Radiation Oncology, Biology, Physics* 1990;19(3):651-60.
14. Gillette SM, Gillette EL, Powers BE, Withrow SJ. Radiation-induced osteosarcoma in dogs after external beam or intraoperative radiation therapy. *Cancer Research* 1990;50(1):54-7.
15. Sebestyen P, Marcellin-Little DJ, Deyoung BA. Femoral medullary infarction secondary to canine total hip arthroplasty. *Veterinary Surgery* 2000;29(3):227-36.
16. Marcellin-Little DJ, DeYoung DJ, Thrall DE, Merrill CL. Osteosarcoma at the site of bone infarction associated with total hip arthroplasty in a dog. *Veterinary Surgery* 1999;28(1):54-60.
17. Bennett D, Campbell JR, Brown P. Osteosarcoma associated with healed fractures. *Journal of Small Animal Practice* 1979;20(1):13-8.
18. Vasseur PB, Stevenson S. Osteosarcoma at the site of a cortical bone allograft in a dog. *Veterinary Surgery* 1987;16(1):70-4.
19. Endicott M. Principles of treatment for osteosarcoma. *Clinical Techniques in Small Animal Practice* 2003;18(2):110-4.
20. Bhandal J, Boston SE. Pathologic fracture in dogs with suspected or confirmed osteosarcoma. *Veterinary Surgery* 2011;40(4):423-30.
21. Gorlick R, Khanna C. Osteosarcoma. *Journal of Bone and Mineral Research* 2010;25(4):683-91.
22. Kirpensteijn J, Kik M, Rutteman GR, Teske E. Prognostic significance of a new histologic grading system for canine osteosarcoma. *Veterinary Pathology* 2002;39(2):240-6.
23. Berg J, Gebhardt MC, Rand WM. Effect of timing of postoperative chemotherapy on survival of dogs with osteosarcoma. *Cancer* 1997;79(7):1343-50.
24. MacEwen EG, Kurzman ID. Canine osteosarcoma: amputation and chemoimmunotherapy. *Veterinary Clinics of North America: Small Animal Practice* 1996;26(1):123-33.
25. Shapiro W, Fossum T, Kitchell B, Couto C, Theilen G. Use of cisplatin for treatment of appendicular osteosarcoma in dogs. *JAVMA* 1988;192(4):507-11.

26. Berg J, Weinstein MJ, Springfield DS, Rand WM. Results of surgery and doxorubicin chemotherapy in dogs with osteosarcoma. *Journal of the American Veterinary Medical Association* 1995;206(10):1555-60.
27. Bergman PJ, MacEwen EG, Kurzman ID, Henry CJ, Hammer AS, Knapp DW, et al. Amputation and carboplatin for treatment of dogs with osteosarcoma: 48 cases (1991 to 1993). *Journal of Veterinary Internal Medicine* 1996;10(2):76-81.
28. Mauldin GN, Matus RE, Withrow SJ, Patnaik AK. Canine osteosarcoma: treatment by amputation versus amputation and adjuvant chemotherapy using doxorubicin and cisplatin. *Journal of Veterinary Internal Medicine* 1988;2(4):177-80.
29. Kent MS, Strom A, London CA, Seguin B. Alternating carboplatin and doxorubicin as adjunctive chemotherapy to amputation or limb-sparing surgery in the treatment of appendicular osteosarcoma in dogs. *Journal of Veterinary Internal Medicine* 2004;18(4):540-4.
30. LaRue SM, Withrow SJ, Powers BE, Wrigley RH, Gillette EL, Schwartz PD, et al. Limb-sparing treatment for osteosarcoma in dogs. *Journal of the American Veterinary Medical Association* 1989;195(12):1734-44.
31. Straw RC, Withrow SJ, Powers BE. Management of canine appendicular osteosarcoma. *Veterinary Clinics of North America: Small Animal Practice* 1990;20(4):1141-61.
32. McEntee MC. Radiation therapy in the management of bone tumors. *Veterinary Clinics of North America: Small Animal Practice* 1997;27(1):131-8.
33. Green EM, Adams WM, Forrest LJ. Four fraction palliative radiotherapy for osteosarcoma in 24 dogs. *Journal of the American Animal Hospital Association* 2002;38(5):445-51.
34. Ramirez O, Dodge RK, Page RL, Price GS, Hauck ML, Ladue TA, et al. Palliative radiotherapy of appendicular osteosarcoma in 95 dogs. *Veterinary Radiology & Ultrasound* 1999;40(5):517-22.
35. Bateman KE, Catton PA, Pennock PW, Kruth SA. 0-7-21 radiation therapy for the palliation of advanced cancer in dogs. *Journal of Veterinary Internal Medicine* 1994;8(6):394-9.
36. Heidner GL, Page RL, McEntee MC, Dodge RK, Thrall DE. Treatment of canine appendicular osteosarcoma using cobalt 60 radiation and intraarterial cisplatin. *Journal of Veterinary Internal Medicine* 1991;5(6):313-6.

37. O'Brien M, Straw R, Withrow S, Powers B, Jameson V, Lafferty M, et al. Resection of pulmonary metastases in canine osteosarcoma: 36 cases (1983-1992). *Veterinary Surgery* 1993;22(2):105-9.
38. Ehrhart N, Dernell W, Hoffmann W, Weigel R, Powers B, Withrow S. Prognostic importance of alkaline phosphatase activity in serum from dogs with appendicular osteosarcoma: 75 cases (1990-1996). *Journal of the American Veterinary Medical Association* 1998;213(7):1002-6.
39. Garzotto CK, Berg J, Hoffmann WE, Rand WM. Prognostic significance of serum alkaline phosphatase activity in canine appendicular osteosarcoma. *Journal of Veterinary Internal Medicine* 2000;14(6):587-92.
40. Kuntz CA, Asselin TL, Dernell WS, Powers BE, Straw RC, Withrow SJ. Limb salvage surgery for osteosarcoma of the proximal humerus: outcome in 17 dogs. *Veterinary Surgery* 1998;27(5):417-22.
41. Forrest LJ, Dodge RK, Page RL, Heidner GL, McEntee MC, Novotney CA, et al. Relationship between quantitative tumor scintigraphy and time to metastasis in dogs with osteosarcoma. *The Journal of Nuclear Medicine* 1992;33(8):1542-7.
42. Hillers K, Dernell W, Lafferty M, Withrow S, Lana S. Incidence and prognostic importance of lymph node metastases in dogs with appendicular osteosarcoma: 228 cases (1986-2003). *Journal of the American Veterinary Medical Association* 2005;226(8):1364-7.
43. Coomber BL, Denton J, Sylvestre A, Kruth S. Blood vessel density in canine osteosarcoma. *Canadian Journal of Veterinary Research* 1998;62(3):199-204.
44. Sottnik JL, Rao S, Lafferty MH, Thamm DH, Morley PS, Withrow SJ, et al. Association of blood monocyte and lymphocyte count and disease-free interval in dogs with osteosarcoma. *Journal of Veterinary Internal Medicine* 2010;24(6):1439-44.
45. Bailey D, Erb H, Williams L, Ruslander D, Hauck M. Carboplatin and doxorubicin combination chemotherapy for the treatment of appendicular osteosarcoma in the dog. *Journal of Veterinary Internal Medicine* 2003;17(2):199-205.
46. Saam DE, Liptak JM, Stalker MJ, Chun R. Predictors of outcome in dogs treated with adjuvant carboplatin for appendicular osteosarcoma: 65 cases (1996-2006). *Journal of the American Veterinary Medical Association* 2011;238(2):195-206.
47. McMahon M, Mathie T, Stingle N, Romansik E, Vail D, London C. Adjuvant carboplatin and gemcitabine combination chemotherapy postamputation in canine

- appendicular osteosarcoma. *Journal of Veterinary Internal Medicine* 2011;25(3):511-7.
48. Phillips B, Powers BE, Dernell WS, Straw RC, Khanna C, Hogge GS, et al. Use of single-agent carboplatin as adjuvant or neoadjuvant therapy in conjunction with amputation for appendicular osteosarcoma in dogs. *Journal of the American Animal Hospital Association* 2009;45(1):33-8.
 49. Bacon NJ, Ehrhart NP, Dernell WS, Lafferty M, Withrow SJ. Use of alternating administration of carboplatin and doxorubicin in dogs with microscopic metastases after amputation for appendicular osteosarcoma: 50 cases (1999–2006). *JAVMA* 2008;232(10):1504-10.
 50. Chun R, Kurzman ID, Couto CG, Klausner J, Henry C, MacEwen EG. Cisplatin and doxorubicin combination chemotherapy for the treatment of canine osteosarcoma: a pilot study. *Journal of Veterinary Internal Medicine* 2000;14(5):495-8.
 51. Boston SE, Ehrhart NP, Dernell WS, Lafferty M, Withrow SJ. Evaluation of survival time in dogs with stage III osteosarcoma that undergo treatment: 90 cases (1985-2004). *Journal of the American Veterinary Medical Association* 2006;228(12):1905-8.
 52. Jeys L, Grimer R, Carter S, Tillman R, Abudu A. Post operative infection and increased survival in osteosarcoma patients: are they associated? *Annals of Surgical Oncology* 2007;14(10):2887-95.
 53. Sottnik J, U'Ren L, Thamm D, Withrow S, Dow S. Chronic bacterial osteomyelitis suppression of tumor growth requires innate immune responses. *Cancer Immunology, Immunotherapy* 2010;59(3):367-78.
 54. Lascelles B, Dernell W, Correa M, Lafferty M, Devitt C, Kuntz C, et al. Improved survival associated with postoperative wound infection in dogs treated with limb-salvage surgery for osteosarcoma. *Annals of Surgical Oncology* 2005;12(12):1073-83.
 55. Khanna C. Novel targets with potential therapeutic applications in osteosarcoma. *Current Oncology Reports* 2008;10(4):350-8.
 56. Paoloni M, Khanna C. Translation of new cancer treatments from pet dogs to humans. *Nature Reviews Cancer* 2008;8(2):147-56.
 57. Mueller F, Fuchs B, Kaser-Hotz B. Comparative biology of human and canine osteosarcoma. *Anticancer Research* 2007;27(1A):155-64.

58. Withrow SJ, Khanna C. Bridging the gap between experimental animals and humans in osteosarcoma. In: Jaffe N, Bruland OS, Bielack SS, editors. *Pediatric and Adolescent Osteosarcoma, Cancer Treatment and Research*. New York: Springer; 2009.
59. Misdorp W. Skeletal osteosarcoma. animal model: canine osteosarcoma. *American Journal of Pathology* 1980;98(1):285-8.
60. Morello E, Martano M, Buracco P. Biology, diagnosis and treatment of canine appendicular osteosarcoma: similarities and differences with human osteosarcoma. *The Veterinary Journal* 2010;In Press, Corrected Proof.
61. Kansara M, Thomas DM. Molecular pathogenesis of osteosarcoma. *DNA and Cell Biology* 2007;26(1):1-18.
62. Entz-Werlé N, Choquet P, Neuville A, Kuchler-Bopp S, Clauss F, Danse JM, et al. Targeted *apc/twist* double-mutant mice: a new model of spontaneous osteosarcoma that mimics the human disease. *Translational Oncology* 2010;3(6):344-53.
63. Wlodarski K, Kobus M, Luczak M. Orthotopic bone induction at sites of Moloney murine sarcoma virus inoculation in mice. *Nature* 1979;281(5730):386-7.
64. Bergman H. Chromosome counts of ⁹⁰Sr-induced osteosarcomas in mice IV. Variation of chromosome counts when using tumours of predetermined age for transplantation. *Acta Oncologica* 1980;19(4):279-84.
65. Pelfrène AF. A search for a suitable animal model for bone tumors: a review. *Drug and Chemical Toxicology* 1985;8(1-2):83-99.
66. Knowles BB, McCarrick J, Fox N, Solter D, Damjanov I. Osteosarcomas in transgenic mice expressing an alpha-amylase-SV40 T-antigen hybrid gene. *American Journal of Pathology* 1990;137(2):259-62.
67. Thomas R, Scott A, Langford CF, Fosmire SP, Jubala CM, Lorentzen TD, et al. Construction of a 2-Mb resolution BAC microarray for CGH analysis of canine tumors. *Genome Research* 2005;15(12):1831-7.
68. Thomas R, Wang H, Tsai P, Langford C, Fosmire S, Jubala C, et al. Influence of genetic background on tumor karyotypes: evidence for breed-associated cytogenetic aberrations in canine appendicular osteosarcoma. *Chromosome Research* 2009;17(3):365-77.
69. Phillips JC, Stephenson B, Hauck M, Dillberger J. Heritability and segregation analysis of osteosarcoma in the Scottish deerhound. *Genomics* 2007;90(3):354-63.

70. MacEwen EG, Kurzman ID, Rosenthal RC, Smith BW, Manley PA, Roush JK, et al. Therapy for osteosarcoma in dogs with intravenous injection of liposome-encapsulated muramyl tripeptide. *Journal of the National Cancer Institute* 1989;81(12):935-8.
71. Kleinerman ES, Jia SF, Griffin J, Seibel NL, Benjamin RS, Jaffe N. Phase II study of liposomal muramyl tripeptide in osteosarcoma: the cytokine cascade and monocyte activation following administration. *Journal of Clinical Oncology* 1992;10(8):1310-6.
72. Kleinerman ES, Gano JB, Johnston DA, Benjamin RS, Jaffe N. Efficacy of liposomal muramyl tripeptide (CGP 19835A) in the treatment of relapsed osteosarcoma. *American Journal of Clinical Oncology* 1995;18(2):93-9.
73. Anninga JK, Gelderblom H, Fiocco M, Kroep JR, Taminiau AHM, Hogendoorn PCW, et al. Chemotherapeutic adjuvant treatment for osteosarcoma: Where do we stand? *European Journal of Cancer* 2011; In Press, Corrected Proof.
74. Jaffe N. Adjuvant chemotherapy in osteosarcoma. In: Jaffe N, Bruland OS, Bielack SS, editors. *Pediatric and Adolescent Osteosarcoma, Cancer Treatment and Research*. New York: Springer; 2009.
75. Jaffe N. Osteosarcoma: review of the past, impact on the future. The American experience. In: Jaffe N, Bruland OS, Bielack SS, editors. *Pediatric and Adolescent Osteosarcoma, Cancer Treatment and Research*. New York: Springer; 2009.
76. Mirabello L, Troisi RJ, Savage SA. International osteosarcoma incidence patterns in children and adolescents, middle ages and elderly persons. *International Journal of Cancer* 2009;125(1):229-34.
77. Paoloni M, Davis S, Lana S, Withrow S, Sangiorgi L, Picci P, et al. Canine tumor cross-species genomics uncovers targets linked to osteosarcoma progression. 2009. p. 625.
78. Gorlick R. Current concepts on the molecular biology of osteosarcoma. In: Jaffe N, Bielack SS, Bruland OS, editors. *Pediatric and Adolescent Osteosarcoma, Cancer Treatment and Research*. New York: Springer; 2009.
79. Wong FL, Boice JD, Abramson DH, Tarone RE, Kleinerman RA, Stovall M, et al. Cancer incidence After retinoblastoma. *The Journal of the American Medical Association* 1997;278(15):1262-7.
80. Araki Y, Matsuyama Y, Kobayashi Y, Toyokawa S, Inoue K, Suzuki S, et al. Secondary neoplasms after retinoblastoma treatment: retrospective cohort study of 754 patients in Japan. *Japanese Journal of Clinical Oncology* 2011;41(3):373-9.

81. Lohmann D. Retinoblastoma. In: Ahmad SI, editor. Diseases of DNA Repair. New York: Springer 2010. p. 220-7.
82. Woo KI, Harbour JW. Review of 676 second primary tumors in patients with retinoblastoma: association between age at onset and tumor type. *Archives of Ophthalmology* 2010;128(7):865-70.
83. MacCarthy A, Bayne AM, Draper GJ, Eatock EM, Kroll ME, Stiller CA, et al. Non-ocular tumours following retinoblastoma in Great Britain 1951 to 2004. *British Journal of Ophthalmology* 2009;93(9):1159-62.
84. Benassi MS, Molendini L, Gamberi G, Ragazzini P, Sollazzo MR, Merli M, et al. Alteration of pRb/p16/cdk4 regulation in human osteosarcoma. *International Journal of Cancer* 1999;84(5):489-93.
85. Levine RA, Fleischli MA. Inactivation of p53 and retinoblastoma family pathways in canine osteosarcoma cell lines. *Veterinary Pathology* 2000;37(1):54-61.
86. Wadayama B-i, Toguchida J, Shimizu T, Ishizaki K, Sasaki MS, Kotoura Y, et al. Mutation spectrum of the retinoblastoma gene in osteosarcomas. *Cancer Research* 1994;54(11):3042-8.
87. Mendoza S, Konishi T, Dernell WS, Withrow SJ, Miller CW. Status of the p53, Rb and MDM2 genes in canine osteosarcoma. *Anticancer Research* 1998;18(6A):4449-53.
88. Heinsohn S, Evermann U, Stadt UZ, Bielack S, Kabisch H. Determination of the prognostic value of loss of heterozygosity at the retinoblastoma gene in osteosarcoma. *International Journal of Oncology* 2007;30(5):1205-14.
89. Li FP, Fraumeni JF, Mulvihill JJ, Blattner WA, Dreyfus MG, Tucker MA, et al. A cancer family syndrome in twenty-four kindreds. *Cancer Research* 1988;48(18):5358-62.
90. Garber JE, Goldstein AM, Kantor AF, Dreyfus MG, Fraumeni JF, Li FP. Follow-up study of twenty-four families with Li-Fraumeni Syndrome. *Cancer Research* 1991;51(22):6094-7.
91. Malkin D, Jolly KW, Barbier NI, Look AT, Friend SH, Gebhardt MC, et al. Germline mutations of the p53 tumor-suppressor gene in children and young adults with second malignant neoplasms. *New England Journal of Medicine* 1992;326(20):1309-15.

92. Malkin D, Li FP, Strong LC, Fraumeni JF, Nelson CE, Kim DH, et al. Germ line p53 mutations in a familial syndrome of breast cancer, sarcomas, and other neoplasms. *Science* 1990;250(4985):1233-8.
93. Willis A, Jung EJ, Wakefield T, Chen X. Mutant p53 exerts a dominant negative effect by preventing wild-type p53 from binding to the promoter of its target genes. *Oncogene* 2004;23(13):2330-8.
94. Weinberg RA. *The Biology of Cancer*. New York: Garland Science; 2007.
95. Chandar N, Billig B, McMaster J, Novak J. Inactivation of p53 gene in human and murine osteosarcoma cells. *British Journal of Cancer* 1992;65(2):208-14.
96. Miller CW, Aslo A, Tsay C, Slamon D, Ishizaki K, Toguchida J, et al. Frequency and structure of p53 rearrangements in human osteosarcoma. *Cancer Research* 1990;50(24):7950-4.
97. Setoguchi A, Sakai T, Okuda M, Minehata K, Yazawa M, Ishizaka T, et al. Aberrations of the p53 tumor suppressor gene in various tumors in dogs. *American Journal of Veterinary Research* 2001;62(3):433-9.
98. Johnson AS, Couto CG, Weghorst CM. Mutation of the p53 tumor suppressor gene in spontaneously occurring osteosarcomas of the dog. *Carcinogenesis* 1998;19(1):213-7.
99. Diller L, Kassel J, Nelson CE, Gryka MA, Litwak G, Gebhardt M, et al. p53 functions as a cell cycle control protein in osteosarcomas. *Molecular and Cellular Biology* 1990;10(11):5772-81.
100. Pompetti F, Rizzo P, Simon RM, Freidlin B, Mew DJ, Pass HI, et al. Oncogene alterations in primary, recurrent, and metastatic human bone tumors. *Journal of Cellular Biochemistry* 1996;63(1):37-50.
101. Park HR, Park YK. Expression of p53 protein, PCNA, and Ki-67 in osteosarcomas of bone. *J Korean Med Sci* 1995;10(5):360-7.
102. Ueda Y, Dockhorn-Dworniczak B, Blasius S, Mellin W, Wuisman P, Böcker W, et al. Analysis of mutant P53 protein in osteosarcomas and other malignant and benign lesions of bone. *Journal of Cancer Research and Clinical Oncology* 1993;119(3):172-8.
103. Kirpensteijn J, Kik M, Teske E, Rutteman GR. TP53 gene mutations in canine osteosarcoma. *Veterinary Surgery* 2008;37(5):454-60.
104. Loukopoulos P, Thornton JR, Robinson WF. Clinical and pathologic relevance of p53 index in canine osseous tumors. *Veterinary Pathology* 2003;40(3):237-48.

105. Scholz RB, Kabisch H, Weber B, Röser K, Delling G, Winkler K. Studies of the RB1 gene and the p53 gene in human osteosarcomas. *Pediatric Hematology-Oncology* 1992;9(2):125-37.
106. Larizza L, Roversi G, Volpi L. Rothmund-Thomson syndrome. *Orphanet Journal of Rare Diseases* 2010;5(1):2.
107. Wang LL, Gannavarapu A, Kozinetz CA, Levy ML, Lewis RA, Chintagumpala MM, et al. Association between osteosarcoma and deleterious mutations in the RECQL4 gene in rothmund thomson syndrome. *Journal of the National Cancer Institute* 2003;95(9):669-74.
108. Nishijo K, Nakayama T, Aoyama T, Okamoto T, Ishibe T, Yasura K, et al. Mutation analysis of the RECQL4 gene in sporadic osteosarcomas. *International Journal of Cancer* 2004;111(3):367-72.
109. Goto M, Miller RW, Ishikawa Y, Sugano H. Excess of rare cancers in Werner syndrome (adult progeria). *Cancer Epidemiology, Biomarkers & Prevention* 1996;5(4):239-46.
110. Ishikawa Y, Miller RW, Machinami R, Sugano H, Goto M. Atypical osteosarcomas in Werner Syndrome (adult progeria). *Cancer Science* 2000;91(12):1345-9.
111. Mao FJ, Sidorova JM, Lauper JM, Emond MJ, Monnat RJ. The human WRN and BLM RecQ helicases differentially regulate cell proliferation and survival after chemotherapeutic DNA damage. *Cancer Research* 2010;70(16):6548-55.
112. Watt PM, Hickson ID. Genome stability: failure to unwind causes cancer. *Current Biology* 1996;6(3):265-7.
113. Blander G, Kipnis J, Leal JFM, Yu C-E, Schellenberg GD, Oren M. Physical and functional interaction between p53 and the Werner's syndrome protein. *The Journal of Biological Chemistry* 1999;274(41):29463-9.
114. Wang XW, Tseng A, Ellis NA, Spillare EA, Linke SP, Robles AI, et al. Functional interaction of p53 and BLM DNA helicase in apoptosis. *The Journal of Biological Chemistry* 2001;276(35):32948-55.
115. Garkavtsev IV, Kley N, Grigorian IA, Gudkov AV. The Bloom syndrome protein interacts and cooperates with p53 in regulation of transcription and cell growth control. *Oncogene* 2001;20(57):8276-80.
116. Miller CW, Aslo A, Campbell MJ, Kawamata N, Lampkin BC, Koeffler HP. Alterations of the p15, p16, and p18 genes in osteosarcoma. *Cancer Genetics and Cytogenetics* 1996;86(2):136-42.

117. Nielsen GP, Burns KL, Rosenberg AE, Louis DN. CDKN2A gene deletions and loss of p16 expression occur in osteosarcomas that lack RB alterations. *The American Journal of Pathology* 1998;153(1):159-63.
118. Oh JH, Kim HS, Kim HH, Kim WH, Lee SH. Aberrant methylation of p14ARF gene correlates with poor survival in osteosarcoma. *Clinical Orthopaedics and Related Research* 2006;442:216-22.
119. Wei G, Lonardo F, Ueda T, Kim T, Huvos AG, Healey JH, et al. CDK4 gene amplification in osteosarcoma: Reciprocal relationship with INK4A gene alterations and mapping of 12q13 amplicons. *International Journal of Cancer* 1999;80(2):199-204.
120. Khan S, Guevara C, Fujii G, Parry D. p14ARF is a component of the p53 response following ionizing irradiation of normal human fibroblasts. *Oncogene* 2004;23(36):6040-6.
121. Zhang Y, Xiong Y, Yarbrough WG. ARF promotes MDM2 degradation and stabilizes p53: ARF-INK4a locus deletion impairs both the Rb and p53 tumor suppression pathways. *Cell* 1998;92(6):725-34.
122. Benassi MS, Molendini L, Gamberi G, Magagnoli G, Ragazzini P, Gobbi GA, et al. Involvement of INK4A gene products in the pathogenesis and development of human osteosarcoma. *Cancer* 2001;92(12):3062-7.
123. Miller CW, Aslo A, Won A, Tan M, Lampkin B, Koefflar HP. Alterations of the p53, Rb and MDM2 genes in osteosarcomas *Journal of Cancer Research and Clinical Oncology* 1996;122(9):559-65.
124. Chen J, Wu X, Lin J, Levine AJ. Mdm-2 inhibits the G1 arrest and apoptosis functions of the p53 tumor suppressor protein. *Molecular and Cellular Biology* 1996;16(5):2445-52.
125. Mejia-Guerrero S, Quejada M, Gokgoz N, Gill M, Parkes RK, Wunder JS, et al. Characterization of the 12q15 MDM2 and 12q13-14 CDK4 amplicons and clinical correlations in osteosarcoma. *Genes, Chromosomes and Cancer* 2010;49(6):518-25.
126. Wunder JS, Eppert K, Burrow SR, Gogkoz N, Bell RS, Andrulis IL. Co-amplification and overexpression of CDK4, SAS and MDM2 occurs frequently in human parosteal osteosarcomas. *Oncogene* 1999;18(3):783-8.
127. van Dartel M, Hulsebos TJM. Amplification and overexpression of genes in 17p11.2~p12 in osteosarcoma. *Cancer Genetics and Cytogenetics* 2004;153(1):77-80.

128. Bogenmann E, Moghadam H, DeClerck YA, Mock A. c-myc amplification and expression in newly established human osteosarcoma cell lines. *Cancer Research* 1987;47(14):3808-14.
129. Ioannidis P, Trangas T, Dimitriadis E, Samiotaki M, Kyriazoglou I, Tsiapalis CM, et al. C-MYC and IGF-II mRNA-binding protein (CRD-BP/IMP-1) in benign and malignant mesenchymal tumors. *International Journal of Cancer* 2001;94(4):480-4.
130. Gamberi G, Benassi MS, Bohling T, Ragazzini P, Molendini L, Sollazzo MR, et al. C-myc and c-fos in human osteosarcoma: prognostic value of mRNA and protein expression. *Oncology* 1998;55(6):556-63.
131. Scionti I, Michelacci F, Pasello M, Hattinger CM, Alberghini M, Manara MC, et al. Clinical impact of the methotrexate resistance-associated genes C-MYC and dihydrofolate reductase (DHFR) in high-grade osteosarcoma. *Annals of Oncology* 2008;19(8):1500-8.
132. Xie X-K, Yang D-S, Ye Z-M, Tao H-M. Recombinant antisense c-Myc adenovirus increase in vitro sensitivity of osteosarcoma MG-63 cells to cisplatin. *Cancer Investigation* 2006;24(1):1-8.
133. Jain M, Arvanitis C, Chu K, Dewey W, Leonhardt E, Trinh M, et al. Sustained loss of a neoplastic phenotype by brief inactivation of MYC. *Science* 2002;297(5578):102-4.
134. Levine RA. Overexpression of the Sis oncogene in a canine osteosarcoma cell line. *Veterinary Pathology* 2002;39(3):411-2.
135. Noubissi FK, Elcheva I, Bhatia N, Shakoori A, Ougolkov A, Liu J, et al. CRD-BP mediates stabilization of [beta]TrCP1 and c-myc mRNA in response to [beta]-catenin signalling. *Nature* 2006;441(7095):898-901.
136. Zhang J, Li F, Liu X, Shen L, Liu J, Su J, et al. The repression of human differentiation-related gene NDRG2 expression by Myc via Miz-1-dependent interaction with the NDRG2 core promoter. *Journal of Biological Chemistry* 2006;281(51):39159-68.
137. Amente S, Gargano B, Diolaiti D, Della Valle G, Lania L, Majello B. p14ARF interacts with N-Myc and inhibits its transcriptional activity. *FEBS Letters* 2007;581(5):821-5.
138. Datta A, Nag A, Pan W, Hay N, Gartel AL, Colamonici O, et al. Myc-ARF (alternate reading frame) interaction inhibits the functions of myc. *The Journal of Biological Chemistry* 2004;279(35):36698-707.

139. Gregory MA, Qi Y, Hann SR. The ARF tumor suppressor: keeping Myc on a leash. *Cell Cycle* 2005;4(2):248-51.
140. Amente S, Gargano B, Varrone F, Ruggiero L, Dominguez-Sola D, Lania L, et al. p14ARF directly interacts with Myc through the Myc BoxII domain. *Cancer Biology & Therapy* 2006;5(3):287-91.
141. Macias E, Jin A, Deisenroth C, Bhat K, Mao H, Lindström MS, et al. An ARF-independent c-MYC-activated tumor suppression pathway mediated by ribosomal protein-Mdm2 interaction. *Cancer Cell* 2010;18(3):231-43.
142. Li YG, Geng X. A meta-analysis on the association of HER-2 overexpression with prognosis in human osteosarcoma. *European Journal of Cancer Care* 2010;19(3):313-6.
143. Shang J, Bi Z-g, Ji H-f, Wang W-b. Integrated assessment of potential value of erbB-2 amplification or expression status as novel therapy target in Chinese children and adolescents with osteosarcoma. *Chinese Medical Journal* 2009;122(13):1521-4.
144. Stein U, Eder C, Karsten U, Haensch W, Walther W, Schlag PM. GLI gene expression in bone and soft tissue sarcomas of adult patients correlates with tumor grade. *Cancer Research* 1999;59(8):1890-5.
145. Roberts WM, Douglass EC, Peiper SC, Houghton PJ, Look AT. Amplification of the Gli gene in childhood sarcomas. *Cancer Research* 1989;49(19):5407-13.
146. Hirotsu M, Setoguchi T, Sasaki H, Matsunoshita Y, Gao H, Nagao H, et al. Smoothed as a new therapeutic target for human osteosarcoma. *Molecular Cancer* 2010;9(5).
147. Nagao H, Ijiri K, Hirotsu M, Ishidou Y, Yamamoto T, Nagano S, et al. Role of GLI2 in the growth of human osteosarcoma. *The Journal of Pathology* 2011;224(2):169-79.
148. Naski MC, Colvin JS, Coffin JD, Ornitz DM. Repression of hedgehog signaling and BMP4 expression in growth plate cartilage by fibroblast growth factor receptor 3. *Development* 1998;125(24):4977-88.
149. Gupta S, Takebe N, LoRusso P. Review: targeting the Hedgehog pathway in cancer. *Therapeutic Advances in Medical Oncology* 2010;2(4):237-50.
150. Warzecha J, Göttig S, Chow KU, Brüning C, Percic D, Boehrer S, et al. Inhibition of osteosarcoma cell proliferation by the Hedgehog-inhibitor cyclopamine. *Journal of Chemotherapy* 2007;19(5):554-61.

151. Lee J-S, Thomas DM, Gutierrez G, Carty SA, Yanagawa S-i, Hinds PW. HES1 cooperates with pRb to activate RUNX2-dependent transcription. *Journal of Bone and Mineral Research* 2006;21(6):921-33.
152. Ducy P, Zhang R, Geoffroy V, Ridall AL, Karsenty G. *Osf2/Cbfa1*: a transcriptional activator of osteoblast differentiation. *Cell* 1997;89(5):747-54.
153. Thomas DM, Johnson SA, Sims NA, Trivett MK, Slavin JL, Rubin BP, et al. Terminal osteoblast differentiation, mediated by *runx2* and *p27KIP1*, is disrupted in osteosarcoma. *Journal of Cell Biology* 2004;167(5):925-34.
154. Wagner ER, Luther G, Zhu G, Luo Q, Shi Q, Kim KH, et al. Defective osteogenic differentiation in the development of osteosarcoma. *Sarcoma* 2011;2011.
155. Pereira BP, Zhou Y, Gupta A, Leong DT, Aung KZ, Ling L, et al. *Runx2*, *p53*, and *pRB* status as diagnostic parameters for deregulation of osteoblast growth and differentiation in a new pre-chemotherapeutic osteosarcoma cell line (OS1). *Journal of Cellular Physiology* 2009;221(3):778-88.
156. Nathan S, Pereira B, Zhou Y-f, Gupta A, Dombrowski C, Soong R, et al. Elevated expression of *Runx2* as a key parameter in the etiology of osteosarcoma. *Molecular Biology Reports* 2009;36(1):153-8.
157. Sadikovic B, Yoshimoto M, Chilton-MacNeill S, Thorner P, Squire JA, Zielenska M. Identification of interactive networks of gene expression associated with osteosarcoma oncogenesis by integrated molecular profiling. *Human Molecular Genetics* 2009;18(11):1962-75.
158. Sadikovic B, Thorner P, Chilton-MacNeill S, Martin J, Cervigne N, Squire J, et al. Expression analysis of genes associated with human osteosarcoma tumors shows correlation of *RUNX2* overexpression with poor response to chemotherapy. *BMC Cancer* 2010;10(1):202.
159. Cao Y, Zhou Z, de Crombrughe B, Nakashima K, Guan H, Duan X, et al. *Osterix*, a transcription factor for osteoblast differentiation, mediates antitumor activity in murine osteosarcoma. *Cancer Research* 2005;65(4):1124-8.
160. Tu Q, Valverde P, Chen J. *Osterix* enhances proliferation and osteogenic potential of bone marrow stromal cells. *Biochemical and Biophysical Research Communications* 2006;341(4):1257-65.
161. Pollak MN, Polychronakos C, Richard M. Insulin-like Growth Factor I: a potent mitogen for human osteogenic sarcoma. *Journal of the National Cancer Institute* 1990;82(4):301-5.

162. Hassan SE, Bekarev M, Kim MY, Lin J, Piperdi S, Gorlick R, et al. Cell surface receptor expression patterns in osteosarcoma. *Cancer* 2011;n/a-n/a.
163. Kolb EA, Gorlick R, Lock R, Carol H, Morton CL, Keir ST, et al. Initial testing (stage 1) of the IGF-1 receptor inhibitor BMS-754807 by the pediatric preclinical testing program. *Pediatric Blood & Cancer* 2011;56(4):595-603.
164. Bagatell R, Herzog CE, Trippett TM, Grippo JF, Cirrincione-Dall G, Fox E, et al. Pharmacokinetically guided phase 1 trial of the IGF-1 receptor antagonist RG1507 in children with recurrent or refractory solid tumors. *Clinical Cancer Research* 2011;17(3):611-9.
165. Dong J, Demarest SJ, Sereno A, Tamraz S, Langley E, Doern A, et al. Combination of two Insulin-Like Growth Factor-I Receptor inhibitory antibodies targeting distinct epitopes leads to an enhanced antitumor response. *Molecular Cancer Therapeutics* 2010;9(9):2593-604.
166. Kurmasheva RT, Dudkin L, Billups C, Debelenko LV, Morton CL, Houghton PJ. The Insulin-like Growth Factor-1 Receptor targeting antibody, CP-751,871, suppresses tumor-derived VEGF and synergizes with rapamycin in models of childhood sarcoma. *Cancer Research* 2009;69(19):7662-71.
167. Kubo T, Piperdi S, Rosenblum J, Antonescu CR, Chen W, Kim H-S, et al. Platelet-derived growth factor receptor as a prognostic marker and a therapeutic target for imatinib mesylate therapy in osteosarcoma. *Cancer* 2008;112(10):2119-29.
168. Sulzbacher I, Birner P, Trieb K, Lang S, Chott A. Expression of osteopontin and vascular endothelial growth factor in benign and malignant bone tumors. *Virchows Archiv* 2002;441(4):345-9.
169. Kaya M, Wada T, Akatsuka T, Kawaguchi S, Nagoya S, Shindoh M, et al. Vascular endothelial growth factor expression in untreated osteosarcoma is predictive of pulmonary metastasis and poor prognosis. *Clinical Cancer Research* 2000;6(2):572-7.
170. Boulytcheva I, Soloviev Y, Kushlinskii N, Mahson A. Expression of molecular markers in the tumor and survival prognosis in osteosarcoma. *Bulletin of Experimental Biology and Medicine* 2010;150(2):237-42.
171. Mendoza S, David H, Gaylord GM, Miller CW. Allelic loss at 10q26 in osteosarcoma in the region of the BUB3 and FGFR2 genes. *Cancer Genetics and Cytogenetics* 2005;158(2):142-7.
172. Sobue T, Gravely T, Hand A, Min YK, Pilbeam C, Raisz LG, et al. Regulation of Fibroblast Growth Factor 2 and Fibroblast Growth Factor receptors by

- Transforming Growth Factor β in human osteoblastic MG-63 cells. *Journal of Bone and Mineral Research* 2002;17(3):502-12.
173. Fieten H, Spee B, Ijzer J, Kik MJ, Penning LC, Kirpensteijn J. Expression of hepatocyte growth factor and the proto-oncogenic Receptor c-Met in canine osteosarcoma. *Veterinary Pathology* 2009;46(5):869-77.
 174. De Maria R, Miretti S, Iussich S, Olivero M, Morello E, Bertotti A, et al. Met oncogene activation qualifies spontaneous canine osteosarcoma as a suitable pre-clinical model of human osteosarcoma. *The Journal of Pathology* 2009;218(3):399-408.
 175. MacEwen EG, Kutzke J, Carew J, Pastor J, Schmidt J, Tsan R, et al. C-Met tyrosine kinase receptor expression and function in human and canine osteosarcoma cells. *Clinical and Experimental Metastasis* 2003;20(5):421-30.
 176. Hanahan D, Weinberg Robert A. Hallmarks of cancer: the next generation. *Cell* 2011;144(5):646-74.
 177. Hanahan D, Weinberg RA. The hallmarks of cancer. *Cell* 2000;100(1):57-70.
 178. Ferrante K, Winograd B, Canetta R. Promising new developments in cancer chemotherapy. *Cancer Chemotherapy and Pharmacology* 1999;43(0):S61-S8-S8.
 179. Kleiner DE, Stetler-Stevenson WG. Matrix metalloproteinases and metastasis. *Cancer Chemotherapy and Pharmacology* 1999;43(0):S42-S51.
 180. Sato H, Okada Y, Seiki M. Membrane-type matrix metalloproteinases (MT-MMPs) in cell invasion. *Thrombosis and Haemostasis* 1997;78(1):497-500.
 181. Munshi H, Stack M. Reciprocal interactions between adhesion receptor signaling and MMP regulation. *Cancer and Metastasis Reviews* 2006;25(1):45-56.
 182. Brown PD, Bloxidge RE, Stuart NSA, Galler KC, Carmichael J. Association between expression of activated 72-kilodalton gelatinase and tumor spread in non-small-cell lung carcinoma. *Journal of the National Cancer Institute* 1993;85(7):574-8.
 183. Zeng ZS, Huang Y, Cohen AM, Guillem JG. Prediction of colorectal cancer relapse and survival via tissue RNA levels of matrix metalloproteinase-9. *Journal of Clinical Oncology* 1996;14(12):3133-40.
 184. Mueller MM, Fusenig NE. Tumor-stroma interactions directing phenotype and progression of epithelial skin tumor cells. *Differentiation* 2002;70(9-10):486-97.

185. Bjørnland K, Flatmark K, Pettersen S, Aaasen AO, Fodstad Ø, Mælandsmo GM. Matrix metalloproteinases participate in osteosarcoma invasion. *The Journal of Surgical Research* 2005;127(2):151-6.
186. Uchibori M, Nishida Y, Nagasaka T, Yamada Y, Nakanishi K, Ishiguro N. Increased expression of membrane-type matrix metalloproteinase-1 is correlated with poor prognosis in patients with osteosarcoma. *International Journal of Oncology* 2006;28(1):33-42.
187. van de Vijver MJ, He YD, van 't Veer LJ, Dai H, Hart AAM, Voskuil DW, et al. A gene-expression signature as a predictor of survival in breast cancer. *New England Journal of Medicine* 2002;347(25):1999-2009.
188. Khanna C, Khan J, Nguyen P, Prehn J, Caylor J, Yeung C, et al. Metastasis-associated differences in gene expression in a murine model of osteosarcoma. *Cancer Research* 2001;61(9):3750-9.
189. Folkman J. Role of angiogenesis in tumor growth and metastasis. *Seminars in oncology* 2002;29(6):15-8.
190. Hillen F, Griffioen A. Tumour vascularization: sprouting angiogenesis and beyond. *Cancer and Metastasis Reviews* 2007;26(3):489-502.
191. Burri PH, Hlushchuk R, Djonov V. Intussusceptive angiogenesis: Its emergence, its characteristics, and its significance. *Developmental Dynamics* 2004;231(3):474-88.
192. Asahara T, Masuda H, Takahashi T, Kalka C, Pastore C, Silver M, et al. Bone marrow origin of endothelial progenitor cells responsible for postnatal vasculogenesis in physiological and pathological neovascularization. *Circulation Research* 1999;85(3):221-8.
193. Asahara T, Takahashi T, Masuda H, Kalka C, Chen D, Iwaguro H, et al. VEGF contributes to postnatal neovascularization by mobilizing bone marrow-derived endothelial progenitor cells. *The EMBO Journal* 1999;18(14):3964-72.
194. Pezzella F, Pastorino U, Tagliabue E, Andreola S, Sozzi G, Gasparini G, et al. Non-small-cell lung carcinoma tumor growth without morphological evidence of neo-angiogenesis. *American Journal of Pathology* 1997;151(5):1417-23.
195. Döme B, Paku S, Somlai B, Tímár J. Vascularization of cutaneous melanoma involves vessel co-option and has clinical significance. *The Journal of Pathology* 2002;197(3):355-62.

196. Holash J, Maisonpierre PC, Compton D, Boland P, Alexander CR, Zagzag D, et al. Vessel cooption, regression, and growth in tumors mediated by angiopoietins and VEGF. *Science* 1999;284(5422):1994-8.
197. Kim ES, Serur A, Huang J, Manley CA, McCrudden KW, Frischer JS, et al. Potent VEGF blockade causes regression of coopted vessels in a model of neuroblastoma. *Proceedings of the National Academy of Sciences* 2002;99(17):11399-404.
198. Maniotis AJ, Folberg R, Hess A, Seftor EA, Gardner LMG, Pe'er J, et al. Vascular channel formation by human melanoma cells in vivo and in vitro: vasculogenic mimicry. *The American Journal of Pathology* 1999;155(3):739-52.
199. Mei J, Gao Y, Zhang L, Cai X, Qian Z, Huang H, et al. Vegf-siRNA silencing induces apoptosis, inhibits proliferation and suppresses vasculogenic mimicry in osteosarcoma in vitro. *Experimental Oncology* 2008;30(1):29-34.
200. Zhang L-Z, Mei J, Qian Z-K, Cai X-S, Jiang Y, Huang W-D. The role of VE-cadherin in osteosarcoma cells. *Pathology & Oncology Research* 2010;16(1):111-7.
201. Wallez Y, Vilgrain I, Huber P. Angiogenesis: The VE-Cadherin switch. *Trends in Cardiovascular Medicine* 2006;16(2):55-9.
202. Demicheli R, Retsky MW, Hrushesky WJM, Baum M, Gukas ID. The effects of surgery on tumor growth: a century of investigations. *Annals of Oncology* 2008;19(11):1821-8.
203. Chiang AC, Massagué J. Molecular basis of metastasis. *New England Journal of Medicine* 2008;359(26):2814-23.
204. Chambers AF, Groom AC, MacDonald IC. Metastasis: dissemination and growth of cancer cells in metastatic sites. *Nature Reviews Cancer* 2002;2(8):563-72.
205. Paget S. The distribution of secondary growths in cancer of the breast. *Lancet* 1889;133(571-573).
206. Khanna C, Wan X, Bose S, Cassaday R, Olomu O, Mendoza A, et al. The membrane-cytoskeleton linker ezrin is necessary for osteosarcoma metastasis. *Nature Medicine* 2004;10(2):182-6.
207. Wan X, Kim SY, Guenther LM, Mendoza A, Briggs J, Yeung C, et al. Beta4 integrin promotes osteosarcoma metastasis and interacts with ezrin. *Oncogene* 2009;28(38):3401-11.

208. Hughes DP. How the NOTCH pathway contributes to the ability of osteosarcoma cells to metastasize. In: Jaffe N, Bruland OS, Bielack SS, editors. *Pediatric and Adolescent Osteosarcoma, Cancer Treatment and Research*. New York: Springer; 2009. p. 479-96.
209. Worth LL, Lafleur EA, Jia S-F, Kleinerman ES. Fas expression inversely correlates with metastatic potential in osteosarcoma cells. *Oncology Reports* 2002;9(4):823-7.
210. Rodriguez CO, Crabbs TA, Wilson DW, Cannan VA, Skorupski KA, Gordon N, et al. Aerosol gemcitabine: preclinical safety and in vivo antitumor activity in osteosarcoma-bearing dogs. *Journal of Aerosol Medicine and Pulmonary Drug Delivery* 2009;23(4):197-206.
211. Lafleur EA, Koshkina NV, Stewart J, Jia S-F, Worth LL, Duan X, et al. Increased Fas expression reduces the metastatic potential of human osteosarcoma cells. *Clinical Cancer Research* 2004;10(23):8114-9.
212. Gordon N, Arndt CAS, Hawkins DS, Doherty DK, Inwards CY, Munsell MF, et al. Fas expression in lung metastasis from osteosarcoma patients. *Journal of Pediatric Hematology/Oncology* 2005;27(11):611-5.
213. Gordon N, Kleinerman ES. The role of Fas/FasL in the metastatic potential of osteosarcoma and targeting this pathway for the treatment of osteosarcoma lung metastases. In: Jaffe N, Bruland OS, Bielack SS, editors. *Pediatric and Adolescent Osteosarcoma, Cancer Treatment and Research*. New York: Springer; 2009. p. 497-508.
214. Venter JC, Adams MD, Myers EW, Li PW, Mural RJ, Sutton GG, et al. The sequence of the human genome. *Science* 2001;291(5507):1304-51.
215. Maskos U, Southern EM. Oligonucleotide hybridisations on glass supports: a novel linker for oligonucleotide synthesis and hybridisation properties of oligonucleotides synthesised in situ. *Nucleic Acids Research* 1992;20(7):1679-84.
216. Affymetrix. GeneChip® Canine Genome 2.0 Array data sheet.
217. McCormick K, Willmann M, Meyers B. Experimental design, preprocessing, normalization and differential expression analysis of small RNA sequencing experiments. *Silence* 2011;2(2).
218. Pollack JR, Perou CM, Alizadeh AA, Eisen MB, Pergamenschikov A, Williams CF, et al. Genome-wide analysis of DNA copy-number changes using cDNA microarrays. *Nature Genetics* 1999;23(1):41-6.

219. Costa V, Angelini C, De Feis I, Ciccodicola A. Uncovering the complexity of transcriptomes with RNA-Seq. *Journal of Biomedicine and Biotechnology* 2010;Epub ahead of print.
220. Dhahbi JM, Atamna H, Boffelli D, Magis W, Spindler SR, Martin DIK. Deep sequencing reveals novel microRNAs and regulation of microRNA expression during cell senescence. *PLoS ONE* 2011;6(5):e20509.
221. Affymetrix. Guide to probe logarithmic intensity error (PLIER) estimation. 2005.
222. Owzar K, Barry WT, Jung S-H, Sohn I, George SL. Statistical challenges in preprocessing in microarray experiments in cancer. *Clinical Cancer Research* 2008;14(19):5959-66.
223. Eisenstein M. Microarrays: quality control. *Nature* 2006;442(7106):1067-70.
224. Gyorffy B, Molnar B, Lage H, Szallasi Z, Eklund AC. Evaluation of microarray preprocessing algorithms based on concordance with RT-PCR in clinical samples. *PLoS ONE* 2009;4(5):e5645.
225. Klopffleisch R, Klose P, Weise C, Bondzio A, Multhaup G, Einspanier R, et al. Proteome of metastatic canine mammary carcinomas: similarities to and differences from human breast cancer *Journal of Proteome Research* 2010;9(12):6380-91.
226. Gupta N, Tanner S, Jaitly N, Adkins JN, Lipton M, Edwards R, et al. Whole proteome analysis of post-translational modifications: Applications of mass-spectrometry for proteogenomic annotation. *Genome Research* 2007;17(9):1362-77.
227. Brodeur GM, Seeger RC, Schwab M, Varmus HE, Bishop JM. Amplification of N-myc in untreated human neuroblastomas correlates with advanced disease stage. *Science* 1984;224(4653):1121-4.
228. Roux-Dosseto M, Romain S, Dussault N, Martin PM. Correlation of erbB-2 gene amplification with low levels of estrogen and/or progesterone receptors in primary breast cancer : do erbB-2 products delineate hormone-independent tumors? *Biomedecine & Pharmacotherapy* 1989;43(9):641-9.
229. Mohseny AB, Tiekens C, van der Velden PA, Szuhai K, de Andrea C, Hogendoorn PCW, et al. Small deletions but not methylation underlie CDKN2A/p16 loss of expression in conventional osteosarcoma. *Genes, Chromosomes and Cancer* 2010;49(12):1095-103.
230. Huang H-Y, Illei PB, Zhao Z, Mazumdar M, Huvos AG, Healey JH, et al. Ewing sarcomas with p53 mutation or p16/p14ARF homozygous deletion: a highly lethal

- subset associated with poor chemoresponse. *Journal of Clinical Oncology* 2005;23(3):548-58.
231. Sakai T, Ohtani N, McGee TL, Robbins PD, Dryja TP. Oncogenic germ-line mutations in Sp1 and ATF sites in the human retinoblastoma gene. *Nature* 1991;353(6339):83-6.
 232. Pietenpol JA, Munger K, Howley PM, Stein RW, Moses HL. Factor-binding element in the human c-myc promoter involved in transcriptional regulation by transforming growth factor beta 1 and by the retinoblastoma gene product. *Proceedings of the National Academy of Sciences* 1991;88(22):10227-31.
 233. Tarunina M, Jenkins JR. Human p53 binds DNA as a protein homodimer but monomeric variants retain full transcription transactivation activity. *Oncogene* 1993;8(11):3165-73.
 234. Herceg Z, Ushijima T. Introduction: epigenetics and cancer. In: Herceg Z, Ushijima T, editors. *Advances in Genetics*. San Diego, CA: Academic Press; 2010. p. 1-23.
 235. Ulaner GA, Vu TH, Li T, Hu J-F, Yao X-M, Yang Y, et al. Loss of imprinting of IGF2 and H19 in osteosarcoma is accompanied by reciprocal methylation changes of a CTCF-binding site. *Human Molecular Genetics* 2003;12(5):535-49.
 236. Rubin EM, Guo Y, Tu K, Xie J, Zi X, Hoang BH. Wnt Inhibitory Factor 1 decreases tumorigenesis and metastasis in osteosarcoma. *Molecular Cancer Therapeutics* 2010;9(3):731-41.
 237. Sawan C, Herceg Z. Histone modifications and cancer. In: Herceg Z, Ushijima T, editors. *Advances in Genetics*. San Diego, CA: Academic Press; 2010. p. 57-85.
 238. Wittenburg L, Bisson L, Rose B, Korch C, Thamm D. The histone deacetylase inhibitor valproic acid sensitizes human and canine osteosarcoma to doxorubicin. *Cancer Chemotherapy and Pharmacology* 2011;67(1):83-92.
 239. McManus MT. MicroRNAs and cancer. *Seminars in Cancer Biology* 2003;13(4):253-8.
 240. Moberg KH, Hariharan IK. Big things from a little RNA. *Trends in Cell Biology* 2003;13(9):455-7.
 241. Zhang B, Pan X, Cobb GP, Anderson TA. microRNAs as oncogenes and tumor suppressors. *Developmental Biology* 2007;302(1):1-12.
 242. Saito Y, Jones P. Epigenetic activation of tumor suppressor microRNAs in human cancer cells. *Cell Cycle* 2006;5(19):2220-2.

243. Creighton CJ, Fountain MD, Yu Z, Nagaraja AK, Zhu H, Khan M, et al. Molecular profiling uncovers a p53-associated role for microRNA-31 in inhibiting the proliferation of serous ovarian carcinomas and other cancers. *Cancer Research* 2010;70(5):1906-15.
244. Ziyan W, Shuhua Y, Xiufang W, Xiaoyun L. MicroRNA-21 is involved in osteosarcoma cell invasion and migration. *Medical Oncology* 2010;Epub ahead of print:1-6.
245. Mayr C, Bartel DP. Widespread shortening of 3'UTRs by alternative cleavage and polyadenylation activates oncogenes in cancer cells. *Cell* 2009;138(4):673-84.
246. Vucic D, Dixit VM, Wertz IE. Ubiquitylation in apoptosis: a post-translational modification at the edge of life and death. *Nature Reviews Molecular & Cellular Biology* 2011;12(7):439-52.
247. Strongin A. Mislocalization and unconventional functions of cellular MMPs in cancer. *Cancer and Metastasis Reviews* 2006;25(1):87-98.
248. Epstein J, Breslow JL. Human osteogenic sarcoma cells exhibit enhanced protein phosphorylation. *Biochimica et Biophysica Acta (BBA) - General Subjects* 1981;676(1):68-76.
249. Chen P-L, Scully P, Shew J-Y, Wang JYJ, Lee W-H. Phosphorylation of the retinoblastoma gene product is modulated during the cell cycle and cellular differentiation. *Cell* 1989;58(6):1193-8.
250. Bergman PJ. Mechanisms of anticancer drug resistance. *Veterinary Clinics of North America: Small Animal Practice* 2003;33(3):651-67.
251. Goto A, Kanda H, Ishikawa Y, Matsumoto S, Kawaguchi N, Machinami R, et al. Association of loss of heterozygosity at the p53 locus with chemoresistance in osteosarcomas. *Cancer Science* 1998;89(5):539-47.
252. Asada N, Tsuchiya H, Tomita K. De novo deletions of p53 gene and wild-type p53 correlate with acquired cisplatin-resistance in human osteosarcoma OST cell line. *Anticancer Research* 1999;19(6B):5131-7.
253. Gagiannis S, Müller M, Uhlemann S, Koch A, Melino G, Krammer PH, et al. Parathyroid hormone-related protein confers chemoresistance by blocking apoptosis signaling via death receptors and mitochondria. *International Journal of Cancer* 2009;125(7):1551-7.
254. Song B, Wang Y, Xi Y, Kudo K, Bruheim S, Botchkina GI, et al. Mechanism of chemoresistance mediated by miR-140 in human osteosarcoma and colon cancer cells. *Oncogene* 2009;28(46):4065-74.

255. Song B, Wang Y, Titmus MA, Botchkina G, Formentini A, Kornmann M, et al. Molecular mechanism of chemoresistance by miR-215 in osteosarcoma and colon cancer cells. *Molecular Cancer* 2010;9(96).
256. Takeshita H, Kusuzaki K, Ashihara T, Gebhardt MC, Mankin HJ, Hirasawa Y. Intrinsic resistance to chemotherapeutic agents in murine osteosarcoma cells. *The Journal of Bone and Joint Surgery* 2000;82(7):936-69.
257. Gomes CMF, van Paassen H, Romeo S, Welling MM, Feitsma RIJ, Abrunhosa AJ, et al. Multidrug resistance mediated by ABC transporters in osteosarcoma cell lines: mRNA analysis and functional radiotracer studies. *Nuclear medicine and biology* 2006;33(7):831-40.
258. Wang G, Rong J, Zhou Z, Duo J. A novel gene P28GANK confers multidrug resistance by modulating the expression of MDR-1, Bcl-2, and bax in osteosarcoma cells. *Molecular Biology* 2000;44(6):898-906.
259. Huang G, Mills L, Worth LL. Expression of human glutathione S-transferase P1 mediates the chemosensitivity of osteosarcoma cells. *Molecular Cancer Therapeutics* 2007;6(5):1610-9.
260. Yin Z, Ivanov VN, Habelhah H, Tew K, Ronai Ze. Glutathione S-Transferase P elicits protection against H₂O₂-induced cell death via coordinated regulation of stress kinases. *Cancer Research* 2000;60(15):4053-7.
261. Bruheim S, Xi Y, Ju J, Fodstad O. Gene expression profiles classify human osteosarcoma xenografts according to sensitivity to doxorubicin, cisplatin, and ifosfamide. *Clinical Cancer Research* 2009;15(23):7161-9.
262. Man T-K, Chintagumpala M, Visvanathan J, Shen J, Perlaky L, Hicks J, et al. Expression profiles of osteosarcoma that can predict response to chemotherapy. *Cancer Research* 2005;65(18):8142-50.
263. Mintz MB, Sowers R, Brown KM, Hilmer SC, Mazza B, Huvos AG, et al. An expression signature classifies chemotherapy-resistant pediatric osteosarcoma. *Cancer Research* 2005;65(5):1748-54.
264. Ochi K, Daigo Y, Katagiri T, Nagayama S, Tsunoda T, Myoui A, et al. Prediction of response to neoadjuvant chemotherapy for osteosarcoma by gene-expression profiles. *International Journal of Oncology* 2004;24(3):647-55.
265. Selvarajah GT, Kirpensteijn J, Wolferen MEv, Rao NA, Fieten H, Mol JA. Gene expression profiling of canine osteosarcoma reveals genes associated with short and long survival times. *Molecular Cancer* 2009;8:72-90.

266. Walters DK, Steinmann P, Langsam B, Schmutz S, Born W, Fuchs B. Identification of potential chemoresistance genes in osteosarcoma. *Anticancer Research* 2008;28(2A):673-80.
267. Wittenburg LA. Chemosensitization of osteosarcoma by the histone deacetylase inhibitor valproic acid. Fort Collins, CO: Colorado State University; 2010.
268. American Type Culture Collection Standards Development Organization Workgroup ASN-0002: 2010, cell line misidentification: the beginning of the end. *Nature Reviews Cancer*;10(6):441-8.
269. Gartler SM. Apparent HeLa cell contamination of human heteroploid cell lines. *Nature* 1968;217(5130):750-1.
270. Lacroix M. Persistent use of “false” cell lines. *International Journal of Cancer* 2008;122(1):1-4.

Chapter 2

Expression profiling in canine osteosarcoma: identification of biomarkers and pathways associated with outcome

SYNOPSIS

Background: Osteosarcoma (OSA) spontaneously arises in the appendicular skeleton of large breed dogs and shares many physiological and molecular biological characteristics with human OSA. The standard treatment for OSA in both species is amputation or limb-sparing surgery, followed by chemotherapy. Unfortunately, OSA is an aggressive cancer with a high metastatic rate. Characterization of OSA with regard to its metastatic potential and chemotherapeutic resistance will improve both prognostic capabilities and treatment modalities. **Methods:** We analyzed archived primary OSA tissue from dogs treated with limb amputation followed by doxorubicin or platinum-based drug chemotherapy. Samples were selected from two groups: dogs with disease free intervals (DFI) of less than 100 days (n=8) and greater than 300 days (n=7). Gene expression was assessed with Affymetrix Canine 2.0 microarrays and analyzed with a two-tailed t-test. A subset of genes was confirmed using qRT-PCR and used in classification analysis to predict prognosis. Systems-based gene ontology analysis was conducted on genes selected using a standard J5 metric. The genes identified using this approach were

converted to their human homologues and assigned to functional pathways using the GeneGo MetaCore platform. **Results:** Potential biomarkers were identified using gene expression microarray analysis and 11 differentially expressed ($p < 0.05$) genes were validated with qRT-PCR ($n = 10/\text{group}$). Statistical classification models using the qRT-PCR profiles predicted patient outcomes with 100% accuracy in the training set and up to 90% accuracy upon stratified cross validation. Pathway analysis revealed alterations in pathways associated with oxidative phosphorylation, hedgehog and parathyroid hormone signaling, cAMP/Protein Kinase A (PKA) signaling, immune responses, cytoskeletal remodeling and focal adhesion. **Conclusions:** This profiling study has identified potential new biomarkers to predict patient outcome in OSA and new pathways that may be targeted for therapeutic intervention.

INTRODUCTION

Osteosarcoma (OSA) is the most common malignant primary bone tumor of children and accounts for roughly 5% of all childhood cancers in the United States. Characteristically, OSA is found in the metaphyseal regions of long bones in the appendicular skeleton. More than 15% of patients present with clinically detectable pulmonary metastases and it is estimated that 80% or more have micrometastases at presentation (1). Advances in treatment such as multi-agent chemotherapy have improved prognosis over the last several decades with five-year survival rates up to 70%. Despite these advances, patients that present with metastases or those whose tumors are refractory to neoadjuvant chemotherapy continue to have a poor prognosis (1). This suggests that within the same histologic type of tumor, different genetic mechanisms may

be operating, altering response to chemotherapy and metastatic capability in some tumors.

Osteosarcoma is also the most common primary bone malignancy in dogs. The majority of these tumors occur in the appendicular skeleton of middle-aged large and giant breeds. Roughly 10,000 new cases of OSA are identified in dogs annually. Standard treatment involves amputation or limb-sparing surgery followed by adjuvant chemotherapy with doxorubicin, a platinum-based drug, or a combination of the two drug types (2). Median disease-free interval (DFI) following amputation has ranged from 165 to 470 days depending on adjuvant chemotherapy protocol and study size (3-7). Median survival time in dogs undergoing amputation alone ranges from 134 to 175 days (3-7). Like their human companions, pulmonary metastases are typically the cause of terminal morbidity. It has been suggested that up to 90% of canine patients may present with microscopic metastases that are undetectable via routine imaging (2). The high variability in DFI suggests that canine OSA exhibits variable metastatic capability, rate and/or resistance to adjuvant chemotherapy, similar to the disease in humans.

Canine OSA shares many features with human OSA, making dogs a valuable comparative model. Pet dogs develop OSA primarily in the metaphyseal regions of long bones, as do human patients. The lesions are histologically identical (2). The similarities between the molecular characteristics of human and canine OSA have been established (see (8) for review). Furthermore, Thomas and colleagues recently demonstrated that some of the same genetic aberrations identified in human OSA are also seen in canine OSA with both breed-dependent and independent associations (9). Among the genetic changes identified, Wilms tumor 1 (*WT1*), tumor protein p53 (*TP53*), cyclin-dependent

kinase inhibitor 2A (*CDKN2A*), phosphatase and tensin homolog (*PTEN*) and retinoblastoma 1 (*RBI*) tumor suppressors as well as v-myc myelocytomatosis viral oncogene homolog (*MYC*) and v-kit Hardy-Zuckerman 4 feline sarcoma viral oncogene homolog (*KIT*) oncogenes were shown to be affected by cytogenetic abnormalities in 76% of their samples (9). Similarly, comparative analysis of gene expression profiles in human and canine OSA determined that the diseases were indistinguishable by hierarchical clustering (10). Treatment and chemotherapeutic regimens are also similar with the notable exception that most amputee dogs do not undergo neoadjuvant chemotherapy, so tumors collected at the time of amputation are naïve to drugs. Dogs also provide a valuable model system in that their tumors arise “naturally,” they share an environment with humans, and they metabolize drugs at a similar rate. Finally, dogs are more genetically diverse than mouse model systems and share more genetic homology with humans than mice (8). Thus, genetic prognostic screening in dogs has strong potential applicability to the human disease (11).

In recent years, it has become clear that the tumor microenvironment plays a strong role in metastatic events even if metastatic subclones are only a small proportion of tumor cells (12, 13). For example, van de Vijver and colleagues demonstrated that gene expression analysis of primary tumors can divide breast cancer patients into “good” and “poor” prognostic groups based on the tumors’ intrinsic metastatic ability (14). Thus, gene expression profiles of primary tumors provide information about metastatic potential and patient prognosis even if distant disease is not detectable or present.

Gene expression analysis of primary tumors can also elucidate novel chemotherapeutic targets by defining individual gene changes and/or whole pathway

derangements (15, 16). Identification of such differences between “good” and “poor” prognostic groups in OSA will allow for more personalized treatment of disease based on an individual’s tumor expression profile.

The current study utilized Affymetrix GeneChip Canine Genome 2.0 arrays to explore differences in gene expression between primary OSA tumors taken from client dogs with a DFI of less than 100 days (“poor responders”) and those with a DFI greater than 300 days (“good responders”) following definitive treatment and chemotherapy. Individual genes with significant changes in expression were validated using qRT-PCR and explored for their ability to correctly classify good and poor responders using four different machine learning schemes. A broader, systems approach was used to identify changes in groups of interacting genes or pathways that may contribute to metastatic progression and resistance to therapy. We have found evidence of altered expression of several genes and pathways and have verified that the Hedgehog signaling pathway is comparatively downregulated in the poor responding group.

METHODS

Chemotherapy-naïve primary tumor samples were selected from the Colorado State University Animal Cancer Center’s tissue archive based on the criteria that the patient had undergone surgical amputation followed by chemotherapy with doxorubicin and/or a platinum-based drug (Table 2.1). Limb-spare surgical samples were excluded from the study as differences in DFI are associated with post operative infections common to the procedure (17, 18). Samples were collected at the time of amputation with the written consent of the owners (between 1996 and 2006), flash-frozen in liquid

Table 2.1 – Study Population.

Unique ID	DFI	Age at Dx (yrs)	Sex	Breed	Tumor Site	Tumor Subtype	Chemotherapy Received
184844	40	4.4	MC	Greyhound	L Prox Humerus	Osteoblastic	Doxorubicin
208911	60	8.0	FS	Doberman	L Prox Humerus	Giant cell	Carboplatin
173175	69	5.0	MC	Rottweiler	L Dist Femur	Osteoblastic	Cisplatin
223986	77	7.0	MC	Greyhound	L Dist Femur	Osteoblastic	Carboplatin
153599	90	9.0	FS	Mix	L Tibia	Giant cell	Cisplatin
222189	91	6.1	FS	Greyhound	L Prox Humerus	Osteoblastic	Doxo & Carbo
204714	94	8.0	FS	Greyhound	L Prox Tibia	Giant Cell	Doxorubicin
208756	95	10.2	FS	Labrador Ret.	L Dist Humerus	Osteoblastic	Cisplatin
146719	97	8.8	MC	Mix	R Dist Femur	Fibroblastic	Doxorubicin
212759	97	10.8	MC	Golden Ret.	L Prox Humerus	Osteoblastic	Doxorubicin
177466	307	7.6	FS	Mix	L Dist Radius	Osteoblastic	Cisplatin
188084	329	10.4	MC	Rottweiler	R Dist Radius	PD	Doxorubicin
190030	356	13.4	MC	Mix	L Dist Humerus	Osteoblastic	Doxorubicin
180223	384	11.5	FS	Mix	R Prox Femur	Osteoblastic	Cisplatin
208513	467	7.1	MC	Greyhound	L Prox Humerus	Osteoblastic	Doxorubicin
180119	619	10.4	FS	Mix	R Dist Femur	Osteoblastic	Cisplatin
193231	694	12.4	MC	Mix	L Dist Radius	Osteoblastic	Doxorubicin
174513	734	10.1	FS	Malamute	L Dist Radius	Osteoblastic	Doxo & Carbo
155214	787	8.7	MC	Labrador Ret.	R Tibia	Osteoblastic	Doxorubicin
168327	885	8.0	FS	Golden Ret.	L Dist Radius	Osteoblastic	Carboplatin

DFI = disease-free interval, Dx = diagnosis, MC = castrated male, FS = spayed female, L = left, Dist = distal, Prox = proximal, R = right, PD = poorly-differentiated, “Doxo & Carbo” = Doxorubicin and Carboplatin combination therapy,

nitrogen and stored at -80°C. Disease-free intervals (DFI) were calculated based upon the presence of metastatic disease and samples were divided into cohorts of DFI<100 days and DFI>300 days. These cohorts were defined to select samples distant from the median DFI of 200 days so that expression differences could be analyzed in very good and very poor responders.

Samples were freeze-fractured, homogenized, extracted with Trizol reagent (Invitrogen, Carlsbad, CA, USA) and purified with RNeasy clean up (Qiagen, Valencia, CA, USA) per the manufacturers' protocols. Resultant RNA was quantified via spectrophotometry and assayed for quality on Agilent (Santa Clara, CA, USA) and Bio-Rad (Hercules, CA, USA) bioanalyzers at the Rocky Mountain Regional Center for Excellence (RMRCE) Genomics Core at CSU. Only samples exhibiting minimal degradation as evidenced by RNA Integrity Numbers (RIN) greater than 8 were used for microarrays.

Eight samples from each DFI cohort were selected and array analysis with GeneChip Canine 2.0 Genome Arrays (Affymetrix, Santa Clara, CA, USA) was performed in two batches (batch 1, n=6; batch 2, n=10) at CSU's RMRCE Genomics Core per Affymetrix protocols. One sample was removed from analysis after data collection based upon pathologist review and review of hospital records that determined the sample was not OSA but hyperreactive osteoid tissue. Briefly, the One-Cycle Target Labeling and Control Reagents package (Affymetrix, Santa Clara, CA, USA) was used to synthesize cDNA from total RNA spiked with prokaryotic Poly-A RNA as a control. The Sample Cleanup Module (Affymetrix, Santa Clara, CA, USA) was used to purify the cDNA which was then used for synthesis of biotin-labeled cRNA. cRNA was purified, quantified and fragmented before hybridization with the GeneChips. Hybridized chips were washed, stained using streptavidin-conjugated phycoerythrin dye (Invitrogen, Carlsbad, CA, USA) and enhanced with biotinylated goat anti-streptavidin antibody (Vector Laboratories, Burlingame, CA, USA) using an Affymetrix GeneChip Fluidics

Station 450 and Genechip Operating Software. The Affymetrix GeneChip scanner 3000 was used to acquire images.

Microarray data was preprocessed using Probe Logarithmic Intensity Error (PLIER) estimation (19) and Robust Multichip Average (RMA) (20) algorithms with \log_2 transformations. PLIER and RMA methods were compared as part of the data discovery. A standard unpaired 2-tailed t-test with a false discovery rate correction for multiple comparisons was used. Uncorrected p-values were used to rank probesets. CIMminer was used to generate clustered images of the data with the following parameters: unsupervised clustering on both axes, average linkage and Euclidean distance (21).

Quantitative RT-PCR was performed on an expanded set of 20 OSA samples including the same 15 samples used in the array analysis plus an additional five samples that met the selection criteria of amputation, chemotherapy, appendicular location of tumor and DFI (n=3 in the DFI>300 cohort and n=2 in the DFI<100 cohort). These additional 5 samples increased the number of samples in each cohort to ten. The sample set was expanded so that expression of genes of interest could be assessed in independent samples in addition to those from the microarray study. cDNA was synthesized using the QuantiTect Reverse Transcription Kit (Qiagen, Valencia, CA, USA) with 1 μ g input RNA. Quantitative real time PCR was performed in duplicate using iQ SYBR Green Supermix (Bio-Rad, Hercules, CA, USA) and 25 ng equivalent RNA input in 25 μ L reactions on a Stratagene Mx3000P instrument. Thermal cycling was performed on the Mx3000p instrument (Stratagene) with the following parameters: 95°C for 10m followed by 40 cycles of 95°C for 30s and 60°C for one minute. Data collection was performed at the end of the 60°C step. Dissociation curve ramps were performed at the end of the

cycle to verify that only a single product was generated. Data analysis was performed with the Mx3000p software. Primers (Table 2.2) were designed based upon NCBI RefSeq mRNA sequences with PrimerQuest (Integrated DNA Technologies, Coralville, IA, USA) and were cross-checked for specificity using UCSC In-Silico PCR (22, 23).

Where possible, primers were designed to be intron spanning and in a central

Table 2.2 – Primer sequences and amplicon size for selected genes.

Primer	Sequence (5' to 3')	Size of Amplicon
HPRT1 S	TGC TCG AGA TGT GAT GAA GG	191 bp
HPRT1 AS	TCC CCT GTT GAC TGG TCA TT	
ADHFE1 S	CCA ACA GTG GCT TCG ATG TGC TTT	104 bp
ADHFE1 AS	TGC TGG CCG AGT GAT AGG ATT TGA	
AGTR1 S	TGA CTT TGC CAC TAT GGG CTG TCT	178 bp
AGTR1 AS	AGG CGG GAC TTC ATT GGA TGA ACA	
CCDC3 S	TGA ACC AGA AGC TCA GCG AGA AGT	162 bp
CCDC3 AS	TAG ATT CCC TGG CAA GAG GCA ACA	
DHH S	ACA ACC CGG ACA TCA TCT TCA AGG	109 bp
DHH AS	ATG TTC ATC ACC GCA ATG GCC AAG	
FBP1 S	TCC TGT ACC CAG CGA ACA AGA AGA	89 bp
FBP1 AS	TGC CTT CTC CAT GAT GTA GGC CAT	
IGF2 S	TCG TGG AAG AGT GCT GTT TCC GTA	154 bp
IGF2 AS	TCG TAT TGG AAG AAC TTG CCC ACG	
IMP1 S	TTG CAG AAT TTG ACA GCG GCT GAG	118 bp
IMP1 AS	TTT GGT GCA GCT GCT TAA CTT GGG	
NDRG2 S	ATA AGT CTT GCT TCC AGC CGC TCT	183 bp
NDRG2 AS	TCA GGT ACT GCA GAA TGC AAG GGA	
PTCH2 S	CAT ATT CCT GCT GGC ACA TGC CTT	229 bp
PTCH2 AS	GAA GAC AAG CAT CAC GGC TGC AAA	
SCN1B S	TCG TGG CAG AGA TGG TTT ACT GCT	121 bp
SCN1B AS	ACA CCC GTA CAG TTC TCC TTG CTT	
SMO S	TGG TGC TCA TTG TGG GAG GTT ACT	210 bp
SMO AS	ACT CAG CCT GGT TGA AGA AGT CGT	

S = sense, AS = antisense, bp = base pairs

region of the gene. Primers were designed to amplify all possible isoforms noted in NCBI and were not specific to the Affymetrix probe region. Expression levels were normalized to hypoxanthine phosphoribosyltransferase 1 (HPRT1) expression as it was consistently expressed at a moderate level in our arrays and has previously been used as a canine housekeeping gene (24) (primer sequences courtesy of Dr. Luke Wittenburg, CSU). Standard curves, dissociation curves and amplification data were collected using Mx3000P (Stratagene, La Jolla, CA, USA) software and analyzed with the $2^{(-\Delta\Delta Ct)}$ method (25) followed by an unpaired 2-tailed t-test as well as REST2009 software (26, 27). In all cases, amplification efficiencies were greater than 90%. Quantitative RT-PCR products were electrophoresed on a 2% agarose gel in 1x TBE and visualized under UV light with ethidium bromide to verify product size.

The pathway analysis pipeline used in this study has been previously described (28). Briefly, the University of Pittsburgh Gene Expression Data Analysis suite (caGEDA) (29) with a standard J5 metric, a threshold of 4 and a jackknife of 4 was used to select unique genes for pathway analysis following both PLIER and RMA preprocessing. The DAVID Gene ID conversion tool was used to link canine identifiers to their human counterparts (30, 31) and identifiers absent from the database were hand-annotated by BLAST and BLAT comparisons of the target sequence; GeneGo MetaCore was used to assign functional pathways. Pathways were assigned independently to PLIER and RMA preprocessed data and the resulting pathways were compared.

WEKA software was used to generate classification models to test the analytical value of qRT-PCR-derived expression changes (32). Classification models were built using a Support Vector Machine (SVM), a J48 decision tree, and logistic regression (33).

Models were generated with the full (n=20) data set and tested for sensitivity and specificity using stratified tenfold cross-validation. Tenfold cross-validation randomly selects 90% of the data for training the model, and uses the other 10% of the data to test the model. The process is repeated ten times and the ten model error rates are averaged to compute an overall error rate.

RESULTS

Tumor Donors

The DFI<100 group was composed of 5 castrated males and 5 spayed females with an average age of 7.73 years (range: 4.4-10.8) at the time of diagnosis. The DFI>300 group was also composed of 5 castrated males and 5 spayed females with an average age of 9.96 years (range: 7.1-13.4) at the time of diagnosis. The samples used in the microarray study were a subset of these as described in the “Methods” section. Dog breed, chemotherapy type, tumor phenotype and tumor location are included in Table 1.

Affymetrix Canine 2.0 Genome Array Analysis

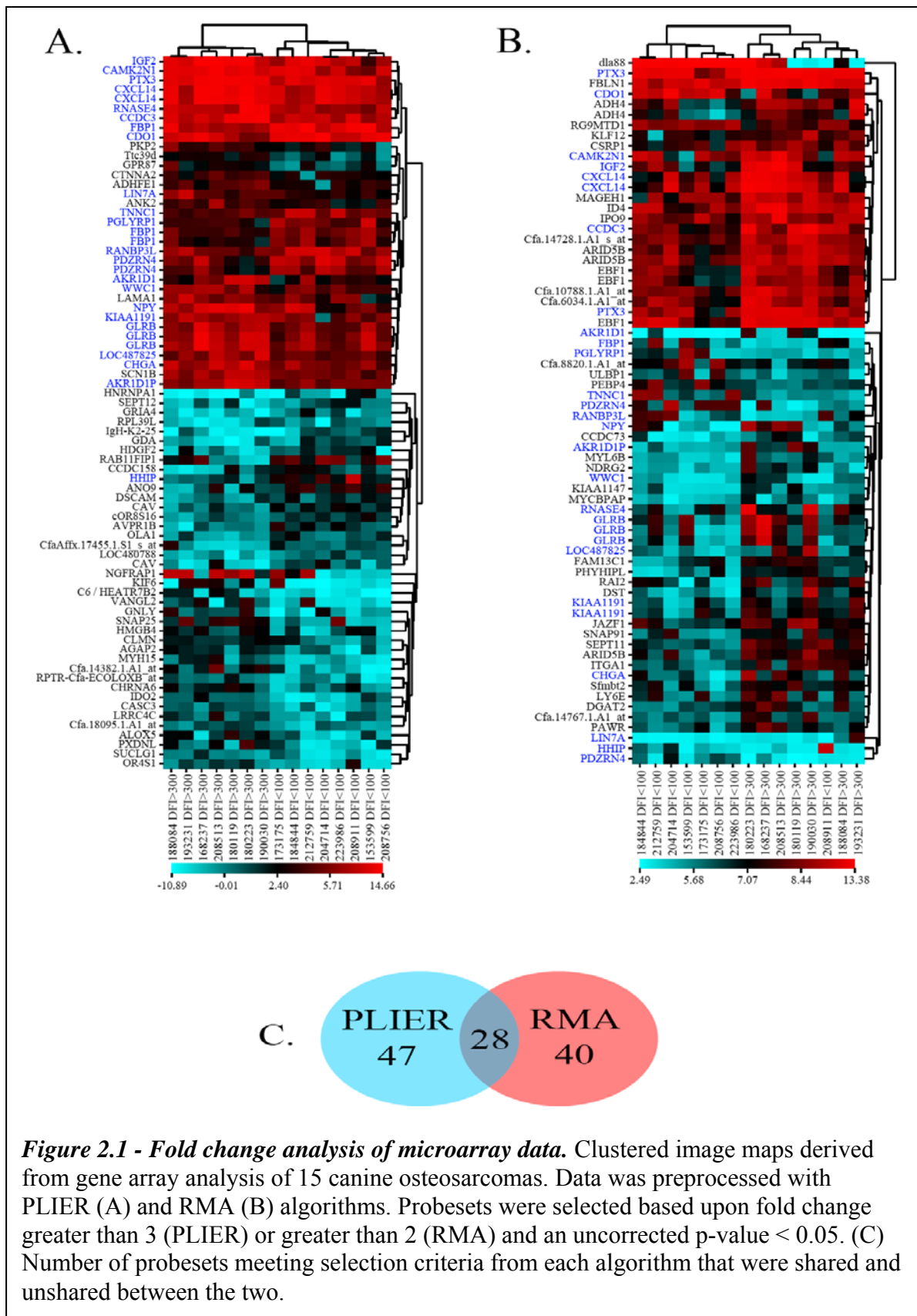
Criteria for assessing differential regulation of probesets were based on the preprocessing algorithm used as both PLIER and RMA have benefits and drawbacks. Briefly, PLIER exhibits higher signal reproducibility and differential sensitivity for low expressing genes yet the variance can be unstable on a log scale, whereas RMA demonstrates fold change compression at the low end of expression, but the variance is stable on a log scale (19). Thus, selection criteria for genes to validate with qRT-PCR were: PLIER fold change greater than 3 with an uncorrected p-value less than 0.05 and/or RMA fold change greater than 2 with an uncorrected p-value less than 0.05. False

discovery rate correction yielded no significant genes so uncorrected p-values were used: this is not surprising in this natural, diverse patient population.

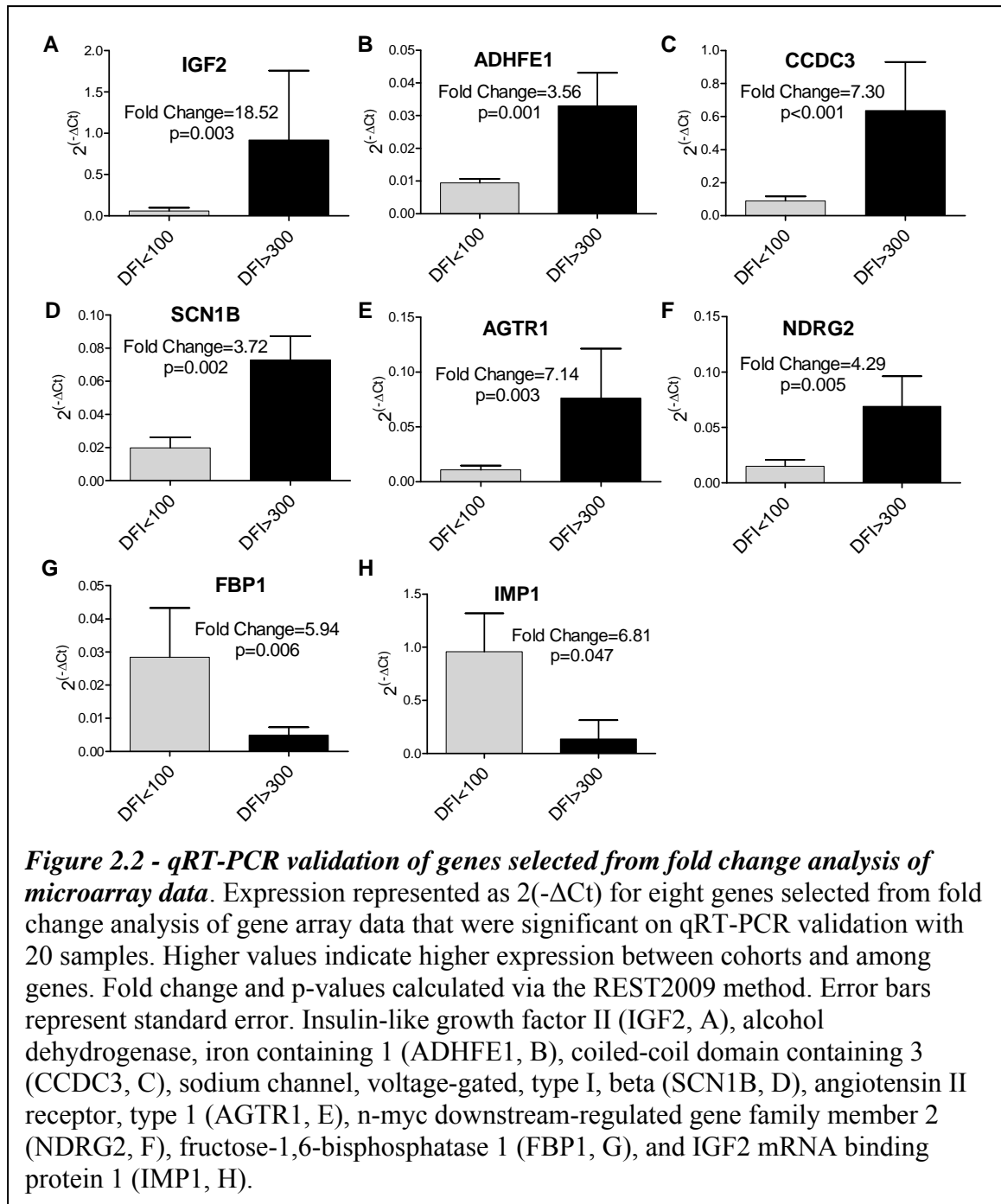
Affymetrix Canine 2.0 gene array analysis yielded 75 probesets matching the PLIER criteria and 68 probesets matching the RMA criteria. Twenty-eight probesets and twenty-three genes were shared (Figure 2.1A & 2.1B, blue labels) between the two selection criteria yielding 115 total probesets for further investigation (Figure 2.1C). Unsupervised hierarchical clustering of the 75 PLIER-selected probesets grouped the dogs according to their respective disease free interval groups (Figure 2.1A, X-axis). This hierarchical clustering also grouped the probesets relative to fold change differences between the DFI<100 day group and the DFI>300 day group (Figure 2.1A, Y-axis). This pattern indicates that, based on the genes showing the greatest expression differences, dogs that have a longer disease-free interval (X-axis, left half) have more-similar primary tumor gene expression to each other than to dogs with a short DFI (X-axis, right half), even those of the same breed. Hierarchical clustering of the 68 RMA-selected probesets yielded similar results with all but one of the dogs (208911 DFI<100) clustering in their respective DFI groups. (Figure 2.1B). The differences in sample clustering, the ranges of expressed values, and the differences in shared gene clustering (i.e. genes shared between the two algorithms are clustered primarily in half of the PLIER dendrogram but spread throughout the RMA dendrogram) underscore the fact that different algorithms yield different results and illustrate the value of applying multiple algorithms.

Quantitative RT-PCR Analysis of Putative Biomarkers and Array Validation

Thirty-six genes were assayed for expression via qRT-PCR in 20 OSA samples to both correlate array data to qRT-PCR as well as explore potential biomarker expression



via a method not subject to multiple sampling errors. Of these, 8 demonstrated significantly different ($p < 0.05$) expression between the two cohorts as calculated by both the $2^{(-\Delta\Delta Ct)}$ method (25) with a 2-tailed t-test and the REST2009 (27) iterative method that accounts for amplification efficiency. qRT-PCR expression is plotted as $2^{(-\Delta Ct)}$ in Figure 2.2. Higher expression levels between cohorts and among genes can be visualized as an increased $2^{(-\Delta Ct)}$ value. Fold changes and statistical calculations stated in the text were calculated with REST2009 as this program consistently demonstrated higher stringency for significance than the $2^{(-\Delta\Delta Ct)}$ method with t-test. We observed significant down-regulation of insulin-like growth factor II (IGF2, fold change=18.52, $p=0.003$, Figure 2.2A) in our poor-responder cohort (DFI <100). Other significantly down-regulated genes in the DFI <100 cohort were: alcohol dehydrogenase, iron containing 1 (ADHFE1, fold change=3.56, $p=0.001$, Figure 2.2B), coiled-coil domain containing 3 (CCDC3, fold change=7.30, $p < 0.001$, Figure 2.2C), sodium channel, voltage-gated, type I, beta (SCN1B, fold change= 3.72, $p=0.002$, Figure 2.2D), angiotensin II receptor, type 1 (AGTR1, fold change=7.14, $p=0.003$, Figure 2.2E), and n-myc downstream-regulated gene family member 2 (NDRG2, fold change=4.29, $p=0.005$, Figure 2.2F). Up-regulated genes in the DFI <100 cohort were: fructose-1,6-bisphosphatase 1 (FBP1, fold change=5.94, $p=0.006$, Figure 2.2G) and IGF2 mRNA binding protein 1 (IMP1, fold change=6.81, $p=0.047$, Figure 2.2H). The remaining 28 genes displayed qRT-PCR fold changes similar in amplitude and direction to at least one of the applicable Affymetrix probesets with only one exception. Although these genes did not meet significance criteria on qRT-PCR, there is a strong correlation between the qRT-PCR data and the microarray data (data not shown).



Pathway Analysis

Pathway analysis was utilized to examine the microarray data in a biologically relevant manner and to rule out the false positives commonly found in fold change analysis. To select differentially-expressed genes from the greater-than 40,000 probesets in an unbiased fashion, we utilized the J5 metric as described previously (29). For the PLIER-processed data, this yielded 3179 total probesets and 1783 unique annotated or identifiable gene identities with human homologs. The RMA-processed data yielded 1374 total probesets with 764 unique identifiers. Probesets that were not associated with a human homolog in the Affymetrix or DAVID databases were hand-annotated, where possible, using NCBI BLAST and/or UCSC BLAT. These datasets were then analyzed with the MetaCore platform to assign functional pathways to each individual dataset as well as to the identifiers common to both PLIER and RMA datasets. Figure 2.3 displays significantly altered pathways ($p < 0.001$) by ascending p-value for PLIER (a), RMA (b), and combined RMA/PLIER (c) analyses. Sixty-nine significant pathways were identified using the PLIER dataset (Figure 2.3A) and eight significant pathways were identified using the RMA dataset (Figure 2.3B). Analysis of identifiers common to both RMA and PLIER datasets yielded 379 shared identifiers and ten significant pathways (Figure 2.3C).

The pathway expression differences between good and poor responders primarily involved genes associated with oxidative phosphorylation, bone development, cAMP/Protein Kinase A (PKA) signaling, cell adhesion, cytoskeletal remodeling and immune response. Many of the pathways show modulation in commonly observed “cancer” signatures including matrix metalloproteinases, transforming growth factors, wntless-type MMTV integration site family members (WNTs) and nuclear factor kappa-

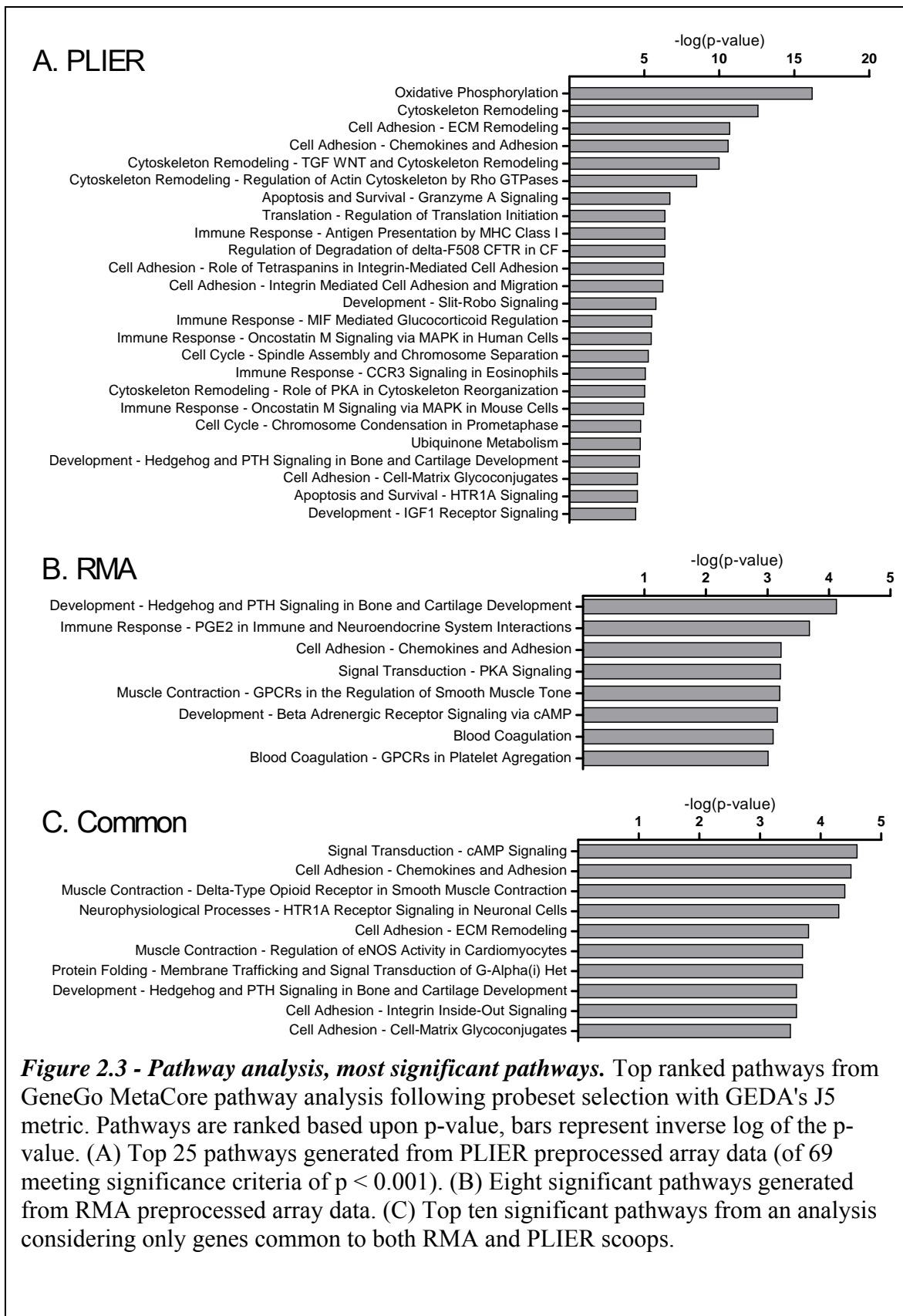


Figure 2.3 - Pathway analysis, most significant pathways. Top ranked pathways from GeneGo MetaCore pathway analysis following probeset selection with GEDA's J5 metric. Pathways are ranked based upon p-value, bars represent inverse log of the p-value. (A) Top 25 pathways generated from PLIER preprocessed array data (of 69 meeting significance criteria of $p < 0.001$). (B) Eight significant pathways generated from RMA preprocessed array data. (C) Top ten significant pathways from an analysis considering only genes common to both RMA and PLIER scoops.

light-chain-enhancer of activated B cells (NF- κ B) downstream targets, as well as actin and myosin cytoskeletal components (Appendix A, Figures A.1-A.3).

qRT-PCR Analysis of the Hedgehog Pathway

The identification of hedgehog pathway components in each pathway (Figure 2.4) and fold change analysis (HHIP, Figure 2.1A and 2.1B), led us to examine expression of nine genes in the pathway via qRT-PCR: hedgehog interacting protein (HHIP), patched (PTCH1 and PTCH2), smoothed (SMO), glioma-associated oncogene family zinc fingers (GLI1 and GLI3), and hedgehog ligands (DHH, SHH, and IHH). Three of these

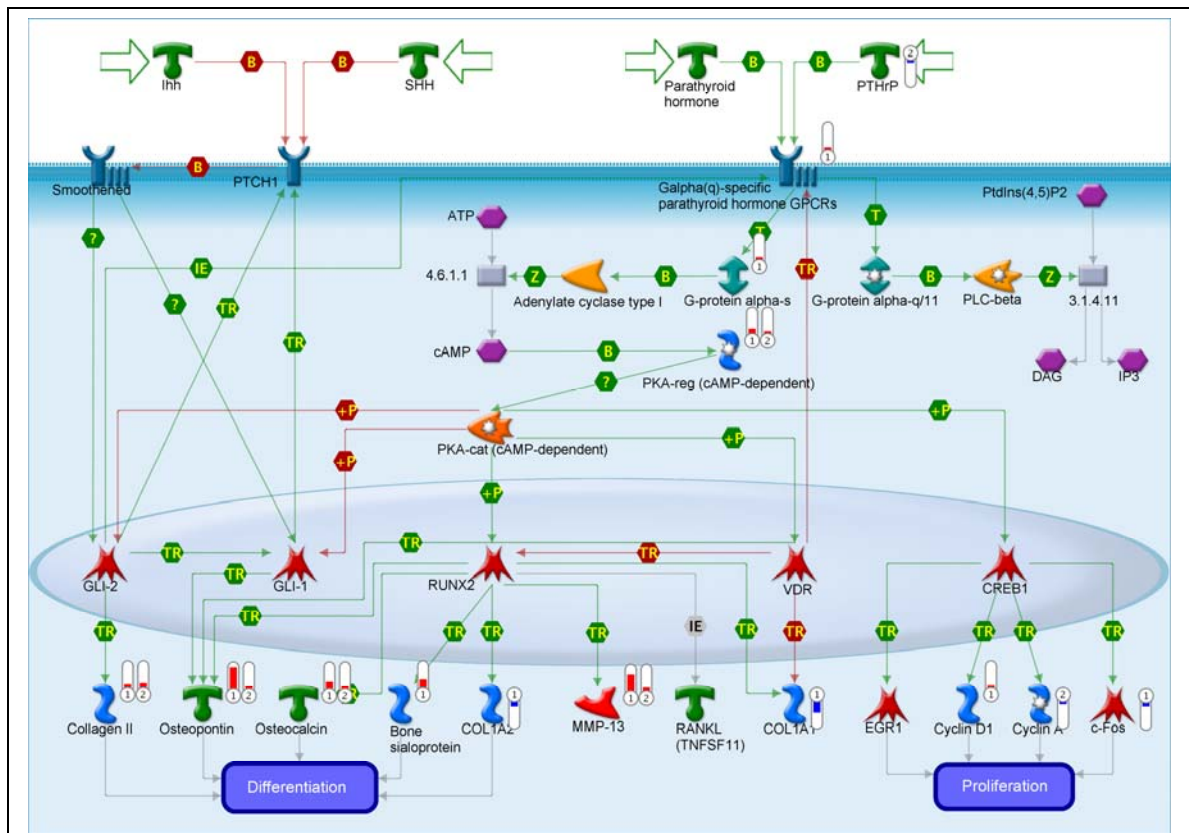
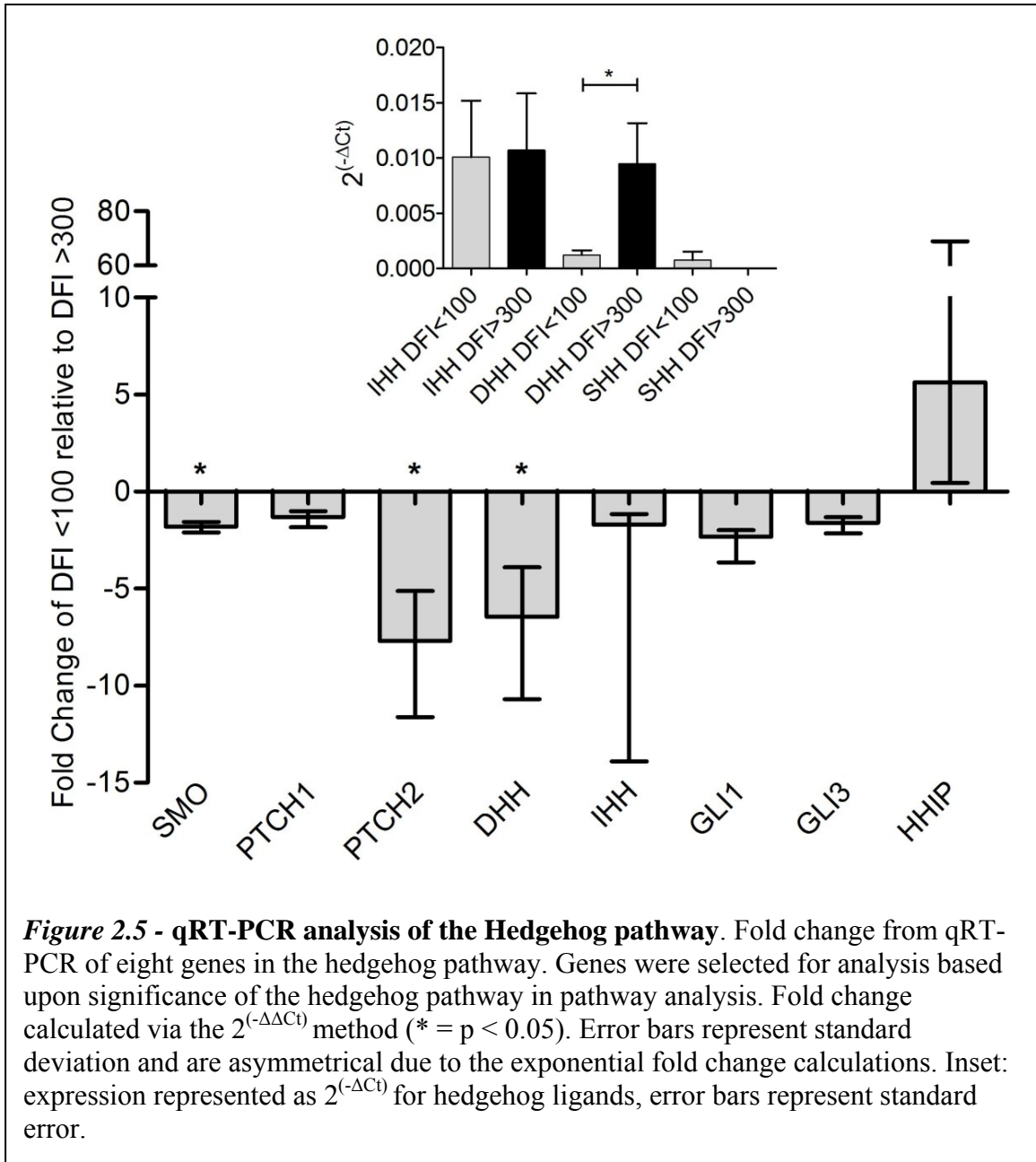


Figure 2.4 - Hedgehog and Parathyroid Hormone Signaling Pathways in Bone and Cartilage Development. Red symbols indicate degree of up-regulation of gene target in DFI < 100 days relative to DFI > 300 days, blue symbols indicate relative down-regulation. Numbers in symbols indicate specific array processing algorithm, 1 = PLIER, 2 = RMA.

genes, DHH, SMO, and PTCH2, demonstrated significant down-regulation in the poor-responder cohort (Figure 2.5). Sonic hedgehog was unexpressed in 17 of 20 samples and only minimally expressed in the remaining three (Figure 2.5 inset).



Data Classification

Four classification models were generated based on the qRT-PCR gene expression patterns of fifteen genes, the eleven significant genes plus four genes that were members of the Hedgehog signaling pathway or were selected in the fold-change analysis of both the RMA and PLIER normalized data sets: GLI3, HHIP, RAN binding protein 3-like (RANBP3L) and peptidoglycan recognition protein 1 (PGLYRP1). The accuracies for each of these models during model generation and cross validation are listed (Table 2.3). Stratified cross-validation in each of these models was repeated 10

Table 2.3 – Results of classification modeling.

	<u>Classifier Model</u>			
	J48 Decision Tree (15 Genes)	Support Vector Machine (15 Genes)	Logistic Regression (3 Genes)	Support Vector Machine (3 Genes)
Full Training Set ^a	100% ^c	100%	100%	100%
Stratified Cross-Validation ^b	75%	90%	90%	90%

^a Full training sets included data for all 20 samples to both build and test the model.

^b Stratified cross-validation models were built with 90% of the samples and tested with the remaining 10% through multiple iterations.

^c Percent of samples correctly classified by the model.

times using 90% of the samples to train the model and 10% to test the model. The J48 decision tree selected two genes that were most predictive for all samples: ADHFE1 and NDRG2. It successfully predicted cohort for all of the 20 samples. When the same model was built with stratified cross-validation using 90% of samples to train the model and 10% to test the model, it predicted cohort with a 75% success rate. A Support Vector Machine algorithm was used to generate two models. The first, incorporating all 15

genes, predicted cohort with a 100% success rate and 90% in cross-validation. The second SVM model incorporated only the 3 most heavily weighted genes from the previous model, CCDC3, FBP1 and ADHFE1. It also predicted cohort with 100% success rate and 90% in cross-validation. Logistic regression including the three most predictive genes from the SVM model predicted cohort with a 100% success rate and 90% in cross-validation.

DISCUSSION

In this study, we analyzed gene expression in chemotherapy-naïve primary OSA tumors from 20 dogs with the aim of identifying a gene signature of aggressive metastasis and/or resistance to chemotherapy following definitive treatment with limb amputation and adjuvant therapy with doxorubicin and/or a platinum drug. The purpose of this aim was 3-fold. First, it provides a basis for development of a prognostic screen; such a tool would be of great value to the clinicians diagnosing and treating the more than 8,000 new cases of canine OSA every year. Additionally, pet owners would benefit greatly from a more accurate projected survival time when weighing their dog's quality of life and their own monetary obligations in treatment decisions. Secondly, analysis of gene signatures may allow elucidation of single genes or genetic pathways that may be manipulated for treatment purposes. Finally, dogs are an excellent model for human OSA and identification of markers and pathways leading to disease progression and resistance to therapy in dogs may be translated to the pediatric clinical setting to improve prognosis and treatment of human OSA.

We utilized qRT-PCR to confirm the differential expression of eleven genes between primary OSA from good (DFI>300 days) and poor (DFI<100 days) responding dogs (Figs. 2 and 5). Transcriptional profiles of an additional 28 genes selected from fold change analysis of the microarray data were assessed via qRT-PCR and, although differential expression was observed in many, significance criteria for the qRT-PCR analysis were not met (data not shown). Nineteen of these qRT-PCR targets were selected for analysis before pathologist review identified one of the “tumors” as hyperplastic tissue without neoplasia. Removal of that sample and subsequent reprocessing of microarray data removed some of these targets from the RMA and PLIER fold change lists. Despite their failure to achieve significance in our fold-change analysis, the qRT-PCR data for these targets still correlates strongly with the array data on a sample-by-sample basis. Two of these genes, IMP1 and AGTR1, were verified as differentially expressed by qRT-PCR analysis (Figure 2), possibly due to the increased sample number used in each group for this analysis. From the additional 28 genes that failed to show statistically significant differences by qRT-PCR, eleven of these gene targets were selected by the fold change analysis of either RMA or PLIER processed data shown in Figure 1. The failure of these gene targets to reach significance in the qRT-PCR analysis may reflect the variability in microarray preprocessing algorithms as well as differences in expression values based on primer design as primers used in this study were not designed to align with Affymetrix probe locations. In addition, since our qRT-PCR analysis used a larger number of samples than the microarray study, some of the microarray hits may have been false positives that have now been removed from the list of putative biomarkers thanks to the qRT-PCR analysis.

Although these genes were primarily assessed by qRT-PCR for their prognostic potential, they may also have functional roles in metastatic progression and resistance to chemotherapy. IMP1 (6.93 fold up-regulated in the poor-responders), also known as IGF2BP1 and not to be confused with the family of IGF binding proteins, is a member of a family of three oncofetal proteins (IMP1-3) whose function is to bind and regulate mRNA stability in the cytoplasm during development. IMP1 expression is stimulated by Wnt/ β -catenin signaling and has many regulatory targets, some of which are implicated in cancer: stabilization of c-myc (34, 35) and CD44 mRNAs (36), translational suppression of IGF2 (37), and localization of β -actin mRNA to sites of actin polymerization (38). These targets can affect cell growth and survival as well as metastatic mechanisms such as invadopodia formation and cell adhesion (39). IMP1 over-expression has been associated with poor prognosis in numerous cancer types including human ovarian and colorectal carcinomas (39, 40).

IGF2 (15.4 fold down-regulated in the poor-responders) has been shown to be down-regulated in response to IMP1 as well as to hedgehog pathway inhibition and the observed alterations in these factors/pathways may account for some down-regulation of IGF2 (41). Additionally, IGF2 expression is modulated by numerous other factors including parathyroid hormone (PTH), cortisol, and transforming growth factor beta (TGF- β) (42). Finally, our pathway analysis shows reduction in PTH related protein (PTHrP) and subsequent modulation of the PTH pathway suggesting IGF2 may be comparatively under-expressed in poor-responders due to decreased PTHrP expression in that cohort. It is important to note that the observed down-regulation of IGF2 (and all

other genes discussed here) is relative between cohorts and that the mRNA was expressed in all samples, but to a lesser degree in poor-responders.

FBP1 (5.94 fold up-regulated in the poor-responders) is involved in gluconeogenesis and is expressed in the liver and, to a lesser extent, most other cell types. Its action opposes that of phosphofructokinase and its expression can lead to increased cellular glutathione and an apoptosis-resistant phenotype (43). Bigl and colleagues examined FBP1 expression in several types of breast cancer and found it to be up-regulated in invasive lobular carcinoma when compared to normal tissue but down-regulated in other tumor types suggesting a variable role depending on tumor type (44).

ADHFE1 is an iron-activated alcohol dehydrogenase with widely conserved motifs that is found in multiple tissue types. It has been shown to oxidize gamma-hydroxybutyrate and is 3.50 fold down-regulated in the poor-responders (45). CCDC3, also down-regulated in the poor-responders (7.10 fold), encodes a 270 amino acid protein with a putative coiled-coil domain near the C-terminus. Recent reports indicate that this protein is secreted by both adipocytes and endothelial cells and is under both hormonal and nutritional control (46). Interestingly, CCDC3 was identified as a factor contributing to ifosfamide resistance in a mouse xenograft model using human OSA cell lines. Bruheim and colleagues reported a 40-fold down-regulation of this gene in resistant tumor cells(47). As none of the dogs in the current study received ifosfamide, this gene may contribute generally to both metastasis and chemotherapeutic resistance.

Chioni *et al.* recently elucidated a role for SCN1B in cellular adhesion and migration in breast cancer cell lines. Their mildly metastatic cell line demonstrated increased expression of SCN1B compared to the highly metastatic cell line; furthermore,

siRNA-mediated knockdown of SCN1B decreased adhesion and increased migration in the mildly metastatic line (48). Our observed 3.70 fold down-regulation of SCN1B in the poor-responders indicates that the tumor environment may become more pro-migratory due to reduced expression of this factor.

The putative tumor suppressor gene NDRG2 (4.57 fold down-regulated in the poor-responders) is expressed in an inverse relationship to proliferation in normal tissues and has been observed to be down-regulated in numerous tumor types, especially in response to myc oncogene expression (See (49) for review). Recent cytogenetic analysis of canine OSA revealed breed independent myc amplification in 40% of the cases, suggesting this is a common chromosomal aberration in both canine (9) and human OSA (50). Tepel and colleagues demonstrated epigenetic promoter modifications as a mechanism for suppression of this gene in glioblastoma (51). Recent evidence has identified numerous mechanisms by which NDRG2 acts as a tumor suppressor and invasion attenuator: anti-proliferative suppression of AP-1 in colorectal carcinoma (52), anti-invasive suppression of NF- κ B in fibrosarcoma and melanoma cell lines (53), pro-apoptotic involvement in the p53 pathway (54), and reduction in invasion and intracellular β -catenin in NDRG2-transfected cell lines (55). Kim and colleagues demonstrated that NDRG2 expression decreases with increasing tumor stage in colon carcinoma, indicating that this may be an excellent marker for molecular staging (55). Furthermore, recent studies have shown that the myc oncogene stimulates mitochondrial glutaminolysis resulting in reprogramming of mitochondrial metabolism to depend on glutamine catabolism to sustain cellular viability (56). In support of this hypothesis, our

pathway analysis associated both upregulation of the Myc oncogene and alterations in mitochondrial oxidative phosphorylation with poor outcome.

To identify the prognostic potential of these genes, we built several classification models to identify genes with the most predictive power. Of the four models tested, all classified the samples with 100% accuracy when the model was built from all 20 samples. However, when stratified cross-validation was used, the two SVMs and the linear regression model were 90% correct whereas the J48 decision tree was only 75% correct. These stratified cross-validation results are generally thought to more accurately reflect results in subsequent applications of the model. The two SVM models classified with the same success rate regardless of whether built with all fifteen genes or the three most heavily weighted contributors, suggesting that CCDC3, ADHFE1 and FBP1 are highly predictive in this data set and are likely to be robust classifiers in future OSA studies.

While biomarker identification can be successful using traditional fold change methodology, as evidenced by our gene hits above, understanding of the processes of metastasis and chemoresistance can be furthered by all-inclusive pathway analysis. Thus, to eliminate some of the arbitrary nature of traditional fold change analysis, we also examined our microarray data via this methodology. Over 4,000 probesets were selected from microarray data using the J5 metric, annotated and converted to human identifiers using public-access tools including DAVID, and assigned to pathways with the GeneGo MetaCore program. This program assigns pathway significance based upon the number of genes represented within a pathway and the direction of change. The overwhelming benefit to this methodology is that change in a single gene will be ignored unless related

genes also demonstrate altered expression. Thus, the downstream impact of chip anomalies, probeset inefficiencies and differences in preprocessing algorithms can be dramatically reduced. This type of analysis allows integration of the typical microarray methodology examining highly expressed genes with the systems biology approach of examining large numbers of genes, some of which may be expressed only at low levels despite their importance to a given pathway (28). One pertinent example is PTEN deletion which was identified as a chromosomal aberration in 40 % of canine OSA (9). However, loss of PTEN was not detected in our fold change analysis, but was associated with poor outcome by pathway analysis (Additional File 2).

Although discussing each of the modulated pathways is beyond the scope of this study, some notable generalizations can be addressed. Cell adhesion and cytoskeletal remodeling are both strongly represented in pathways we have identified as significantly altered between our two cohorts; this suggests that the aggressiveness of tumor cells with regard to these two elements of metastasis may be just as important as chemoresistance mechanisms in this population. Bone-related developmental and immune-response pathways are also represented, much as one would expect in these osteoblastic/osteolytic tumors. Finally, cAMP/PKA signaling pathways also have strong representation in these analyses. Similar alterations in cAMP/PKA signaling with upregulation of the PKA regulatory subunit 1 α have been described in other cancers (57). However, the differences between good and poor responders are notable and provide evidence for variation in molecular phenotype contributing to aggressiveness within the same histologic subtype of tumor.

The pathway analysis converged with the traditional fold change analysis at the hedgehog signaling pathway. The hedgehog signaling pathway appears to act upstream of Wnt/ β -catenin signaling during bone development and aberrant hedgehog signaling has been associated with cancer development and progression (58). As a result, we decided to examine other genes in the hedgehog pathway with qRT-PCR. Of the eight hedgehog-related genes examined, three were significantly down regulated in the poor responder cohort. These three genes, SMO, PTCH2 and DHH, were not identified on traditional fold change analysis and this is likely due to two factors. First, DHH is not annotated in the canine genome so primers were designed based on a region of the canine genome homologous to the gene in other species. Considering this, the Canine 2.0 microarray does not have a probe for this gene. Probes were present for the SMO and PTCH2 genes, however, in this study, raw array expression values for these genes were very low suggesting that the signal may be nearing the detection limit of the microarrays.

Hedgehog interacting protein (HHIP) was identified by fold change criteria in both RMA and PLIER preprocessed arrays. The up-regulation in the poor responder cohort was also observed as a trend in qRT-PCR but did not meet significance criteria. HHIP antagonizes all three of the hedgehog family of ligands (SHH, DHH and IHH) and has been shown to be down-regulated in numerous epithelial tumor types (59) with the notable exception of basal cell carcinoma where it is upregulated (60). HHIP is also abundant in endothelial cells but is suppressed during angiogenesis through a VEGF mediated pathway (61). The up-regulation of HHIP observed in our poor-responders likely has some causative relationship to the down-regulation of DHH and, through feedback loops, SMO and PTCH2 in the same cohort.

Three studies have examined gene expression in primary human OSA to identify chemotherapy-resistance signatures by comparing good and poor responders (62-64). Among them, they identified over 200 differentially regulated genes but each gene set was unique to each study (i.e. there was no overlap in expression signatures). More recently, Walters and colleagues (65) assayed expression patterns in OSA cell lines with differing aggressiveness and identified 252 differentially regulated genes, four of which overlapped with the Mintz *et al.* study's gene signature (63). This lack of similarity in expression patterns is observed in array analyses of various tumor types and is not at all surprising when one contemplates the differences in array preprocessing algorithms. Considering the disparity between the heat maps presented in Figure 1A and 1B, it is plausible that the exact same data processed in two different ways may yield two very different sets of candidate genes. Thus, in addition to traditional fold change analysis of microarray data for biomarker identification, a broader, unbiased systems-biology approach, such as we have done here, is likely to identify biological changes that can be reliably verified in multiple data sets. In fact, this approach was used to analyze multiple independent data sets to show that genes involved in the oxidative phosphorylation pathway were reduced in metastases compared to primary solid carcinomas (28). Interestingly, in the current comparison of primary sarcomas, increased expression of genes in the oxidative phosphorylation pathway was associated with a poor outcome, suggesting that different metabolic factors may contribute to the initiation of metastasis from a primary tumor and the implantation and successful growth of metastasis at a distant site.

Given the small sample size of the study, we acknowledge that this data serves primarily as a road map for future studies. Our sample size was small primarily due to the stringent selection criteria set forth in Methods limiting our samples to dogs that had appendicular osteosarcoma, undergone amputation and received chemotherapy. Furthermore, we limited our samples to those from dogs with either very low or very high DFIs; the 100 and 300-day cutoffs were intended to straddle our facility's average DFI of 200 days. Selvarajah and colleagues recently studied gene expression in a group of dogs with OSA with good and poor outcome (66). They utilized a larger sample size (n=32) but included dogs with axial OSA as well as dogs that did not receive adjuvant chemotherapy. Although they did not observe differences in outcome due to these factors, previous studies have established an effect on DFI (2, 3, 5, 7). They also based their good and poor responder groups on survival time instead of DFI: this can greatly affect outcome groups in a field of medicine where euthanasia is practiced. Beyond study-design differences, we applied a systems-based model for biomarker/pathway discovery by using the J5 metric to enrich for high to medium expressing genes that are most appropriate for selection as diagnostic/prognostic biomarkers, as opposed to fold-change based input. Hand annotation of many probesets based upon sequence homology allowed us to input a very large and complete data set into the MetaCore pathway analysis. Despite these differences in study design and analysis methods, we identified some pathways with similarity to those they identified in their PANTHER analysis, including hedgehog signaling, WNT signaling and chemokine signaling. Considering the differences in chemotherapy requirements between the two studies, these pathways may

be most indicative of increased metastatic potential as opposed to chemotherapeutic resistance.

Work by Paoloni and colleagues provides strong evidence for the validity of dogs as a model for human OSA. They found that canine and human OSA are more similar to each other than to normal tissues from the same species (10). This, in concert with our growing body of knowledge regarding gene and pathway derangements in canine OSA provides insights into the mechanisms of OSA progression and chemoresistance.

CONCLUSIONS

The present study has examined gene expression in primary canine OSA via both traditional fold change analysis and systems-based pathway analysis and found significant differences between dogs that responded poorly to chemotherapy following definitive treatment and dogs that responded well as evidenced by a long disease-free interval. This study has identified candidate biomarkers of aggressive tumors as well as pathways that are deranged in poor responders relative to good responders, opening the door for molecular prognostic screening in canine OSA and further molecular comparison between the human and canine disease. Although further studies, such as protein expression analysis will be necessary to solidify the role of these genes and pathways in OSA, targets identified here provide a strong foundation from which to identify druggable targets and markers of progression in OSA.

ACKNOWLEDGEMENTS

This work was originally published in *BMC Cancer*. We acknowledge Erin Petrilli and the Genomics Core at the Rocky Mountain Regional Center for Excellence at CSU for generating the microarray data. We would also like to thank Irene Mok at CSU's Animal Cancer Center for coordinating sample retrieval from the tissue archive and Drs. Douglas Thamm and Gerrit Bouma for manuscript editing. This work was supported by grants to DLD from the Morris Animal Foundation (MAF D08CA-053), the CSU College Research Council - Miki Society, and Infinity Pharmaceuticals, and to LEO from the CSU Center for Companion Animal Studies PVM Student Grant Program.

REFERENCES

1. Jaffe N. Adjuvant chemotherapy in osteosarcoma: An odyssey of rejection and vindication. In: Jaffe N, Bielack SS, Bruland OS, editors. *Pediatric and Adolescent Osteosarcoma, Cancer Treatment and Research*. New York: Springer; 2009.
2. Dernell WS, Ehrhart NP, Straw RC, Vail DM. Tumors of the skeletal system. In: Withrow SJ, Vail DM, editors. *Withrow and MacEwen's Small Animal Clinical Oncology*. 4th ed. St. Louis: Saunders Elsevier; 2007. p. 540-67.
3. Bacon NJ, Ehrhart NP, Dernell WS, Lafferty M, Withrow SJ. Use of alternating administration of carboplatin and doxorubicin in dogs with microscopic metastases after amputation for appendicular osteosarcoma: 50 cases (1999–2006). *JAVMA* 2008;232(10):1504-10.
4. Chun R, Kurzman ID, Couto CG, Klausner J, Henry C, MacEwen EG. Cisplatin and doxorubicin combination chemotherapy for the treatment of canine osteosarcoma: a pilot study. *Journal of Veterinary Internal Medicine* 2000;14(5):495-8.
5. Mauldin GN, Matus RE, Withrow SJ, Patnaik AK. Canine osteosarcoma: treatment by amputation versus amputation and adjuvant chemotherapy using doxorubicin and cisplatin. *Journal of Veterinary Internal Medicine* 1988;2(4):177-80.
6. Shapiro W, Fossum T, Kitchell B, Couto C, Theilen G. Use of cisplatin for treatment of appendicular osteosarcoma in dogs. *JAVMA* 1988;192(4):507-11.
7. Spodnick GJ, Berg J, Rand WM, Schelling SH, Couto G, Harvey HJ, *et al.* Prognosis for dogs with appendicular osteosarcoma treated by amputation alone: 162 cases (1978-1988). *JAVMA* 1992;200(7):995-9.
8. Mueller F, Fuchs B, Kaser-Hotz B. Comparative biology of human and canine osteosarcoma. *Anticancer Research* 2007;27(1A):155-64.
9. Thomas R, Wang H, Tsai P, Langford C, Fosmire S, Jubala C, *et al.* Influence of genetic background on tumor karyotypes: evidence for breed-associated cytogenetic aberrations in canine appendicular osteosarcoma. *Chromosome Research* 2009;17(3):365-77.

10. Paoloni M, Davis S, Lana S, Withrow S, Sangiorgi L, Picci P, *et al.* Canine tumor cross-species genomics uncovers targets linked to osteosarcoma progression. *BMC Genomics* 2009;10(1):625.
11. Sutter NB, Ostrander EA. Dog star rising: the canine genetic system. *Nature Reviews Genetics* 2004;5(12):900-10.
12. Fidler IJ. The pathogenesis of cancer metastasis: the 'seed and soil' hypothesis revisited. *Nature Reviews Cancer* 2003;3(6):453-8.
13. Van'tVeer LJ, Weigelt B. Road map to metastasis. *Nature Medicine* 2003;9(8):999-1000.
14. van de Vijver MJ, He YD, van 't Veer LJ, Dai H, Hart AAM, Voskuil DW, *et al.* A gene-expression signature as a predictor of survival in breast cancer. *New England Journal of Medicine* 2002;347(25):1999-2009.
15. Collins I, Workman P. New approaches to molecular cancer therapeutics. *Nature Chemical Biology* 2006;2(12):689-700.
16. Varmus H. The new era in cancer research. *Science* 2006;312(5777):1162-5.
17. Jeys L, Grimer R, Carter S, Tillman R, Abudu A. Post operative infection and increased survival in osteosarcoma patients: are they associated? *Annals of Surgical Oncology* 2007;14(10):2887-95.
18. Lascelles B, Dernell W, Correa M, Lafferty M, Devitt C, Kuntz C, *et al.* Improved survival associated with postoperative wound infection in dogs treated with limb-salvage surgery for osteosarcoma. *Annals of Surgical Oncology* 2005;12(12):1073-83.
19. Affymetrix. Guide to probe logarithmic intensity error (PLIER) estimation. 2005.
20. Irizarry RA, Hobbs B, Collin F, Beazer-Barclay YD, Antonellis KJ, Scherf U, *et al.* Exploration, normalization, and summaries of high density oligonucleotide array probe level data. *Biostatistics* 2003;4(2):249-64.
21. Weinstein JN, Myers TG, O'Connor PM, Friend SH, Jr. AJF, Kohn KW, *et al.* An information-intensive approach to the molecular pharmacology of cancer. *Science* 1997;275(5298):343-9.
22. Karolchik D, Baertsch R, Diekhans M, Furey TS, Hinrichs A, Lu YT, *et al.* The UCSC genome browser database. *Nucleic Acids Research* 2003;31(1):51-4.
23. Kent WJ. BLAT---the BLAST-like alignment tool. *Genome Research* 2002;12(4):656-64.

24. Thomson SAM, Kennerly E, Olby N, Mickelson JR, Hoffmann DE, Dickinson PJ, *et al.* Microarray analysis of differentially expressed genes of primary tumors in the canine central nervous system. *Veterinary Pathology* 2005;42:550-8.
25. Livak KJ, Schmittgen TD. Analysis of relative gene expression data using real-time quantitative PCR and the $2^{-\Delta\Delta C_t}$ method. *Methods* 2001;25(4):402-8.
26. Pfaffl MW. A new mathematical model for relative quantification in real-time RT-PCR. *Nucleic Acids Research* 2001;29(9):e45.
27. Pfaffl MW, Horgan GW, Dempfle L. Relative expression software tool (REST) for group-wise comparison and statistical analysis of relative expression results in real-time PCR. *Nucleic Acids Research* 2002;30(9):e36.
28. Ptitsyn A, Weil M, Thamm D. Systems biology approach to identification of biomarkers for metastatic progression in cancer. *BMC Bioinformatics* 2008;9(Suppl 9):S8.
29. Patel S, Lyons-Weiler J. caGEDA: a web application for the integrated analysis of global gene expression patterns in cancer. *Applied Bioinformatics* 2004;3(1):49-62.
30. Dennis G, Sherman B, Hosack D, Yang J, Gao W, Lane HC, *et al.* DAVID: database for annotation, visualization, and integrated discovery. *Genome Biology* 2003;4(5):P3.
31. Huang DW, Sherman BT, Lempicki RA. Systematic and integrative analysis of large gene lists using DAVID bioinformatics resources. *Nature Protocols* 2008;4(1):44-57.
32. Witten I, Frank E. *Data Mining: practical machine learning tools and techniques*. 2nd ed. San Francisco: Morgan Kaufmann; 2005.
33. Depeursinge A, Iavindrasana J, Hidki A, Cohen G, Geissbuhler A, Platon A, *et al.* Comparative performance analysis of state-of-the-art classification algorithms applied to lung tissue categorization. *Journal of Digital Imaging* 2008;23(1):18-30.
34. Lemm I, Ross J. Regulation of c-myc mRNA decay by translational pausing in a coding region instability determinant. *Molecular and Cellular Biology* 2002;22(12):3959-69.
35. Noubissi FK, Elcheva I, Bhatia N, Shakoory A, Ougolkov A, Liu J, *et al.* CRD-BP mediates stabilization of $[\beta]$ TrCP1 and c-myc mRNA in response to $[\beta]$ -catenin signalling. *Nature* 2006;441(7095):898-901.

36. Vikesaa J, Hansen TVO, Jønson L, Borup R, Wewer UM, Christiansen J, *et al.* RNA-binding IMPs promote cell adhesion and invadopodia formation. *The EMBO Journal* 2006;25(7):1456-68.
37. Nielsen J, Christiansen J, Lykke-Andersen J, Johnsen AH, Wewer UM, Nielsen FC. A family of Insulin-Like Growth Factor II mRNA-binding proteins represses translation in late development. *Molecular and Cellular Biology* 1999;19(2):1262-70.
38. Hüttelmaier S, Zenklusen D, Lederer M, Dichtenberg J, Lorenz M, Meng X, *et al.* Spatial regulation of β -actin translation by Src-dependent phosphorylation of ZBP1. *Nature* 2005;438(7067):512-5.
39. Kobel M, Weidensdorfer D, Reinke C, Lederer M, Schmitt WD, Zeng K, *et al.* Expression of the RNA-binding protein IMP1 correlates with poor prognosis in ovarian carcinoma. *Oncogene* 2007;26(54):7584-9.
40. Dimitriadis E, Trangas T, Milatos S, Foukas PG, Gioulbasanis I, Courtis N, *et al.* Expression of oncofetal RNA-binding protein CRD-BP/IMP1 predicts clinical outcome in colon cancer. *International Journal of Cancer* 2007;121(3):486-94.
41. Yang Y, Tian X, Xie X, Zhuang Y, Wu W, Wang W. Expression and regulation of hedgehog signaling pathway in pancreatic cancer *Langenbeck's Archives of Surgery* 2009;Epub ahead of print.
42. Minuto F, Palermo C, Arvigo M, Barreca AM. The IGF system and bone. *Journal of Endocrinological Investigation* 2005;28(8 Suppl):8-10.
43. Voehringer DW, Hirschberg DL, Xiao J, Lu Q, Roederer M, Lock CB, *et al.* Gene microarray identification of redox and mitochondrial elements that control resistance or sensitivity to apoptosis. *Proceedings of the National Academy of Sciences* 2000;97(6):2680-5.
44. Bigl M, Jandrig B, Horn L-C, Eschrich K. Aberrant methylation of human L- and M-fructose 1,6-bisphosphatase genes in cancer. *Biochemical and Biophysical Research Communications* 2008;377(2):720-4.
45. Lyon RC, Johnston SM, Panopoulos A, Alzeer S, McGarvie G, Ellis EM. Enzymes involved in the metabolism of [γ]-hydroxybutyrate in SH-SY5Y cells: Identification of an iron-dependent alcohol dehydrogenase ADHFe1. *Chemico-Biological Interactions* 2009;178(1-3):283-7.
46. Kobayashi S, Fukuhara A, Taguchi T, Matsuda M, Tochino Y, Otsuki M, *et al.* Identification of a new secretory factor, CCDC3/Favine, in adipocytes and endothelial cells. *Biochemical and Biophysical Research Communications* 2010;392(1):29-35.

47. Bruheim S, Xi Y, Ju J, Fodstad O. Gene expression profiles classify human osteosarcoma xenografts according to sensitivity to doxorubicin, cisplatin, and ifosfamide. *Clinical Cancer Research* 2009;15(23):7161-9.
48. Chionia A-M, Brackenburyb WJ, Calhounb JD, Isomb LL, Djamgoza MBA. A novel adhesion molecule in human breast cancer cells: Voltage-gated Na⁺ channel β 1 subunit. *The International Journal of Biochemistry & Cell Biology* 2009;41(5):1216-27.
49. Yao L, Zhang J, Liu X. NDRG2: a Myc-repressed gene involved in cancer and cell stress. *Acta Biochimica et Biophysica Sinica* 2008;40(7):625-35.
50. Squire J, Pei J, Marrano P, Beheshti B, Bayani J, Lim G, *et al.* High-resolution mapping of amplifications and deletions in pediatric osteosarcoma by use of CGH analysis of cDNA microarrays. *Genes Chromosomes Cancer* 2003;38(3):215-25.
51. Tepel M, Roerig P, Wolter M, Gutmann DH, Perry A, Reifenberger G, *et al.* Frequent promoter hypermethylation and transcriptional downregulation of the NDRG2 gene at 14q11.2 in primary glioblastoma. *International Journal of Cancer* 2008;123(9):2080-6.
52. Kim YJ, Yoon SY, Kim J-T, Choi SC, Lim J-S, Kim JH, *et al.* NDRG2 suppresses cell proliferation through down-regulation of AP-1 activity in human colon carcinoma cells. *International Journal of Cancer* 2009;124(1):7-15.
53. Kim A, Kim M-J, Yang Y, Kim JW, Yeom YI, Lim J-S. Suppression of NF- κ B activity by NDRG2 expression attenuates the invasive potential of highly malignant tumor cells. *Carcinogenesis* 2009;Epub ahead of print: bgp072.
54. Liu N, Wang L, Li X, Yang Q, Liu X, Zhang J, *et al.* N-Myc downstream-regulated gene 2 is involved in p53-mediated apoptosis. *Nucleic Acids Research* 2008;36(16):5335-49.
55. Kim Y-J, Yoon SY, Kim J-T, Song EY, Lee HG, Son HJ, *et al.* NDRG2 expression decreases with tumor stages and regulates TCF/ β -catenin signaling in human colon carcinoma. *Carcinogenesis* 2009;30(4):598-605.
56. Wise DR, DeBerardinis RJ, Mancuso A, Sayed N, Zhang X-Y, Pfeiffer HK, *et al.* Myc regulates a transcriptional program that stimulates mitochondrial glutaminolysis and leads to glutamine addiction. *Proceedings of the National Academy of Sciences* 2008;105(48):18782-7.
57. Naviglio S, Caraglia M, Abbruzzese A, Chiosi E, Gesto DD, Marra M, *et al.* Protein kinase A as a biological target in cancer therapy. *Expert Opinion on Therapeutic Targets* 2009;13(1):83-92.

58. Day TF, Yang Y. Wnt and hedgehog signaling pathways in bone development. *The Journal of Bone and Joint Surgery* 2008;90(Suppl 1):19-24.
59. Katoh Y, Katoh M. Comparative genomics on HHIP family orthologs. *International Journal of Molecular Medicine* 2006;17(2):391-5.
60. Tojo M, Kiyosawa H, Iwatsuki K, Kaneko F. Expression of a sonic hedgehog signal transducer, hedgehog-interacting protein, by human basal cell carcinoma. *British Journal of Dermatology* 2002;146(1):69-73.
61. Olsen C, Hsu P-P, Glienke J, Rubanyi G, Brooks A. Hedgehog-interacting protein is highly expressed in endothelial cells but down-regulated during angiogenesis and in several human tumors. *BMC Cancer* 2004;4(1):43-53.
62. Man T-K, Chintagumpala M, Visvanathan J, Shen J, Perlaky L, Hicks J, *et al.* Expression profiles of osteosarcoma that can predict response to chemotherapy. *Cancer Research* 2005;65(18):8142-50.
63. Mintz MB, Sowers R, Brown KM, Hilmer SC, Mazza B, Huvos AG, *et al.* An expression signature classifies chemotherapy-resistant pediatric osteosarcoma. *Cancer Research* 2005;65(5):1748-54.
64. Ochi K, Daigo Y, Katagiri T, Nagayama S, Tsunoda T, Myoui A, *et al.* Prediction of response to neoadjuvant chemotherapy for osteosarcoma by gene-expression profiles. *International Journal of Oncology* 2004;24(3):647-55.
65. Walters DK, Steinmann P, Langsam B, Schmutz S, Born W, Fuchs B. Identification of potential chemoresistance genes in osteosarcoma. *Anticancer Research* 2008;28(2A):673-80.
66. Selvarajah GT, Kirpensteijn J, Wolferen MEv, Rao NA, Fieten H, Mol JA. Gene expression profiling of canine osteosarcoma reveals genes associated with short and long survival times. *Molecular Cancer* 2009;8:72-90.

Chapter 3

Gaining perspective: Gene expression analysis of canine osteosarcoma in relation to normal bone.

SYNOPSIS

Osteosarcoma (OSA) is the most common primary bone tumor in humans and dogs. The genomic and transcriptomic nature of the disease is best characterized as chaotic with aneuploidy and inconsistent gene expression patterns frequently observed among samples. Technological advances allowing screening of an ever-increasing number of genes and chromosome regions offer the opportunity for identification of new molecular contributors to the disease. Thus, we compared microarray expression profiles of primary canine OSA tumors to normal bone samples to gain insight into genes that contribute to tumorigenesis as well as disease progression and chemoresistance. We also investigated genomic copy number status in primary tumors relative to matched normal tissue via array comparative genomic hybridization. Microarray profiling identified over 2,000 genes that were dysregulated in tumors relative to normal bone and aCGH studies identified regions of copy number alterations that may contribute to some of this dysregulation. This integrated screening approach provides insight into the complex

mechanisms of OSA tumorigenesis and progression and may help to identify new gene targets for treatment and prognostic purposes.

INTRODUCTION

Osteosarcoma (OSA) is the most common primary bone malignancy in both dogs and humans. Roughly 800 new human cases occur annually and greater than 10-times that many occur in dogs (1, 2). The disease in dogs is increasingly recognized as an excellent model for the human disease; thus, we previously sought to identify biomarkers of disease progression and chemotherapeutic resistance in canine patients (3). Having identified several promising gene and pathway signatures, we next sought to gain perspective on this dysregulation by comparing OSA gene expression signatures to those of normal bone tissue.

A number of gene expression profiling studies aimed at identifying molecular features of OSA have been performed in humans (4-6). Similarly, human OSA-derived *in vitro* models and mouse model systems have been used to seek out gene expression signatures that may identify the most aggressive or chemoresistant OSA types (7-10). Although several genes of importance in OSA progression have been identified (e.g. Ezrin), the greatest unifying factor of these studies is the lack of concordance between the resulting lists of prognostic or chemoresistance-related genes. This is due, partly, to the multifactorial nature of OSA but also to very limited numbers of sample tissues available. The large number of dogs affected by this cancer as well as new initiatives by nationwide tumor archiving consortia to bank veterinary tumors offer unique study opportunities for biomarker identification (1, 11-14).

Studies have examined OSA gene expression relative to normal tissues other than bone yet expression studies involving normal bone are lacking due to the low cellularity of this tissue and resulting difficulty of RNA extraction (14). Thus, we set out to devise an effective method for high quality RNA extraction from bone and to analyze gene expression in this tissue via microarray and quantitative RT-PCR. Additionally, we performed array comparative genomic hybridization (aCGH) studies on genomic DNA from tumors and normal muscle tissue to determine to what extent copy number alterations (CNAs) were contributing to observed gene expression changes.

METHODS

Canine Tissues

Canine tissues used in these studies were obtained from animals presenting to Colorado State University (CSU) for treatment of OSA. Owner consent for tissue archiving was obtained prior to definitive surgical treatment. Good- and poor-responder primary tumors were archived at the Animal Cancer Center between 1996 and 2006 - snap frozen tissues and formalin-fixed paraffin embedded (FFPE) tissues were archived. Good and poor responder groups were defined based upon patient disease-free-interval (DFI): good-responders had a DFI greater than 300 days and poor-responders had a DFI less than 100 days following amputation of the affected limb and chemotherapy with doxorubicin and/or a platinum-based drug . Normal bone and matched tumor samples were obtained from limbs post-amputation and harvested so that “normal” bone included in the study was distant from the tumor site and separated from the tumor by a joint (e.g. a femoral tumor would have matched distal tibia bone collected). A one to two

centimeter section of normal bone was collected for each sample; marrow and medullary fat was removed at collection. Tissue was snap frozen in liquid nitrogen and stored at -80°C until processing. Inclusion in good and poor responder studies required limb amputation followed by doxorubicin and/or platinum drug adjuvant therapy whereas inclusion in normal bone studies required limb amputation. Patient details are provided in Tables 2.1 and 3.1

RNA Extraction

As many researchers are skeptical about the possibility of obtaining high quality RNA from normal bone tissue, we first set out to devise a method for efficient RNA isolation from normal bone. Normal bone samples were collected as above then returned to liquid nitrogen immediately prior to extraction. Bone samples were freeze fractured and powdered in a liquid-nitrogen cooled Biopulverizer (RPI Corp., Mount Prospect, IL). Up to 1 cm³ of the resulting powder was then added to 3 mL Trizol (Invitrogen, Cat# 15596-026) and homogenized with a mechanical homogenizer for 60 s. The resulting slurry was centrifuged at 2000 rpm in a swinging bucket rotor for 15 s to remove osseous particulates. The supernatant was transferred to a new tube and was subjected to phase separation RNA extraction per the manufacturer's instructions. RNA pellets were resuspended in nuclease free water, pre-treated with the RNase-Free DNase Set (Qiagen, Cat# 79254) then purified with the RNeasy cleanup protocol per the manufacturer's instructions (Qiagen, Cat# 74104). Tumor samples were purified in a similar fashion, only with significantly less tissue input. RNA was quantified via spectrophotometry and, prior to microarray, tissue and tumor RNA was bioanalyzed for quality at the Rocky Mountain Regional Center for Excellence (RMRCE) Genomics Core at CSU. Only high

Table 3.1 – Signalment, tumor location and treatment information for patients included in the normal bone versus matched tumor studies.

Unique ID	Sex	Breed	DOB	Amputation Date	Tumor Location	Normal Bone Location	Chemotherapy	Histology Diagnosis	Follow Up
N1	FS	Labrador Ret.	6/15/1996	9/10/2009	Proximal Right Tibia	Proximal Right Femur	None	Giant Cell OSA	Last F/U NSF 12/2009
N2	MC	Mix	9/29/1999	9/30/2009	Distal Femur	Distal Tibia	None	OSA	Mets present at amp, PTS 2/19/2010
N3	FS	Labrador Ret.	2/14/2000	10/5/2009	Distal Left Tibia	Proximal Left Femur	Carboplatin	OSA	Positive met check 2/3/2010
N5	FS	Labrador Ret.	1/1/2000	1/28/2010	Proximal Right Humerus	Distal Right Radius/Ulna	None	Osteoblastic OSA	Mets present at 1-month F/U
N6	FS	Mix	2/12/2001	1/19/2010	Proximal Left Tibia	Proximal Left Femur	Carboplatin, Mitoxantrone	Telangiectatic OSA	Possible met 7/15/10
N7	MC	Mix	1/1/2005	2/23/2010	Proximal Left Humerus	Distal Left Radius/Ulna	Carboplatin	Chondroblastic OSA	No mets as of 9/24/2010
N8	MC	Mix	9/1/2003	2/24/2010	Proximal Left Humerus	Distal Left Radius/Ulna	Carboplatin	OSA	NA
N9	FS	Coonhound	5/24/2001	4/30/2010	Distal Left Radius	Proximal Left Humerus	Carboplatin	Osteoblastic OSA	No mets as of 6/30/2010
N10	MC	Labrador Ret.	3/19/2003	4/30/2010	Proximal Right Humerus	Distal Right Radius/Ulna	None	OSA	NA

FS = spayed female, MC = castrated male, DOB = date of birth, OSA = osteosarcoma, Met(s) = metastases, NSF = no significant findings

quality RNA with RNA Integrity Numbers (RINs) greater than 8 were used in microarray studies.

Microarray

Eight normal bone samples were analyzed with Affymetrix Canine 2.0 GeneChips as previously described (3). Resultant data was compiled with data from 15 good and poor-responder primary tumor samples obtained previously and analyzed with ArrayTrack (15). Data was preprocessed with the Probe Logarithmic Intensity Error (PLIER) estimation algorithm with a Log_2 transformation then analyzed for fold change based on two scenarios: normal bone versus all tumors or normal bone versus good responders versus poor responders. The first scenario was analyzed with a Bonferroni adjusted unpaired 2-tailed t-test, thresholds of corrected p-value <0.05 and fold-change >3 were applied. The second scenario was analyzed with pairwise t-test comparisons and the same p-value and fold-change thresholds. Heat maps were generated with the ArrayTrack software using average Euclidean distance estimators and unsupervised clustering for all axes.

Array Comparative Genomic Hybridization

Genomic DNA was extracted from patient-matched normal tissue (muscle, skin) using the DNeasy (Qiagen, Cat# 69504) kit per the manufacturer's instructions. Array-CGH was performed by Dr. Matthew Breen's laboratory at North Carolina State University as previously described (16). Amplification of each probe region was expressed as Log_2 tumor tissue relative to normal tissue. gDNA hybridization intensities were compared to microarray expression data from good and poor responder groups as well as all tumors relative to normal bone.

RESULTS AND DISCUSSION

Gene Expression Profiling in Normal Bone: A Valuable Reference for OSA Studies

Having previously identified a number of genes that were dysregulated between good and poor-responder canine patients' primary OSA tumors, we sought to determine the degree of dysregulation of these genes relative to an applicable baseline: normal bone. Using the methods described here, ample quantities of RNA were obtained from non-tumor-bearing bone; Affymetrix Canine 2.0 expression arrays were then performed on these samples to provide perspective for tumor gene expression profiles. Comparing all tumors as a group (n=15) to all normal bone samples yielded 2,549 differentially expressed probesets (FC>3, p<0.05, unpaired, 2-tailed t-test). Hierarchical unsupervised clustering of these probesets grouped all normal bone samples together and all tumor samples together (Figure 3.1a). Principal components analysis of this data also clustered tumors together, separated from normal bone, on the basis of one principal component (Figure 3.1b).

Pairwise comparisons of the three groups (good responders, poor responders and normal bone) yielded 4,587 significant probesets when comparing normal bone to good responders, 4,982 differentially regulated probesets when comparing normal bone to poor responders, and 114 significantly different probesets when comparing good and poor responders. Intersection of these gene groups was visualized with a Venn diagram based upon gene IDs (Figure 3.2). Multiple probesets were often present for one gene ID and probesets without an assigned ID were excluded, reducing the total number of probesets analyzed. Twenty-two genes were differentially regulated in all three comparisons

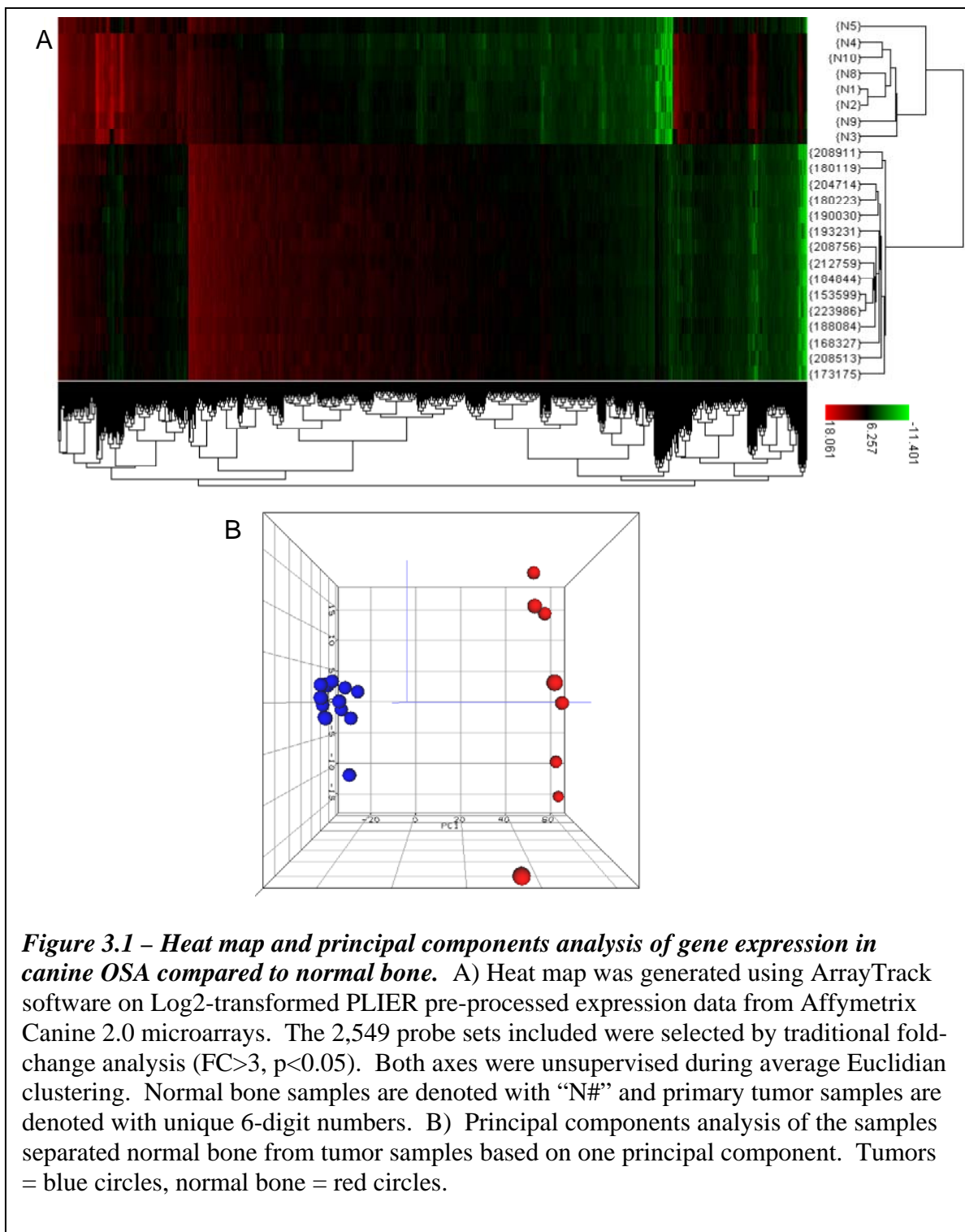
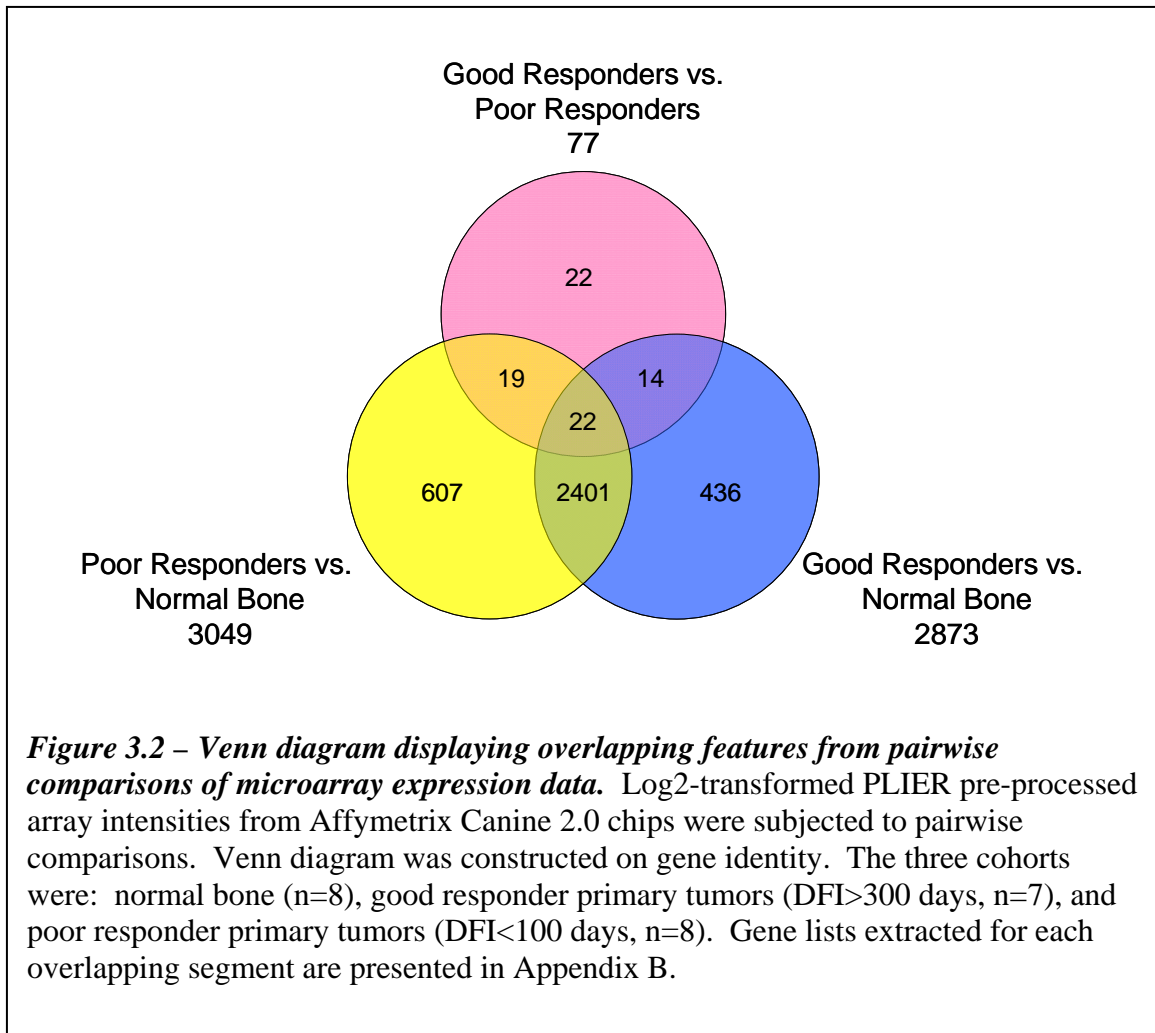


Figure 3.1 – Heat map and principal components analysis of gene expression in canine OSA compared to normal bone. A) Heat map was generated using ArrayTrack software on Log₂-transformed PLIER pre-processed expression data from Affymetrix Canine 2.0 microarrays. The 2,549 probe sets included were selected by traditional fold-change analysis (FC>3, p<0.05). Both axes were unsupervised during average Euclidian clustering. Normal bone samples are denoted with “N#” and primary tumor samples are denoted with unique 6-digit numbers. B) Principal components analysis of the samples separated normal bone from tumor samples based on one principal component. Tumors = blue circles, normal bone = red circles.

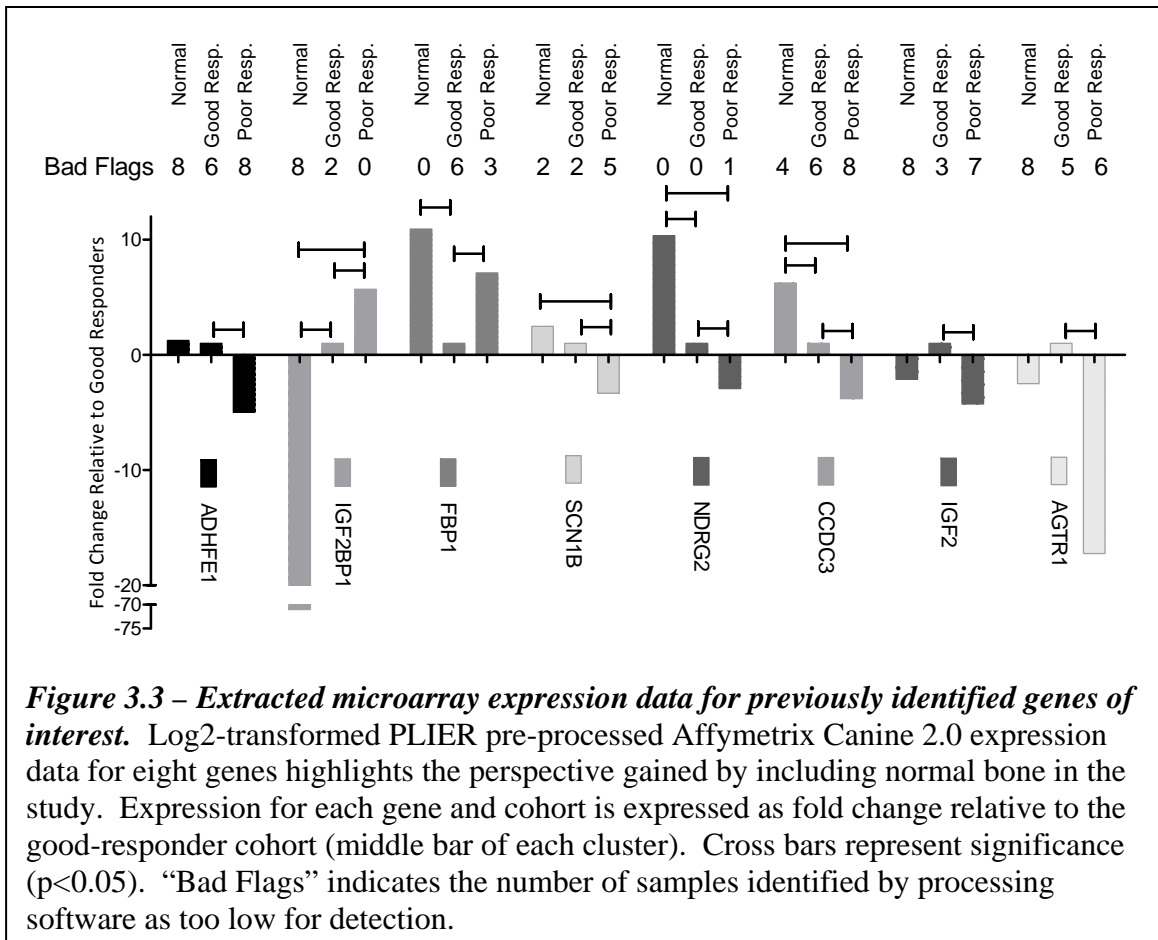
(middle segment) flagging these genes as those that have progressively altered expression patterns with increasing tumor aggressiveness. 2,401 significant genes were shared when comparing each responder group to normal bone (bottom middle wedge). As these genes



demonstrated no differences between good and poor responders, they are not likely to be related to progression but are tumor-specific and may contribute to tumorigenesis and maintenance of the primary tumor. Nineteen genes were identified in the comparisons between poor responders vs. normal bone and good responders vs. poor responders (left wedge). These genes are unchanged in good responders relative to normal bone but have altered expression in the worst tumors, suggesting they may play a role as mediators of invasion, metastasis and/or chemoresistance. Fourteen genes were shared in the comparisons between good responders vs. normal bone and good responders vs. poor

responders (right wedge). As these genes were dysregulated in good responders but not poor, it suggests they may be positive prognostic indicators or merely incidental findings. Gene lists generated by the intersection of these pairwise comparisons are provided in Appendix B.

Fold change values were extracted for several previously-identified genes of interest; additionally, bad-flag calls were examined to interpret their relevance to the study (Figure 3.3). Even in the cases where greater than 50% of calls were flagged as



"bad," gene expression differences were verified by qRT-PCR (Figure 2.2). Thus, even at low hybridization signal, this platform offers excellent sensitivity. This method of analysis provided valuable perspective on these genes that had previously been analyzed

in only good and poor responder groups. For instance, the targets fructose 1,6 bisphosphatase (FBP1) and insulin-like growth factor 2 (IGF2) were less-attractive as biomarkers following inclusion of normal bone expression in the analysis. While normal bone and poor responders both demonstrated significant expression differences from good responders for these two genes, no differences between normal bone and poor responders were observed. This finding suggests that the observed dysregulation may be natural variance or unrelated to tumor progression. Other targets, however, became even more promising following this analysis. The oncofetal gene IGF2 mRNA binding protein 1 (*IGF2BP1*) was overexpressed in all tumors relative to normal bone and significantly more so in poor-responder tumors relative to good-responder tumors. All normal bone samples were denoted as bad flags by the analysis software but, as this gene is wholesale suppressed in most normal tissues, this is to be expected. Exclusion of these "bad" flags would have truncated valuable data. Additionally, the putative tumor suppressor gene n-Myc downstream regulated gene 2 (*NDRG2*) demonstrated a similar stair-step pattern of regulation but progressing from highest expression in normal bone to least expression in poor-responder tumors. Finally, this study identified several genes that demonstrate a progressive downregulation similar to *NDRG2* yet have received limited or no attention in cancer: alcohol dehydrogenase, iron-containing 1 (*ADHFE1*), sodium channel, voltage-gated, type I, beta (*SCN1B*) and coiled coil domain containing 3 (*CCDC3*).

Array Comparative Genomic Hybridization Highlights the Chaotic Nature of OSA

Copy number alterations (CNAs) are a well-established means of genetic dysregulation and OSA is often described as having a high degree of aneuploidy (12, 17,

18). Thus, aCGH was used to assay a subset of good and poor-responder tumors relative to paired normal tissue to determine the extent of CNAs and related expression alterations in this system. A total of eight primary tumors with paired muscle samples (n=4 from each cohort) were analyzed. No software capable of comparing one-color microarrays (e.g the Affymetrix array used here) to the employed aCGH platform in the context of the canine genome is currently available. Thus, individual chromosome maps were generated to compare aCGH relative hybridization intensities to microarray expression data. Appendix C presents each chromosome as an aCGH intensity figure paired with a fold-change of tumor relative to normal bone microarray expression figure. Appendix D presents each chromosome as an aCGH intensity of good and poor responder cohorts figure paired with a fold-change of poor responders relative to good responders microarray expression figure. These chromosome profiles provide a visual means by which to assess regions in which gene over- or under-expression may be related to chromosomal amplification or deletion.

Locus regions that were identified in previous studies as important to OSA tumorigenesis or progression as well as several other regions identified in the pairwise comparison conducted here have been labeled with green boxes in Appendix C figures. *Ezrin*, found on Cfa 1, is associated with invasion and metastasis and only shows one case of amplification whereas several samples show deletion (19). The tumor suppressor tumor protein p53 (*TP53*) is located on Cfa 5: several samples show deletion in the region of this locus and two samples show amplification. Deletion of portions of the *TP53* gene have been observed in several systems although dominant negative mutations unrelated to CNAs are also common tumorigenic events (20-22). The oncofetal gene

IGF2BP1 is located on Cfa 9 in close proximity to the breast cancer associated oncogene v-erb-b2 erythroblastic leukemia viral oncogene homolog 2 (*ERBB2/HER2*). *IGF2BP1* was identified in the pairwise comparison analysis above, but demonstrates no CNAs in the eight samples examined here. Previous studies of these two genes have determined that amplification often occurs in this region in human breast cancers, but, despite the proximity of these two loci, they are often amplified independently of each other (23).

Mouse double minute 2 (*MDM2*), located on Cfa 10, is often amplified in human OSA; overexpression of the gene product results in inappropriate down-regulation of the p53 tumor suppressor protein (24-26). Two cases of amplification and three cases of deletion were observed in the region of this locus. The cyclin-dependent kinase inhibitor 2A (*CDKN2A*, Cfa 11) locus encodes two alternate gene products, both of which serve as tumor suppressors by interacting with the p53 and retinoblastoma (Rb) pathways (27-30). Deletion at this locus was observed in a majority of samples and has previously been identified as contributing to tumorigenesis in a number of different tumor types.

Similarly, the *RB* tumor suppressor gene, found on Cfa 22, demonstrates copy number loss in three samples tested. Thus, while genes involved in p53 and Rb control are not uniformly experiencing CNAs in this population, amplification or deletion at one of many related loci in different tumors are likely contributing to OSA development (31).

The runt-related transcription factor 2 (*RUNX2*) gene is a bone-development-specific gene often observed to be upregulated in OSA (32-35). The precise location of this gene has not been defined in dogs but a BLAST search of the human homolog coding sequence suggests that Cfa 12 is the likely chromosome. The locus in question is

LOC474923 and demonstrates amplification in the majority of samples analyzed here. Corresponding overexpression of nearby mRNAs is also observed.

Previous work by Thomas and colleagues identified a number of common karyotypic aberrations in canine OSA (17). These include loci of some genes already discussed as well as oncogenes such as v-myc myelocytomatosis viral oncogene homolog (*c-Myc*), v-kit Hardy-Zuckerman 4 feline sarcoma viral oncogene homolog (*KIT*) and the rat sarcoma viral oncogene homologs (*HRAS* and *KRAS*). They also identified CNAs in the tumor suppressor genes Wilms tumor 1(*WT1*) and phosphatase and tensin homolog (*PTEN*). The current study supports their findings: *c-Myc* and *KIT* both occupy regions of Cfa 13 and amplification in multiple samples is seen at each locus. Similarly, microarray probes for these genes demonstrated significant two- and four-fold upregulation, respectively, when comparing all tumors to normal bone. *NDRG2*, a gene identified in pairwise analysis as common to all three test groups, is regulated by c-Myc and also shows copy number loss in two samples tested here (Cfa 15)(36). Thus, dysregulation of c-Myc targets may be caused by amplification at the *c-Myc* locus or deletion of one of its downstream targets, such as *NDRG2*. *PTEN* and *WT1* also show evidence of copy number loss in the current study (Cfa 26 and Cfa 18, respectively).

CONCLUSIONS

The chromosome maps generated here highlight the extreme variance in CNAs among individuals' tumors. Despite this variance, amplification of oncogenes and deletion of tumor suppressor genes is a recurrent theme. Furthermore, CNAs in genes involved in these pathways can cause the same phenotypes even when the oncogene or

tumor suppressor loci are unaffected. Comparison of aCGH plots to microarray expression plots has provided further insight: in some cases, gene expression tracks with CNAs, however, in others it does not, suggesting that, for these genes, other mechanisms of gene regulation are at work. One such gene is *NDRG2*; mechanisms of its regulation and its role in OSA are further explored in Chapter 6.

REFERENCES

1. Mueller F, Fuchs B, Kaser-Hotz B. Comparative biology of human and canine osteosarcoma. *Anticancer Research* 2007;27(1A):155-64.
2. Withrow SJ, Khanna C. Bridging the gap between experimental animals and humans in osteosarcoma. In: Jaffe N, Bruland OS, Bielack SS, editors. *Pediatric and Adolescent Osteosarcoma, Cancer Treatment and Research*. New York: Springer; 2009.
3. O'Donoghue LE, Ptitsyn AA, Kamstock DA, Siebert J, Thomas RS, Duval DL. Expression profiling in canine osteosarcoma: identification of biomarkers and pathways associated with outcome. *BMC Cancer* 2010;10(1):506.
4. Man T-K, Chintagumpala M, Visvanathan J, Shen J, Perlaky L, Hicks J, *et al.* Expression profiles of osteosarcoma that can predict response to chemotherapy. *Cancer Research* 2005;65(18):8142-50.
5. Mintz MB, Sowers R, Brown KM, Hilmer SC, Mazza B, Huvos AG, *et al.* An expression signature classifies chemotherapy-resistant pediatric osteosarcoma. *Cancer Research* 2005;65(5):1748-54.
6. Ochi K, Daigo Y, Katagiri T, Nagayama S, Tsunoda T, Myoui A, *et al.* Prediction of response to neoadjuvant chemotherapy for osteosarcoma by gene-expression profiles. *International Journal of Oncology* 2004;24(3):647-55.
7. Sadikovic B, Yoshimoto M, Chilton-MacNeill S, Thorner P, Squire JA, Zielenska M. Identification of interactive networks of gene expression associated with osteosarcoma oncogenesis by integrated molecular profiling. *Human Molecular Genetics* 2009;18(11):1962-75.
8. Walters DK, Steinmann P, Langsam B, Schmutz S, Born W, Fuchs B. Identification of potential chemoresistance genes in osteosarcoma. *Anticancer Research* 2008;28(2A):673-80.
9. Bruheim S, Xi Y, Ju J, Fodstad O. Gene expression profiles classify human osteosarcoma xenografts according to sensitivity to doxorubicin, cisplatin, and ifosfamide. *Clinical Cancer Research* 2009;15(23):7161-9.
10. Khanna C, Khan J, Nguyen P, Prehn J, Caylor J, Yeung C, *et al.* Metastasis-associated differences in gene expression in a murine model of osteosarcoma. *Cancer Research* 2001;61(9):3750-9.
11. Selvarajah GT, Kirpensteijn J, Wolferen MEv, Rao NA, Fieten H, Mol JA. Gene expression profiling of canine osteosarcoma reveals genes associated with short and long survival times. *Molecular Cancer* 2009;8:72-90.

12. Angstadt AY, Motsinger-Reif A, Thomas R, Kisseberth WC, Guillermo Couto C, Duval DL, *et al.* Characterization of canine osteosarcoma by array comparative genomic hybridization and RT-qPCR: Signatures of genomic imbalance in canine osteosarcoma parallel the human counterpart. *Genes, Chromosomes and Cancer* 2011;n/a-n/a.
13. Scott MC, Sarver AL, Gavin KJ, Thayanithy V, Getzy DM, Newman RA, *et al.* Molecular subtypes of osteosarcoma identified by reducing tumor heterogeneity through an interspecies comparative approach. *Bone* 2011;49(3):356-67.
14. Paoloni M, Davis S, Lana S, Withrow S, Sangiorgi L, Picci P, *et al.* Canine tumor cross-species genomics uncovers targets linked to osteosarcoma progression. *BMC Genomics* 2009;10(1):625.
15. Tong W, Cao X, Harris S, Sun H, Fang H, Fuscoe J, *et al.* ArrayTrack--supporting toxicogenomic research at the U.S. Food and Drug Administration National Center for Toxicological Research. *Environmental Health Perspectives* 2003;111(15).
16. Thomas R, Scott A, Langford CF, Fosmire SP, Jubala CM, Lorentzen TD, *et al.* Construction of a 2-Mb resolution BAC microarray for CGH analysis of canine tumors. *Genome Research* 2005;15(12):1831-7.
17. Thomas R, Wang H, Tsai P, Langford C, Fosmire S, Jubala C, *et al.* Influence of genetic background on tumor karyotypes: evidence for breed-associated cytogenetic aberrations in canine appendicular osteosarcoma. *Chromosome Research* 2009;17(3):365-77.
18. Selvarajah S, Yoshimoto M, Ludkovski O, Park PC, Bayani J, Thorner P, *et al.* Genomic signatures of chromosomal instability and osteosarcoma progression detected by high resolution array CGH and interphase FISH. *Cytogenetic and Genome Research* 2008;122(1):5-15.
19. Khanna C, Wan X, Bose S, Cassaday R, Olomu O, Mendoza A, *et al.* The membrane-cytoskeleton linker ezrin is necessary for osteosarcoma metastasis. *Nature Medicine* 2004;10(2):182-6.
20. Chandar N, Billig B, McMaster J, Novak J. Inactivation of p53 gene in human and murine osteosarcoma cells. *British Journal of Cancer* 1992;65(2):208-14.
21. Miller CW, Aslo A, Tsay C, Slamon D, Ishizaki K, Toguchida J, *et al.* Frequency and structure of p53 rearrangements in human osteosarcoma. *Cancer Research* 1990;50(24):7950-4.
22. Willis A, Jung EJ, Wakefield T, Chen X. Mutant p53 exerts a dominant negative effect by preventing wild-type p53 from binding to the promoter of its target genes. *Oncogene* 2004;23(13):2330-8.
23. Doyle GA, Bourdeau-Heller JM, Coulthard S, Meisner LF, Ross J. Amplification in human breast cancer of a gene encoding a c-myc mRNA-binding protein. *Cancer Research* 2000;60(11):2756-9.

24. Levine RA, Fleischli MA. Inactivation of p53 and retinoblastoma family pathways in canine osteosarcoma cell lines. *Veterinary Pathology* 2000;37(1):54-61.
25. Mendoza S, Konishi T, Dernell WS, Withrow SJ, Miller CW. Status of the p53, Rb and MDM2 genes in canine osteosarcoma. *Anticancer Research* 1998;18(6A):4449-53.
26. Miller CW, Aslo A, Won A, Tan M, Lampkin B, Koefflar HP. Alterations of the p53, Rb and MDM2 genes in osteosarcomas *Journal of Cancer Research and Clinical Oncology* 1996;122(9):559-65.
27. Miller CW, Aslo A, Campbell MJ, Kawamata N, Lampkin BC, Koeffler HP. Alterations of the p15, p16, and p18 genes in osteosarcoma. *Cancer Genetics and Cytogenetics* 1996;86(2):136-42.
28. Nielsen GP, Burns KL, Rosenberg AE, Louis DN. CDKN2A gene deletions and loss of p16 expression occur in osteosarcomas that lack RB alterations. *The American Journal of Pathology* 1998;153(1):159-63.
29. Oh JH, Kim HS, Kim HH, Kim WH, Lee SH. Aberrant methylation of p14ARF gene correlates with poor survival in osteosarcoma. *Clinical Orthopaedics and Related Research* 2006;442:216-22.
30. Benassi MS, Molendini L, Gamberi G, Magagnoli G, Ragazzini P, Gobbi GA, *et al.* Involvement of INK4A gene products in the pathogenesis and development of human osteosarcoma. *Cancer* 2001;92(12):3062-7.
31. Gorlick R. Current concepts on the molecular biology of osteosarcoma. In: Jaffe N, Bielack SS, Bruland OS, editors. *Pediatric and Adolescent Osteosarcoma, Cancer Treatment and Research*. New York: Springer; 2009.
32. Martin JW, Zielenska M, Stein GS, van Wijnen AJ, Squire JA. The role of RUNX2 in osteosarcoma oncogenesis. *Sarcoma* 2011;vol. 2011(Article ID 282745):13 pages.
33. Thomas DM, Johnson SA, Sims NA, Trivett MK, Slavin JL, Rubin BP, *et al.* Terminal osteoblast differentiation, mediated by runx2 and p27KIP1, is disrupted in osteosarcoma. *Journal of Cell Biology* 2004;167(5):925-34.
34. Pereira BP, Zhou Y, Gupta A, Leong DT, Aung KZ, Ling L, *et al.* Runx2, p53, and pRB status as diagnostic parameters for deregulation of osteoblast growth and differentiation in a new pre-chemotherapeutic osteosarcoma cell line (OS1). *Journal of Cellular Physiology* 2009;221(3):778-88.
35. Nathan S, Pereira B, Zhou Y-f, Gupta A, Dombrowski C, Soong R, *et al.* Elevated expression of Runx2 as a key parameter in the etiology of osteosarcoma. *Molecular Biology Reports* 2009;36(1):153-8.
36. Zhang J, Li F, Liu X, Shen L, Liu J, Su J, *et al.* The repression of human differentiation-related gene NDRG2 expression by Myc via Miz-1-dependent interaction with the NDRG2 core promoter. *Journal of Biological Chemistry* 2006;281(51):39159-68.

Chapter 4

Validation of *in vitro* models for canine osteosarcoma

SYNOPSIS

Canine osteosarcoma is an excellent model for the disease in humans and an increasing amount of research is being pursued in both primary tumors and immortal cell lines derived from these tumors. Previously, we analyzed gene expression in canine osteosarcoma (OSA) with the intent of identifying biomarkers of tumor aggressiveness and chemoresistance; here we pursue validation of *in vitro* models prior to embarking on further mechanistic studies of biomarkers. Cell line cross-contamination as well as genetic drift during passaging have been acknowledged as widespread problems since the 1960s. Thus, a highly sensitive polymerase chain reaction (PCR)-based approach and short tandem repeat (STR) profiling were used to examine the prevalence of inter- and intraspecies cell line contamination and to verify that canine cell lines to be used in future studies were canine and unique. Furthermore, the availability of anti-canine antibodies is limited, thus, we have tested anti-human antibodies to ADHFE1 and SCN1B for specificity to canine proteins via both western blot and immunohistochemistry. Sixty cell lines from six laboratories were tested with multiplex species-specific PCR capable of identifying six commonly used species. Of these, three were determined to be misidentified by species. To identify intraspecies contamination among canine cancer

cell lines, 29 canine lines from three different laboratories were analyzed with STR fingerprinting. Using this methodology, three canine cell lines were determined to be misidentified or cross-contaminated by other canine cell lines and genetic drift was observed within one cell line. These findings emphasize the importance of cell line validation as a critical component of “good cell culture practice” and add detail to the body of knowledge regarding two canine genes that may be important in the tumorigenesis and progression of osteosarcoma.

INTRODUCTION

Osteosarcoma (OSA) is the most common primary bone malignancy in both humans and dogs affecting roughly 800 adolescents and 8,000 companion dogs annually (1, 2). Diseases in veterinary patients, including OSA, are becoming widely acknowledged as valid translational models for similar diseases in humans and, as such, veterinary research facilities are performing an increasing number of *in vitro* and *in vivo* clinical trials using models from a variety of species (3). Thus, it is crucial for the veterinary community to possess the resources to fully study these models and to undertake the necessary steps to validate all cell lines in use. Prior studies by our laboratory identified several genes that may contribute to cancer progression and chemoresistance in canine OSA (4). Following up that study with investigations into the roles of identified genes required validation of *in vitro* models with regard to species and tumor of origin as well as validation of the specificity of anti-human antibodies in canine samples.

Cell lines are widely used in biomedical research as *in vitro* models for disease. HeLa cells were established in 1952 and, as early as 1958, interspecies cross-

contamination between these cells and other lines was observed (5). In the 1960's, karyotyping, examination of biochemical polymorphisms and immunological approaches were developed to test cell line identity (6) within and between species but the early pioneers of cell line validation generally met with resistance from the scientific community (5). More recently, it has been estimated that 18% to 36% of cell lines may be contaminated or misidentified (7). With the advent of relatively simple PCR-based DNA fingerprinting techniques, a new drive for cell line validation was initiated, aimed at providing a solution for eradication of cell line misidentification (8).

In addition to misidentification, problems with excessive sub-culturing of cells have also been identified (9). As cell lines are maintained in culture for long periods of time, selective pressures are being exerted on them and, thus, lines are subject to genetic drift, especially at higher passage numbers. Therefore, even when a cell line has not been contaminated, it can take on new attributes, skewing experimental data. Currently, an increasing number of journals require cell-line validation prior to publication as examples emerge of cell lines with false identities being used and published about long after they have been identified as problematic (10).

With the recent sequencing of the canine genome, in-depth gene expression studies have become more-feasible in canine models; however, many resources specific to canine samples are relative to those available for humans and mouse and rat models (11). In order to investigate mechanisms of disease and progression, antibodies need to be generated or validated for the canine model and expressed sequences need to be confirmed.

Researchers at the Colorado State University (CSU) Animal Cancer Center (ACC) use a variety of cell lines from a number of different species, including a panel of canine cancer cell lines. Because of this diversity, it was determined that testing for both inter- and intraspecies cell line contamination was necessary. Multiplex polymerase chain reaction (PCR) has been demonstrated to be effective at determining species contamination (12) and short tandem repeat (STR) profiling is commonly used in animal breed detection and parentage testing as well as human forensics to differentiate between individuals of the same species. Utilizing these relatively simple and robust methods, the current study has identified instances of both inter- and intraspecies cell line contamination. Sixty cell lines from multiple species of origin, 29 of which were canine, were tested via PCR. Subsequent STR screening of the 29 canine cell lines has allowed development of a database of canine STR profiles for comparison to other investigators' cell lines and periodic cell line revalidation. Additionally, presumptive OSA cell lines were assayed for expression of the osteoblast differentiation factor, runt-related transcription factor 2 (RUNX2), to verify they were truly OSA derived. Finally, anti-human antibodies to Alcohol Dehydrogenase Iron Containing 1 (ADHFE1) and Sodium Channel, Voltage-Gated Type I β (SCN1B) have been validated for use in canine samples.

METHODS

Canine Tissues

Canine tissues in this study were collected from dogs presenting to CSU or other veterinary teaching hospitals for treatment of OSA. Owner consent for tissue archiving was obtained prior to definitive treatment. Good- and poor-responder primary tumors

were archived at the Animal Cancer Center between 1996 and 2006 - snap frozen tissues and formalin-fixed paraffin embedded (FFPE) tissues were archived. Good and poor responder groups were defined based upon patient disease-free-interval (DFI): good-responders had a DFI greater than 300 days and poor-responders had a DFI less than 100 days. This is the same primary tumor sample set used in a previous publication (4). Samples of each primary tumor were collected at the time of limb amputation, flash frozen for nucleic acid extraction and/or formalin fixed and paraffin embedded for histology and IHC.

Mammalian Cell Lines

Cell lines used in this study were graciously provided by several laboratories in the CSU ACC. They were received either as a cryopreserved vial or phosphate-buffered-saline-washed pellets. Cryopreserved cells were cultured in "C10" media: DMEM high glucose with 6 mM L-glutamine, 1x each of sodium pyruvate, MEM vitamins, MEM non-essential amino acids and antibiotic-antimycotic, 10% fetal bovine serum (FBS) and Plasmocin prophylactic (Invivogen, Cat# ant-mpp). Cell cultures were detached from plates with 3 mM ethylenediaminetetraacetic acid (EDTA) in phosphate-buffered saline (PBS) or 0.25% trypsin in PBS with EDTA, pelleted by centrifugation for 5 minutes at 500 x g and extracted as described below.

Polymerase Chain Reaction Species Validation

Considering the variety of species of cell lines currently in use at the ACC, a multiplex PCR test was adapted from previous work to differentiate among cell lines from dogs, cats, mice, rats, Chinese hamsters, and humans (12). Genomic DNA from 60 cell lines from six laboratories with multiple presumed species of origin was extracted

with the DNeasy kit per the manufacturer's protocol (Qiagen, 69504) from cells grown to 90% confluency on 10 cm culture dishes or from pelleted cells. For the purposes of comparison, this screen tested cell line duplicates from different laboratories. PCR reactions were performed using 1 μ L (50-400 ng) of genomic DNA in a reaction mixture adapted from previous work (12) containing 20 mM Tris-HCl pH 8.4, 50 mM KCl, 6 mM MgCl₂, 0.5% glycerol, 0.006% NP40/Tween 20 (1:1 v:v), 500 μ M dNTPs, primers and 1.25 U GoTaq polymerase (Promega, M5005). Primers were synthesized by Integrated DNA Technologies; sequences and concentrations were as previously published (12) except for the Chinese hamster antisense primer which was adapted to 5'-GCG TAG GCG AAC AGG AAG TAT C-3' to match the currently published genomic sequence. Internal control primers that detect a 70 bp amplicon in all species were also included. Thermal cycling conditions were: 95°C for 5 minutes followed by 30 cycles of 95°C for 30 s, 60°C for 15 s and 72°C for 30 s and completed with a 7 minute final elongation at 72°C. PCR products were run on a 2% agarose gel in TBE at 100 v for 60 minutes and visualized under ultraviolet light by ethidium bromide staining. A ladder containing PCR of gDNA from all six species was run concurrently. To validate the sensitivity of the multiplex PCR, each species' DNA was artificially contaminated with 10% and 1% of another species' DNA and tested.

Short Tandem Repeat Profiling of Canine Cell Lines

Short tandem repeat (STR) profiling was performed on cell lines that PCR testing identified as canine in origin to assess the frequency of intraspecies contamination among cell lines. One μ L of genomic DNA prepared as above was input into multiplex STR PCR reactions using the StockMarks kit (Applied Biosystems, PN 4307481) per the

manufacturer's protocol. Two separate runs were performed to test a total of 29 cell lines (20 presumed unique lines, 9 duplicates from different laboratories). A positive control sample from the kit was included in each run. Thermal cycling conditions were as recommended by the manufacturer without controlled ramping. PCR products were analyzed via capillary electrophoresis (Applied Biosystems, Genetic Analyzer 3130xl) per manufacturer's protocols except as follows: 1 μ L of PCR product was mixed with 9 μ L water to lower signal intensity during the run and 1.5 μ L of diluted PCR product was then mixed with 0.5 μ L size standard^f and 10 μ L highly deionized formamide. Additionally, POP7 polymer was used instead of POP4 and the array length was 50 cm. Run conditions were identical to the default run module except the injection time was increased from 15 to 24 seconds and the scan number was shortened from 1800 scans to 1750. Data interpretation was performed by manually binning alleles into size groupings and assigning allele designations.

RNA Extraction and qRT-PCR

Following pelleting of cells, RNA was extracted using the RNeasy kit (Qiagen, Cat# 74104) per the manufacturer's instructions. Resultant RNA was quantified via spectrophotometry and 1 μ g was added to reverse transcription (RT) reactions using the Quantitect Reverse Transcription kit (Qiagen, Cat# 05313). Quantitative RT-PCR was performed as previously described using previously published primers (4) for ADHFE1, SCN1B and HPRT1 (hypoxanthine phosphoribosyltransferase 1, housekeeping gene). RUNX2 primer sequences were as follows: forward - 5'- TGT TTA GCC CTG CAG TGA AGA CGA -3', reverse - 5'- ACT GAG GCG GTC AGA GAA CAA ACT -3'.

Gene expression data from canine tissues was previously published (4). Fold change was calculated using the $2^{(-\Delta\Delta Ct)}$ method (13).

Western Blot Validation of Antibodies

Western blot analysis was performed on whole-cell lysates obtained by repeatedly passing cell pellets through a 26-gauge needle in Tris pH 7.5 buffer with cOmplete™, EDTA-free Protease Inhibitor Cocktail Tablets (Roche, Cat# 04693132001). Total protein was quantified with a BCA Assay kit (Pierce, Cat# 23227) and 25 µg protein denatured in 1x Laemli Buffer was loaded for each sample. Proteins were electrophoresed on 12% SDS-PAGE gels with 5% stacking gels at 180 v for 50 minutes and were then transferred to PVDF membranes with a semi-dry transfer unit. Membranes were dried with methanol then blocked in 5% milk in Tris-buffered saline with Tween-20 (TBST) for one hour at room temperature. Membranes were incubated with primary antibody in blocking buffer over night at 4°C, washed in TBST and incubated with secondary antibody in blocking buffer for one hour at room temperature. Following an additional wash step, SuperSignal West Pico Chemiluminescent Substrate (Pierce, Cat# 34078) was used for development and images were captured on a Bio-Rad ChemiDoc XRS system. α -tubulin was used as a loading control: primary antibody (Sigma Cat# T5168 mouse monoclonal anti-human) incubation was performed for one hour at a 1:5,000 dilution in 5% milk/TBST, secondary antibody (BioRad Cat# 170-6516, HRP-conjugated goat anti-mouse IgG) incubation was performed for one hour at room temperature at a 1:10,000 dilution in 5% milk/TBST. Western blotting was performed on a selection of canine OSA cell lines: Abrams, D17, Gracie, McKinley, Moresco, Vogel and Yamane.

Specificity of the primary antibodies was verified using blocking peptides per standard protocols. Briefly, primary antibody was incubated with 10x (by mass) blocking peptide in blocking buffer overnight at 4°C with agitation before being applied to the membrane. In parallel, unblocked primary was applied to a second, identical membrane. The western blot was completed as above and membrane signals were compared between the two membranes.

The anti-human primary antibodies tested here were both generated in rabbit and were polyclonal to the targets, ADHFE1 and SCN1B. The ADHFE1 antibody was obtained from Abcam (Cat# ab84313), the blocking peptide from Aviva Systems Biology (Cat# ARP52720_P050), and was targeted to an epitope that was 98% homologous to the equivalent canine peptide. The SCN1B antibody was obtained from Sigma (Cat# AV35028), the blocking peptide from Aviva Systems Biology (ARP35028_P050), and was targeted to an epitope that was 100% homologous to the equivalent canine peptide. Goat anti-rabbit IgG secondary was obtained from Sigma (Cat# 170-6516)

Immunohistochemistry

Immunohistochemistry (IHC) was performed on canine kidney sections and a pilot group of FFPE OSA tissues (n=17) to optimize antibody and assess staining patterns. The primary antibodies were the same as used for western blotting. The secondary antibody and ABC reagents used were components of the Vectastain Elite Rabbit kit (Vector Laboratories, Cat#PK-6101). Final development was performed with ImmPACT DAB Peroxidase Substrate (Vector Laboratories, Cat# SK-4105). Slides with 5 µm thick sections were deparaffinized and rehydrated in serial alcohol baths. Antigen retrieval was performed in a pressure-cooker with citric acid-based antigen unmasking

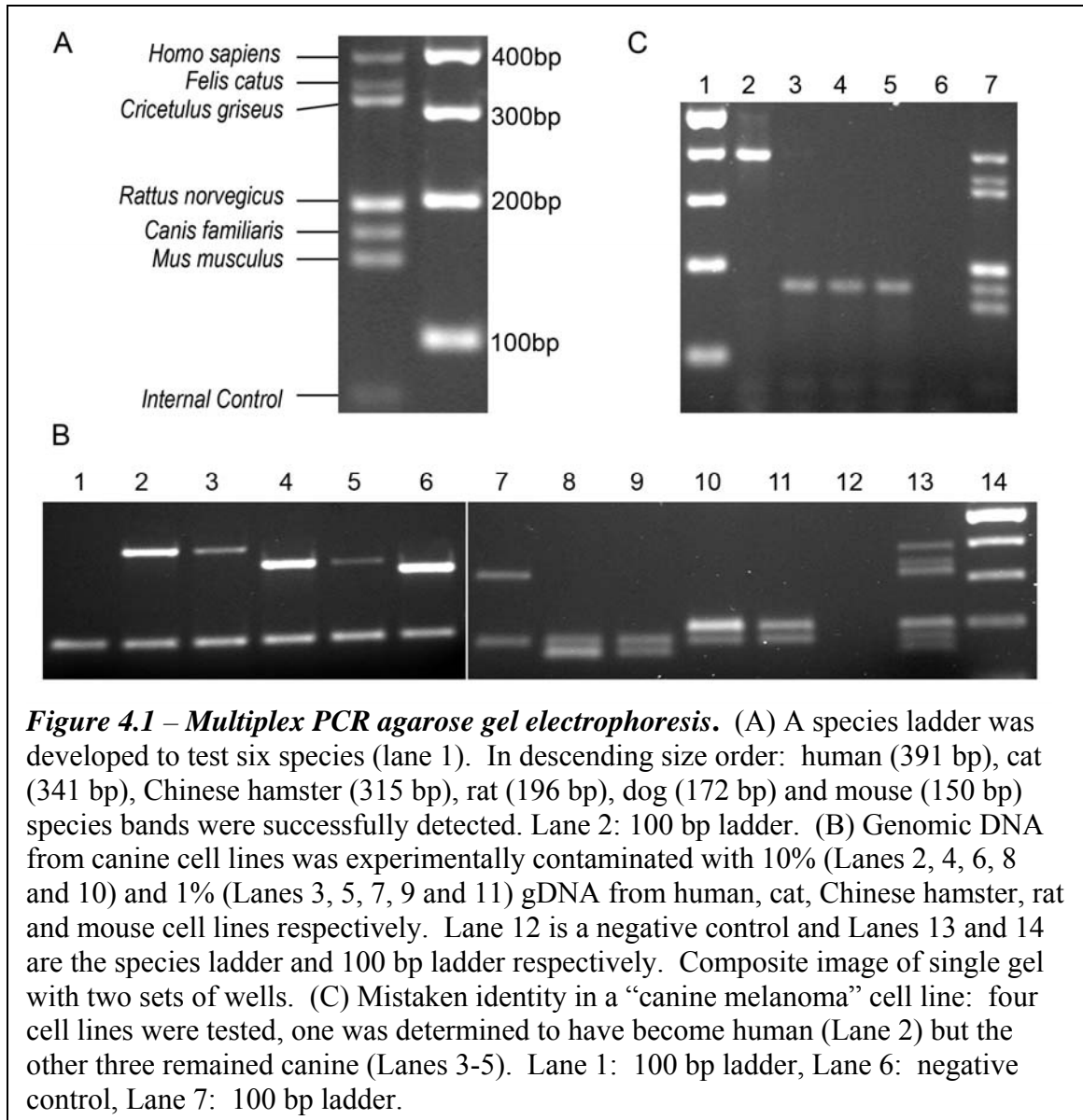
solution (Vector Laboratories, Cat# H-3300): the unit was brought to boiling, slides were added and the lid was secured. After five minutes of full-pressure heating, slides were allowed to cool to room temperature before washing in deionized water. Endogenous peroxidase activity was quenched in 3% hydrogen peroxide followed by water and TBST washes. Sections were isolated with a hydrophobic pen and blocking was performed with 1.5% goat serum in TBST for one hour at room temperature. Blocking buffer was aspirated and primary antibody was applied at a 1:500 to 1:10,000 dilution (depending on the antibody) in blocking buffer; sections were incubated overnight at 4°C in a humidified chamber. Slides were washed 3 times for 3 minutes in TBST before application of secondary antibody. Secondary antibody was diluted 1:1,000 in blocking buffer, applied to all sections and incubated for 1 hour at room temperature. Slides were again washed and ABC reagent was applied per the manufacturer's instructions. Following a 30-minute incubation, the ABC reagent was washed off the slides and DAB reagent was applied. Development was allowed to proceed for one minute. Slides were washed and counterstained with hematoxylin, dehydrated and mounted per standard protocols. Negative controls lacking primary antibody as well as blocking-peptide blocked primary controls were included.

RESULTS

Multiplex PCR Species Validation

The multiplex PCR was successfully able to identify all six tested species and the internal control amplicon at previously published amplicon sizes (Fig. 4.1) (12). Furthermore, when each species of interest was contaminated with 10% and 1% gDNA from a different species, the PCR detected this contamination with 100% success rate.

Figure 4.1B demonstrates this contamination study with canine gDNA as the primary input alone (lane 1) and contaminated with 10% (even lanes) and 1% (odd lanes) of human (lanes 2-3), cat (lanes 4-5), Chinese hamster (lanes 6-7), rat (lanes 8-9) and mouse (lanes 10-11) DNA. Lane 12 is a negative control with no input gDNA and the final two lanes are the species ladder and a 100bp ladder respectively.



Multiplex PCR testing of a total of 60 cell lines yielded three cases of mistaken identity. The first, a slow-growing canine osteosarcoma cell line “Yamane” was identified by PCR as murine in origin. A sample of this cell line from a different laboratory tested as canine indicating that the first laboratory had experienced a previous mislabeling or contamination event. The second case of mistaken identity was observed in another slow-growing canine cell line: the “Parks” melanoma tested as human in origin by PCR (Figure 4.1C). The investigator working with this line had noticed a change in morphology and proliferation rate and, thus, requested the validation. As with the “Yamane” cell line, a different laboratory’s stock of the “Parks” cell line tested as canine. Finally, another presumed canine osteosarcoma line, “Grey,” was identified by PCR as human in origin. None of these three samples demonstrated any evidence that the original species was still present in the sample. This result was not surprising as previous studies have shown that contaminating cell lines can completely overgrow cultures in as few as four or five passages (5).

Table 4.1 – Observed allele sizes in 29 canine cell lines.

	Allele Designation										
	A	B	C	D	E	F	G	H	I	J	K
PEZ 1	107	115	119	123	127						
PEZ 3	112	115	118	121	124	127	128	131	134	136	139
PEZ 5	103	107	111	115							
PEZ 6	171	175	179	180	183	184	187	188	191	199	
PEZ 8	227	228	229	232	233	236	238	240	245	249	
PEZ 12	263	267	270	274	277	285	288	290	297	301	
PEZ 20	172	176	180								
FHC 2010	227	231	235	239							
FHC 2054	147	151	156	160	164	168	172	176			
FHC 2079	272	275	279	287	291						

Short Tandem Repeat Profiling of Canine Cell Lines

Short tandem repeat analysis of verified canine cell lines yielded three additional cases of mistaken identity. The STR kit tested ten different loci; up to 11 different alleles were observed among the samples (Table 4.1). Alleles were designated by sequential lettering because a set nomenclature utilizing allelic ladders for canine STRs has not yet been established. This tactic allows comparisons between different cell lines or multiple samples from the same cell line to validate identity within a species. Cancer cell lines can contain many genetic alterations including loss of heterozygosity or the gain or loss of allele copies, thus, sub-lines of the same cell line may not have identical STR profiles. Considering this, looser criteria are required for the comparison of cancer cell line STR profiles. Previous work comparing STR alleles in human cell lines determined that a threshold of 75% identity was sufficient to identify all cell lines known to derive from a single source. Virally transformed and drug-resistant sublines also conformed to this threshold (14). Cell lines isolated from different individuals showed no greater than 50% identity (14).

In the first case of mistaken identity, two samples of the widely-used D17 canine osteosarcoma cell line had vastly different STR profiles (Figure 4.2). In order to determine the correct STR profile, two additional samples of the D17 cell line were analyzed, including a sample obtained from the supplier (ATCC). Comparisons of the STR profiles between multiple samples obtained from a total of 8 osteosarcoma cell lines allowed the determination that the STR profile of one of these “D17” cell lines matched that of another canine osteosarcoma line, the Moresco line (Table 4.2). The other “D17” cell line matched the STR profile of the D17 sample obtained from the supplier (ATCC).

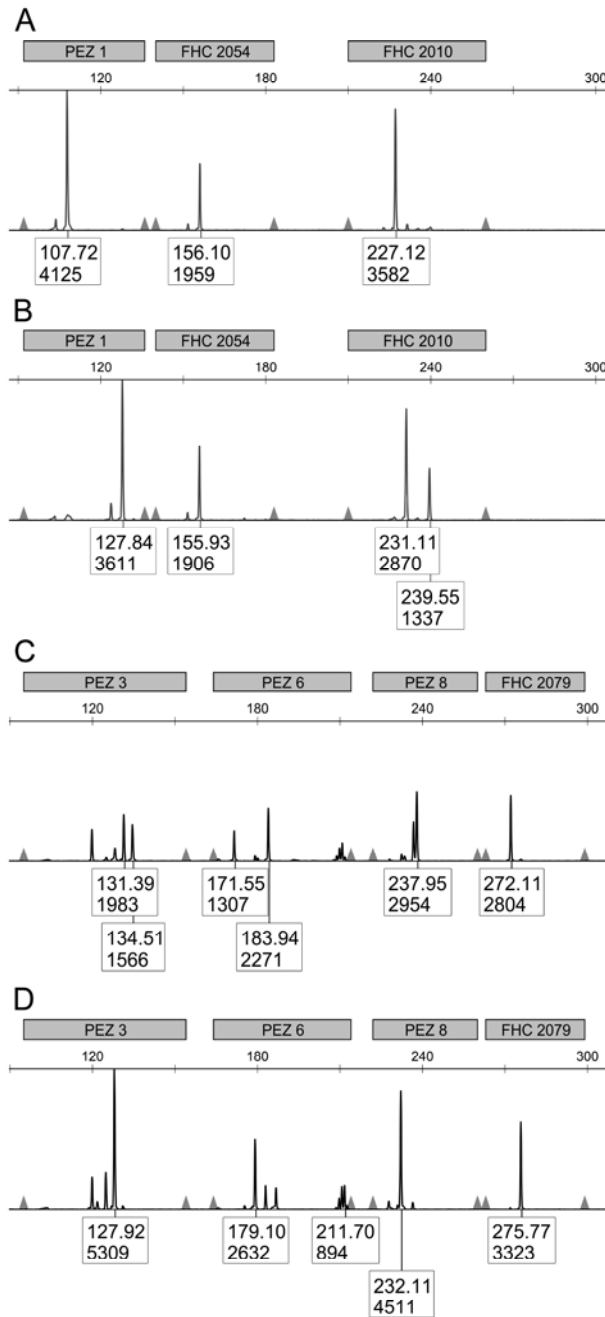


Figure 4.2 – Abbreviated STR profile of two cell lines originally presumed to both be D17. A) Three STR loci from the sentinel D17 cell line from one laboratory compared to the same 3 loci (B) of the original D17 cell line from the provider (reference cell line)^g. The lines share the same FHC2054 allele but the other two loci do not match. Four additional loci from the sentinel (C) and reference (D) D17 cell lines do not share alleles. Further testing demonstrated that the sentinel line (A&C) was identical to the “Moresco” cell line and that a D17 line from another laboratory matched the reference D17 line (B&D).

Table 4.2 – Allele distribution in 29 cell lines as determined by STR analysis.

Cell Line	PEZ1	FHC 2054	FHC 2010	PEZ5	PEZ20	PEZ12	PEZ3	PEZ6	PEZ8	FHC 2079
C2(1195) ^b	A	A,C	B	C	B	C	C,K*	E,H	C,D	A
Moresco ^b	A	C	A	A	0	A,I	H	A,F	G	A
D17 ^b	A	C	A	A	0	A,I	H,I	A,F	G	A
Abrams[r] ^{1,b}	A,C	D,H	A,C	A	B	D,J	E	C,G	B,G	D,E
Abrams ^a	A,C	D,H	A,C	A	B	D,J	E	C,G	B,G	D,E
Abrams ^{2,b}	A,C	D,H	A,C	A	B	D,J	E	C	B,G	D,E
CMT27 ^b	B	B,C	C	A	B	E	A,D	B	I,J	A
CMT12 ^b	B	B	C	A	B	E	A,D	B	E,I	A
CML6M ^b	B	B	C	A	B	E	A,D*	B	E,I	A
Gracie ^b	B	C,G	B,C	C	C	C,D	F,G	C,E	H	B,C
Vogel ^a	B,C	C,G	C,D	A	B	D	B,H	B,F	C,F	A,B
Vogel ^b	B,C	C,G	C,D	A	B	D	B,H	B,F	C,F	A,B
OSW ^b	B,D	C	D	A	C	C,G	E,J	B,E	H	C
OSW ^b	B,D	C	D	A	C	C,G	E,J	B,E	H	C
DEN-HSA ^{1,b}	B,D	F,G	B,C	A	B,C	F,G	E	E,G	C,H	B,C
DEN-HSA ^{2,b}	B,D	F,G	B,C	A	0	F,G	E	E,G	C,H	B,C
Fitz-HSA ^b	B,D	F,G	B,C	A	B,C	F,G	E	E,G	C,H	B,C
CTAC ^b	C	E	A,B	D	B	E	H,I	E	A	B
McKinley ^a	C,D	B,C	B,C	A	B	D,F	G,H	G,J	B	A,B
McKinley ^b	C,D	B,C	B,C	A	B	D,F	G,H	G,J	B	A,B
Dog Control	C,D	B,G	C	A	A,C	A,I	B,E	D,G	D,H	B
Yamane ^a	C,D	B	A	A	B	C	E,H	A	C	B
DH82 ^b	C,D	C,F	B	B	B	C,F	E	C	D,H	B
K9TCC ^b	C,D	H	B	D	B	B	C	E	F	C
1771[r] ^b	C,E	B	B	A	0	D,E	K	I	F,J	A
CML6M ^c	C,E	B	C,D	A	0	E,I	G,I	C	F,H	B
CML10C2 ^b	D	C	B	D	B	C,D	C	C,E	B,H	A,E
CML84- 10C2 ^c	D	C	B	D	B	C,D	C	C,E	B,H	A,E
D17 ^a	E	C	B,D	A	0	A,H	G	C	D	B
D17 ^{3,b}	E	C	B,D	A	A,C	A,H	G	C	D	B

* = allele call missed by analysis software, a = “Laboratory 1”, b = “Laboratory 2”, c = “Laboratory 3”,
 1 = Oldest passage of cell line, 2 = Recent passage of cell line, 3 = Sentinel cell line from supplier

In the second case, the STR profile for the canine Fitz-HSA hemangiosarcoma cell line exactly matched both early and late passage number samples from the DEN-HSA hemangiosarcoma line, indicating the three samples are derived from the same source.

A third case of mistaken identity occurred when two separate samples of a putative canine melanoma cell line, CML6M, did not have similar STR profiles. However, one sample shared an identical STR profile with the mammary tumor cell line, CMT12, indicating contamination or mislabeling. Interestingly, the CMT12 and CMT27 cell lines had STR profiles that were 90% conserved, showing differences in only two alleles, indicating that they were likely derived from the same donor. This change in alleles may represent genetic drift of a single cell line or the difference between a primary tumor and a metastatic site. Additional information regarding the derivation of these cell lines or comparisons to earlier passages will help to resolve these questions. The other CML6M sample had a unique STR profile when compared to all the canine cell lines tested to date and is presumed to be correct.

Short tandem repeat profiling is also useful for the detection of genetic drift among different passages of the same cell line. In the current study, one such case of genetic drift was observed. Comparison of three Abrams canine osteosarcoma cell line

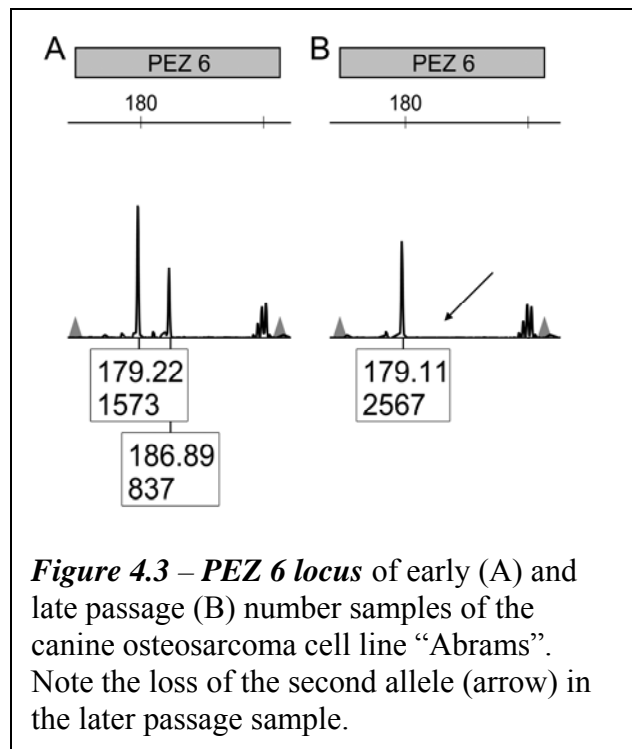


Figure 4.3 – PEZ 6 locus of early (A) and late passage (B) number samples of the canine osteosarcoma cell line “Abrams”. Note the loss of the second allele (arrow) in the later passage sample.

samples indicated that one later passage sample had lost one PEZ 6 allele resulting in 95% identity with the other two samples (Figure 4.3). In all, seven of 60 cell lines tested (12%) were misidentified or altered. Although this is lower than suggested averages (7), it still validates the necessity of good cell culture practices including periodic cell line validation. The observed misidentifications may be due to contamination or accidental mislabeling. Thus, it is imperative to practice excellent cell culture techniques and regular testing to prevent cases of misidentification from wasting valuable time and money.

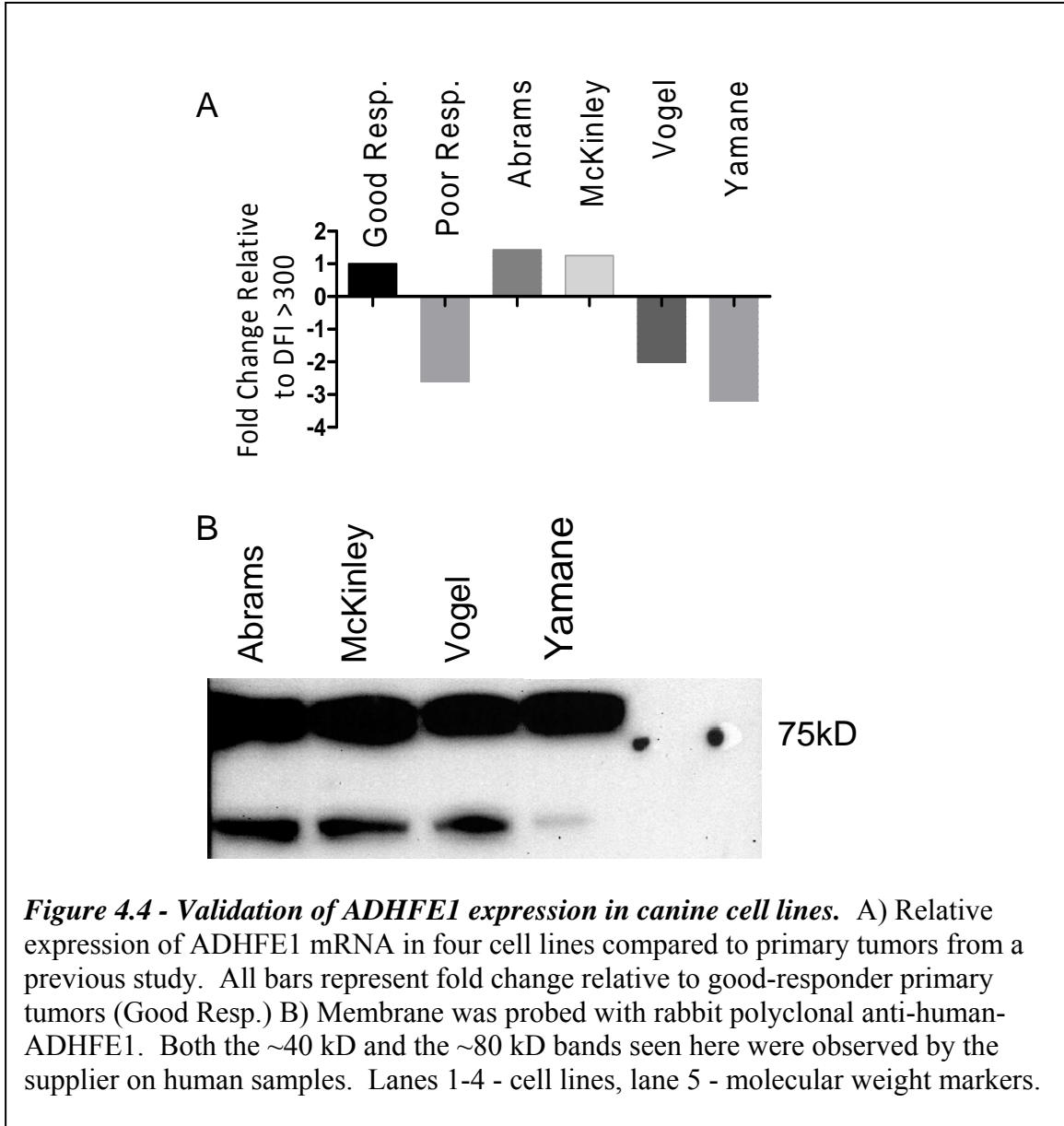
RUNX2 Expression as a Means to Validate OSA Origin of Cell Lines

In order to validate that all canine OSA cell lines used in this study were, indeed, derived from OSA, we tested expression of the bone/OSA marker, RUNX2. RUNX2 is a well-established marker of OSA and typically shows strong up-regulation in these tumors [see (15) for review]. Via qRT-PCR, we determined that RUNX2 was, indeed, detectable in all presumed OSA cell lines (Ct < 37 cycles, data not shown).

ADHFE1 Expression in Canine OSA Cell Lines

ADHFE1 was previously identified as a dysregulated gene in canine OSA and it was determined to be an attractive target for model generation. Thus, we analyzed protein and mRNA expression of this gene in cell lines for future *in vitro* studies. qRT-PCR in the Abrams, McKinley, Vogel and Yamane (verified canine) cell lines identified a range of expression levels spanning those observed in good and poor responder dogs (Figure 4.4A). The ADHFE1 antibody tested successfully probed the target protein: the expected band size of 40-45 kD was observed as was a larger band, roughly 80 kD in size (Figure 4.4B). Blocking peptide blocked signal from both of these bands, and the

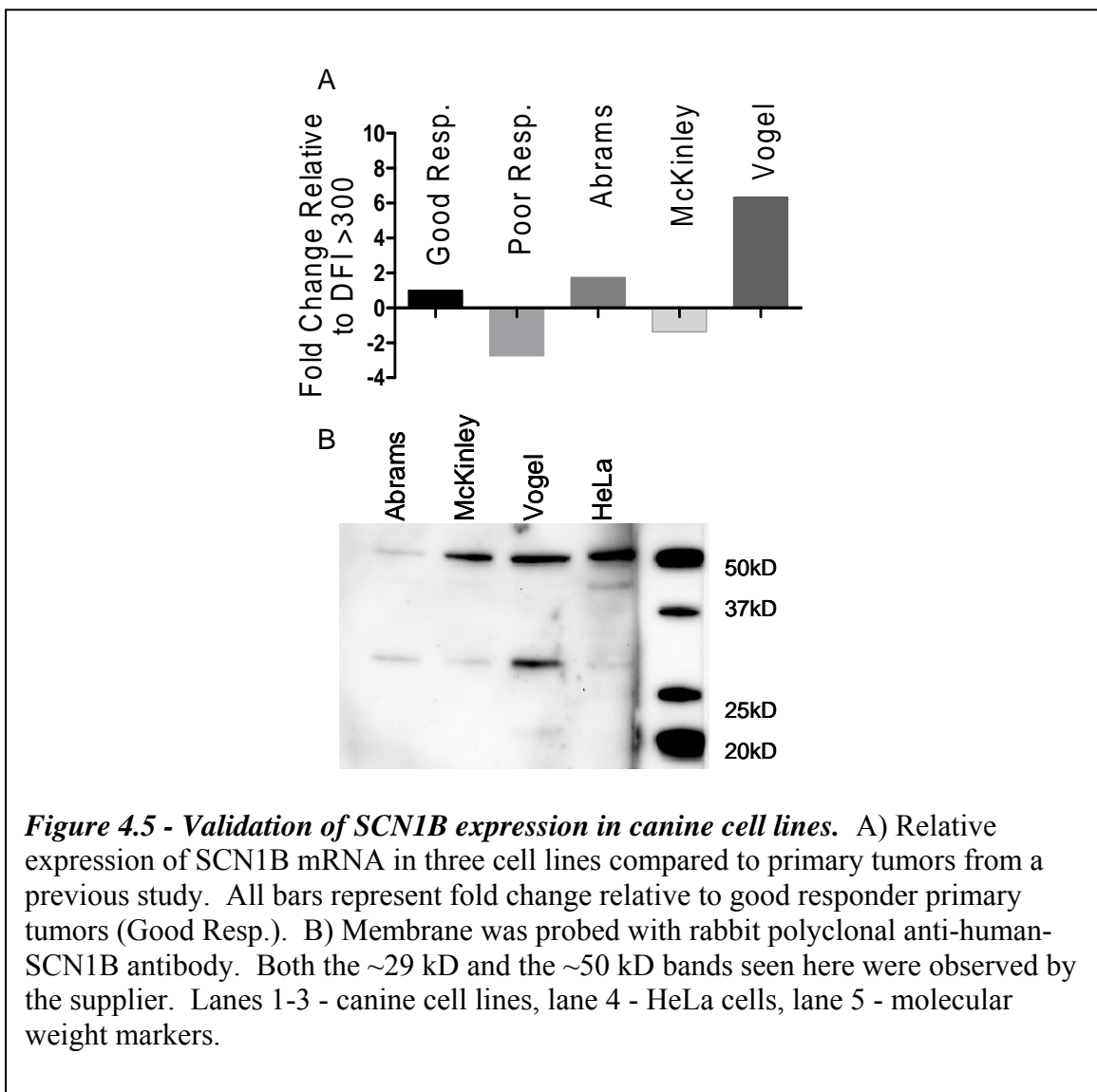
information from the supplier indicates that this larger band is present in human samples as well. However, it is worth noting that only the intensity of the smaller band tracks with observed mRNA expression levels.



SCN1B Expression in Canine Cell Lines

SCN1B expression levels were also examined relative to good and poor responder dogs. qRT-PCR identified a range of expression in cell lines with the Vogel line

expressing far greater quantities of SCN1B mRNA than observed in any primary tumors tested thus far (Figure 4.5A). The SCN1B antibody that was tested also successfully probed the target protein but, again, generated two bands. The expected band size was observed at 29 kD as was a 50 kD band that was also observed by the supplier (Figure 4.5B). HeLa cells (Lane 4) were included in this blot as a positive control and demonstrated similar banding patterns to the canine samples. Blocking peptide successfully blocked signal from both predominant bands.



Immunohistochemical Validation of Antibodies in Canine Samples

To determine if antibody functionality observed in western blots translated to IHC procedures, primary canine tumors as well as control tissues were stained using the antibodies that had been determined to be specific above. Blocking peptide and negative controls lacking primary antibody were used to optimize antibody concentrations. The ADHFE1 antibody was optimized in canine kidney sections. Initial staining with 1:1,000 dilution of primary antibody was successful and demonstrated membranous and nuclear

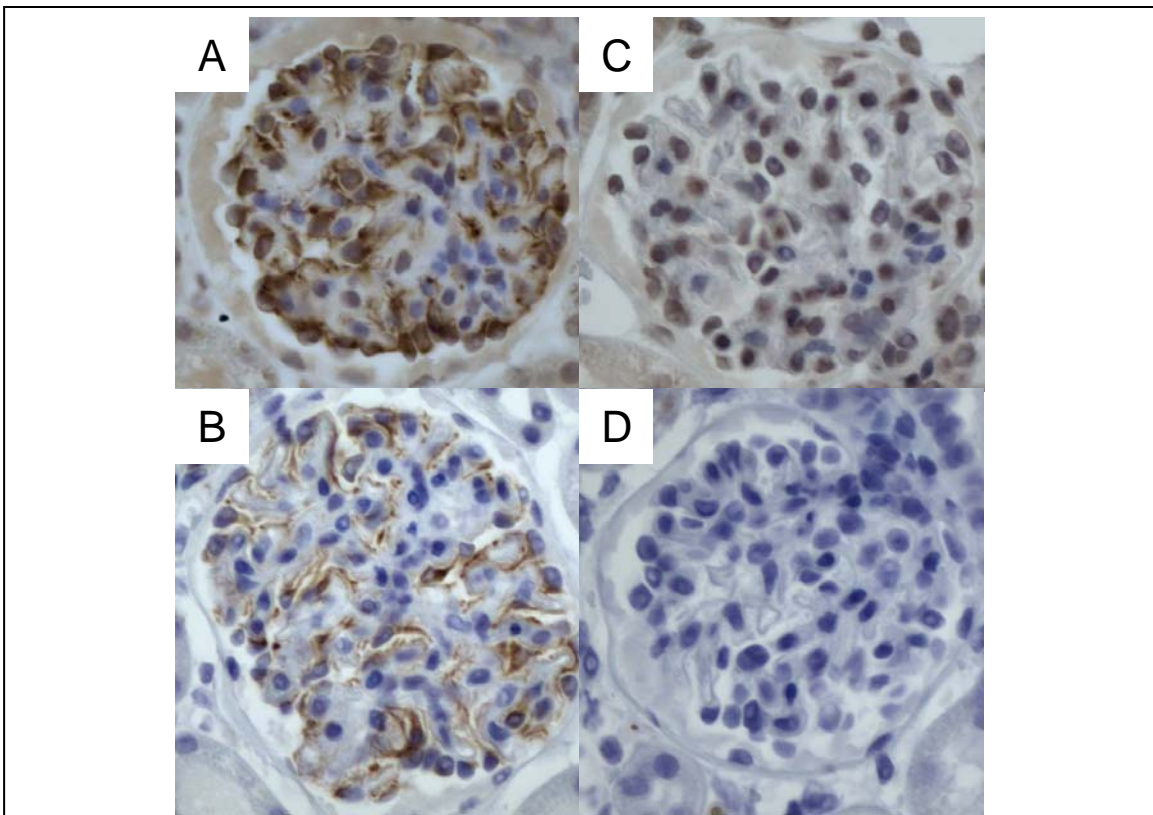


Figure 4.6 - Immunohistochemical staining of canine kidney sections with anti-ADHFE1 antibody. All images are 400x. 5 μ m sections of primary tumor tissue were stained for ADHFE1 using the same polyclonal antibody used for western blotting. Positive signal is indicated by brown staining (DAB development), hematoxylin (blue) counter-stain (A-D). Primary antibody concentrations of 1:1,000 (A,C) and 1:10,000 (B,D) were tested. Blocking peptide blocking of primary antibody specific activity (C,D) indicated that 1:1,000 was too high of a concentration as it produced non-specific nuclear staining (C). 1:10,000 dilution, however, yielded specific staining as all staining was blocked by the blocking peptide (D).

staining (Figure 4.6A). Staining with a 1:10,000 dilution of primary antibody, however, abolished all nuclear staining yet maintained membranous staining (Figure 4.6B). To determine which pattern was specific, blocking peptide was used to block specific binding of primary antibody to the targeted epitope. This experiment determined that the nuclear staining observed with the more concentrated primary antibody was non-specific as only membranous staining was blocked by blocking peptide (Figure 4.6C-D).

SCN1B antibody staining of control tissues (kidney and skin) indicated that SCN1B is localized to a subpopulation of tubule cells (Figure 4.7A) and is present in sebaceous glands and hair follicles (Figure 4.7B). Staining of primary OSA tumors indicated that the protein was localized to the cytoplasm and was present in the vast majority of tumors (Figure 4.7C,E). Blocking peptide studies indicated that slight background staining was present in those tumors demonstrating the strongest staining (Figure 4.7D) but not in tumors with less-intense or less-frequent staining (Figure 4.7F).

DISCUSSION

In the current study, we have validated canine species, STR identity and RUNX2 expression for seven canine OSA cell lines to be used in future studies and validated two anti-human antibodies for use in canine samples. Additionally, we have tested a variety of other cell lines for species identity and STR genotype, in the process, establishing a database of these findings as a resource for other researchers.

The pet dog population is a uniquely ideal model group for many diseases in humans, especially cancers. Their large body size and similar metabolic rate make for easy translation of drugs and surgical techniques to the human population. Furthermore,

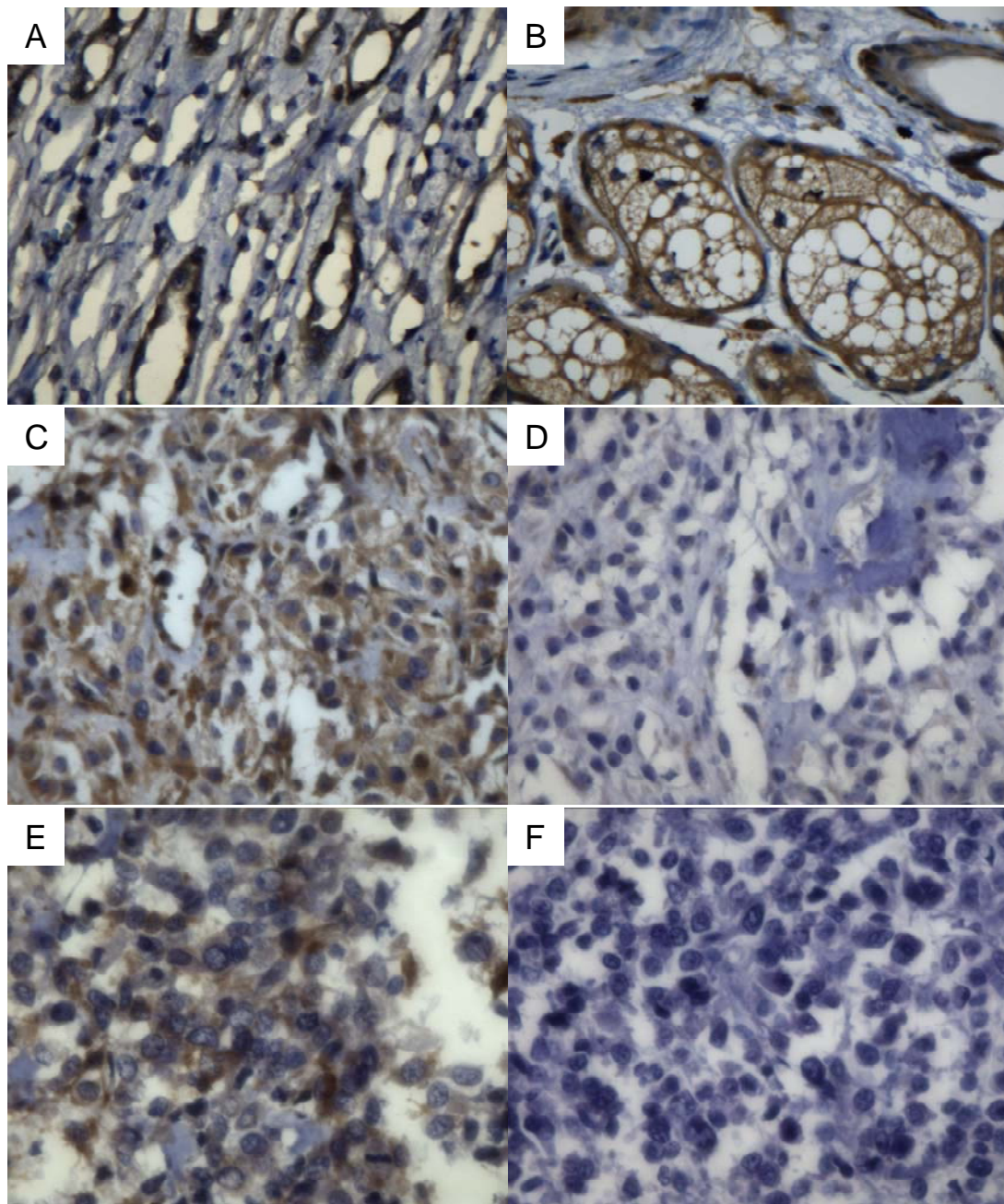


Figure 4.7 - Immunohistochemical staining of canine kidney, skin and tumor sections with anti-SCN1B antibody. All images are 400x. 5 μ m sections of primary tumor tissue were stained for ADHFE1 using the same polyclonal antibody used for western blotting. Positive signal is indicated by brown staining (DAB development), hematoxylin (blue) counter-stain (A-F). Canine normal tissues: (A) Canine kidney tubules, (B) canine skin section with sebaceous gland and hair follicle. Canine OSA sections: C) unblocked SCN1B staining, D) blocked SCN1B antibody used for staining in a sample from the same dog. E&F) Same as C & D but with tumor from a different patient.

they share a living environment with humans and are more closely genetically related to people than are mice. Compared to humans, dogs are a relatively inbred population; this may lend itself to successful identification of disease-causing genetic factors that are otherwise obscured in the human population. Finally, unlike mouse models, diseases in dogs are spontaneous and more likely to reflect similar human diseases (1, 3, 16, 17).

Multiplex PCR testing using species specific primers is a simple and inexpensive way to begin the species validation process in any facility where multiple species of cell lines are used. Following species validation, PCR-based STR profiling is the current “gold standard” for cell line validation within a species. Commercial microsatellite kits are not currently available for all species. However, the increased use of STR analysis in forensics and parentage testing for breed registries has resulted in the development of STR panels for a growing variety of species.(18-25) Both forensic and parentage testing require the STR panels to be sufficiently complex to allow for the identification of individuals in a population and within specific breeds. The selected loci must also exhibit efficient, repeatable amplification in and between laboratories. Typically, tetranucleotide repeats have proven to be the least susceptible to error.(23) The STR panel used in this study exceeded 99% power of exclusion for canine parentage verification in 61% of the breeds tested in a previous study.(26)

For the effective development of searchable databases, a standardized nomenclature for a consistent set of microsatellite markers is required. For such nomenclature to be developed, allelic ladders for each locus must be generated so that allele size can be standardized across different facilities. As these are not currently available for the canine species, the allele sizes presented in Table 1 are specific to the

capillary electrophoresis instrument and methodology used at CSU. The control canine DNA (Table 2) that was included with the STR kit may, to a limited extent, be used as an inter-facility reference point. However, the control DNA is not sufficiently precise to supplant an allelic ladder because DNA migration in capillary electrophoresis is dependent upon both size and sequence. Thus, the use of an allelic ladder would greatly enhance size measurement accuracy (23).

The average standard deviation in allele size for this control was ± 0.176 bp between runs indicating that there was a high degree of repeatability when the same instrument was used. However, different instruments and polymers may result in as much as a 4 bp shift. As a consequence, most laboratories conducting parentage testing require that the samples for offspring and all possible parents are tested concurrently to minimize error. The consistency in allele size between runs suggests that this will not be a problem for cell line validation within CSU's core facility; however, control samples will be monitored to detect deviations in the observed allelic sizes.

Standard cell culture practices that should be implemented to avoid contamination include maintenance of separate culture media stocks for each cell line, never having multiple cell lines in the hood at the same time, and thoroughly cleaning the hood and associated cell culture equipment between cell lines. Beyond these basic practices, validation of cell lines before beginning a new study is highly recommended. To further the precision of cell line validation, it is recommended that, whenever a new cell line is cultured from tissue, a sample from the tissue donor be analyzed with STR profiling so that all future passages of the resulting cell line may be compared against the donor's profile. Furthermore, to avoid genetic drift, it is advantageous to maintain low passage

number stocks to which an experimenter can return when cultured cell lines reach a high passage number or show evidence of genetic drift on STR analysis.

Despite these current limitations, STR analysis provides a simple, inexpensive method to validate cell line consistency and identity. The development of a database of STR profiles and comparison of cell line profiles from multiple sources including early passage samples or donor tissues will improve the quality, consistency, and validity of research studies utilizing canine cell lines.

Quantitative RT-PCR for the RUNX2 gene was a fast and effective method of verifying that OSA cell lines were, indeed, derived from OSA. Up-regulation of this gene is not unique to OSA but the only other system in which it is commonly observed is acute myeloid leukemia. Thus, RUNX2 expression must be evaluated in the context of cell morphology - as OSA cells are adherent and spindle-shaped and leukemic cells are, generally, non-adherent and round, they are easy to differentiate. Using this methodology, the seven OSA cell lines addressed in this study have been validated as OSA-derived.

Only a very limited number of anti-canine antibodies are commercially available as the dog model system is only recently gaining acceptance. Thus, short of generating new antibodies, the only way to study protein expression in canine samples is to validate currently available antibodies. Many of these are anti-human antibodies and, considering the high degree of homology between dogs and humans, have a good chance of working in the canine system. We approached antibody validation by first verifying that there was a significant amount of conservation between the target epitope and the canine protein sequence. This, undoubtedly, contributed to the validation success rate shown here.

The importance of blocking peptides for optimization of IHC is often omitted in standard protocols. The false background staining observed in canine kidney sections stained with anti-ADHFE1 (Figure 4.6) emphasizes that having a blocking peptide for every antibody is crucial if one wishes to generate true and correct data. An additional two antibodies were validated for use in canine samples; data for these are presented in the chapters focused on the genes *IGF2BP1* (Ch. 5) and *NDRG2* (Ch. 6).

ACKNOWLEDGEMENTS

This chapter was expanded from a short report that was originally published in *JVDI* (27). Jason P. Rivest was included as an author on that publication due to his significant input on the canine STR portion of this work. The author would like to thank Jessica Prenni at CSU's Proteomics and Metabolomics Core facility for assistance with the Canine STR analysis. The Molecular Oncology Laboratory at the CSU Animal Cancer Center in collaboration with the Proteomics and Metabolomics Core will facilitate species verification and canine STR analysis as a fee-for-service for interested investigators. This work was funded by a grant from the Colorado State University Cancer Supercluster Program.

REFERENCES

1. Dernell WS, Ehrhart NP, Straw RC, Vail DM. Tumors of the skeletal system. In: Withrow SJ, Vail DM, editors. *Withrow and MacEwen's Small Animal Clinical Oncology*. 4th ed. St. Louis: Saunders Elsevier; 2007. p. 540-67.
2. Jaffe N. Adjuvant chemotherapy in osteosarcoma: An odyssey of rejection and vindication. In: Jaffe N, Bielack SS, Bruland OS, editors. *Pediatric and Adolescent Osteosarcoma, Cancer Treatment and Research*. New York: Springer; 2009.
3. Sutter NB, Ostrander EA. Dog star rising: the canine genetic system. *Nature Reviews Genetics* 2004;5(12):900-10.
4. O'Donoghue LE, Ptitsyn AA, Kamstock DA, Siebert J, Thomas RS, Duval DL. Expression profiling in canine osteosarcoma: identification of biomarkers and pathways associated with outcome. *BMC Cancer* 2010;10(1):506.
5. Shapiro W, Fossum T, Kitchell B, Couto C, Theilen G. Use of cisplatin for treatment of appendicular osteosarcoma in dogs. *JAVMA* 1988;192(4):507-11.
6. Gartler SM. Apparent HeLa cell contamination of human heteroploid cell lines. *Nature* 1968;217(5130):750-1.
7. Lacroix M. Persistent use of "false" cell lines. *International Journal of Cancer* 2008;122(1):1-4.
8. Nardone R. Eradication of cross-contaminated cell lines: A call for action. *Cell Biology and Toxicology* 2007;23(6):367-72.
9. Hughes P, Marshall D, Reid Y, Parkes H, Gelber C. The costs of using unauthenticated, over-passaged cell lines: how much more data do we need? *BioTechniques* 2007;43(5):575-86.
10. American Type Culture Collection Standards Development Organization Workgroup ASN-0002: 2010, cell line misidentification: the beginning of the end. *Nature Reviews Cancer*;10(6):441-8.
11. Paoloni M, Khanna C. Translation of new cancer treatments from pet dogs to humans. *Nature Reviews Cancer* 2008;8(2):147-56.

12. Cooper J, Sykes G, King S, Cottrill K, Ivanova N, Hanner R, *et al.* Species identification in cell culture: a two-pronged molecular approach. *In Vitro Cellular & Developmental Biology - Animal* 2007;43(10):344-51.
13. Livak KJ, Schmittgen TD. Analysis of relative gene expression data using real-time quantitative PCR and the 2- $\Delta\Delta$ Ct method. *Methods* 2001;25(4):402-8.
14. Masters JR, Thomson JA, Daly-Burns B, Reid YA, Dirks WG, Packer P, *et al.* Short tandem repeat profiling provides an international reference standard for human cell lines. *Proceedings of the National Academy of Sciences* 2001;98(14):8012-7.
15. Martin JW, Zielenska M, Stein GS, van Wijnen AJ, Squire JA. The role of RUNX2 in osteosarcoma oncogenesis. *Sarcoma* 2011;vol. 2011(Article ID 282745):13 pages.
16. Withrow SJ, Khanna C. Bridging the gap between experimental animals and humans in osteosarcoma. In: Jaffe N, Bruland OS, Bielack SS, editors. *Pediatric and Adolescent Osteosarcoma, Cancer Treatment and Research*. New York: Springer; 2009.
17. Mueller F, Fuchs B, Kaser-Hotz B. Comparative biology of human and canine osteosarcoma. *Anticancer Research* 2007;27(1A):155-64.
18. Chen JW, Uboh CE, Soma LR, Li X, Guan F, You Y, *et al.* Identification of racehorse and sample contamination by novel 24-plex STR system. *Forensic Science International: Genetics* 2010;4(3):158-67.
19. Coomber N, David VA, O'Brien SJ, Menotti-Raymond M. Validation of a short tandem repeat multiplex typing system for genetic individualization of domestic cat samples. *Croatian Medical Journal* 2007;48(4):547-55.
20. Kanthaswamy S, Tom BK, Mattila AM, Johnston E, Dayton M, Kinaga J, *et al.* Canine population data generated from a multiplex STR kit for use in forensic casework. *Journal of Forensic Sciences* 2009;54(4):829-40.
21. van Asch B, Alves C, Gusmao L, Pereira V, Pereira F, Amorim A. A new autosomal STR nineplex for canine identification and parentage testing. *Electrophoresis* 2009;30(2):417-23.
22. van Asch B, Pinheiro R, Pereira R, Alves C, Pereira V, Pereira F, *et al.* A framework for the development of STR genotyping in domestic animal species: characterization and population study of 12 canine X-chromosome loci. *Electrophoresis* 2010;31(2):303-8.
23. van Asch B, Pereira F. State-of-the-art and future prospects of canine STR-based genotyping. *The Open Forensic Science Journal* 2010;3:45-52.

24. van de Goor LH, Koskinen MT, van Haeringen WA. Population studies of 16 bovine STR loci for forensic purposes. *International Journal of Legal Medicine* 2009.
25. van de Goor LH, Panneman H, van Haeringen WA. A proposal for standardization in forensic bovine DNA typing: allele nomenclature of 16 cattle-specific short tandem repeat loci. *Animal Genetics* 2009;40(5):630-6.
26. DeNise S, Johnston E, Halverson J, Marshall K, Rosenfeld D, McKenna S, *et al.* Power of exclusion for parentage verification and probability of match for identity in American kennel club breeds using 17 canine microsatellite markers. *Animal Genetics* 2004;35(1):14-7.
27. O'Donoghue LE, Rivest JP, Duval DL. Polymerase chain reaction-based species verification and microsatellite analysis for canine cell line validation. *Journal of Veterinary Diagnostic Investigation* 2011;23(4):780-5.

Chapter 5

Expression of the oncofetal protein IGF2BP1 contributes to an invasive phenotype in canine osteosarcoma.

SYNOPSIS

Background: Osteosarcoma (OSA) is a highly aggressive bone malignancy that affects both dogs and humans. Previous identification of IGF2BP1 as a negative prognostic indicator in canine OSA led us to investigate possible mechanisms of control for this gene as well as the effects of modulating its expression in this system. **Methods:** Normal bone mRNA expression of IGF2BP1 was compared to that of tumors using microarrays and qRT-PCR. Intracellular localization of IGF2BP1 protein was examined via immunohistochemistry and *in vitro* invasion was assayed following siRNA-mediated knockdown. Genomic DNA was analyzed to determine if amplification of the IGF2BP1 locus was amplified and 3' UTR analysis was performed to determine if UTR shortening was responsible for over-expression of this gene. **Results:** IGF2BP1 transcript was found to be virtually undetectable in normal bone with microarray and qRT-PCR but up-regulated in the vast majority of tumor samples tested. Protein was localized to the

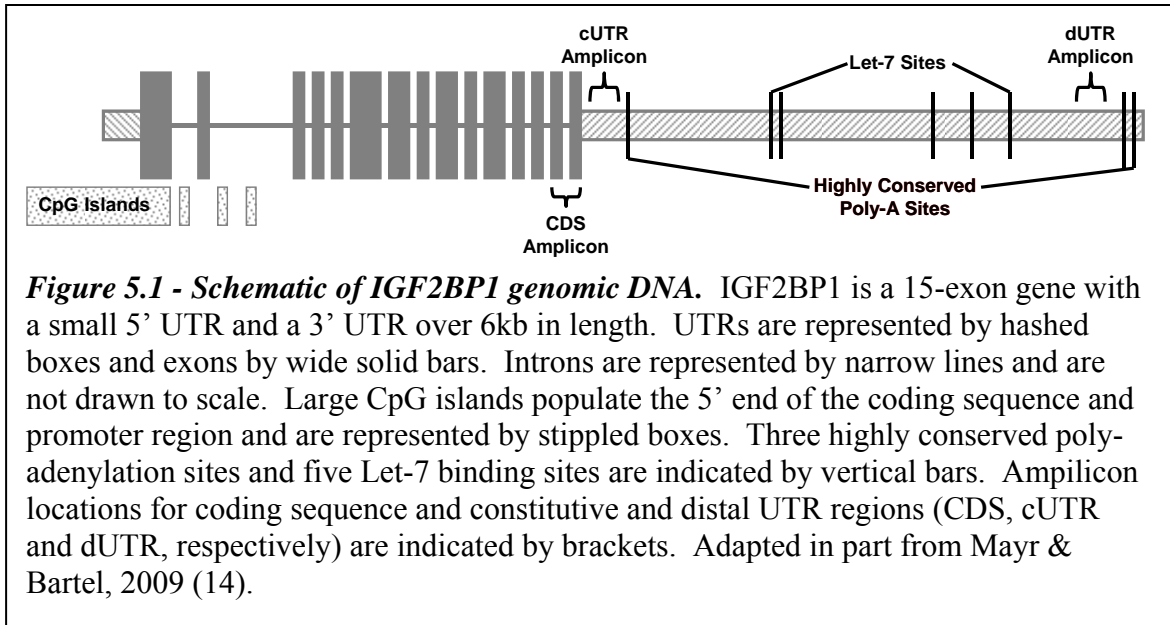
cytoplasm in many tumor samples but extended into the nucleus in others. siRNA-mediated knockdown was successful and reduced invasion in the Abrams canine OSA cell line. Genomic amplification of the IGF2BP1 locus does not appear to be a mechanism of over-expression in this system but 3' UTR truncation may contribute to increased mRNA half life. **Conclusions:** IGF2BP1 is up-regulated in canine OSA, most-so in dogs that respond poorly to definitive treatment and adjuvant chemotherapy. When modulated *in vitro*, IGF2BP1 contributes to invasion in canine OSA and over-expression of the gene is likely influenced by 3' UTR shortening *in vivo*.

INTRODUCTION

Osteosarcoma (OSA) is the most common primary bone malignancy in both humans and dogs affecting roughly 800 adolescents and 8,000 companion dogs annually (1, 2). Standard of care in both species involves resection of the tumor either by amputation or limb sparing surgery followed by adjuvant chemotherapy. Neoadjuvant chemotherapy is commonly utilized in human medicine but less-so in canine patients. The majority of OSA tumors in both dogs and humans occur in the metaphyseal regions of long bones in the appendicular skeleton. Histological classifications are shared between species as are many molecular characteristics of the disease (1, 3-6). Metastatic disease of the lungs is the most common cause of morbidity and mortality and is a strong negative prognostic indicator (1, 2, 7). Roughly 10-15% of patients of both species present with clinically detectable metastases and it is estimated that over 80% of patients may have undetectable micrometastatic disease at presentation. Thus, systemic chemotherapy aimed at diminishing distant disease is included in most protocols.

Considering the similarities between canine and human living environments, their genomes and the pathology of OSA, this disease in dogs is increasingly recognized as a valuable model for the human disease (3, 8). Previous studies by our laboratory identified Insulin-Like Growth Factor II (IGF2) mRNA Binding Protein I (IGF2BP1) as a gene that was highly expressed in primary OSA tumors from dogs that rapidly developed metastatic disease following definitive treatment when compared to dogs that exhibited slower disease progression (9). IGF2BP1 has been identified in a number of different systems and, as such, is known by many names including Zipcode-Binding Protein 1 (ZBP1), Coding Region Determinant Binding Protein (CRD-BP) and IMP-1, an alternate acronym for its IGF2 binding capability (10-13). The genomic DNA encoding this protein is located on human chromosome 17q21 and on canine chromosome 9; in both species, the promoter region has extensive CpG islands. A 15-exon transcript has been identified in both dogs and humans and an additional 13-exon splice variant has been identified in humans. The gene has an extensive 3' untranslated region (6.7 kb) with three highly conserved poly-adenylation signals and five highly-conserved Let-7 binding sites (14). Additional miRNA binding sites are also present. The translated protein is 577 aa long with 6 conserved domains: two K-homology (KH) domains and four RNA recognition motifs (RRM) (Figure 5.1). This gene has been termed "oncofetal" as it is only expressed in cancer and fetal tissues, expression is extremely limited in normal adult tissues (12, 15).

A number of studies have identified IGF2BP1 as a poor prognostic factor in several different cancer types. Doyle and colleagues identified chromosomal amplification of the IGF2BP1 region in human breast carcinomas; this was particularly



notable as this gene is near Her-2 yet they found amplification of the two genes to be independent of each other. They also found that IGF2BP1 amplification correlated with increased tumor grade, projecting a poor outcome (16). Ioannidis and colleagues supported this finding in breast carcinomas (17) and found this gene to be overexpressed in brain and lung cancers (18). This latter group did note that upregulation is not unique to malignancy as it was also observed in some benign masses. From this, they hypothesized that activation of IGF2BP1 may be an early step in tumorigenesis. IGF2BP1 has been linked to progression in lung, colorectal and ovarian carcinomas (19-22) and was found to be expressed in 72% of malignant mesenchymal tumors tested in one study as compared to 40% of benign masses (23).

As an mRNA binding protein, IGF2BP1 interacts with and modulates the expression of a number of different targets. CRD-BP was first discovered by Jeffrey Ross's group at UW Madison when they were investigating the stability of c-myc mRNA. They found a region of the c-myc RNA within the coding sequence (CRD) that, when

disrupted, decreased the half life of this mRNA by 4 to 8 fold (10). From this, they determined that a protein (CRD-BP) binds to this region and protects it from endonucleolytic cleavage. ZBP1 was first discovered by Robert Singer's group in the context of its binding to and localization of β -actin mRNAs in chick embryo fibroblasts (13). In a number of elegant mRNA trafficking studies, they determined that ZBP1 plays a crucial role in cell polarization and lamellapodia formation by directing localization of β -actin mRNAs (24-26). Additionally, they determined that the interaction of β -actin and ZBP1 is controlled by Src-mediated phosphorylation of a tyrosine residue of ZBP1 causing cargo release at the periphery of the cell (27). In 1999, Nielsen and colleagues coined yet another acronym for this protein, IMP-1, after they discovered it associating with the insulin-like growth factor II leader 3 mRNA (11, 12). In this initial study, they determined that multiple IMP-1 proteins bind to and repress translation of the IGFII leader 3 mRNA during key stages of embryonic development. With so many potential regulatory targets, it is unsurprising that dysregulation of IGF2BP1 could play a major role in tumorigenesis and cancer progression.

As the body of knowledge regarding miRNAs has dramatically increased in recent years, IGF2BP1 has gained more attention due to its lengthy 3' UTR with multiple Let-7 and other miRNA binding sites. Let-7 has been identified as tumor suppressor miRNA capable of suppressing oncogene expression as well as cell-cycle factors. Recent literature indicates it also downregulates IGF2BP1 which, in turn, may actually be a master regulator of cell-cycle-progression factors that are downstream of MYC including Cyclin D2 (*CCND2*), Cyclin-Dependent Kinase 6 (*CDK6*) and Cyclin-Dependent Kinase (*CDC2*) among others (28, 29). In a 2009 publication, Mayr & Bartel identified one

possible mechanism by which IGF2BP1 can escape Let-7 regulation: alternative cleavage and polyadenylation of the 3' UTR that removes all Let-7 binding sites from the transcript (14). Thus, dysregulation of Let-7 can lead to a release of IGF2BP1 expression and/or early cleavage of the UTR can be favored by conditions in the cell, effectively removing the ability of Let-7 to suppress the half-life of IGF2BP1. In either scenario, massive disruption in the normal control cascades of the cell ensues and the diverse IGF2BP1 downstream targets are released from their normal regulation.

The current study compares previously determined OSA primary tumor expression patterns of IGF2BP1 with those of normal bone via both microarray and quantitative reverse transcription PCR (qRT-PCR) as well as exploring IGF2BP1 expression in canine OSA cell lines. Array CGH analysis comparing normal tissue (muscle, skin) to a subset of OSA primary tumors was also performed to investigate if IGF2BP1 dysregulation was caused by gene amplification. Immunohistochemical staining of primary OSA sections was utilized to determine if staining of this factor could be used as a prognostic indicator. Additionally, we sought to elucidate the effect of IGF2BP1 expression in these cells with respect to invasion and migration. Finally, we examine relative expression levels of different 3' UTR segments to determine if truncation of the UTR is an active mechanism of IGF2BP1 release in this model.

METHODS

Canine Tissues

Canine tissues used in microarray and PCR studies were obtained from animals presenting to Colorado State University (CSU) for treatment of OSA. Owner consent for tissue archiving was obtained prior to definitive surgical treatment. Good- and poor-

responder primary tumors were archived at the Animal Cancer Center between 1996 and 2006 - snap frozen tissues and formalin-fixed paraffin embedded (FFPE) tissues were archived. Good and poor responder groups were defined based upon patient disease-free-interval (DFI): good-responders had a DFI greater than 300 days and poor-responders had a DFI less than 100 days. Normal bone and matched tumor samples were obtained from limbs post-amputation and harvested so that “normal” bone included in the study was distant from the tumor site and separated from the tumor by a joint (i.e. a femoral tumor would have matched distal tibia bone collected). Tissue was collected, snap frozen in liquid nitrogen and stored at -80°C until processing. Tumor tissues for an independent data set used for immunohistochemistry (n=64) were collected at various veterinary teaching hospitals and archived at CSU as FFPE blocks. Inclusion in these studies required limb amputation followed by doxorubicin and/or platinum drug adjuvant therapy.

Canine Cell Lines

Canine cell lines used in this study were graciously provided by Dr. Douglas Thamm and all cell lines were validated for species and short-tandem-repeat identities as previously described (30). Abrams cells were derived from metastatic OSA nodules whereas McKinley, Vogel and Yamane were derived from primary tumors. Cells were cultured in C10 media (DMEM high glucose with 6mM L-glutamine, 1x each of sodium pyruvate, MEM vitamins, MEM non-essential amino acids and antibiotic-antimycotic, 10% fetal bovine serum (FBS) and Plasmocin prophylactic (Invivogen, ant-mpp)). C0.1 media (identical to C10 but with 0.1% FBS) was utilized in invasion and migration assays.

RNA Extraction

Tumor and normal tissues were freeze-fractured, homogenized, extracted in Trizol per the manufacturer's instructions and purified with the RNeasy cleanup protocol. Cell cultures were detached from plates with 3mM ethylenediaminetetraacetic acid (EDTA) in phosphate-buffered saline (PBS) or 0.25% trypsin in PBS with EDTA, pelleted by centrifugation for 5 minutes at 500 x g and extracted using the RNeasy kit per the manufacturer's protocol. RNA was quantified via spectrophotometry and, prior to microarray, tissue RNA was bioanalyzed for quality at the Rocky Mountain Regional Center for Excellence (RMRCE) Genomics Core at CSU. Only high quality RNA with RNA Integrity Numbers (RINs) greater than 8 were used in microarray studies.

Microarray

Eight normal bone samples were analyzed with Affymetrix Canine 2.0 GeneChips as previously described (9). Resultant data was compiled with data from 15 good and poor-responder primary tumor samples obtained previously and analyzed with ArrayTrack (31). Data was preprocessed with the Probe Logarithmic Intensity Error (PLIER) estimation algorithm with a \log_2 transformation then analyzed for fold change based on two scenarios: normal bone versus all tumors or normal bone versus good responders versus poor responders. The first scenario was analyzed with a Bonferroni adjusted unpaired 2-tailed t-test, thresholds of corrected p-value <0.05 and fold-change >3 were applied. The second scenario was analyzed with pairwise t-tests and the same p-value and fold-change thresholds. \log_2 -transformed PLIER IGF2BP1 expression values were extracted for this study.

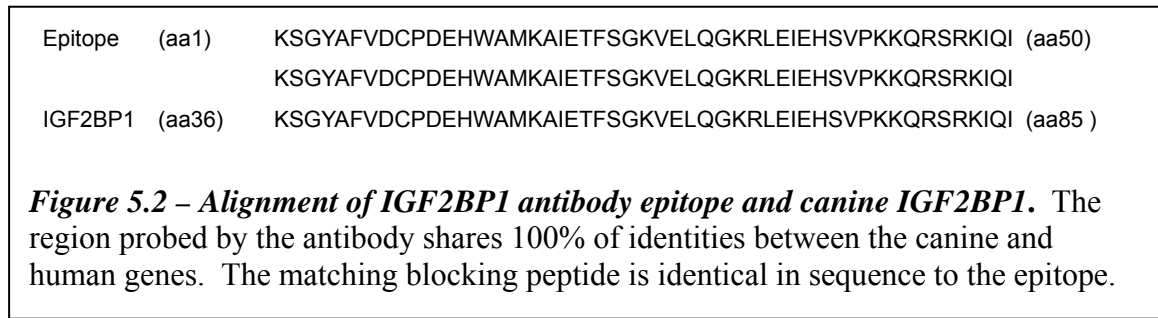
Quantitative RT-PCR

Reverse transcription (RT) was performed on RNA samples with the QuantiTect Reverse Transcription kit (Qiagen, 05313) per the manufacturer's instructions with 1 µg RNA input, a ten-minute gDNA digest incubation and a 30-minute RT incubation. No-RT controls were included for each sample as was one no-transcript control per RT reaction. Real-time quantitative PCR was performed using the iQ SYBR Green Supermix (Bio-Rad, 170-8880) in 25 µL reactions with 25 ng equivalent cDNA input. IGF2BP1 and housekeeping gene (HPRT-1) primers were as previously published (9) and were included in the reactions at 100 nM forward and 300 nM reverse primer concentrations. Standard curves for the two primer sets over two orders of magnitude were within 5% efficiency of each other. Thermal cycling was performed on the Mx3000p instrument (Stratagene) with the following parameters: 95°C for 10 m followed by 40 cycles of 95°C for 30 s and 60°C for one minute. Data collection was performed at the end of the 60°C step. Dissociation curve ramps were performed at the end of the cycle to verify that only a single product was generated. Data analysis was performed with the Mx3000p software. IGF2BP1 expression was normalized to HPRT-1 and fold change was calculated using the $2^{(-\Delta\Delta Ct)}$ method (32).

Western Blotting

Western blotting was performed on whole-cell lysates obtained by repeatedly passing cell pellets through a 26-gauge needle in Tris pH 7.5 buffer with cOmplete™, EDTA-free Protease Inhibitor Cocktail Tablets (Roche, 04693132001). Total protein was quantified with a BCA Assay kit (Pierce, 23227) and 25 µg protein was loaded for each sample. Proteins were electrophoresed on 12% SDS-PAGE gels with 5% stacking gels at

180 v for 50 minutes and were then transferred to PVDF membranes with a semi-dry transfer unit. Membranes were dried with methanol then blocked in 0.5% milk in Tris-buffered saline with Tween-20 (TBST) for one hour at room temperature. The primary antibody was obtained from Abcam (ab82968 - rabbit polyclonal to human); the targeted epitope is 100% homologous to the canine protein (Figure 5.2). Membranes were



incubated overnight at 4°C with primary antibody diluted 1:1,000 in 0.5% milk/TBST and were then washed 3 times for five minutes each in TBST. Secondary antibody (HRP-conjugated goat anti-rabbit IgG, Bio-Rad, 172-1019) was applied at a dilution of 1:10,000 in 5% milk/TBST for a one-hour, room-temperature incubation followed by TBST washes. SuperSignal West Pico Chemiluminescent Substrate (Pierce, 34078) was used for development and images were captured on a Bio-Rad ChemiDoc XRS system. Specificity of the primary antibody was verified using a blocking peptide (Abcam ab100852) per standard protocols. Briefly, primary antibody was incubated with 10x (by mass) blocking peptide in blocking buffer overnight at 4°C with agitation before being applied to the membrane. In parallel, unblocked primary was applied to a second, identical membrane. The western blot was completed as above and membrane signals were compared between the two membranes. α -tubulin was used as a loading control: primary antibody (Sigma Cat# T5168 mouse monoclonal anti-human) incubation was

performed for one hour at a 1:5,000 dilution in 5% milk/TBST, secondary antibody (BioRad Cat# 170-6516, HRP-conjugated goat anti-mouse IgG) incubation was performed for one hour at room temperature at a 1:10,000 dilution in 5% milk/TBST with washing and development steps as above.

Immunohistochemistry

Immunohistochemistry (IHC) was first performed on the good and poor responder groups (n=17) then in the expanded, independent data set. The primary antibody was the same as used for western blotting. The secondary antibody and ABC reagents used were components of the Vectastain Elite Rabbit kit (Vector Laboratories PK-6101). Final development was performed with ImmPACT DAB Peroxidase Substrate (Vector Laboratories, SK-4105). Slides with 5 μ m thick sections were deparaffinized and rehydrated in serial alcohol baths. Antigen retrieval was performed in a pressure-cooker with citric acid-based antigen unmasking solution (Vector Laboratories, H-3300): the unit was brought to boiling, slides were added and the lid was secured. After five minutes of full-pressure heating, slides were allowed to cool to room temperature before washing in deionized water. Endogenous peroxidase activity was quenched in 3% hydrogen peroxide followed by water and TBST washes. Sections were isolated with a hydrophobic pen and blocking was performed with 1.5% goat serum in TBST for one hour at room temperature. Blocking buffer was aspirated and primary antibody was applied at a 1:500 dilution in blocking buffer; sections were incubated overnight at 4°C in a humidified chamber. Slides were washed 3 times for 3 minutes in TBST before application of secondary antibody. Secondary antibody was diluted 1:1,000 in blocking buffer, applied to all sections and incubated for 1 hour at room temperature. Slides were

again washed and ABC reagent was applied per the manufacturer's instructions. Following a 30-minute incubation, the ABC reagent was washed off the slides and DAB reagent was applied. Development was allowed to proceed for one minute. Slides were washed and counterstained with hematoxylin, dehydrated and mounted per standard protocols. Negative controls lacking primary antibody were included. Slides were scored by two blinded individuals on several criteria: presence of sufficient tissue to read four or more 400x fields, percent and intensity of cytoplasmic staining and percent and intensity of nuclear staining. Scorers were instructed to avoid tissue edges to decrease artifactual findings. Good- and poor-responder scores were analyzed with Fisher's Exact Test; the larger, independent dataset was analyzed by generating Kaplan-Meier survival curves followed by log-rank analysis to compare groups.

Array Comparative Genomic Hybridization

Genomic DNA was extracted from tumors and patient-matched normal tissue (muscle, skin) using the DNeasy (Qiagen, Cat# 69504) kit per the manufacturer's instructions. Low yield tissue samples were digested overnight in proteinase K, salt extracted per standard protocols and precipitated in ethanol prior to DNeasy cleanup. Array-CGH was performed by Dr. Matthew Breen's laboratory at North Carolina State University as previously described (33). Relative amplification of the IGF2BP1 region was determined by dividing signal of each tumor sample by its matched normal sample.

IGF2BP1 Knockdown

Transient knockdown with siRNA was pursued in the Abrams cell line. Stealth pre-annealed siRNAs were designed with the BLOCK-iT RNAi design software and purchased from Invitrogen; sequences were: Scrambled, 5'-CAG GUG UGU GGU ACC

UUA CGA UGC A-3' with complement 5'-UGC AUC GUA AGG UAC CAC ACA CCU G; si1, UUC CCU UGC AAU UCG ACU UUC CCG G-3' with complement 5'-CCG GGA AAG UCG AAU UGC AAG GGA A-3'; si2, 5'-UGC CAA UGA UGG CAC CCA CAU ACU G-3' with complement 5'-CAG UAU GUG GGU GCC AUC AUU GGC A-3'. Cells were split onto 24-well, 6-well or 6cm plates and allowed to adhere overnight. The following day, HiPerFect transfection reagent (0.86 $\mu\text{L}/\text{cm}^2$ plate surface area, Qiagen, 301705) was mixed with siRNA duplexes (0.33 $\mu\text{L}/\text{cm}^2$ of a 20 μM solution) in DMEM and allowed to incubate for 15 minutes at room temperature for complex formation. This solution was then added, dropwise, to the plates and gently mixed. A Cy3 labeled siRNA (10 nM) was used as a transfection control (Integrated DNA Technologies - IDT). Cells were incubated for 6-72 hours with the siRNA before being harvested or split for further experiments. Knockdown was verified with qRT-PCR and western blot.

Invasion and Migration Assays

Abrams cells that had been transfected with either scrambled or targeted siRNAs were split onto 24-well FluoroBlok BioCoat Matrigel invasion or FluoroBlok migration plates (BD Biosciences, 354166 and 351158) 24 or 48 hours following transfection at a density of 2,000 cells/chamber in 500 μL C0.1 media. 750 μL C10 media (chemoattractant) was added to the bottom chamber of half of the wells whereas C0.1 was added to the other half. 24 hours following plating, media from the chambers was removed and 4 $\mu\text{g}/\text{mL}$ Calcein AM (BD Biosciences, 354216) in Hank's Buffered Salt Solution was added to the bottom chamber. Plates were incubated at 37°C in 5% CO₂ for 1 hour then read on a fluorescence plate reader at 494/517 nm (Excitation/Emission).

Three replicates of each treatment were performed. Net invasion was determined by dividing invasion signal by migration signal.

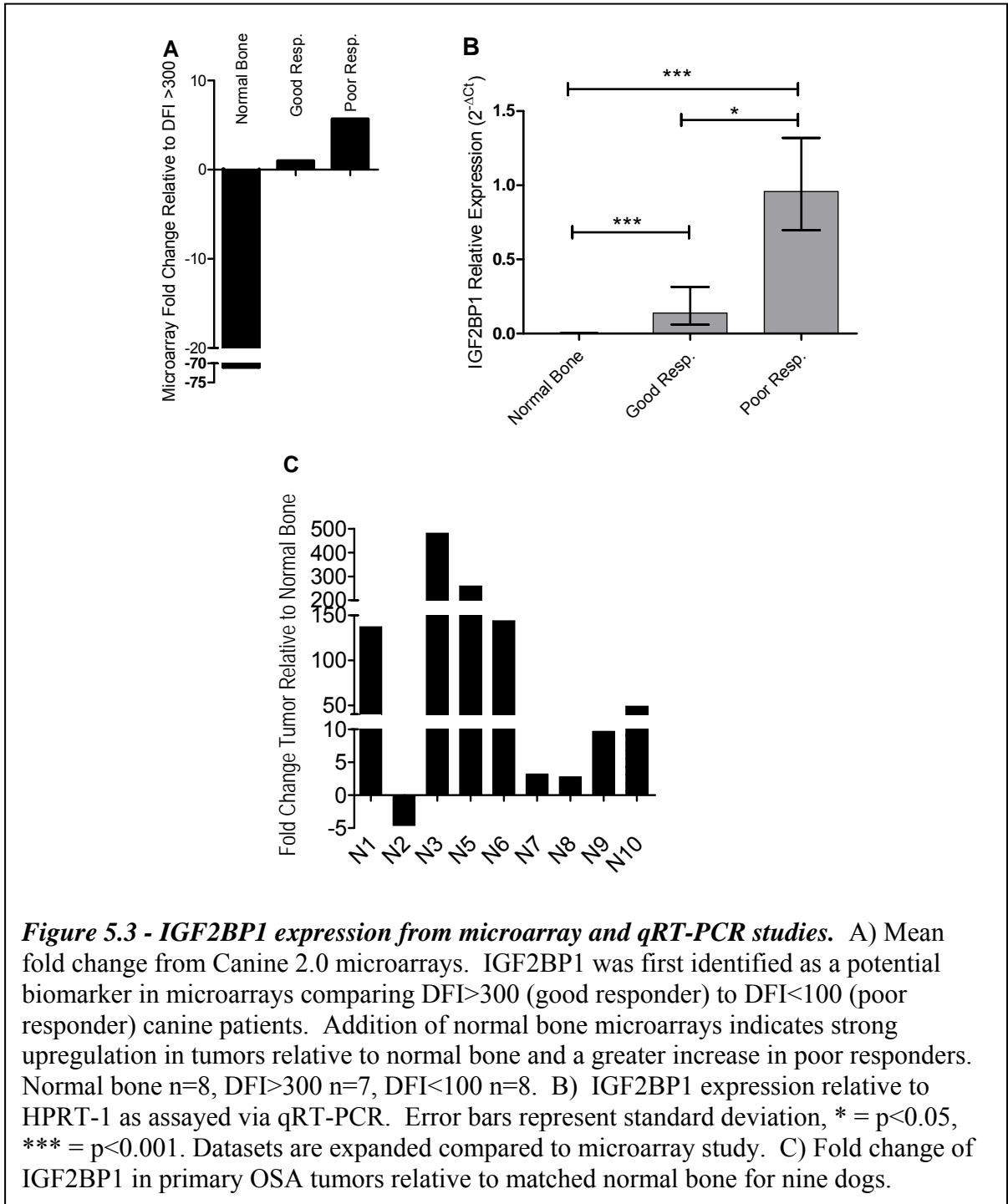
3' Untranslated Region Analysis

In order to determine the prevalence of 3' untranslated region (UTR) shortening in IGF2BP1 transcripts, primers were designed for qRT-PCR to generate amplicons in the constitutive UTR (cUTR) and the distal UTR (dUTR). Amplicon locations are diagrammed in Figure 5.1. Primer sequences were: cUTR Fwd 5'-AAG GAC AAC GGG CTG AAA TCG AGA-3', Rev 5'-CAA GCA AGT GGG CAA ACC TGA TCT-3' and dUTR Fwd 5'-TGA GAG AGG CCG CTT CTG AAT CAA-3', Rev 5'-TCA GAA GGG AAG GGA CGC ATC TTT-3'. qRT-PCR was performed as above with reactions for both UTR amplicons, the translated-region amplicon and the housekeeping gene performed concurrently to minimize inter-run variability. Expression relative to HPRT-1 was calculated and expressed as $2^{(-\Delta Ct)}$; fold-change was calculated using the $2^{(-\Delta\Delta Ct)}$ method.

RESULTS

Microarray and qRT-PCR Analysis

IGF2BP1 has been identified as an oncofetal protein and, thus, we wished to compare previously-observed tumor expression levels to that of normal bone. Toward this end, we performed microarray and qRT-PCR analysis of normal bone and compared it to the DFI cohorts and to matched tumor samples. IGF2BP1 transcript was virtually undetectable on microarray, with all 8 samples being flagged as "bad" by standard analysis procedures. When this small expression was compared to DFI cohorts, a greater-than 70-fold down regulation was observed relative to both tumor sets (Figure



5.3A). We validated this with qRT-PCR and observed a similar stair-step pattern with normal bone having virtually no IGF2BP1 expression, good-responder tumors having increased expression and poor-responder tumors demonstrating dramatically increased

expression (Figure 5.3B). When we compared normal bone samples to matched tumors via qRT-PCR, we observed a dramatic upregulation in 6 of 9 tumors, exceeding 400-fold in one case (Figure 5.3C). The other three tumors demonstrated no or limited upregulation of IGF2BP1 indicating that dysregulation of this gene may not be an important factor in those individuals.

Immunohistochemical Analysis

Considering the observed mRNA expression pattern of IGF2BP1 (i.e. highest in poor-responders) and previous reports indicating prognostic significance, we pursued immunohistochemical staining of tumor sections with the aim of developing a widely-applicable prognostic screen. As a pilot experiment, tumor sections from dogs included in the DFI cohorts were probed for IGF2BP1 staining. Cellular localization of the protein varied between samples with some only demonstrating cytoplasmic staining while others demonstrated both cytoplasmic and nuclear staining (Figure 5.4A-D). In this group of samples, presence of nuclear staining in greater than 25% of cells was predictive of outcome (Fisher's Exact Test, $p=0.009$). Immunohistochemistry was then pursued in a larger, independent set of 80 primary tumors from dogs with known DFIs and treatment histories. Neither cellular localization of IGF2BP1 nor intensity and frequency of staining were prognostic in this data set (Figure 5.4E-F).

IGF2BP1 Expression in Canine Cell Lines

With the aim of examining mechanisms and results of IGF2BP1 dysregulation *in vitro*, mRNA and protein product expression of this gene were assayed in four canine OSA cell lines. Using qRT-PCR, mRNA expression of IGF2BP1 was compared to previously-observed expression in the DFI cohorts. The Abrams line, originally derived

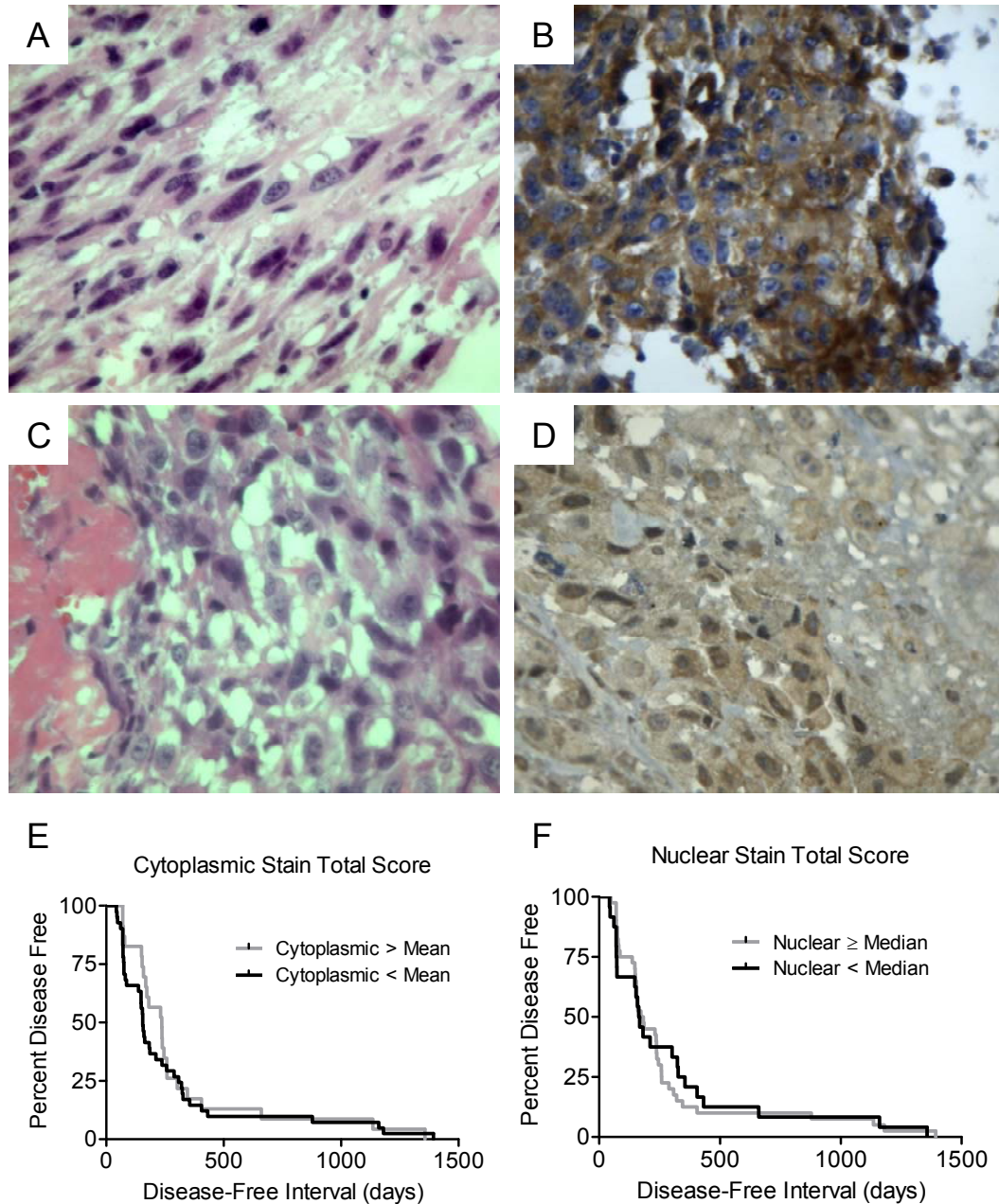
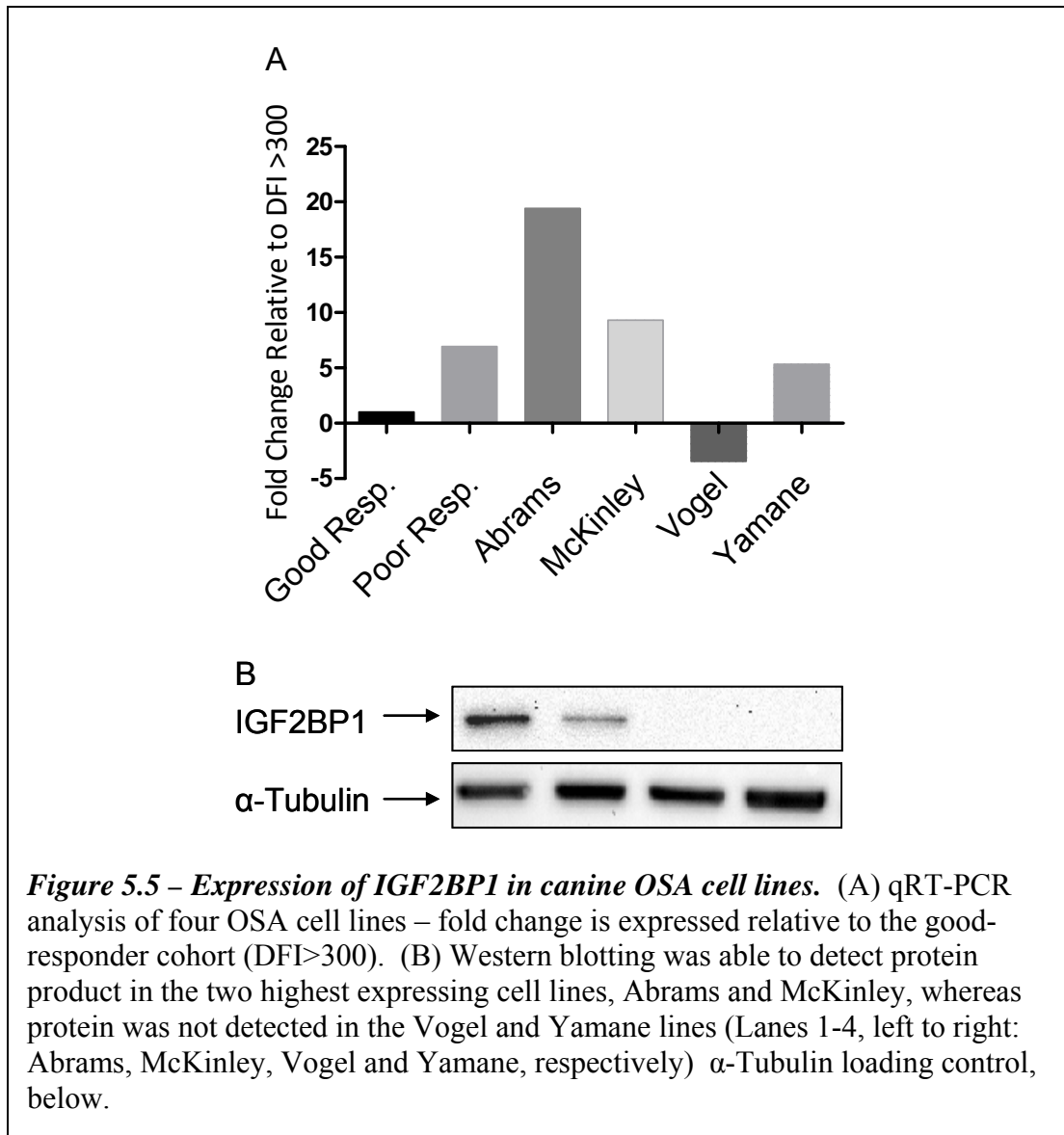


Figure 5.4 – Immunohistochemical staining of primary OSA sections for IGF2BP1 and survival curves based on IHC scores. (A & B) H&E and IGF2BP1 staining, respectively, of a representative tumor sample (#184844). Note the strong cytoplasmic staining but lack of nuclear staining. 400x magnification. (C & D) H&E and IGF2BP1 staining of a tumor sample (#223986) representative of those with frequent nuclear staining. 400x magnification. Initial study of DFI cohorts (n=17) indicated that nuclear staining in >25% of cells correlated with poor outcome (Fisher’s exact test, p=0.009). Considering these initial findings, the IHC study was expanded to an independent data set (n=64) and survival curves based upon cytoplasmic and nuclear staining were constructed (E & F). No significant differences between staining patterns were found.

from a metastatic nodule, demonstrated the highest expression at a 20-fold increase over good-responder primary tumors (Figure 5.5A). The Vogel line expressed the least



IGF2BP1 mRNA with a 4-fold decrease relative to the DFI>300 cohort and a 10-fold decrease relative to the DFI<100 cohort. Upon western blot, only the two highest expressing cell lines (Abrams and McKinley) had detectable protein levels of IGF2BP1 (Figure 5.5B)

siRNA Knockdown of IGF2BP1

In order to examine what benefits IGF2BP1 overexpression may confer to OSA cells, we knocked down transcripts of this gene using siRNA methodology in the highest-expressing cell line (Abrams). Scrambled (negative control) and two targeted siRNAs were designed and introduced into Abrams cultures with lipid-based transient transfection. qRT-PCR analysis of cells between 6 and 72 hours post-transfection indicated that IGF2BP1 was rapidly and effectively knocked down by this strategy with an observed 6-fold down-regulation of mRNAs after 24 hours and 10-fold down-regulation after 72 hours relative to scrambled controls (Figure 5.6A & B). IGF2BP1-si1 was most effective at knocking down the target and demonstrated the most long-lived effects. IGF2BP1-si2 was also effective but not to the extent of IGF2BP1-si1 and mRNA expression began to recover 72 hours following transfection (Figure 5.6B). Western blot was used to verify protein knockdown 48 to 116 hours following transfection. As with mRNA expression, IGF2BP1-si1 was the most effective and lasting siRNA (Figure 5.6C).

Invasion & Migration Assays

To determine the effect of IGF2BP1 expression on tumor progression and metastasis, Abrams cells that had been transfected with siRNAs were assayed for invasion and migration capabilities. Cells that had been transfected 24-hours previously were plated onto invasion or migration chambers and allowed to incubate for 24 hours. The resulting data showed little difference between scrambled and targeted siRNAs (Figure 5.6D, black bars). A subsequent western blot of a sample of these cells indicated that effective knockdown was not observed at the 24-hour post-transfection time point.

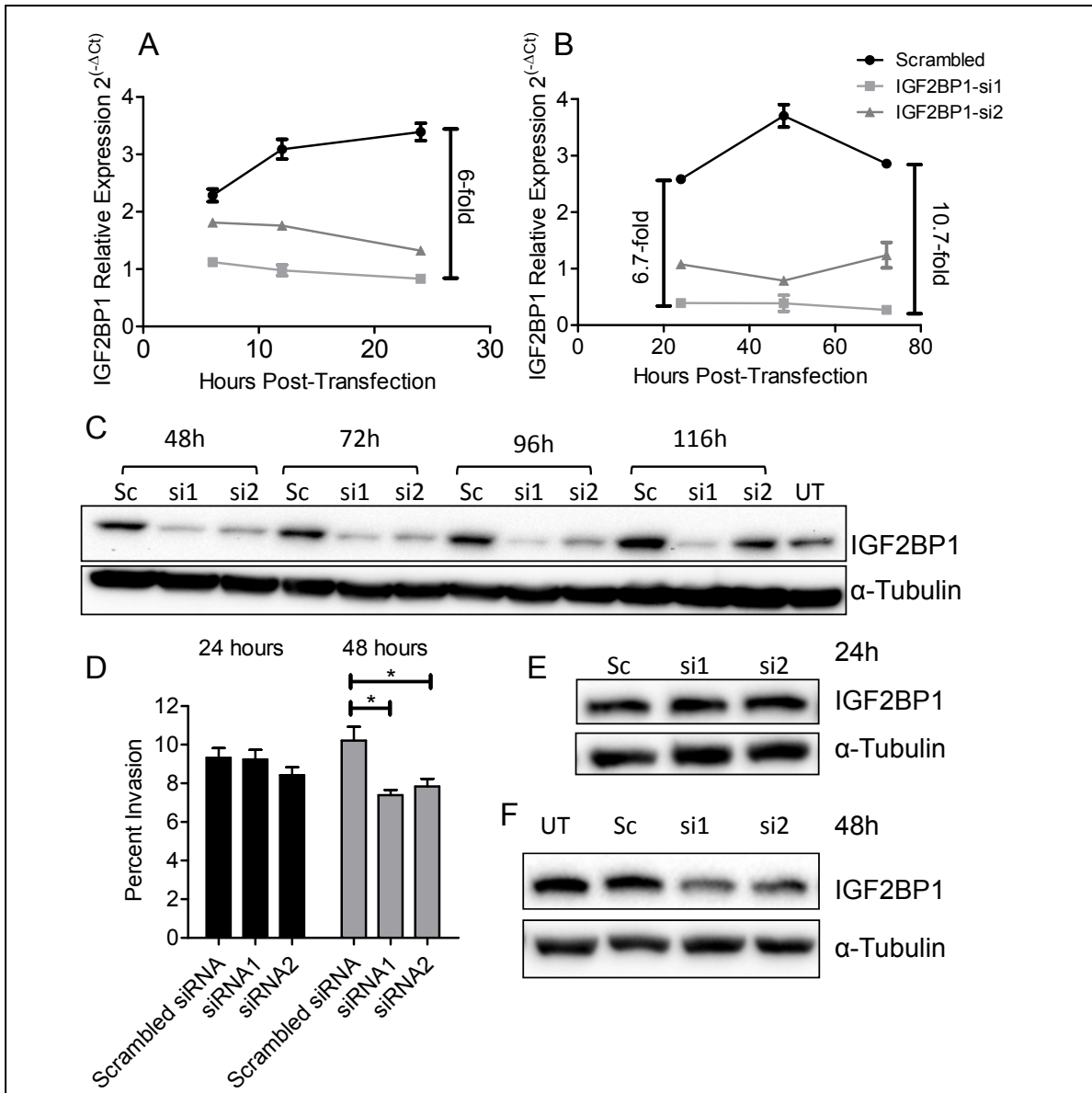
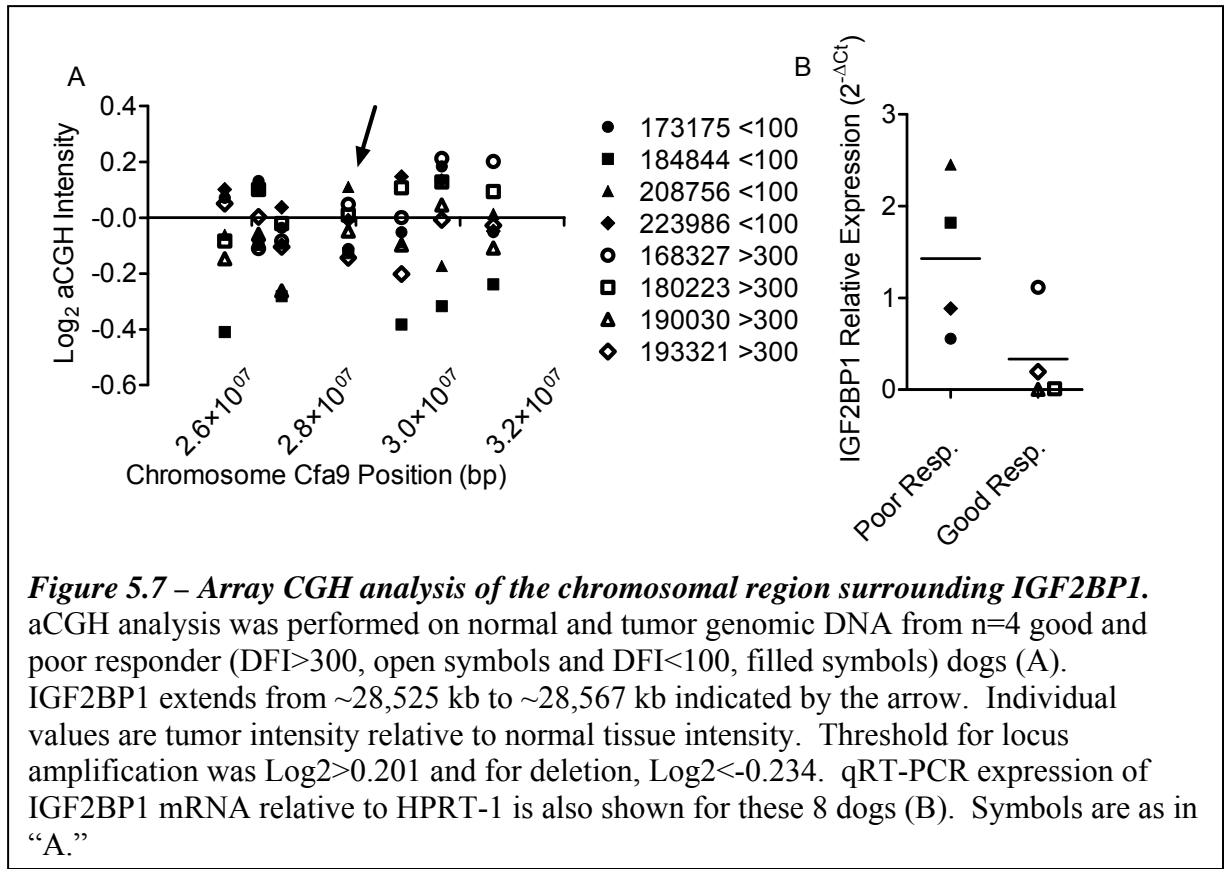


Figure 5.6 – IGF2BP1 knockdown and subsequent invasion and migration assays in the Abrams cell line. Successful knockdown was confirmed at 6, 12, 24, 48 and 72 hours post transfection via qRT-PCR in two separate experiments (n=3 biological replicates per treatment, A & B, IGF2BP1 expression relative to HPRT1). Knockdown was also confirmed via western blot of whole-cell lysates at 48, 72, 96 and 116 hours post transfection (C), α -Tubulin was used as a loading control. Sc = scrambled siRNA, si1 = IGF2BP1-si1, si2 = IGF2BP1-si2, UT = untransfected. D) Two separate invasion/migration assays were performed: they were initiated either 24 h or 48 h following transfection and allowed to incubate for 24 hours prior to development (n=3/treatment, * = p<0.05). Percent invasion was calculated as $RFU(\text{invasion})/RFU(\text{migration})$ where RFU=Relative Fluorescence Units. Western blot follow-up with samples of cells that had been transfected concurrently to experimental cells indicated that knockdown of IGF2BP1 was not apparent at the protein level 24h after transfection (E). Knockdown was apparent at 48 h post-transfection (F).

Thus, the experimental window was shifted so that cells were plated into invasion or migration chambers at 48 hours post transfection and incubated for 24 hours. A significant reduction in percent invasive cells was observed for both targeted siRNAs relative to the scrambled control (Figure 5.6D, gray bars). Furthermore, a trend showing fewer invasive cells in the IGF2BP1-si1 treated group relative to the IGF2BP1-si2 treated group correlated with the relative levels of knockdown between these two treatments. Subsequent western blotting of samples of these cells showed detectable knockdown with both targeted siRNA treatments relative to scrambled and untransfected cells (Figure 5.6F).

Array Comparative Genomic Hybridization

Array CGH was pursued as a methodology for determining genomic amplification in tumor tissues relative to normal tissues. This assay was performed by Dr. Matthew Breen's laboratory with their 2 Mb resolution canine BAC array. Genomic DNA was extracted from primary tumors and matched normal muscle tissue in a subset of the DFI cohort samples (n=4 from each group). Intensity of tumor DNA relative to somatic DNA was calculated and plotted for a region surrounding the IGF2BP1 locus (Figure 5.7A). Thresholds for locus amplification or deletion relative to somatic DNA were: $\text{Log}_2 > 0.201$ (amplification) and $\text{Log}_2 < -0.234$ (deletion). In these 8 samples, no amplification was observed at any of the loci surrounding IGF2BP1, in fact, deletion was observed at several probe regions, however, not in the region closest to the IGF2BP1 gene (Figure 5.7A, arrow). mRNA expression of IGF2BP1 for these 8 tumor samples was plotted to compare relative expression to locus intensity (Figure 5.7B). Two of the higher expressing samples, 208756 and 168327 (closed triangle and open circle,



respectively) also demonstrated higher aCGH signals but these did not meet thresholds for amplification. Thus, although IGF2BP1 locus amplification has been observed in breast cancers, it does not appear to be the underlying cause of overexpression in these samples of canine OSA.

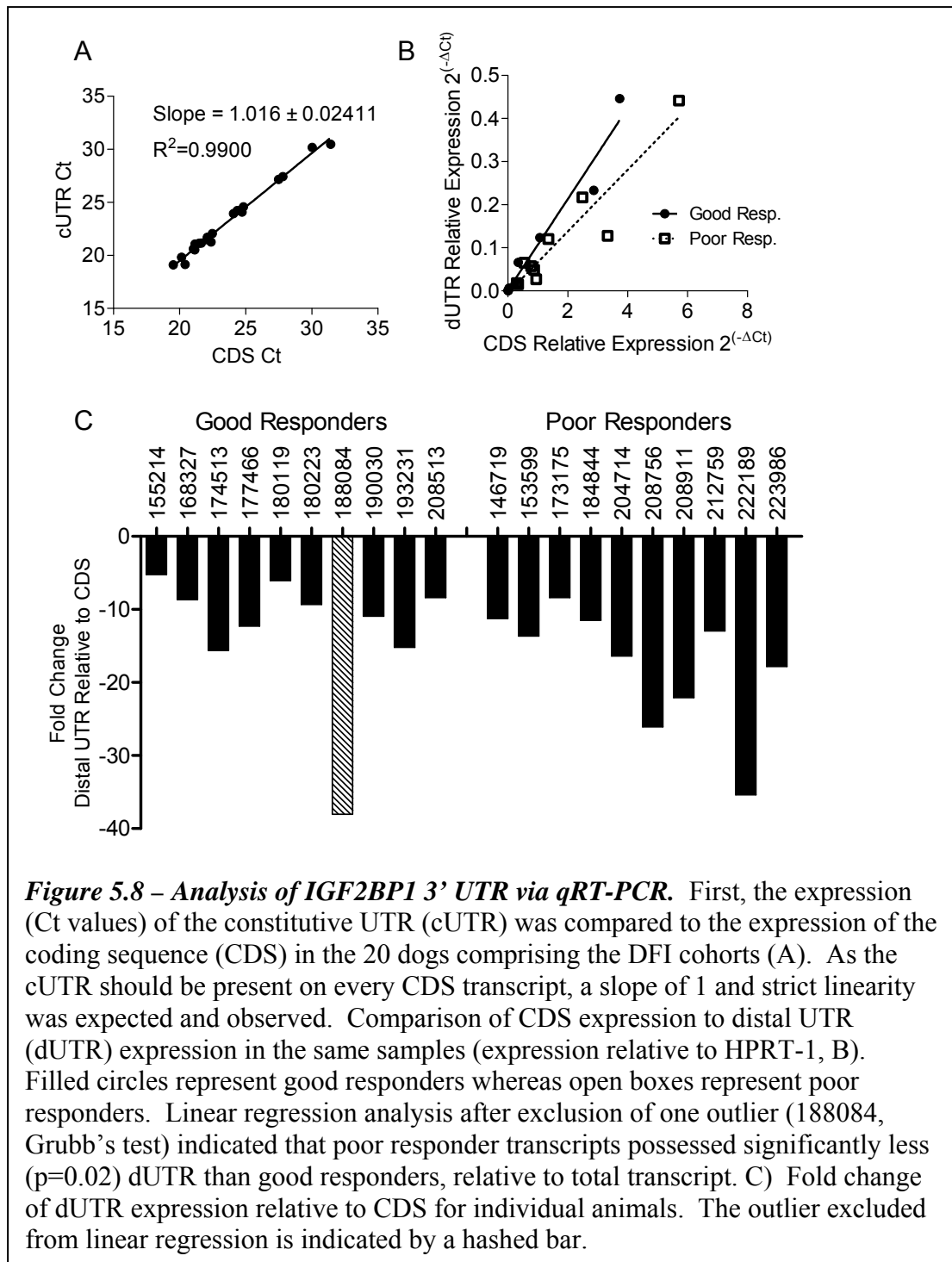
3' Untranslated Region Analysis

Recent reports of miRNA interaction with and truncation of the extensive IGF2BP1 3'UTR in human samples led us to investigate whether this mechanism of transcript control is active in canine OSA. Predicted sequences of the canine IGF2BP1 3'UTR do not describe a region equivalent to that found in humans so an *in silico* investigation comparing human to canine genomic contigs was undertaken. Alignment of the sequences following the stop codons in both species demonstrated a greater than 70%

homology with 100% conservation of the location and sequence of poly-adenylation signals and Let-7 binding sites diagrammed in Figure 5.1. Thus, primers were designed to interrogate canine constitutive UTR (cUTR) and distal UTR (dUTR) prevalence. As the cUTR is expected to be present in every transcript, expression of the cUTR was first compared to coding sequence (CDS) expression to validate the qRT-PCR methodology. Indeed, expression of the cUTR precisely correlated to the CDS expression as evidenced by a linear regression with a slope that was not significantly different from 1 (Figure 5.8A, $R^2=0.99$). Next, CDS expression (and cUTR by proxy) was compared to dUTR expression in the good- and poor-responder cohorts. One "good-responder" sample (188084) was excluded from linear regression analysis following an outlier test (Grubb's). Linear regression indicated that significantly less dUTR relative to CDS was present in the poor-responder cohort (slope = 0.07147 ± 0.009084 , $R^2=0.89$, Figure 5.8B, dashed line) than in the good-responder cohort (slope = 0.1056 ± 0.008824 , $R^2=0.95$, Figure 5.8B, solid line, slope difference $p=0.02141$). Fold-change of dUTR relative to CDS was also calculated for all samples (Figure 5.8C); in general, far more IGF2BP1 transcripts lack dUTR in poor-responders than in good-responders.

DISCUSSION

Previously, via microarray, we identified overexpression of IGF2BP1 in primary tumors as a negative prognostic indicator for disease free interval in dogs with OSA (9). In this study, we examined expression levels of this oncofetal gene in canine OSA and normal bone as well as its contribution to invasion and migration in this system. Immunohistochemical staining patterns were investigated with the aim of providing a prognostic screen that would be functional for veterinarians without access to RNA



preservation technology. We also examined two possible mechanisms of dysregulation, one of which may, indeed, be a factor in the increased expression of IGF2BP1 common to the majority of tumors studied.

Although IGF2BP1 expression has been assayed in a number of tumor (*in vitro* and *in vivo*) and normal tissue systems, its expression in the canine model or evaluation in osteosarcoma samples compared to normal bone had not been investigated prior to the current study (14, 17-19, 21, 23, 28, 34-40). Our findings indicate that IGF2BP1 in canine bone is not expressed except in the case of transformation where it is expressed at high levels in the majority of tumors. Expression is further elevated in dogs that respond poorly to definitive treatment as evidenced by shorter disease-free intervals. Thus, in this system, IGF2BP1 displays an oncofetal expression pattern as has been observed in other systems.

Interestingly, protein localization patterns vary among samples with some tumors demonstrating cytoplasmic localization while others show both nuclear and cytoplasmic (but not nucleolar) localization. Previous studies have identified primarily cytoplasmic localization of this protein, especially at the leading edge of cells where it is involved in actin mRNA localization (19, 25, 26, 38, 39, 41). However it has also, rarely, been observed in the nucleus and possesses a canonical nuclear export signal (NES) (26, 42). It has been hypothesized that IGF2BP1 protein binds to target mRNAs in the nucleus and, thus, guides their export, final destination, longevity and translatability (42, 43). That being said, one can speculate about potential causes of the observed nuclear staining in some of the samples tested here. Perhaps a mutation has damaged a subset of IGF2BP1 proteins' NES so that they inappropriately remain in the nucleus or perhaps it is simply a reflection of target mRNA upregulation and, hence, increased demand for IGF2BP1 transit services. Future mechanistic studies could provide much insight into this inconsistent distribution pattern. Based upon the current findings,

immunohistochemistry does not appear to be a feasible prognostic screen. However, a previous study identified the related protein, IGF2BP2, as an auto-antigen in 21% of hepatocellular carcinomas (44). Thus, development of an ELISA screen for IGF2BP1 auto-antibodies may yet hold promise as a prognostic or early-detection screen.

Small interfering RNA-mediated knockdown of IGF2BP1 and subsequent invasion and migration assays indicate that IGF2BP1 promotes invasion relative to migration in this system. Interestingly, the body of literature regarding IGF2BP1 and cell invasion is highly contradictory and likely reflects the different systems studied. In HeLa cells, knockdown of IGF2BP1 has been shown to inhibit invadopodia formation through a CD44-dependent mechanism, indicating that IGF2BP1 is pro-metastatic in this system (38). Similarly, in a colorectal carcinoma system, IGF2BP1 has been shown to promote lamellipodia and ruffle formation, encouraging invasion. However, in a rat mammary adenocarcinoma model, increased polarity but *reduced* chemotaxis in response to IGF2BP1 overexpression was observed. The authors hypothesize that IGF2BP1 interacting with β -actin stabilizes the cells' polarity in an anti-metastatic fashion (34). Wang and colleagues also identified IGF2BP1 as an anti-metastatic factor in primary human breast cancers as well as the same rat adenocarcinoma model (45, 46). In two recent papers, Gu and colleagues examined a positive feedback loop between IGF2BP1 and β -catenin in additional breast cancer systems (28, 35). They determined that β -catenin can promote transcription of IGF2BP1 and, in turn, IGF2BP1 stabilizes β -catenin transcripts. Furthermore they found that IGF2BP1 was suppressed by hypermethylation of the promoter region in highly metastatic cell lines yet was over-expressed in non-metastatic lines. Again, identifying IGF2BP1 as an anti-metastatic factor. It has been

suggested that these different conclusions arise because the action of IGF2BP1 is highly system-centric and primarily acts through different targets in different tissue types (22, 35). Indeed, this is likely the case as a *negative* feedback loop between IGF2BP1 and β -catenin via the intermediary F-box and WD repeats protein, β -TrCP, has been identified in colorectal carcinomas (47). Thus, we have determined that IGF2BP1 promotes invasion in a canine OSA model but this finding does not necessarily extend to other systems.

Previous studies identified genomic amplification of the IGF2BP1 locus as one cause of over-expression of the protein in breast carcinomas (16, 17). Here, we investigated genomic amplification via aCGH in eight primary tumors and matched muscle tissue and did not identify significant levels of gene amplification at the IGF2BP1 locus in any of these samples despite clear increases in gene expression. Based upon the recent findings of Mayr & Bartel, we also investigated 3' UTR shortening (14). Their study found that this was a common event for the IGF2BP1 transcript in transformed cells and, as this region is a target for Let-7-based suppression, shortening may allow over-expression (28, 29). The current findings indicate that this mechanism does contribute to IGF2BP1 regulation in the canine OSA model as our poor-responder cohort had significantly greater transcript relative to dUTR than our good responder cohort. Upon identifying the significant outlier in our good-responder group, we investigated why this sample appeared more similar to the poor-responder group. Review of veterinary records indicated that this sample may be misclassified: one radiologist identified a possible lung mass within 150 days of definitive treatment but this mass was not identified on a follow-up radiograph. Within six months, metastatic disease was

diagnosed. Thus, uncertainty regarding DFI for this patient encourages its exclusion from future studies.

Let-7 evasion certainly appears to be a mechanism of IGF2BP1 over-expression in this model and this encourages speculation as to whether *de novo* events lead to 3' UTR shortening in tumors or if specific individuals are predisposed due to other factors. Large body size and rapid growth have been identified as factors in the development of OSA in both dogs and man, indeed, the Lin28/Let-7/IGF2BP1 signaling axis may contribute to both large body size and the pathogenesis of OSA. In one recent study, Lin28a transgenic mice (with resultant Let-7 suppression, and presumably increased IGF2BP1 expression) demonstrated increased body size and endocrine phenotypes including delayed puberty and increased glucose utilization (48). Similarly, IGF2BP1-deficient mice demonstrate a dwarf phenotype with impaired gut development. Taken together, these studies suggest that Lin28a may be acting through IGF2BP1 to modulate size phenotypes (15). Thus, one may speculate that individuals with even slightly overactive Lin28 genes will have less-active Let-7 signaling that directly translates into increased IGF2BP1 half life and larger body size. Such a precarious balance in expression levels may be easily tipped into tumorigenesis by mutation or trauma to the system. This axis deserves further investigation in OSA as targeted therapies aimed at IGF2BP1 may be able to right the system and prevent distant disease.

ACKNOWLEDGEMENTS

We acknowledge Erin Petrilli and the Genomics Core at the Rocky Mountain Regional Center for Excellence at CSU for generating the microarray data. We

would also like to thank Irene Mok and Kristen Grunerud at CSU's Animal Cancer Center for coordinating sample retrieval from the tissue archive and amputees. Deanna Dailey and Debra Kamstock deserve many thanks for their reading of IHC slides. This work was supported by grants to DLD from the Morris Animal Foundation (MAF D08CA-053) and the CSU College Research Council - Miki Society.

REFERENCES

1. Dernell WS, Ehrhart NP, Straw RC, Vail DM. Tumors of the skeletal system. In: Withrow SJ, Vail DM, editors. *Withrow and MacEwen's Small Animal Clinical Oncology*. 4th ed. St. Louis: Saunders Elsevier; 2007. p. 540-67.
2. Jaffe N. Adjuvant chemotherapy in osteosarcoma: An odyssey of rejection and vindication. In: Jaffe N, Bielack SS, Bruland OS, editors. *Pediatric and Adolescent Osteosarcoma, Cancer Treatment and Research*. New York: Springer; 2009.
3. Mueller F, Fuchs B, Kaser-Hotz B. Comparative biology of human and canine osteosarcoma. *Anticancer Research* 2007;27(1A):155-64.
4. Paoloni M, Davis S, Lana S, Withrow S, Meltzer P, Khanna C. Comparative gene expression analysis of canine and human osteosarcoma. *Genes, Dogs & Cancer: 4th International Canine Cancer Conference*; 2006; Chicago, IL; 2006. p. 19.
5. Paoloni M, Davis S, Lana S, Withrow S, Sangiorgi L, Picci P, *et al.* Canine tumor cross-species genomics uncovers targets linked to osteosarcoma progression. *BMC Genomics* 2009;10(1):625.
6. Thomas R, Wang H, Tsai P, Langford C, Fosmire S, Jubala C, *et al.* Influence of genetic background on tumor karyotypes: evidence for breed-associated cytogenetic aberrations in canine appendicular osteosarcoma. *Chromosome Research* 2009;17(3):365-77.
7. Link MP, Goorin AM, Miser AW, Green AA, Pratt CB, Belasco JB, *et al.* The effect of adjuvant chemotherapy on relapse-free survival in patients with osteosarcoma of the extremity. *New England Journal of Medicine* 1986;314(25):1600-6.
8. Sutter NB, Ostrander EA. Dog star rising: the canine genetic system. *Nature Reviews Genetics* 2004;5(12):900-10.
9. O'Donoghue LE, Ptitsyn AA, Kamstock DA, Siebert J, Thomas RS, Duval DL. Expression profiling in canine osteosarcoma: identification of biomarkers and pathways associated with outcome. *BMC Cancer* 2010;10(1):506.

10. Bernstein PL, Herrick DJ, Prokipcak RD, Ross J. Control of c-myc mRNA half-life in vitro by a protein capable of binding to a coding region stability determinant. *Genes & Development* 1992;6(4):642-54.
11. Nielsen FC, Nielsen J, Christiansen J. A family of IGF-II mRNA binding proteins (IMP) involved in RNA trafficking. *Scandinavian Journal of Clinical and Laboratory Investigations* 2001;61(Suppl 234):93-9.
12. Nielsen J, Christiansen J, Lykke-Andersen J, Johnsen AH, Wewer UM, Nielsen FC. A family of Insulin-Like Growth Factor II mRNA-binding proteins represses translation in late development. *Molecular and Cellular Biology* 1999;19(2):1262-70.
13. Ross AF, Oleynikov Y, Kislauskis EH, Taneja KL, Singer RH. Characterization of a β -actin mRNA zipcode-binding protein. *Molecular and Cellular Biology* 1997;17(4):2158-65.
14. Mayr C, Bartel DP. Widespread shortening of 3'UTRs by alternative cleavage and polyadenylation activates oncogenes in cancer cells. *Cell* 2009;138(4):673-84.
15. Hansen TVO, Hammer NA, Nielsen J, Madsen M, Dalbaeck C, Wewer UM, *et al.* Dwarfism and impaired gut development in Insulin-Like Growth Factor II mRNA-Binding Protein 1-deficient mice. *Molecular and Cellular Biology* 2004;24(10):4448-64.
16. Doyle GA, Bourdeau-Heller JM, Coulthard S, Meisner LF, Ross J. Amplification in human breast cancer of a gene encoding a c-myc mRNA-binding protein. *Cancer Research* 2000;60(11):2756-9.
17. Ioannidis P, Mahaira L, Papadopoulou A, Teixeira MR, Heim S, Andersen JA, *et al.* 8q24 Copy number gains and expression of the c-myc mRNA stabilizing protein CRD-BP in primary breast carcinomas. *International Journal of Cancer* 2003;104(1):54-9.
18. Ioannidis P, Kottaridi C, Dimitriadis E, Courtis N, Mahaira L, Talieri M, *et al.* Expression of the RNA-binding protein CRD-BP in brain and non-small cell lung tumors. *Cancer Letters* 2004;209(2):245-50.
19. Dimitriadis E, Trangas T, Milatos S, Foukas PG, Gioulbasanis I, Courtis N, *et al.* Expression of oncofetal RNA-binding protein CRD-BP/IMP1 predicts clinical outcome in colon cancer. *International Journal of Cancer* 2007;121(3):486-94.
20. Kato T, Hayama S, Yamabuki T, Ishikawa N, Miyamoto M, Ito T, *et al.* Increased expression of Insulin-like Growth Factor-II Messenger RNA Binding Protein 1 is associated with tumor progression in patients with lung cancer. *Clinical Cancer Research* 2007;13(2):434-42.

21. Kobel M, Weidensdorfer D, Reinke C, Lederer M, Schmitt WD, Zeng K, *et al.* Expression of the RNA-binding protein IMP1 correlates with poor prognosis in ovarian carcinoma. *Oncogene* 2007;26(54):7584-9.
22. Vainer G, Vainer-Mosse E, Pikarsky A, Shenoy SM, Oberman F, Yeffet A, *et al.* A role for VICKZ proteins in the progression of colorectal carcinomas: regulating lamellipodia formation. *The Journal of Pathology* 2008;215(4):445-56.
23. Ioannidis P, Trangas T, Dimitriadis E, Samiotaki M, Kyriazoglou I, Tsiapalis CM, *et al.* C-MYC and IGF-II mRNA-binding protein (CRD-BP/IMP-1) in benign and malignant mesenchymal tumors. *International Journal of Cancer* 2001;94(4):480-4.
24. Farina KL, Hüttelmaier S, Musunuru K, Darnell R, Singer RH. Two ZBP1 KH domains facilitate β -actin mRNA localization, granule formation, and cytoskeletal attachment. *Journal of Cell Biology* 2003;160(1):77-87.
25. Oleynikov Y, Singer RH. Real-time visualization of ZBP1 association with β -actin mRNA during transcription and localization. *Current Biology* 2003;13(3):199-207.
26. Pan F, Huttelmaier S, Singer RH, Gu W. ZBP2 facilitates binding of ZBP1 to β -Actin mRNA during transcription. *Molecular and Cellular Biology* 2007;27(23):8340-51.
27. Hüttelmaier S, Zenklusen D, Lederer M, Dictenberg J, Lorenz M, Meng X, *et al.* Spatial regulation of β -actin translation by Src-dependent phosphorylation of ZBP1. *Nature* 2005;438(7067):512-5.
28. Boyerinas B, Park S-M, Shomron N, Hedegaard MM, Vinther J, Andersen JS, *et al.* Identification of Let-7-regulated oncofetal genes. *Cancer Research* 2008;68(8):2587-91.
29. Hafner M, Landthaler M, Burger L, Khorshid M, Hausser J, Berninger P, *et al.* Transcriptome-wide identification of RNA-binding protein and microRNA target sites by PAR-CLIP. *Cell* 2010;141:129-41.
30. O'Donoghue LE, Rivest JP, Duval DL. Polymerase chain reaction-based species verification and microsatellite analysis for canine cell line validation. *Journal of Veterinary Diagnostic Investigation* 2011;23(4):780-5.
31. Tong W, Cao X, Harris S, Sun H, Fang H, Fuscoe J, *et al.* ArrayTrack--supporting toxicogenomic research at the U.S. Food and Drug Administration National Center for Toxicological Research. *Environmental Health Perspectives* 2003;111(15).

32. Livak KJ, Schmittgen TD. Analysis of relative gene expression data using real-time quantitative PCR and the 2- $\Delta\Delta$ Ct method. *Methods* 2001;25(4):402-8.
33. Thomas R, Scott A, Langford CF, Fosmire SP, Jubala CM, Lorentzen TD, *et al.* Construction of a 2-Mb resolution BAC microarray for CGH analysis of canine tumors. *Genome Research* 2005;15(12):1831-7.
34. Lapidus K, Wyckoff J, Mouneimne G, Lorenz M, Soon L, Condeelis JS, *et al.* ZBP1 enhances cell polarity and reduces chemotaxis. *Journal of Cell Science* 2007;120(18):3173-8.
35. Gu W, Pan F, Singer RH. Blocking beta-catenin binding to the ZBP1 promoter represses ZBP1 expression, leading to increased proliferation and migration of metastatic breast-cancer cells. *Journal of Cell Science* 2009;122(11):1895-905.
36. Ross J, Lemm I, Berberet B. Overexpression of an mRNA-binding protein in human colorectal cancer. *Oncogene* 2001;20(45):6544-50.
37. Tessier CR, Doyle GA, Clark BA, Pitot HC, Ross J. Mammary tumor induction in transgenic mice expressing an RNA-binding protein. *Cancer Research* 2004;64(1):209-14.
38. Vikesaa J, Hansen TVO, Jønson L, Borup R, Wewer UM, Christiansen J, *et al.* RNA-binding IMPs promote cell adhesion and invadopodia formation. *The EMBO Journal* 2006;25(7):1456-68.
39. Hammer NA, Hansen TvO, Byskov AG, Meyts ER-D, Grøndahl ML, Bredkjær HE, *et al.* Expression of IGF-II mRNA-binding proteins (IMPs) in gonads and testicular cancer. *Reproduction* 2005;130(2):203-12.
40. Ioannidis P, Mahaira LG, Perez SA, Gritzapis AD, Sotiropoulou PA, Kavalakis GJ, *et al.* CRD-BP/IMP1 expression characterizes cord blood CD34+ stem cells and affects c-myc and IGF-II expression in MCF-7 cancer cells. *The Journal of Biological Chemistry* 2005;280(20):20086-93.
41. Nielsen FC, Nielsen J, Kristensen MA, Koch G, Christiansen J. Cytoplasmic trafficking of IGF-II mRNA-binding protein by conserved KH domains. *Journal of Cell Science* 2002;115(Pt 10):2087-97.
42. Nielsen J, Adolph SK, Rajpert-De Meyts E, Lykke-Andersen J, Koch G, Christiansen J, *et al.* Nuclear transit of human zipcode-binding protein IMP1. *Biochemical Journal* 2003;376(Pt 2):383-91.
43. Jønson L, Vikesaa J, Krogh A, Nielsen LK, Hansen Tv, Borup R, *et al.* Molecular composition of IMP1 ribonucleoprotein granules. *Molecular & Cellular Proteomics* 2007;6(5):798-811.

44. Zhang J-Y, Chan EKL, Peng X-X, Tan EM. A novel cytoplasmic protein with RNA-binding motifs is an autoantigen in human hepatocellular carcinoma. *The Journal of Experimental Medicine* 1999;189(7):1101-10.
45. Wang W, Goswami S, Lapidus K, Wells AL, Wyckoff JB, Sahai E, *et al.* Identification and testing of a gene expression signature of invasive carcinoma cells within primary mammary tumors. *Cancer Research* 2004;64(23):8585-94.
46. Wang W, Wyckoff JB, Frohlich VC, Oleynikov Y, Hüttelmaier S, Zavadil J, *et al.* Single cell behavior in metastatic primary mammary tumors correlated with gene expression patterns revealed by molecular profiling. *Cancer Research* 2002;62(21):6278-88.
47. Noubissi FK, Elcheva I, Bhatia N, Shakoory A, Ougolkov A, Liu J, *et al.* CRD-BP mediates stabilization of [beta]TrCP1 and c-myc mRNA in response to [beta]-catenin signalling. *Nature* 2006;441(7095):898-901.
48. Zhu H, Shah S, Shyh-Chang N, Shinoda G, Einhorn WS, Viswanathan SR, *et al.* Lin28a transgenic mice manifest size and puberty phenotypes identified in human genetic association studies. *Nature Genetics* 2010;42(7):626-31.

Chapter 6

Suppression of the putative tumor suppressor gene, n-Myc Downstream Regulated Gene 2 (*NDRG2*), contributes to doxorubicin resistance in canine osteosarcoma.

SYNOPSIS

Background: Osteosarcoma (OSA) is a highly aggressive bone malignancy that affects both dogs and humans. Previous identification of *NDRG2* mRNA suppression as a negative prognostic indicator in canine OSA led us to investigate possible mechanisms of control for this gene as well as the effects of modulating its expression in this system.

Methods: Normal bone mRNA expression of *NDRG2* was compared to that of tumors using microarrays and qRT-PCR. Genomic DNA was analyzed to determine if copy number alterations of the *NDRG2* locus caused loss of expression and demethylating agent effects on *NDRG2* expression were explored. Stable transfectants expressing *NDRG2* were generated and tested for chemosensitivity to doxorubicin and carboplatin

Results: *NDRG2* was dramatically downregulated in tumors relative to normal bone. Two different expressed isoforms of *NDRG2* were identified and characterized and three possible mechanisms of this suppression were identified: c-Myc overexpression, copy

number loss at the NDRG2 locus and gDNA methylation. NDRG2 expressing clones demonstrated enhanced doxorubicin sensitivity. **Conclusions:** NDRG2 is down-regulated in canine OSA, most-so in dogs that respond poorly to definitive treatment and adjuvant chemotherapy. This suppression may play a significant role in tumor invasion and metastasis as well as resistance to chemotherapy that leads to treatment failures.

INTRODUCTION

Osteosarcoma (OSA) is a highly aggressive primary bone malignancy that affects both dogs and humans. Roughly 800 adolescents and over ten times as many companion dogs are diagnosed annually (1, 2). Standard of care in both species involves resection of the tumor either by amputation or limb sparing surgery followed by adjuvant chemotherapy. Neoadjuvant chemotherapy is commonly utilized in human medicine but less-so in canine patients. The majority of OSA tumors in both dogs and man occur in the metaphyseal region of long bones in the appendicular skeleton. Histological classifications are shared between species as are many molecular characteristics of the disease (1, 3-6). Metastatic disease of the lungs is the most common cause of morbidity and mortality and is a strong negative prognostic indicator (1, 2, 7). Roughly 10-15% of patients of both species present with clinically detectable metastases and it is estimated that over 80% of patients may have undetectable micrometastatic disease at presentation. Thus, systemic chemotherapy aimed at diminishing distant disease is included in most protocols.

Considering the similarities between canine and human living environments, their genomes and the pathology of OSA, this disease in dogs is increasingly recognized as a

valuable model for the human disease (3, 8). Previous studies by our laboratory identified n-Myc Downstream Regulated Gene 2 (*NDRG2*) as a gene that was suppressed in primary OSA tumors from dogs that responded poorly to definitive treatment when compared to dogs that responded well (9). *NDRG2* maps to human chromosome 14q11.2 and to the equivalent locus on chromosome 15 in dogs. The gene encodes 16 exons with up to eight isoforms predicted in humans and seven in dogs. The promoter region has a substantial CpG island and several studies have found genomic DNA methylation to be important in transcriptional control of this gene, especially in cancer (10, 11). Mutations in the promoter region that presumably affect transcription factor assembly have also been identified and result in gene suppression. Additionally, transcripts have an ~850 bp 3' untranslated region with several conserved micro-RNA recognition sites that influence mRNA half life (10). At least two protein isoforms have been identified in humans, dogs and mice; the protein contains a conserved alpha-beta hydrolase (ABH) domain but its precise function in cells is unknown. The protein is typically localized in the plasma membrane and cytosol with a small nuclear population (12). Enhanced nuclear translocation of the protein has been demonstrated in response to Hypoxia Inducible Factor 1 (HIF1) expression in hypoxic tumor cells but no nuclear import element was identified (13). Three highly conserved phosphorylation sites are present in the translated protein (Thr 330, Ser 332 and Thr 348) and are substrates for multiple kinases (14). The recent elucidation of the crystal structure of this protein has provided some clues as to its behavior in cells (12). The catalytic residues common to most ABH proteins are not present in *NDRG2*, thus, it likely lacks enzymatic activity. It does, however, appear to interact with other molecules and α -helix 6 is important in that role, notably in the

suppression of β -catenin signaling (12). Additionally, helix $\alpha 6$ may be responsible for the nuclear translocation of NDRG2 under hypoxic conditions. Two studies have identified Matrix Metalloproteinase 9 (*MMP9*) inhibition as a downstream target of NDRG2; one of these determined that Bone Morphogenetic Protein 4 (*BMP4*) was an intermediate regulator in that activity, suggesting a role for NDRG2 in inhibition of invasion and metastasis (15, 16).

NDRG2 expression has been identified as a prognostic factor in a variety of tumors including breast, thyroid, colorectal, lung and brain cancer where it has been dubbed a tumor suppressor (17-22). Furthermore, even patients with a good prognosis often have reduced NDRG2 expression in tumor samples when compared to normal tissue. Although the name of the gene implies it is regulated by n-Myc, it has been firmly established that it is, in fact, downstream of c-Myc in most tissues (10, 23, 24).

In this study, we sought to identify expression changes of NDRG2 in canine OSA and to further elucidate its role in these tumors. NDRG2 has received only limited attention in sarcomas thus far but the current study determines that it does, indeed, play a role in mesenchymal tumors (15). We identify two cases of gene deletion as well as provide evidence that gDNA methylation is involved in *NDRG2* downregulation. Additionally, we present the first evidence correlating NDRG2 suppression with doxorubicin resistance.

METHODS

Canine Tissues

Canine tissues used in microarray and PCR studies were obtained from animals presenting to Colorado State University (CSU) for treatment of OSA. Owner consent for

tissue archiving was obtained prior to definitive surgical treatment. Good- and poor-responder primary tumors were archived at the Animal Cancer Center between 1996 and 2006 - snap frozen tissues and formalin-fixed paraffin embedded (FFPE) tissues were archived. Good and poor responder groups were defined based upon patient disease-free-interval (DFI): good-responders had a DFI greater than 300 days and poor-responders had a DFI less than 100 days. Inclusion in these studies required limb amputation followed by doxorubicin and/or platinum drug adjuvant therapy. Normal bone and matched tumor samples were obtained from limbs post-amputation and harvested so that “normal” bone included in the study was distant from the tumor site and separated from the tumor by a joint (e.g. a femoral tumor would have matched distal tibia bone collected). Tissue was collected, snap frozen in liquid nitrogen and stored at -80°C until processing.

Canine Cell Lines

Canine OSA cell lines used in this study were graciously provided by Dr. Douglas Thamm and all cell lines were validated for species and short-tandem-repeat identities as previously described (25). Abrams and D17 cells were derived from metastatic OSA nodules whereas Gracie, McKinley, Moresco and Vogel were derived from primary tumors. Cells were cultured in "C10" media: DMEM high glucose with 6 mM L-glutamine, 1x each of sodium pyruvate, MEM vitamins, MEM non-essential amino acids and antibiotic-antimycotic, 10% fetal bovine serum (FBS) and Plasmocin prophylactic (Invivogen, Cat# ant-mpp).

RNA Extraction

Tumor and normal tissues were freeze-fractured, homogenized, extracted in Trizol (Invitrogen, Cat# 15596-026) per the manufacturer's instructions and purified with the RNeasy (Qiagen, Cat# 74104) cleanup protocol. Cell cultures were detached from plates with 3 mM ethylenediaminetetraacetic acid (EDTA) in phosphate-buffered saline (PBS) or 0.25% trypsin in PBS with EDTA, pelleted by centrifugation for 5 minutes at 500 x g and extracted using the RNeasy kit per the manufacturer's protocol. RNA was quantified via spectrophotometry and, prior to microarray, tissue RNA was bioanalyzed for quality at the Rocky Mountain Regional Center for Excellence (RMRCE) Genomics Core at CSU. Only high quality RNA with RNA Integrity Numbers (RINs) greater than 8 were used in microarray studies.

Microarray

Eight normal bone samples were analyzed with Affymetrix Canine 2.0 GeneChips as previously described (9). Resultant data was compiled with data from 15 good and poor-responder primary tumor samples obtained previously and analyzed with ArrayTrack (26). Data was preprocessed with the Probe Logarithmic Intensity Error (PLIER) estimation algorithm with a \log_2 transformation then analyzed for fold change based on two scenarios: normal bone versus all tumors or normal bone versus good responders versus poor responders. The first scenario was analyzed with a Bonferroni adjusted unpaired 2-tailed t-test, thresholds of corrected p-value <0.05 and fold-change >3 were applied. The second scenario was analyzed with a 3-way ANOVA and the same p-value and fold-change thresholds. \log_2 -transformed PLIER NDRG2 expression values were extracted for this study.

Quantitative RT-PCR

Reverse transcription (RT) was performed on RNA samples with the QuantiTect Reverse Transcription kit (Qiagen, Cat# 05313) per the manufacturer's instructions with 1 µg RNA input, a ten-minute gDNA digest incubation and a 30-minute RT incubation. No-RT controls were included for each sample as was one no-transcript control per RT reaction. Real-time quantitative PCR was performed in duplicate using the iQ SYBR Green Supermix (Bio-Rad, Cat# 170-8880) in 25 µL reactions with 25 ng equivalent cDNA input. Any sample where duplicates were not within 0.5 Ct of each other was repeated. NDRG2 and housekeeping gene (HPRT-1) primers were as previously published (9) and were included in the reactions at 100 nM forward and 300 nM reverse primer concentrations. NDRG2 Exon-2 primers were as follows: Fwd 5'-TGA GTT AGC TGC CCG AAT CCT CCT-3', Rev 5'-AGA GCG GCT GGA AGC AAG ACT TAT-3'. Bone Morphogenetic Protein 4 (BMP4) primers were: Fwd 5'-TTA CAT GCG GGA TCT TTA CCG GCT-3', Rev 5'-TGG TCC CTG GGA TGT TCT CCA AAT-3'. We also examined c-Myc mRNA expression in matched tumor and normal samples to determine what proportion of tumors with suppressed NDRG2 may overexpress Myc; primers were: Fwd 5'-TCA ATG ACA GCA GCT CGC CCA A-3', Rev: 5'-TTC GTC CTC TTG TTC TTC CTC CGA-3'. Standard curves for the five primer sets over two orders of magnitude were within 5% efficiency of each other. Thermal cycling was performed on the Mx3000p instrument (Stratagene) with the following parameters: 95°C for 10 m followed by 40 cycles of 95°C for 30 s and 60°C for one minute. Data collection was performed at the end of the 60°C step. Dissociation curve ramps were performed at the end of the cycle to verify that only a single product was generated. Data

analysis was performed with the Mx3000p software. NDRG2 expression was normalized to HPRT-1 and fold change was calculated using the $2^{(-\Delta\Delta Ct)}$ method (27).

Western Blotting

Western blot analysis was performed on whole-cell lysates obtained by repeatedly passing cell pellets through a 26-gauge needle in Tris pH 7.5 buffer with cOmplete, EDTA-free Protease Inhibitor Cocktail Tablets (Roche, 04693132001). For phosphorylation analysis, cell lysates were extracted in the presence of calf intestinal alkaline phosphatase (CIAP) with CIAP buffer (New England Biosystems, M0290S) per standard protocols (28). Total protein was quantified with a BCA Assay kit (Pierce, Cat# 23227) and 25 μ g protein was loaded for each sample. Proteins were electrophoresed on 12% SDS-PAGE gels with 5% stacking gels at 180 v for 50 minutes and were then transferred to PVDF membranes with a semi-dry transfer unit. Membranes were dried with methanol then blocked in 5% milk in Tris-buffered saline with Tween-20 (TBST) for one hour at room temperature. The primary antibody was obtained from Sigma (Cat# HPA002896, rabbit polyclonal anti-human); the targeted epitope is 99% homologous to the canine protein. Membranes were incubated overnight at 4°C with primary antibody diluted 1:10,000 in 5% milk/TBST. The following day, they were washed 3 times for five minutes each in TBST. Secondary antibody (HRP-conjugated goat anti-rabbit IgG, Bio-Rad, Cat# 170-6515) was applied at a dilution of 1:10,000 in 5% milk/TBST for a one-hour, room-temperature incubation followed by TBST washes. SuperSignal West Pico Chemiluminescent Substrate (Pierce, Cat# 34078) was used for development and images were captured on a Bio-Rad ChemiDoc XRS system. Specificity of the primary antibody was verified using a blocking peptide isolated from mammalian cells expressing

cloned NDRG2 as described below and via western blotting of whole cell lysates from cells expressing this cloned NDRG2 protein. Immunoblotting for the V5 epitope was performed to verify size and identity of cloned NDRG2 in transfected cells as above (Invitrogen, Cat# R960-25) with anti-mouse IgG secondary (BioRad Cat# 170-6516, HRP-conjugated goat anti-mouse IgG). For blocking experiments, primary antibody was incubated with 10x (by mass) blocking peptide in blocking buffer overnight at 4°C with agitation before being applied to the membrane. In parallel, unblocked primary was applied to a second, identical membrane. The western blot was completed as above and membrane signals were compared between the two membranes. α -tubulin was used as a loading control: primary antibody (Sigma Cat# T5168 mouse monoclonal anti-human) incubation was performed for one hour at a 1:5,000 dilution in 5% milk/TBST, secondary antibody (BioRad Cat# 170-6516, HRP-conjugated goat anti-mouse IgG) incubation was performed for one hour at room temperature at a 1:10,000 dilution in 5% milk/TBST with washing and development steps as above.

Array Comparative Genomic Hybridization

Genomic DNA was extracted from tumors and patient-matched normal tissue (muscle, skin) using the DNeasy (Qiagen, Cat# 69504) kit per the manufacturer's instructions. Low yield tissue samples were digested overnight in proteinase K, salt extracted per standard protocols and precipitated in ethanol prior to DNeasy cleanup. Array-CGH was performed by Dr. Matthew Breen's laboratory at North Carolina State University as previously described (29). Relative amplification of the NDRG2 region was determined by dividing signal of each tumor sample by its matched normal sample.

Cloning and Transfection of Canine NDRG2

TOPO cloning into the pcDNATM3.2/V5-GW/D-TOPO[®] vector was used to generate plasmids containing the NDRG2 coding sequence per the manufacturer's protocol (Invitrogen, K2440-20). Primers targeted to the start and stop codon regions, with additional sequence necessary for TOPO cloning, were designed based upon RefSeq mRNA sequence. Reverse transcription of mRNA was performed as for qRT-PCR; NDRG2 targeted primers were: Fwd 5'-CAC CAT GGC GGA GCT GCA GGA GGT-3', Rev minus stop codon 5'-GCA GGA GAC CTC CAT GGT ATG CCC-3', and Rev with stop codon 5'-TCA GCA GGA GAC CTC CAT GGT ATG CCC-3'. Vogel and McKinley cell line cDNA was used as the template. Specific cDNAs were amplified in 50 μ L reactions consisting of 5 μ L Thermo Pol buffer (New England BioLabs, Cat# B9004S), 500 μ M dNTPs, 660 nM MgSO₄, 300 nM each forward and reverse primers and 1 u VentR[®] DNA polymerase (New England BioLabs, Cat# M0254S). Thermal cycling parameters were: 95°C for 2 min followed by 35 cycles of 95°C for 30 s, 60°C for 30 s and 72°C for 90 s with a final elongation at 72°C for 5 min. PCR product was electrophoresed on 1% agarose gels with GelGreen (Biotium, Cat# 41005) in 1x TBE buffer for 1 hour; bands were visualized under UV light, excised and purified using the QIAquick Gel Extraction Kit (Qiagen, Cat# 28704). Purified product was combined with the vector and allowed to incubate at room temperature for 5 minutes before being transferred to ice. 2 μ L of this reaction was then added to 50 μ L of DH5 α chemically competent cells (Invitrogen, Cat# 18263-012), incubated on ice for 30 m, heatshocked at 37°C for 45 s, then returned to ice. 250 μ L SOC medium was added and the reaction was incubated at 37°C for 1 h with 225 RPM shaking. The resultant culture was plated onto

LB-Agar plates with 100 µg/mL ampicillin and incubated overnight at 37°C. Individual colonies were picked and cultured in 3 mL LB broth with 100 µg/mL ampicillin at 37°C overnight. The resultant cultures were pelleted and plasmid DNA was extracted using alkaline lysis and the QIAprep Spin Miniprep Kit (Qiagen, Cat# 27104). Restriction digests and sequencing (CSU Proteomics and Metabolomics Facility) of the plasmids was performed to verify the presence and direction of the insert. Plasmids were stably transfected into the Abrams cell line by electroporation of 2.5×10^5 cells in cold PBS with a one-pulse, 220 V, 20 µs protocol. Cells were plated onto 15 cm plates and selected with 750 µg/mL G418 in C10 media for two weeks before selection of stable clones. The same methodology was used to transfect the negative control plasmid, cDNA3.2/V5/GW-CAT into Abrams cells for comparison. No blocking peptide was available for the antibody used in this study so protein product from stable transfections was immunoprecipitated using a V5 tagged protein purification kit per the manufacturer's protocol (MBL International, Cat# 3315A) to use as a blocking peptide.

Chemotherapy Sensitivity Assays

As doxorubicin (DOX) and carboplatin (Carb) are the two primary chemotherapeutic drugs currently used to treat canine OSA at Colorado State University, we assayed the sensitivity of Abrams cells to these drugs when expressing exogenous NDRG2. Clones expressing exogenous NDRG2 or CAT were plated at a density of 2000 cells/well on 96-well plates and allowed to adhere over night. The following day, media was aspirated and replaced with C10 containing a range of drug concentrations: DOX – 200 ng/mL to 195 pg/mL, Carb – 300 µg/mL to 1.17 µg/mL (n=6 biological replicates per dose). Cells were incubated for 72 hours with drug then assayed for viability with a

resazurin-based assay per standard protocols (30). Dose-response curves were generated and analyzed with GraphPad Prism 5.0 software (31).

5-Azacytidine Treatment

Untransfected Abrams cells were plated at 40% confluency and treated with 10 μ M 5-azacytidine in C10 media (n=5 biological replicates). Vehicle controls (0.1% DMSO) were included (n=2 biological replicates). Abrams cells were chosen specifically as, of all cell lines examined, they express the least endogenous NDRG2. Forty-eight hours after treatment, cells were harvested, RNA was extracted and samples were assayed for NDRG2 expression via qRT-PCR.

RESULTS

NDRG2 mRNA Expression is Suppressed in OSA

Previous studies by our laboratory indicated that NDRG2 is down-regulated in dogs that respond poorly to definitive treatment compared to dogs that respond well (9). In order to gain perspective on this dysregulation, we performed microarray and qRT-PCR studies on normal bone samples to compare expression to matched tumor samples as well as previously-analyzed tumor samples. Signalment, tumor location and other details regarding the matched tumor-normal bone study population are outlined in Table 3.1; good and poor responder patient details are as previously published (9). Microarray findings indicate that NDRG2 is dramatically down-regulated in all OSA primary tumors studied relative to normal bone with the lowest levels of expression observed in primary tumors from the poor-responder cohort (DFI<100 days)(Figure 6.1a). Normal bone expresses, on average, 10-fold more NDRG2 mRNA than good-responder primary

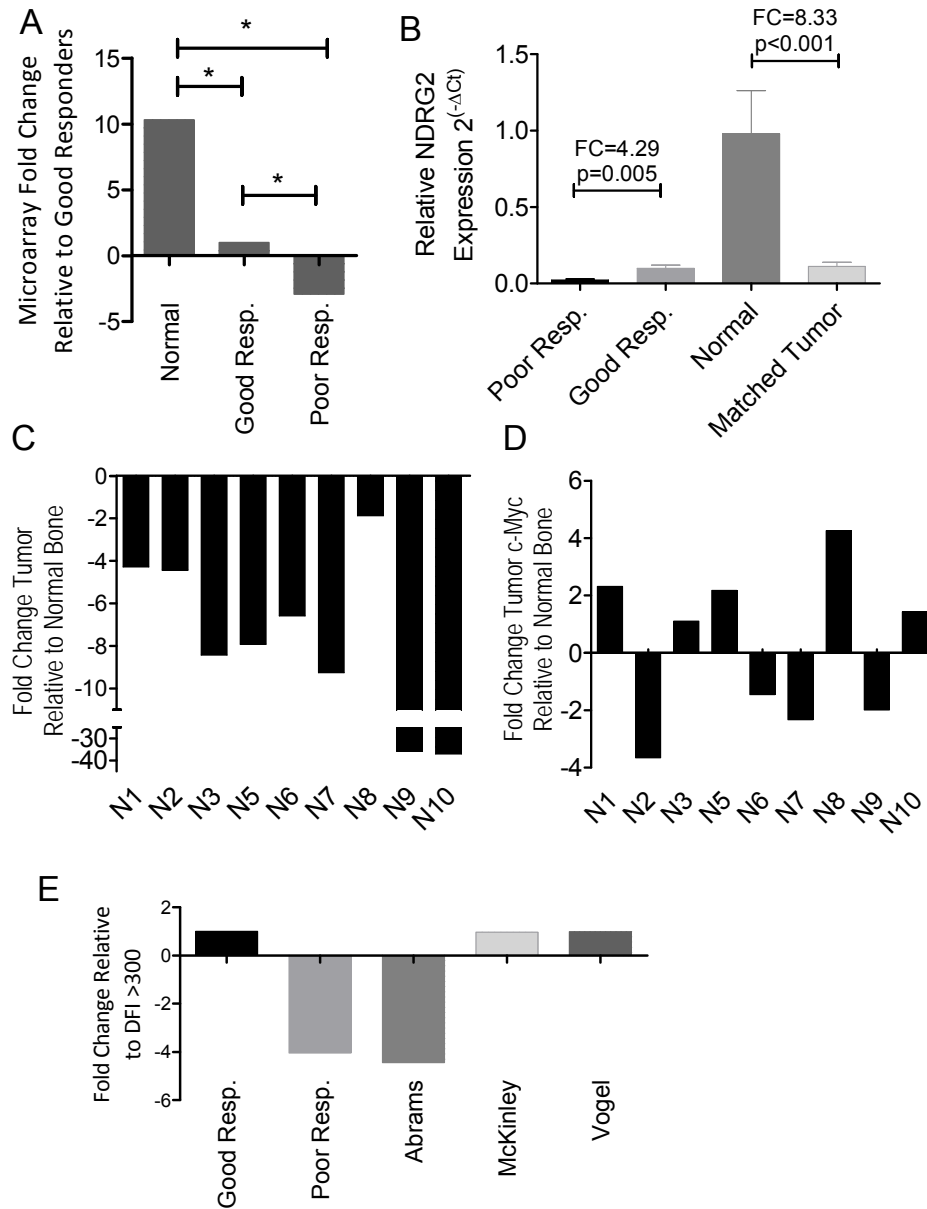


Figure 6.1 – Messenger RNA Expression of NDRG2 in primary OSA tumors, cell lines and normal bone. A) Microarray analysis revealed significant progressive downregulation of NDRG2 in tumors from both good and poor responders relative to normal bone. Normal bone n=8, Poor Resp. n=8, Good Resp. n=7, *=p<0.05. B) qRT-PCR validation of microarray data with NDRG2 transcript expression relative to HPRT-1 expressed as $2^{(-\Delta Ct)}$. Fold change calculations are inset, n=10 for good and poor responder groups and n=9 for normal bone and matched tumor. C) NDRG2 expression in tumors relative to matched normal bone from the same patient as measured by qRT-PCR. D) mRNA expression of c-Myc in tumors relative to matched normal bone as measured by qRT-PCR. E) qRT-PCR analysis of NDRG2 transcript expression in three canine OSA cell lines expressed as fold change relative to good-responder (DFI>300) primary tumor samples.

tumors (Figure 6.1a, left bar) which, in turn, express over 3-fold more NDRG2 than poor responders (Figure 6.1a, middle and right bars) indicating a 30-fold down-regulation in poor responders relative to normal bone. To confirm these findings, we validated mRNA expression levels with qRT-PCR on an expanded sample set of poor- and good-responder primary tumors, normal bone and tumor samples matched to the normal bone samples. This study confirmed significant down-regulation of NDRG2 in all primary tumors relative to normal bone (Figure 6.1b). On a patient-by-patient basis, NDRG2 was also down-regulated in tumor relative to normal bone (Figure 6.1c). In two cases, NDRG2 was down-regulated almost 40-fold in the primary tumor. When comparing c-Myc mRNA expression in this same matched tumor and normal bone sample set, we observed c-Myc upregulation in only four of nine samples (Figure 6.1d, N1, N5, N8 & N10). Thus, while NDRG2 has been shown to be Myc responsive in tumor systems, it is not the only means of NDRG2 suppression in this sample set. With the aim of identifying viable *in vitro* models for this dysregulation, we assayed NDRG2 expression in canine OSA cell lines. Expression levels similar to those observed in both good- and poor-responders were identified in different lines with the Abrams line expressing very low amounts of NDRG2 mRNA, similar to poor-responders, and the Vogel and McKinley lines mimicking good-responder expression levels (Figure 6.1e).

Two NDRG2 Isoforms are Expressed in Cell Lines and Primary Tumors

Initially, we performed immunoblotting on cell lines to determine if NDRG2 protein expression correlated with mRNA expression. This preliminary study resulted in the identification of two distinct protein products, one at ~40 kD and a slightly larger one at ~42 kD (Figure 6.2a). This finding lead to the hypotheses that a) a proportion of

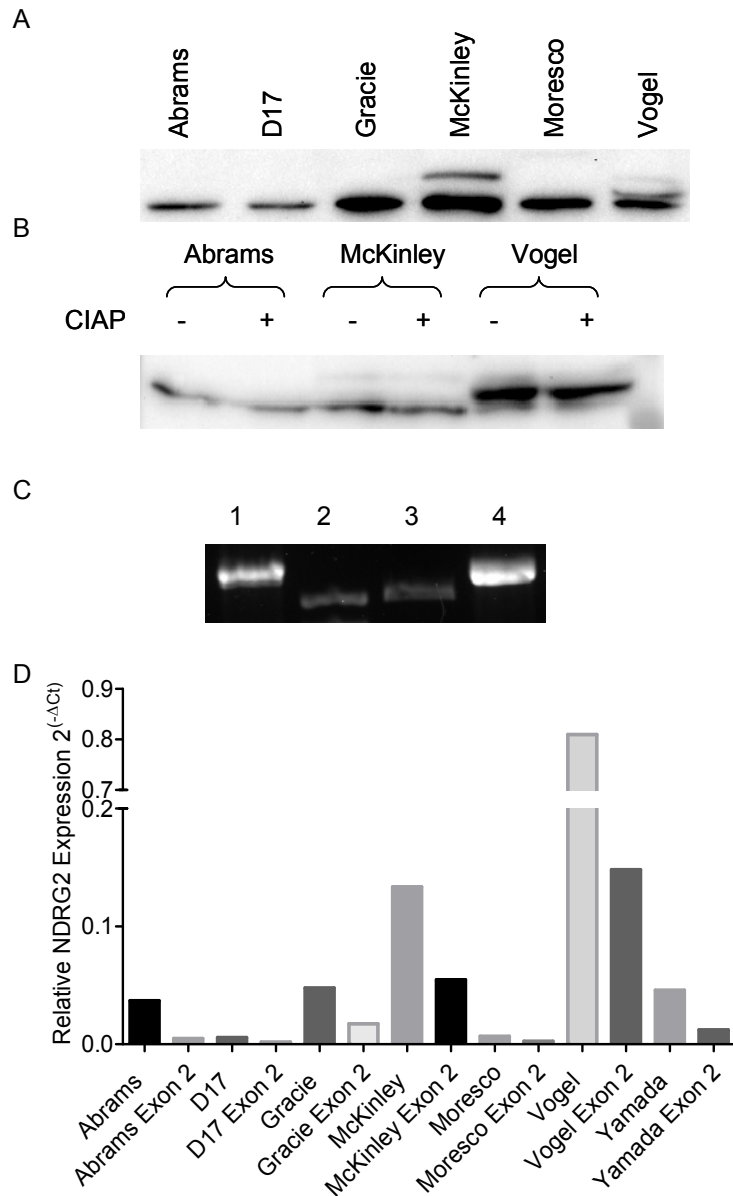
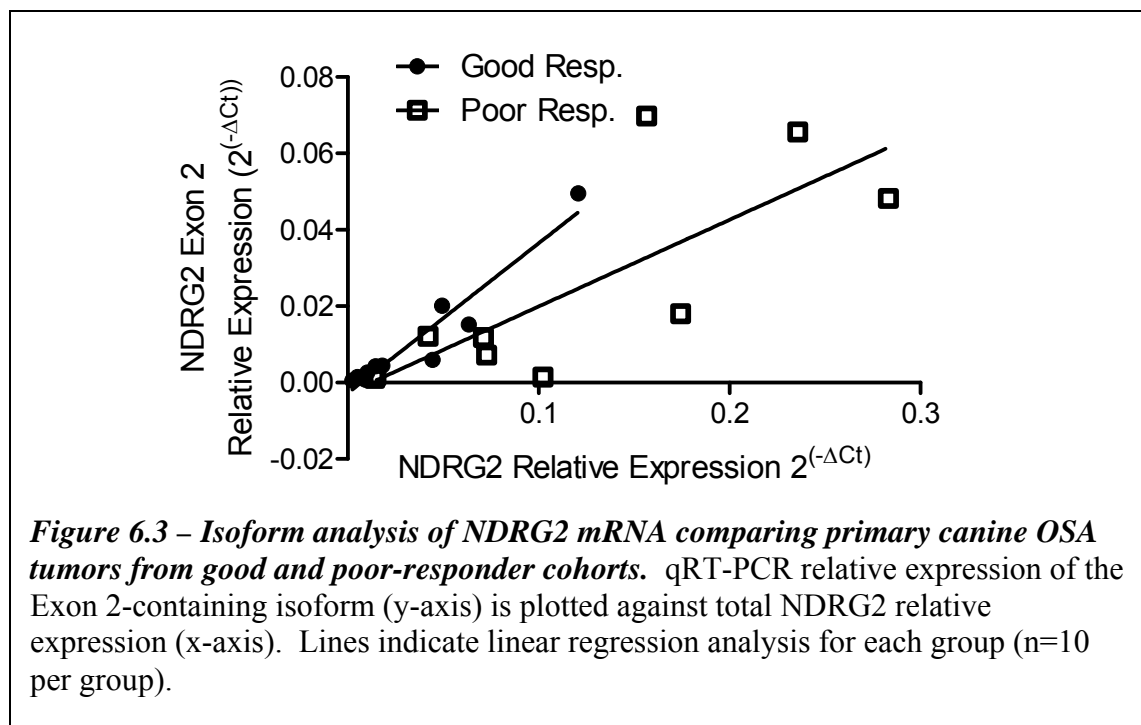


Figure 6.2 – Protein and isoform analysis of NDRG2 in canine OSA cell lines. A) Western blot of whole cell lysates from six canine OSA cell lines yielded two specific bands. 25 μ g protein loaded per well. B) Western blot analysis of NDRG2 lysates untreated (odd lanes), or treated with calf intestinal alkaline phosphatase (CIAP, even lanes). C) Pre-cloning PCR yielded two distinct product sizes: Lane 1 – McKinley cell line amplicon Lane 2 – 100 bp ladder, 1 kb band, Lane 3 – 1 kb ladder, 1 kb band, Lane 4 – Vogel cell line amplicon. D) Quantitative RT-PCR of NDRG2 using primers that amplify all isoforms or Exon 2-specific primers. Expression is relative to HPRT1 and is expressed as $2^{(-\Delta Ct)}$. N=2 technical replicates per expression value.

NDRG2 protein undergoes post-translational modification in some cell lines leading to the observed size shift or b) multiple NDRG2 protein isoforms are present in some OSA cell lines. As NDRG2 has multiple conserved phosphorylation sites, we first investigated whether this size shift was due to phosphorylation by immunoblotting cell lysate that had been treated with calf intestinal alkaline phosphatase (CIAP). This dephosphorylation method did not yield any changes in band distribution on western blot as untreated lysate (Figure 6.2b, odd lanes) ran no differently than CIAP treated lysate (Figure 6.2b, even lanes). In order to determine if expression of multiple isoforms was the cause of the western banding pattern, full-length coding sequence NDRG2 cDNA was amplified using gene specific primers from McKinley and Vogel lines, the two lines with the strongest secondary bands. Although the resulting PCR products were very similar in size, two distinct products were present upon gel electrophoresis (Figure 6.2c)

The resulting PCR products were cloned into the mammalian expression vector pDNATM3.2/V5-GW/D-TOPO® and sequenced with primers flanking the inserts. Two inserts were obtained and the difference between them was the presence (long isoform) or absence (short isoform) of a 14 aa domain following AA 25 (Exon 2). Insert sequences and alignments of encoded proteins are provided in Appendix E. Proteins generated from these coding sequences are predicted to be 371 aa and 357 aa in size. To assess the prevalence of the Exon 2-containing isoform of NDRG2 in canine OSA cell lines, Exon 2 specific primers were designed and qRT-PCR was performed to compare total NDRG2 expression to long isoform expression. In all cell lines examined, the short NDRG2 isoform was predominant, but in some lines (i.e. D17, McKinley, Moresco) the long isoform approached 1/3 to 1/2 of total NDRG2 transcripts (Figure 6.2D).

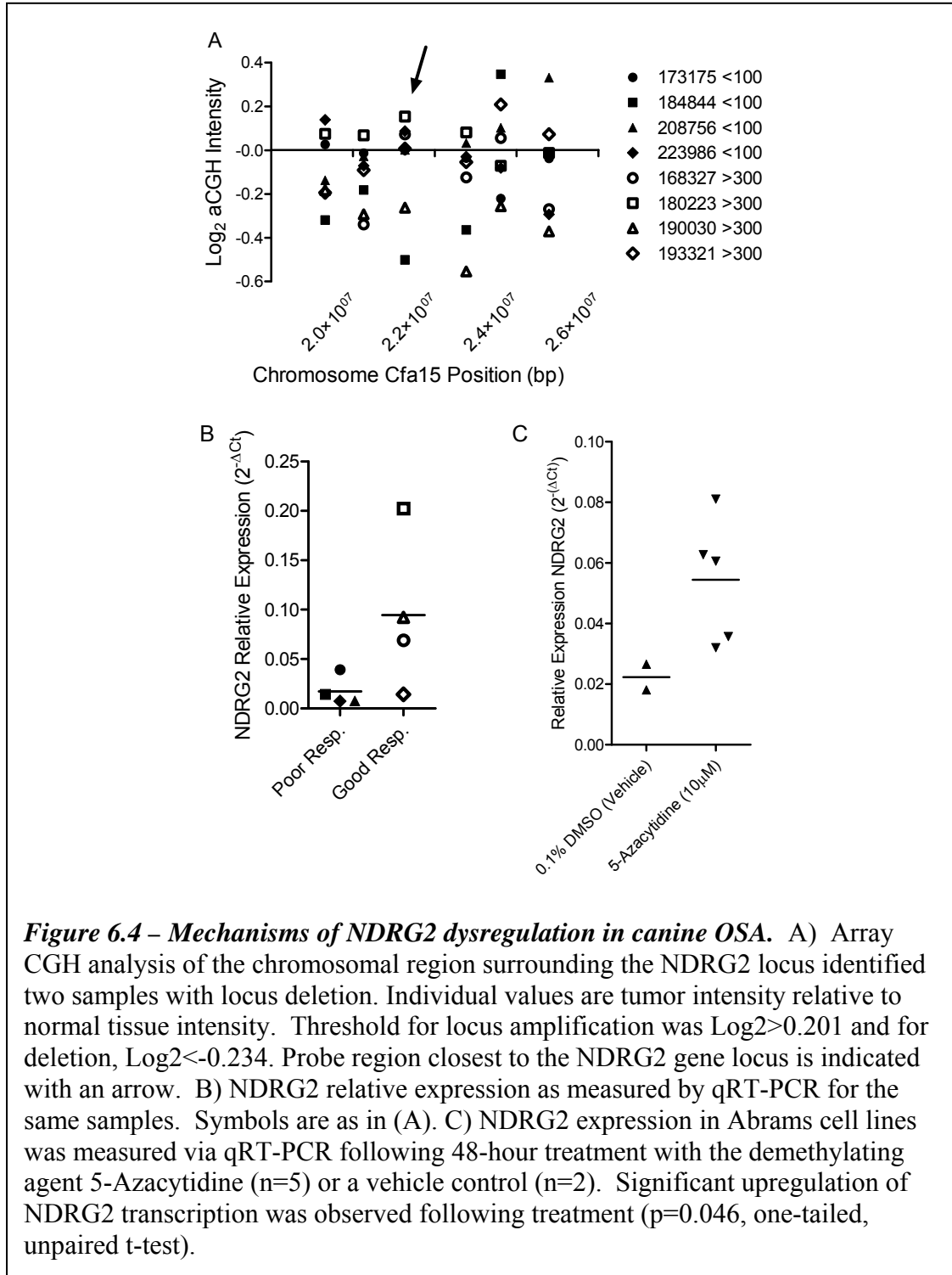
Having identified this splice variant, we hypothesized that Exon 2-containing transcript expression may relate to the prognostic value of NDRG2 expression in canine primary tumors. Thus, exon-specific qRT-PCR expression analysis was performed on the good- and poor-responder primary tumor cohorts. A slight trend demonstrating a smaller proportion of exon 2-containing long isoform transcripts (y-axis) relative to total NDRG2 (x-axis) in good-responder tumors was observed following linear regression analysis (Figure 6.3). This trend, however, did not reach significance thresholds.



Gene Deletion and Methylation: Two Mechanisms of NDRG2 Suppression

Copy number aberrations (CNAs) at the *NDRG2* locus have been previously identified in tumors (11), thus, array CGH was performed to examine this possible mechanism of NDRG2 suppression in canine OSA. Array CGH was performed on four samples each from good- and poor-responder cohorts; hybridization intensities of primary

tumors were compared to matched normal tissue to identify tumor-specific CNAs. Two samples, one from each cohort, demonstrated gene deletion at the probe location closest to the *NDRG2* gene (Figure 6.4a, arrow). Upon comparing chromosomal hybridization



intensities to observed mRNA expression levels, however, it was notable that the extent of mRNA suppression did not correlate with deletion (i.e. tumors without deletion had equal or less NDRG2 mRNA than tumors with CNAs) (Figure 6.4b). Thus, it was clear that additional mechanisms must be involved in NDRG2 suppression, especially in tumors without CNAs.

To investigate whether methylation influences NDRG2 expression in this system, the cell line with the most-suppressed NDRG2 (Abrams) was subjected to 5-Azacytidine treatment. Following 48-hour treatment with this demethylating agent, NDRG2 expression was significantly up-regulated compared to vehicle controls (Figure 6.4c). These findings indicate that methylation may, indeed, suppress transcription of *NDRG2* in OSA.

Exogenous NDRG2 Modulates BMP4 Expression in Transfected Cells

Abrams cells were stably transfected with either short isoform or long isoform expression constructs to further investigate the role of NDRG2 in this system. Resulting short isoform clones were denoted with numbers (i.e. Clone 2) and long isoform clones were denoted with letters (i.e. Clone C). Bone Morphogenetic Protein 4 (BMP4) was previously identified as a downstream target of NDRG2 (16), thus, BMP4 expression was assayed via qRT-PCR to determine if exogenous NDRG2 was active in the cells. This was deemed especially important as all transfected NDRG2 was also expressing a linker and V5 tag at the C-terminus of the protein and it was unknown how this would affect protein functionality. BMP4 expression tracked with NDRG2 expression independent of which NDRG2 isoform was transfected suggesting that exogenous NDRG2 was, indeed, active (Figure 6.5a, black bars vs. gray bars). Exon-specific PCR demonstrated that Exon

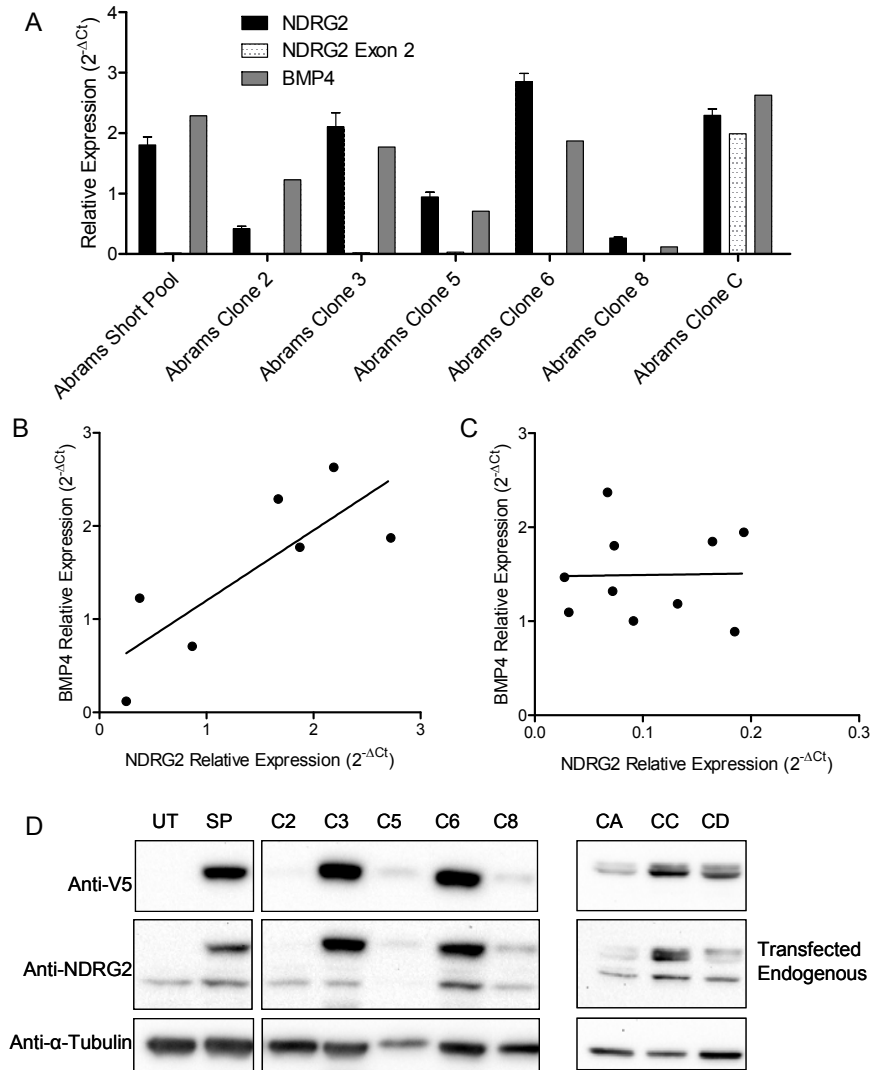


Figure 6.5 – NDRG2 mRNA and protein expression in Abrams transfectants. A) qRT-PCR expression analysis of total NDRG2 expression (black bars), Exon 2-containing NDRG2 isoforms (stipled bars) and BMP4 expression (gray bars). “Short Pool” and numbered clones denote cells transfected with the isoform lacking Exon 2, lettered clones are cells transfected with the Exon 2-containing isoform. n=2 technical replicates per sample, total NDRG2 expression is the mean of two separate experiments, error bars represent SEM. B) Relative mRNA expression of BMP4 (y-axis) plotted against total NDRG2 mRNA expression (x-axis) expressed as $2(-\Delta Ct)$ relative to HPRT1 in Abrams-NDRG2 clones and short pool. Line indicates linear regression analysis, slope is significantly non-zero ($p=0.03$). C) Relative mRNA expression of BMP4 (y-axis) plotted against total NDRG2 mRNA expression (x-axis) in untransfected Abrams cells and Abrams-CAT clones. Line indicates linear regression analysis which was not significantly different from zero. D) Western blots of NDRG2 transfectants. UT=untransfected, SP=short pool, numbered clones are transfected with the short isoform and lettered clones with the long isoform. Figure is a composite of two blots, each stripped and re-probed with the noted antibodies.

2 expression was only up-regulated in clones that were specifically transfected with that isoform (Figure 6.5a, stippled bars). Linear regression analysis of total NDRG2 expression versus BMP4 expression in Abrams-NDRG2 transfectants yielded a significantly non-zero slope ($p= 0.0305$), suggesting the interconnection of these two genes (Figure 6.5b). However, untransfected Abrams cells and Abrams-CAT clones demonstrated inordinately high and variable levels of BMP4 transcript that did not correlate with NDRG2 expression (Figure 6.5c).

To further evaluate the nature of the protein product generated in transfectants, western blotting was performed on whole cell lysates of various clones. Anti-V5 probing identified no bands in untransfected cells, one band in short isoform transfected cells and two bands in long isoform transfected cells (Figure 6.5d, top panel). Similarly, Anti-NDRG2 probing identified the same banding pattern in transfected cells in addition to endogenous NDRG2 (Figure 6.5d, middle panel). Exogenous NDRG2 is notably larger than endogenous NDRG2 due to the attached V5 tag and linker which total an additional 33 aa. Abrams-NDRG2-Clone 5 demonstrated fainter bands than expected from mRNA assays but this was due to insufficient protein loading as evidenced by the α -Tubulin loading control (Figure 6.5d, bottom panel). The distinct doublet observed in long-isoform transfected cells (Figure 6.5d, far right panel) cannot be explained by isoform differences as Exon 2 isoform expression makes up the vast majority of total NDRG2 in these clones (Figure 6.5a, final bars). Thus, this isoform likely undergoes preferential post-translational modification as compared to the short isoform.

NDRG2 Suppression Confers Doxorubicin Resistance

Stable Abrams-NDRG2 clones and control Abrams-CAT clones were assayed for both DOX and Carb sensitivity to determine if NDRG2 modulates this aspect of tumor aggressiveness. Overexpression of NDRG2 did not modulate sensitivity to Carb (data not shown), however, sensitivity to DOX was significantly increased in all short-isoform expressing transfectants as evidenced by reduced half maximal inhibitory concentration values (IC_{50}) (Figure 6.6a-e, Table 6.1). The heterogeneous pool of short-isoform transfected Abrams cells demonstrated the smallest increase in sensitivity relative to Abrams-CAT clones, supporting the idea that this heterogeneous population is likely to have a proportion of low NDRG2 expressing cells still contributing to resistance. Long isoform transfectants demonstrated a range of DOX sensitivities, with two of the clones demonstrating heightened sensitivity while the third, highest expressing clone (Abrams-NDRG2-Clone C), was as resistant as the Abrams-CAT pool (Figure 6.6f-h, Table 6.1).

Four stable clonal Abrams-CAT populations were also generated to determine the extent of inherent variability in DOX resistance for clones selected from this cell line. Three of four of these clones (Table 6.1 Abrams-CAT clones 1, 4, and 6) demonstrated significantly different resistance compared to the pool, however, in all cases, IC_{50} values were greater than those observed for the Abrams-CAT pool (Table 6.1). Thus, while the Abrams cell line demonstrates some natural variability in sensitivity to DOX, overexpression of NDRG2 dramatically increases sensitivity beyond this inherent variation.

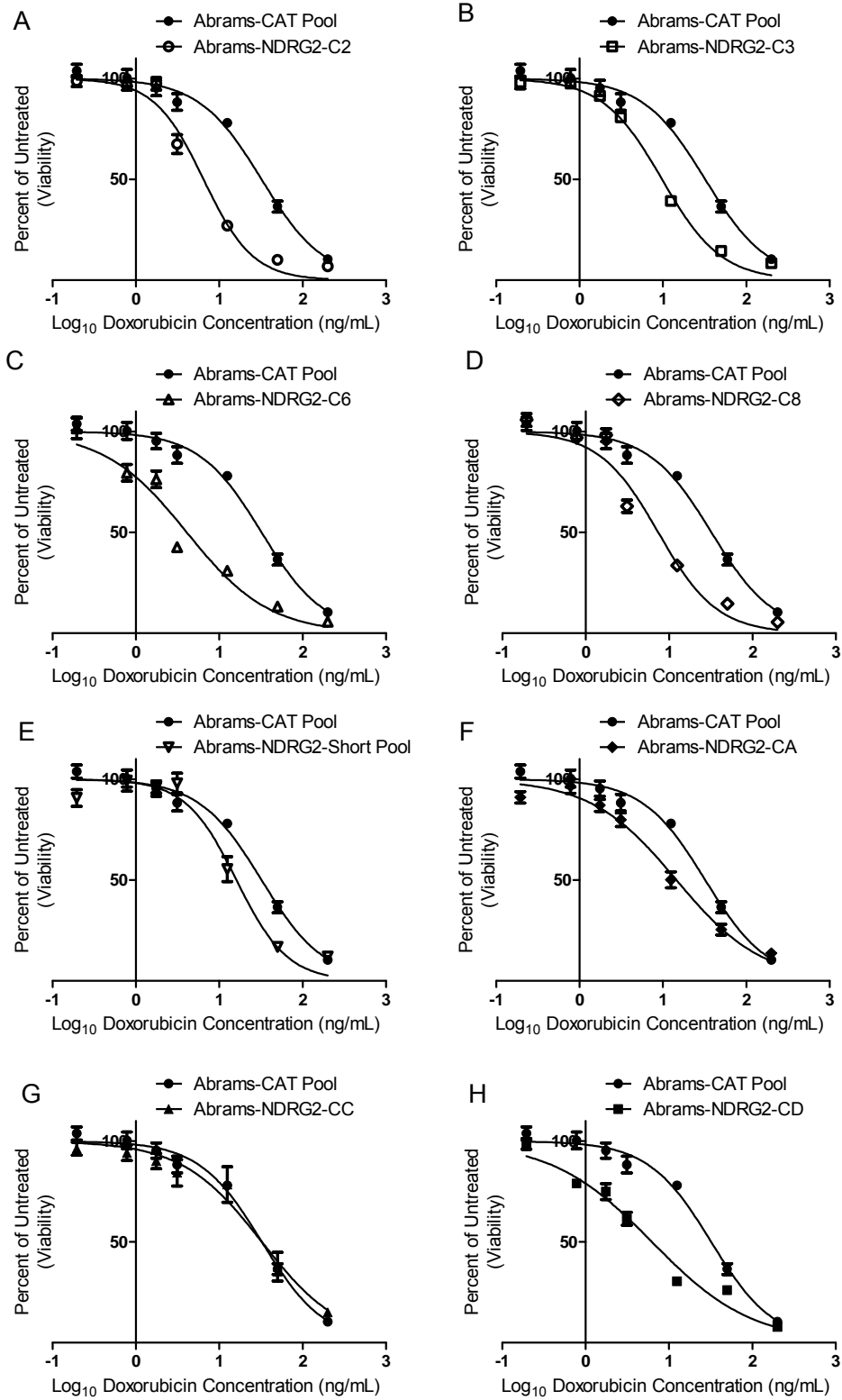


Figure 6.6 – Caption, following page

Figure 6.6 (Preceding Page) – Resazurin-based viability assays of Abrams-NDRG2 and Abrams-CAT cells following DOX treatment. Stable clones of NDRG2 expressing Abrams cells were selected and subjected to 72-hour DOX treatment after which cell viability was measured. From this, half maximal inhibitory concentration values (IC50) were determined as a measure of drug sensitivity. A-D) Four clonal isolates expressing the short isoform of NDRG2. E) The heterogeneous pool of short isoform transfectants. F-H) Three clonal isolates expressing the long isoform of NDRG2.

Table 6.1 – Doxorubicin sensitivity in transfected Abrams cells

	IC ₅₀ ^a	IC ₅₀ Range ^b	IC ₅₀ vs. CAT Pool IC ₅₀ ^c
Abrams-NDRG2-Short Pool ^d	16.09	12.91 to 20.06	<i>P</i> <0.0001
Abrams-NDRG2-Clone 2	6.487	5.557 to 7.573	<i>P</i> <0.0001
Abrams-NDRG2-Clone 3	9.771	8.761 to 10.90	<i>P</i> <0.0001
Abrams-NDRG2-Clone 6	4.077	3.263 to 5.094	<i>P</i> <0.0001
Abrams-NDRG2-Clone 8	7.396	6.109 to 8.954	<i>P</i> <0.0001
Abrams-NDRG2-Clone A ^e	14.54	11.95 to 17.69	<i>P</i> <0.0001
Abrams-NDRG2-Clone C	32.79	23.46 to 45.82	0.9173
Abrams-NDRG2-Clone D	6.259	5.186 to 7.555	<i>P</i> <0.0001
Abrams-CAT Pool ^f	32.18	27.23 to 38.03	NA
Abrams-CAT Clone 1	64.74	54.32 to 77.15	<i>P</i> <0.0001
Abrams-CAT Clone 2	35.47	27.91 to 45.09	0.4117
Abrams-CAT Clone 4	50.14	37.18 to 67.62	0.0082
Abrams-CAT Clone 6	72.25	56.03 to 93.17	<i>P</i> <0.0001

a – Half maximal inhibitory concentration values for DOX, b – 95% confidence interval for IC50, c – significance values for nonlinear regression analysis comparing clone IC50s to CAT Pool IC50, d – “Short Pool” and numbered clones denote transfectants with NDRG2 lacking Exon 2, e – lettered clones denote transfectants with NDRG2 including Exon 2, f – CAT Pool and clones are negative control samples

DISCUSSION

Previously, we identified underexpression of NDRG2 mRNA in primary tumors as a negative prognostic indicator for disease free interval in dogs with OSA (9).

Although NDRG2 expression had been assayed previously in a number of different tumor

systems, this is the first report of dysregulation in OSA relative to normal bone and the first examination of expression in the canine model (10, 11, 15-23, 32-34). We examined expression levels of this tumor suppressor gene in canine OSA and normal bone as well as its contribution to chemotherapeutic resistance in this system. We have identified two expressed isoforms of the mRNA and protein in canine samples. Furthermore, it is likely that one of these isoforms undergoes post-translational modification in the *in vitro* system. We also examined three possible mechanisms of the observed mRNA suppression, all of which may, indeed, be factors in the NDRG2 dysregulation common to all of the tumors studied.

Although its precise mechanism of action remains a mystery, previous association studies have linked NDRG2 to a variety of downstream targets important in cancer progression. For instance, NDRG2 protein has been found to directly interact with β -catenin protein and affect downregulation of TCF/ β -catenin transcriptional targets such as Cyclin D1 and fibronectin (12, 21). Similarly, cells expressing transfected NDRG2 have been shown to secrete enhanced levels of BMP4 which then suppresses matrix metalloproteinase 9 (*MMP9*) activity and cell invasion (16). Alteration in MMP9 expression in response to NDRG2 has also been shown to involve nuclear factor of kappa light polypeptide gene enhancer in B-cells (*NF κ B*) as an intermediary (15). Additionally, NDRG2 transfection led to activation of suppressor of cytokine signaling 1 (*SOCS1*) in breast cancer cells which then reduced phosphorylation and activity of Janus tyrosine kinase 2 (*JAK2*) and signal transducer and activator of transcription 3 (*STAT3*) resulting in decreased cellular proliferation (35). Finally, studies have shown that NDRG2 can enhance apoptosis mediated by hypoxia, p53 and Fas (13, 33, 36).

The role of *BMP4* in OSA has typically been viewed as a negative one: increased expression tends to correlate with less-differentiated tumors and worse outcomes (37). Despite this, even benign bone tumors can express and secrete BMP4, implying that BMP4 is not strictly a marker of aggressive malignancy but may indicate activation of non-tumorous osteoblasts (38). Our findings may provide a clue as to how BMP4 is (dys-)regulated in OSA: untransfected Abrams cells and CAT-transfected Abrams clones with extremely low levels of NDRG2 demonstrated variable but high BMP4 mRNA expression. However, when NDRG2 was transfected into these cells, BMP4 expression was expressed in an NDRG2-positively-responsive fashion. From this, one may hypothesize that, upon NDRG2 suppression, BMP4 is released from this controlling factor and behaves in a tumorigenic, pro-proliferative manner. However, restoration of even a small amount of functional NDRG2 signaling restores proper BMP4 control, reducing the influence of this signaling molecule on reactive bone formation and proliferation. Furthermore, NDRG2 expression has been linked to a BMP4-dependent repression of MMP9 expression in breast cancer, suggesting a role for NDRG2 and BMP4 in invasion and metastasis suppression (16).

NDRG2 and BMP4 have also been identified as upstream regulators and downstream targets, respectively, of NF κ B (15). NDRG2 transfection of murine melanoma cells resulted in suppression of NF κ B and a resultant decrease in metastatic potential (15). Increased NF κ B activity in OSA has been strongly correlated with proliferation and invasion (39, 40). Furthermore, knockdown of NF κ B induced BMP4 expression in OSA cells (39) and suppressed vascular endothelial growth factor (VEGF) and intercellular adhesion molecule 1 (ICAM-1) resulting in reversion of the metastatic

phenotype of the murine OSA cell line LM8 (40). Thus, multiple lines of evidence suggest that, via interactions with NF κ B and its downstream targets, NDRG2 serves as both a tumor suppressor and a metastasis suppressor.

Our findings confirm that NDRG2 is widely suppressed in OSA primary tumors. Similarly, we have confirmed that both *NDRG2* gene deletion as well as methylation can serve as mechanisms for suppression of this gene (10, 11, 41). Furthermore, c-Myc-dependent repression of the *NDRG2* gene via direct binding of the core promoter has been identified in a number of different cell types and it has been determined that this repression is dependent on Myc-interacting zinc finger 1 (ZBTB17 aka Miz-1) association with Myc (24). c-Myc and n-Myc have both been identified as oncogenes that can be overexpressed in OSA and copy number gains of c-Myc have been observed in canine OSA (6, 42-45). Additionally c-Myc expression has been associated with methotrexate and cisplatin resistance in OSA (46, 47) and mouse models of Myc alteration have demonstrated that reduction of Myc expression can cause tumor regression (48). Thus, dysregulation in either of these upstream factors can inhibit NDRG2 expression. Here, we have observed upregulation of c-Myc mRNA relative to normal bone in four of nine matched tumors indicating that over-expression of this oncogene may suppress NDRG2 in a portion of OSA primary tumors. Other gene regulation mechanisms not yet addressed in this system may also be at work. For instance, microRNA regulation of NDRG2 has also been observed (10). As our transfectants lack 3'UTR, they also, undoubtedly lack some of the control mechanisms that may contribute to NDRG2 suppression in OSA. Thus, generation of luciferase-3'UTR constructs may be very informative in future studies aimed at more closely

defining mechanisms of post transcriptional NDRG2 regulation. As mentioned previously, NDRG2 is also a known phosphorylation target for several kinases, thus, modulation in kinase activity or mutation in phosphorylation sites can alter downstream effects without altered transcriptional activity of NDRG2 (14).

For the first time, we have linked NDRG2 suppression to chemoresistance; to date, no other studies have examined this important feature of cancer progression with regard to NDRG2. Interestingly, while our short isoform expressing cells consistently demonstrated enhanced DOX chemosensitivity, long isoform expressing cells were inconsistent. The structure and function of Exon 2 is currently unknown as crystal structure analyses have not included it, thus, it is worth exploring in the future because the short isoform may be far more therapeutically beneficial than the long isoform (12). Our finding that restoration of NDRG2 short isoform expression induces DOX chemosensitivity in OSA makes sense if one considers the interconnection between NDRG2 and NF κ B. NF κ B overexpression has been shown to induce chemoresistance through pro-survival/anti-apoptotic mechanisms, thus, its suppression by NDRG2 may very well be the mechanism of sensitivity induction we see here (49-51). However, as NF κ B responsiveness to NDRG2 has not yet been assessed in this system, future identification of new NDRG2 gene targets and modulators of chemoresistance may yet be possible.

In conclusion, we have identified NDRG2 as a potential prognostic biomarker in canine OSA and followed that up with investigations into mechanisms of its suppression in these tumors. Myc oncogene expression, CNAs and methylation of the *NDRG2* locus likely contribute to gene suppression but other mechanisms may also be identified that

contribute to the profound reduction in mRNA observed in all tumors tested here. NDRG2 involvement with the NF κ B pathway may contribute to both metastases and chemoresistance in OSA, thus, further evaluation of this link will be of great value.

ACKNOWLEDGEMENTS

We acknowledge Erin Petrilli and the Genomics Core at the Rocky Mountain Regional Center for Excellence at CSU for generating the microarray data. We would also like to thank Irene Mok and Kristen Grunerud at CSU's Animal Cancer Center for coordinating sample retrieval from the tissue archive and amputees. Generation of NDRG2 transfectants would not have been possible without the excellent subcloning skills of Anne Handschy. This work was supported by grants to DLD from the Morris Animal Foundation (MAF D08CA-053) and the CSU College Research Council - Miki Society.

REFERENCES

1. Dernell WS, Ehrhart NP, Straw RC, Vail DM. Tumors of the skeletal system. In: Withrow SJ, Vail DM, editors. *Withrow and MacEwen's Small Animal Clinical Oncology*. 4th ed. St. Louis: Saunders Elsevier; 2007. p. 540-67.
2. Jaffe N. Adjuvant chemotherapy in osteosarcoma: An odyssey of rejection and vindication. In: Jaffe N, Bielack SS, Bruland OS, editors. *Pediatric and Adolescent Osteosarcoma, Cancer Treatment and Research*. New York: Springer; 2009.
3. Mueller F, Fuchs B, Kaser-Hotz B. Comparative biology of human and canine osteosarcoma. *Anticancer Research* 2007;27(1A):155-64.
4. Paoloni M, Davis S, Lana S, Withrow S, Meltzer P, Khanna C. Comparative gene expression analysis of canine and human osteosarcoma. *Genes, Dogs & Cancer: 4th International Canine Cancer Conference*; 2006; Chicago, IL; 2006. p. 19.
5. Paoloni M, Davis S, Lana S, Withrow S, Sangiorgi L, Picci P, *et al.* Canine tumor cross-species genomics uncovers targets linked to osteosarcoma progression. *BMC Genomics* 2009;10(1):625.
6. Thomas R, Wang H, Tsai P, Langford C, Fosmire S, Jubala C, *et al.* Influence of genetic background on tumor karyotypes: evidence for breed-associated cytogenetic aberrations in canine appendicular osteosarcoma. *Chromosome Research* 2009;17(3):365-77.
7. Link MP, Goorin AM, Miser AW, Green AA, Pratt CB, Belasco JB, *et al.* The effect of adjuvant chemotherapy on relapse-free survival in patients with osteosarcoma of the extremity. *New England Journal of Medicine* 1986;314(25):1600-6.
8. Sutter NB, Ostrander EA. Dog star rising: the canine genetic system. *Nature Reviews Genetics* 2004;5(12):900-10.
9. O'Donoghue LE, Ptitsyn AA, Kamstock DA, Siebert J, Thomas RS, Duval DL. Expression profiling in canine osteosarcoma: identification of biomarkers and pathways associated with outcome. *BMC Cancer* 2010;10(1):506.

10. Feng L, Xie Y, Zhang H, Wu Y. Down-regulation of NDRG2 gene expression in human colorectal cancer involves promoter methylation and microRNA-650. *Biochemical and Biophysical Research Communications* 2011;406(4):534-8.
11. Liu N, Wang L, Liu X, Yang Q, Zhang J, Zhang W, *et al.* Promoter methylation, mutation, and genomic deletion are involved in the decreased NDRG2 expression levels in several cancer cell lines. *Biochemical and Biophysical Research Communications* 2007;358(1):164-9.
12. Hwang J, Kim Y, Kang HB, Jaroszewski L, Deacon AM, Lee H, *et al.* Crystal structure of the human N-Myc Downstream-Regulated Gene 2 protein provides insight into its role as a tumor suppressor. *Journal of Biological Chemistry* 2011;286(14):12450-60.
13. Wang L, Liu N, Yao L, Li F, Zhang J, Deng Y, *et al.* NDRG2 is a new HIF-1 target gene necessary for hypoxia-induced apoptosis in A549 cells. *Cellular Physiology & Biochemistry* 2008;21(1-3):239-50.
14. Burchfield JG, Lennard AJ, Narasimhan S, Hughes WE, Wasinger VC, Corthals GL, *et al.* Akt mediates insulin-stimulated phosphorylation of NdrG2. *Journal of Biological Chemistry* 2004;279(18):18623-32.
15. Kim A, Kim M-J, Yang Y, Kim JW, Yeom YI, Lim J-S. Suppression of NF- κ B activity by NDRG2 expression attenuates the invasive potential of highly malignant tumor cells. *Carcinogenesis* 2009;Epub ahead of print: bgp072.
16. Shon S-K, Kim A, Kim JY, Kim KI, Yang Y, Lim J-S. Bone morphogenetic protein-4 induced by NDRG2 expression inhibits MMP-9 activity in breast cancer cells. *Biochemical and Biophysical Research Communications* 2009;385(2):198-203.
17. Lorentzen A, Lewinsky R, Bornholdt J, Vogel L, Mitchelmore C. Expression profile of the N-myc Downstream Regulated Gene 2 (NDRG2) in human cancers with focus on breast cancer. *BMC Cancer* 2011;11(1):14.
18. Chu D, Zhang Z, Li Y, Wu L, Zhang J, Wang W, *et al.* Prediction of colorectal cancer relapse and prognosis by tissue mRNA levels of NDRG2. *Molecular Cancer Therapeutics* 2011;10(1):47-56.
19. Shi H, Li N, Li S, Chen C, Wang W, Xu C, *et al.* Expression of NDRG2 in esophageal squamous cell carcinoma. *Cancer Science* 2010;101(5):1292-9.
20. Skiriute D, Tamasauskas S, Asmoniene V, Saferis V, Skauminas K, Deltuva V, *et al.* Tumor grade-related NDRG2 gene expression in primary and recurrent intracranial meningiomas. *Journal of Neuro-Oncology* 2011;102(1):89-94.

21. Kim Y-J, Yoon SY, Kim J-T, Song EY, Lee HG, Son HJ, *et al.* NDRG2 expression decreases with tumor stages and regulates TCF/ β -catenin signaling in human colon carcinoma. *Carcinogenesis* 2009;30(4):598-605.
22. Tepel M, Roerig P, Wolter M, Gutmann DH, Perry A, Reifenberger G, *et al.* Frequent promoter hypermethylation and transcriptional downregulation of the NDRG2 gene at 14q11.2 in primary glioblastoma. *International Journal of Cancer* 2008;123(9):2080-6.
23. Deng Y, Yao L, Chau L, Ng SS-m, Peng Y, Liu X, *et al.* N-Myc downstream-regulated gene 2 (NDRG2) inhibits glioblastoma cell proliferation. *International Journal of Cancer* 2003;106(3):342-7.
24. Zhang J, Li F, Liu X, Shen L, Liu J, Su J, *et al.* The repression of human differentiation-related gene NDRG2 expression by Myc via Miz-1-dependent interaction with the NDRG2 core promoter. *Journal of Biological Chemistry* 2006;281(51):39159-68.
25. O'Donoghue LE, Rivest JP, Duval DL. Polymerase chain reaction-based species verification and microsatellite analysis for canine cell line validation. *Journal of Veterinary Diagnostic Investigation* 2011;23(4):780-5.
26. Tong W, Cao X, Harris S, Sun H, Fang H, Fuscoe J, *et al.* ArrayTrack--supporting toxicogenomic research at the U.S. Food and Drug Administration National Center for Toxicological Research. *Environmental Health Perspectives* 2003;111(15).
27. Livak KJ, Schmittgen TD. Analysis of relative gene expression data using real-time quantitative PCR and the 2- $\Delta\Delta$ Ct method. *Methods* 2001;25(4):402-8.
28. Ausubel FM. *Current Protocols in Molecular Biology*: Greene Publishing Associates and Wiley-Interscience; 2001-2011.
29. Thomas R, Scott A, Langford CF, Fosmire SP, Jubala CM, Lorentzen TD, *et al.* Construction of a 2-Mb resolution BAC microarray for CGH analysis of canine tumors. *Genome Research* 2005;15(12):1831-7.
30. Anoopkumar-Dukie S, Carey JB, Conere T, O'Sullivan E, van Pelt FN, Allshire A. Resazurin assay of radiation response in cultured cells. *The British Journal of Radiology* 2005;78(934):945-7.
31. GraphPad. Prism 5.0. Prism5 Statistics Guide. 5.0 ed. San Diego, CA: GraphPad Software Inc.; 2007.

32. Kim YJ, Yoon SY, Kim J-T, Choi SC, Lim J-S, Kim JH, *et al.* NDRG2 suppresses cell proliferation through down-regulation of AP-1 activity in human colon carcinoma cells. *International Journal of Cancer* 2009;124(1):7-15.
33. Liu N, Wang L, Li X, Yang Q, Liu X, Zhang J, *et al.* N-Myc downstream-regulated gene 2 is involved in p53-mediated apoptosis. *Nucleic Acids Research* 2008;36(16):5335-49.
34. Yao L, Zhang J, Liu X. NDRG2: a Myc-repressed gene involved in cancer and cell stress. *Acta Biochimica et Biophysica Sinica* 2008;40(7):625-35.
35. Park Y, Shon S-K, Kim A, Kim KI, Yang Y, Cho DH, *et al.* SOCS1 induced by NDRG2 expression negatively regulates STAT3 activation in breast cancer cells. *Biochemical and Biophysical Research Communications* 2007;363(2):361-7.
36. Choi S-C, Yoon SR, Park YP, Song EY, Kim JW, Kim WH, *et al.* Expression of NDRG2 is related to tumor progression and survival of gastric cancer patients through Fas-mediated cell death *Experimental & Molecular Medicine* 2007;39(6):705-14.
37. Yoshikawa H, Nakase T, Myoui A, Ueda T. Bone morphogenetic proteins in bone tumors. *Journal of Orthopaedic Science* 2004;9(3):334-40-40.
38. Okuda Sy, Myoui A, Nakase T, Wada E, Yonenobu K, Yoshikawa H. Ossification of the ligamentum flavum associated with osteoblastoma: a report of three cases. *Skeletal Radiology* 2001;30(7):402-6.
39. Andela VB, Sheu T-J, Puzas EJ, Schwarz EM, O'Keefe RJ, Rosier RN. Malignant reversion of a human osteosarcoma cell line, Saos-2, by inhibition of NF[κ]B. *Biochemical and Biophysical Research Communications* 2002;297(2):237-41.
40. Nishimura A, Akeda K, Matsubara T, Kusuzaki K, Matsumine A, Masuda K, *et al.* Transfection of NF-[κ]B decoy oligodeoxynucleotide suppresses pulmonary metastasis by murine osteosarcoma. *Cancer Gene Therapy* 2011;18(4):250-9.
41. Piepoli A, Cotugno R, Merla G, Gentile A, Augello B, Quitadamo M, *et al.* Promoter methylation correlates with reduced NDRG2 expression in advanced colon tumour. *BMC Medical Genomics* 2009;2(1):11.
42. Pompetti F, Rizzo P, Simon RM, Freidlin B, Mew DJ, Pass HI, *et al.* Oncogene alterations in primary, recurrent, and metastatic human bone tumors. *Journal of Cellular Biochemistry* 1996;63(1):37-50.

43. Bogenmann E, Moghadam H, DeClerck YA, Mock A. c-myc amplification and expression in newly established human osteosarcoma cell lines. *Cancer Research* 1987;47(14):3808-14.
44. Ioannidis P, Trangas T, Dimitriadis E, Samiotaki M, Kyriazoglou I, Tsiapalis CM, *et al.* C-MYC and IGF-II mRNA-binding protein (CRD-BP/IMP-1) in benign and malignant mesenchymal tumors. *International Journal of Cancer* 2001;94(4):480-4.
45. Gamberi G, Benassi MS, Bohling T, Ragazzini P, Molendini L, Sollazzo MR, *et al.* C-myc and c-fos in human osteosarcoma: prognostic value of mRNA and protein expression. *Oncology* 1998;55(6):556-63.
46. Scionti I, Michelacci F, Pasello M, Hattinger CM, Alberghini M, Manara MC, *et al.* Clinical impact of the methotrexate resistance-associated genes C-MYC and dihydrofolate reductase (DHFR) in high-grade osteosarcoma. *Annals of Oncology* 2008;19(8):1500-8.
47. Xie X-K, Yang D-S, Ye Z-M, Tao H-M. Recombinant antisense c-Myc adenovirus increase in vitro sensitivity of osteosarcoma MG-63 cells to cisplatin. *Cancer Investigation* 2006;24(1):1-8.
48. Jain M, Arvanitis C, Chu K, Dewey W, Leonhardt E, Trinh M, *et al.* Sustained loss of a neoplastic phenotype by brief inactivation of MYC. *Science* 2002;297(5578):102-4.
49. Chaturvedi MM, Sung B, Yadav VR, Kannappan R, Aggarwal BB. NF-[kappa]B addiction and its role in cancer: "one size does not fit all". *Oncogene* 2011;30(14):1615-30.
50. Li F, Sethi G. Targeting transcription factor NF-[kappa]B to overcome chemoresistance and radioresistance in cancer therapy. *Biochimica et Biophysica Acta (BBA) - Reviews on Cancer* 2010;1805(2):167-80.
51. Yu L-L, Dai N, Yu H-G, Sun L-M, Si J-M. Akt associates with nuclear factor κ B and plays an important role in chemoresistance of gastric cancer cells. *Oncology Reports* 2010;24(1):113-9.

Chapter 7

General Conclusions

The studies presented in this dissertation describe molecular analyses of osteosarcoma (OSA) in canine patients with the aim of identifying novel factors that contribute to disease progression and chemotherapeutic resistance. As OSA is the most common primary bone tumor in both dogs and man, and current treatments provide only a limited cure rate, new therapeutic targets are sorely needed. The high incidence of this cancer in the canine population as well as their genetic and environmental similarities to humans make them an ideal translational study model. Thus, new discoveries in the field of canine OSA research can benefit both veterinary and human patients.

In Chapter 2, we profiled gene expression using Affymetrix Canine 2.0 microarrays in primary tumors taken from two cohorts of canine OSA patients: those with good responses and those with poor responses following definitive treatment by amputation of the affected limb followed by adjuvant therapy with doxorubicin and/or a platinum-based drug. Patients were selected for these cohorts on the basis of disease free intervals (good responders = DFI>300 days, poor responders = DFI<100 days) which were determined from the medical record. The aim of this study was to identify genes and pathways that were dysregulated between the tumors of the two cohorts and

determine a gene signature that predicted the most aggressive or chemoresistant tumors. Microarray analysis and subsequent qRT-PCR validation of this data led to the development of four predictive models that were based on a selection of differentially regulated genes. Additionally, pathway analysis of microarray data identified several dysregulated pathways including hedgehog signaling. This broad survey study laid the groundwork for future investigations into the molecular pathogenesis of OSA.

Having identified several genes of interest in the outcome-based study, we wished to establish applicable baseline data for the dysregulation observed in tumors. Thus, in Chapter 3, we pursued gene expression profiling of normal bone as well as array comparative genomic hybridization (aCGH) to determine what portion of gene (dys)regulation was due to gene copy number alterations (CNAs). Comparing normal bone gene expression to that of primary tumors was strikingly informative as only a subset of previously-identified progression-related genes were significantly altered from normal in all tumors. Furthermore, aCGH analysis of primary tumors relative to normal tissue identified many regions of CNA in primary tumors and emphasized the chaotic nature of OSA chromosome derangements. As a general theme, many tumors demonstrated copy number gain of oncogenes, copy number loss of tumor suppressors and/or CNAs in genes associated with those pathways. These survey experiments provided much-needed perspective on the studies in Chapter 2 and allowed us to move forward with the most-robust targets.

Cell line contamination has gained much attention in recent years and many funding agencies and journals are beginning to require validation of cell lines. Thus, with the aim of generating vigorous and correct data in future *in vitro* work, we pursued

validation of cell lines with respect to species, short tandem repeat (STR), and tissue of origin identities. In Chapter 4, we verified that all cell lines to be used in future studies were derived from different canine individuals and that they had been generated from OSA. Additionally, we identified several instances of cell line contamination in the Animal Cancer Center and generated a database of STR profiles to be used in future validation studies. Finally, we also validated anti-human antibodies for use in canine samples for western blotting and immunohistochemistry.

Having verified the sanctity of the canine *in vitro* models, we next pursued in-depth examination of two genes that had been identified in our outcome-based survey experiments. The first, insulin-like growth factor 2 mRNA binding protein 1 (*IGF2BP1*) is explored in Chapter 5. Previous work had identified *IGF2BP1* as an oncofetal gene: expressed during embryonic development and in some cancers but suppressed in normal adult tissues. Our analysis confirmed this relative to normal bone: mRNA expression was virtually undetectable in normal bone but increased in good-responder primary tumors and was even further elevated in poor-responder primary tumors. Immunohistochemical evaluation of IGF2BP1 expression in primary tumors from our study cohorts revealed increased nuclear localization of IGF2BP1 as a prognostic indicator for poor outcome but application of this screen to a large, independent data set demonstrated no relationship between nuclear or cytoplasmic staining frequency/intensity and outcome. Analysis of CNAs in the region around the *IGF2BP1* locus indicated that gene amplification was not the cause of enhanced expression in tumors. Thus, we investigated an additional mechanism of IGF2BP1 dysregulation: 3' untranslated region (UTR) shortening. Transcript of this gene can possess a 3' UTR of up to 7 kb in length

with multiple micro-RNA response elements. Previous studies identified shortening of this region as a possible mechanism of escape from normal regulation. Our analysis determined that primary tumors from poor outcome patients have a significantly smaller proportion of IGF2BP1 transcripts with full-length 3'UTR compared to patients with good outcomes. Next, we set out to explore functional consequences of IGF2BP1 expression in an *in vitro* model. Knockdown of this gene in the Abrams canine OSA cell line was accomplished with siRNA and resulted in decreased invasive capacity of the cell line. Thus, we determined that truncation of the IGF2BP1 3' UTR can contribute to its overexpression in OSA and this overexpression may result in enhanced metastatic capacity of the tumor.

Finally, in Chapter 6, we investigated the functional role of the putative tumor suppressor gene n-Myc downstream regulated gene 2 (*NDRG2*) in OSA. Expression analysis of the *NDRG2* mRNA identified suppression in good-responder primary tumors and significantly stronger suppression in poor-responder primary tumors relative to normal bone. As this gene has been shown to be downregulated in response to c-Myc, c-Myc expression in matched normal bone and tumor samples was assayed. This study identified upregulation of c-Myc in 4/9 tumors relative to normal bone. *NDRG2* expression, however, was suppressed in 9/9 tumors relative to normal bone indicating that other mechanisms were also causing suppression. aCGH analysis of the region surrounding the *NDRG2* locus identified copy number loss in 2/8 primary tumors (25%) which was unrelated to outcome. Additionally, treatment with the demethylating agent 5-azacytidine increased *NDRG2* mRNA expression in an *in vitro* system. These findings highlighted the importance of multiple factors in the (dys)regulation of *NDRG2* in this

system. To examine the functional role of this gene, we cloned the two expressed NDRG2 isoforms into a mammalian expression construct and generated stable Abrams-NDRG2 expressing cell line clones. Resultant clones demonstrated enhanced sensitivity to doxorubicin compared to negative-control transfected cell lines. Thus, we determined that multiple mechanisms of gene regulation control suppression of NDRG2 in canine OSA and tumors with reduced NDRG2 may exhibit resistance to one of the most common therapeutic agents used to treat this disease.

In conclusion, the work presented in this dissertation defines a pyramid of investigations into the molecular factors in OSA that contribute to disease progression and chemoresistance. We used broad survey experiments to identify novel factors related to outcome then fine-tuned those findings in order to select genes for in-depth investigation. The initial pursuit of a prognostic factor or factors developed, instead, into more-thoroughly defining the roles of two genes that may contribute to outcome: *IGF2BP1* and *NDRG2*. These two genes likely contribute to metastasis and chemotherapeutic resistance yet are not adequate, by themselves, to serve as prognostic indicators. They do, however, emphasize the likely importance of *MYC*-related genes in the pathogenesis of OSA. *IGF2BP1* has been shown to be upstream of *MYC* in some systems whereas *NDRG2* has been shown to be downstream of it. In this system, we observed altered expression of these genes as well as copy number alterations and dysregulation in *MYC*; these changes were most robustly demonstrated by poor responders. Thus, dysregulation of *MYC* and related genes likely contributes to an aggressive OSA phenotype. This contribution, however, cannot account for all observed cases with short time to metastases or limited response to chemotherapy. Therefore,

more work remains to be done to identify molecular features of OSA that contribute to metastasis and chemotherapeutic resistance.

Future Directions

There are a number of additional studies that could be performed to further investigate the roles of *IGF2BP1* and *NDRG2* in OSA. For instance, mammalian expression vectors containing shRNAs specific to IGF2BP1 have already been generated by our laboratory. Stable transfection of IGF2BP1 expressing cell lines with these knockdown vectors would allow long-term chemosensitivity and proliferation assays as well as other studies of tumor aggressiveness (e.g. colony formation, growth in soft agar) to be performed. Similarly, full length IGF2BP1 coding sequence has been generated for cloning and transfection. Stable overexpression of this gene in low IGF2BP1-expressing cell lines may provide further insights into its role in OSA. Additionally, further investigation of the 3' UTR shortening phenomenon in independent sets of primary tumors may lead to the development of prognostic screens or treatment modalities based around this method of dysregulation. Finally, locked nucleic acid technology provides a means by which to knock down gene expression *in vivo*. As this gene is unexpressed in normal tissues, one could hypothesize that systemic knockdown of IGF2BP1 in cancer patients would have only limited side effects and may prove an effective method of limiting tumor cell invasion and metastasis. Assessment of this methodology in mouse models of OSA may provide an excellent platform for development of a new anti-OSA treatment.

There is much work yet to be done with regards to NDRG2 suppression in OSA. Our findings herein indicate that methylation of *NDRG2* may silence this gene in tumors but further investigation with methylation-specific-PCR or sodium bisulfite sequencing would provide definitive evidence to this effect. Also, it has been suggested that NDRG2 pathways control matrix metalloproteinase expression. It would be interesting to determine if these downstream targets are affected in our stable clones through the use of zymography and subsequent invasion assays. Additionally, the means by which NDRG2 regulates its downstream targets is currently unknown. As we have validated an anti-NDRG2 antibody and generated V5-tagged NDRG2 constructs, immunoprecipitation experiments followed by MALDI-TOF identification of NDRG2-associated targets would provide much needed information regarding its interaction network.

Our broad survey experiments also identified several other gene targets of interest: coiled coil domain containing 3 (*CCDC3*), alcohol dehydrogenase iron containing 1 (*ADHFE1*) and sodium channel, voltage-gated, type I, beta (*SCN1B*) to name a few. Our laboratory has already initiated investigations into two of these targets but as there is only a limited body of knowledge regarding these genes, there is much work yet to be done. Similarly, there is much additional knowledge that can be mined from our large survey datasets. One potential application of this data would be to obtain microarray data that has been performed on human samples and examine the intersections of this data with our canine data. Further elucidation of the shared molecular characteristics between human and canine OSA may identify new gene targets that would otherwise be obscured when examining only one species.

Appendix A

Pathway Maps - GeneGo MetaCore Analysis

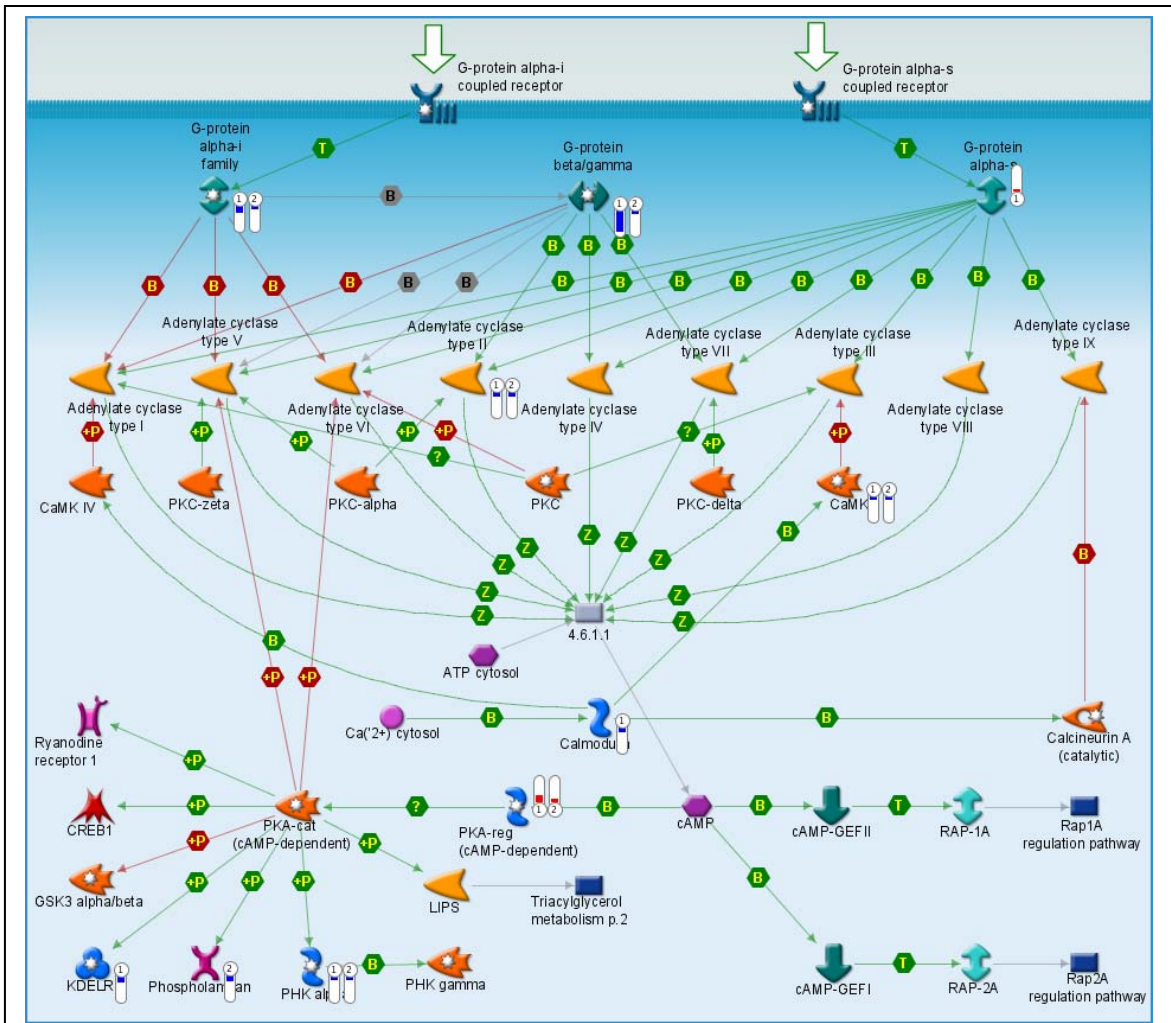


Figure A.1 - Signal transduction - cAMP signaling. Top scored pathway map in the analysis of gene targets common to both PLIER and RMA processing. Red symbols indicate degree of upregulation of gene target in DFI < 100 days relative to DFI > 300 days, blue symbols indicate relative down-regulation. Numbers in symbols indicate specific array processing algorithm, 1 = PLIER, 2 = RMA.

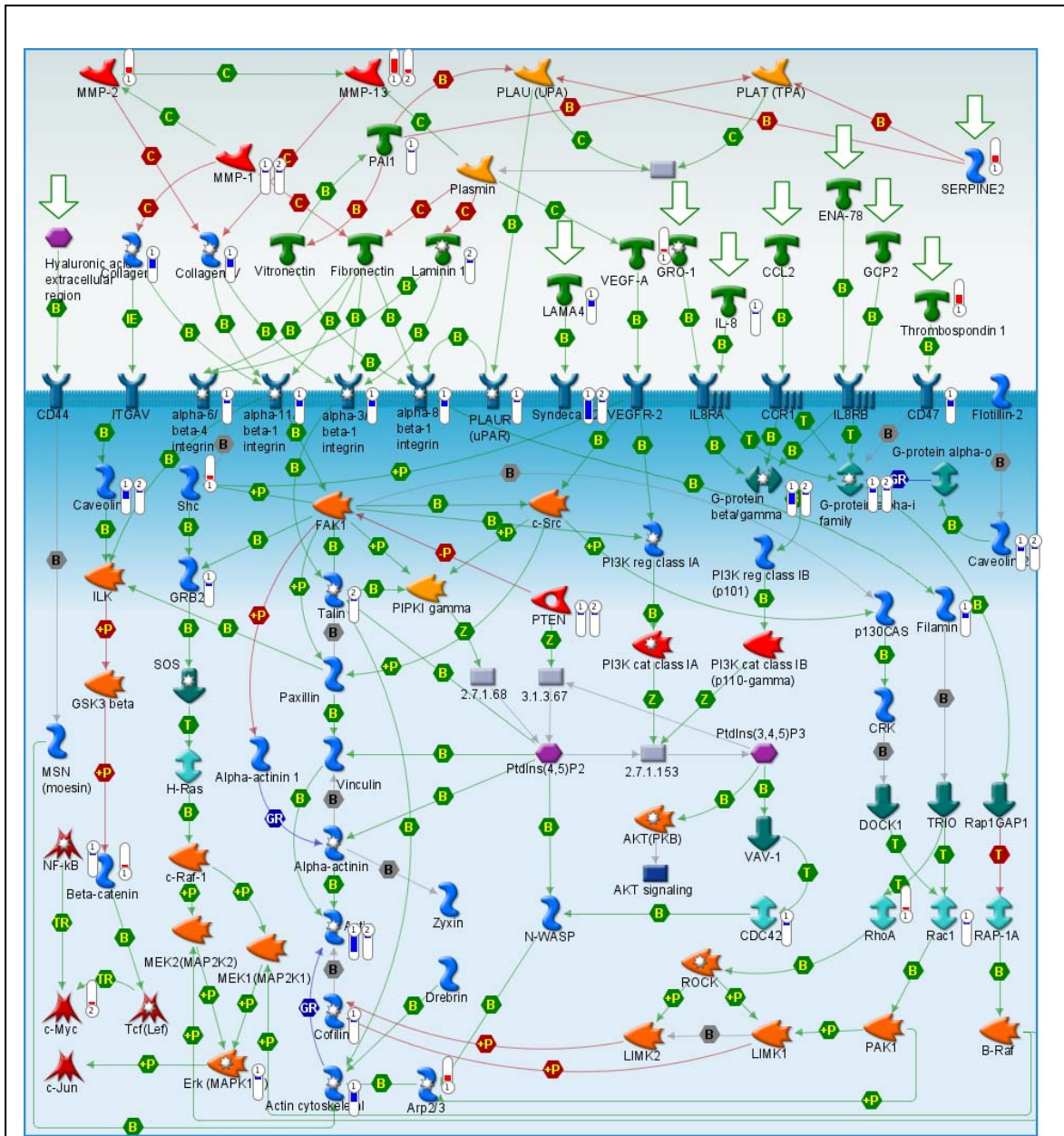


Figure A.2 - Cell Adhesion - Chemokines and Adhesion. Second scored pathway for the analysis of gene targets common to both PLIER and RMA processing. Red symbols indicate degree of upregulation of gene target in DFI < 100 days relative to DFI > 300 days, blue symbols indicate relative down-regulation. Numbers in symbols indicate specific array processing algorithm, 1 = PLIER, 2 = RMA.

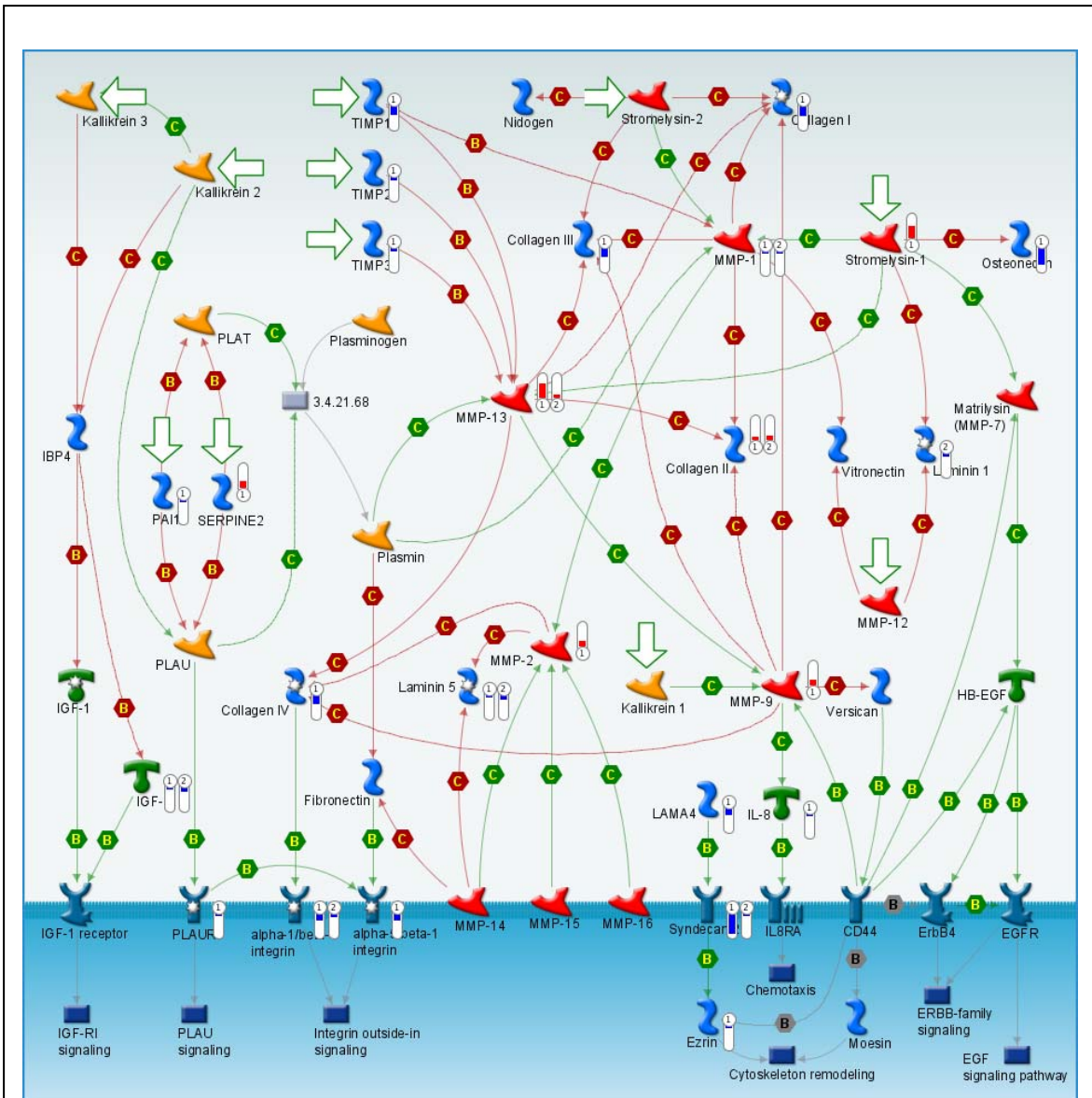


Figure A.3 - Cell adhesion - ECM remodeling. Fifth scored pathway for the analysis of gene targets common to both PLIER and RMA processing. Red symbols indicate degree of upregulation of gene target in DFI < 100 days relative to DFI > 300 days, blue symbols indicate relative down-regulation. Numbers in symbols indicate specific array processing algorithm, 1 = PLIER, 2 = RMA.

Appendix B

Lists of genes obtained from pairwise t-test intersections of three study cohorts: Poor Responder Primary Tumors (DFI<100 days, G1), Good Responder Primary Tumors (DFI>300 days, G2) and Normal Bone (G3). Refer to Chapter 3 for discussion.

Twenty-two genes shared in all three pairwise comparisons (G1 vs. G2, G1 vs. G3, G2 vs. G3)

ADAMTS16
ADPRHL1
ALOX5
C6 /// HEATR7B2
CCDC158
CCDC3
CSRP3
DMGDH
DSCAM
DSCAML1
IGF2BP1
KIF5A
LOC477016
LOC482199 ///
LOC482200
MTSS1L
NDRG2
PGLYRP1
RBP7
RH30
SELL
SULT1B1
TNNC1

Nineteen genes shared between G1 vs. G2 and G1 vs. G3 pairwise comparisons.

ANO9
AVPR1B
CASC3
CLMN
cOR8B15
CXCL14
LOC474658 /// LOC477388 /// LOC478751 ///
LOC480304 /// LOC480973 /// LOC491822 ///
LOC606885 ///
LOC491385
NPY
PACRG
PDZRN4
PRL
RAB11FIP1
RANBP3L
RNASE4
SCN1B
UPF3B
WDR65
WWC1

Fourteen genes shared between G1 vs. G2 and G2 vs. G3 pairwise comparisons.

CCDC7
CDKL1
CDO1
DUSP13
FBP1
FSCN3
GLRB
HMGB4
LOC483943
LOC487825
LOC612877
MC5R
PKP2
SNAP25

2,401 genes shared between G1 vs. G3 and G2 vs. G3 pairwise comparisons.

A2M	ADAMTS14	AMPD1
A2ML1	ADAMTS3	AMPD2
AADACL2	ADAMTS6	AMPD3
AAGAB	ADCY3	ANAPC4
AAMP	ADD1	ANGPTL2
AARS	ADIPOQ	ANK1
AASS	ADIPOR2	ANK3
AATF	ADK	ANKK1
ABCA1	ADNP	ANKLE2
ABCA4	ADORA3	ANKMY2
ABCA6	ADPGK	ANKRA2
ABCA8	ADRB2	ANKRD1
ABCA9	ADSSL1	ANKRD13A
ABCC1	AER61	ANKRD2
ABCD3	AFAP1	ANKRD22
ABCE1	AFG3L2	ANKRD23
ABCF1	AGMAT	ANKRD44
ABCF2	AGPAT2	ANKS1B
ABCG8	AGPAT4	ANO6
ABHD12	AGTRAP	ANP32E
ABHD5	AHCTF1	ANPEP
ABI1	AHI1	ANXA3
ABI3BP	AHNAK	ANXA8
ABLIM1	AHR	ANXA9
ABLIM3	AIDA	AOAH
ABRA	AIF1	AP1G1
ABTB1	AIM1L	AP1S3
ACACA	AK5	AP2B1
ACER2	AKAP11	AP2M1
ACMSD	AKAP9	AP3M1
ACO2	AKR1E2	AP4E1
ACP6	AKT1S1	APLP1
ACPL2	ALAD	APOA1
ACPL2 /// LOC610183	ALAS1	APOBEC2
ACRBP	ALAS2	APOC2
ACSBG2	ALDH18A1	APOC3
ACSL1	ALDH1L1	APOD
ACSL3	ALDH1L2	ARAP2
ACSL5	ALDOC	ARF3
ACSM3	ALG13	ARFGAP2
ACSM4	ALKBH8	ARFGAP3
ACSS1	ALOX12	ARHGAP1
ACTA1 /// ACTB /// LOC489678	ALOX15	ARHGAP15
ACTA2 /// LOC488984	ALOX5AP	ARHGAP25
ACTC1	ALPL	ARHGAP33
ACTN2	ALS2	ARHGAP39
ACTN3	ALX1	ARHGAP9
ACTR2	AMBP	ARHGDIB
ADAM18	AMDHD1	ARHGEF15
ADAM32	AMICA1	ARHGEF6

ARL2BP	BCL3	CACNA2D3
ARL4D	BCR	CACNA2D4
ARL6IP6	BDH1	CACNB4
ARMC6	BEND5	CACNG3
ARMC8	BEND6	CACNG4
ARSE	BEND7	CADM1
ARSJ	BET3L	CADM2
ASAP2	BGN	CADM4
ASB1	BHLHE40	CAFA-T2R10
ASB11	BICC1	CAGE1
ASB12	BICD2	CALU
ASB18	BIN1	CAMK2D
ASB5	BIN2	CAMP
ASCC3	BIRC2	CAP2
ASNS	BIRC5	CAPN2
ASNSD1 /// LOC606866	BLMH	CAPN3
ASPA	BLVRB	CAPN6
ASPH	BMP1	CAPNS1
ASPN	BMPR1A	CAPRIN1
ATAD2	BMX	CARD9
ATF2	BNC2	CARHSP1
ATG13	BNIP3L	CARTPT
ATG16L2	BNIPL	CASC4
ATG4C	BOD1L	CASK
ATG4D	BOLA1	CASP4
ATMIN	BPNT1	CAT
ATP11C	BRD2	CATSPER2
ATP13A5	BSCL2	CATSPERG
ATP1A4	BTD	CAV3
ATP1B3	BTG2	CBLB
ATP2A1	BTK	CBLL1
ATP2A2	BTN2A2	CC2D2A
ATP2C1	BYSL	CCDC108
ATP6AP1	C1QC	CCDC113
ATP7A	C1QTNF2	CCDC114
ATP8A1	C1QTNF3	CCDC115
ATP8B1	C1RL	CCDC21
ATRX	C2CD3 /// LOC609399	CCDC65
ATXN7	C3	CCDC73
AZIN1	C4BPB	CCDC75
B3GALT2	C6	CCDC8
B4GALT1	C7	CCDC83
BACE1	CA1	CCDC87
BAG2	CA2	CCDC88A
BAT2	CA4	CCDC88C
BAZ2B	CA5B	CCDC90A
BCAR1	CA6	CCDC91
BCAT1	CACHD1	CCDC94
BCL11A	CACNA1E	CCDC98
BCL2L14	CACNA1S	CCL14

CCL25	CHD7	COL3A1
CCL28	CHD9	COL4A3
CCNDBP1	CHEK2	COL4A5
CCNI	CHL1	COL5A1
CCNJ	CHMP4B	COL6A1
CCNT2	CHPT1	COL6A3
CCR3	CHRM3	COLEC12
CCRL2	CHRNA4	COPA
CCT5	CHRNA5	COPB1
CD109	CHST10	COPB2
CD164	CHSY1	COR10A3 /// LOC485375 ///
CD177	CIDEA	LOC611322
CD200R1	CIDEC	COR2AG1
CD209	CILP	COR52J7
CD226	CIRBP	COR52N9
CD244	CIRH1A	COR52P2P
CD276	CKMT2	COR6M4
CD2AP	CLCA2	COR8U2 /// OR10G10
CD53	CLDN17	CORO1A
CD5L	CLDND2	CP
CD69	CLEC11A	CPA1
CD79A	CLEC12A	CPA3
CDC40	CLEC1B	CPNE4
CDC42EP1	CLEC2B	CPNE7
CDCA7L	CLEC2D	CPSF2
CDCA8	CLEC5A	CPXM2
CDH9	CLEC9A	CR1
CDIPT	CLIC2	CRABP2
CDK14	CLIC6	CRHR1
CDK16	CLIP3	CRIM1
CDK17	CLIP4	CRIP3
CDK5R2	CLPTM1	CRISP2
CDKN2D	CLPTM1L	CRISP3
CDR2	CMA1	CRNKL1
CDRT4	CMTM5	CROT
CEBPE	CMYA5	CRYM
CEL	CNGA3	CSE1L
CELF2	CNKSR3	CSNK1D
CENPI	CNNM1	CSNK1G1
CEP70	CNNM2	CSNK1G3
CEPT1	CNST	CST7
CES1	CNTNAP5	CSTA
CFB	COG2	CTBS
CFD	COG3	CTNND2
CFH	COL12A1	CTSE
CFI	COL16A1	CTSG
CFP	COL1A1	CUBN
CHAD	COL1A2	CUL1
CHAF1B	COL21A1	CUL2
CHD5	COL24A1	CUL4B
		CXCL12

CXCR7
CYBB
CYP2A13
CYR61
CYTH3
DACH1
DAK
DAP
DAPK1
DAPP1
DARC
DBN1
DBT
DCAKD
DCC
DCLK1
DCUN1D4
DDA1
DDAH1
DDN
DDO
DDX1
DDX31
DDX3X
DDX43
DDX50
DDX6
DECR1
DENND2C
DENND2D
DENND4A
DENND4C
DEPDC5 /// LOC612011
DEPDC7
DERL1
DERL3
DES
DFNB31
DGAT2
DGKG
DGKI
DHRS7C
DHX15
DIO3
DIS3L
DKC1
DLA-12 /// DLA88
DLAT
DLG1
DLK2

DLX4
DMD
DMKN
DMRTA1
DMRTC2
DMTF1
DNAJB1
DNAJC10
DNAJC14
DNAJC16
DNAL1
DNM1L
DNPEP
DNPTT
DOCK11
DOCK2
DOCK8
DOK4
DOK5
DOLPP1
DPAGT1
DPH3
DPH5
DPP10
DPY19L3
DPY19L4
DPYSL3
DRAM1
DSCC1
DSN1
DSPP
DST
DTNA
DUSP10
DUSP26
DUSP27
ECT2
EDN1
EDNRA
EFCAB1
EFCAB6
EFHC2
EFNB1
EFR3A
EGF
EHD4
EHHADH
EHMT2
EIF2A
EIF3B

EIF5
ELANE
ELL
ELMO1
ELMO2
ELOVL2
ELOVL3
ELOVL6
ELP2
EMILIN1
EML1
EMP3
EMR3
ENDOU
ENO3
ENOPH1
ENOX1
ENPEP
ENPP2
ENPP3
ENPP6
EOMES
EPB41
EPB41L1
EPB41L2
EPB41L3
EPB42
EPB49
EPC1
EPCAM
EPHA2
EPHA3
EPHA7
EPHB3
EPHX2
EPO
EPRS
EPS8L3
EPX
ERBB2IP
ERBB4
ERLIN2
ERP27
ERRF1
ESM1
ESRP1
ETV7
EVI2B
EXOC5
EXTL2

EYA3
EZR
F11R
F12
F2RL2
F3
FADS1
FADS1 /// LOC612278
FANK1
FAP
FARP1
FAT1
FAT4
FBLN1
FBLN7
FBP2
FBXL5
FBXO21
FBXO32
FBXO9
FBXW5
FCER1A
FCER1G
FCGR1A
FCN1
FCRLA
FDXR
FECH
FER
FERMT3
FFAR2
FGF14
FGFR1
FGFR2
FGFR2IIIC
FGFR3
FGL1
FGL2
FGR
FHAD1
FHIT
FHL1
FHOD3
FIP1L1
FITM1
FKBP10
FKBP14
FKBP4
FKBP7
FKBP8

FLNA
FLNB
FLNC
FLOT1
FLOT2
FLRT2
FLT3
FMN1
FMNL1
FMNL2
FMNL3
FMO2
FN1
FN3K
FNBP1
FNBP1L
FNDC3B
FOSL2
FOXJ3
FOXK2
FOXR1
FPR2
FRMD3
FRMD6
FRMD7
FRRS1
FRS2
FRY
FSCN1
FSIP1
FST
FSTL1
FSTL5
FTSJ1
FUT5
FXVD2
FYB
FYCO1
FYN
FZD2
FZD6
GAB1
GABRB2
GABRG2
GAD1
GADD45G
GAL3ST4
GALNTL2
GALR1
GAN

GARS
GATA1
GATAD2A
GATM
GBA
GCA
GCH1
GDI1
GDPD2
GF11
GFM1
GFPT1
GGA2
GGT1
GHR
GIGYF1
GIGYF2
GIMAP8
GIP
GJA1
GJB2
GLB1
GLCE
GLG1
GLOD5
GLS
GLT25D1
GMFG
GNA13
GNB4
GNB5
GNL2
GNMT
GNPDA1
GNPTAB
GOLGA2
GOLGA5
GOLT1B
GORASP2
GP1BA
GP6
GP9
GPAT2
GPC2
GPC4
GPD1
GPHA2
GPM6A
GPR110
GPR111

GPR116	HHAT	ICA1L
GPR120	HHATL	ICAM4
GPR125	HIBCH	ICK
GPR141	HIF1A	IFI44
GPR146	HIP1R	IFITM2
GPR152	HIPK2	IFNAR1
GPR171	HK3	IFRD1
GPR176	HMBS	IGF1R
GPR18	HMGCR	IGFBP2
GPR37L1	HMOX1	IGSF10
GPR65	HN1L	IL13RA2
GPR98	HNF1B	IL16
GPSM2	HNRNPA1L2 /// LOC477645	IL17RB
GPSM3	/// LOC607099 /// LOC607135	IL17RD
GPX5	/// LOC607332 /// LOC607650	IL18R1
GRAMD3	/// LOC608035 ///	IL18RAP
GRAP2	HNRNPH2	IL1R2
GRB7	HNRNPR	IL1RAP
GRIA4	HOMER2	IL7R
GRIK3	HORMAD1	IMPA1
GRINA	HOXA1	IMPDH1
GRN	HOXB5	INADL
GRWD1	HOXB7	ING3
GTF2E1	HOXD10	INMT
GTF2I	HP	INPP5F
GTPBP2	HPCAL1	INTS10
GTPBP5	HPGD	INTS2
GXYLT2	HRASLS	INTS6
GYPE	HRC	INTS7
GYS2	HRH2	IPO11
GZF1	HS6ST3	IPO5
GZMK	HSD11B1	IPO8
HAND2	HSD17B7	IPPK
HAUS5	HSD17B8	IQCE
HBD	HSD3B7	IQGAP2
HBD /// LOC609402	HSP70	IRF2
HBE1	HSPA1L	ISG20L2
HBG1	HSPA4L	ISM1
HCFC1	HSPA9	ITCH
HCFC2	HSPB3	ITGA10
HCRTR1	HSPB7	ITGA2B
HDLBP	HSPD1 /// LOC608756	ITGA5
HEATR3	HSPH1	ITGAD
HEATR5A	HTR1D	ITGAV
HECTD3	HTR2A	ITGB2
HEMGN	HTRA1	ITGB5
HEPACAM	HUWE1	ITGB7
HES5	HYAL3	ITIH3
HEY1	HYAL4	ITIH5
HFE2	IARS	ITPKC
	IBTK	

ITSN2	LAMC1	LOC474923
IVNS1ABP	LANCL1	LOC474943
JAG1	LARP1	LOC475048
JAK1	LASP1	LOC475066
JAM3	LATS1	LOC475113
JAZF1	LATS2	LOC475166
JUB	LCA5	LOC475225
K-RAS	LCN2	LOC475236
KALRN	LCP1	LOC475259
KANK3	LDOC1	LOC475269
KBTBD10	LEP	LOC475290
KCNA3	LEPRE1	LOC475563
KCNC4	LEPREL1	LOC475605
KCNH8	LGALS3BP	LOC475615
KCNJ13	LGALS9	LOC475754
KCNJ4	LGI1	LOC475754 /// LOC611906
KCNT1	LGR4	LOC475790
KCTD10	LHB	LOC475815 /// LOC608055
KDELR1	LHX2	LOC475881
KDELR2	LHX8	LOC475935
KDELR3	LIFR	LOC475935 /// LOC475936 ///
KEL	LIM2	LOC483396
KIDINS220	LIMA1	LOC475985
KIF13B	LIMD2	LOC476006
KIF16B	LIMK1	LOC476049
KIF18A	LIN37	LOC476149
KIF1A	LIN54	LOC476233
KIF3C	LIN7C	LOC476320
KIF5B	LLGL1	LOC476397
KIT	LMAN1	LOC476778
KLC3	LMBR1L	LOC477053
KLF10	LMLN	LOC477652
KLHL11	LMNB1	LOC477671
KLK11	LMO2	LOC477720
KLK4	LMO3	LOC477770 /// PECR
KLK7	LMOD3	LOC477831
KLKB1	LOC100049001 /// LOC490080	LOC477837
KLRD1	LOC403447	LOC477867
KMO	LOC474456	LOC477943
KRT18	LOC474524	LOC477964
KRT18 /// LOC486139	LOC474570	LOC478015
KRT24	LOC474642	LOC478059
KRT31	LOC474671	LOC478234
KRT72	LOC474744 /// LOC478576 ///	LOC478277
KY	LOC480791 /// LOC488981 ///	LOC478287
L2HGDH	LOC611805 /// RPS15A	LOC478326
LACTB	LOC474768	LOC478419
LALBA	LOC474790	LOC478449
LAMA4	LOC474791 /// NIPSNAP3A	LOC478524
LAMB1	LOC474811	LOC478556
	LOC474869	LOC478557

LOC478559	LOC481747	LOC606941 /// LOC606953 ///
LOC478802	LOC481825	LOC607152 /// LOC612050 ///
LOC478827	LOC481879	LOC612054 ///
LOC478850	LOC481962	LOC486386 /// LOC491454 ///
LOC478866	LOC482035	LOC606953 /// LOC612050 ///
LOC478959	LOC482172	LOC612054 /// LOC612081 ///
LOC478991	LOC482200	LOC612104 ///
LOC479096	LOC482470	LOC486389
LOC479114	LOC482503	LOC486389 /// LOC491454 ///
LOC479209	LOC482687	LOC606941 /// LOC606953 ///
LOC479261	LOC482844	LOC612050 /// LOC612054 ///
LOC479268	LOC482849	LOC612081 ///
LOC479419	LOC482907	LOC486392
LOC479430	LOC482914	LOC486392 /// LOC491362 ///
LOC479458	LOC482987	LOC491364 /// LOC491454 ///
LOC479693	LOC483142	LOC491494 /// LOC606953 ///
LOC479707	LOC483173	LOC607125 ///
LOC479780	LOC483398	LOC486392 /// LOC491364 ///
LOC479825	LOC483474	LOC491494 /// LOC607125 ///
LOC479837	LOC483480	LOC607213 /// LOC612135
LOC479917	LOC483501	LOC486393
LOC479920	LOC483559	LOC486394 /// LOC491405
LOC479927	LOC483676	LOC486394 /// LOC607364 ///
LOC479983	LOC483842	LOC607394 /// LOC607415 ///
LOC479987	LOC483843	LOC607424 /// LOC607441 ///
LOC480010	LOC483869	LOC607465 ///
LOC480053	LOC484082	LOC486404
LOC480156	LOC484187	LOC486414
LOC480336	LOC484249	LOC486459
LOC480437	LOC484338	LOC486474 /// LOC607364 ///
LOC480441	LOC484356	LOC607541 /// LOC607551 ///
LOC480469	LOC484362	LOC607558 /// LOC607582 /// VPREB1
LOC480469 /// LOC608024 /// LOC607213 /// LOC611705	LOC484560	LOC486484
LOC480487	LOC484560	LOC486528
LOC480550	LOC484866	LOC486632 /// LOC491723 ///
LOC480602	LOC484877	LOC608476
LOC480665	LOC484994	LOC486736
LOC480692	LOC485302	LOC487557
LOC480699	LOC485316	LOC487601
LOC480760 /// LOC483173 ///	LOC485372	LOC487697
LOC488267 /// LOC488279 ///	LOC485645 /// TMEM106B	LOC487888
LOC488290 /// LOC488303 ///	LOC485973	LOC488130
LOC488309 ///	LOC486214	LOC488247
LOC480784	LOC486374 /// LOC486377 ///	LOC488248
LOC480804	LOC486386 /// LOC486387 ///	LOC488359
LOC480885	LOC486389 /// LOC491362 /// LOC491364 ///	LOC488474
LOC481273	LOC486380	LOC488486
LOC481446	LOC486381	LOC488621
LOC481569	LOC486382	LOC488709
LOC481704 /// LOC488909 ///	LOC486384	LOC488882
LOC608835	LOC486386 /// LOC491454 ///	LOC488984
		LOC489024
		LOC489167

LOC489353	LOC606953 /// LOC612054	LOC609308
LOC489446	LOC607010	LOC609334
LOC489575	LOC607013 /// LOC609925	LOC609433
LOC489616	LOC607020 /// LOC612115	LOC609447
LOC489680	LOC607055	LOC609455
LOC489992	LOC607079	LOC609534
LOC490143	LOC607125	LOC609573
LOC490390	LOC607137	LOC609577
LOC490399	LOC607153	LOC609582
LOC490653	LOC607179	LOC609596
LOC490669	LOC607188	LOC609646
LOC490674 /// PKM2	LOC607200	LOC609688
LOC490782	LOC607202	LOC609690
LOC490888 /// LOC606869 ///	LOC607236	LOC609701
LOC606943	LOC607239	LOC609737
LOC490891 /// LOC606916 ///	LOC607255	LOC609741
LOC606943 /// LOC607028 ///	LOC607113 /// LOC607188	LOC609826
LOC491035	LOC607279	LOC609861
LOC491203	LOC607343	LOC609897
LOC491240	LOC607368	LOC610071
LOC491298	LOC607380	LOC610188
LOC491391 /// LOC491492 ///	LOC607395	LOC610299
LOC491686 /// LOC607996 ///	LOC607460	LOC610324
LOC608202 /// LOC608379 ///	LOC607558 /// LOC607582	LOC610339
LOC609845 ///	LOC607662	LOC610447
LOC491427 /// WNK1	LOC607731	LOC610577
LOC491454	LOC607775	LOC610618
LOC491454 /// LOC606941 ///	LOC607812	LOC610658
LOC606953 /// LOC607152 ///	LOC607964	LOC610749 /// ST3GAL3
LOC612050 /// LOC612054 ///	LOC608007	LOC610769
LOC612081 ///	LOC608031	LOC610927
LOC491492	LOC608051	LOC610994
LOC491494 /// LOC607125	LOC608313	LOC611062 /// RBMX
LOC491504	LOC608387	LOC611076
LOC491506	LOC608388 /// LOC610188 ///	LOC611079
LOC491596	LOC611971 /// LOC612667 ///	LOC611134
LOC491696	PSMA1	LOC611270
LOC491813 /// LOC609154 ///	LOC608434	LOC611361
LOC610238 /// LOC611215 ///	LOC608476	LOC611428
LOC612844	LOC608537	LOC611455
LOC491868	LOC608636	LOC611514 /// NME4
LOC492155	LOC608656	LOC611542
LOC492181	LOC608702	LOC611558
LOC492199	LOC608848	LOC611583
LOC606810	LOC608881	LOC611624
LOC606842	LOC608883	LOC611632
LOC606845	LOC608999	LOC611634
LOC606893	LOC609034	LOC611694
LOC606928	LOC609038	LOC611707
LOC606941 /// LOC606953 ///	LOC609251	LOC611708
LOC607152 /// LOC612050 ///	LOC612054 /// LOC612081 ///	
LOC606943	LOC609254	
	LOC609277	

LOC611771	LYSMD3	MEN1
LOC611775	LYST	MEPE
LOC611796	LYZ	MEST
LOC611867	LYZL1	METTLL14
LOC611874	MAD1L1	MFAP2
LOC611906	MAEA	MFAP3
LOC611912	MAGEB10	MFGE8
LOC612050	MAGED1	MFN1
LOC612055	MAGED2	MFSD1
LOC612065	MAGEE2	MFSD11
LOC612086 /// LOC612131	MAGI3	MGAM
LOC612135	MAGT1	MGAT1
LOC612322	MAL	MGLL
LOC612347	MAMDC2	MGST1
LOC612347 /// LOC613010	MAN2B1	MIA3
LOC612366	MAOB	MICAL2
LOC612394	MAP1B	MID1
LOC612513	MAP2	MIOX
LOC612534	MAP2K4	MIS12
LOC612640	MAP3K4	MKNK2
LOC612982	MAP3K5	MKRN2
LOX	MAP3K8	MLF2
LOXL2	MAP4K2	MLLT3
LOXL4	MAP4K5	MLXIPL
LPAR1	MAP7	MMD
LPAR3	MAPK1	MME
LPAR5	MAPK12	MMGT1
LRCH2	MAPK8	MMP16
LRG1	MAPRE1	MMP2
LRGUK		MMP27
LRMP	MARK4	MMP3
LRP10	MARVELD3	MMP8
LRP12	MAT1A	MMRN1
LRPPRC	MATN3	MOGAT1
LRRC1	MB	MOGAT2
LRRC3	MBNL2	MORF4L2
LRRC39	MBOAT2	MOSC1
LRRC49	MBP	MPO
LRRC58	MBTD1	MPP6
LRRC8B	MCF2L2	MPPED2
LRRC8D	MCM2	MPRIP
LTB	MCM4	MRAP2
LTF	MCTP1	MRPS10
LY6G6F	MDGA1	MRPS28
LY75	MDGA2	MS4A1
LY86	MEAF6	MS4A2
LYG1	MED12	MSRA
LYPD1	MED16	MST4
LYPLA1	MEF2A	MSX2
LYSMD1	MEGF9	MTRF1

MTHFD1	NAPB	NPHS2
MTHFD2	NAPSA	NPR3
MTMR15	NARFL	NPY1R
MTMR6	NARS	NQO1
MTRR	NAV3	NR0B2
MUC16	NBEAL1	NR1D2
MUC2	NCAPG	NR1H4
MUC4	NCF1	NR2C1
MUDENG	NCF2	NRAP
MUL1	NCF4	NRAS
MUT	NCKAP1	NRG1
MXD1	NCS1	NRP1
MXRA5	NCSTN	NRXN1
MXRA8	NDE1	NSD1
MYADM	NDUFA4L2	NT5C1A
MYBPC1	NDUFS1	NT5C3
MYBPC2	NEBL	NT5DC1
MYEF2	NEDD1	NTN3
MYF6	NEFH	NTRK2
MYH1	NEIL1	NTSR2
MYH11	NEIL2	NUAK1
MYH2	NEK4	NUCB1
MYH3	NEK9	NUDC
MYH7	NELL1	NUS1
MYH7B	NES	NXPH2
MYL1	NETO2	NXT2
MYL10	NEXN	OAF
MYL2	NF1	OAS2
MYL3	NFE2	OCIAD1
MYL6B	NFIA	OCRL
MYLK2	NFIL3	ODF1
MYLPF	NFYA	ODZ2
MYO10	NHLH1	ODZ3
MYO15A	NINL	OGN
MYO18B	NIP7	OLFML3
MYO1B	NIPAL2	OLR1
MYO1E	NIPSNAP3A	OPA1
MYO3A	NKD1	OR12C09
MYO5A	NKG7	ORC2L
MYO9A	NKX3-2	ORC3L
MYOC	NLRP10	ORMDL1
MYOM1	NMD3	OSBPL9
MYOT	NME2	OTOR
MYOZ1	NMNAT3	OVCH1
MYPN	NNAT	P4HA1
MYSM1	NNT	P4HA2
NAA10	NOC4L	P4HA3
NACC1	NOP2	P4HB
NALCN	NOSTRIN	PADI1
NAPA	NOTUM	PADI2

PADI4	PLA2G16	PPL
PAF1	PLAC8	PPP1CB
PAG1	PLAU	PPP1R15A
PAICS	PLAUR	PPP1R3B
PALLD	PLBD1	PPP2R5C
PALM2	PLCD3	PPP4R1
PALMD	PLEC	PPP4R4
PAPOLA	PLEKHA1	PPP5C
PARD6G	PLEKHA6	PPPDE1
PARP12	PLEKHG2	PRAF2
PARP4	PLIN1	PRAM1
PARP8	PLIN5	PRC1
PARVA	PLK1S1	PRCC
PAX8	PLK3	PREPL
PBRM1	PLN	PRICKLE1
PCNX	PLOD1	PRICKLE2
PCSK7	PLOD2	PRKAA1
PCTP	PLOD3	PRKAB1
PCYOX1	PLS3	PRKAR2B
PCYOX1L	PLSCR1	PRKCB
PDE4D	PLSCR3	PRKCD
PDE4DIP	PLVAP	PRKCE
PDE8A	PLXNB2	PRKCQ
PDGFRA	PLXND1	PRKCSH
PDIA6	PM20D1	PRKCZ
PDK4	PMEPA1	PRKD1
PDLIM4	PMPCA	PRKG2
PDLIM5	PMS1	PRMT3
PDP1	PNMAL1	PRMT5
PDS5B	PNOC	PRPF4B
PFKFB1	PNPLA2	PRPF6
PFKFB3	POGK	PRPS1
PGAM2	POLA1	PRPS2
PGM3	POLK	PRR11
PGR	POLR1A	PRR15
PHEX	POLR2B	PRRC1
PHKG1	POMGNT1	PRSS45 /// PRSS50
PHLDB3	POMT2	PRSS48
PHTF2	POSTN	PRSSL1
PHYH	POT1	PSAT1
PICALM	POU4F3	PSMA8
PIGT	PPARG	PSMB8
PIGV	PPARGC1A	PSMC1
PIP	PPAT	PSMD2
PIP5K1A	PPBP	PTCD3
PIP5KL1	PPEF2	PTGDR
PITPNB	PPFIA2	PTGER3
PJA2	PPFIBP1	PTGER4
PKIA	PPHLN1	PTGIS
PKLR	PPIP5K1	PTGS1

PTGS2	RBM12	RRAS2
PTK7	RBM28	RRM2B
PTMS	RBM39	RTF1
PTN	RBM45	RUNX1
PTP4A3	RBM9	RUNX2
PTPLAD2	RBPMS	RUVBL2
PTPN14	RCAN3	RYK
PTPN2	RCN3	S100A5
PTPN21	RCSD1	S100A8
PTPN6	RDH11	S100A9
PTPRB /// PTPRR	RDH16	S100B
PTPRCAP	REEP3	S100P
PTPRN	REL	SACS
PTPRS	RERG	SAMD11
PTPRT	REST	SAMSN1
PUS10	RETN	SAR1A
PYCARD	RFC1	SAT2
PYCR1	RFESD	SBNO1
PYGL	RGS1	SCAF1
PYGM	RGS14	SCAMP3
PYGO1	RGS16	SCAND3
QSER1	RGS18	SCGB1A1
QTRTD1	RGS7BP	SCN8A
RAB10	RHAG	SCOC
RAB23	RHBDL2	SCUBE2
RAB25	RIN1	SDCBP
RAB27B	RIPK4	SDK2
RAB40AL	RIPPLY2	SEC16A
RAB5A	RND3	SEC23A
RABGAP1L	RNF10	SEC23B
RABIF	RNF112	SEC24B
RABL5	RNF2	SEC24D
RAC1	RNF6	SEC61A2
RAC2	RNPS1	SELENBP1
RAD23A	ROBO1	SELI
RAI14	ROBO2	SELP
RAI16	ROD1	SEMA6D
RARRES2	ROGDI	SEPP1
RARS	RORA	
RASAL3	RPA1	SEPX1
RASD2	RPF1	SERAC1
RASEF	RPGRIP1L	SERINC1
RASGRP2	RPL3L	SERPINA4
RAVER2	RPL7L1	SERPINB1
RAX2	RPN2	SERPINB10
RB1	RPRD1B	SERPINB4
RBAK	RPS6KA3	SERPINB5
RBBP8	RPS6KA5	SERPINC1
RBEL1	RPS6KC1	SERPINE1
RBL2	RPUSD1	SERPINI1

SERPINI2	SLC22A4	SMG1
SERTAD4	SLC25A16	SMO
SESN1	SLC25A2	SMPX
SESTD1	SLC25A25	SMTN
SF3B3	SLC25A32	SMTNL2
SF3B4	SLC25A37	SMYD1
SF4	SLC26A2	SNCAIP
SFRP2	SLC26A8	SNCG
SFRS13B	SLC27A2	SND1
SFRS18	SLC27A6	SNRPF
SFXN1	SLC2A1	SNX13
SFXN3	SLC30A4	SNX29
SGCB	SLC30A6	SNX4
SGCD	SLC35A5	SOBP
SGK3	SLC35B2	SOCS5
SGPL1	SLC35F1	SON
SGTA	SLC35F2	SORL1
SGTB	SLC35F5	SOX12
SH3GL2	SLC37A1	SOX2
SH3PXD2B	SLC38A2	SOX5
SHANK2	SLC39A14	SOX6
SHC1	SLC39A9	SOX9
SHH	SLC43A1	SP100
SHISA5	SLC43A2	SPAG11
SHMT2	SLC46A3	SPAG6
SHOX2	SLC4A1	SPARCL1
SHPK	SLC4A2	SPATA18
SHQ1	SLC4A7	SPATA20
SIGMAR1	SLC5A3	SPEF2
SIK3	SLC5A6	SPIC
SIN3A	SLC6A17	SPIN1
SIRT7	SLC6A8	SPINK4
SIX1	SLC7A11	SPOCK2
SIX3	SLC7A6	SPP2
SKAP1	SLC8A3	SPRY2
SKP2	SLC9A5	SPSB1
SLA	SLC9A6	SPTA1
SLC12A1	SLFN14	SPTB
SLC13A5	SLIT3	SPTBN1
SLC14A1	SLITRK2	SPTLC1
SLC15A4	SLITRK6	SQLE
SLC16A1	SLK	SQRDL
SLC17A5	SLPI	SRCAP
SLC17A7	SLURP1	SREBF2
SLC17A8	SMAD1	SRGN
SLC19A2	SMAD5	SRPR
SLC22A1	SMAD9	SRPRB
SLC22A16	SMARCC1	SS18
SLC22A17	SMARCE1	SSH2
SLC22A3	SMEK2	SSPO

SSR1	TBC1D12	TMC6
SSTR1	TBC1D4	TMEM109
ST6GALNAC1	TBC1D8	TMEM129
ST6GALNAC5	TBC1D8B	TMEM168
STAC3	TBCCD1	TMEM169
STAP1	TBL2	TMEM178
STARD7	TBX18	TMEM182
STAT1	TBX19	TMEM19
STAT4	TCEAL3	TMEM194B
STAU1	TCF7	TMEM195
STBD1	TCN1	TMEM20
STCH	TCP1	TMEM209
STEAP2	TCTE1	TMEM33
STIP1	TEAD2	TMEM39A
STK17A	TECPR1	TMEM43
STK3	TEKT2	TMEM45A
STK32B	TEKT4	TMEM49
STK35	TES	TMEM52
STK39	TESC	TMEM56
STOM	TF	TMEM67
STOML3	TFAP2A	TMEM68
STRA6	TFAP2B	TMLHE
STRADA	TFAP2C	TMOD1
STRADB	TFDP2	TMOD3
STT3A	TFF1	TMOD4
STT3B	TFF2	TMTC3
STX16	TFG	TMX1
STX1B	TFPI	TMX2
STX7	TFPI2	TNFAIP1
STXBP2	TGFB111	TNFAIP2
STYK1	TGFB3	TNFAIP8
SUCNR1	TGFBR1	TNFAIP8L3
SUN1	TGIF2LX	TNFRSF14
SUN5	TGM2	TNFRSF19
SUSD1	THBS4	TNFSF11
SUSD3	THOX2	TNFSF12-TNFSF13
SVEP1	THY1	TNFSF18
SVIP	TIAM2	TNN
SYDE1	TIMD4	TNNC2
SYT3	TKTL1	TNNI2
TAAR5	TLE1	TNNT1
TADA1	TLK1	TNNT3
TAF6	TLN1	TOR1AIP1
TAF9B	TLR4	TOR1B
TAGLN3	TM6SF1	TOX4
TAOK3	TM9SF1	TP53BP1
TAP2	TM9SF2	TPBG
TARS	TM9SF3	TPCR71
TAT	TM9SF4	TPM3
TATDN2	TMBIM4	TPPP3

TPX2	TULP4	VPREB1
TRAF3IP3	TUSC5	VPS13A
TRAFD1	TWF1	VPS52
TRAM1	TYK2	VSTM1
TRAM2	TYR	VSTM2B
TRAPPC9	TYRO3	VTN
TRDN	TYW1	VWA1
TREM1	UBA1	VWA2
TREML1	UBA6	WARS
TRIM10	UBAP2	WASF3
TRIM17	UBASH3A	WBP2
TRIM23	UBP1	WBP4
TRIM28	UBQLN2	WDFY2
TRIM4	UBR2	WDR11
TRIM54	UBR5	WDR35
TRIM58	UBXN2A	WDR45L
TRIM63	UBXN7	WDR46
TRIM65	UCHL1	WDR49
TRIP12	UCN3	WFDC2
TRIP13	UCP2	WISP1
TRPC4	UCP3	WNT11
TRPC4AP	UGDH	WNT5B
TRPM7	UHRF1BP1L	WRB
TRPS1	UNC45B	WWP1
TSGA14	UNC93A	WWTR1
TSHB	UPF1	XDH
TSHZ2	USO1	XIRP2
TSNAX	USP10	XPNPEP1
TSPAN2	USP11	XPO7
TSPAN32	USP18	XYLT2
TSPAN33	USP20	YARS
TSPAN5	USP24	YBX2
TSPAN8	USP25	YES1
TSPO2	USP30	YIF1B
TSTD1	USP33	YIPF3
TTC18	USP37	YIPF5
TTC23	USP44	YIPF7
TTC23L	USP5	YTHDF3
TTC29	USP6NL	ZBED4
TTC3	USPL1	ZBTB16
TTC4	UST	ZBTB2
TTLL12	UTRN	ZBTB8A
TTN	VARS2	ZC3H13
TUBA3E	VASH2	ZCCHC12
TUBA4A	VAT1L	ZCCHC16
TUBA8	VCAM1	ZDHHC14
TUBB	VCAN	ZDHHC2
TUBB3	VEGFA	ZFAND2A
TUBGCP2	VIL1	ZFP106
TUFT1	VNN1	ZFP36L1

ZG16B
ZMAT1
ZMYM1
ZMYM2
ZMYND17
ZNF157
ZNF181
ZNF207
ZNF208
ZNF25
ZNF277
ZNF280C
ZNF300
ZNF322A
ZNF367
ZNF385D
ZNF429
ZNF449
ZNF474
ZNF536
ZNF564
ZNF569
ZNF655
ZNF688
ZNF706
ZNF726
ZNF791
ZNF804B
ZNF836
ZNHIT6
ZRANB3
ZSWIM6
ZUFSP
ZYG11A
ZZZ3

Appendix C

Chrosomal Expression Maps: Array Comparative Genomic Hybridization versus Microarrays for Tumor and Normal Bone

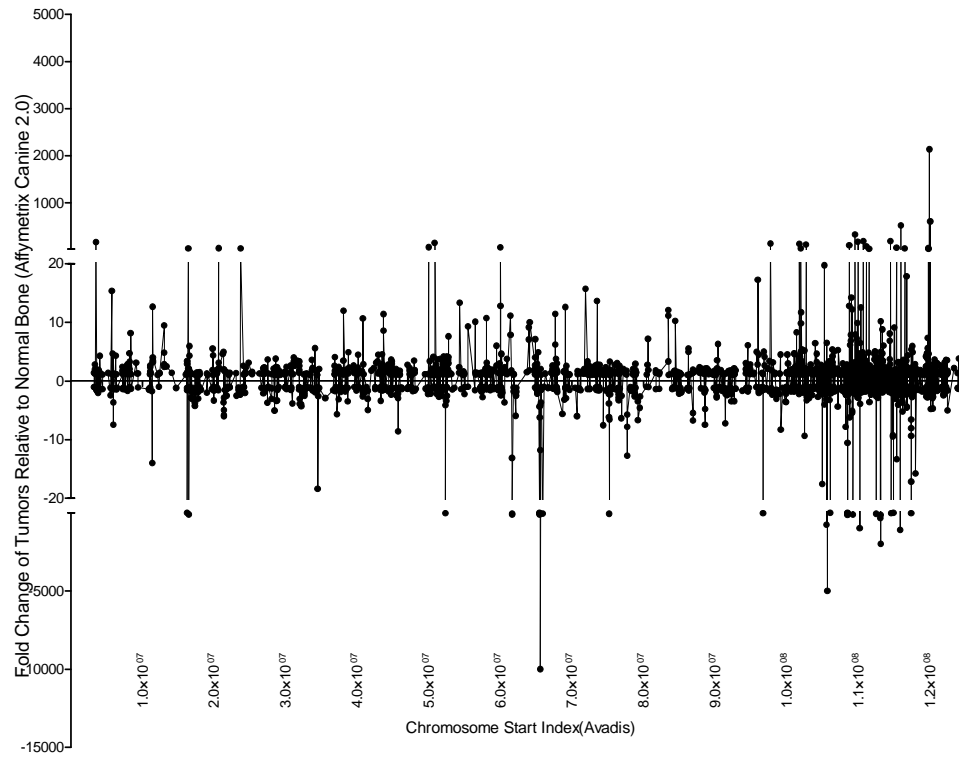
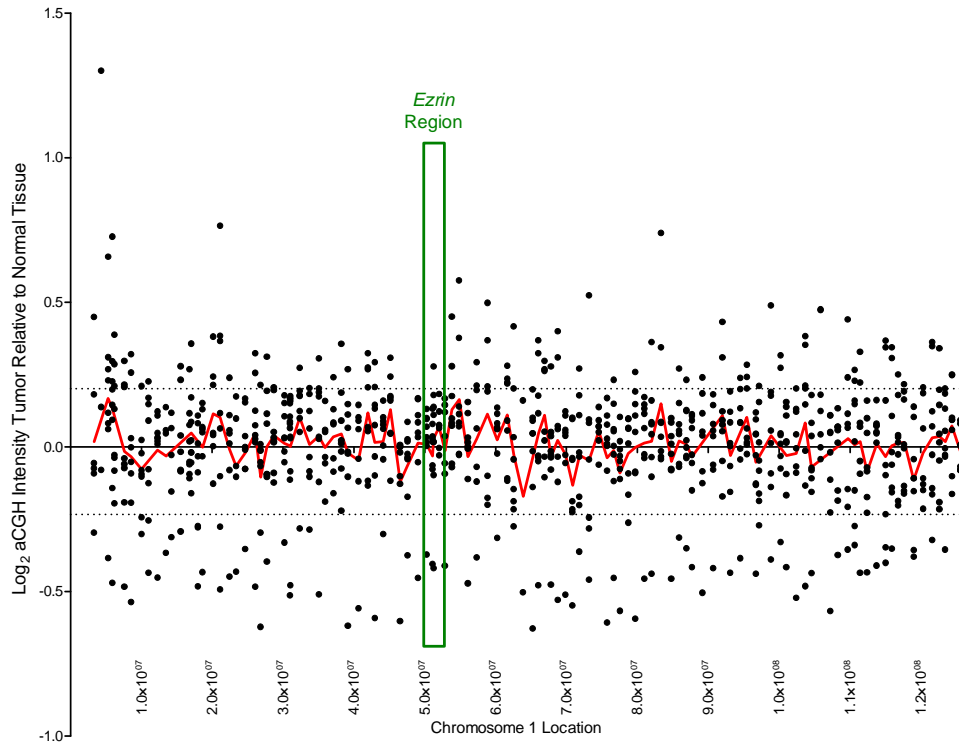
X-axes = chromosomal location of probe

Y-axis (aCGH, top half of page) = hybridization intensity tumor (n=8) relative to normal tissue (n=8). Thresholds for amplification and deletion are represented by dashed lines intersecting the Y axis at 0.201 and -0.234 respectively. Each sample is represented by a point at each probe. Mean intensities are represented by the continuous red line.

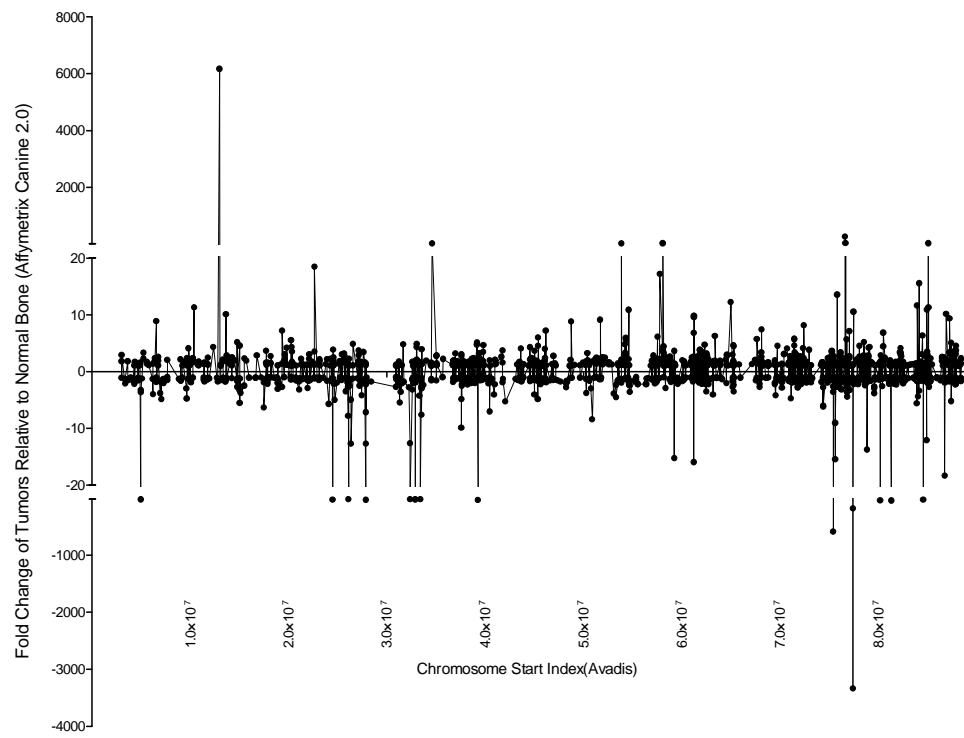
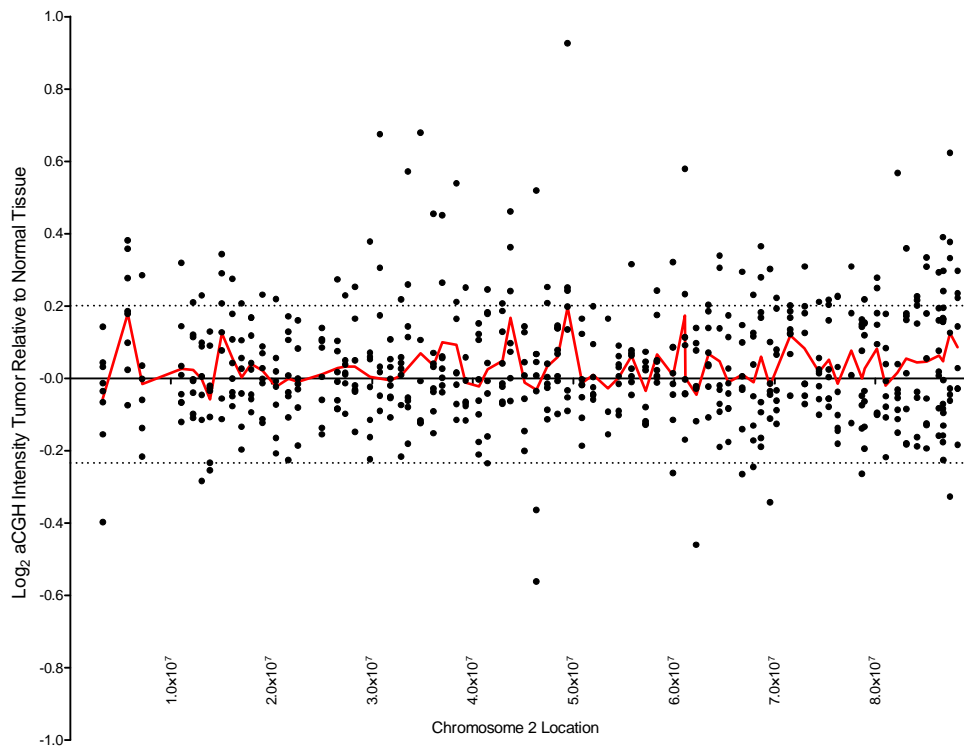
Y-axis (Affymetrix, bottom half of page) = fold change tumors (n=15) relative to normal bone (n=8).

Some locus regions of interest outlined in the text are indicated on figures with boxes and gene name labels.

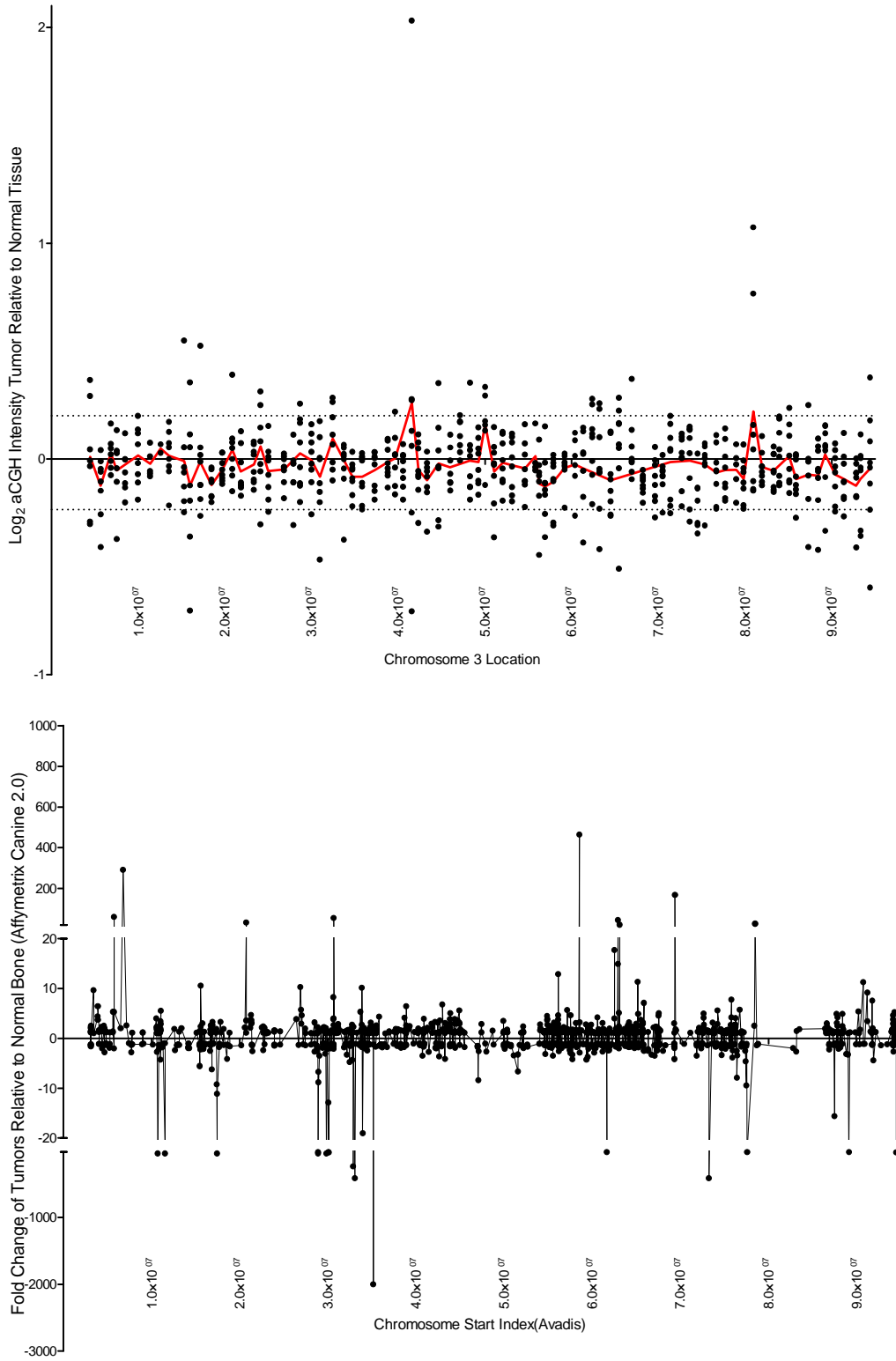
Chromosome 1



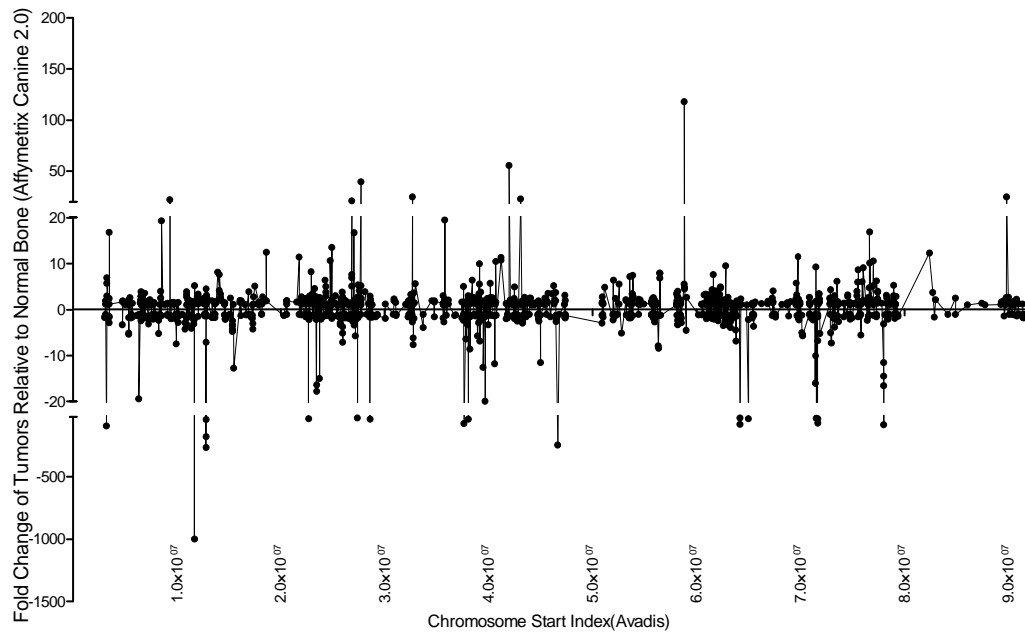
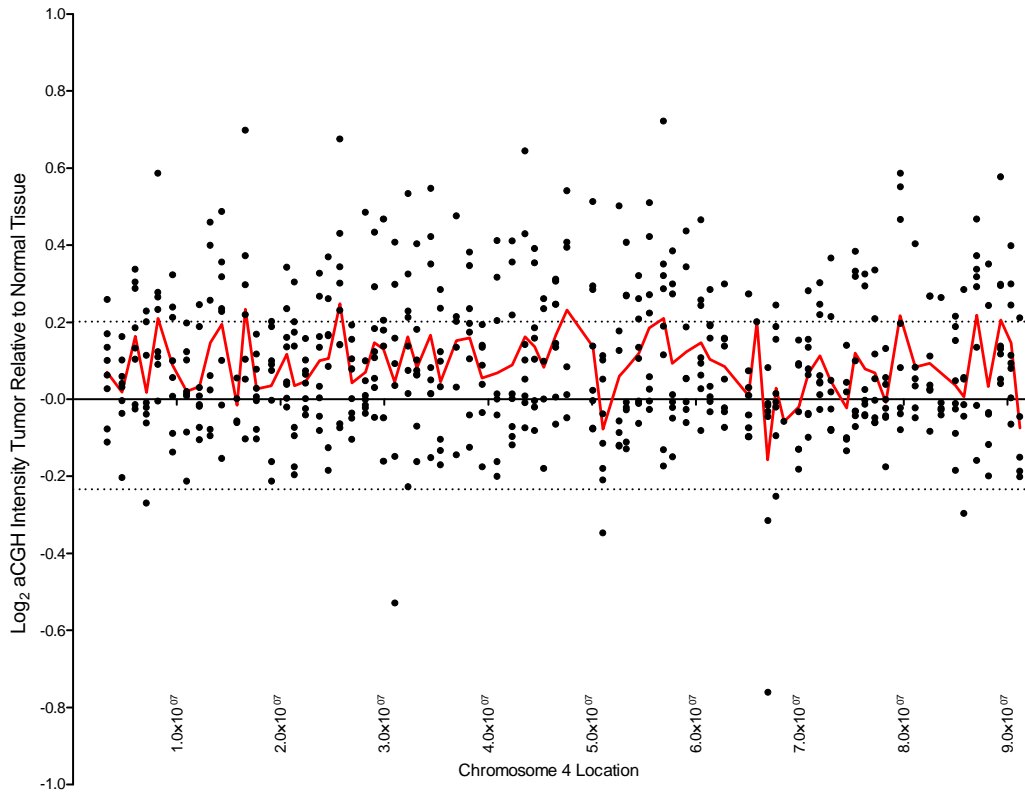
Chromosome 2



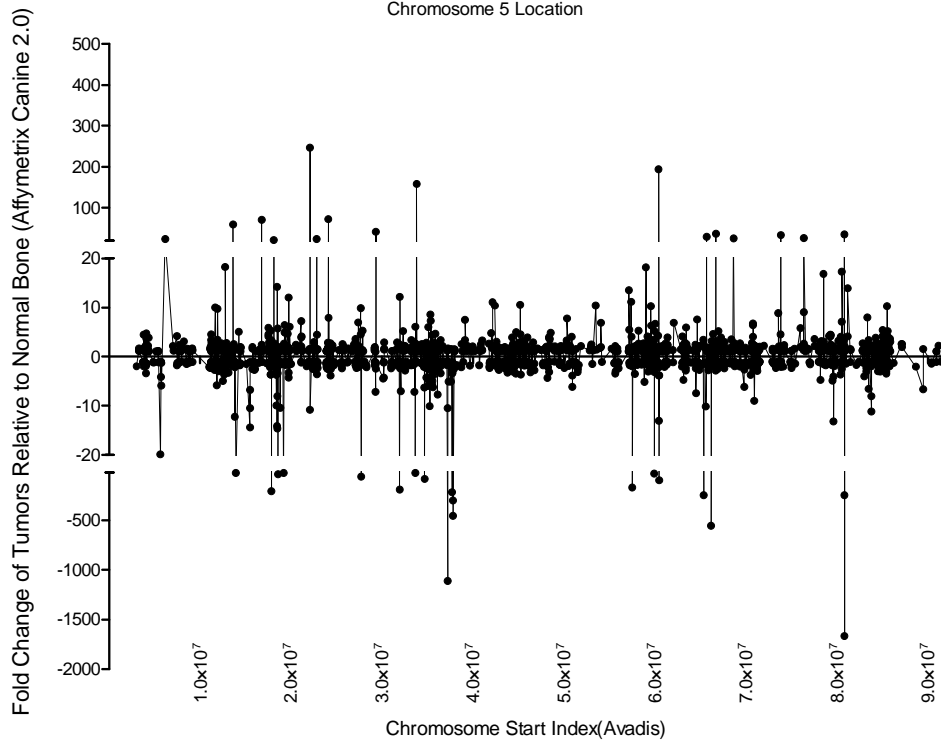
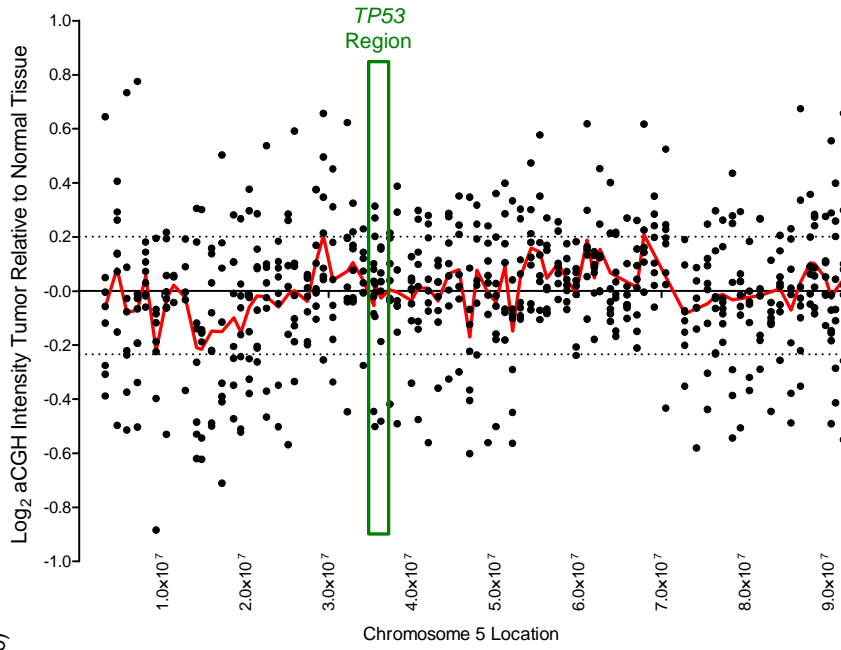
Chromosome 3



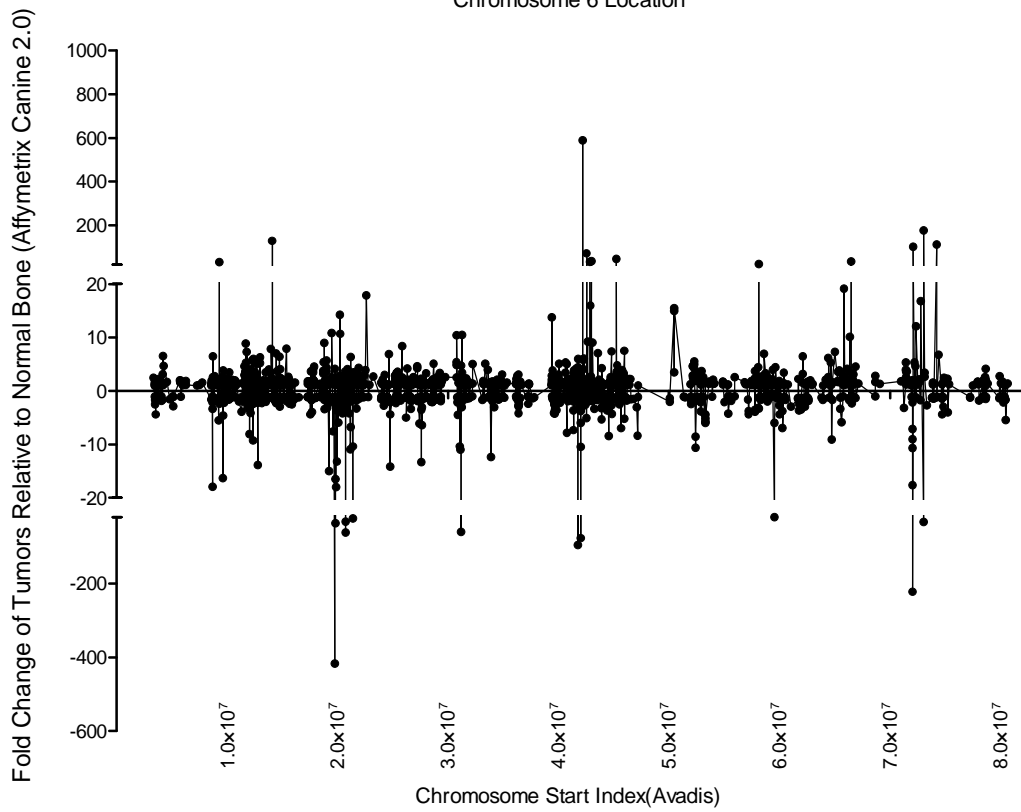
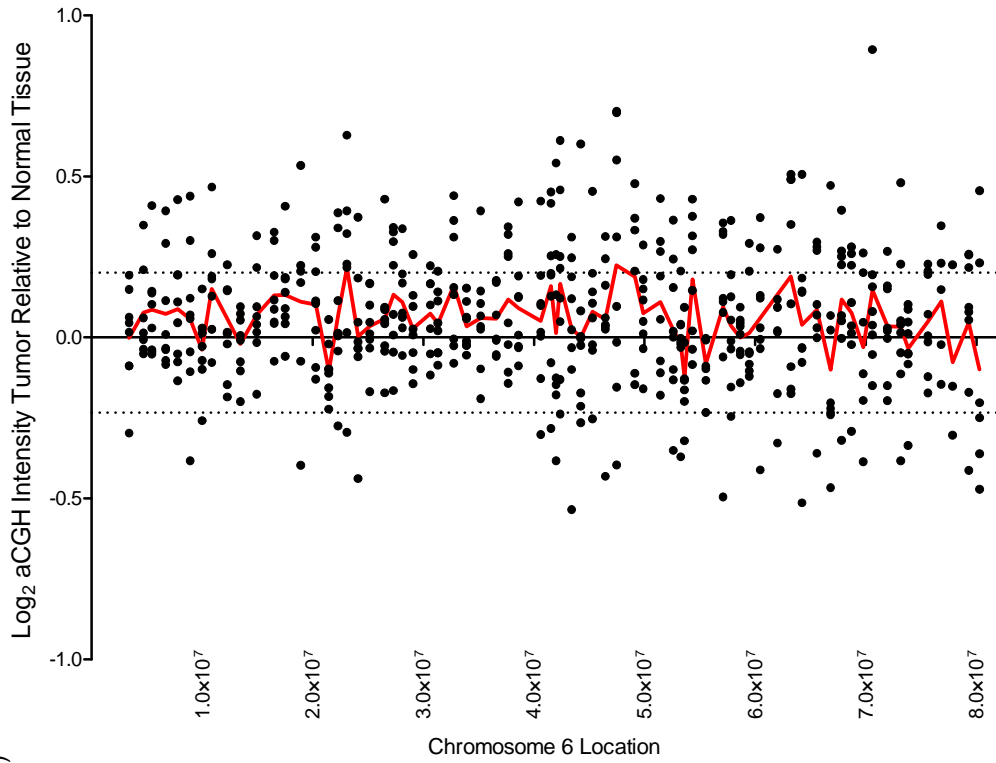
Chromosome 4



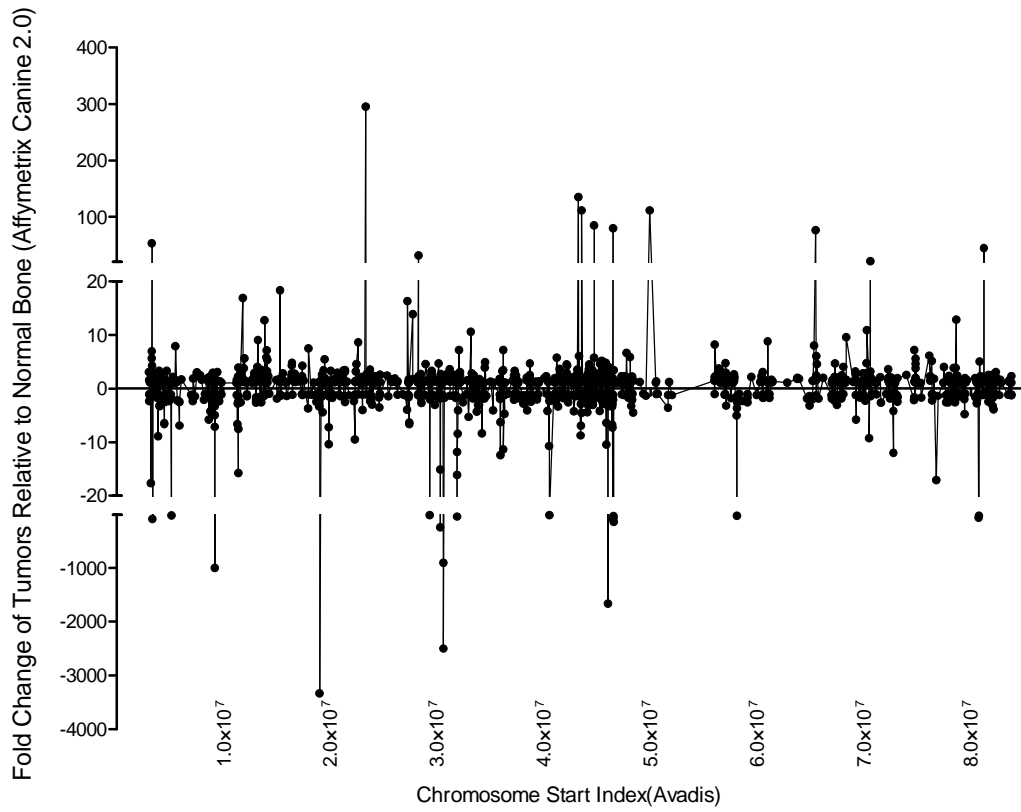
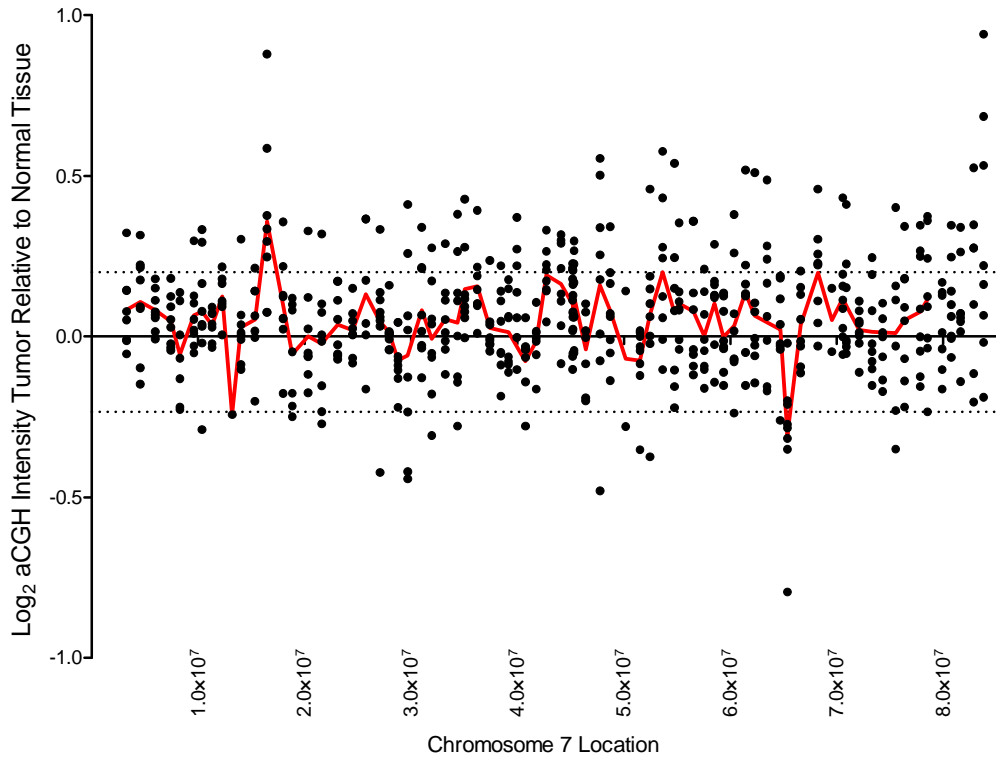
Chromosome 5



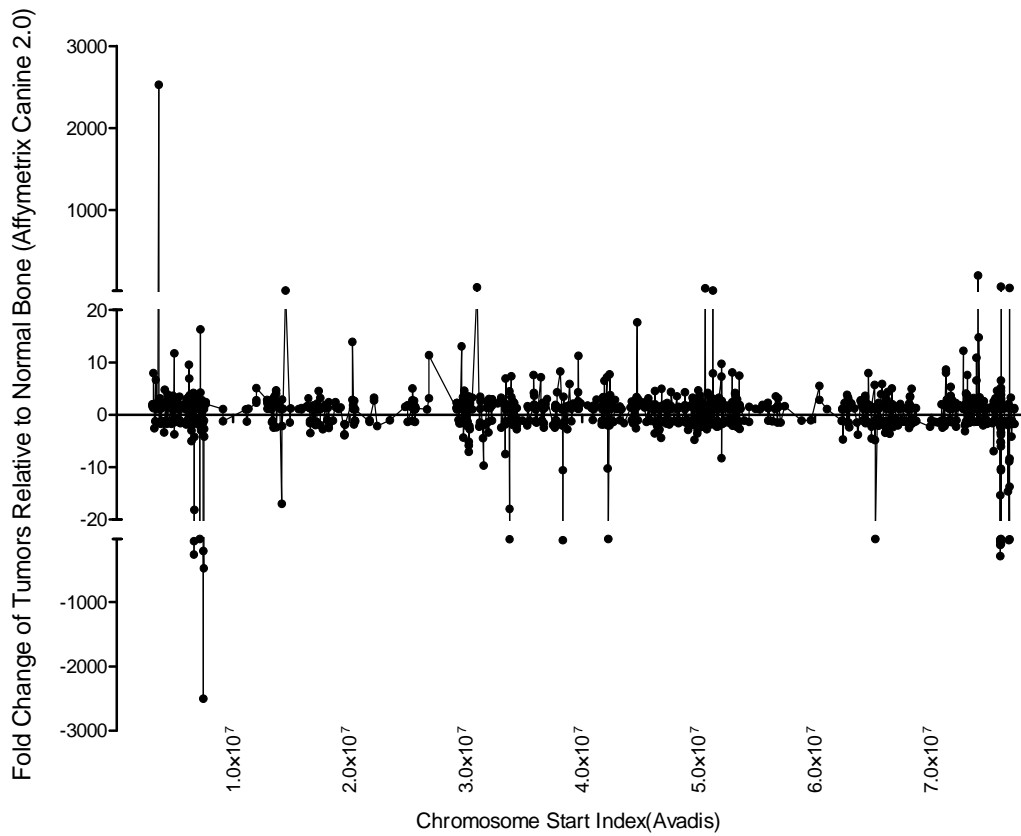
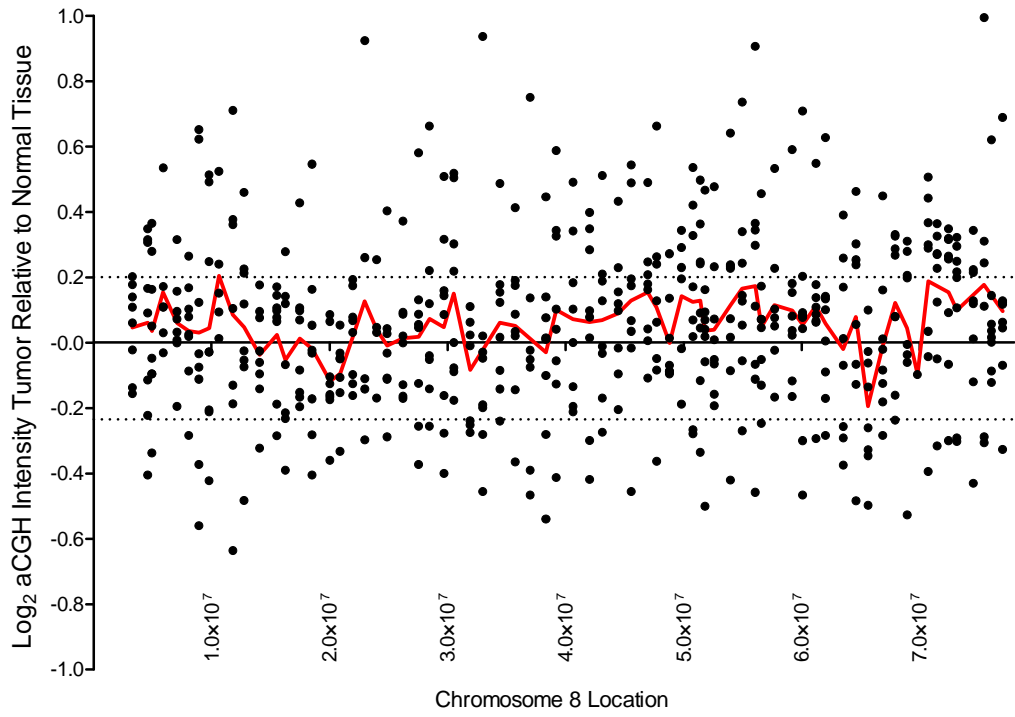
Chromosome 6



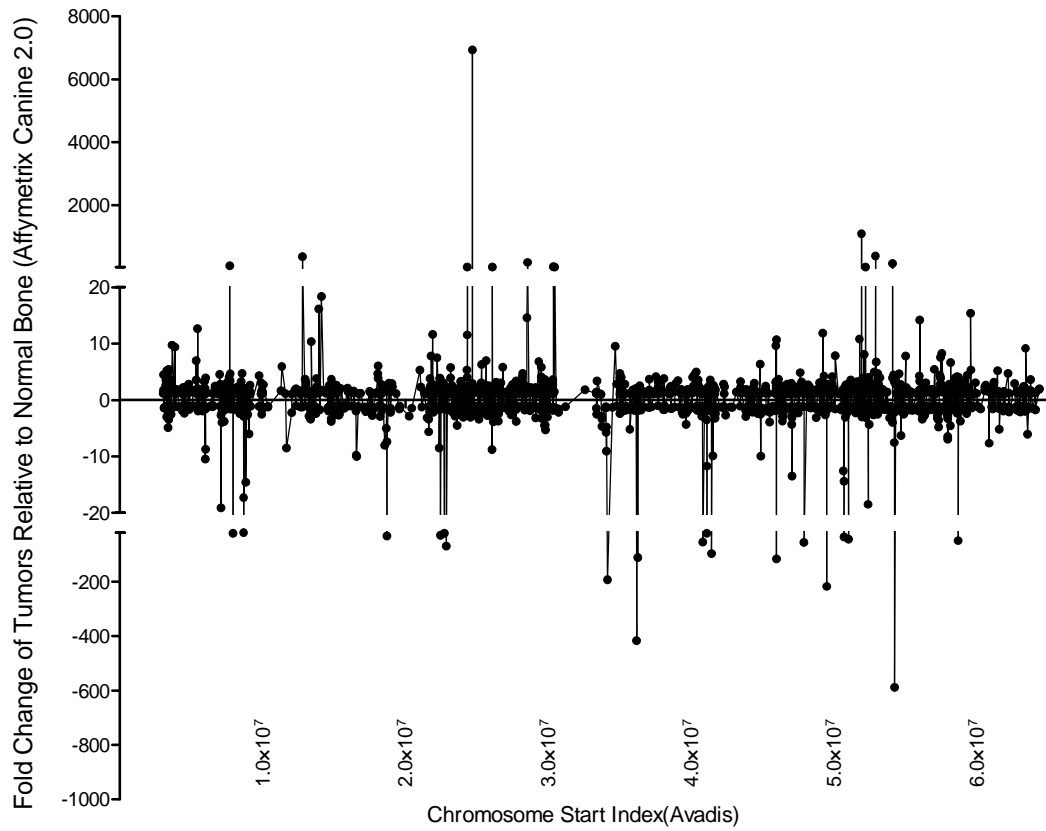
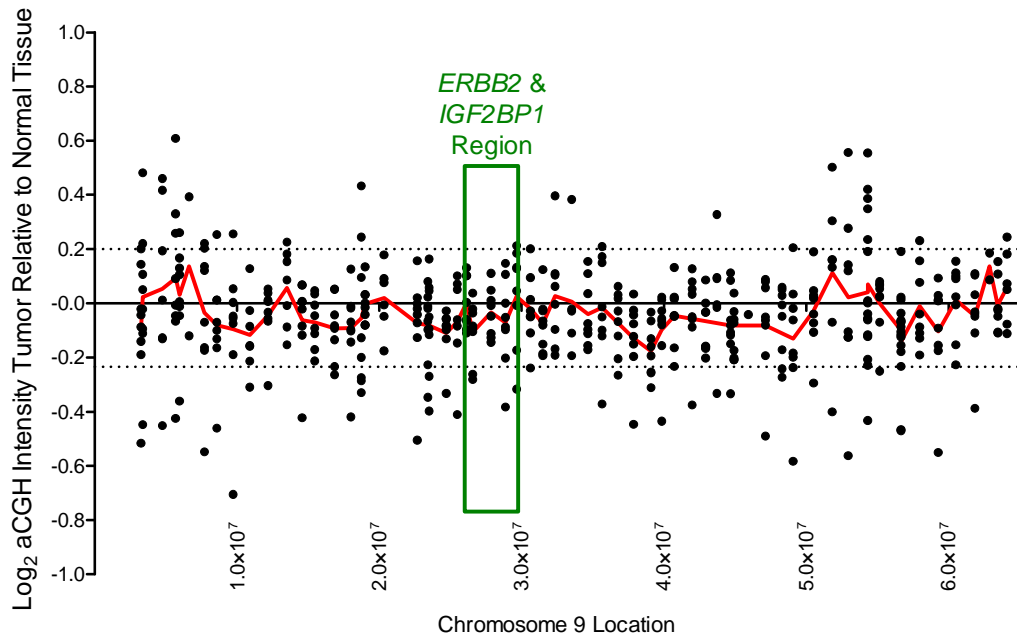
Chromosome 7



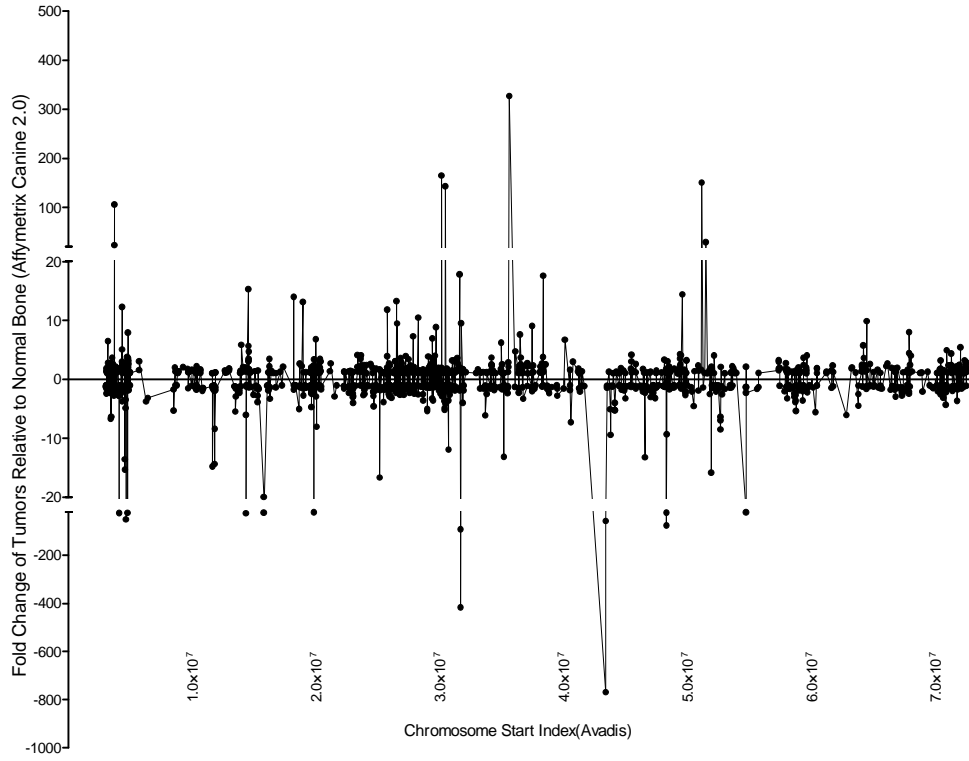
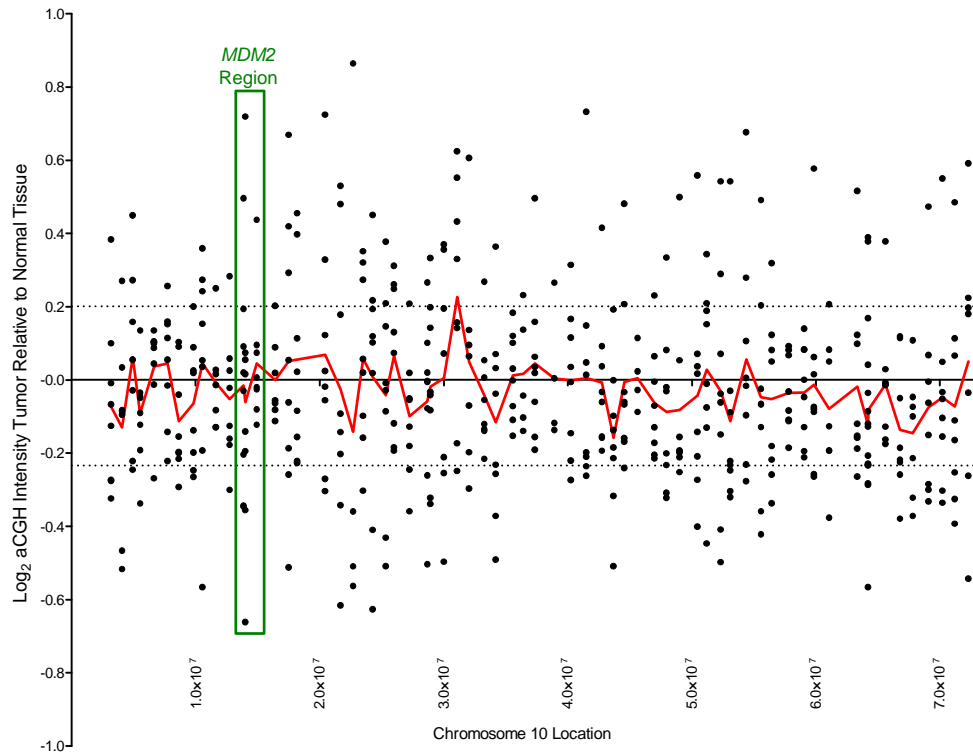
Chromosome 8



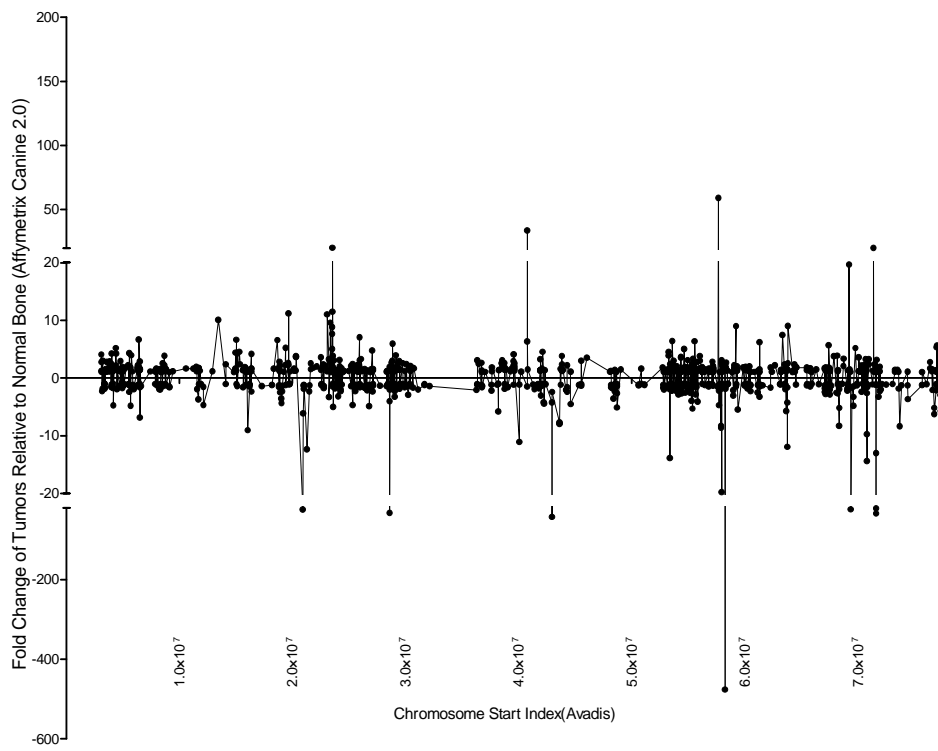
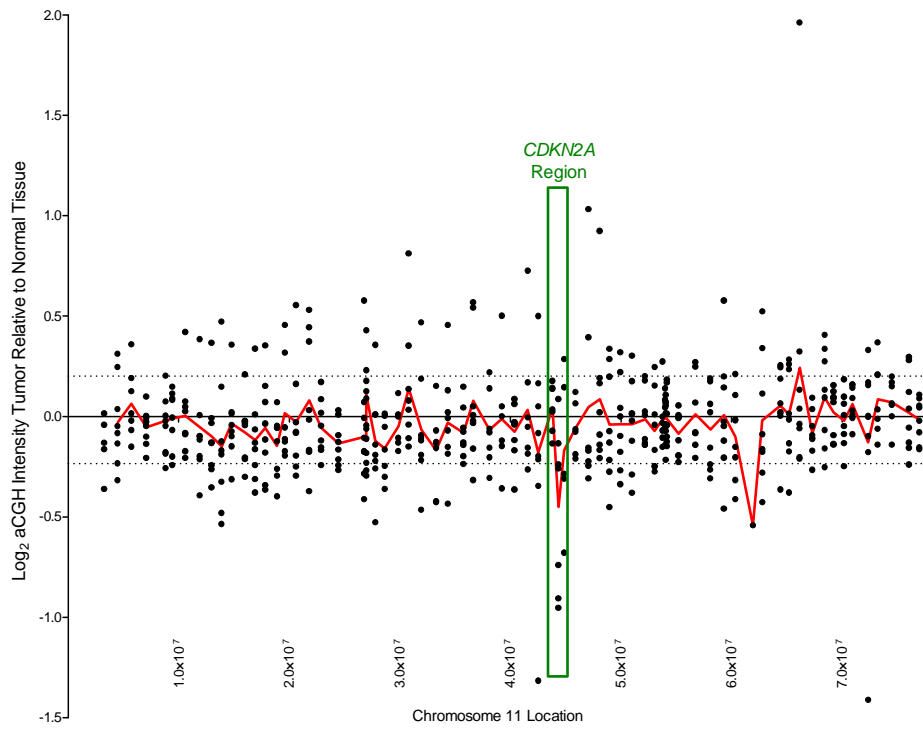
Chromosome 9



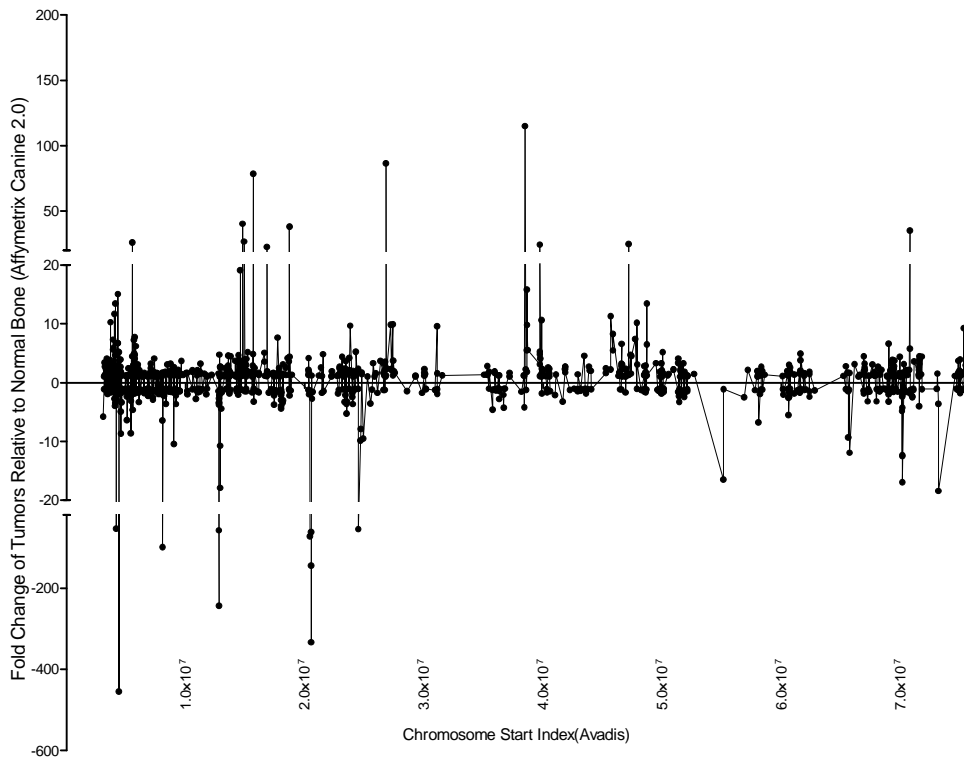
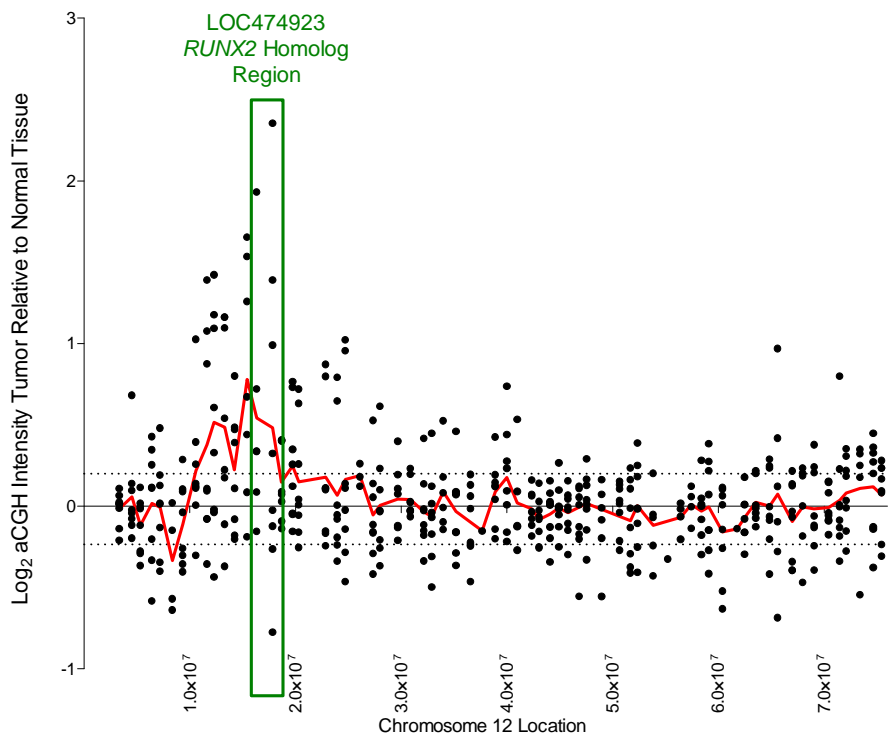
Chromosome 10



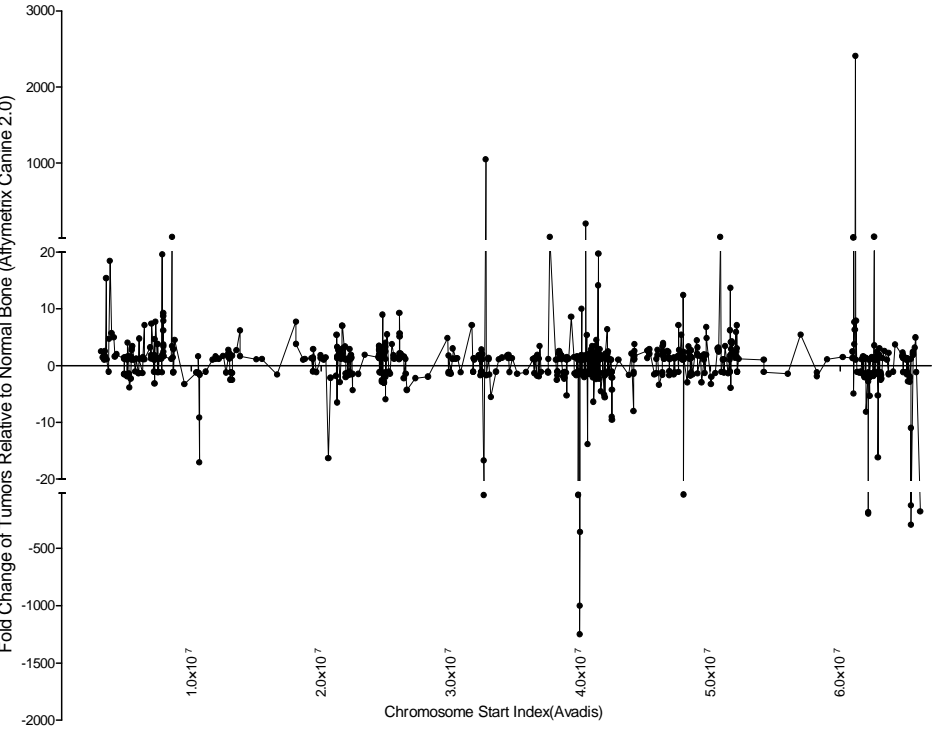
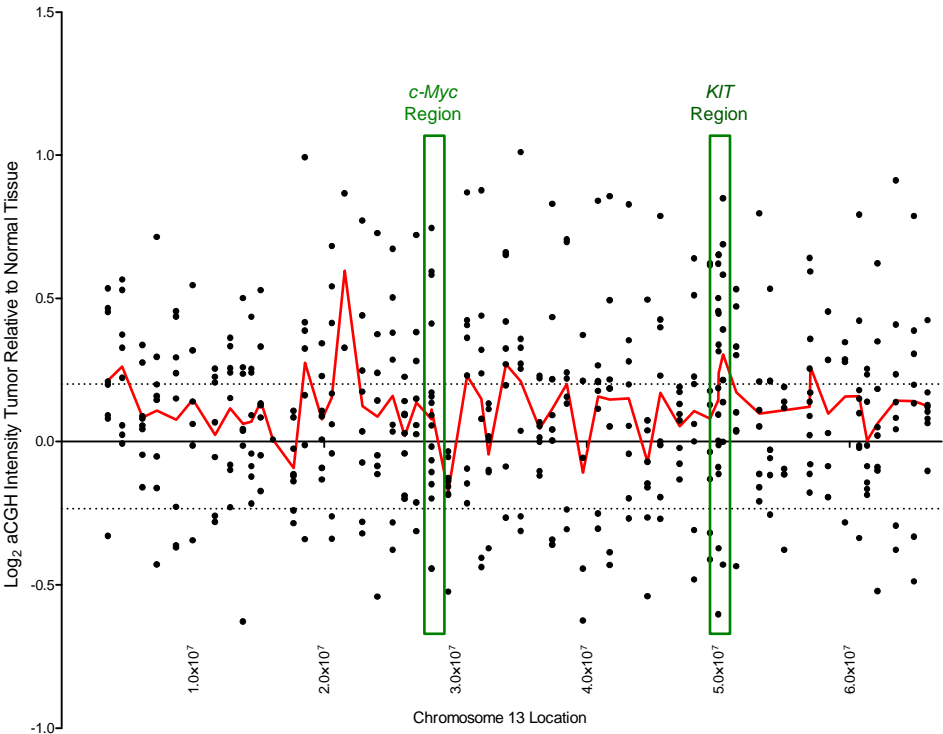
Chromosome 11



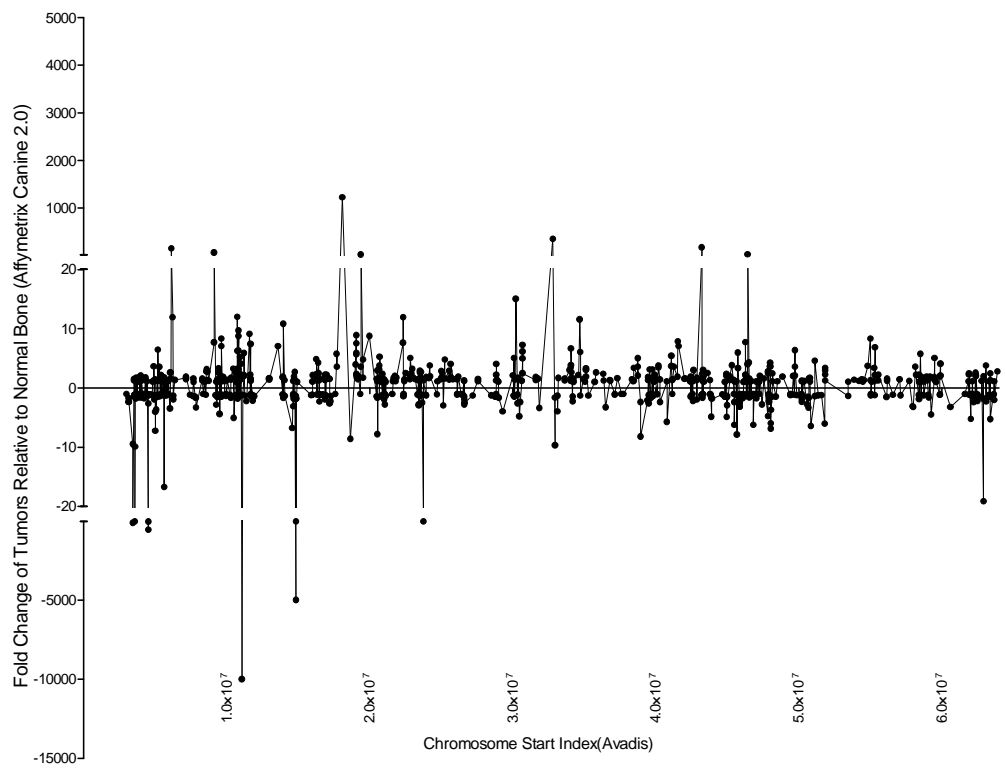
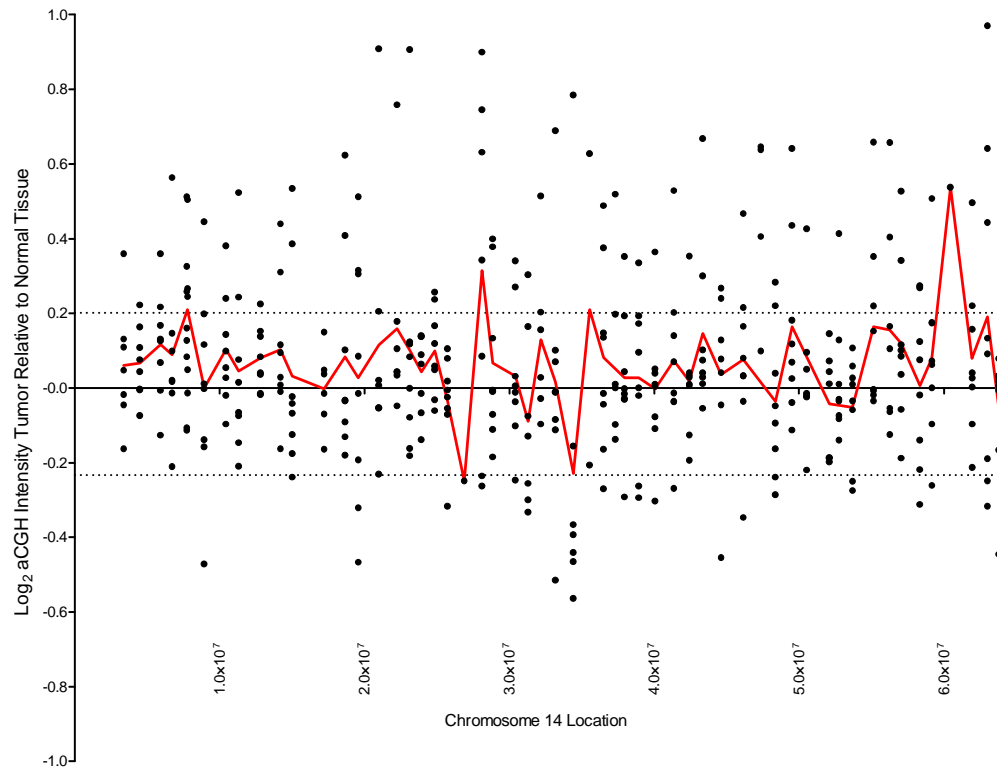
Chromosome 12



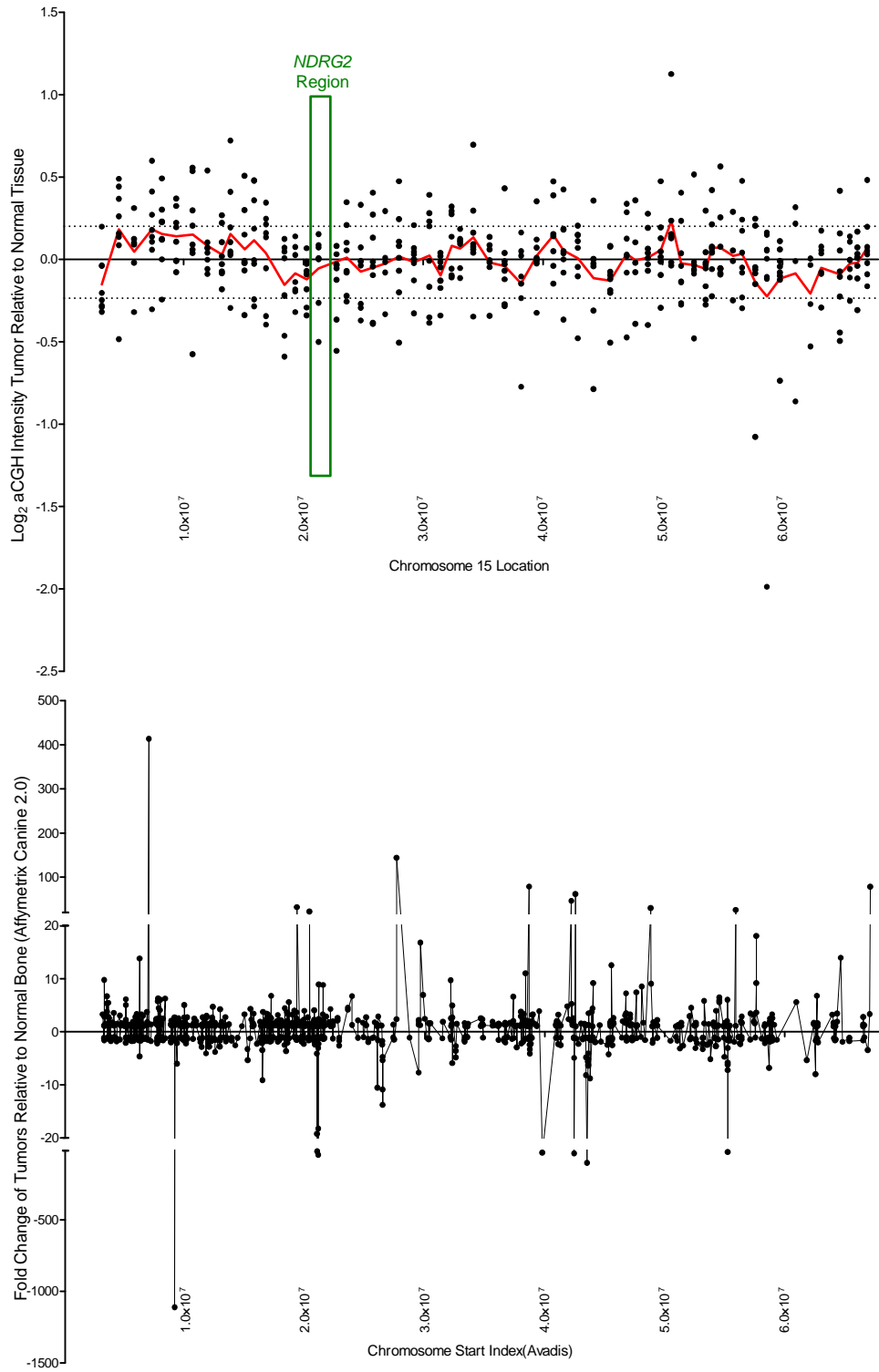
Chromosome 13



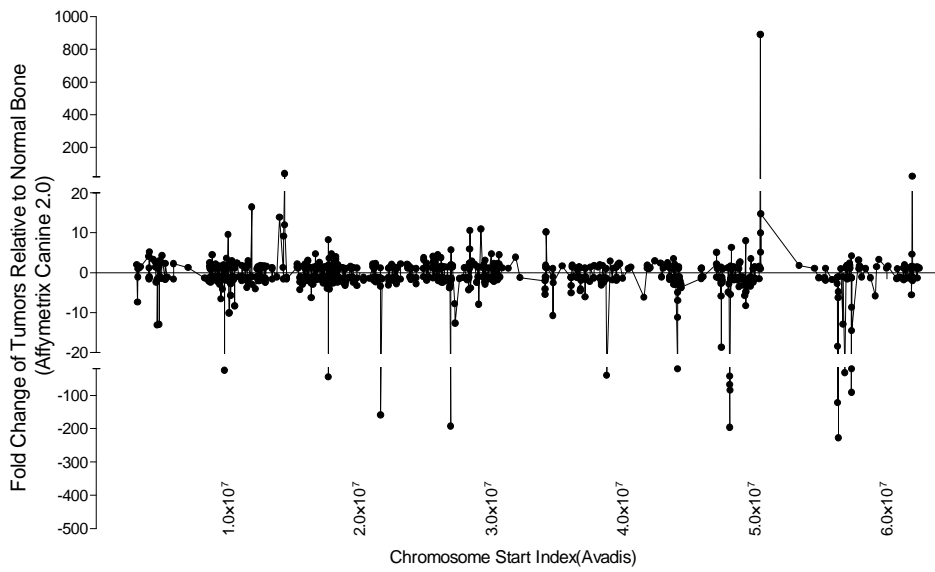
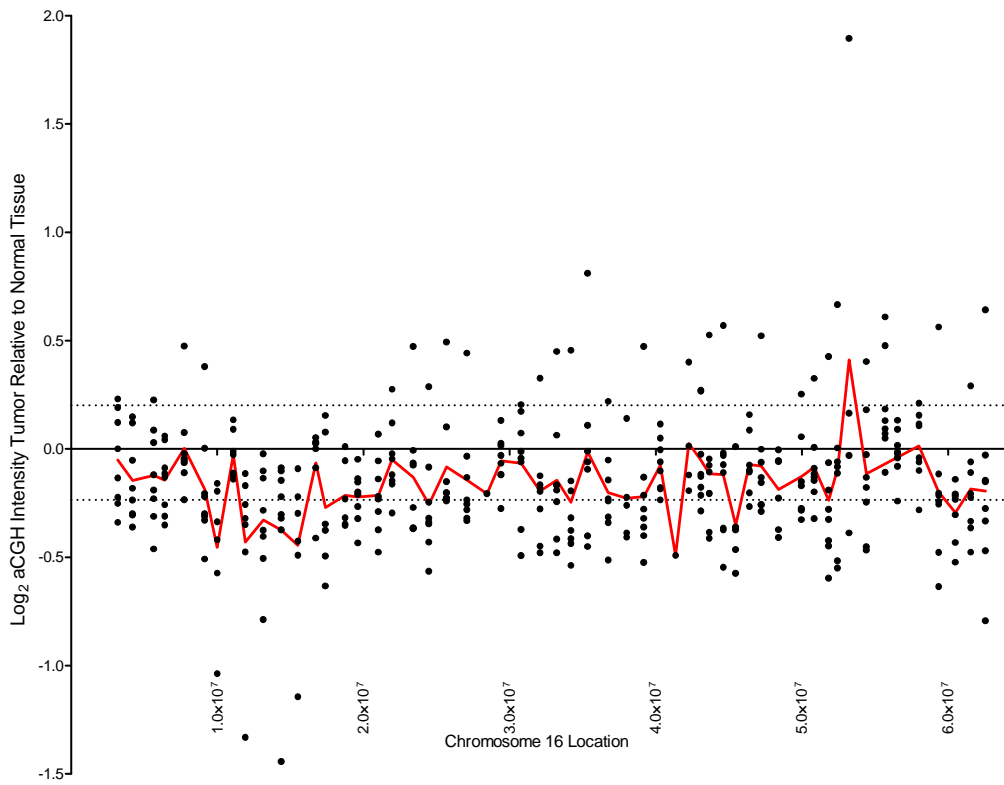
Chromosome 14



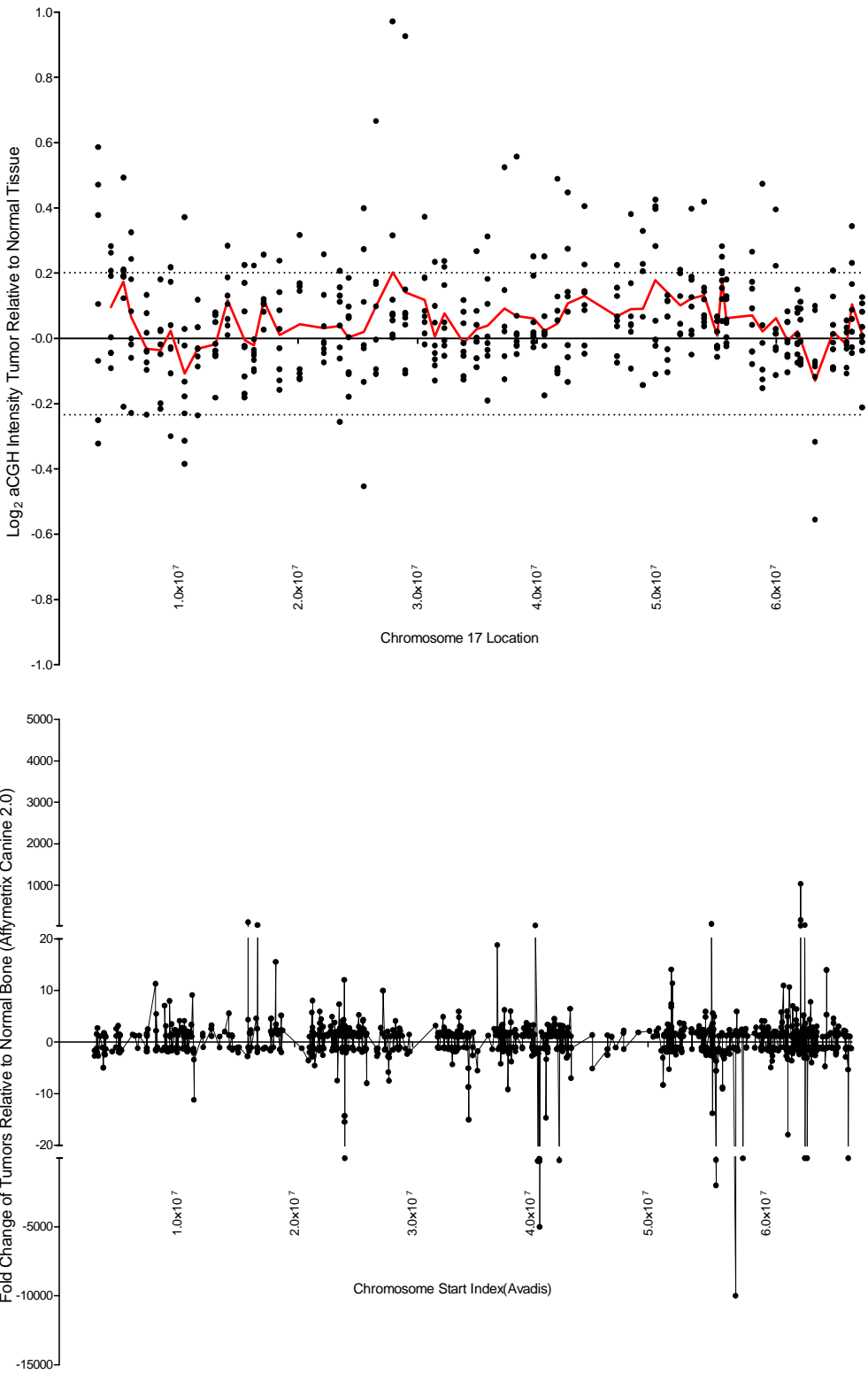
Chromosome 15



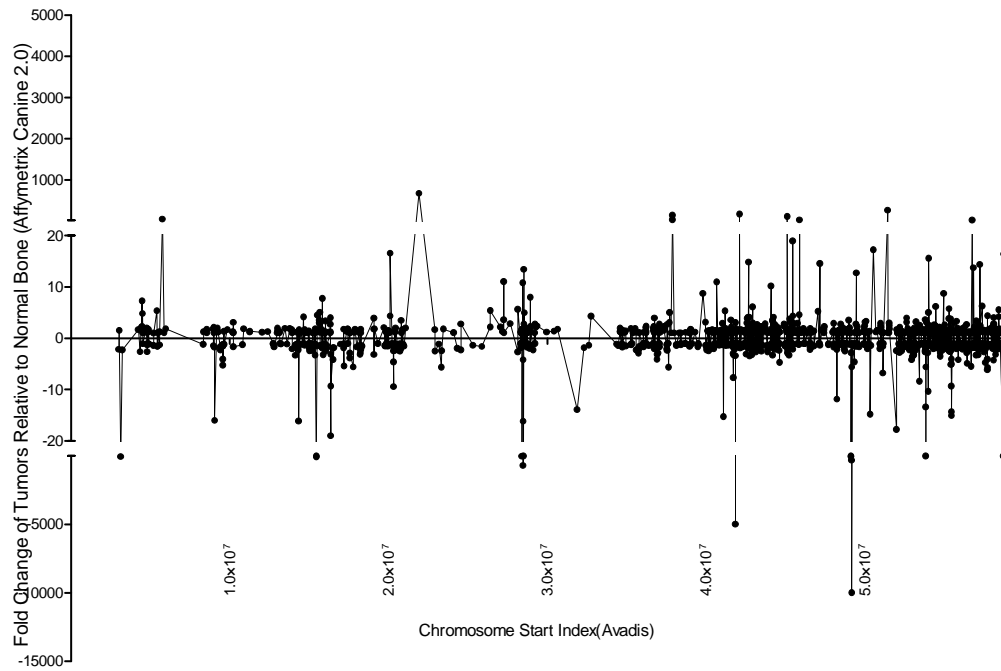
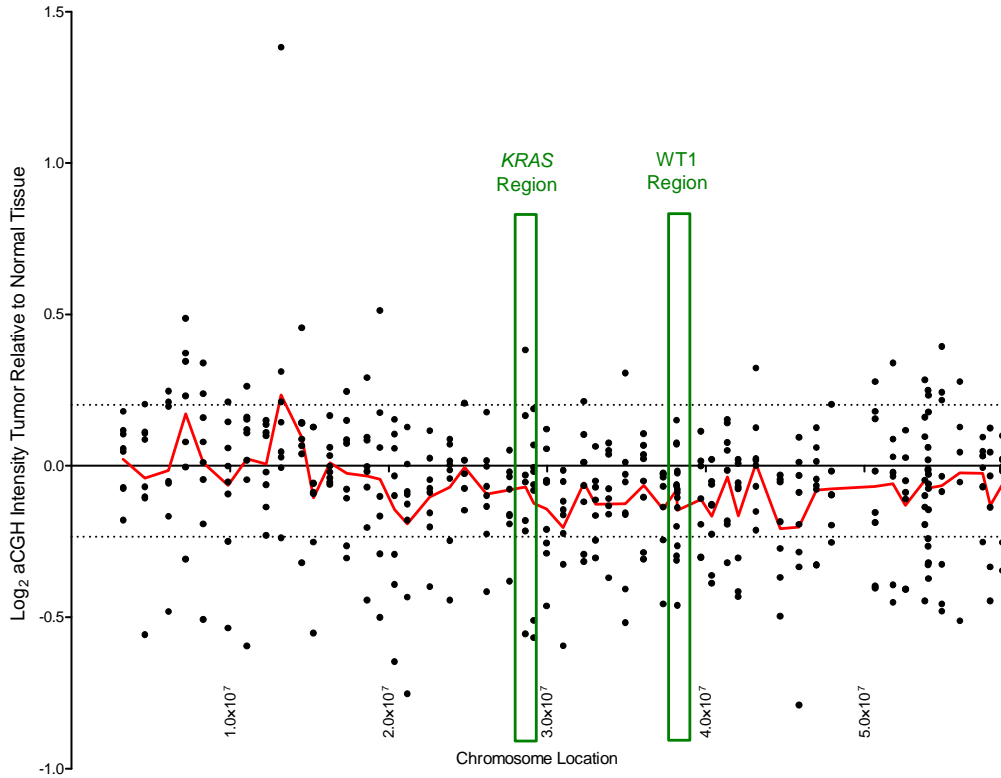
Chromosome 16



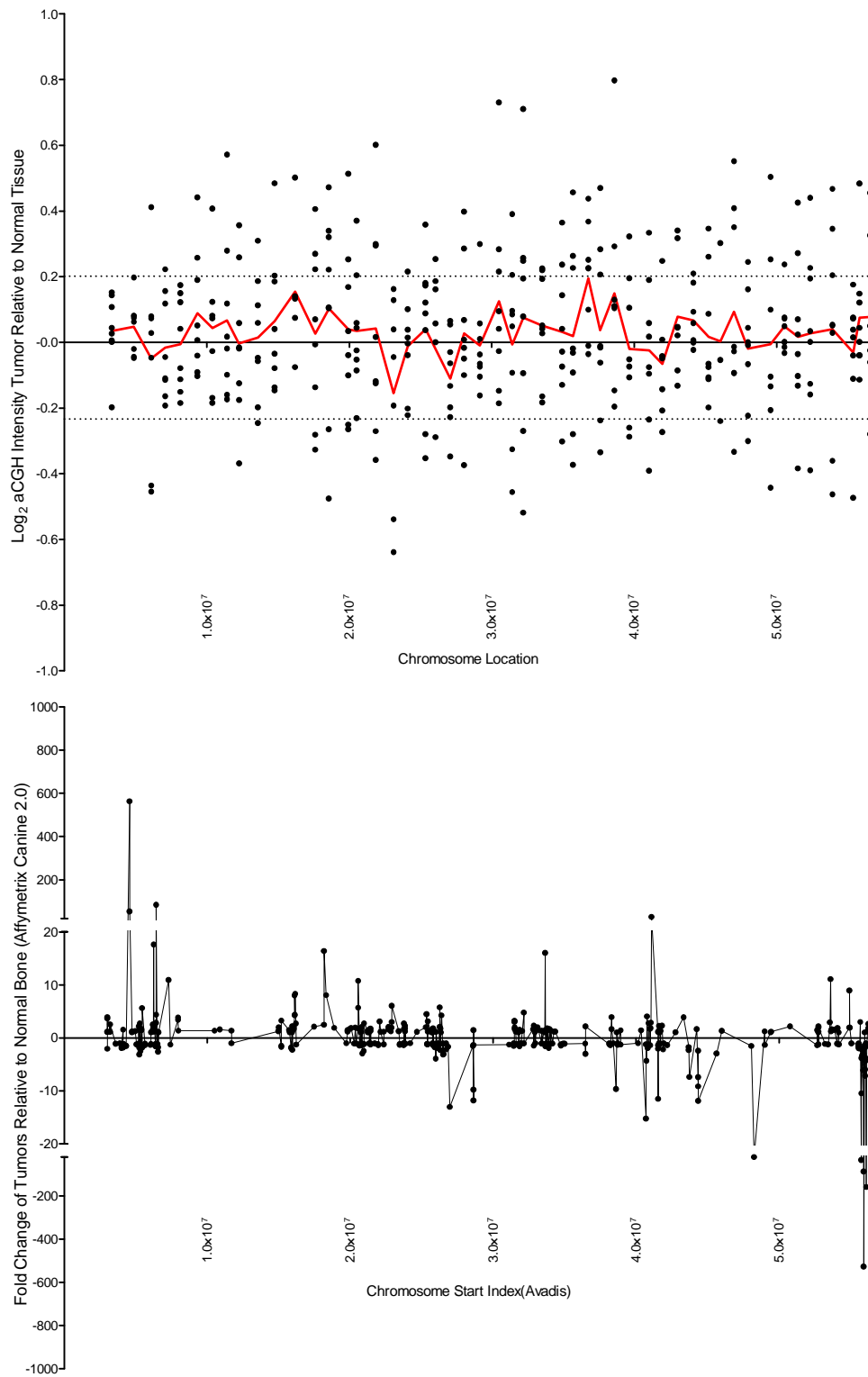
Chromosome 17



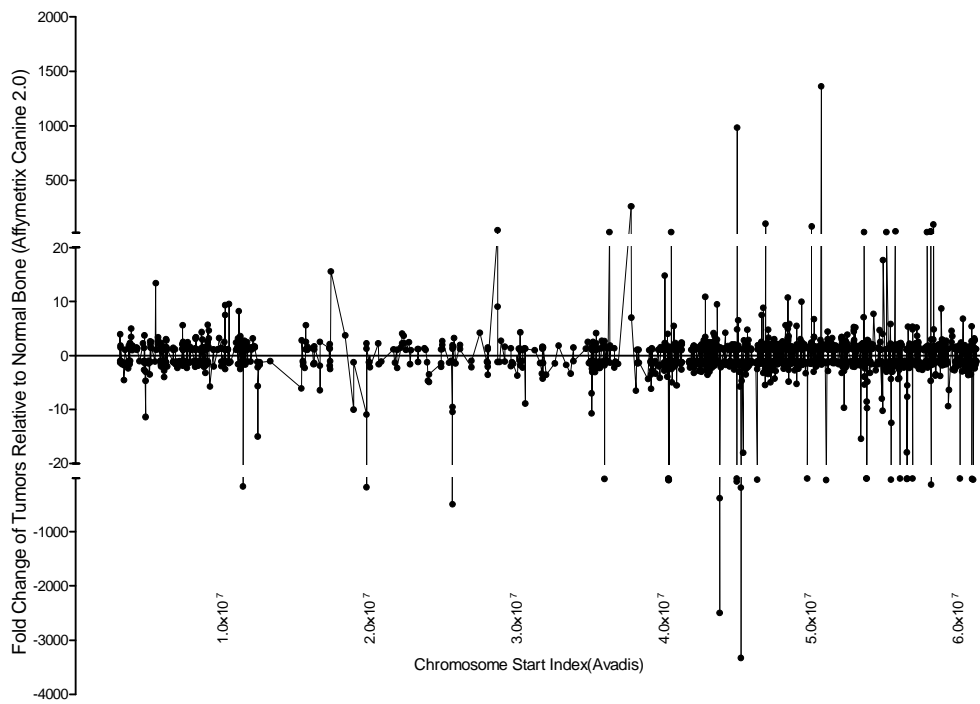
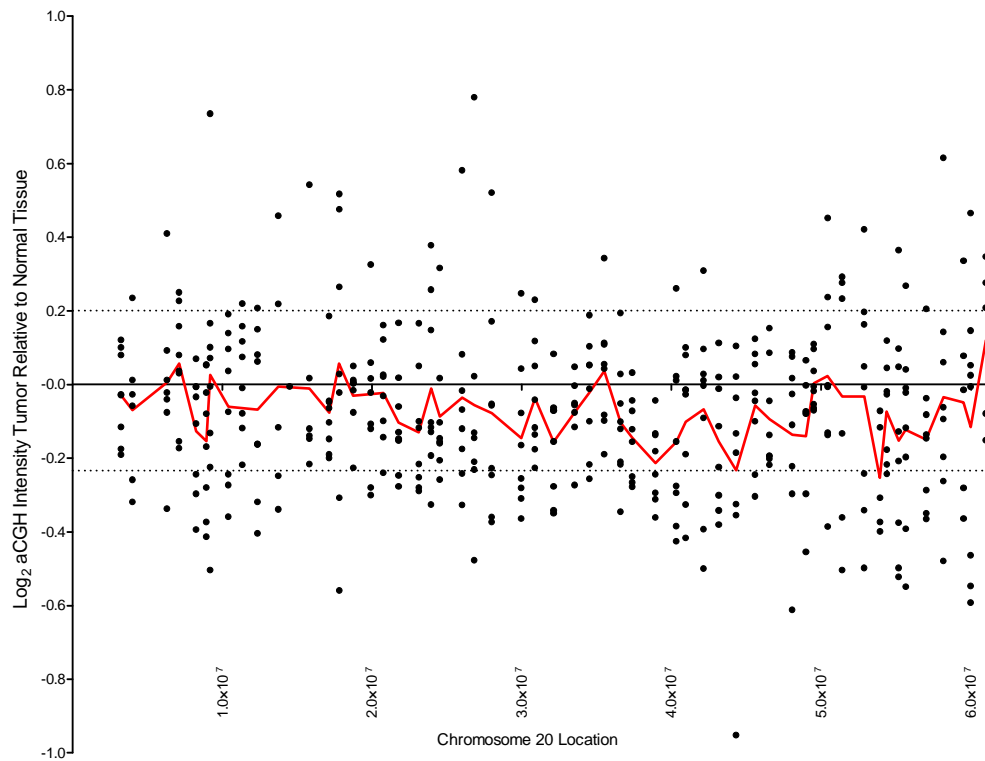
Chromosome 18



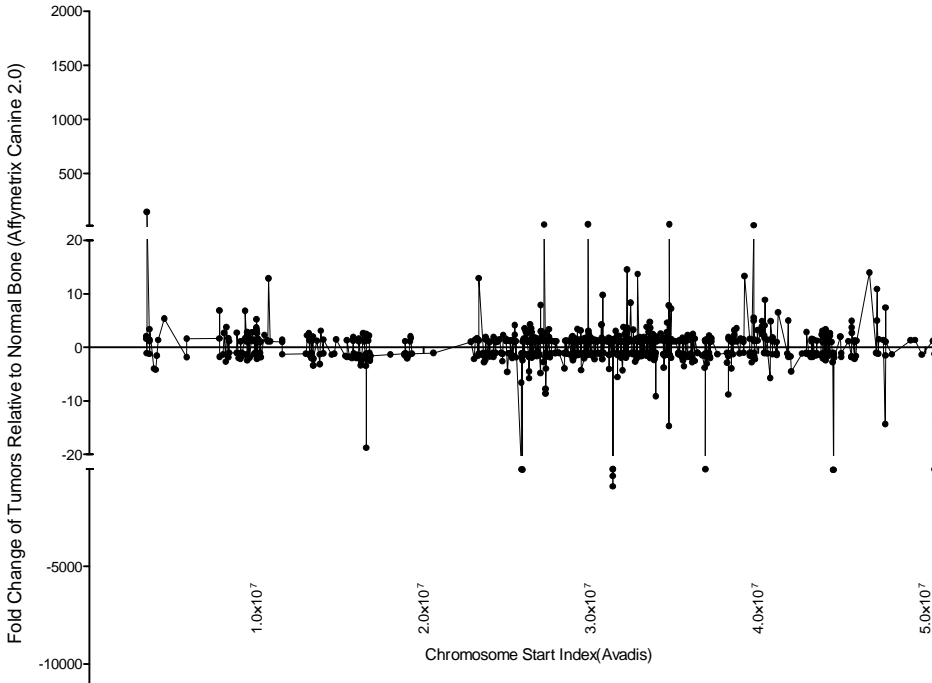
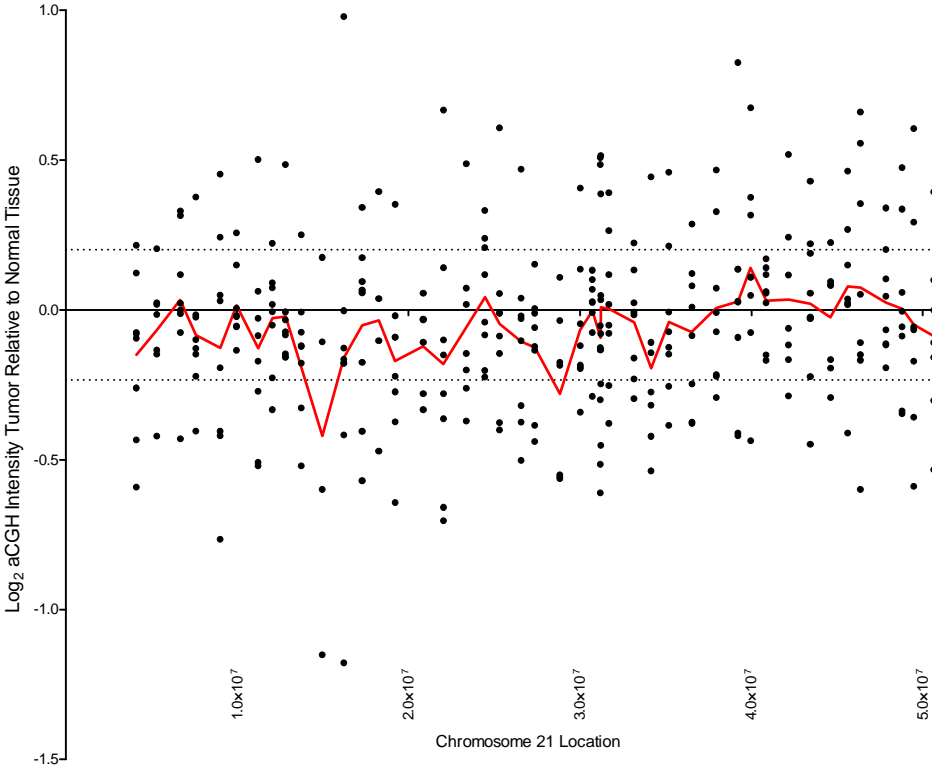
Chromosome 19



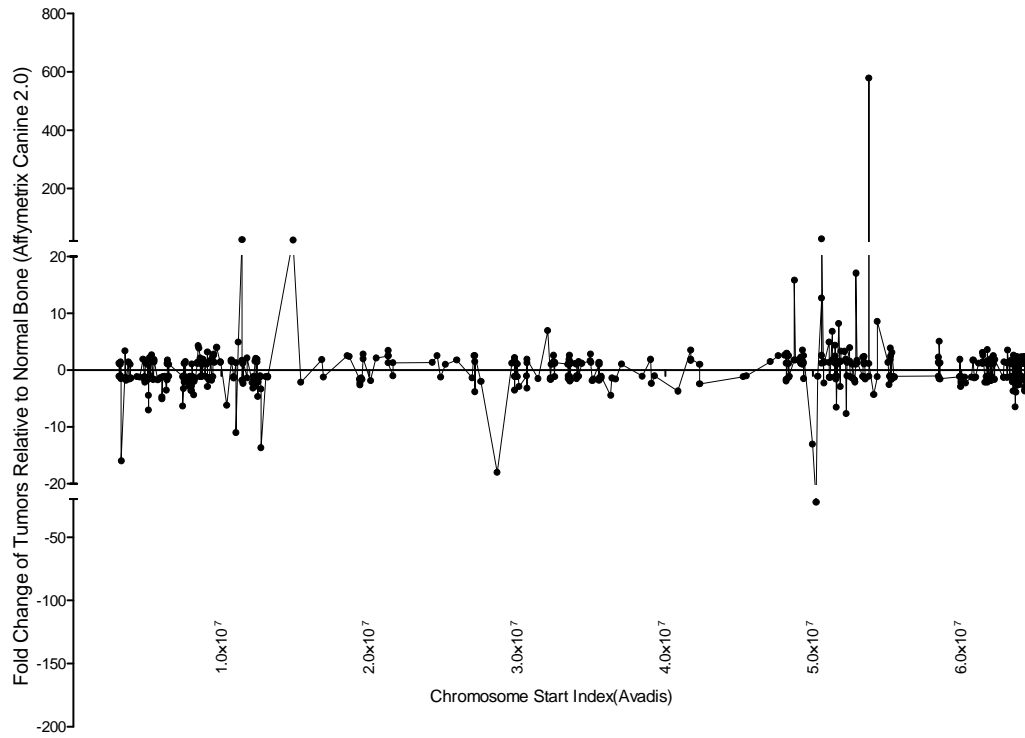
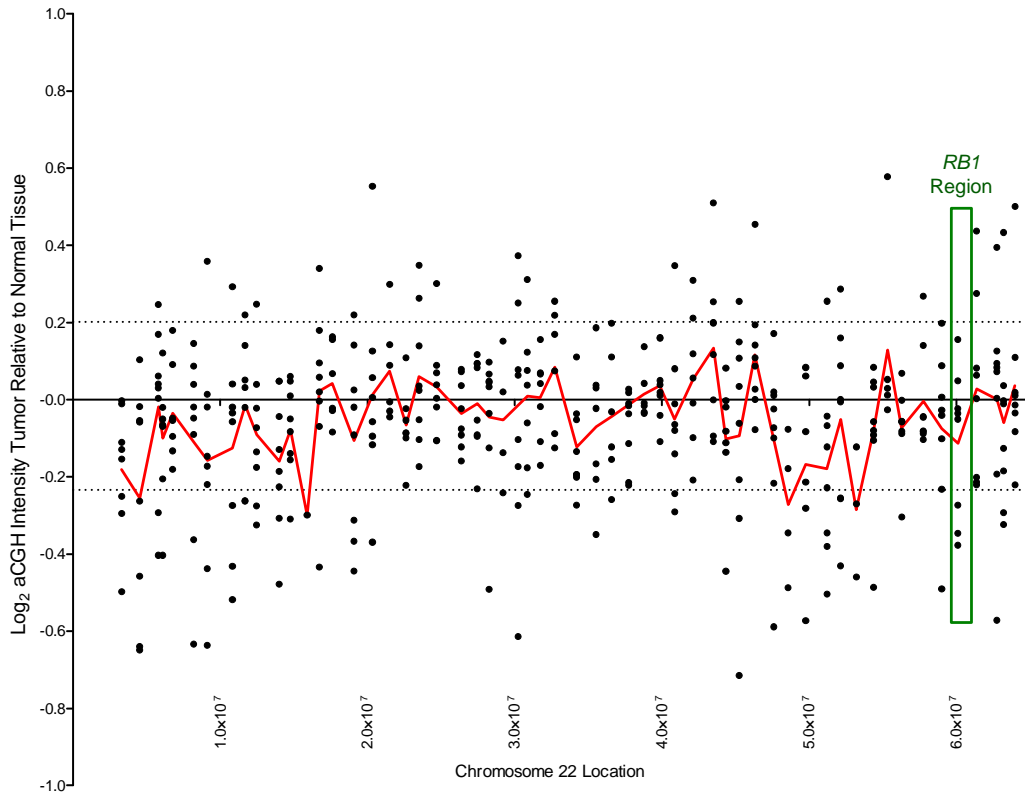
Chromosome 20



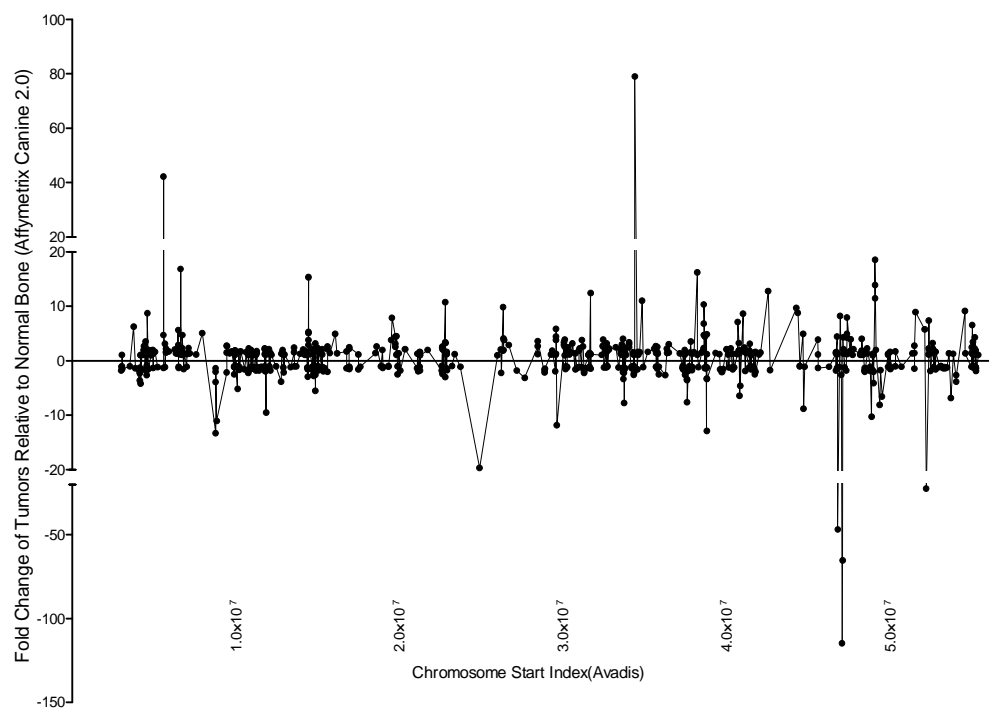
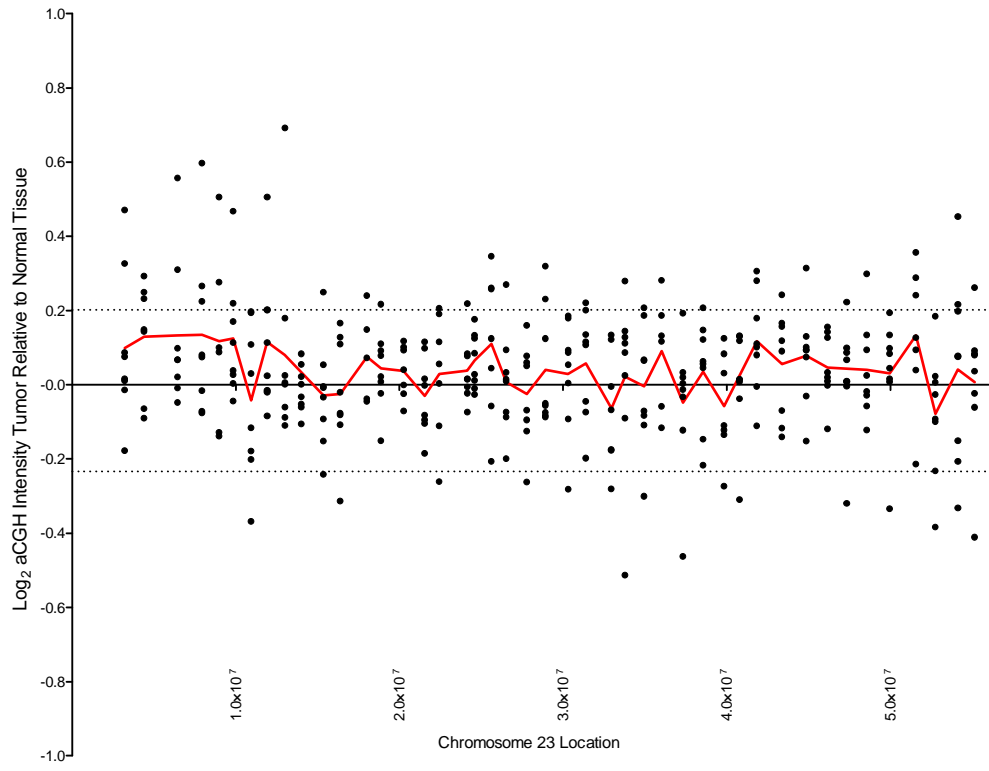
Chromosome 21



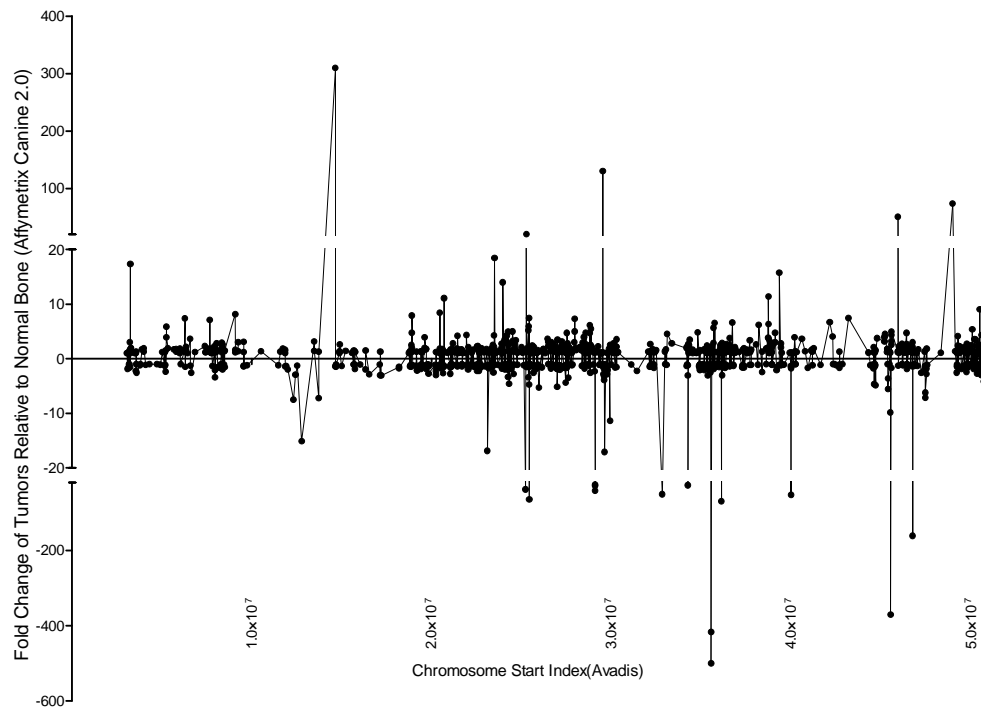
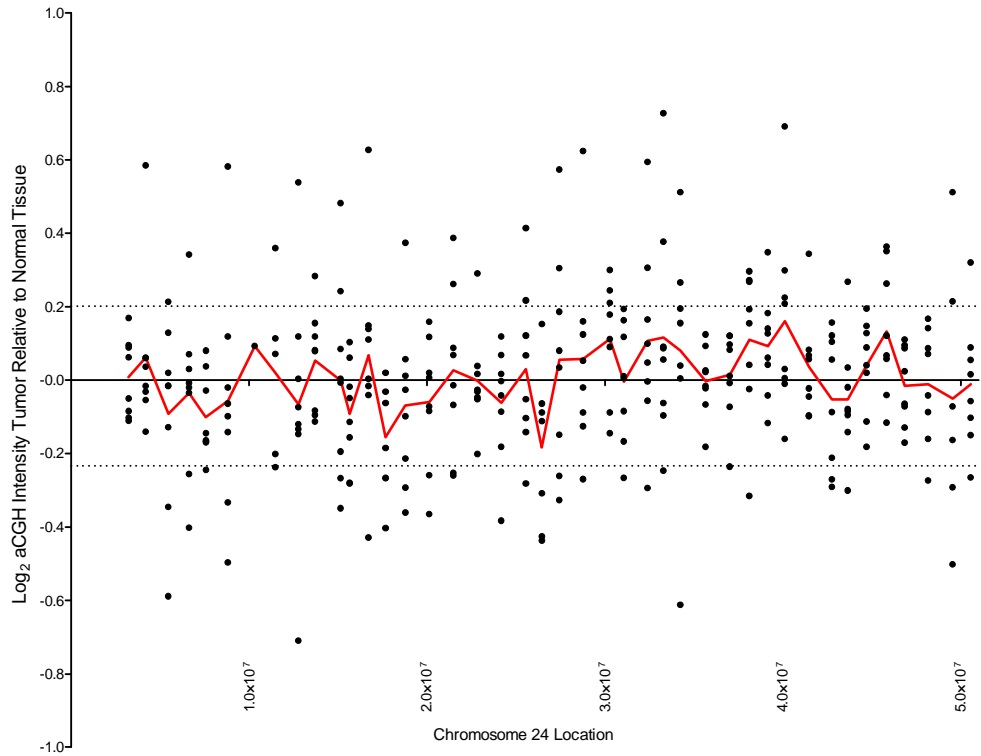
Chromosome 22



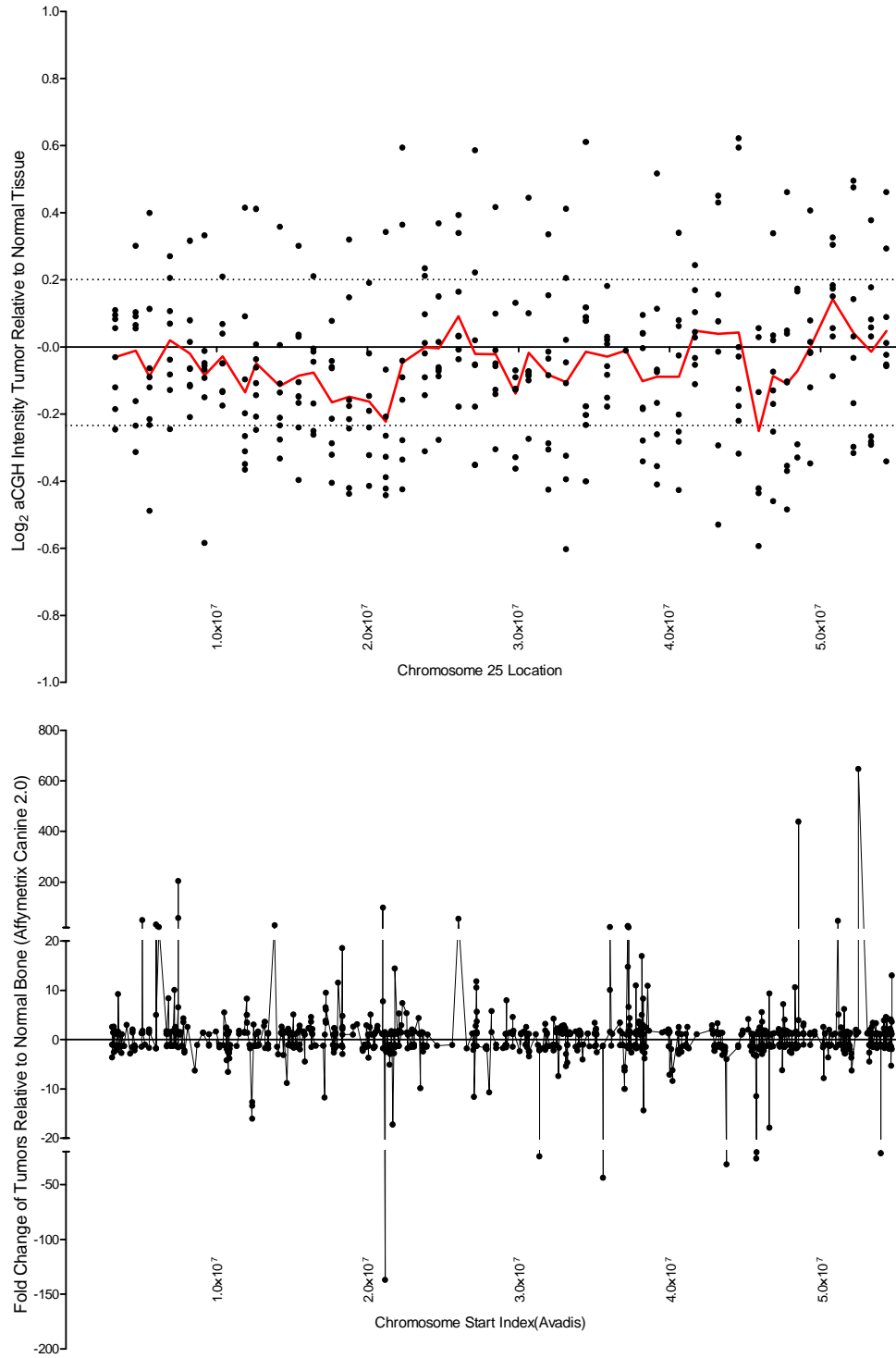
Chromosome 23



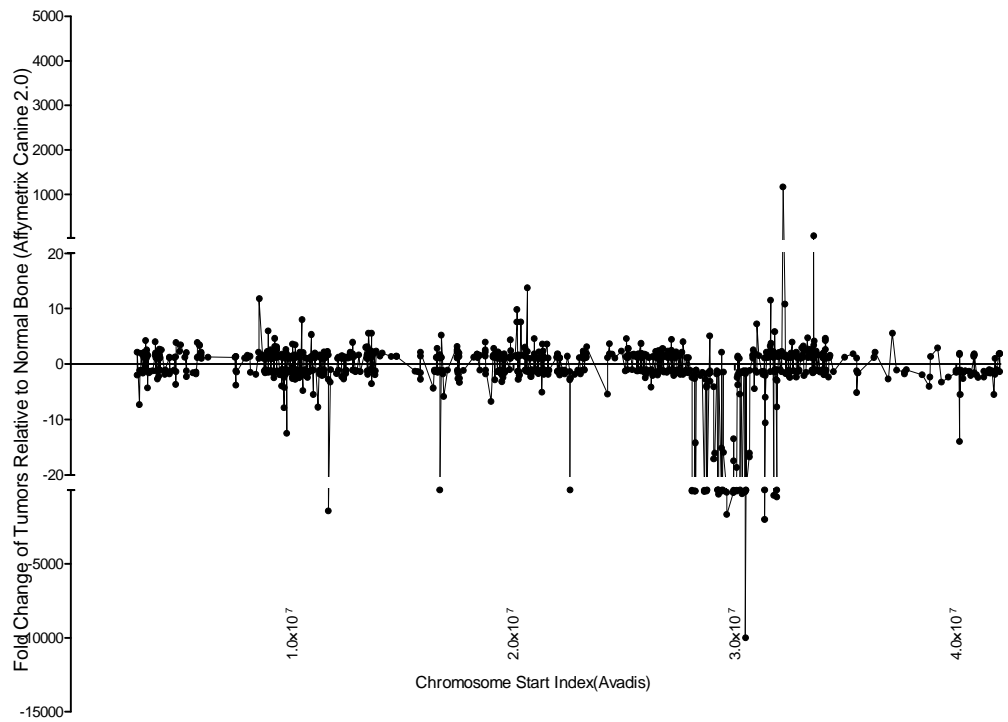
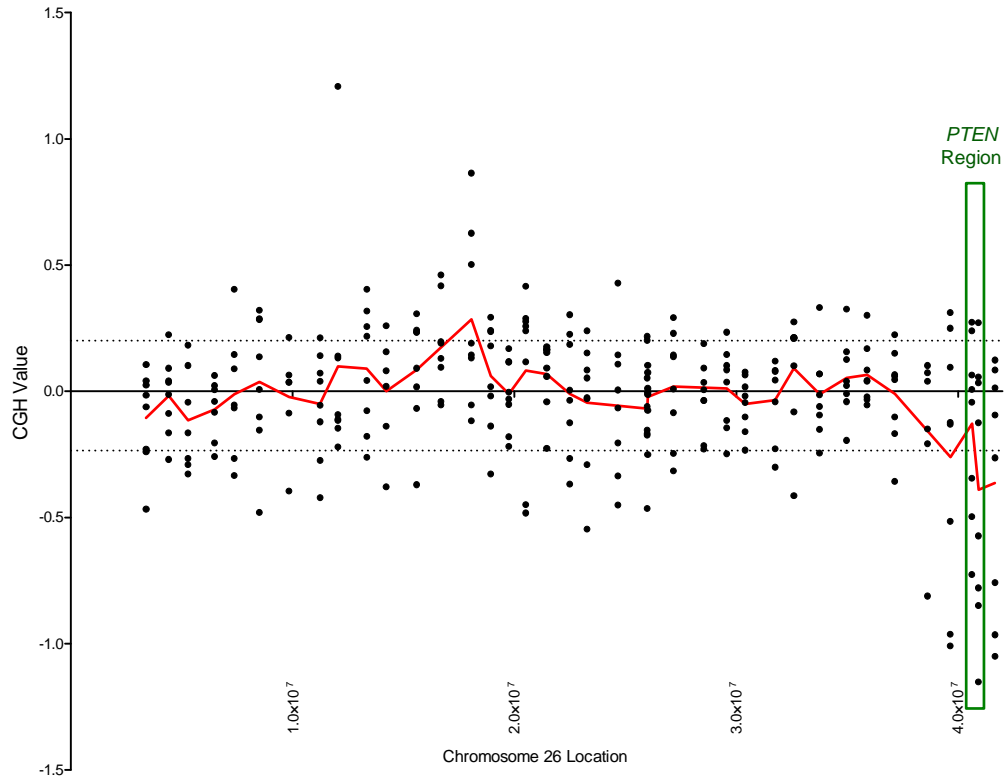
Chromosome 24



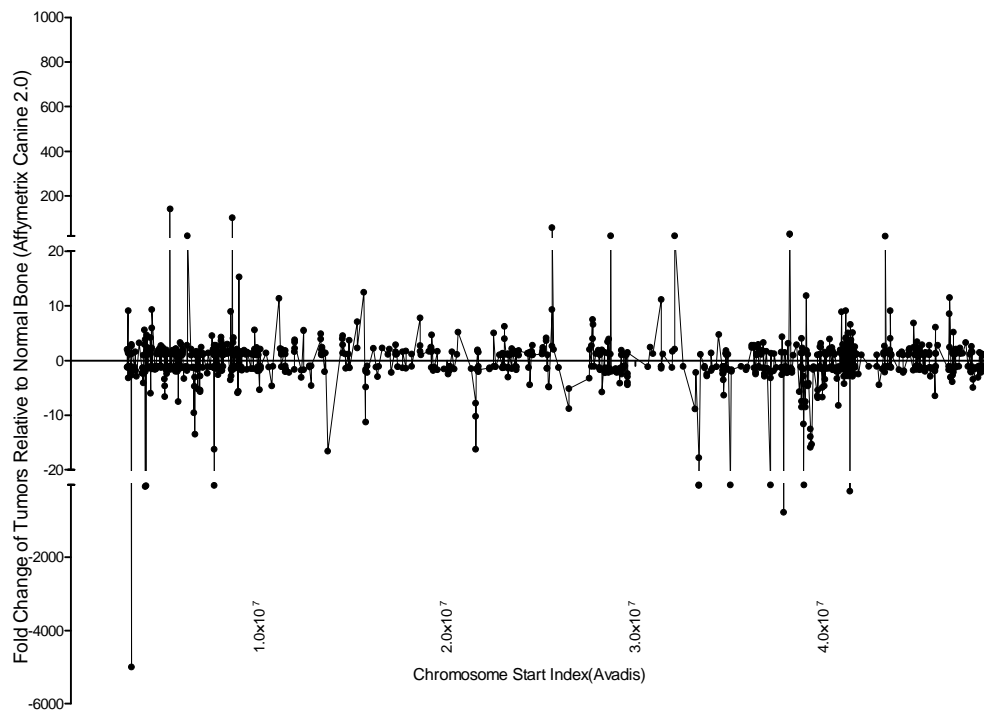
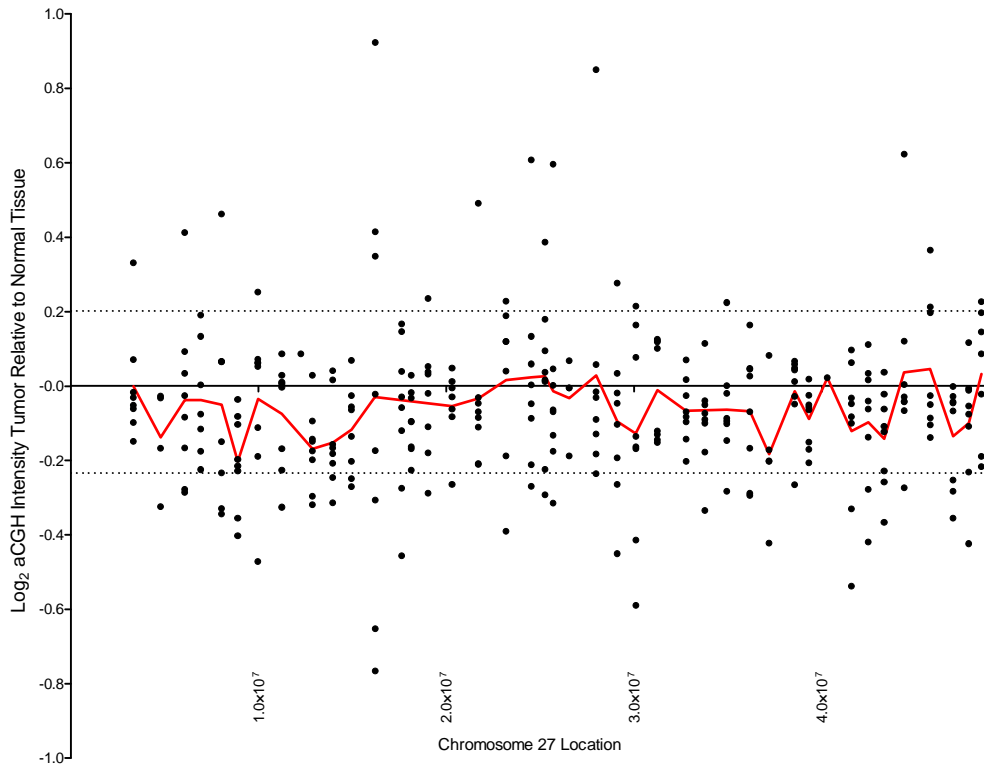
Chromosome 25



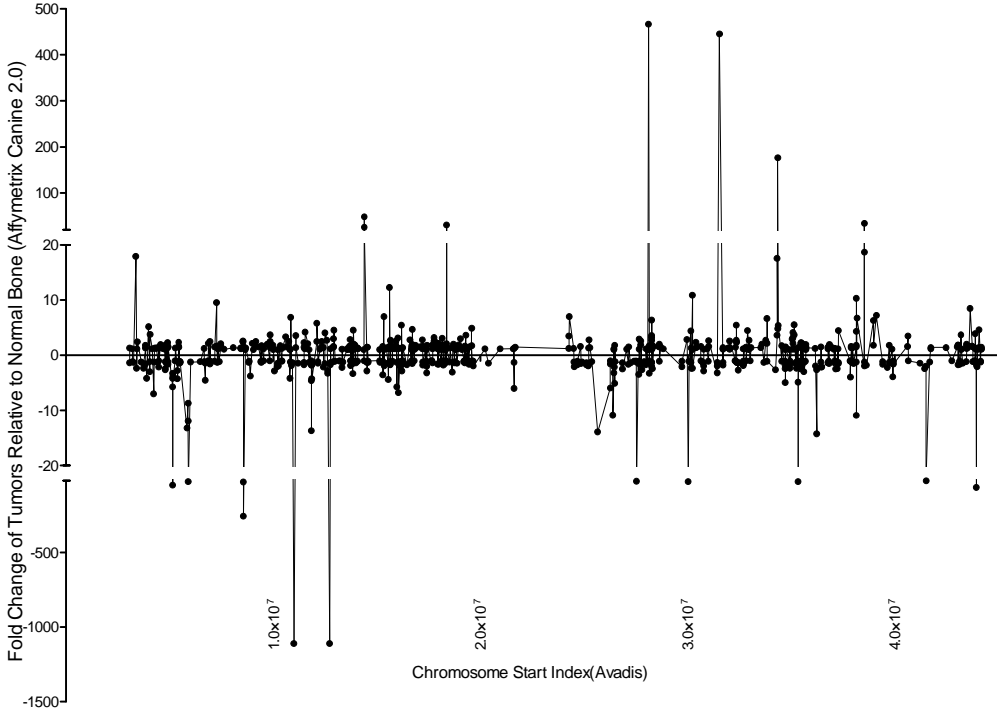
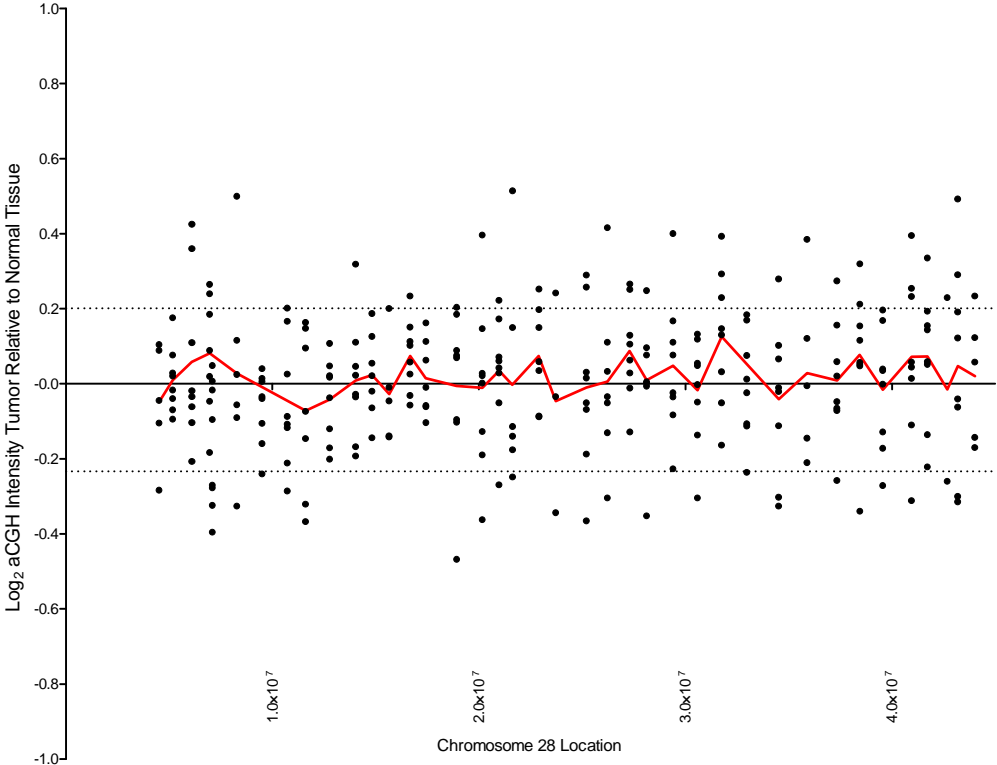
Chromosome 26



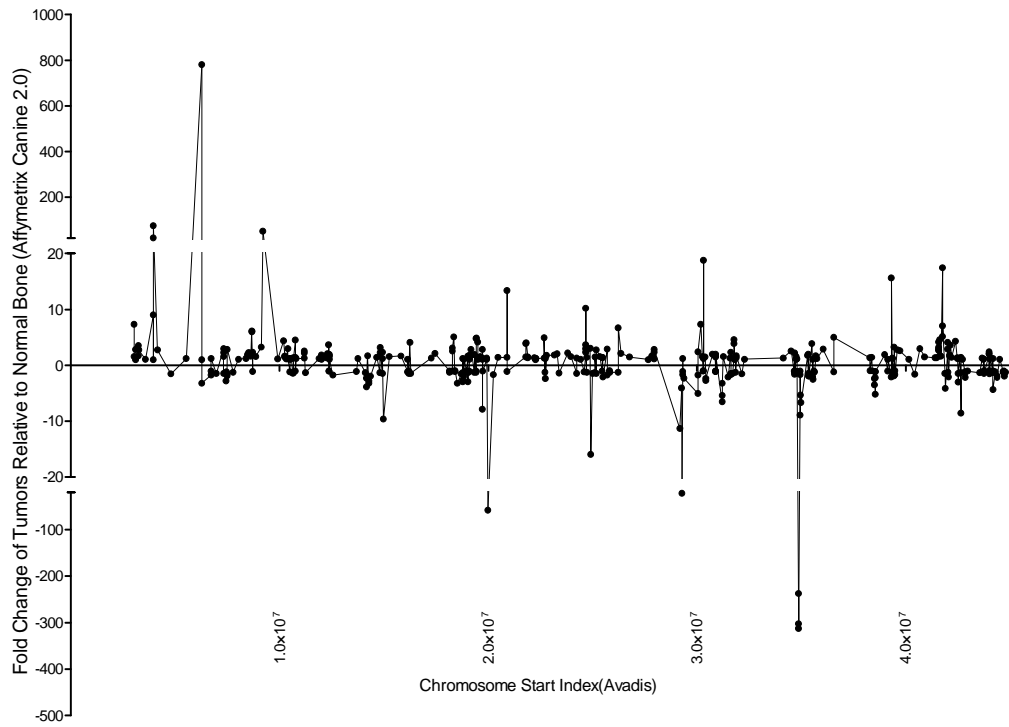
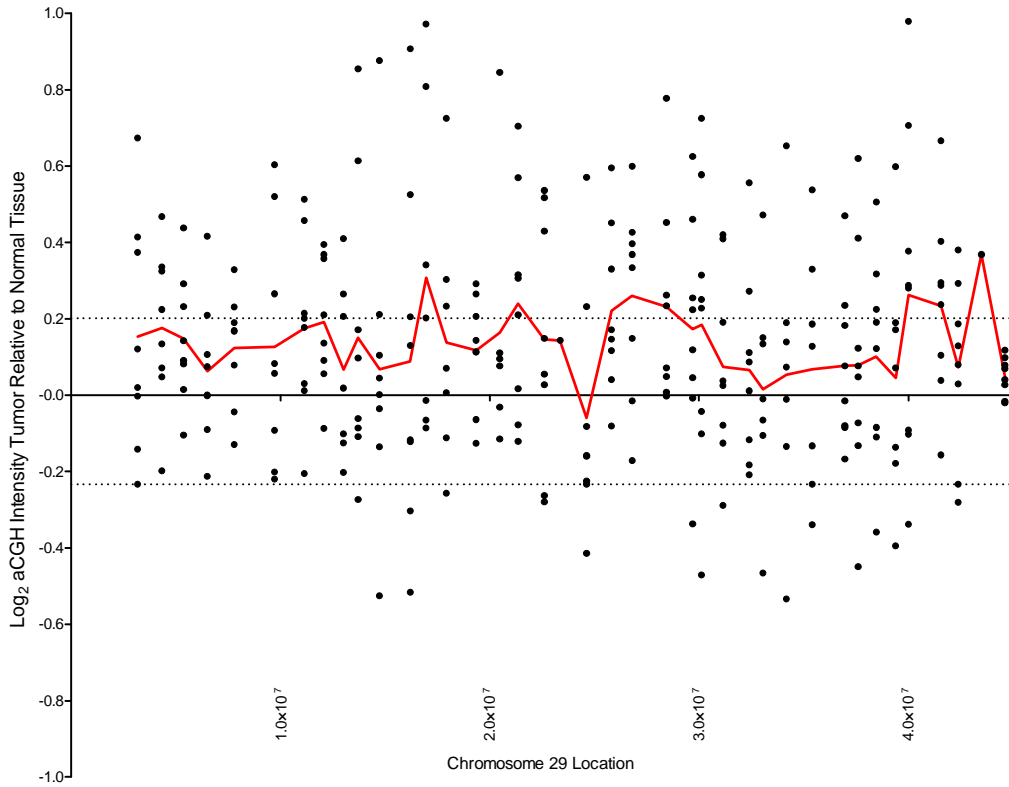
Chromosome 27



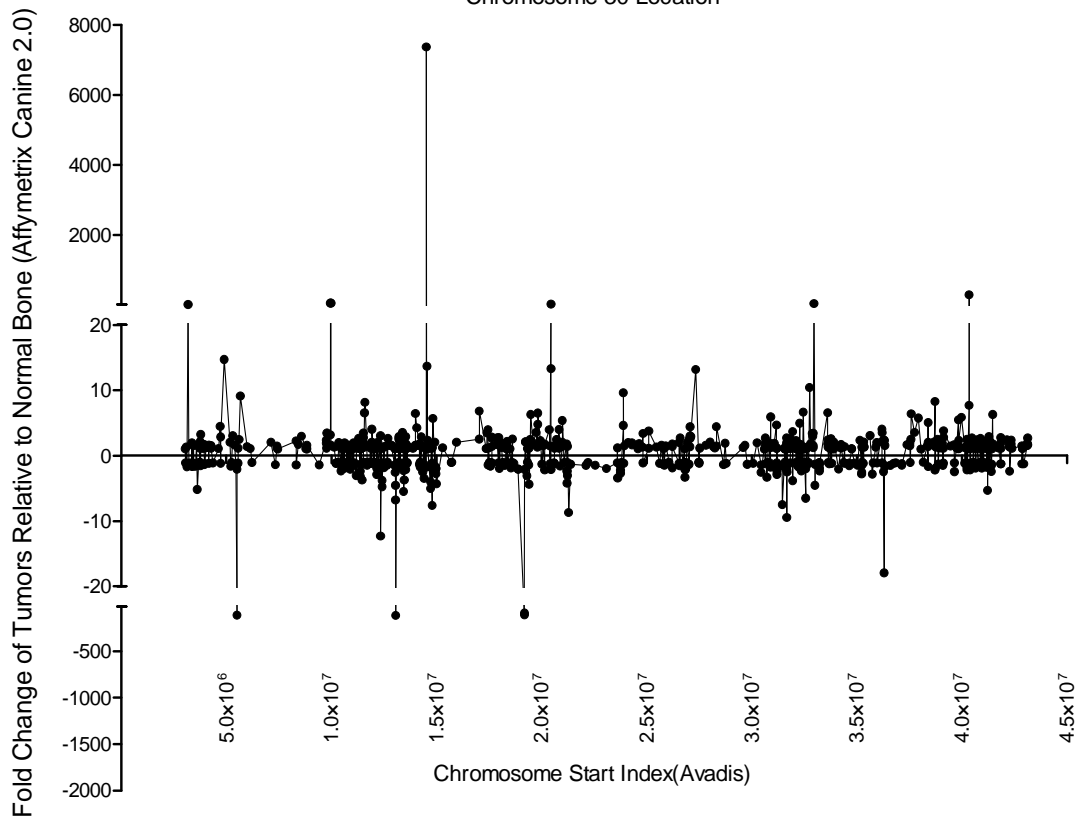
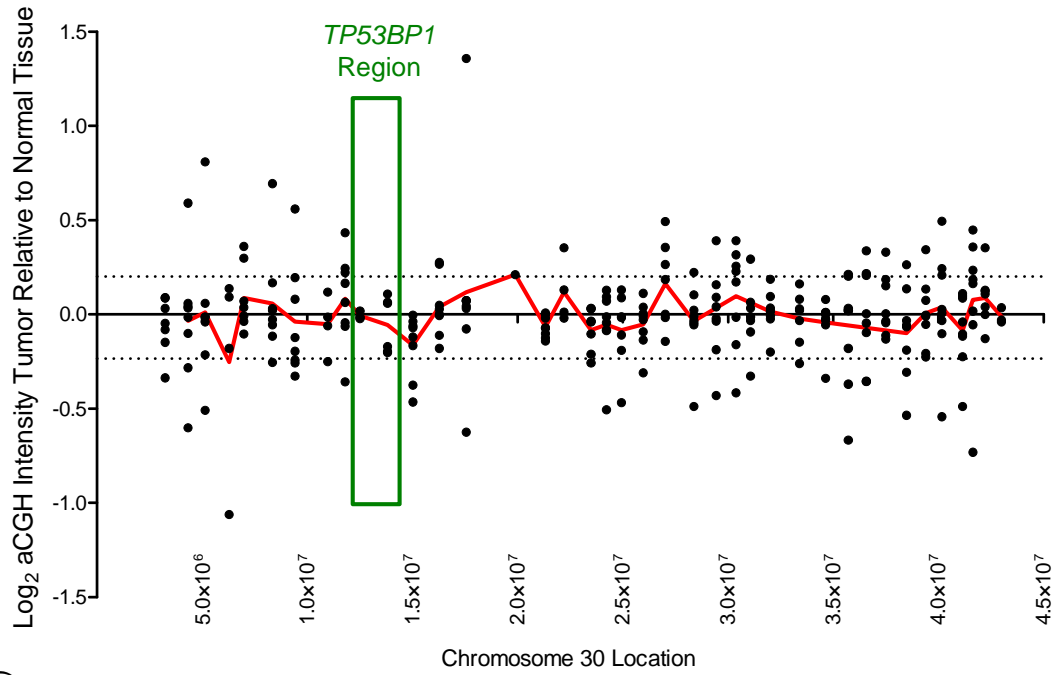
Chromosome 28



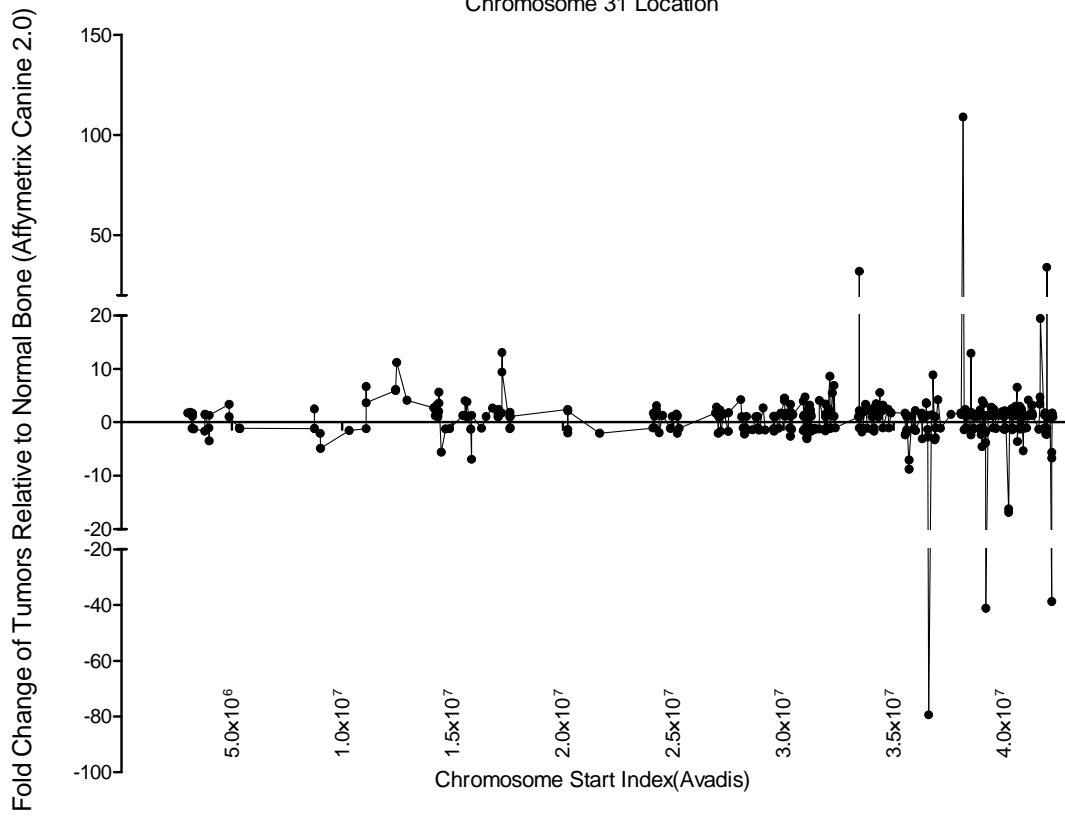
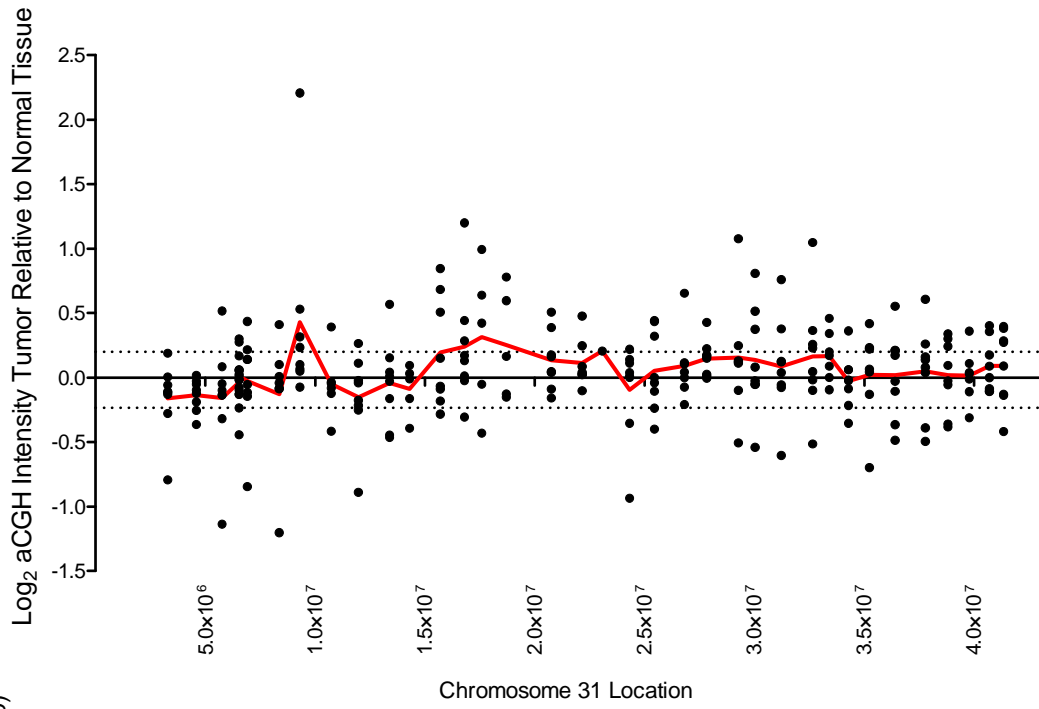
Chromosome 29



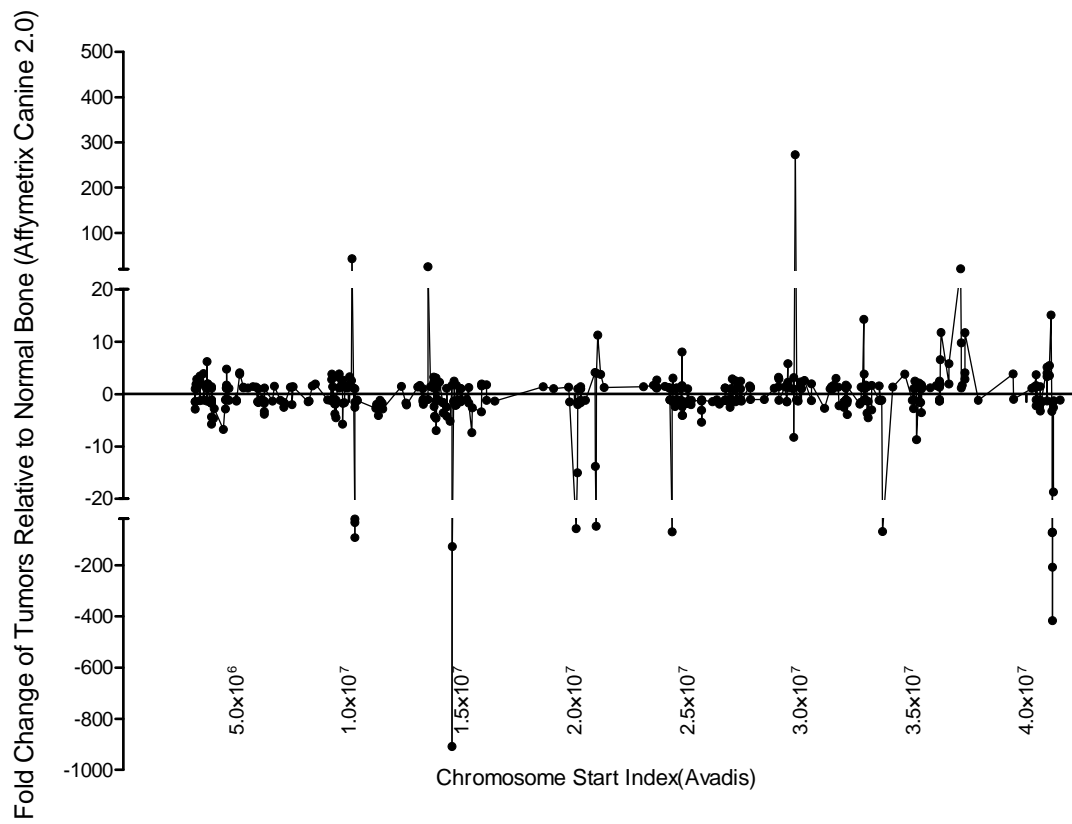
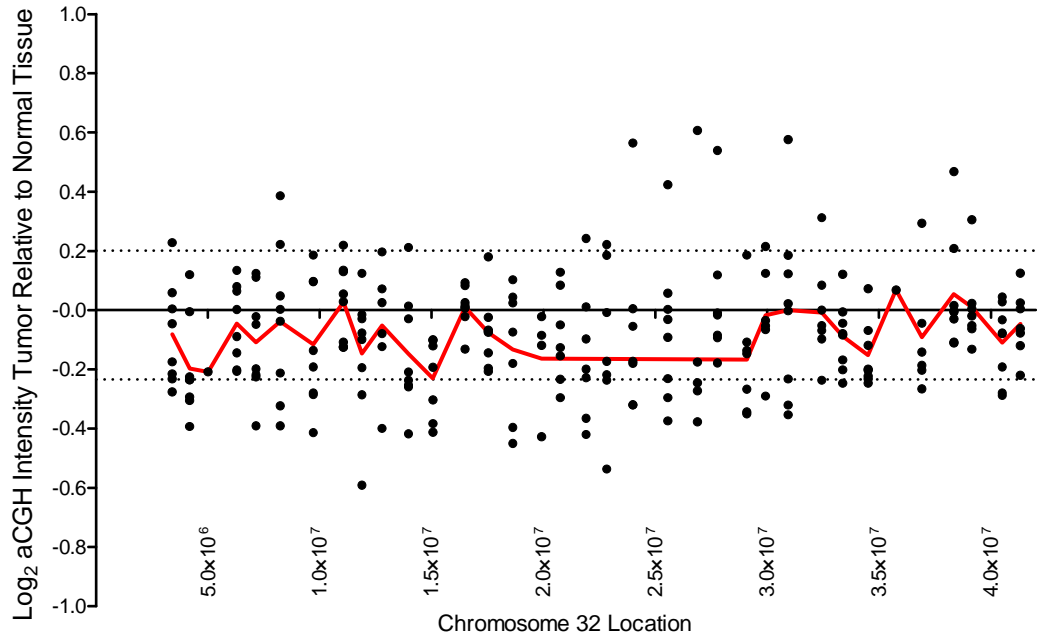
Chromosome 30



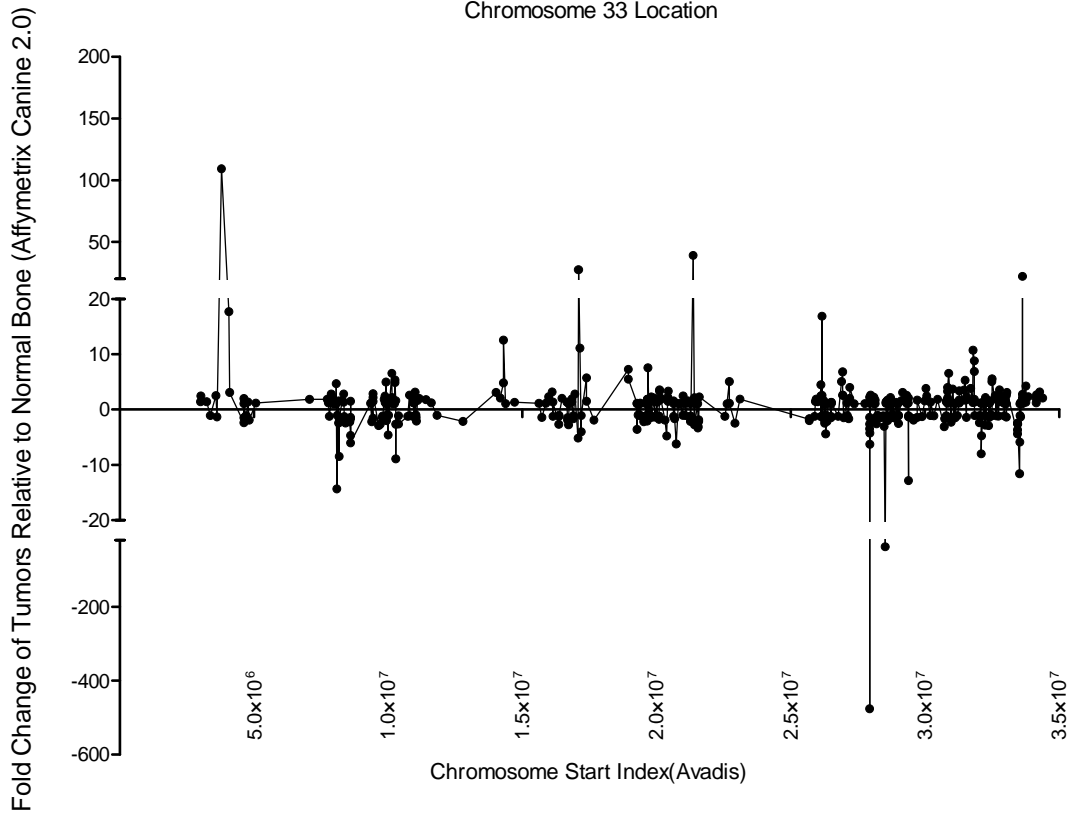
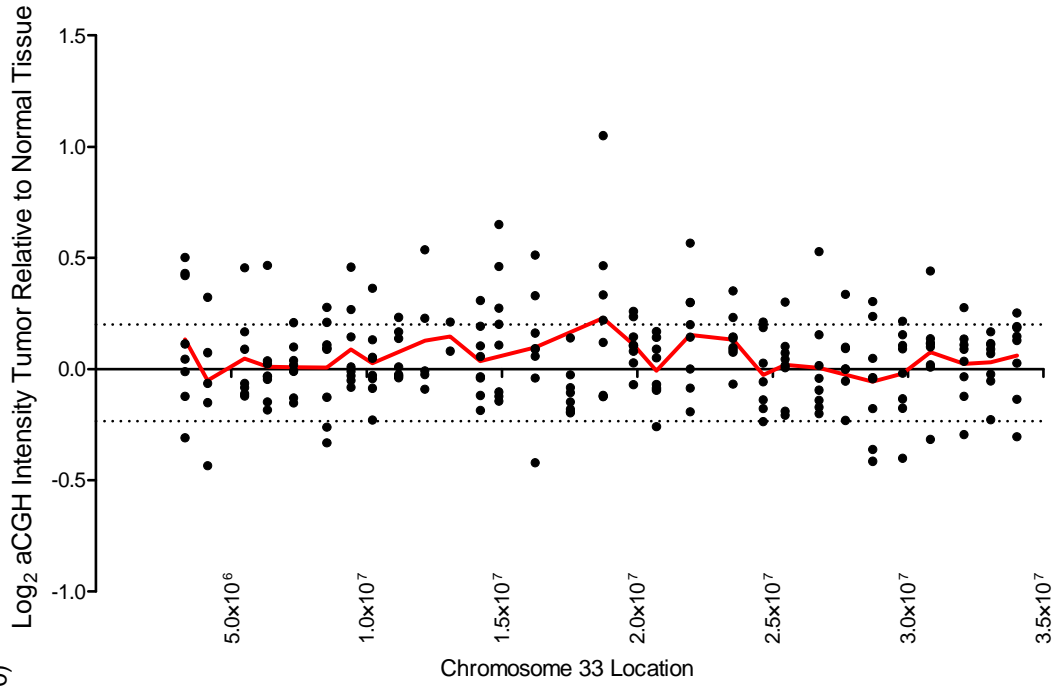
Chromosome 31



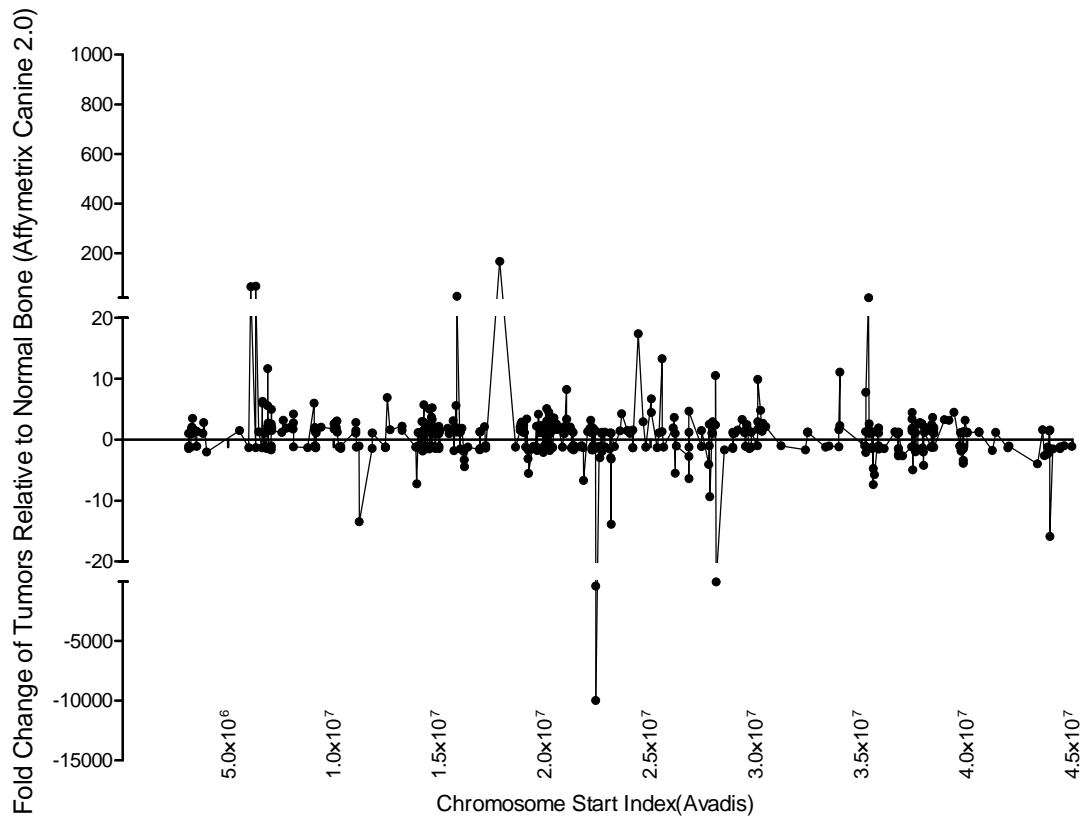
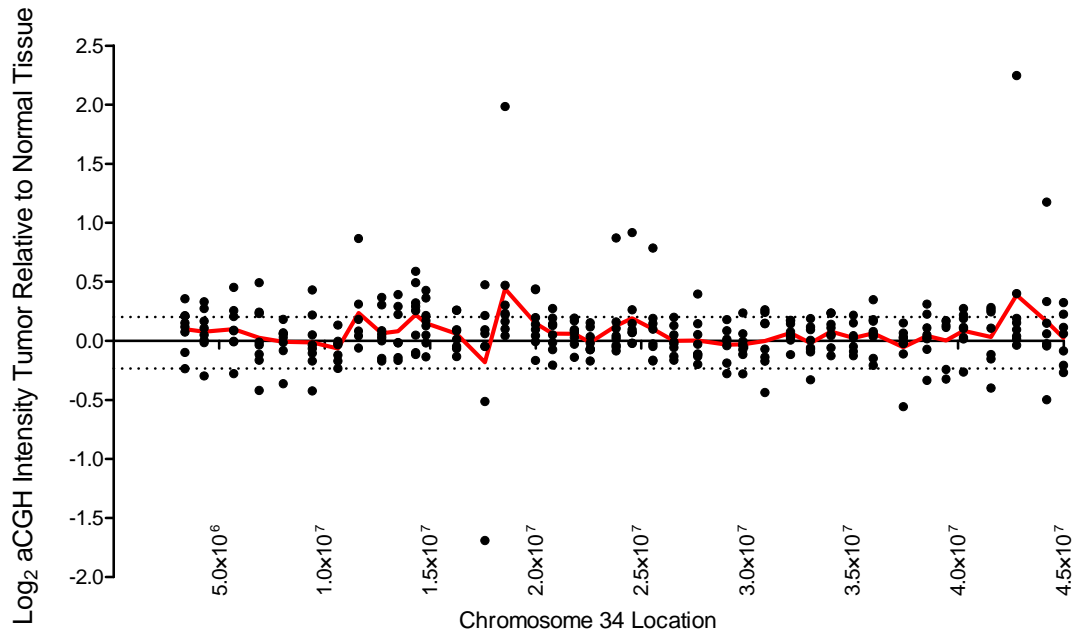
Chromosome 32



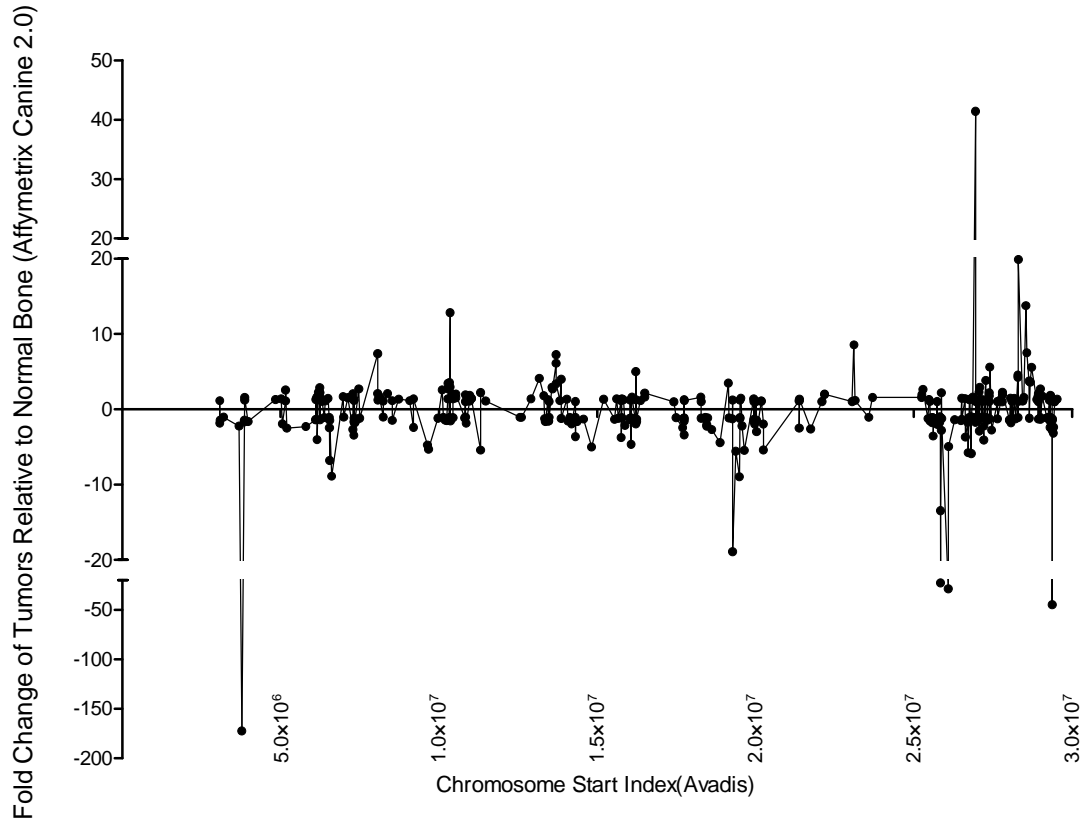
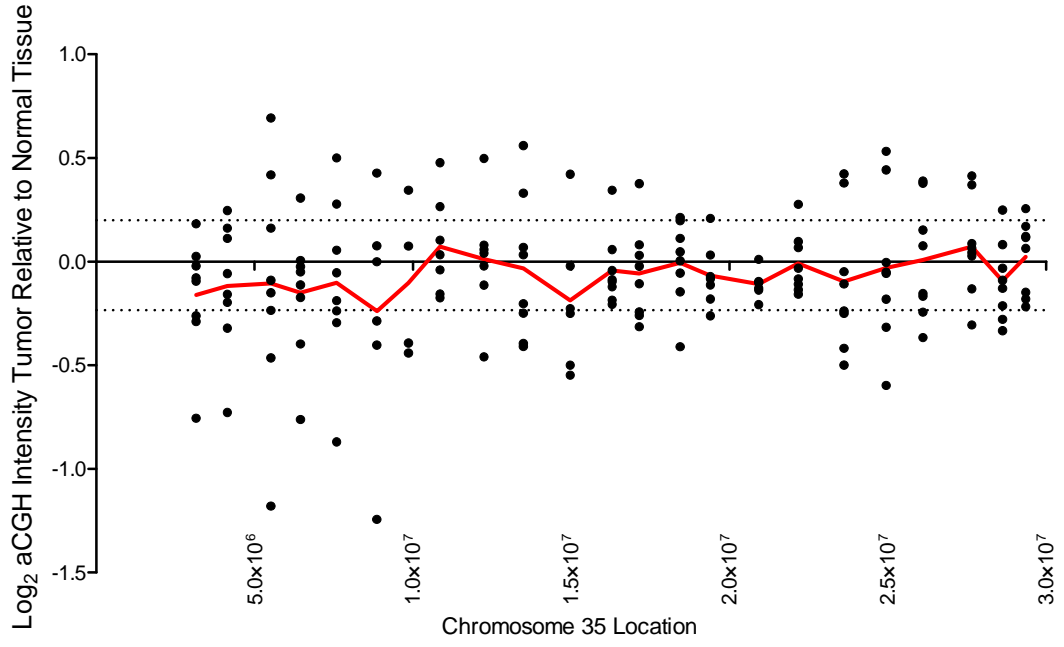
Chromosome 33



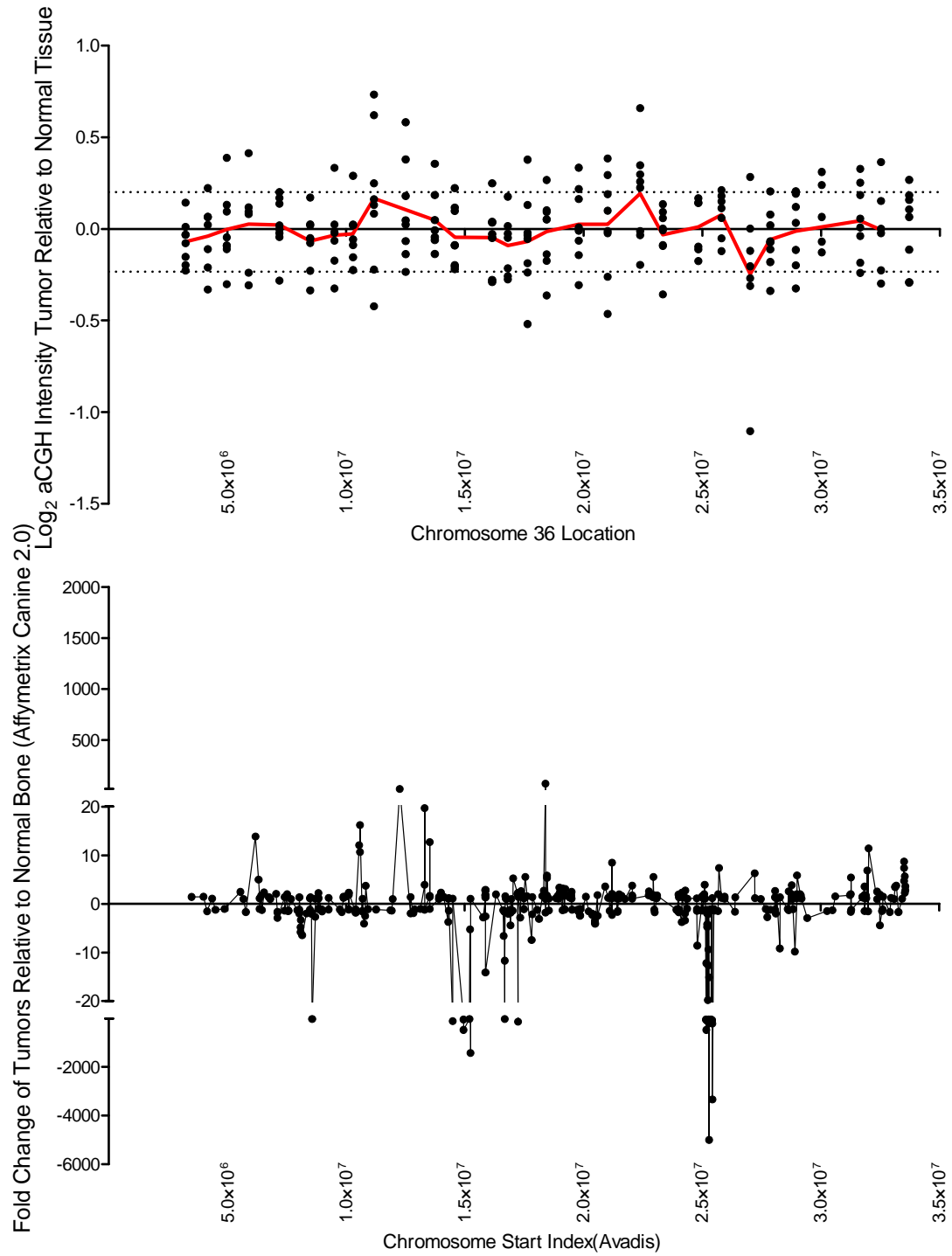
Chromosome 34



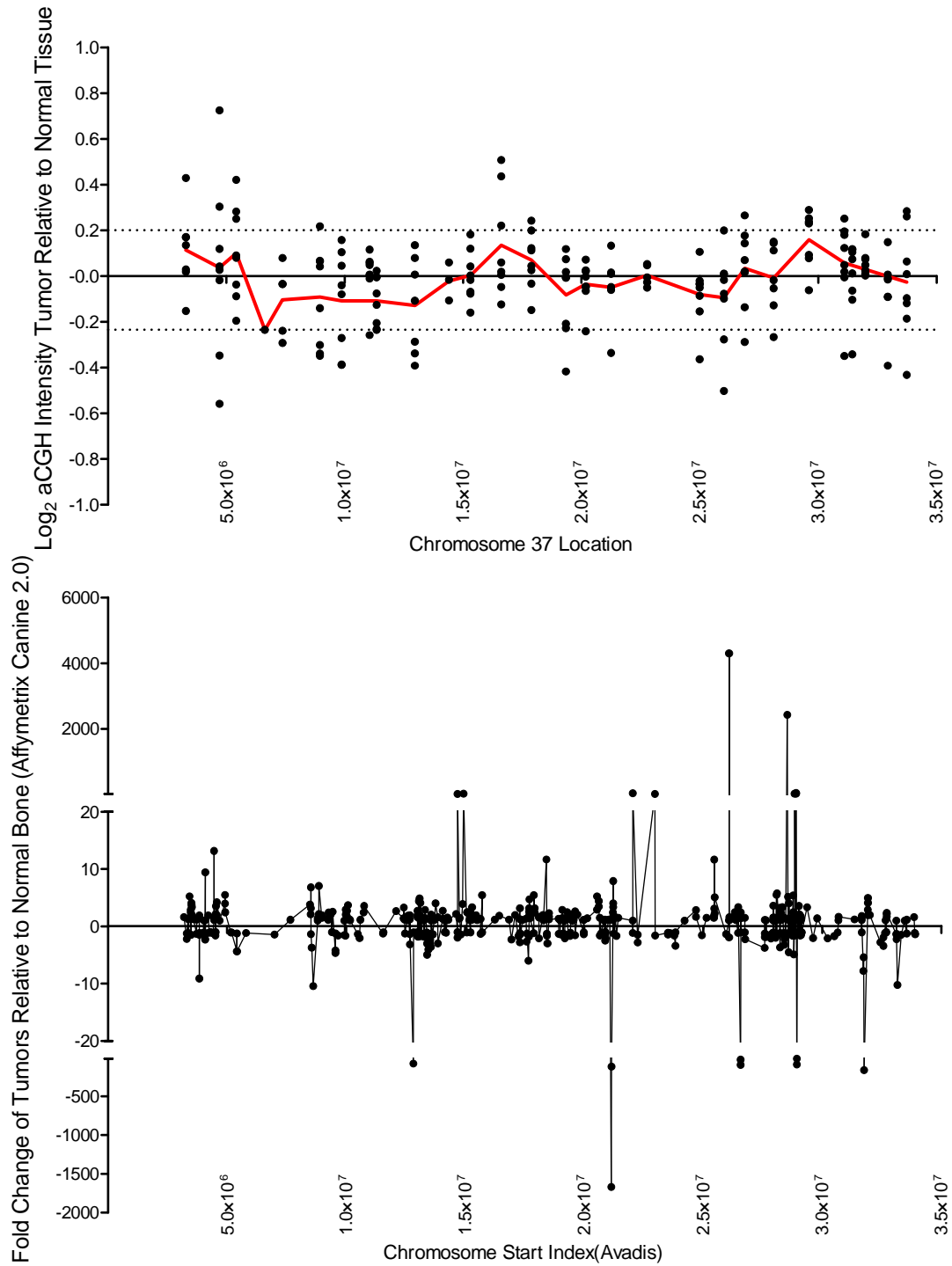
Chromosome 35



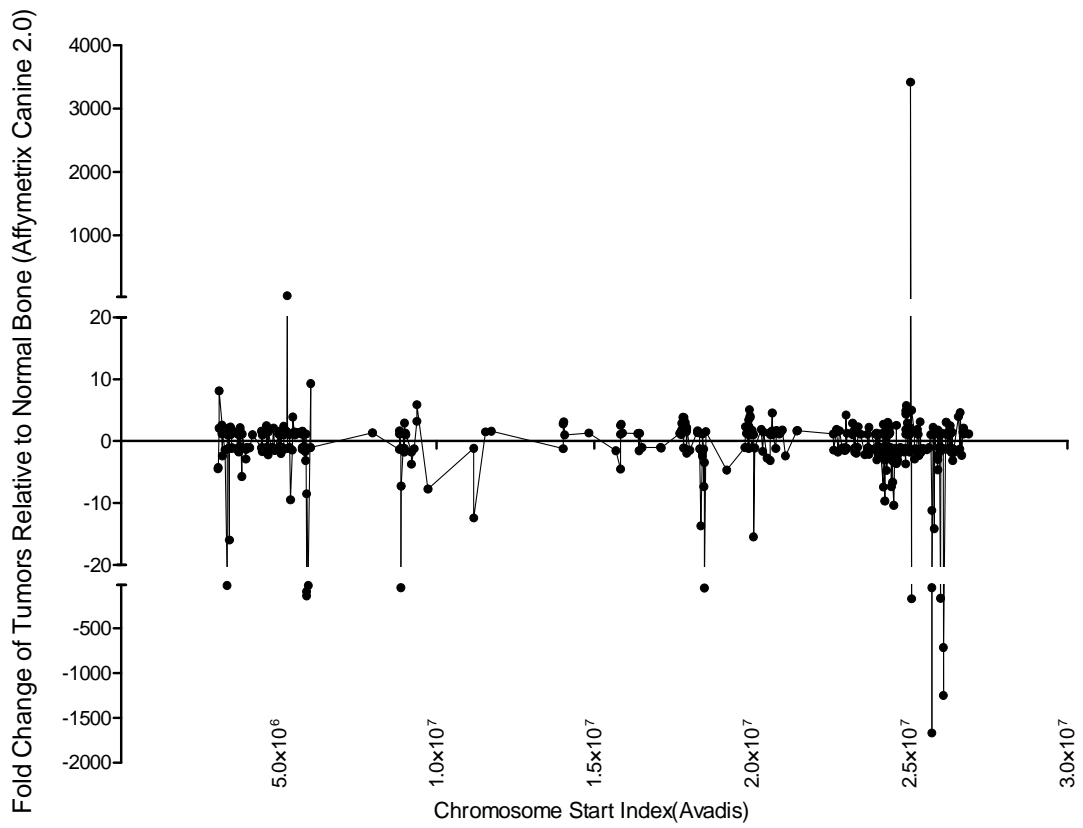
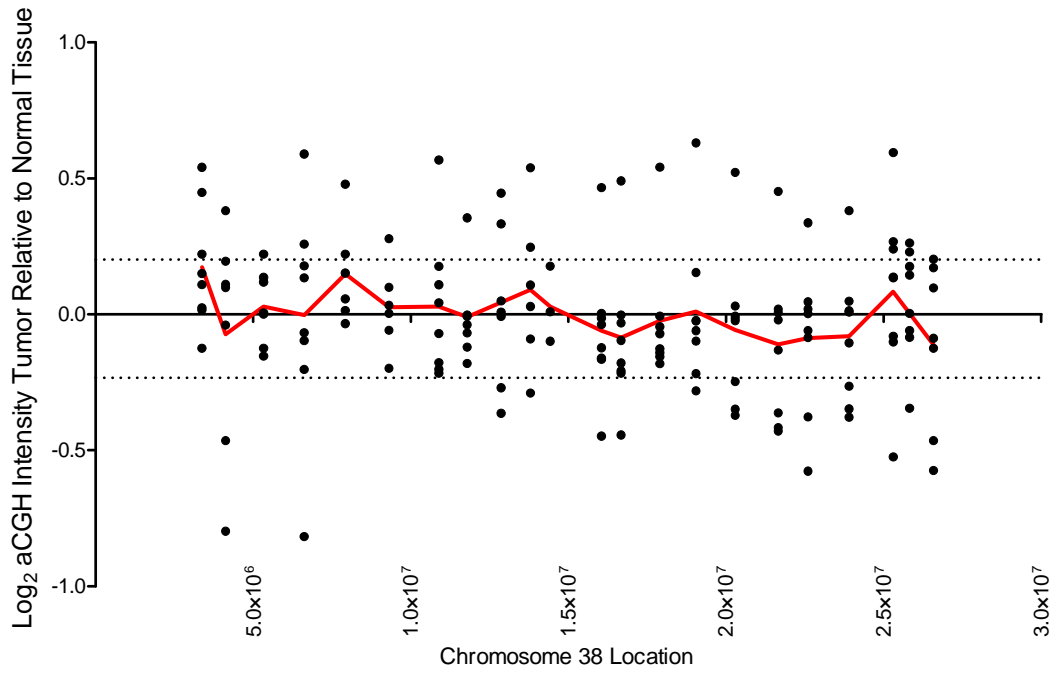
Chromosome 36



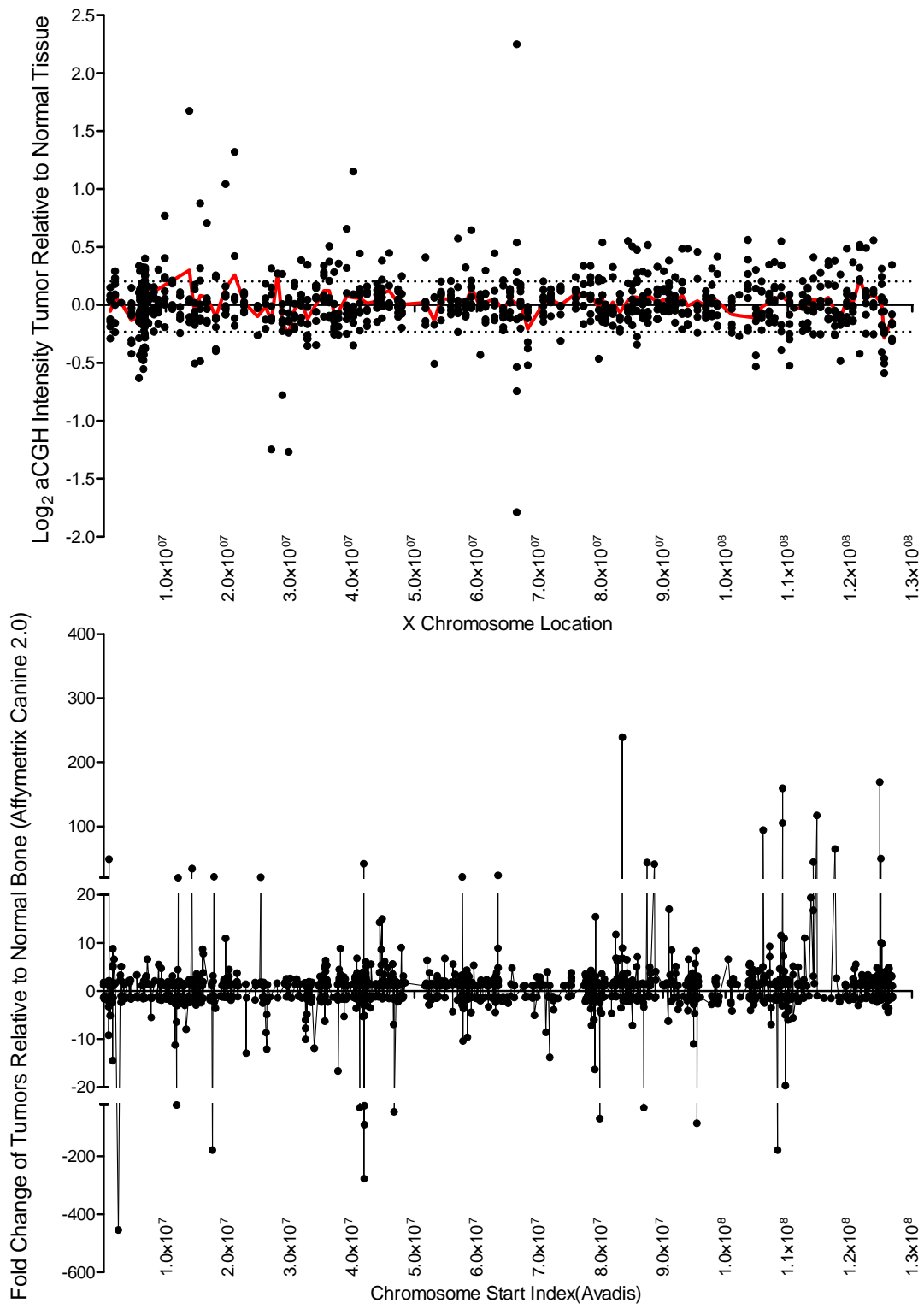
Chromosome 37



Chromosome 38



X Chromosome



Appendix D

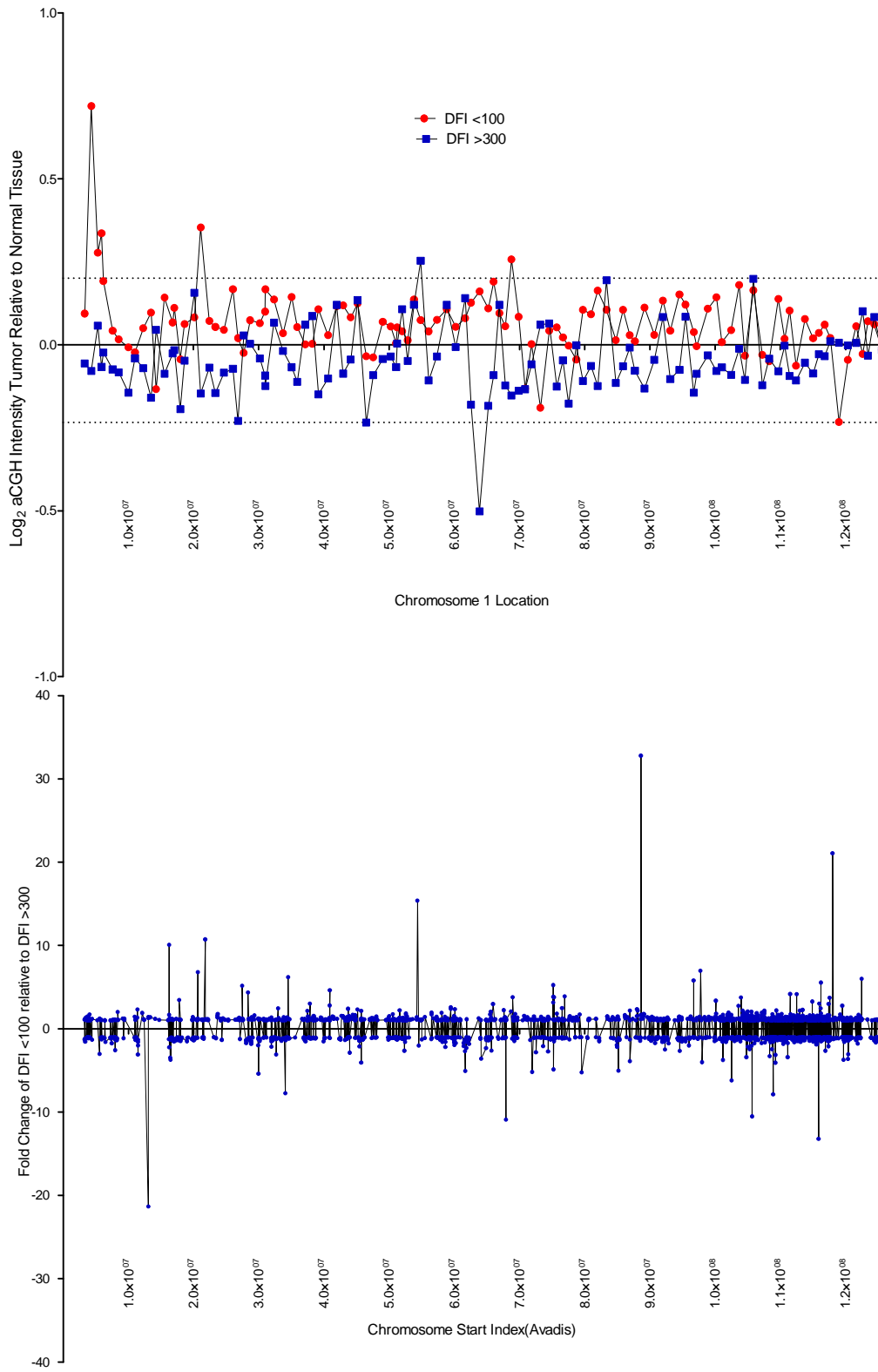
Chrosomal Expression Maps: Array Comparative Genomic Hybridization versus Microarrays for Good- and Poor-Responder Tumors

X-axes = chromosomal location of probe

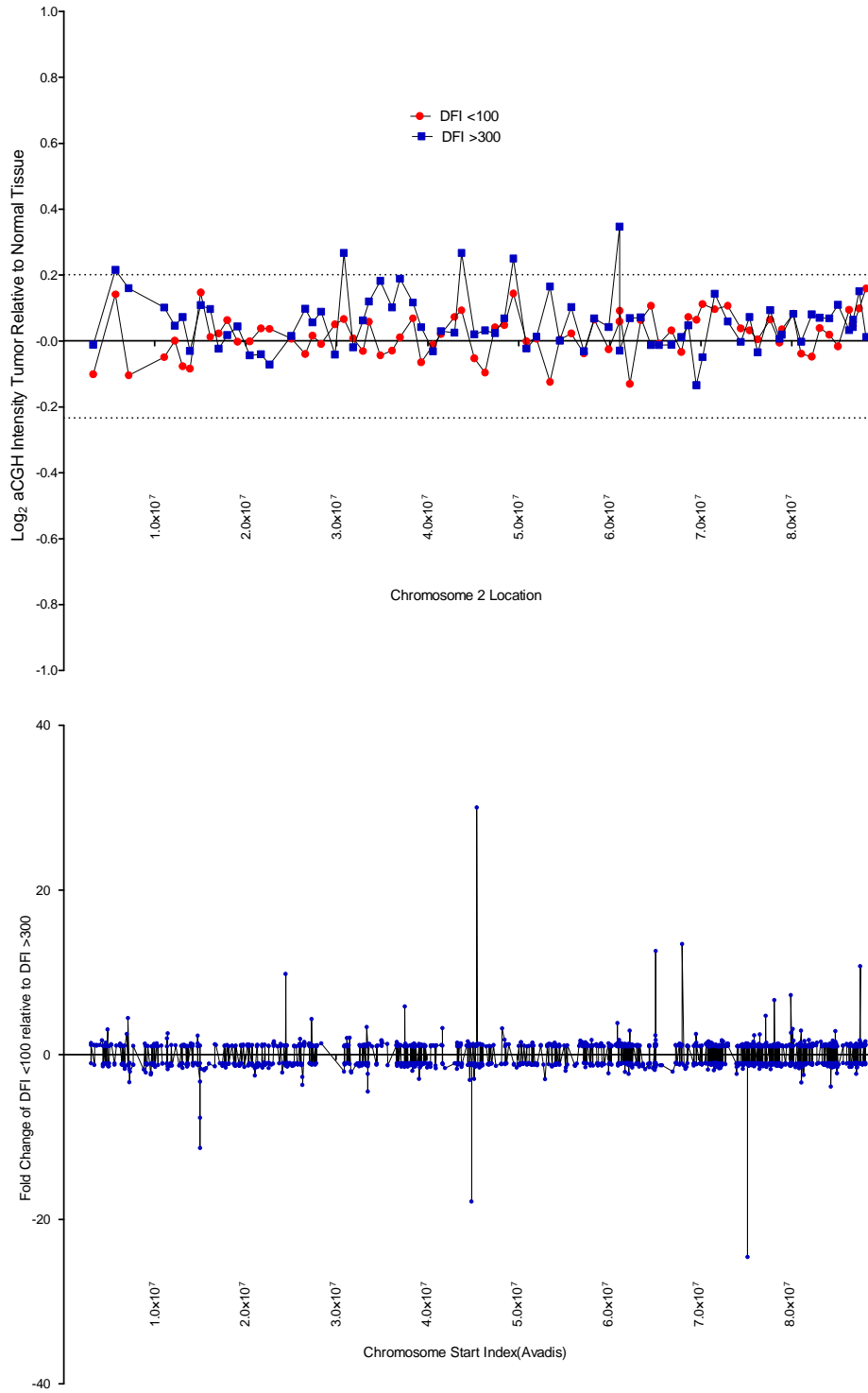
Y-axis (aCGH, top half of page) = hybridization intensity poor-responder tumor (DFI<100, n=4, red circles) relative to paired normal tissue and good responder tumor (DFI>300, n=4, blue squares) relative to paired normal tissue. Thresholds for amplification and deletion are represented by dashed lines intersecting the Y axis at 0.201 and -0.234 respectively. Means of four samples per group are plotted.

Y-axis (Affymetrix, bottom half of page) = fold change poor-responder primary tumors (n=8) relative to good-responder primary tumors (n=7)

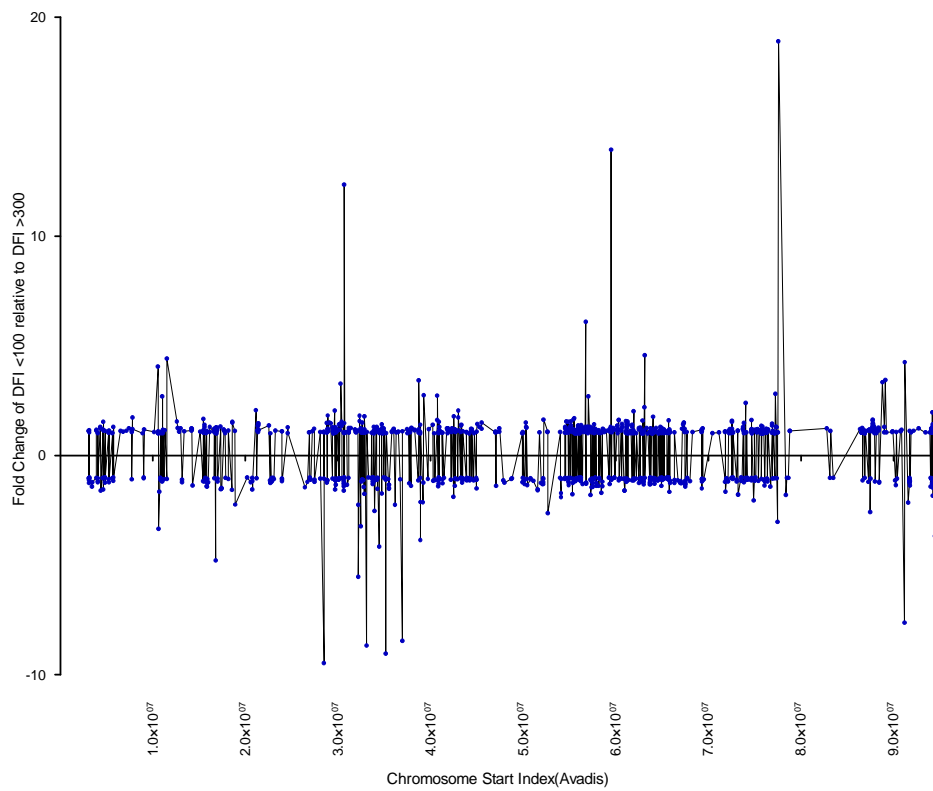
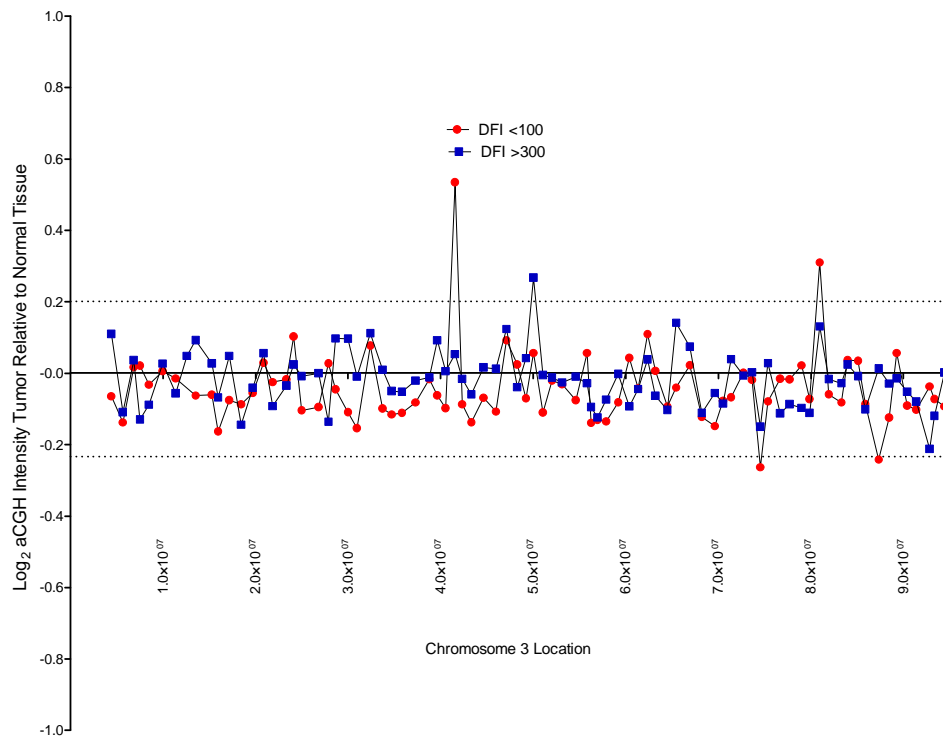
Chromosome 1



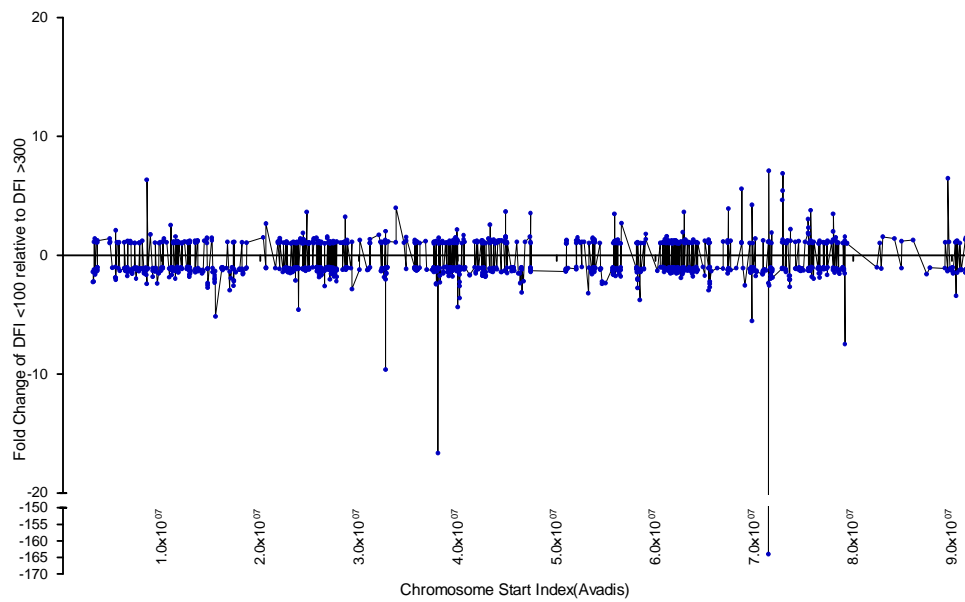
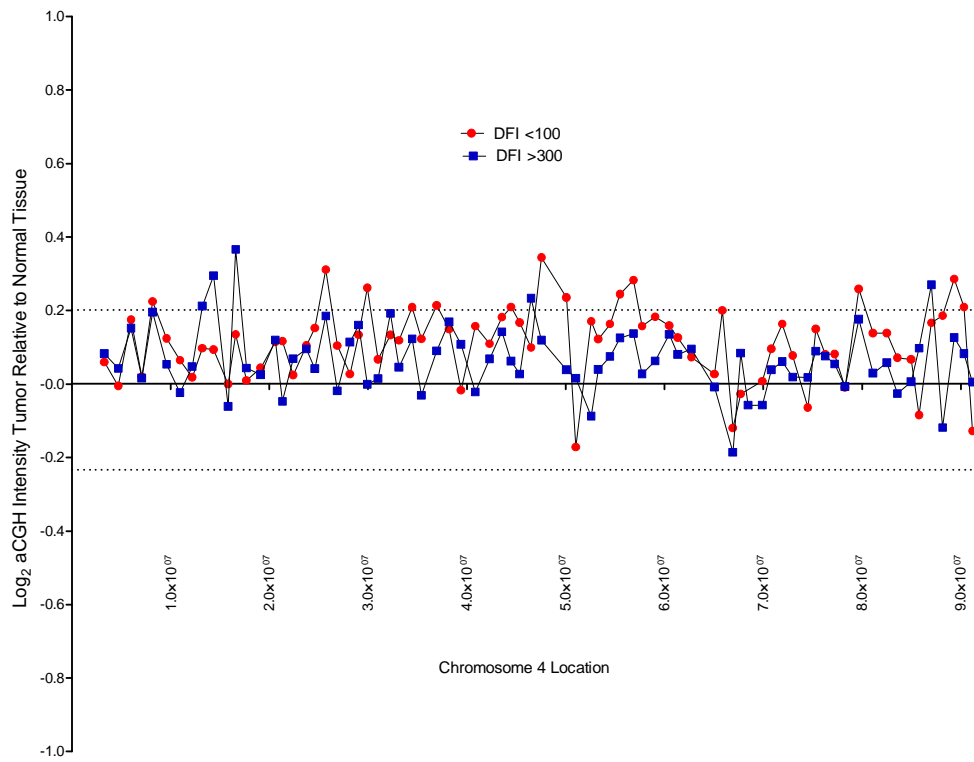
Chromosome 2



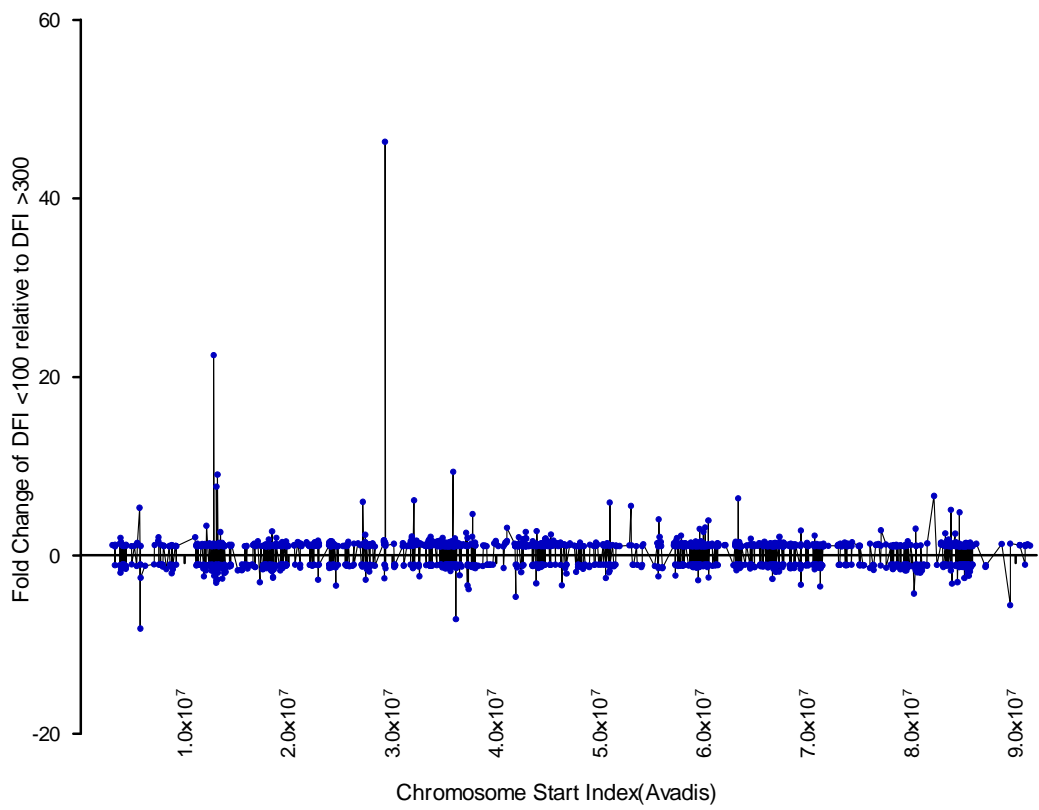
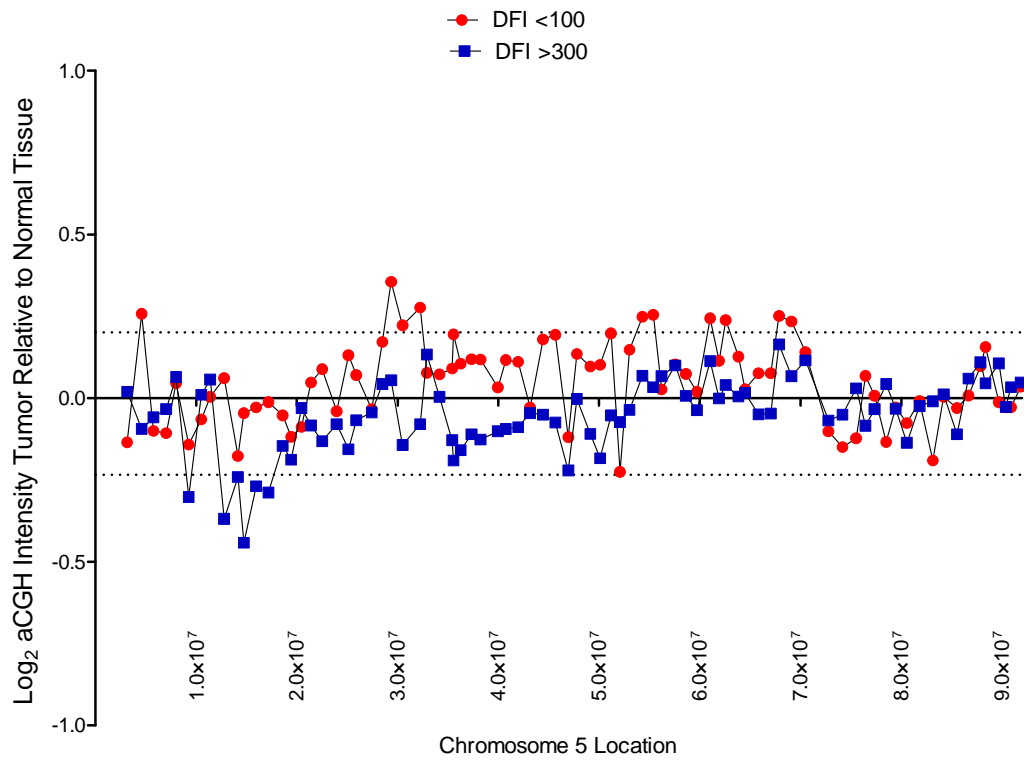
Chromosome 3



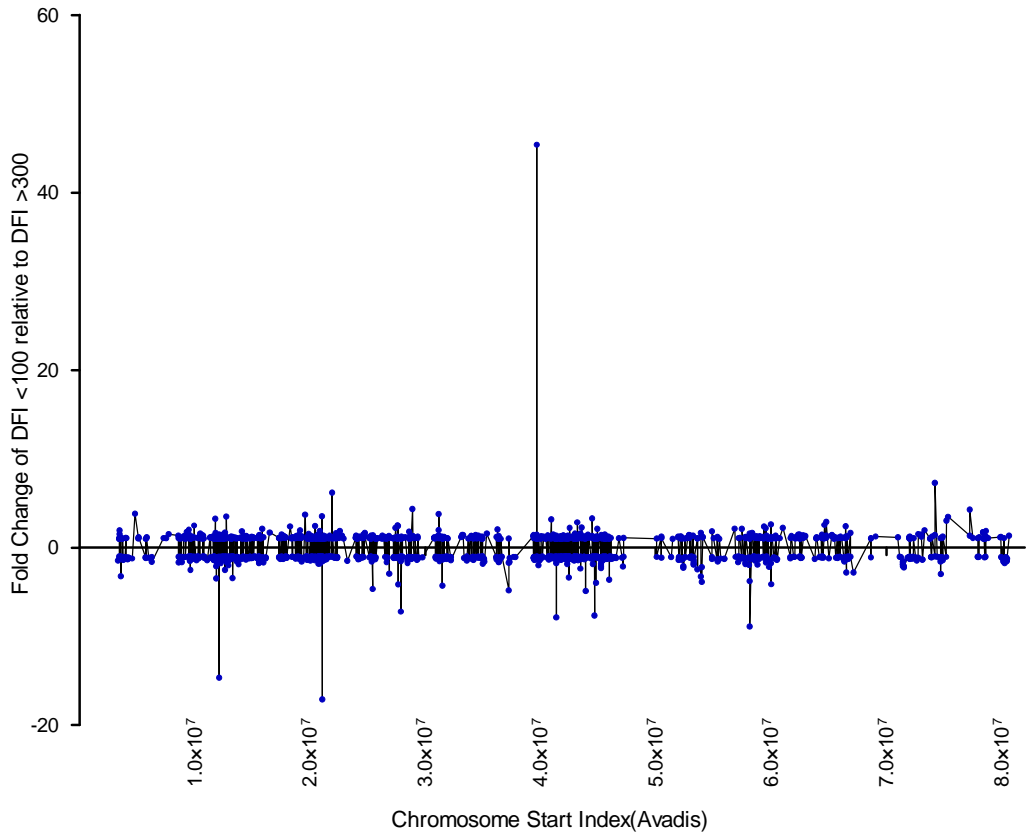
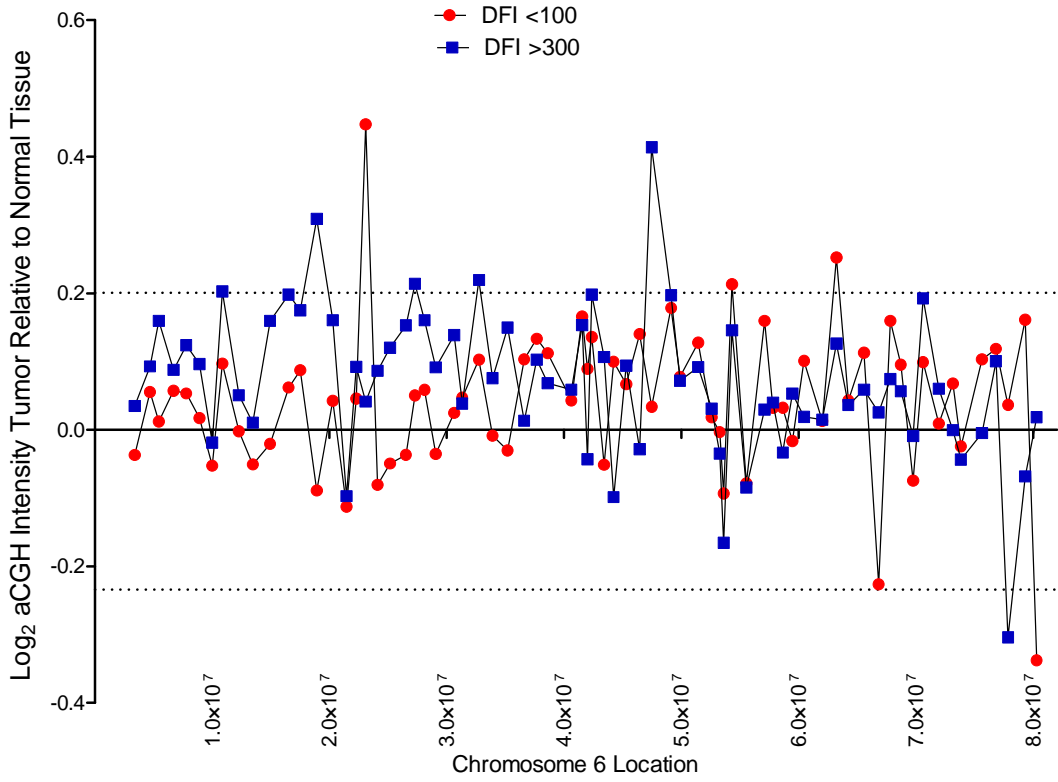
Chromosome 4



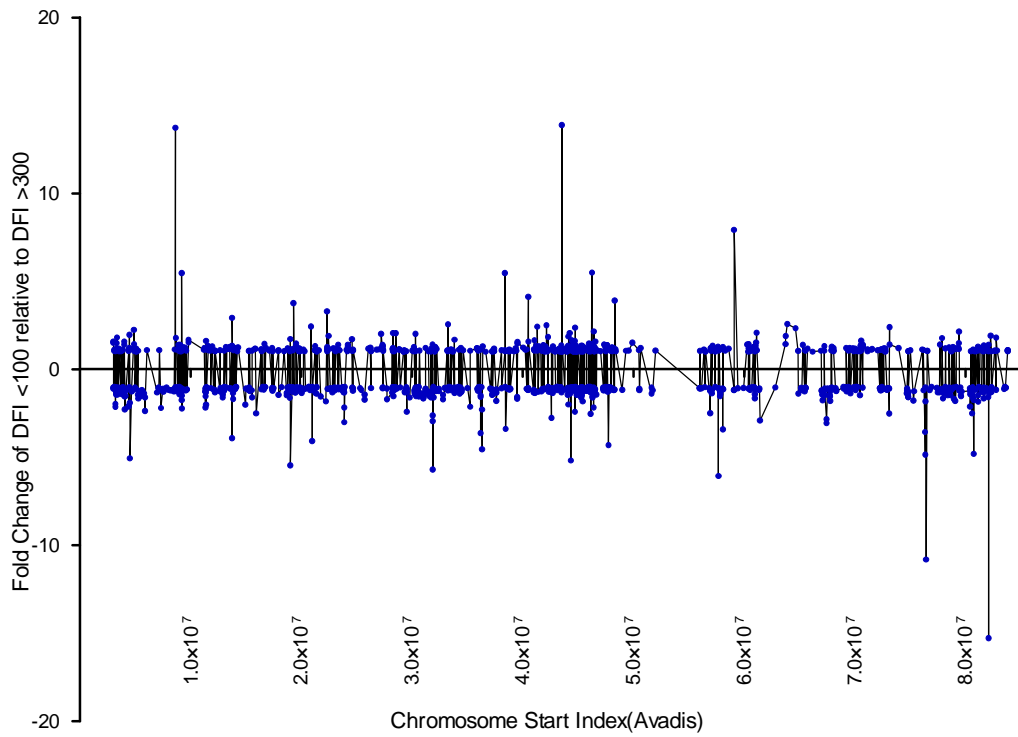
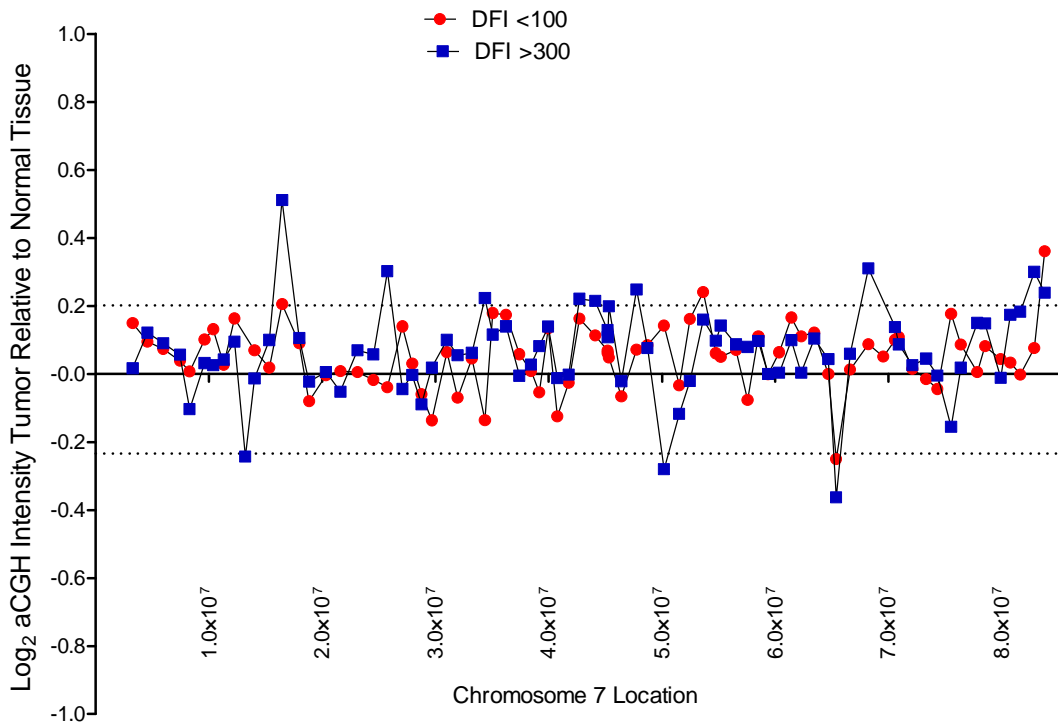
Chromosome 5



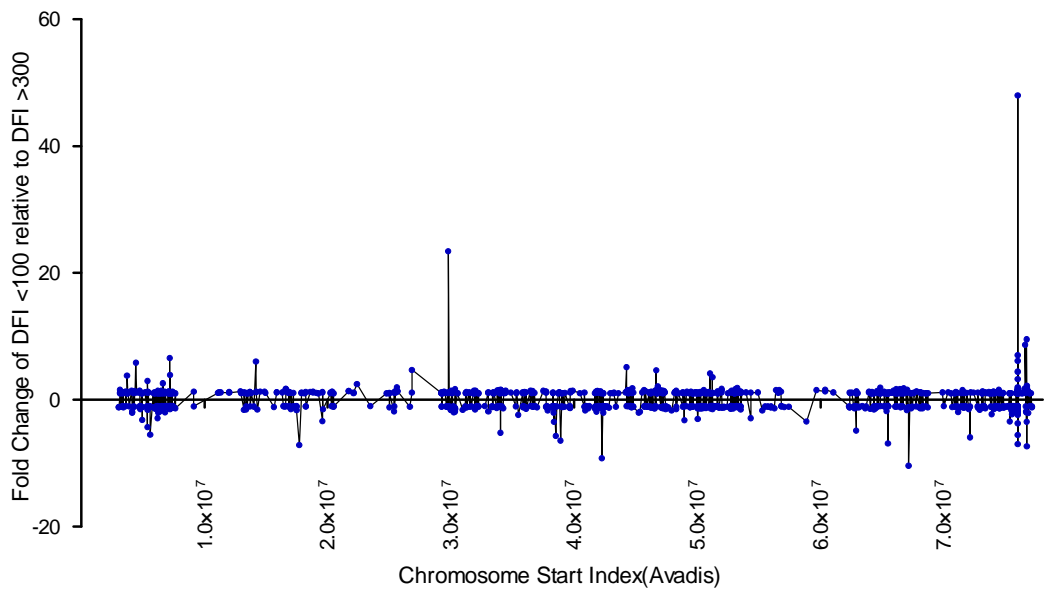
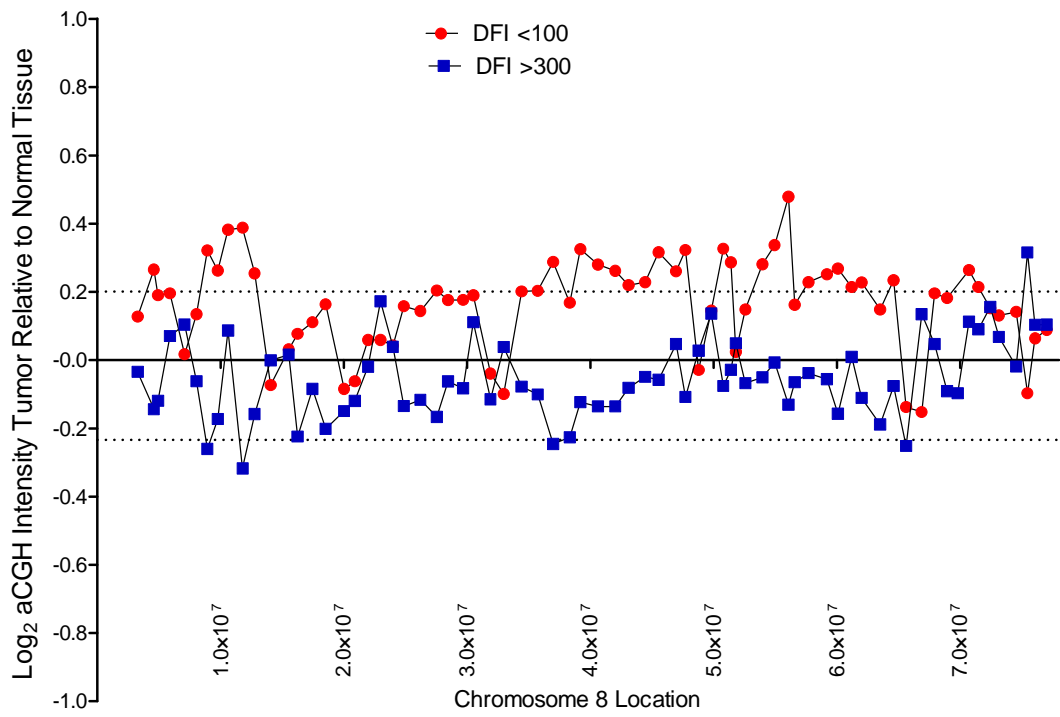
Chromosome 6



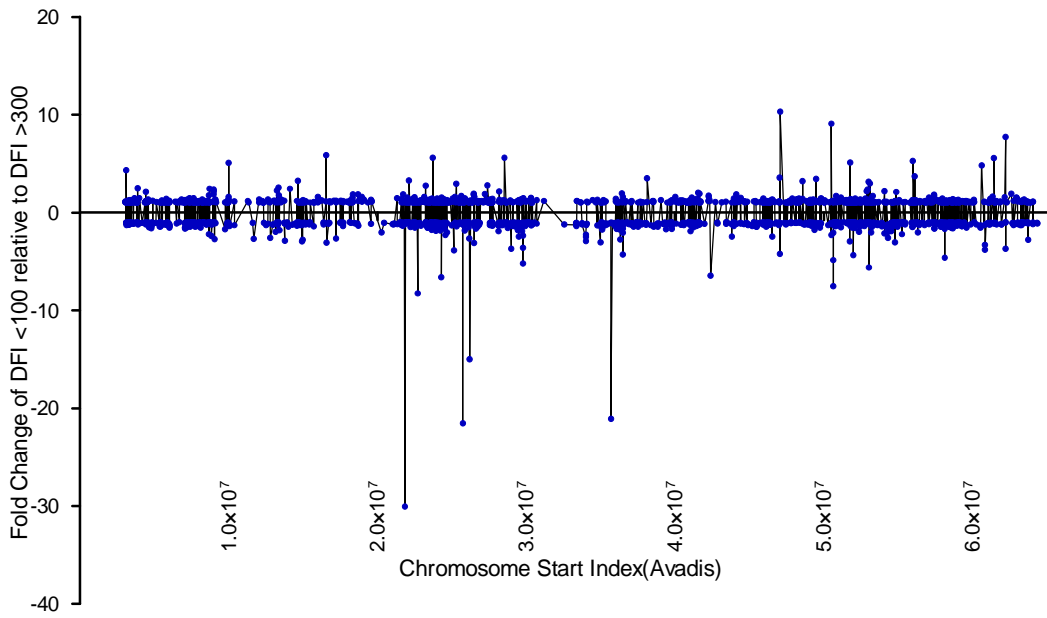
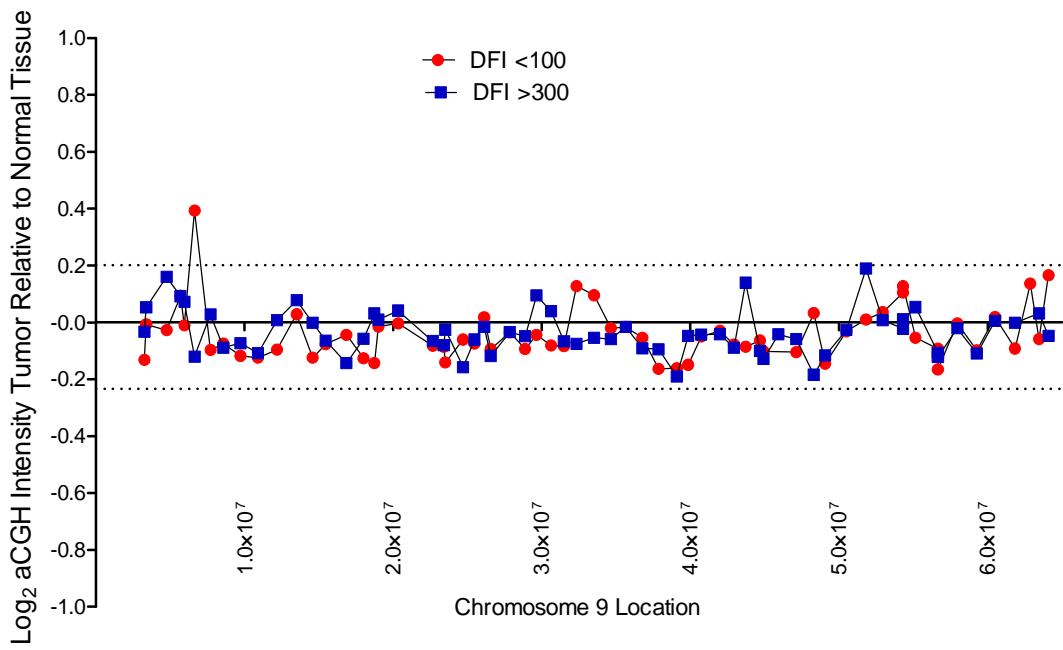
Chromosome 7



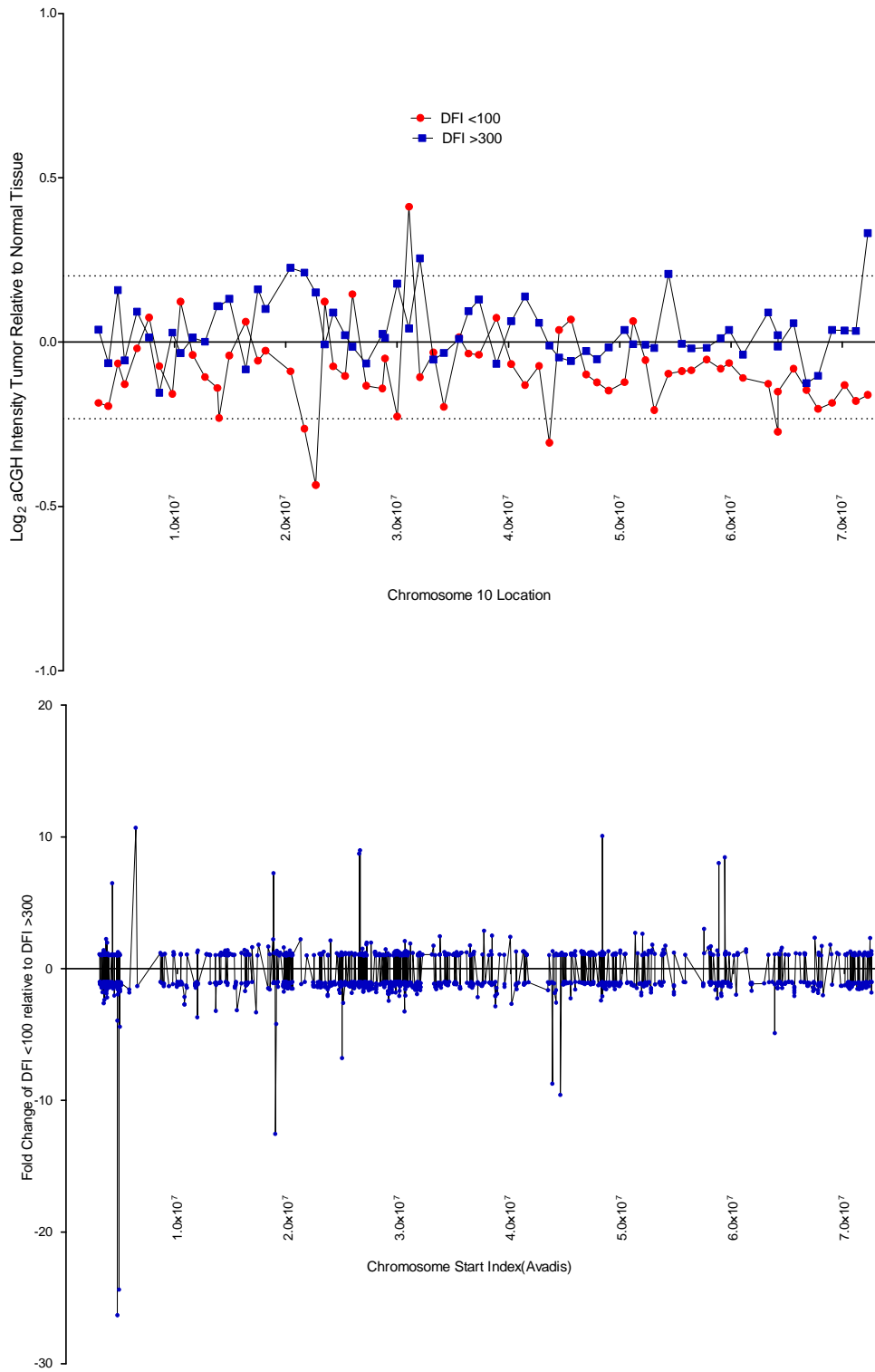
Chromosome 8



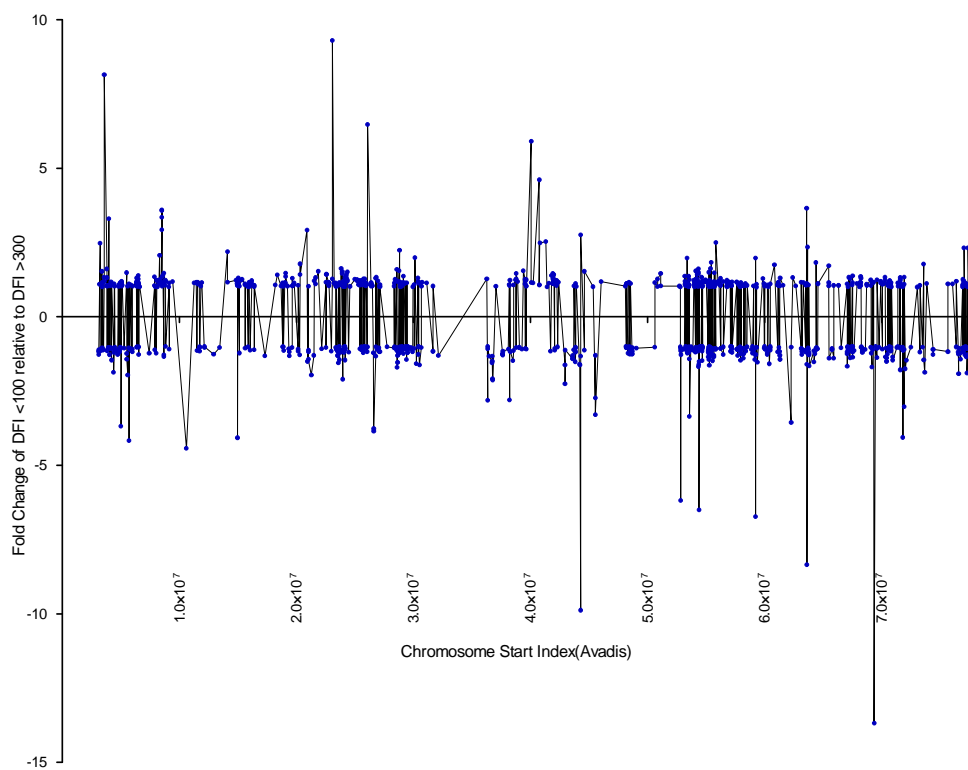
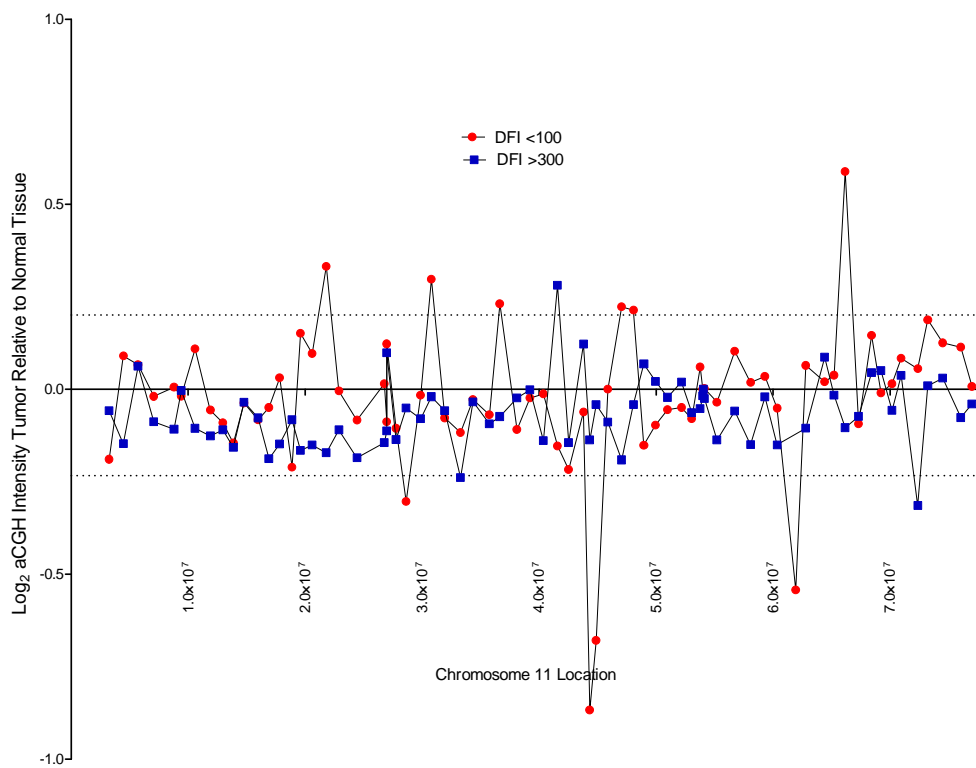
Chromosome 9



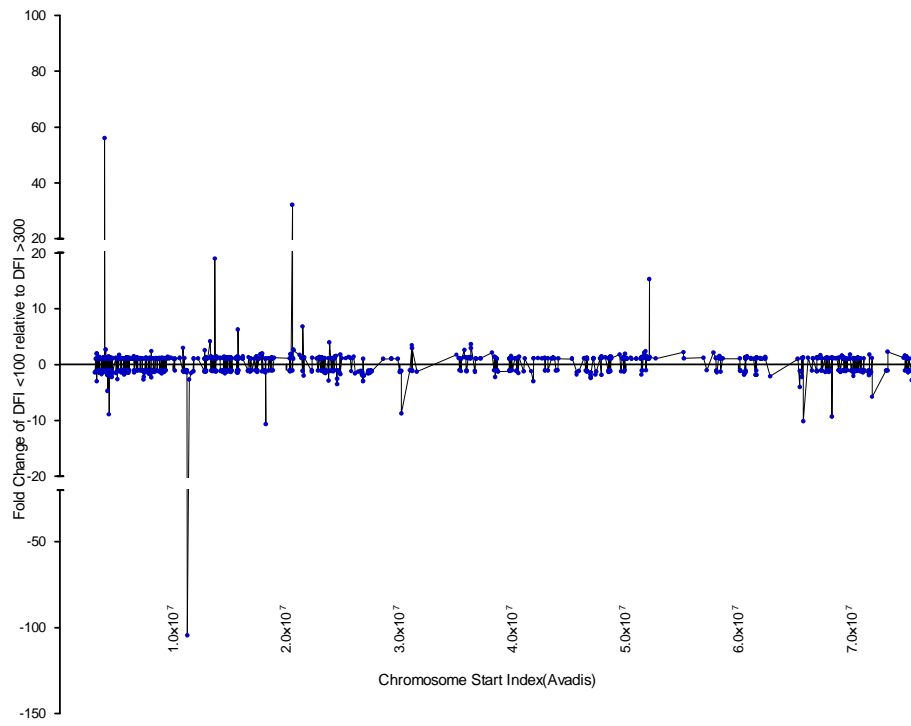
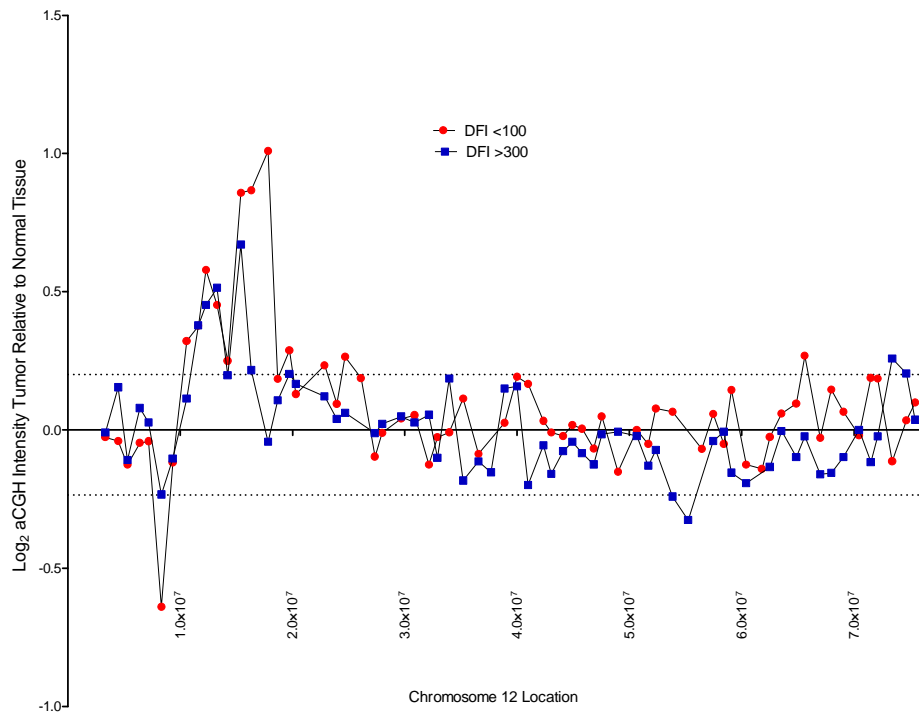
Chromosome 10



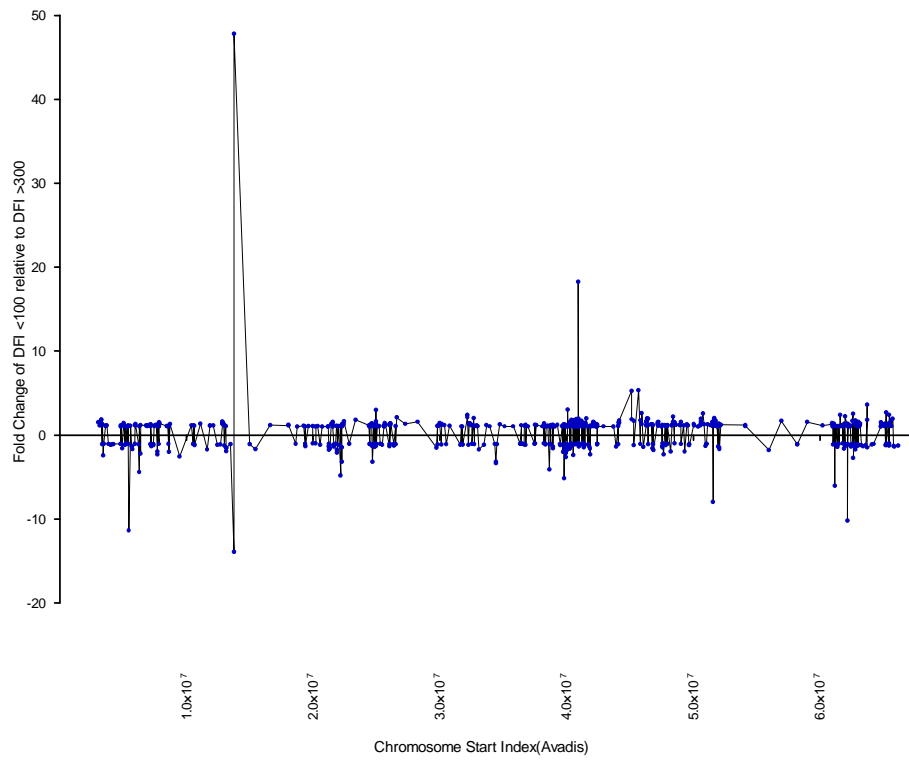
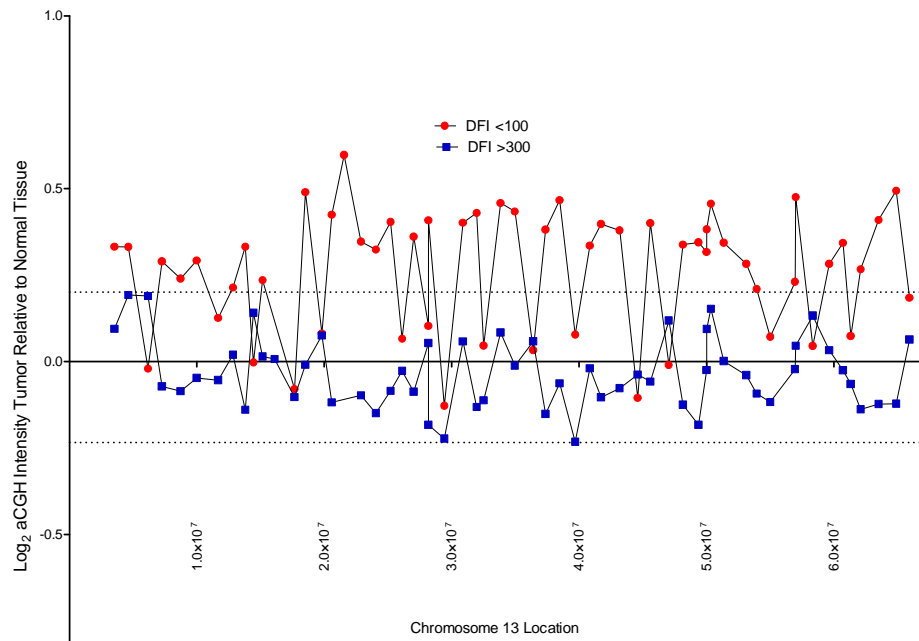
Chromosome 11



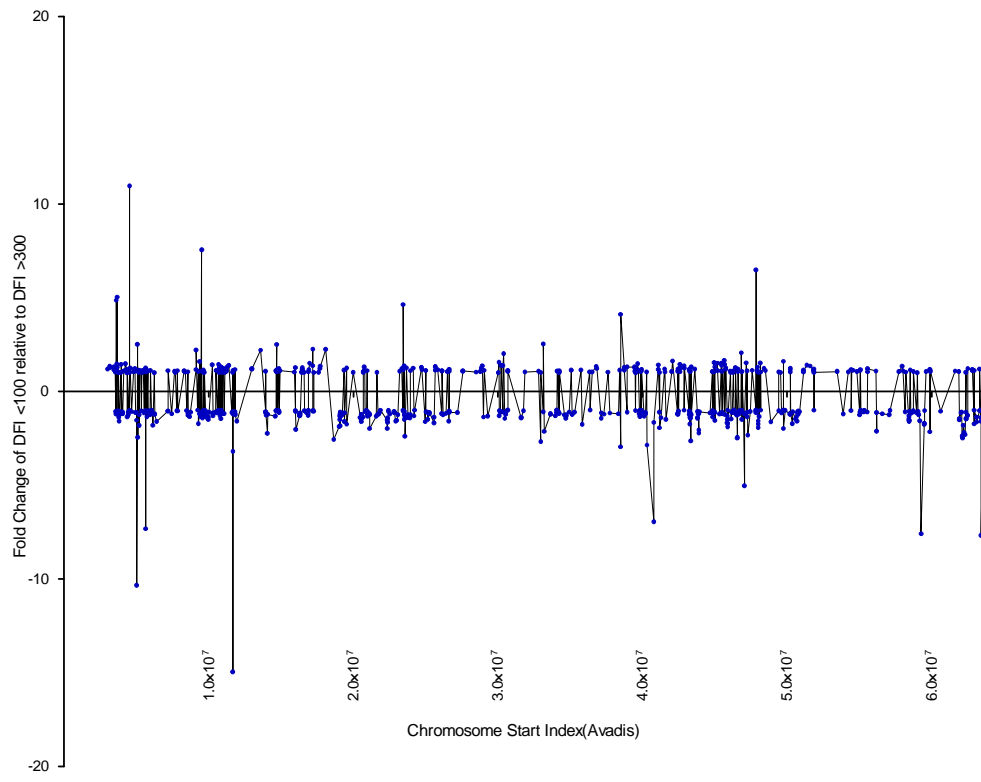
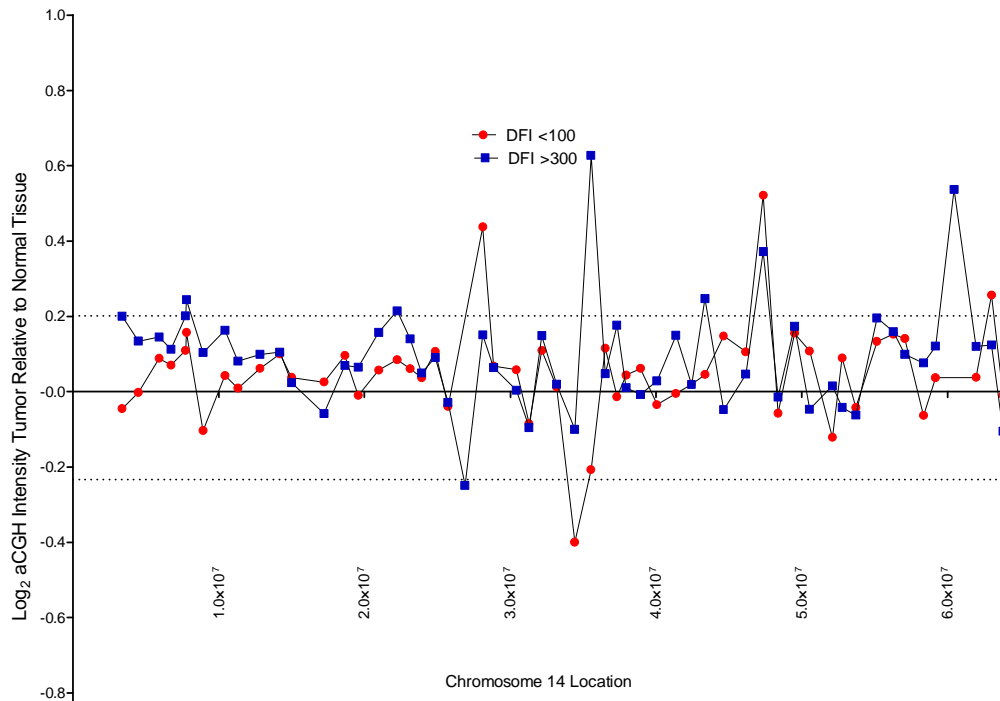
Chromosome 12



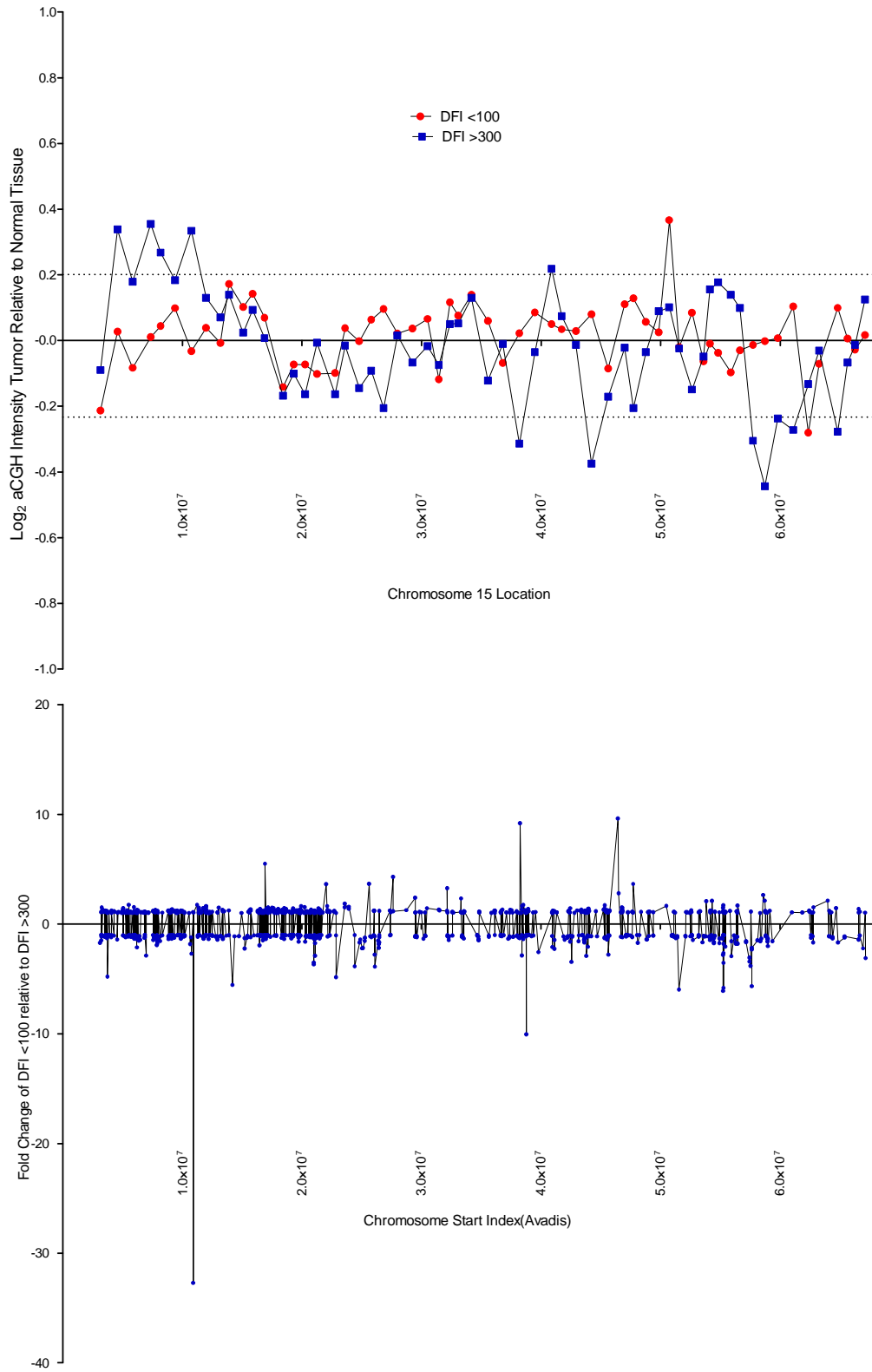
Chromosome 13



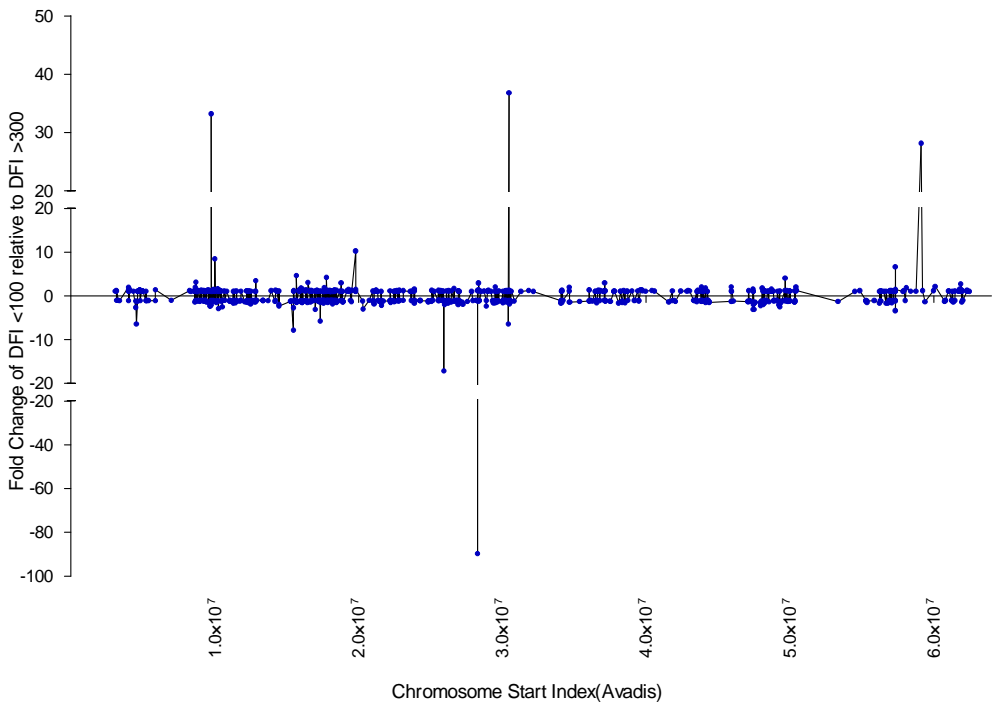
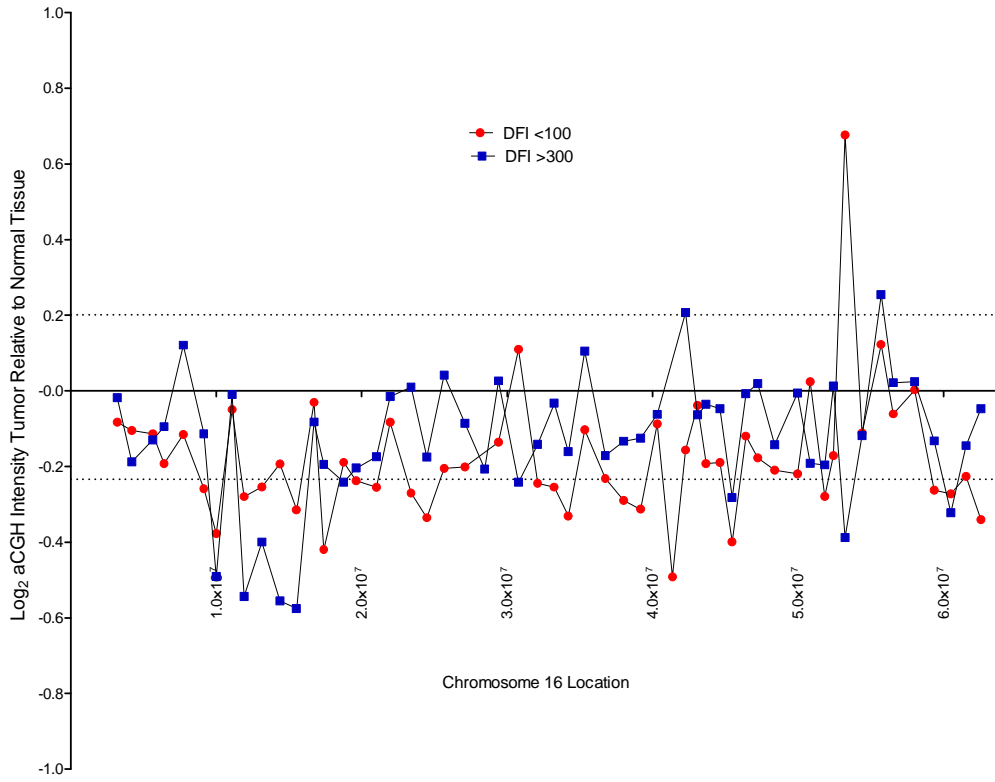
Chromosome 14



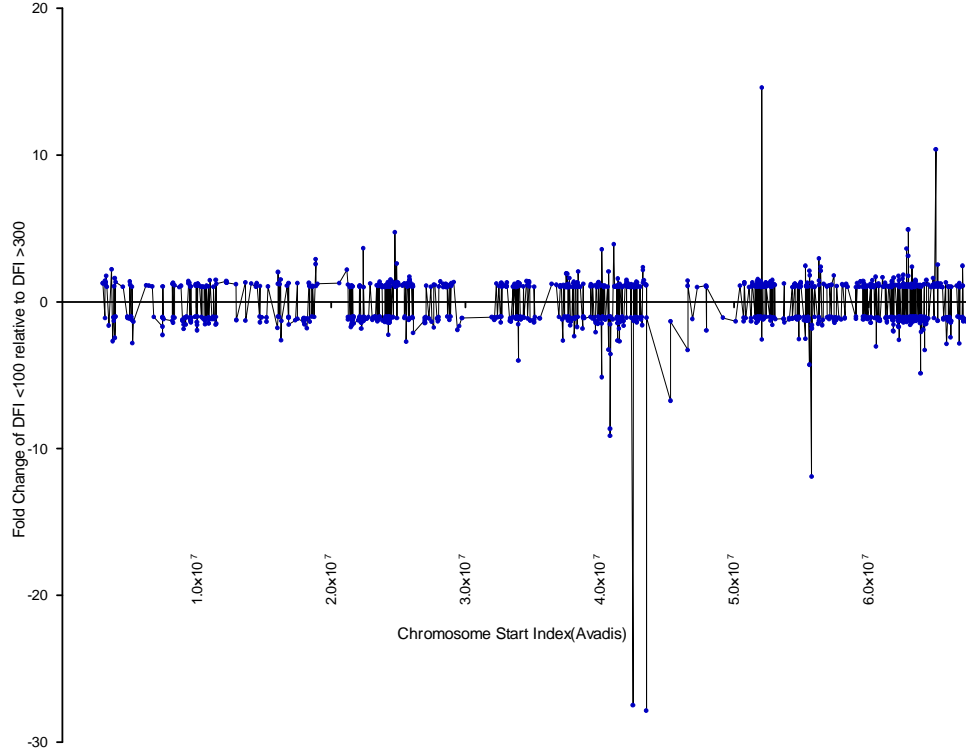
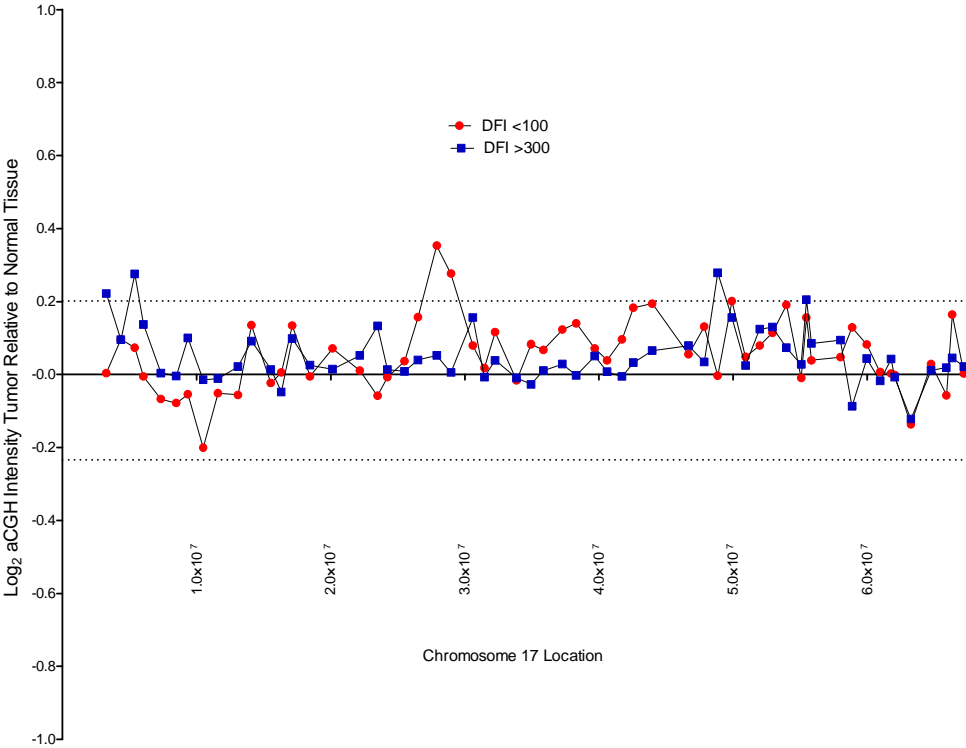
Chromosome 15



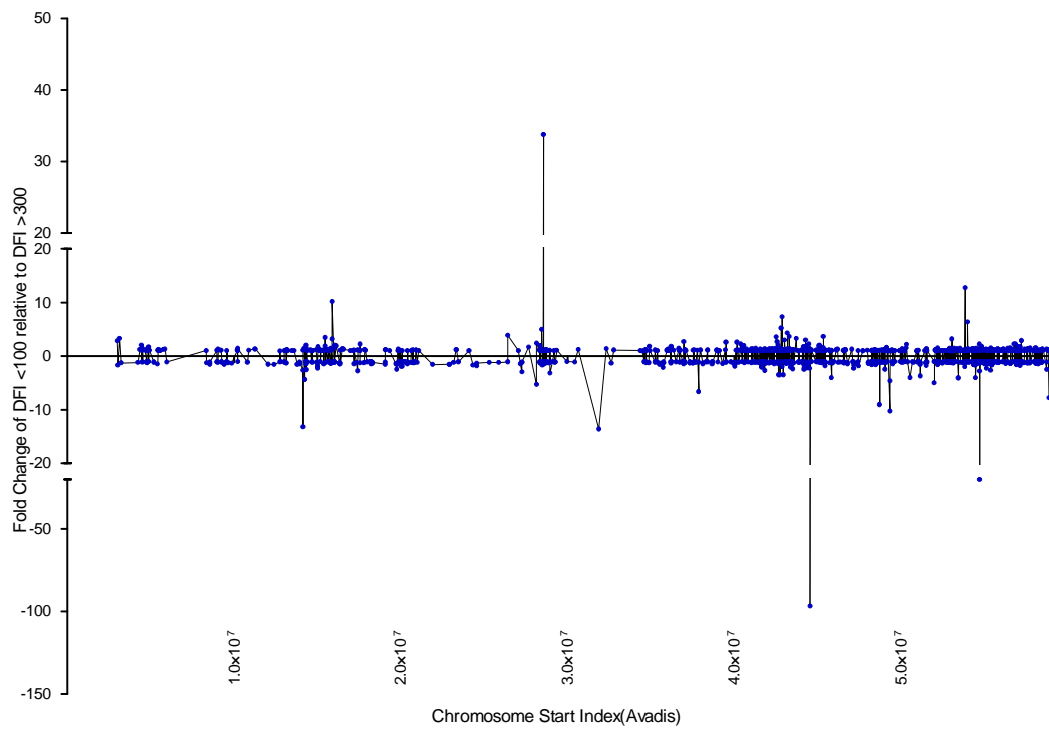
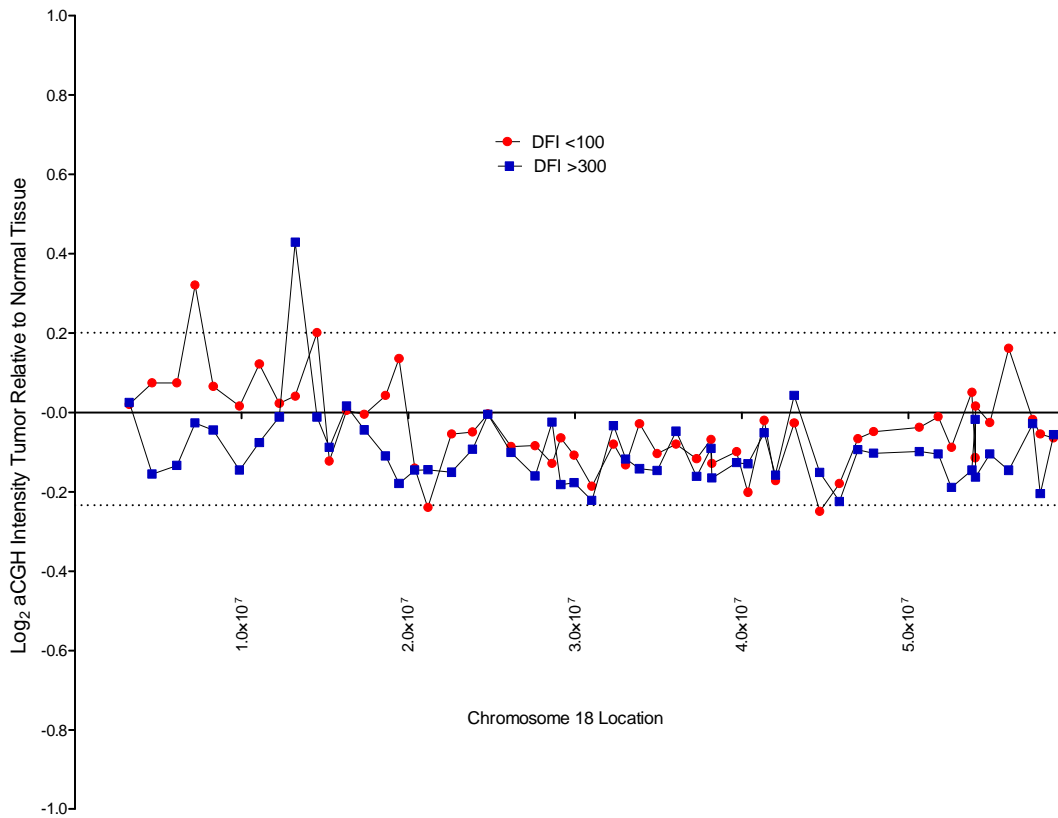
Chromosome 16



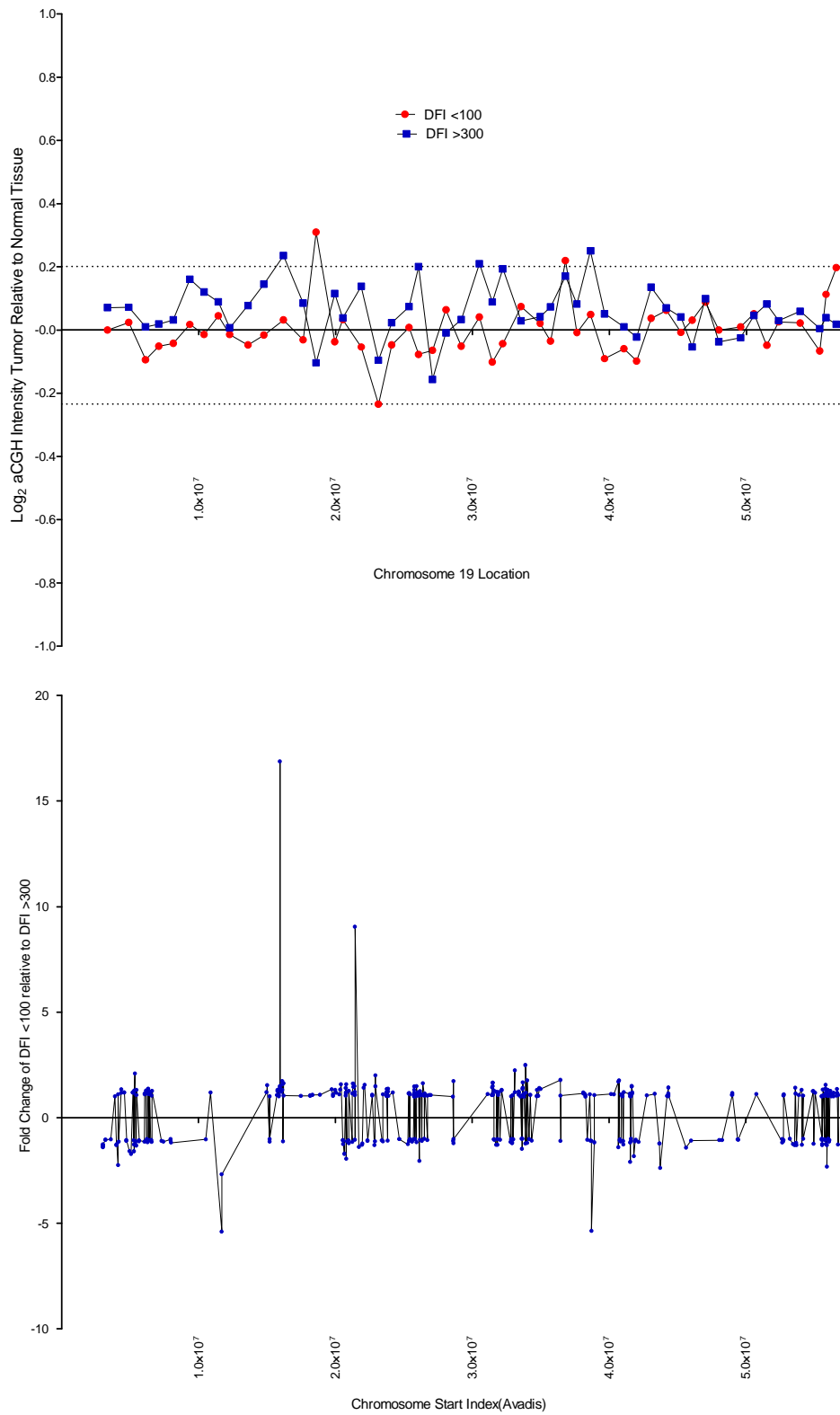
Chromosome 17



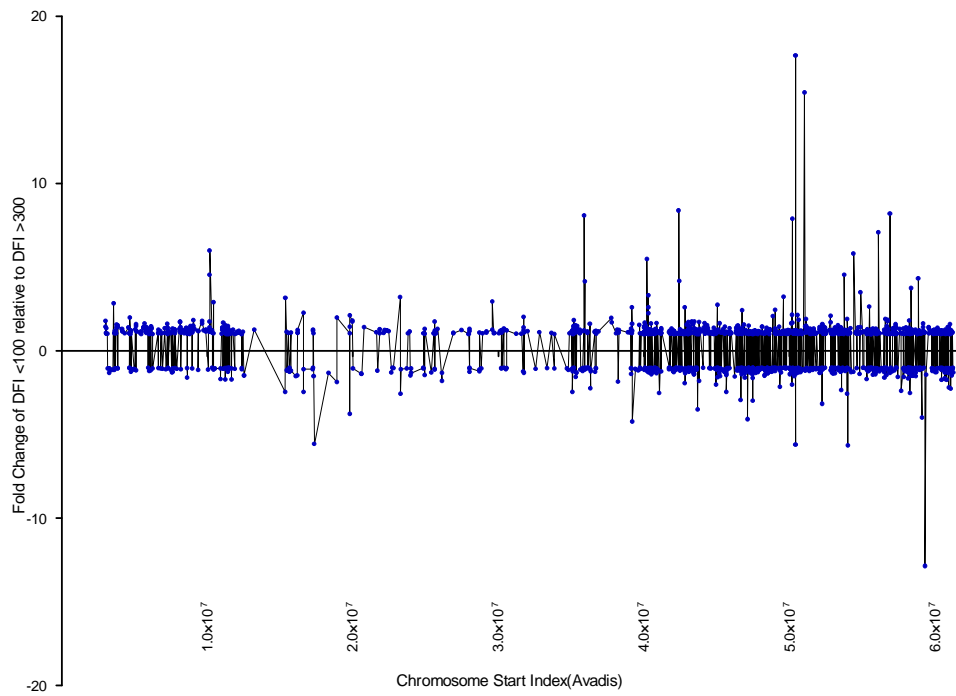
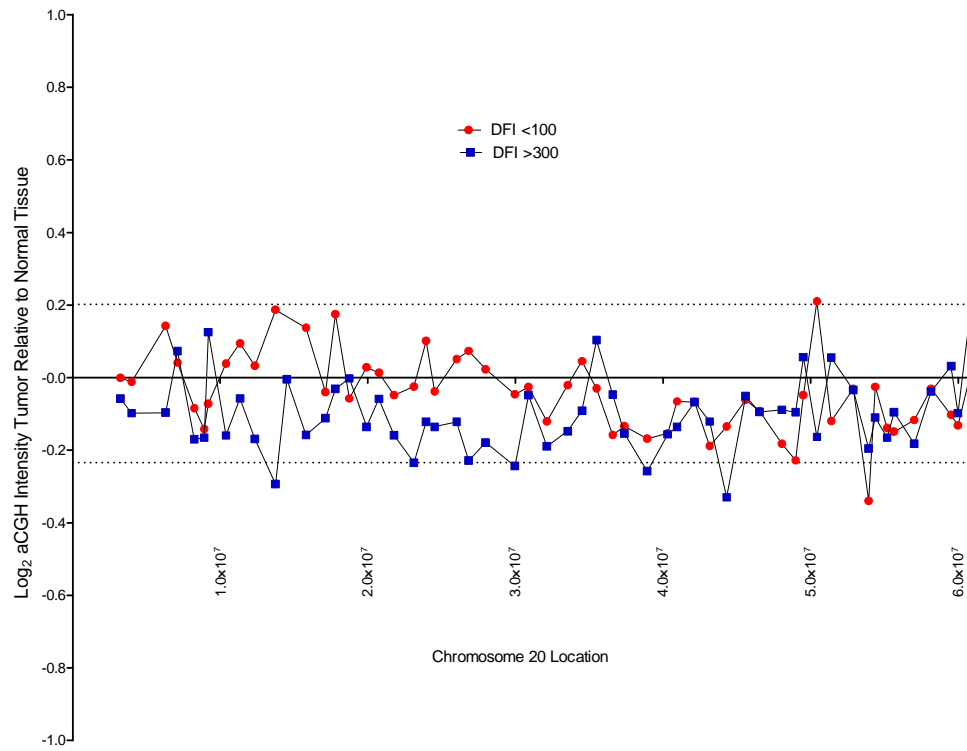
Chromosome 18



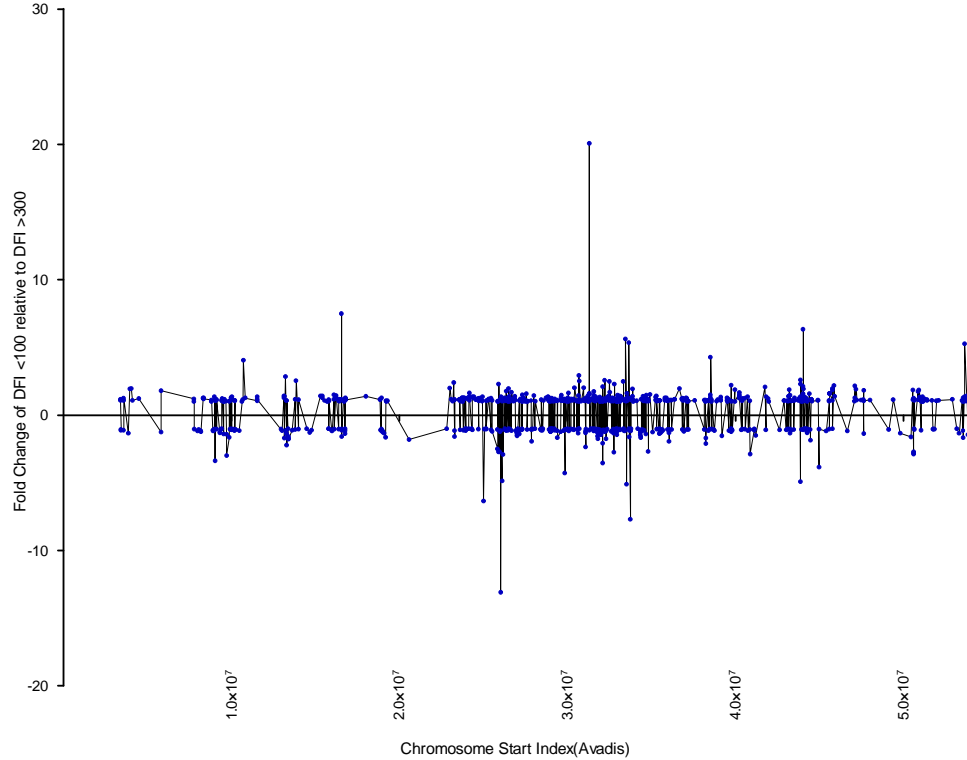
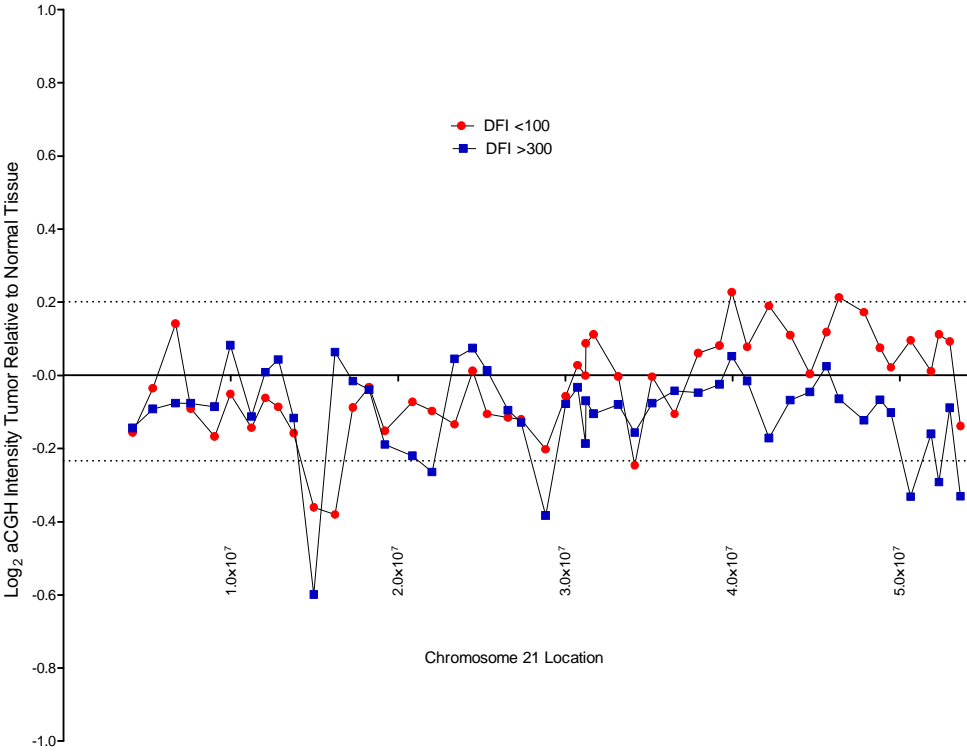
Chromosome 19



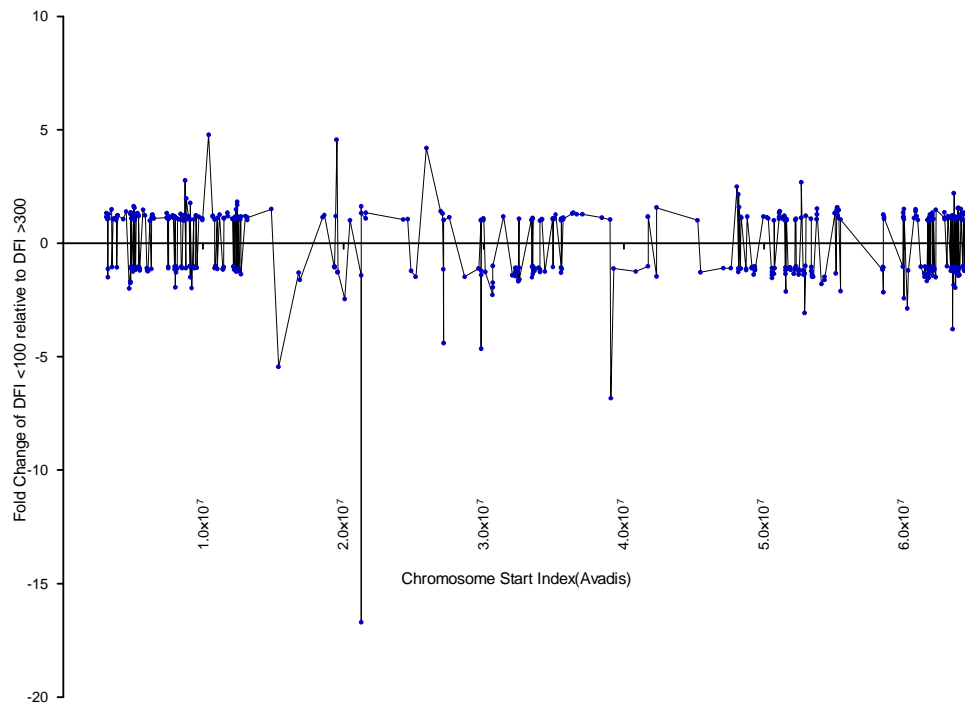
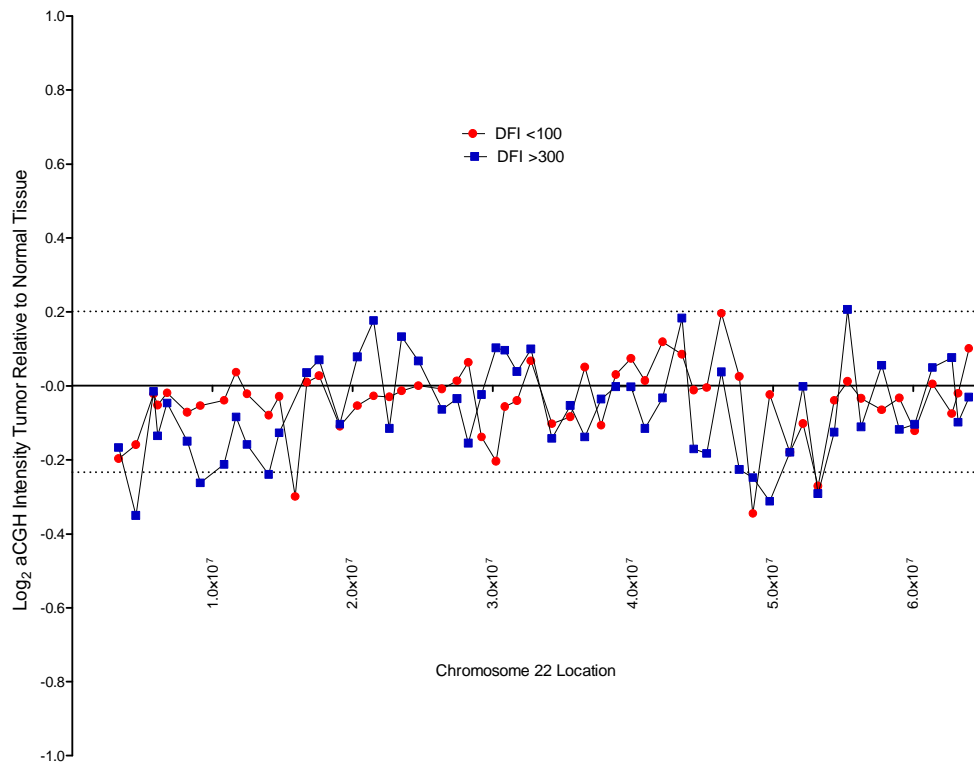
Chromosome 20



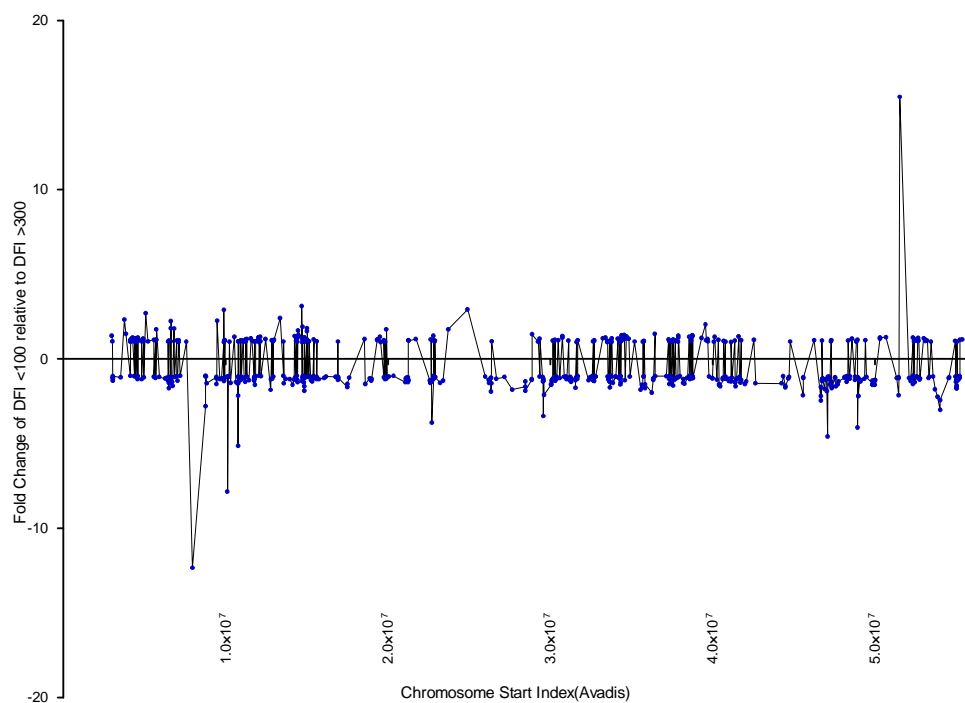
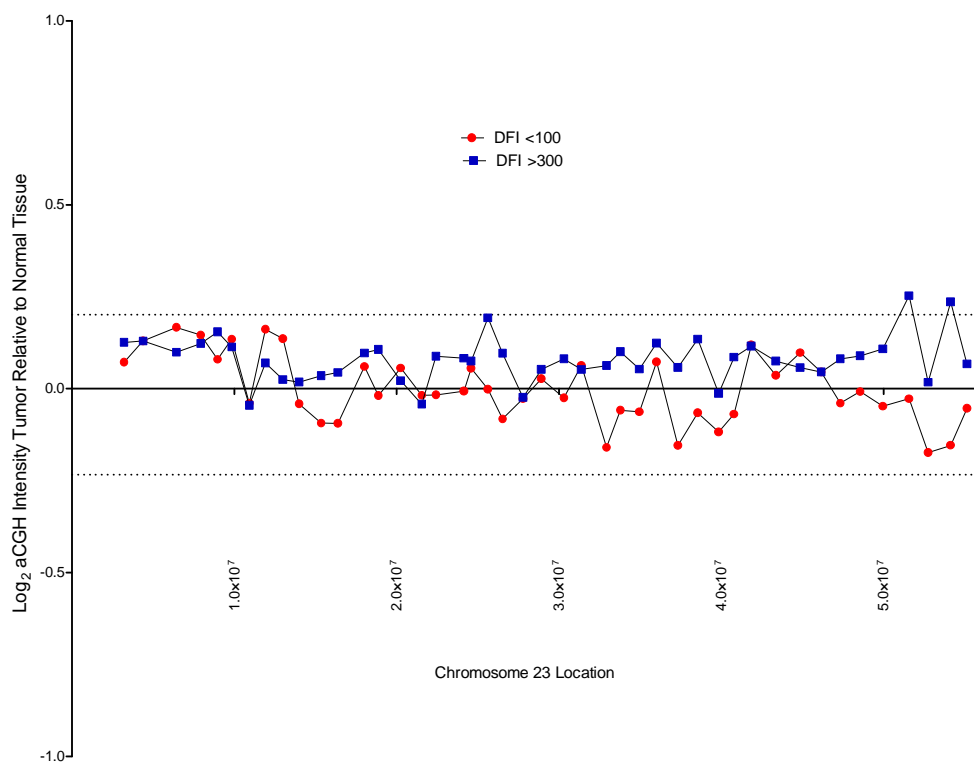
Chromosome 21



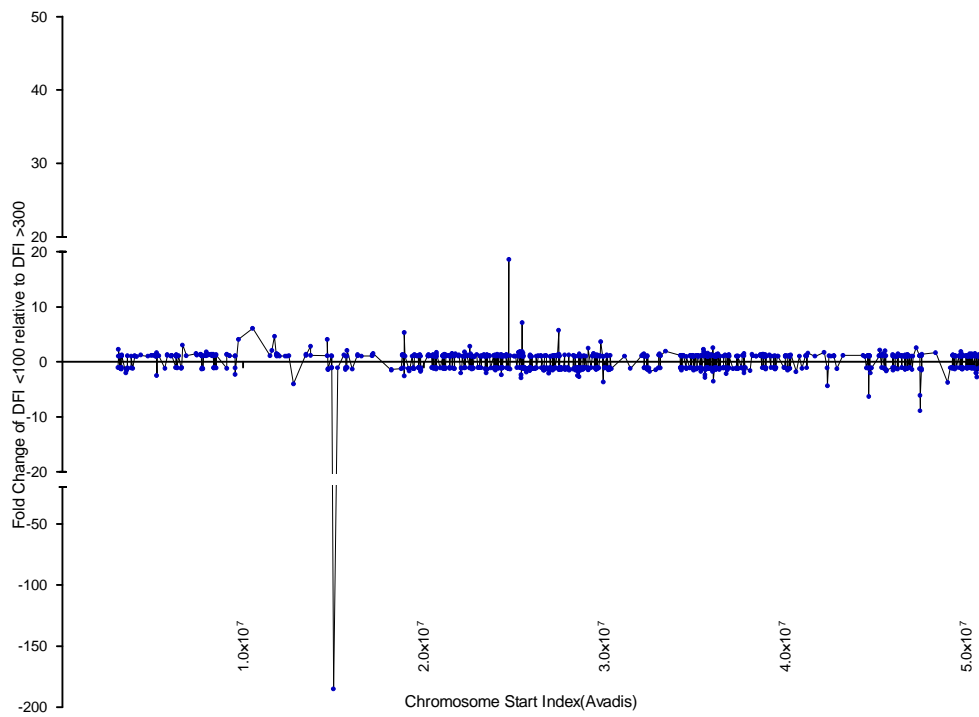
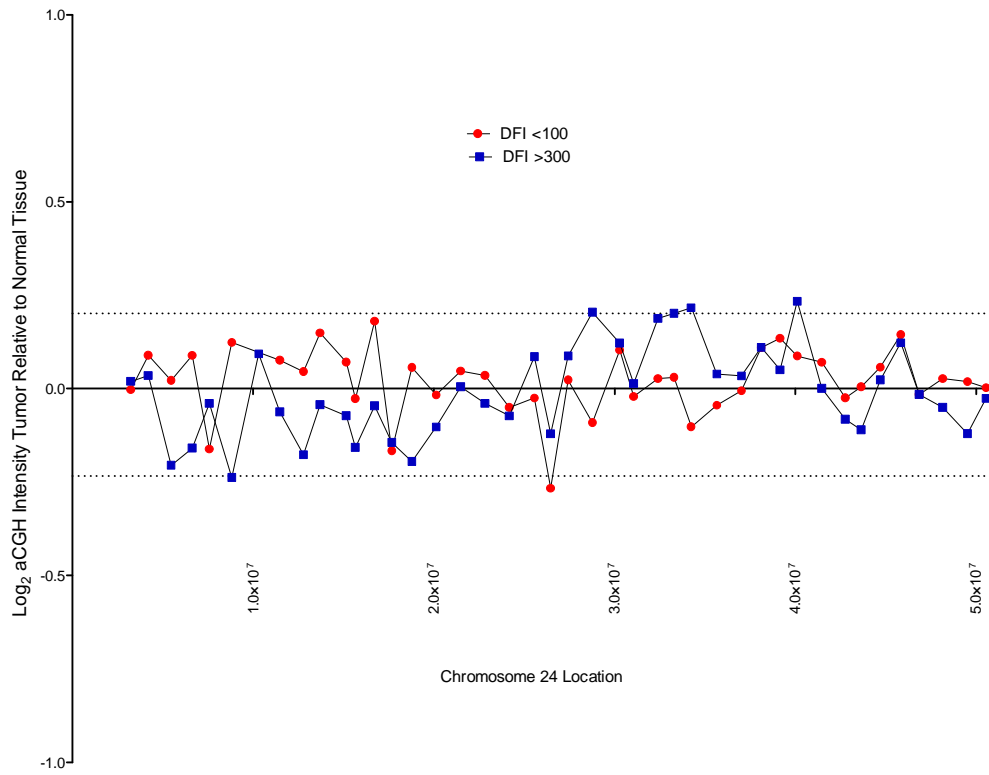
Chromosome 22



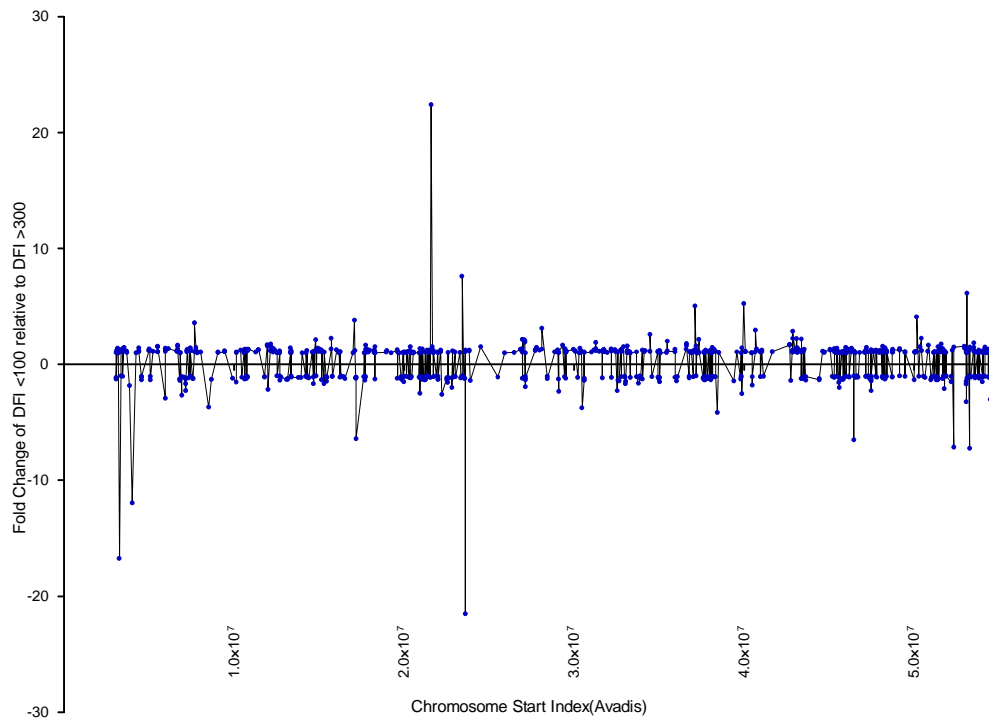
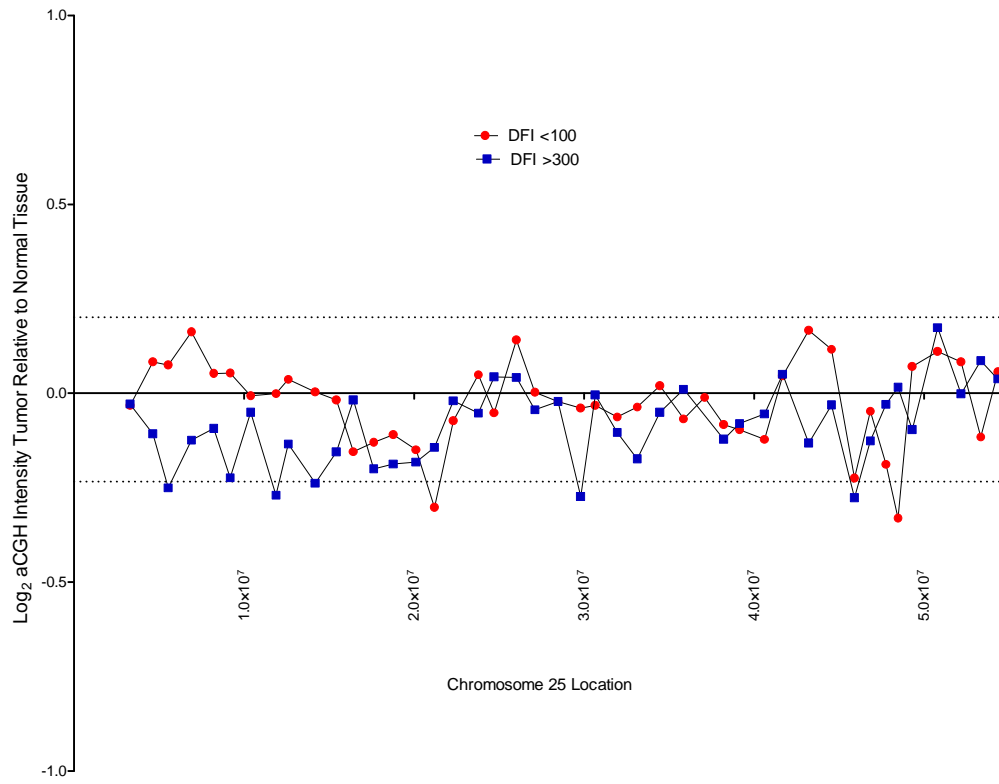
Chromosome 23



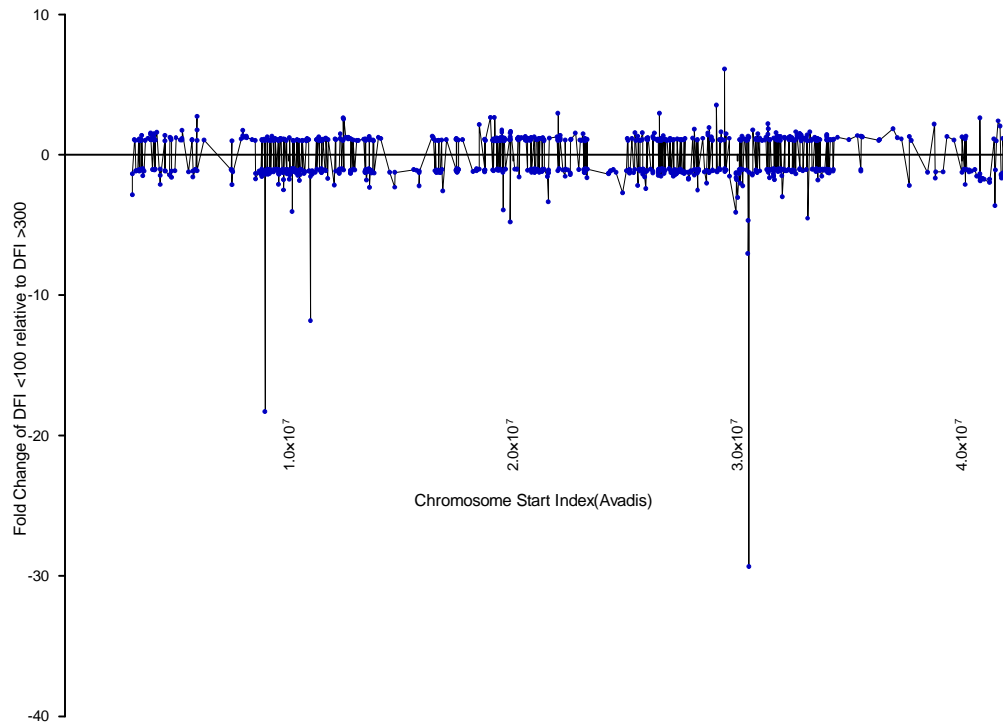
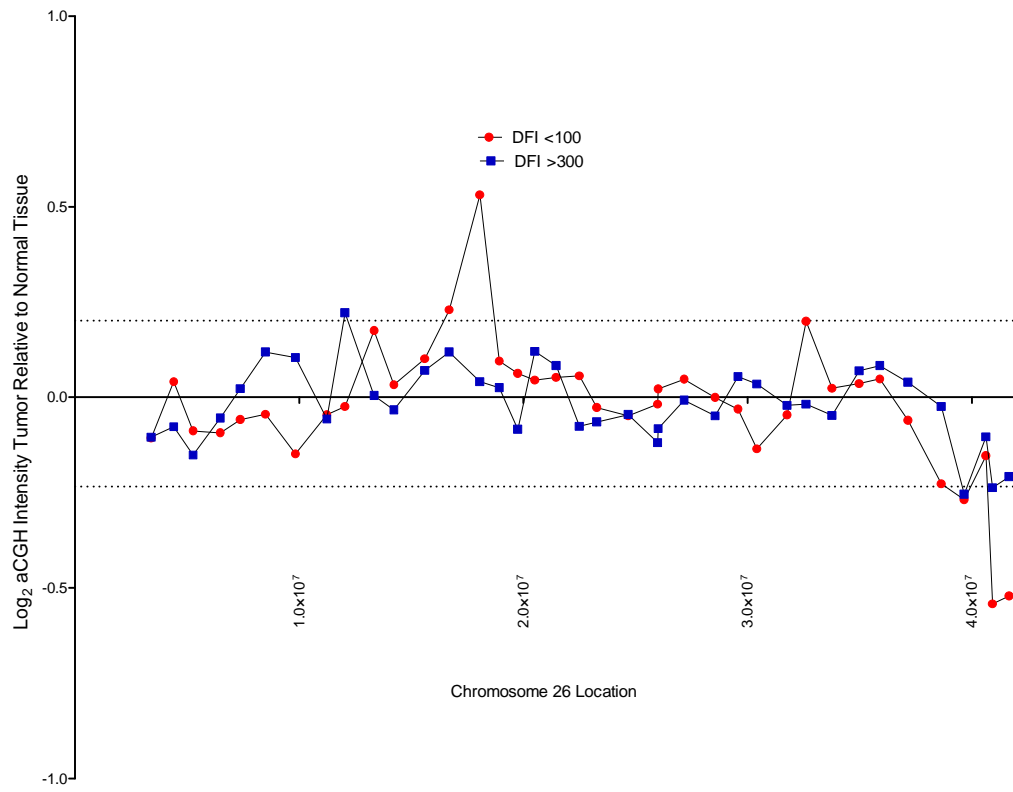
Chromosome 24



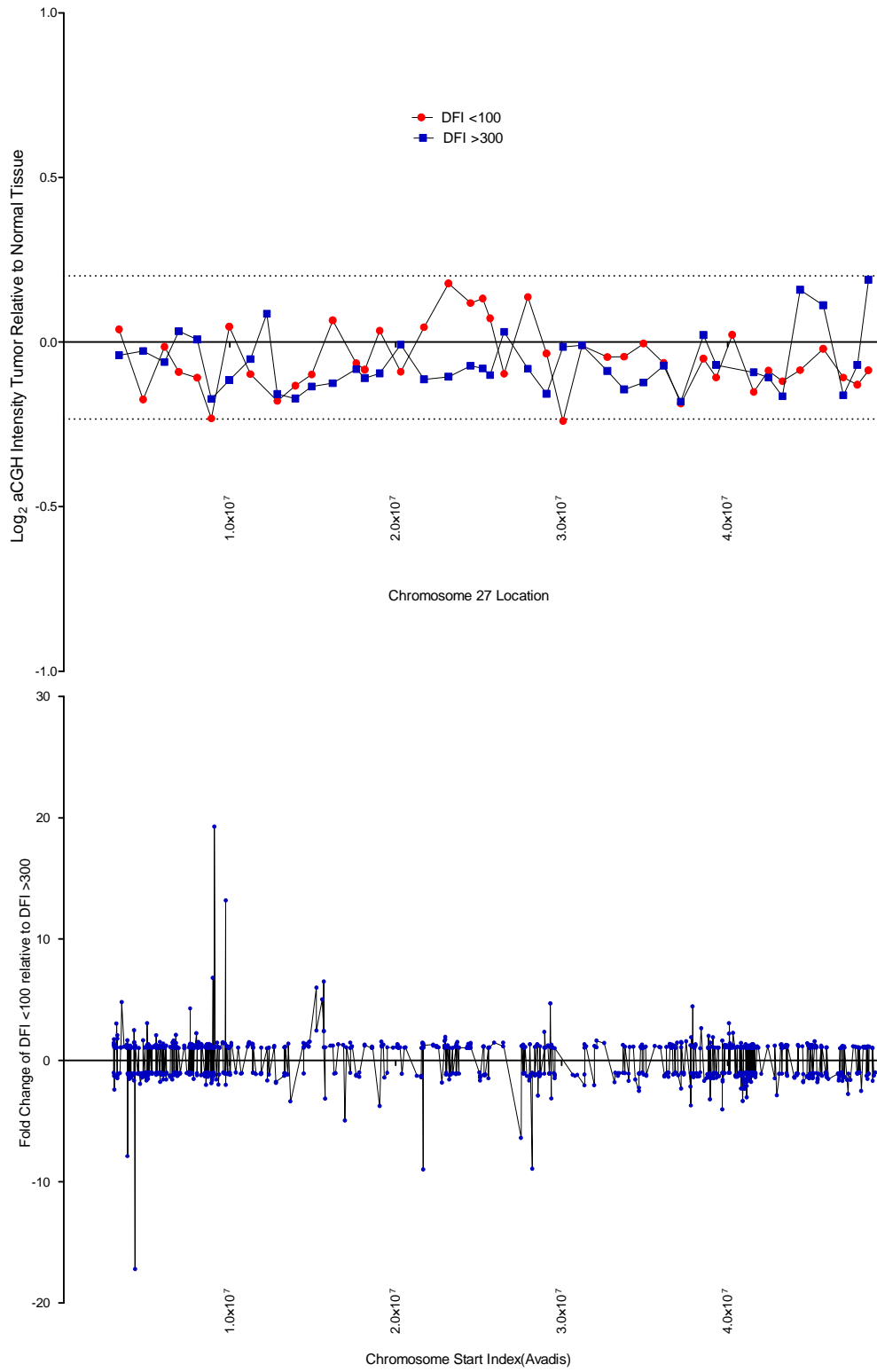
Chromosome 25



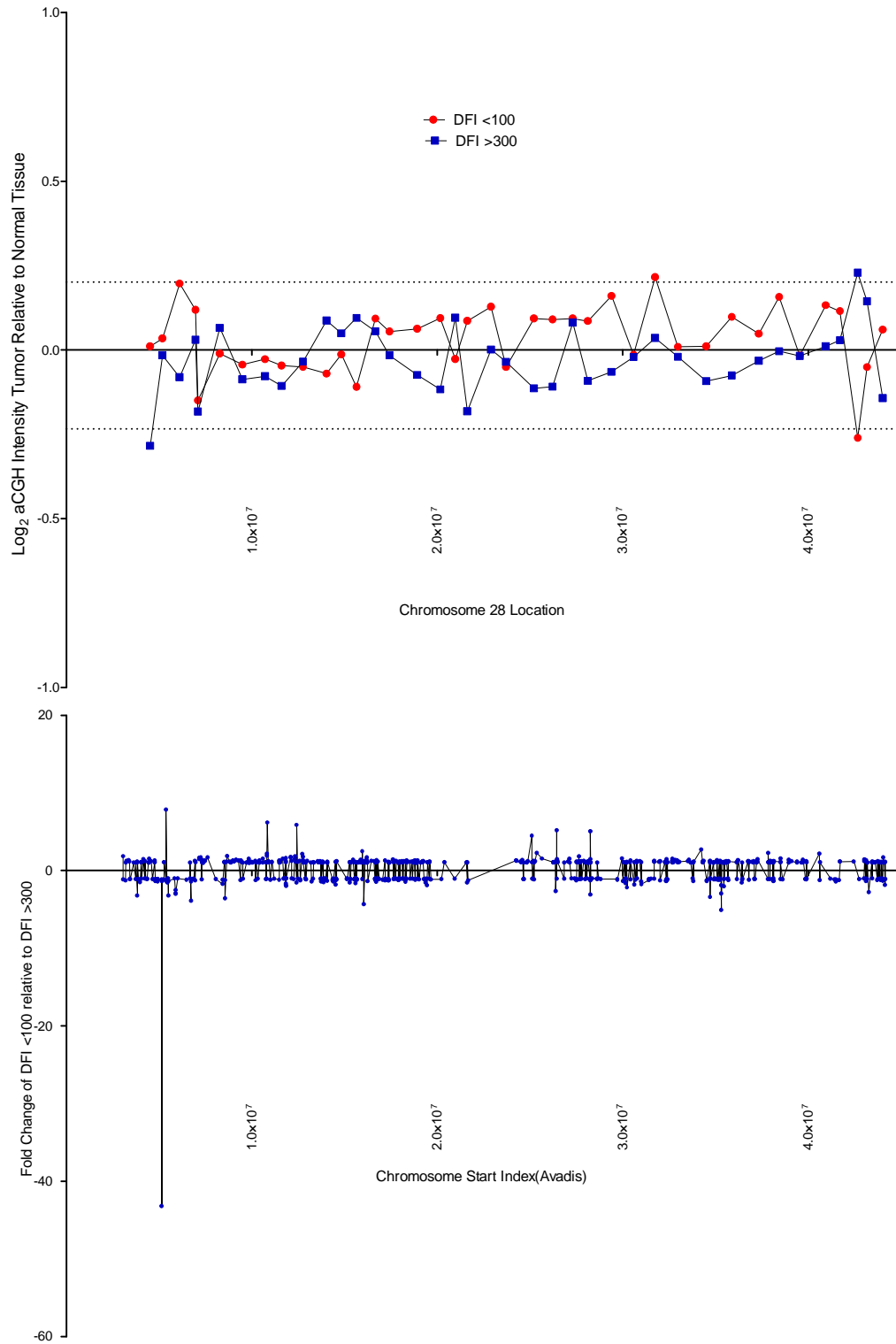
Chromosome 26



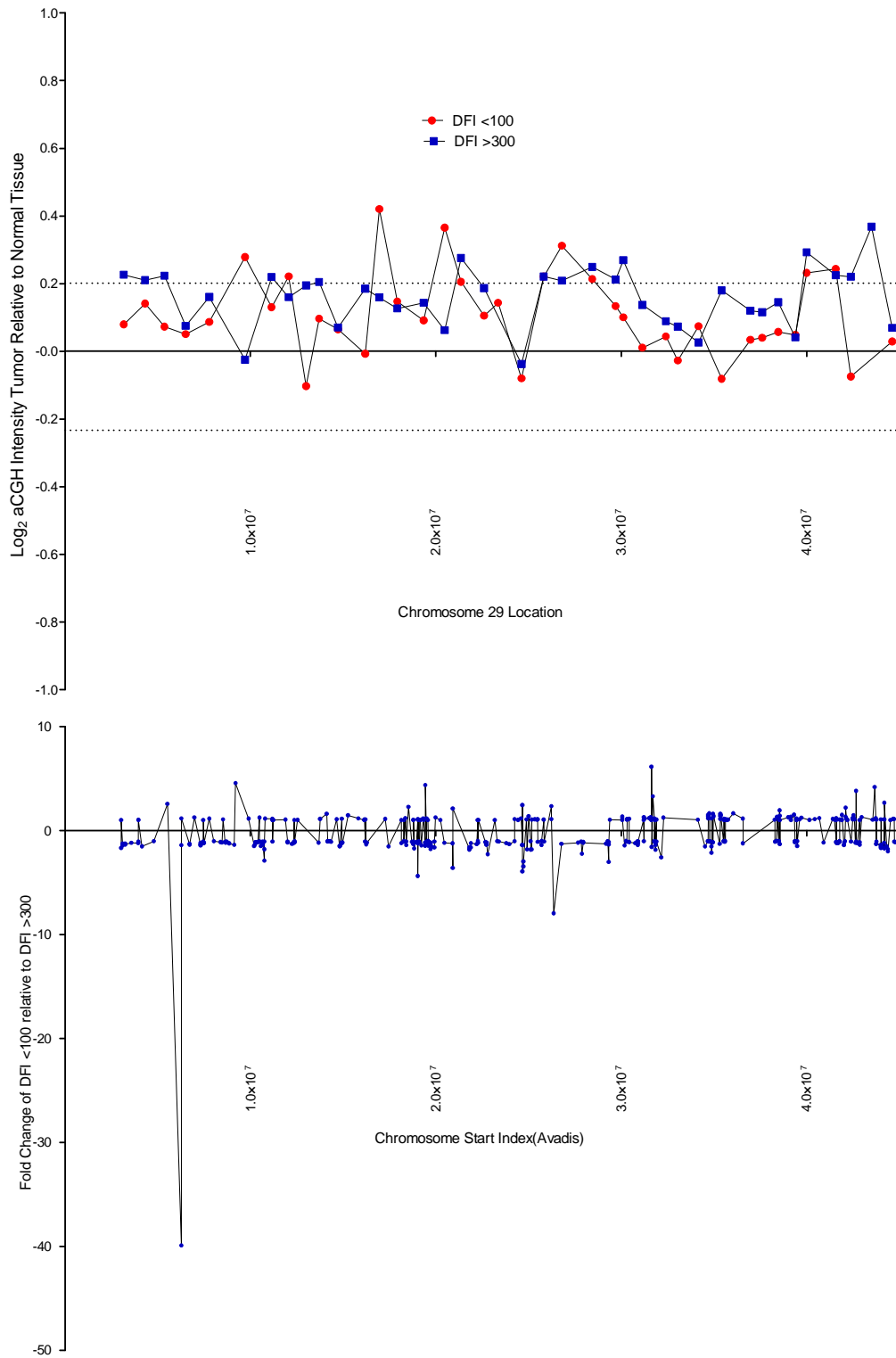
Chromosome 27



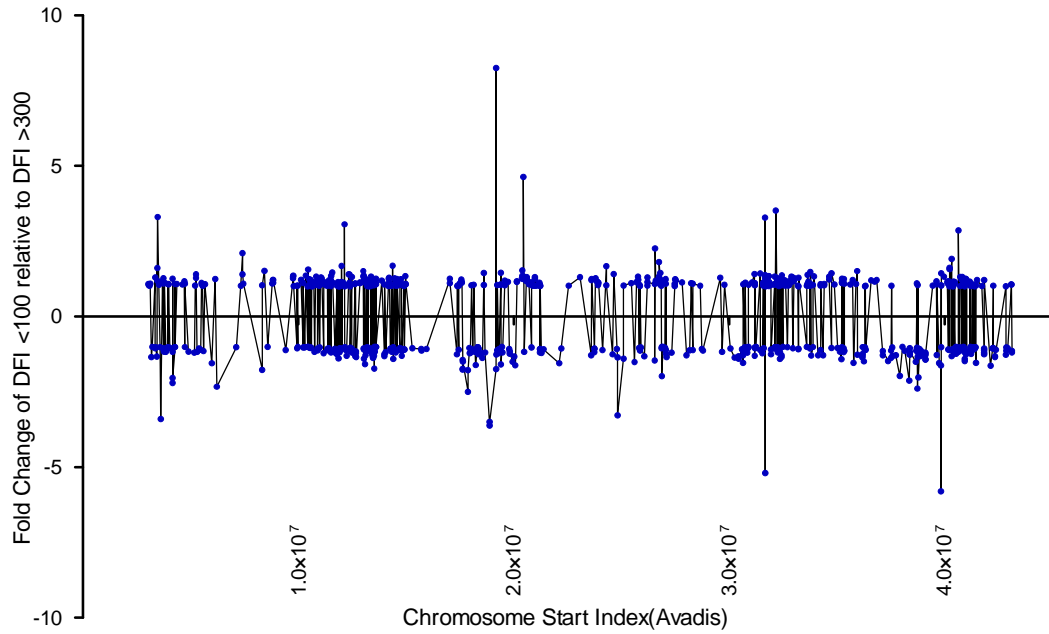
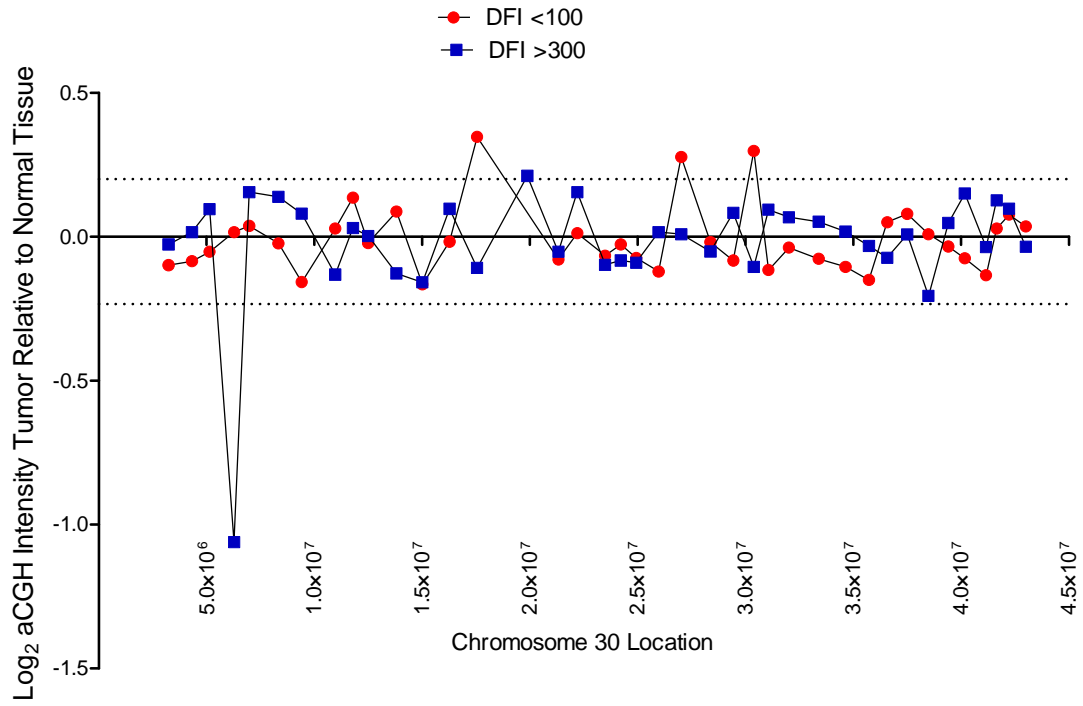
Chromosome 28



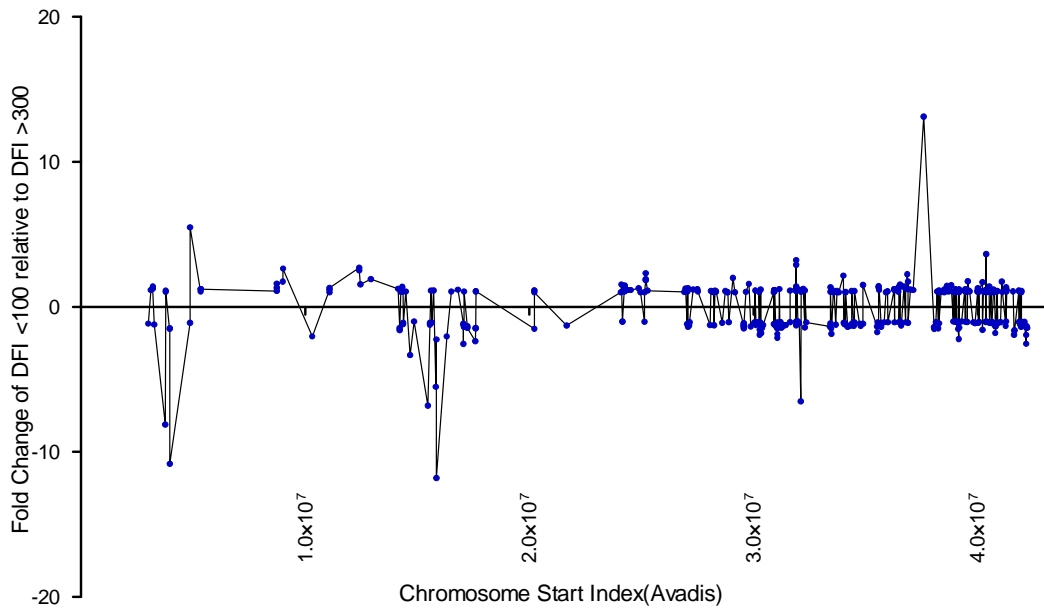
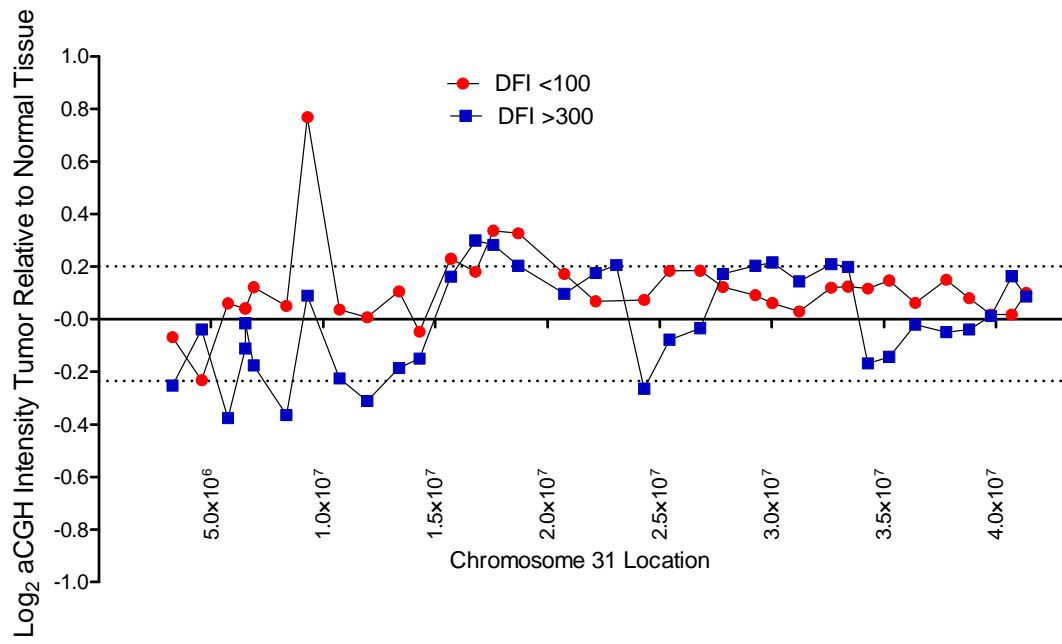
Chromosome 29



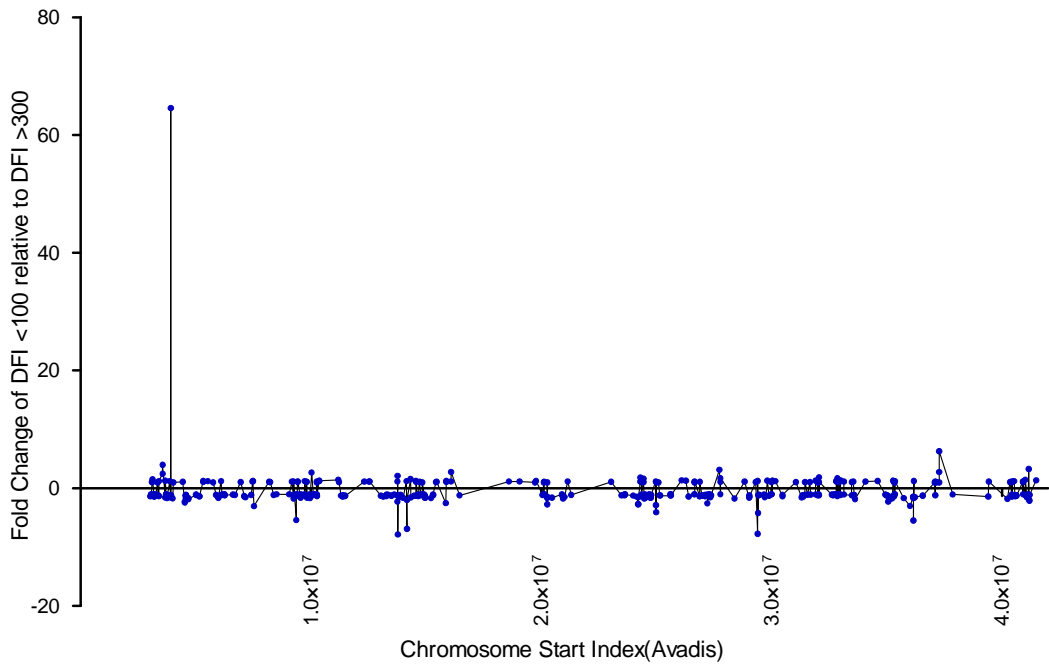
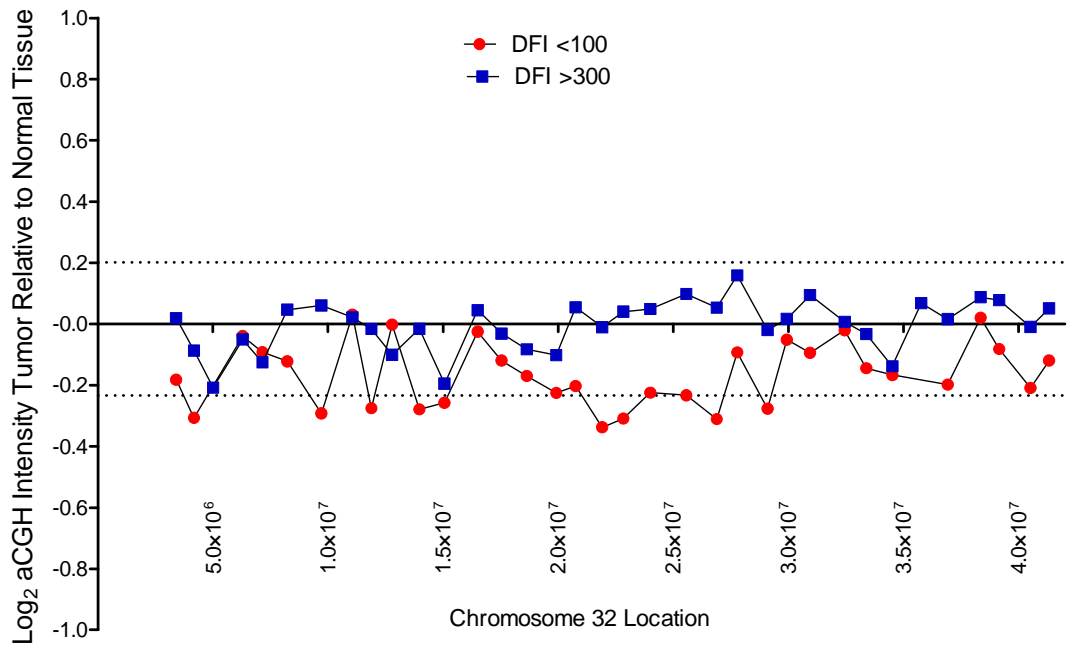
Chromosome 30



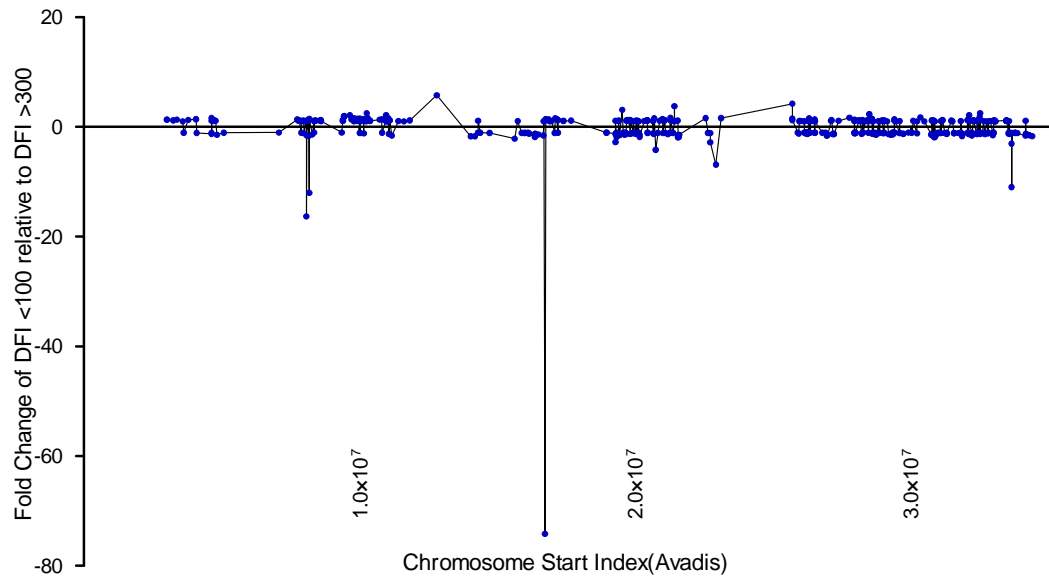
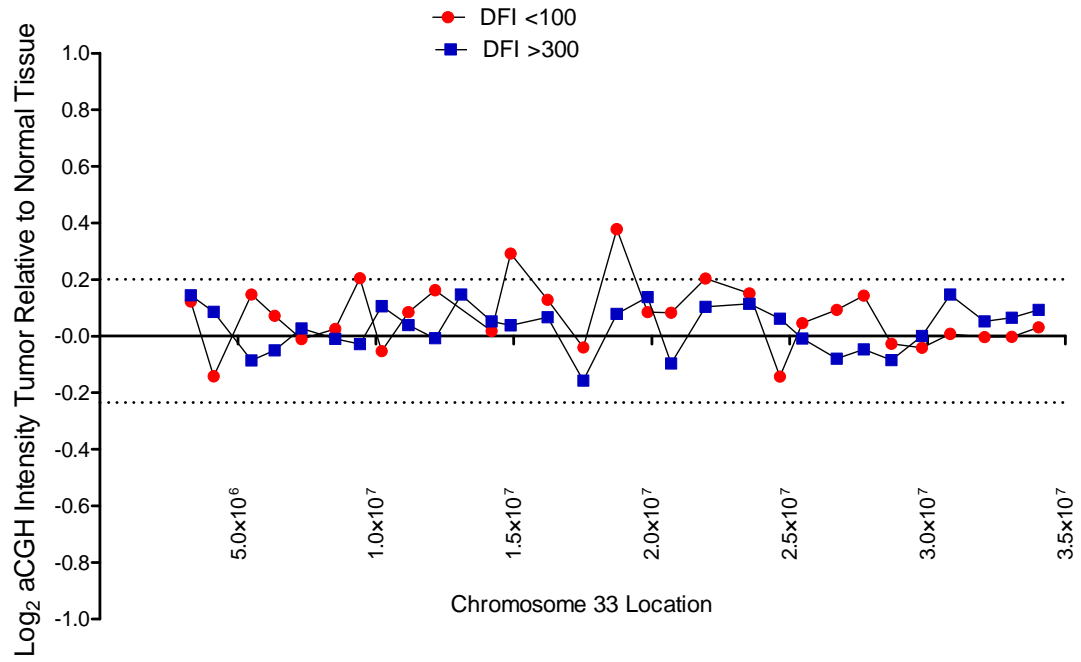
Chromosome 31



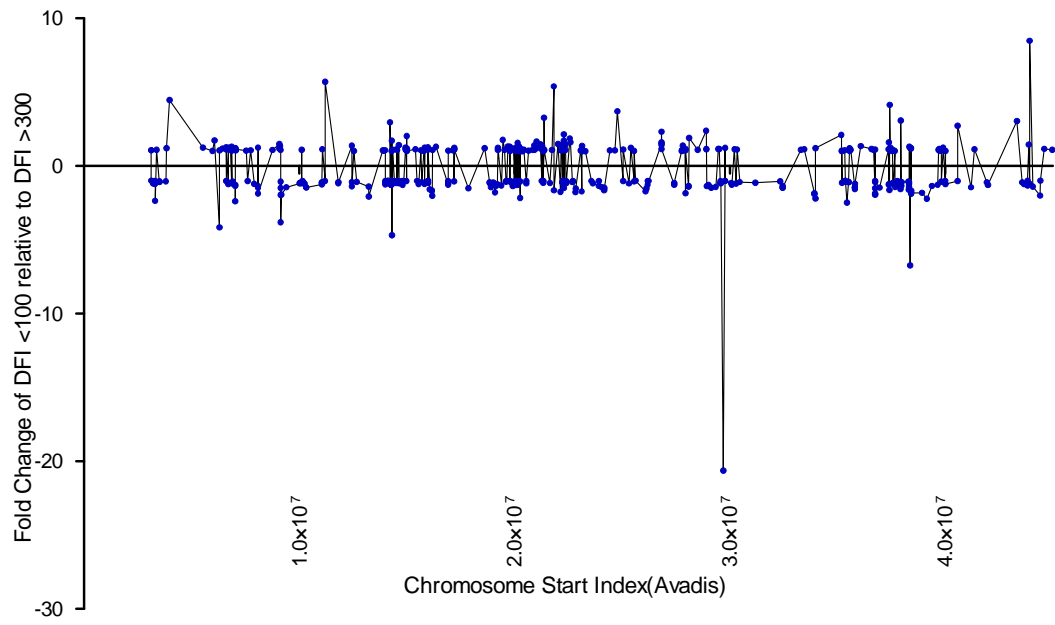
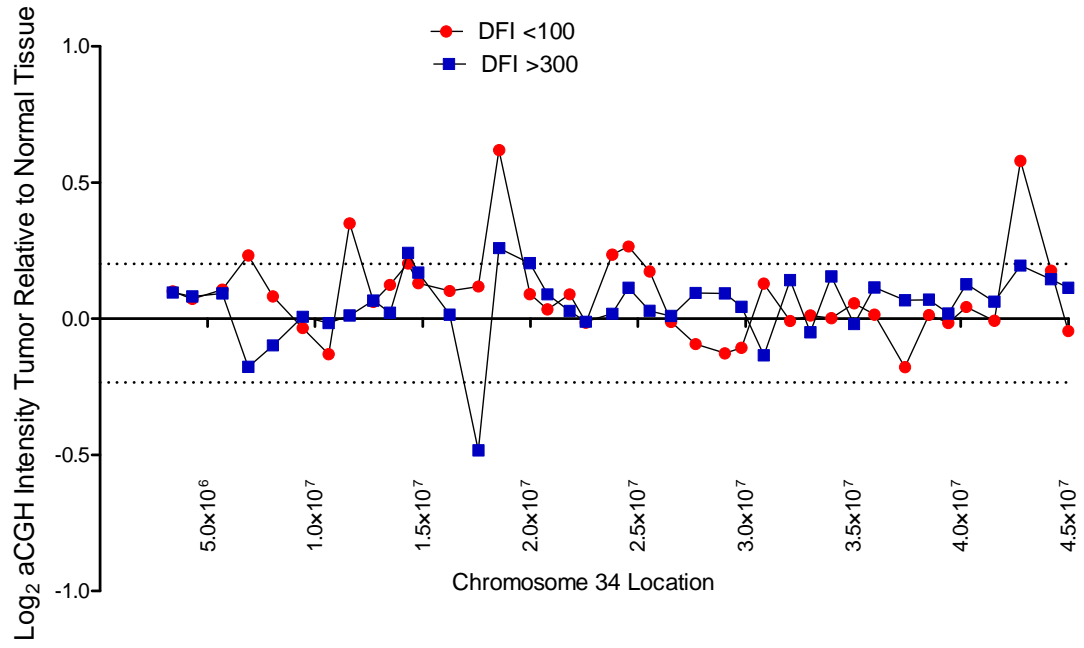
Chromosome 32



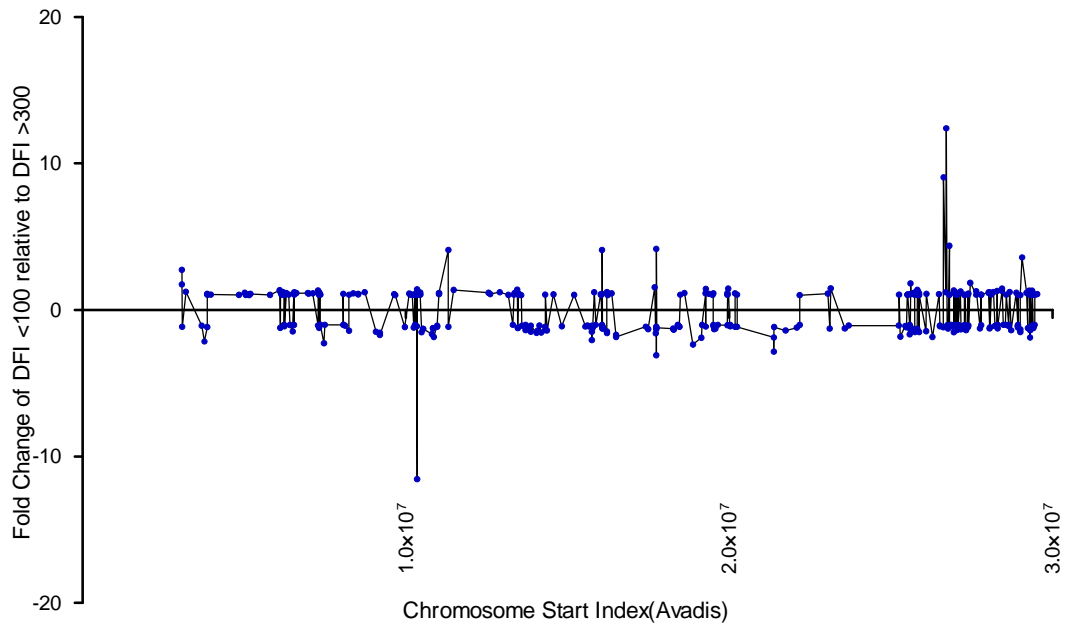
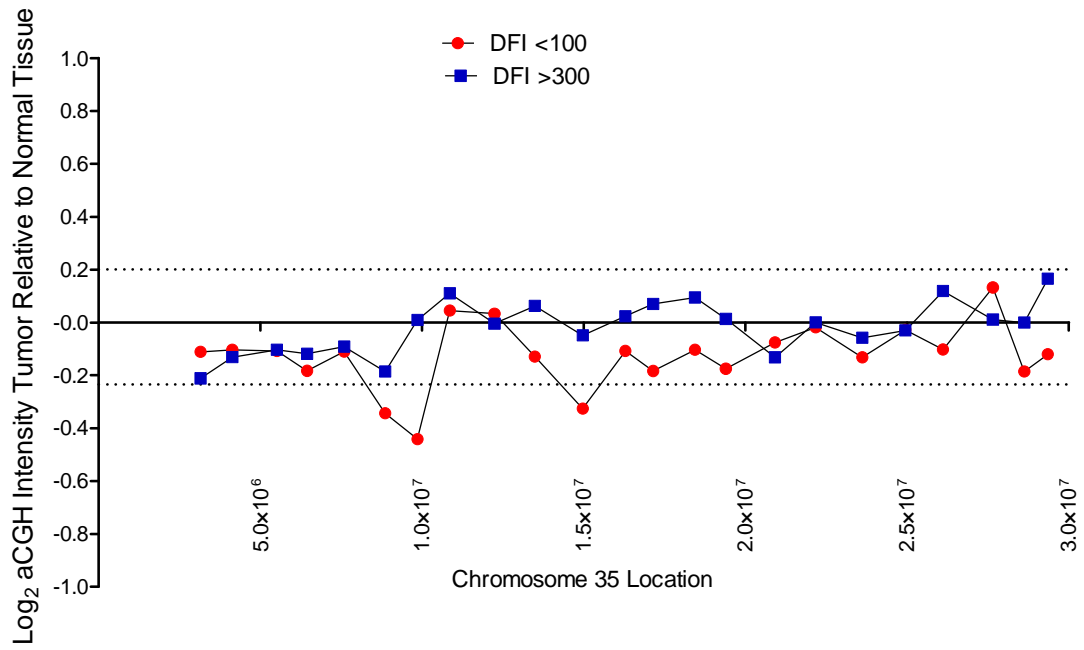
Chromosome 33



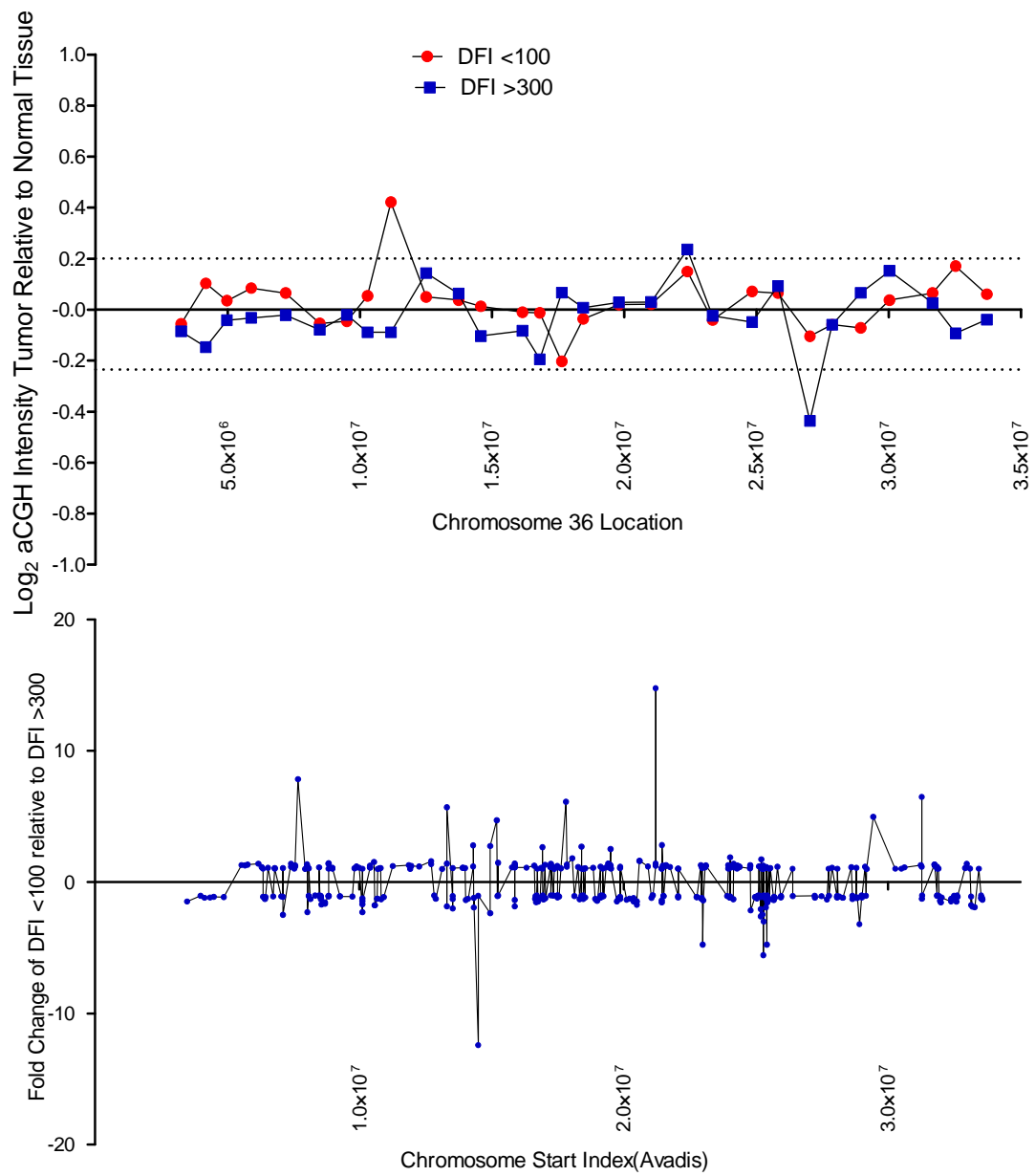
Chromosome 34



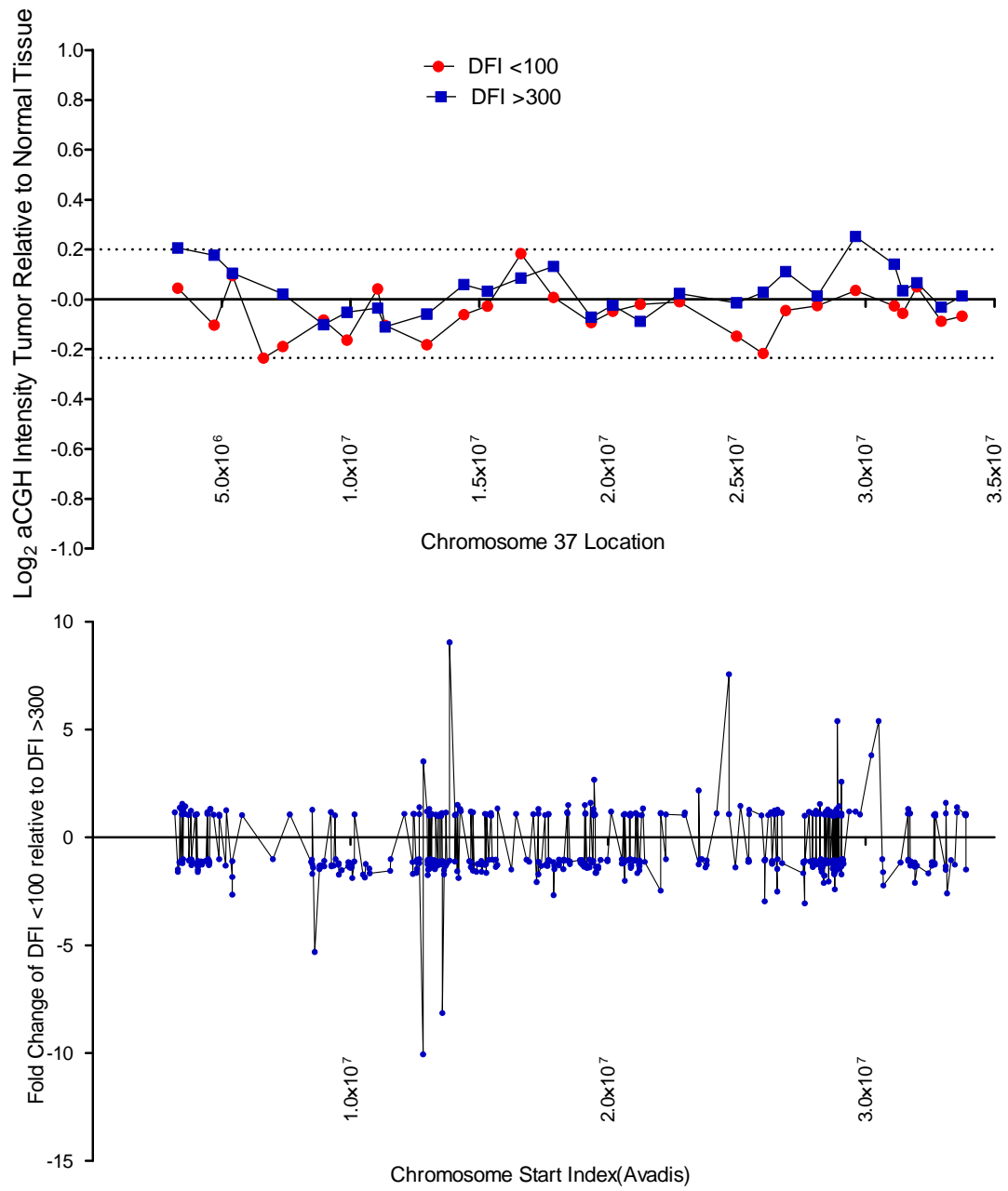
Chromosome 35



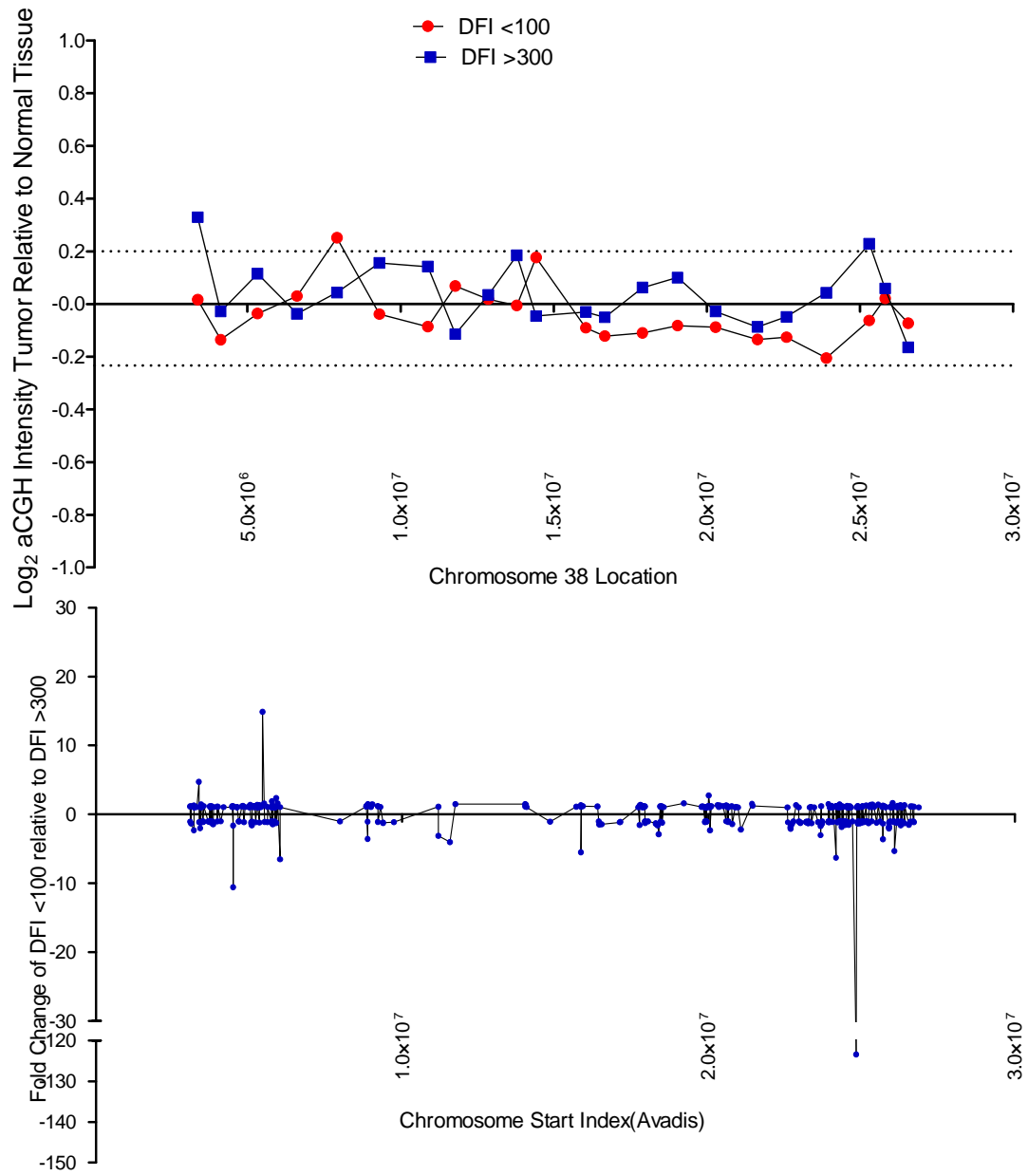
Chromosome 36



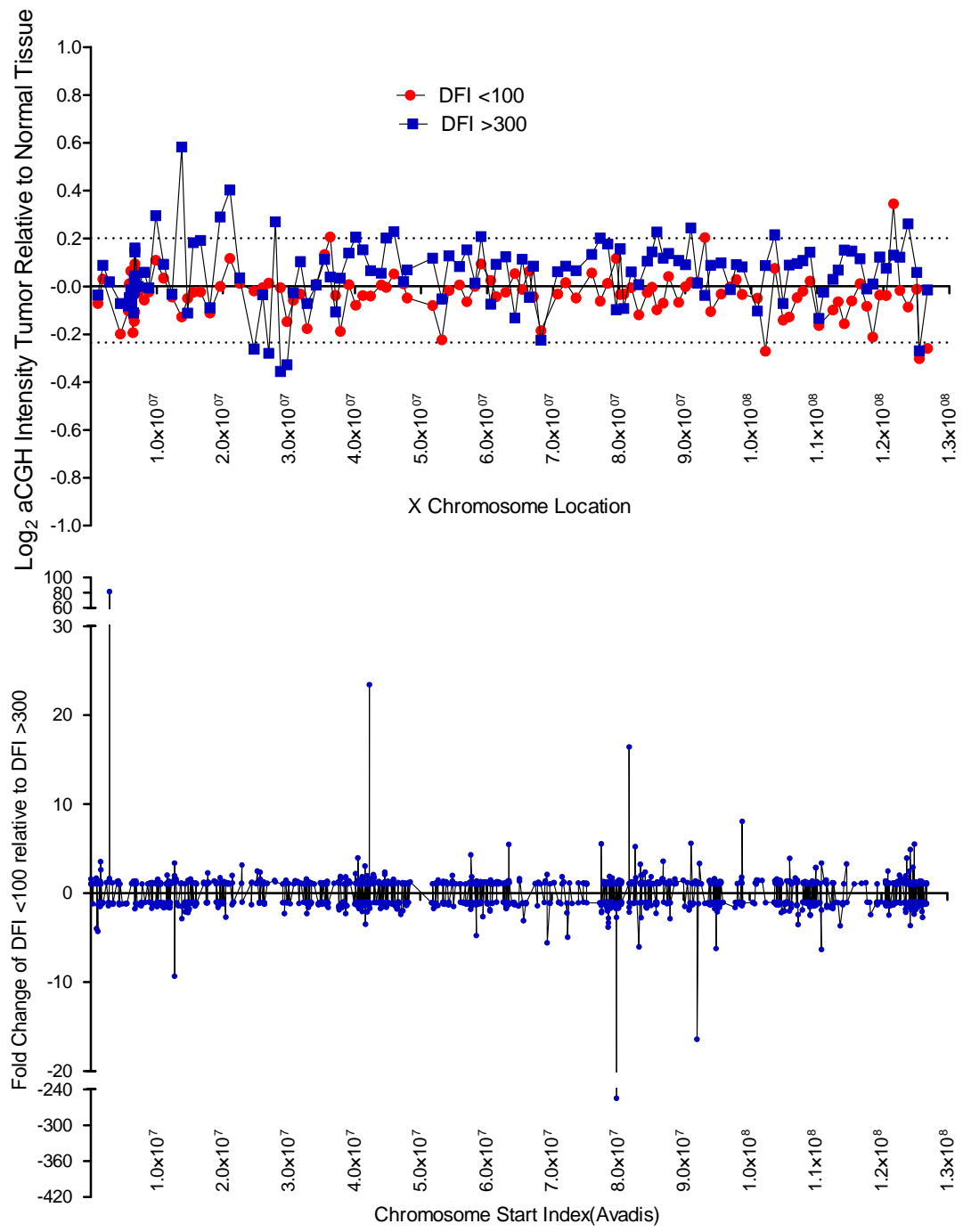
Chromosome 37



Chromosome 38



X Chromosome



Appendix E

NDRG2 Sequences: Expression Constructs

DNA sequencing results and translated protein sequence alignments for the two expression constructs used to generate stable Abrams-NDRG2 clones in Chapter 6. The short clone lacks coding sequence Exon 2, a 14-amino acid domain that follows the first 25 amino acids of the protein. Stop codons were excluded in both constructs to attach V5 tags to the resultant proteins.

NDRG2 short clone sequence - Blue letters indicate the first base of each exon, red letters indicate the last base of each exon. Lower-case letters highlighted in yellow indicate silent mutations present in the plasmid sequence. Numbers to the right of each line indicate base position relative to CDS start codon

```

ATGGCGGAGC TGCAGGAGGT GCAGATCACA GAGGAGAAGC CGCTGTTGCC 50
AGGGCAGACG CCCGAGACGG CCAAGACTCA CTCTGTGGAG ACACCGTATG 100
GCTCTGTAC TTTTACTGTC TATGGGACCC CCAAGCCCAA ACGCCCAGCG 150
ATACTCACCT ACCATGATGT AGGACTCAAC TATAAGTCTT GCTTCCAGCC 200
GCTCTTTCAG TTCGGGGACA TGCAGGAAAT CATTCAGAAC TTCGTGCGGG 250
TTCATGTGGA TGCCCCTGGA ATGGAAGAGG GGGCTCCCGT GTTCCCTTTG 300
GGGTATCAGT ACCCGTCTCT GGACCAGCTC GCGGACATGA TCCCTTGCAT 350
TCTGCAGTAC CTGAATTCTT CCACAATAAT TGGAGTTGGT GTTGGAGCTG 400
GAGCCTACAT CCTGTACGA TATGCTCTGA CCCACCCGGA TACAGTCGAG 450
GGGCTTGTCC TCATCAACAT TGATCCCAAT GCCAAGGGTT GGATGGACTG 500
GGCGGCCAC AAGCTAACAG GTCTCACCTC TTCCATTCCG GAGATGATCC 550
TCGGACATCT TTTTCAGCCAG GAGGAGCTGT CTGGAAACTC GGAGCTGATA 600
CAGAAGTACA GAAACATCAT CACACATGCG CCCAACCTGG AGAACATTGA 650
ACTGTACTGG AACAGCTACA ACAATCGCCG AGACCTGAAC CTGGAGCGTG 700
GCGGTGCCGT CACCCTCAGG TGCCCTGTGA TGCTGGTGGT GGGAGACCAA 750
GCACCCCATG AAGATGCAGT GGTGGAGTGT AACTCAAAGC TGGACCCAC 800
CCAGACCTCT TTTCTCAAGA TGGCCGACTC TGGAGGTCAG CCCCAGCTGA 850
CGCAGCCAGG CAAGCTGACC GAGGCCTTCA AGTACTTCTT GCAAGGCATG 900
GGCTACATGG CCTCGTCCTG CATGACTCGC CTGTGCGGAT CGCGCACGGC 950
CTCGCTGACC AGTGCGGCGT CCATTGATGG CAACCGGTCC CGCTCCCACA 1000
CCCTATCGCA GGGCAGCGAG TCTGGGACTC TCCCTTCAGG GCCGCCAGG 1050
CATACCATGG AAGTCTCCTG C

```

NDRG2 long clone sequence - Colors are as above, CDS Exon 2 is dark blue.

```

ATGGCGGAGC TGCAGGAGGT GCAGATCACA GAGGAGAAGC CGCTGTTGCC 50
AGGGCAGACG CCCGAGACGG CCAAGGAGGC TGAATTAGCT GCCCGAATCC 100
TCCTGGACCG GGGACAGACT CACTCTGTGG AGACACCGTA TGGCTCTGTC 150
ACTTTTACTG TCTATGGGAC CCCCAAGCCC AAACGCCAG CGATACTCAC 200
CTACCATGAT GTAGGACTCA ACTATAAGTC TTGCTTCCAG CCGCTCTTTC 250
AGTTCGGGGG CATGCAGGAA ATCATTGAGA ACTTCGTGCG GGTTCATGTG 300
GATGCCCCTG GAATGGAAGA GGGGGCTCCC GTGTTCCCTT TGGGTATCA 350
GTACCCGTCT CTGGACCAGC TCGCGGACAT GATCCCTTGC ATTCTGCAGT 400
ACCTGAATTT CTCCACAATA ATTGGAGTTG GTGTTGGAGC TGGAGCCTAC 450
ATCCTGTCAC GATATGCTCT GACCCACCCG GATACAGTCG AGGGGCTTGT 500
CCTCATCAAC ATTGATCCCA ATGCCAAGGG TTGGATGGAC TGGGCGGCC 550
ACAAGCTAAC AAGTCTCACC TCTTCCATTC CGGAGATGAT CCTCGGACAT 600
CTTTTCAGCC AGGAGGAGCT GTCTGGAAAC TCGGAGCTGA TACAGAAGTA 650
CAGAAACATC ATCACACATG CGCCCAACCT GGAGAACATT GAACTGTACT 700
GGAACAGCTA CAACAATCGC CGAGACCTGA ACCTGGAGCG TGGCGGTGCC 750
GTCACCCTCA GGTGCCCTGT GATGTTGGTG GTGGGAGACC AAGCACCCCA 800
TGAAGATGCA GTGGTGGAGT GTAACTCAA GCTGGACCCC ACCCAGACCT 850
CTTTTCTCAA GATGGCCGAC TCTGGAGGTC AGCCCAGCT GACGCAAGCA 900
GGCAAGCTGA CCGAGGCCTT CAAGTACTTC CTGCAAGGCA TGGGCTACAT 950
GGCCTCGTCC TGCATGACTC GCCTGTGCGG ATCGCGCACG GCCTCGCTGA 1000
CCAGTGCAGG GTCCATTGAT GGCAACCGGT CCCGCTCCCG CACCCTGTCT 1050
CAGGGCAGCG AGTCTGGGAC TCTCCCTTCA GGGCCGCCGG GGCATACCAT 1100
GGAGGTCTCC TGC

```

NDRG2 short clone protein alignment - NCBI blastx alignment of translated nucleotide sequence for the short construct with NDRG2 isoform protein sequence. 100% of residues align with transcript variants 6 and 7. These two isoforms share identical coding sequences but differ in untranslated region sequence. Mutations identified in coding sequence do not result in residue changes.

ref|XP_863342.1| PREDICTED: similar to N-myc downstream-regulated gene 2 isoform b isoform 6 [Canis familiaris]

ref|XP_863366.1| PREDICTED: similar to N-myc downstream-regulated gene 2 isoform b isoform 7 [Canis familiaris]

Length=357

GENE ID: 609390 NDRG2 | NDRG family member 2 [Canis lupus familiaris]

Score = 672 bits (1733), Expect = 0.0
 Identities = 357/357 (100%), Positives = 357/357 (100%), Gaps = 0/357 (0%)
 Frame = +1

Query	1	MAELQEVQITEEKPLLPGQTPETAKTHSVETPYGSVTFVYGTPKPKRPAILTYHDVGLN	180
Sbjct	1	MAELQEVQITEEKPLLPGQTPETAKTHSVETPYGSVTFVYGTPKPKRPAILTYHDVGLN	60
Query	181	YKSCFQPLFQFGDMQEIIQNFVRVHVDAPGMEEGAPVFPLGYQYPSLDQLADMIPCILQY	360
Sbjct	61	YKSCFQPLFQFGDMQEIIQNFVRVHVDAPGMEEGAPVFPLGYQYPSLDQLADMIPCILQY	120
Query	361	LNFSTIIGVGVGAGAYILSRYALTHPDTVEGLVLINIDPNAKGWMDWAAHKLTLTSSIP	540
Sbjct	121	LNFSTIIGVGVGAGAYILSRYALTHPDTVEGLVLINIDPNAKGWMDWAAHKLTLTSSIP	180
Query	541	EMILGHLFSQEELSGNSELIQYRNIITHAPNLENIELYWNSYNNRRDLNLERGGAVTLR	720
Sbjct	181	EMILGHLFSQEELSGNSELIQYRNIITHAPNLENIELYWNSYNNRRDLNLERGGAVTLR	240
Query	721	CPVMLVVG DQAPHEDAVVECN SKLDPTQTSFLKMADSGGQPQLTQPGKLTEAFKYFLQGM	900
Sbjct	241	CPVMLVVG DQAPHEDAVVECN SKLDPTQTSFLKMADSGGQPQLTQPGKLTEAFKYFLQGM	300
Query	901	GYMASSCMTRLSRSRTASL TSAASIDGNRSRRTLSQGS E SGTLP SGPPGHTMEVSC	1071
Sbjct	301	GYMASSCMTRLSRSRTASL TSAASIDGNRSRRTLSQGS E SGTLP SGPPGHTMEVSC	357

NDRG2 long clone protein alignment - NCBI blastx alignment of translated nucleotide sequence for the long construct with NDRG2 isoform protein sequence. 100% of residues align with transcript variant 1. Mutations identified in coding sequence do not result in residue changes. Exon 2 is denoted by **dark blue** font.

ref|XP_851185.1|PREDICTED: similar to NDRG2 protein (Syld709613 protein) isoform 1 [Canis familiaris]

Length=371

GENE ID: 609390 NDRG2 | NDRG family member 2 [Canis lupus familiaris]

Score = 697 bits (1798), Expect = 0.0
 Identities = 371/371 (100%), Positives = 371/371 (100%), Gaps = 0/371 (0%)
 Frame = +1

Query	1	MAELQEVQITEEKPLLPGQTPETAK EAELAARILLDRGQ THSVETPYGSVTFVYGTPKP	180
Sbjct	1	MAELQEVQITEEKPLLPGQTPETAK EAELAARILLDRGQ THSVETPYGSVTFVYGTPKP	60
Query	181	KRPAILTYHDVGLNYKSCFQPLFQFGDMQEIIQNFVVRVHVDAPGMEEGAPVFPLGYQYPS	360
Sbjct	61	KRPAILTYHDVGLNYKSCFQPLFQFGDMQEIIQNFVVRVHVDAPGMEEGAPVFPLGYQYPS	120
Query	361	LDQLADMIPCILQYLNFSSTIIGVGVGAGAYILSRYALTHPDTVEGLVLINIDPNAKGWMD	540
Sbjct	121	LDQLADMIPCILQYLNFSSTIIGVGVGAGAYILSRYALTHPDTVEGLVLINIDPNAKGWMD	180
Query	541	WAAHKLTGLTSSIPEMILGHLFSQEELSGNSELIQKYRNIITHAPNLENIELYWNSYNNR	720
Sbjct	181	WAAHKLTGLTSSIPEMILGHLFSQEELSGNSELIQKYRNIITHAPNLENIELYWNSYNNR	240
Query	721	RDLNLERGGAVTLRCPVMLVVGDAQPHEDAVVECNSKLDPTQTSFLKMADSGGQPQLTQP	900
Sbjct	241	RDLNLERGGAVTLRCPVMLVVGDAQPHEDAVVECNSKLDPTQTSFLKMADSGGQPQLTQP	300
Query	901	GKLTEAFKYFLQGMGYMASSCMTRLSRSRTASLTSAA SIDGNRSRSRTLSQGSESGTLPS	1080
Sbjct	301	GKLTEAFKYFLQGMGYMASSCMTRLSRSRTASLTSAA SIDGNRSRSRTLSQGSESGTLPS	360
Query	1081	GPPGHTMEVSC 1113	
		GPPGHTMEVSC	
Sbjct	361	GPPGHTMEVSC 371	